A 3D seismic interpretation of mud volcanoes within the western slope of the Nile Cone

Christopher Brian Kirkham

Submitted in partial fulfilment of the requirements for the degree of Ph.D.

Cardiff University

September 2015

DECLARATION

This work has not been submitted in substance for any other degree or award at this or any other university or place of learning, nor is being submitted concurrently in candidature for any degree or other award.

Signed ……(candidate) Date …….

STATEMENT 1

This thesis is being submitted in partial fulfillment of the requirements for the degree of PhD.

Signed ……(candidate) Date …….

STATEMENT 2

This thesis is the result of my own independent work/investigation, except where otherwise stated. Other sources are acknowledged by explicit references. The views expressed are my own.

Signed ……(candidate) Date …….

STATEMENT 3

I hereby give consent for my thesis, if accepted, to be available online in the University's Open Access repository and for inter-library loan, and for the title and summary to be made available to outside organisations.

Signed ……(candidate) Date …….

STATEMENT 4: PREVIOUSLY APPROVED BAR ON ACCESS

I hereby give consent for my thesis, if accepted, to be available online in the University's Open Access repository and for inter-library loans **after expiry of a bar on access previously approved by the Academic Standards & Quality Committee.**

Signed ……(candidate) Date …….

Acknowledgments

First and foremost I wish to thank my main supervisor Professor Joe Cartwright for providing me with fantastic supervision throughout my PhD. Thanks to this opportunity and Joe's guidance and encouragement, I now stand in a position where I feel that I have achieved something great and produced a piece of research that I am very proud of. This project has given me the chance to challenge myself and develop as an individual and as an academic, all of which I owe Joe a lot of thanks for.

A big thanks goes to Christian Hermanrud and Christopher Jebsen who really helped get this project off the ground. Their deep knowledge and insight have been greatly appreciated during meetings in Norway and via various correspondences. I would also like to thank Statoil for the grant and provision of the data used in this study and NERC for award number BW22003102 that has supported this research.

Thank you to all the members of the Cardiff University 3D seismic lab past and present, whom I have very much enjoyed the company of during my time at Cardiff and shared numerous helpful conversations. Special thanks go out to Dr Tiago Alves and Gwen Pettigrew for the wealth of IT and academic support that they have given me over the many years that I have been in Cardiff University.

I would finally like to thank my family for their continued support, encouragement and unwavering faith in my ability to successfully achieve my goals. I would especially like to thank my partner Stacey Wood for her continued understanding of the pressures exerted on me from this PhD and for supporting me till the end of the project. Sorry for all the long days and late nights working.

Table of contents

CHAPTER 2

CHAPTER 3

CHAPTER 4

CHAPTER 5

CHAPTER 7

List of figures

CHAPTER 1

List of tables

CHAPTER 1

List of equations

CHAPTER 1

Abstract

Mud volcanoes are found within a variety of settings both terrestrial and submarine around the world. The extrusion of mud forms topographic features at the surface that are representative of the focused release of fluids and mud and overpressure. An understanding of mud volcanoes is important for numerous reasons, which include, the insight they provide into overpressure systems and the presence of hydrocarbons, and their potential as a geological hazard.

The research that is presented within this thesis focuses on a large number of mud volcanoes within the western slope of the Nile Cone, Eastern Mediterranean. The analysis of these mud volcanoes is based on interpretation using 3D seismic data. The core themes of this research involve analysing these mud volcanoes in order to better understand their geometry and seismic character, timing and distribution, source region and depletion zone, and understand the mechanisms behind the formation of their conduits and ultimately their extruded bodies.

This research has led to the discovery of a suite of giant mud volcanoes that are irregular in shape and are among the largest to have been recorded thus far. These mud volcanoes formed directly on top of the Messinian evaporites within the western slope of the Nile Cone at the climax of the Messinian Salinity Crisis. Their interpretation presents significant evidence for a major overpressure release event at the end of the Messinian Salinity Crisis.

As many as 386 smaller and conical mud volcanoes have also been interpreted within the western slope of the Nile Cone. Hosting such a large number of mud volcanoes, it could be argued that this region of the Eastern Mediterranean should be considered as amongst the largest mud volcano provinces in the world. Analysis of these mud volcano conduits, depletion zones and volumetric balance calculations, combined with evidence from published literature present a strong case for a pre-salt source for these mud volcanoes. This implies that significant volumes of mud and fluid have bypassed what many previously considered to be a near impermeable barrier.

Chapter 1

1 Introduction

1.1 Rationale

Subsurface sediment and fluid mobilisation is an important naturally occurring geological phenomenon, the products of which occur in a variety of sedimentary basins and are becoming increasingly observed (Huuse et al., 2010; Judd and Hovland, 2007) (Figure 1.1). Forms of subsurface sediment mobilisation include soft sediment deformations, sand injections, shale diapirs and mud volcanoes (Van Rensbergen et al., 2003; Huuse et al., 2010; Huuse et al., 2005; Brown, 1990; Kopf, 2002). Recent advancements in the fidelity of subsurface imaging via 3D seismic data (Cartwright and Huuse, 2005) has led to an increase in the documentation of features associated with the mobilisation of subsurface sediments (Van Rensbergen et al., 1999; Cartwright et al., 2007; Stewart and Davies, 2006; Huuse et al., 2010; Løseth et al., 2001; Evans et al., 2007) (Figure 1.2). Mud volcanoes in particular have received a significant amount of attention in recent years, due to the fact that they are relatively easy to observe physically on land and offshore, as well as via 3D seismic analysis (Roberts et al., 2010; Evans et al., 2008; Van Rensbergen et al., 2005; Graue, 2000; Huguen et al., 2009), but also due to the eruption of the Lusi mud volcano in Indonesia, the impact of which has added significant societal relevance to the study of mud volcanoes (Davies et al., 2008; Davies et al., 2011; Davies et al., 2007; Rudolph et al., 2013; Rudolph et al., 2011; Mazzini et al., 2012; Mazzini et al., 2009; Mazzini et al., 2007; Tanikawa et al., 2010; Istadi et al., 2009; Fukushima et al., 2009).

Understanding and analysing mud volcanoes is of importance for numerous reasons including: 1) they are a source of hydrocarbon gas and CO_2 flux, and emit into the atmosphere a significant percentage of the world's greenhouse gases (Etiope et al., 2002; Etiope et al., 2004b; Etiope and Klusman, 2002; Milkov, 2000; Dimitrov, 2002; Haese et al., 2003); 2) they deposit clasts from deeper lithologies onto the surface, which provides information on the rocks present at depth (Giresse et al., 2010; Milkov, 2000); 3) they can seep hydrocarbons and act as a potential indicator for active

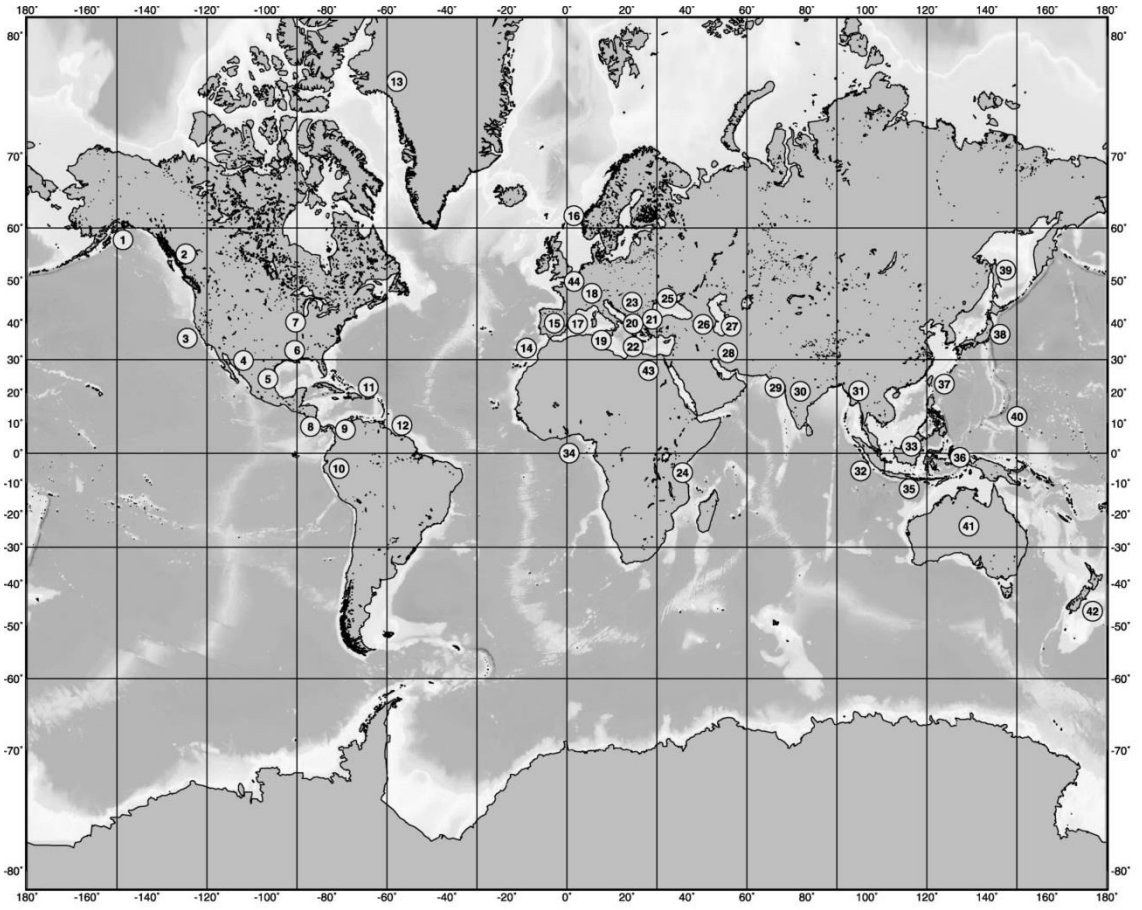

Figure 1.1 A map showing the occurrence of mud volcanoes on earth (From Kopf (2002))

hydrocarbon plays deep within the subsurface (Pierre et al., 2014; Dupré et al., 2014; Huguen et al., 2009; Milkov, 2000; MacDonald et al., 2000; Berndt, 2005); 4) gas hydrates can be found in association with deep-water mud volcanoes, which is a potential energy source (Deville et al., 2010; Dimitrov, 2002; Milkov, 2000); 5) they present a potential geologic hazards, as demonstrated by the modern eruption of the Lusi mud volcano (Davies et al., 2008; Deville and Guerlais, 2009; Giresse et al., 2010; Milkov, 2000; Mazzini et al., 2012). They also offer a unique insight into deep basin overpressure systems since high pore fluid pressure is a vital requirement for large scale mud mobilisation (Kopf, 2002; Maltman and Bolton, 2003; Van Rensbergen et al., 2003). An understanding of overpressure associated with mud volcanoes can be of vital importance for the oil and gas industry, as subsurface overpressure presents a significant hazard for drilling, and the eruption of a mud volcano could potentially impact rig installations and pipeline routings (Reilly and Flemings, 2010; Roberts, 2010; Osborne and Swarbrick, 1997; Milkov, 2000; Yusifov and Rabinowitz, 2004).

1.1.1 Aims

This PhD project uses three-dimensional (3D) seismic reflection data to primarily investigate mud volcanism within the El Dabaa study area, which is located within the western province of the Eastern Mediterranean (See Chapter 3 for full location details). The aims of this chapter are to:

1. Present an introduction to mud volcanoes.
2. Describe the various subdivisions of mud volcano systems.
3. Describe the potential mechanisms that drive mud mobilisation and the formation of mud volcanoes.
4. Describe how mud volcano conduits and other structural features associated with mud volcanoes present types of seal bypass system.
5. Describe the geophysical indicators and various hydrocarbon indicators associated with mud volcanoes in 3D seismic data.
6. Outline the aims for this research and structure of the thesis.

1.2 Mud volcanoes

1.2.1 Defining mud volcanoes

Mud volcanoes of the order of several thousand have been observed within a variety of settings across the Earth, both terrestrial and submarine (Kopf, 2002) (Figure 1.1). A mud volcano is defined as a superficial topographic structure, formed through natural processes within cold seep environments where fluid rich and fine grained sediments such as clay produce a mud slurry (a muddy mass made from fluids, gas and sediments of different age, composition, structure) that ascends through a lithological succession, until piercing the surface or seafloor where it is extruded and produces varied morphological expressions (Dimitrov, 2002; Kopf, 2002; Gontharet et al., 2007a; Judd and Hovland, 2007) (Figure 1.2).

The volcano part of the name mud volcano is used in reference to the similarities in the geometry of mud extrusions and that of igneous volcanoes (Kopf, 2002; Judd and Hovland, 2007). However, the comparable extruded geometry between mud volcanoes and igneous volcanoes is where the similarity ends. Mud volcanoes are in fact rarely observed in connection with igneous activity (Chiodini et al., 1996; Kopf, 2002). The scale of individually described and measured mud volcanoes has been recorded to be as great 22.5 km^3 (Davies and Stewart, 2005) and igneous volcanoes have been measured to have total volumes greater by four orders of magnitude (Bryan et al., 2010; Robinson and Eakins, 2006). However, despite the thousands of mud volcanoes that have been discovered on Earth and the extensive literature on mud volcanoes, quantitative information on the scale by volume of mud volcanoes is surprisingly limited.

Mud volcanoes act as a pathway for degassing and dewatering deeper lithologies; therefore, they can have a major influence on fluctuations in pore fluid pressure at depth and can encourage hydrocarbon migration if the overpressuring of their source unit is associated with the generation of hydrocarbons or if their conduits

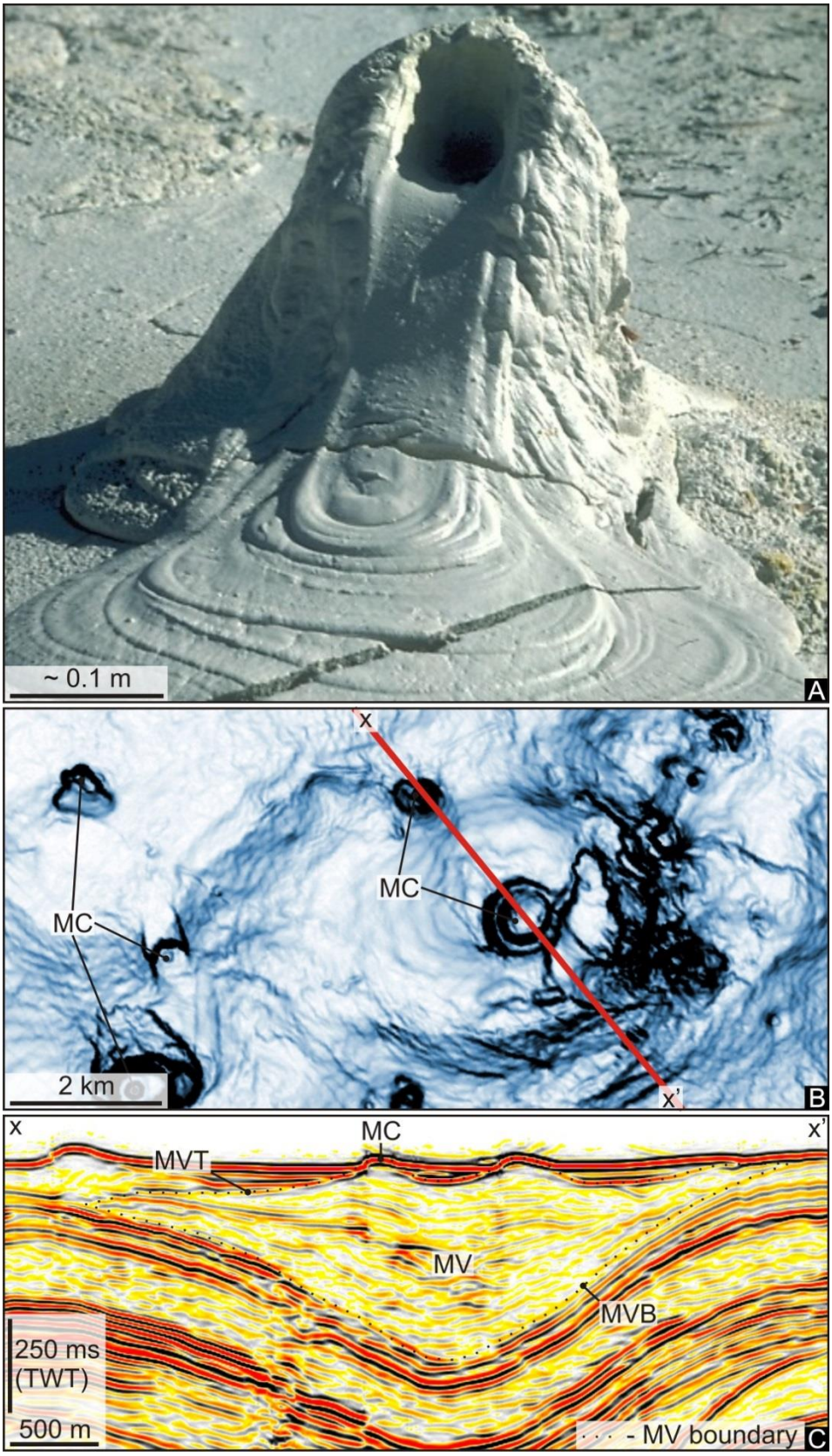

Figure 1.2 The appearance of a mud volcano. A: A mud volcano gryphon from Norris Geyser Basin, Yellowstone National Park, Wyoming. Photograph by S.R. Brantley (September1983) (http://volcanoes.usgs.gov/about/pglossary/MudVolcano.php). B: A time-dip map of the seafloor in the El Dabaa study area showing numerous mud cones. C: A seismic profile through a mud volcano within the El Dabaa study area. MV – Mud volcano; MC – Mud cone; MVB – Mud volcano base; MVT – Mud volcano top.

penetrate through active hydrocarbon plays (Milkov, 2000; Osborne and Swarbrick, 1997; Cartwright et al., 2007; Kopf and Behrmann, 2000). A strong relationship between areas of active generation of buoyant hydrocarbons and the formation mud volcanoes has often been observed (Hedberg, 1980; Charlou et al., 2003; Dimitrov, 2002; Kopf, 2002; Wilford, 1967; Humphrey, 1963; Stamatakis et al., 1987). It has previously been suggested that the very first documentations of mud volcanoes were in fact undertaken as a result of their intimate association with hydrocarbons and hence hydrocarbon provinces (Abikh, 1863; Goubkin and Fedorov, 1938; Dadashev, 1963; Roberts, 2010).

1.2.2 Occurrence and typical setting for mud volcanism

Mud volcanoes occur in various settings worldwide, particularly compressional tectonic settings and areas with high sedimentation rates (Deville and Guerlais, 2009; Kopf, 2002; Milkov, 2000; Dimitrov, 2002). Typically, mud volcanoes occur on convergent plate margins where fluid rich sediments are rapidly deposited within deep sea trenches before entering the subduction factory, where high compaction stress and temperature force liquids and volatiles to be released (Kopf, 2002). They also occur on passive margins and deltaic settings where sediment accumulation rates are high (Milkov, 2000; Graue, 2000; Loncke et al., 2004).

Submarine mud volcanoes are more common than subaerial, however, considering about two thirds of the world are covered by seas and oceans this fact is relatively unsurprising (Milkov, 2000) (Figure 1.1). Examples of areas of active mud volcanism include submarine mud volcanoes discovered offshore Barbados, the Gulf of Mexico, offshore Nigeria and in the Norwegian, Mediterranean, Black and Caspian seas (Milkov, 2000). The region with the greatest amount of mud volcanism to date is the Mediterranean Sea and Tethyan Belt, which spans from the south of Greece, over the Black and Caspian Sea into Azerbaijan, the Crimea and Taman Peninsulas, Iran and Turkmenistan into the Makran coast (Kopf, 2002). Mud volcanoes are in abundance within the Eastern Mediterranean particularly on the Mediterranean Ridge (Kopf et al.,

2001; Kopf, 2002). Within the Nile Deep Sea Fan more than 150 mud cones and pockmarks have also been observed by Loncke et al. (2004) within water depths of about 2500-3000m.

1.2.3 Subdivision of mud volcano systems

In an attempt to categorise the various components of a 'mud volcano system', Stewart and Davies (2006) subdivided the system into a source stratigraphic succession, an intrusive domain (here referred to as the mud volcano conduit) and the extrusive domain (here referred to as the mud volcano) (Figure 1.3).

Thick mud dominated formations typically form the source stratigraphic succession for mud volcanoes (Figure 1.3). These successions are usually comprised of fine grained sediments and are of low permeability, which is one of the prime reasons for fluids being trapped in the muds during burial, which can lead to undercompaction and overpressuring (Brown, 1990; Kopf, 2002). The analysis of clasts within the extruded body of a mud volcano can provide information on the types of sediment that have been extruded, which could also give an indication as to the sediment and fluid source (Giresse et al., 2010; Kopf, 2002; Deville et al., 2003; Deville et al., 2010; Deville et al., 2006; Robertson, 1996; Kopf et al., 1998). Definitively ascertaining the primary source of mud from extruded samples alone can be challenging and in some cases it has been interpreted that the fluids and sediment feeding some mud volcanoes could be sourced from numerous levels within a succession (Mazzini et al., 2009; Mazzini et al., 2007; Tanikawa et al., 2010; Deville et al., 2003; Deville et al., 2010; Deville et al., 2006).

If the depth from which mud has been withdrawn during mud volcanism can be identified, it may give some indications as to the mechanisms behind its mobilisation and outline the vertical extent that the mud volcano conduit must have transected in order to connect the source stratigraphic succession and the extruded mud volcano (Cartwright et al., 2007; Cartwright and Santamarina, 2015). Downsagging reflections and the thinning of a succession, which are observable in 3D seismic data, have

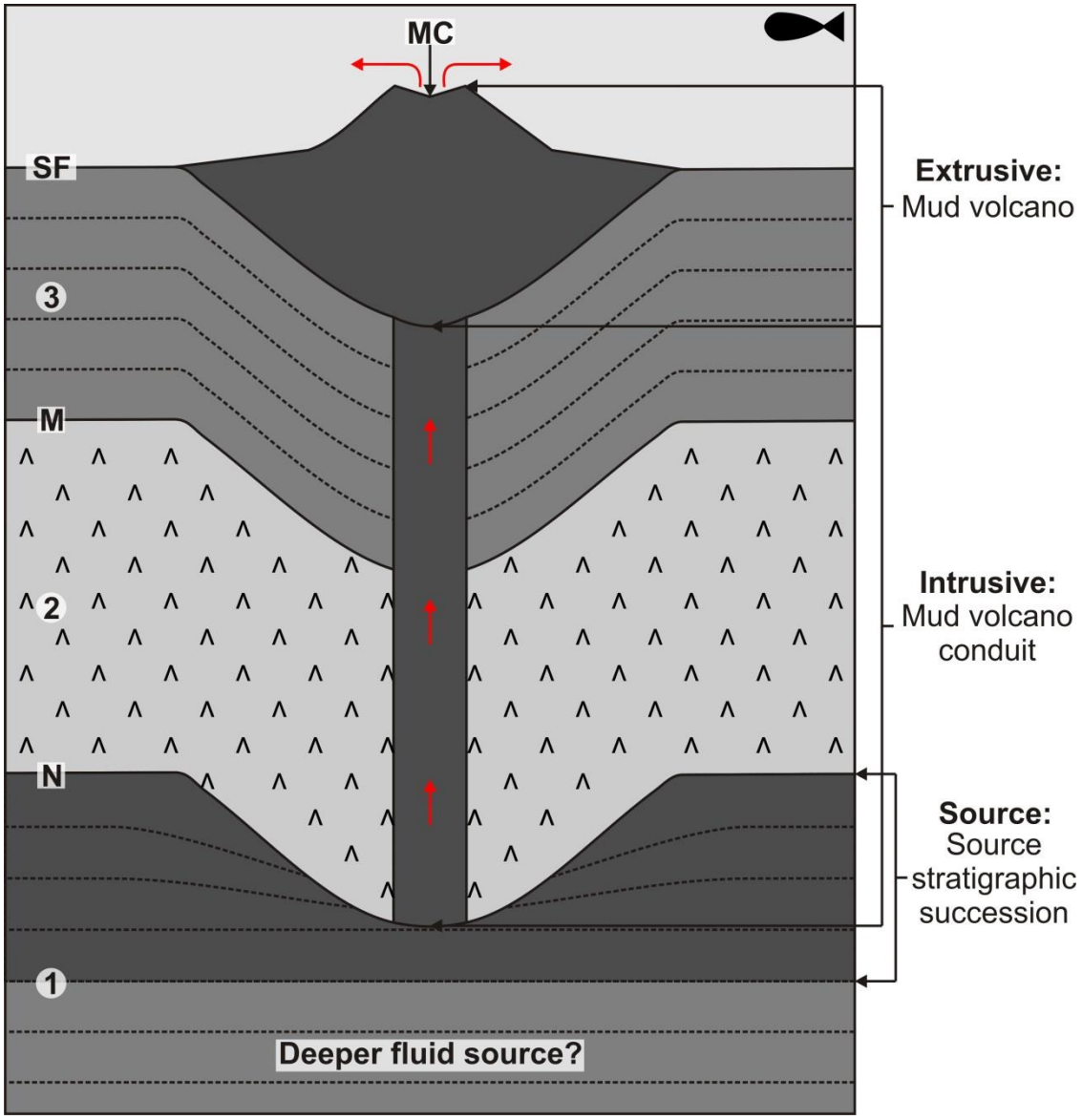

Figure 1.3 A schematic diagram of a mud volcano within the study area for this thesis. The schematic highlights subdivisions of a mud volcano system. The red arrows represent fluid and mud migration. MC – Mud cone; SF – Seafloor; M – Horizon M; N – Horizon N; 1 – Pre-salt succession; 2 – Messinian evaporites; 3 – Pliocene to Recent succession (See section 3.5 of Chapter 3 for description of the seismic stratigraphy).

previously been documented as depletion related geometries associated with the mobilisation and withdrawal of sediments from a succession (Stewart and Davies, 2006; Istadi et al., 2009; Fukushima et al., 2009) (Figure 1.3).

Mud volcano conduits represent a form of seal bypass system that is highly effective in facilitating the migration of fluids and fine grained sediment through a sedimentary succession (Cartwright et al., 2007). This conduit connects the source stratigraphic succession and the extruded mud volcano (Roberts et al., 2010; Stewart and Davies, 2006; Cartwright et al., 2007). Similar to descriptions of fluid escape pipes, the root zone of the mud volcano conduit will be the upper margin of the source stratigraphic succession and so the identification of the root zone can give an indication as to where the mud and fluids have been sourced (Huuse et al., 2010; Moss and Cartwright, 2010a; Cartwright and Santamarina, 2015) (Figure 1.3). The upper termination of a mud volcano conduit is the point at which it pierces the surface or seafloor, which then leads to the extrusion of mud during the construction of a mud volcano (Fowler et al., 2000; Graue, 2000; Stewart and Davies, 2006; Reiche et al., 2014) (Figure 1.3).

Several types of connection between a source stratigraphic succession and an extruded mud volcano have been observed over the years, which include large diapirs (Brown, 1990), steep mud injections or diatremes (Pickering et al., 1988; Robertson and Kopf, 1998; Clari et al., 2004) and narrow vertical pipes (Graue, 2000; Roberts et al., 2010; Kopf, 2002; Reiche et al., 2014). Secondary pathways off the primary conduit have also previously been documented and result in small mud cones or craters towards the margins of a mud volcano known as gryphons. The geometry of mud volcano conduits and the mechanisms behind their formation remain one of the least analysed and least understood aspects of mud volcanoes (Roberts, 2010; Roberts et al., 2010). It is thought that the geometry of the conduit and vent, which forms the main breach of the seal, controls the rate at which mud ascends through a lithological succession and has a significant impact on the mud volcanoes expression at the surface (Cartwright et al., 2007; Kopf, 2002).

There has to date been limited detailed analysis of the geometry and expression of mud volcano conduits via 3D seismic data. This may perhaps be in part associated with previous limitations in the imaging of mud volcano conduits using seismic data (Dimitrov, 2002; Yusifov and Rabinowitz, 2004). However, recent improvements in the resolution and imaging quality of highly disruptive zones such as mud volcano conduits implies that a more detailed and quantitative account of these highly complex zones should be undertaken (Stewart and Davies, 2006; Davies and Stewart, 2005; Kopf, 2002; Fowler et al., 2000; Cartwright et al., 2007; Van Rensbergen, 2003). While improved analysis of conduit margins and overall geometry is possible, the potential for seismic artefacts should be considered. Acoustic blanking or amplitude attenuation (see section 5.3.2 and Figure 5.7) shrouds the centre of mud volcano conduits, potentially due to a combination of disruption to the host succession and the presence of gas (Judd and Hovland, 1992; Judd and Hovland, 2007). Detailed analysis from field mapping of exhumed mud volcano conduits has, however, documented the internal character of some mud volcanoes (Roberts et al., 2010).

The extruded and constructional mud volcano that forms at the upper terminus of mud volcano conduits represent the part of the mud volcano system that a significant amount of research to date has focused on (Davies and Stewart, 2005; Loncke et al., 2004; Dupre et al., 2007; Dupré et al., 2014; Evans et al., 2007; Evans et al., 2008; Huguen et al., 2009; Milkov, 2000; Murton and Biggs, 2003; Etiope et al., 2004a; Kopf, 2002; Yusifov and Rabinowitz, 2004) (Figure 1.3). This is most probably because mud volcanoes represent the surface expression of mud mobilisation and so are more easily observed on land or in submarine settings than mud volcano conduits.

It has previously been suggested that despite the varied geometry of mud volcanoes they can be loosely subdivided as either mud cones/domes or mud pies (Kopf, 2002) (Figure 1.4). The distinction between the two is based predominately on the angle of the flanks of the mud volcano. Mud pies are generally considered to be low angled with a slope of <5° and the conduit for a mud pie is thought to be usually wider than that of mud domes (Kopf, 2002) (Figure 1.4). The viscosity of the erupted mud is thought to be a key factor in governing whether the extruded mud volcano is either a mud cone or mud pie, based on the classification set by Kopf (2002). If the

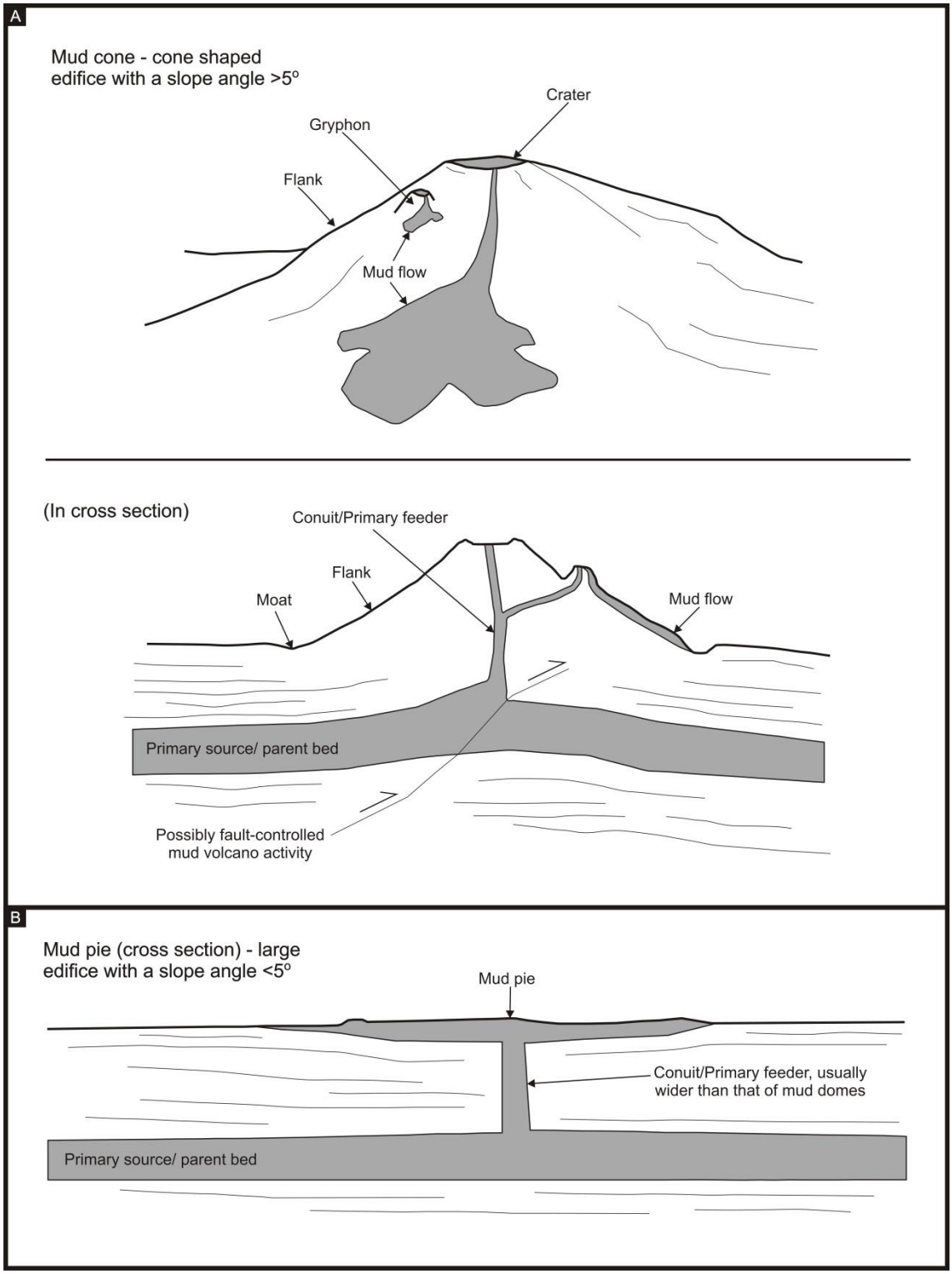

Figure 1.4 A schematic diagram of two types of mud volcano. A: A mud cone/dome schematic and cross section. B: A mud pie cross section. The name originates from its pie-shape (Modified from Kopf (2002).

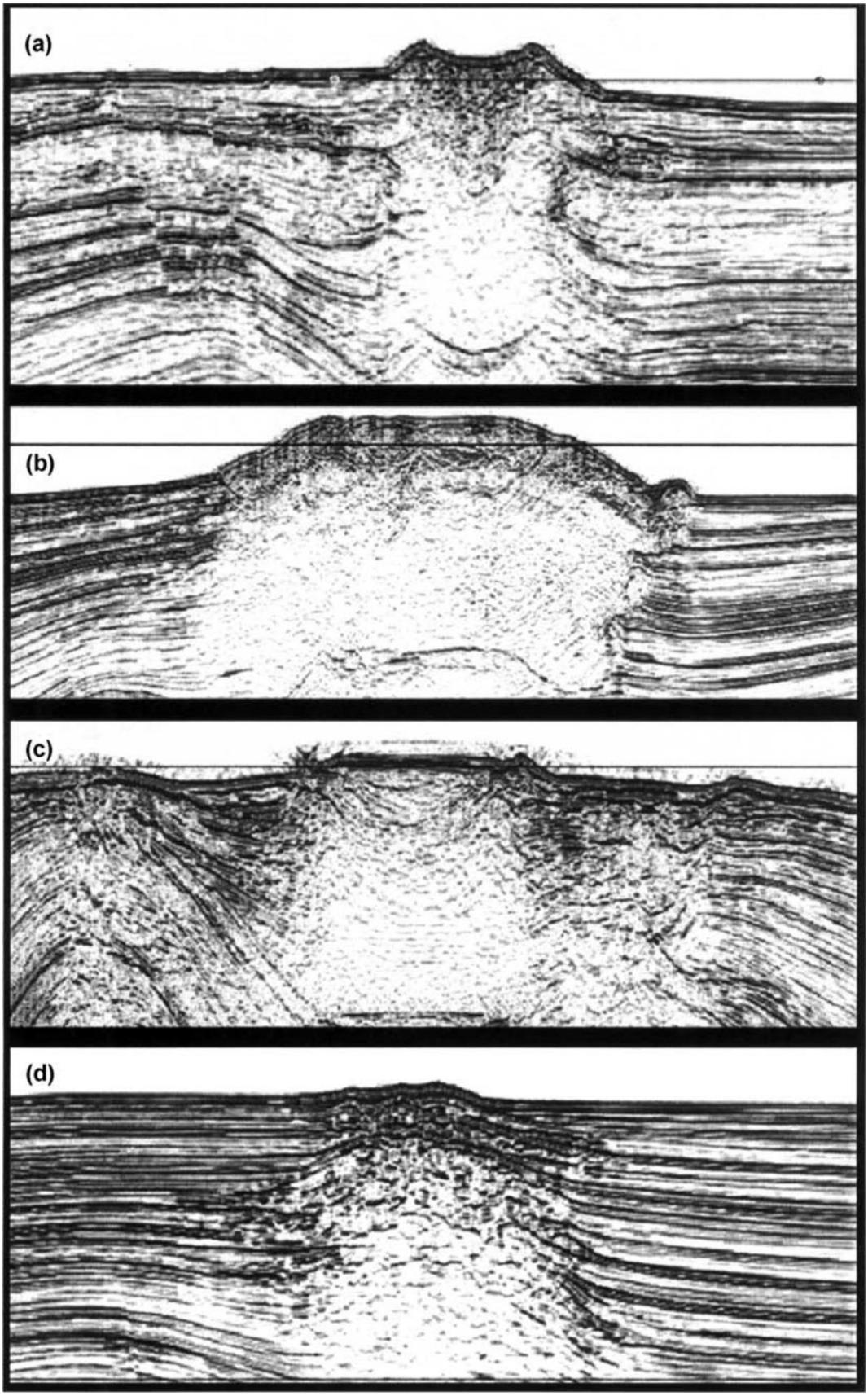

Figure 1.5 Classification of mud volcanoes by Yusifov and Rabinowitz (2004) based on shape and appearance in seismic profile. a) concave; b) convex; c) flat; d) buried (From Yusifov and Rabinowitz (2004)).

mud eruption has a high viscosity it is most probable that it will form a steep sided cone and if the erupted mud has a low viscosity it may form a mud pie (Kopf, 2002; Kopf et al., 2001). Yusifov and Rabinowitz (2004) also attempted to classify mud volcanoes within Azerbaijan, based on whether their general shape is: A) concave; B) convex; C) flat; D) buried (Figure 1.5). It has been suggested that the areal extent of these mud volcanoes is governed by local morphology and slope angle and the viscosity of the erupted mud, which is thought to be less viscous in submarine mud volcanoes than in onshore mud volcanoes (Yusifov and Rabinowitz, 2004)

The extrusion of mud volcanoes within some regions can result in a 'Christmas tree' geometry, which is formed via a stack of overlapping mud volcanoes (Stewart and Davies, 2006; Deville and Guerlais, 2009). This geometry has been observed in mud volcanoes offshore Trinidad and is thought to potentially have formed as a result of the interaction of mud extrusion and high sedimentation rates, whereby the mud volcanoes form on flat surfaces during periods of low sedimentation and are progressively covered during periods of high sedimentation (Deville and Guerlais, 2009; Deville et al., 2006).

Over recent years evidence has been presented that demonstrates that the eruption of mud volcanoes is generally episodic with cyclic phases of activity (Deville and Guerlais, 2009; Deville et al., 2006; Deville et al., 2010) (Figure 1.6). These eruptive episodes are essentially controlled by the local pressure regime within the source stratigraphic succession, resulting in times of high and low fluid and mud flux (Deville and Guerlais, 2009). This can be seen onshore Trinidad where mud volcanoes have shown different phases of activity, which include catastrophic events followed by periods of moderate activity during which the mud and gas flows expelled are reduced (Deville and Guerlais, 2009; Higgins and Saunders, 1974) (Figure 1.6). The amount of overpressure and fluid released at a given time depends on the point in the mud volcanoes cyclic phase (Figure 1.6). Low frequency cycles are likely the result of excess pore pressure at depth, which leads to hydraulic fracturing and the formation of a hydraulic fracture network and allows for successive fluid release and cyclic pressure decrease.

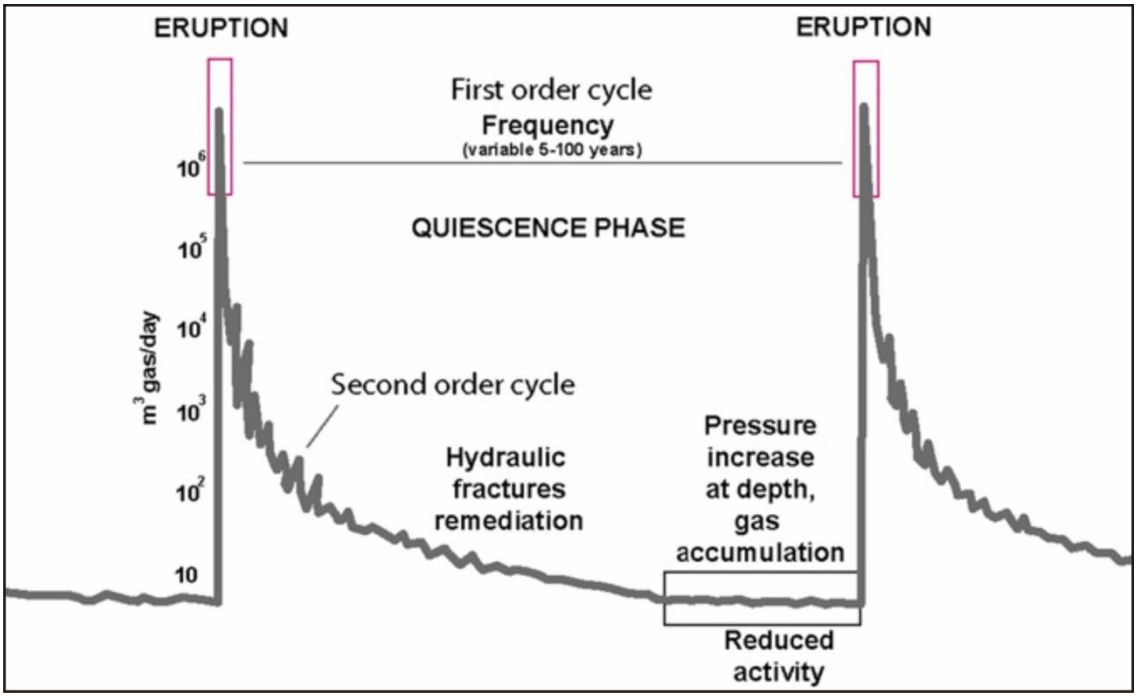

Figure 1.6 A conceptual model of over-imposed cycles of mud volcano flux in which catastrophic eruptions occurred (From Deville and Guerlais (2009)).

1.3 Mechanisms driving mud volcanism

The mobilisation of sediment requires a mechanism that renders the sediment within the source stratigraphic succession capable of moving as a fluidised slurry (Maltman and Bolton, 2003; Davies et al., 2008; Tanikawa et al., 2010). One of the core requirements often thought to be the driving force behind the mobilisation and extrusion of mud from a source stratigraphic succession that is undercompacted and fluid rich, is overpressure (Kopf, 2002).

Pore fluid pressure, also known as the formation pressure, is defined as the pressure acting on fluids within the pore spaces of the formation. Under normal burial conditions, loading of sediments by newly deposited sediments results in the progressive expulsion of fluids as a direct response to the increase in sedimentary load (Maltman et al., 2000; Evans, 2007). Pore fluid is defined as overpressured when the pressure exceeds that of the hydrostatic gradient at a given depth (Figure 1.7). The definition of hydrostatic pressure is the pressure exerted by the weight of a static column of fluid. Where the pore fluid pressure equals the hydrostatic pressure, the formation is normally pressured (Figure 1.7). It is a function of the fluid density and vertical height of the fluid column (Judd and Hovland, 2007; Osborne and Swarbrick, 1997; Swarbrick, 1999). The equation for hydrostatic pressure (P_{hydro}) is expressed as;

Equation 1.1

$$P_{hydro} = (p_{water}.g.h) + P_{atmos}$$

Where p_{water} is the average fluid density, g is the acceleration due to gravity and h is the vertical height of the fluid column measured from a datum and P_{atmos} is the atmospheric pressure (normally 101 kPa are the sea surface).

The pressure that is exerted by the weight of the overlying sediments, including the contained fluids within sediment pore spaces, defines what is referred to as the lithostatic pressure (Osborne and Swarbrick, 1997; Swarbrick, 1999) (Figure 1.7). This is also known as the overburden pressure or overburden stress. As the weight of the overlying sediments govern the lithostatic pressure, increases in depth result in an increase in lithostatic pressure along the lithostatic gradient.

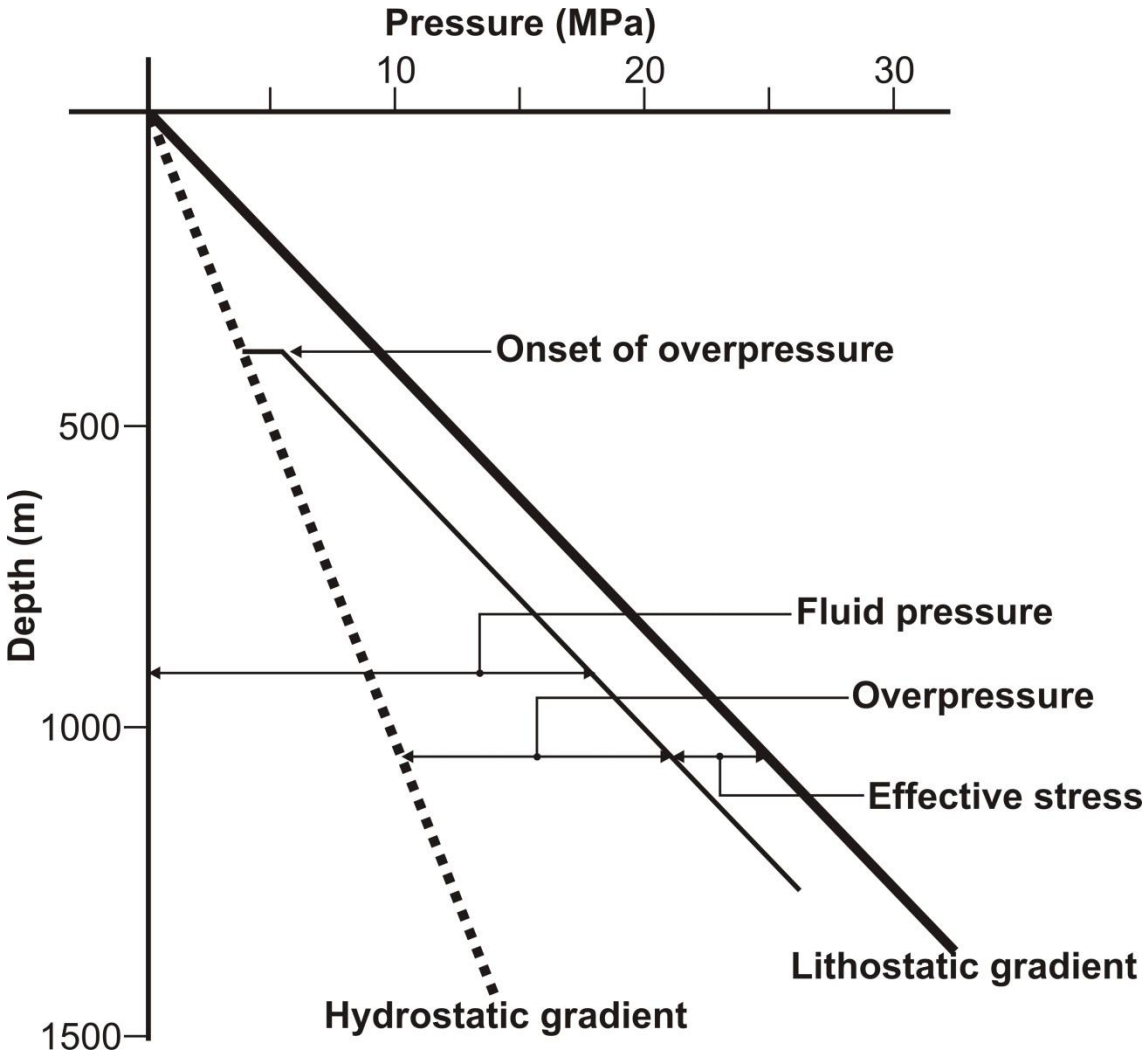

Figure 1.7 Pressure versus depth plot for a sedimentary succession. Pressure vs. depth plots allow the opportunity to determine formation pressure with respects to hydrostatic, fracture and lithostatic pressures, to evaluate fluid density and type and to establish fluid contacts. The schematic demonstrates the relationship between lithostatic pressure, pore fluid pressure, overpressure and effective stress. The thinner black line represents an idealised depth-pore fluid pressure path for a sand body that has become overpressured as a result of disequilibrium compaction (Modified from (Jolly and Lonergan, 2002)).

The equation for the overburden stress (S) is expressed as;

Equation 1.2

$$S = h \times pbg$$

Where *h* is the vertical thickness of the overlying sediments, *pb* is the average bulk density and *g* is the gravitational force (Osborne and Swarbrick, 1997). Some of the weight of the overburden is borne by the fluids within pore spaces. Any additional load that is exerted on the sediment particles is known as the effective stress (Figure 1.7). This means that an increase in pore fluid pressure leads to a decrease in effective stress. When pore fluid pressure reaches lithostatic pressure, the entire weight of the overburden is supported by the fluids and is effectively not matrix support. This relationship between effective stress (σ) and the overburden is expressed in Terzaghi's equation;

Equation 1.3

$$\sigma = S - P_f$$

Where *S* is the overburden stress and P_f is the fluid pressure.

The porosity of sediment during burial is governed by the effective stress. If effective stress is low and the pore fluid pressure is high, porosity values will remain high. However, if effective stress increases, porosity will decrease and the sediment will compact (Osborne and Swarbrick, 1997). The overburden stress increases with depth along the lithostatic gradient (Osborne and Swarbrick, 1997) (Figure 1.7). At any point the lithostatic pressure is determined by the density of the overlying sediment, which is expressed as;

Equation 1.4

$$\sigma_{v'} = S = \sum_z^0 [d_s(1-\phi) + d_f(\phi)]$$

Where $\sigma_{v'}$ is the vertical stress, d_s is the density of the rock, d_f is the density of the fluid and φ is the porosity.

It is possible that an increase in fluid overpressure to near lithostatic pressure gradient levels, could cause the overburden to hydraulically fracture and allow fluids and mud to mobilise and bypass an overlying succession (Deville and Guerlais, 2009;

Morley et al., 1998; Cartwright and Santamarina, 2015). The amount of pore fluid pressure that a rock can withstand or is required before it fails is known as the fracture pressure. The fracture pressure is, therefore, defined as the amount of pore fluid pressure a rock can withstand before its tensile strength (T) and the minimum principal stress (σ_{min}) is exceeded and hydraulic fracturing can occur (Osborne and Swarbrick, 1997; Swarbrick, 1999), which is expressed as;

Equation 1.5

$$P_f > \sigma_{\min} + T$$

The fracture gradient is generally lower than the lithostatic pressure gradient. Evaluating the fracture gradient requires information on the in-situ stresses, which are a function of sedimentation and the regions tectonic history during basin formation. The orientation of hydraulic fractures is primarily governed by the direction of minimum compressive stress (Jolly and Lonergan, 2002; Delaney et al., 1986; Hubbert and Willis, 1972). Within a tectonically relaxed setting such as a passive margin, the direction of minimum compressive stress is typically horizontal, as the direction of maximum compressive stress is usually vertical due to the lithostatic load (Cosgrove, 2001; Cartwright and Santamarina, 2015). Where the minimum compressive stress direction is vertical, hydraulic fractures will form in a horizontal orientation, which could lead to the development of sedimentary sills (Jolly and Lonergan, 2002).

1.3.1 Generating overpressure

Two important factors behind the generation and distribution of overpressure are: 1) the permeability, which is as a function of the sealing properties of a rock allowing it to retain fluid and overpressure; 2) The amount and rate at which overpressure accumulates or dissipates, which is directly related to the mechanism behind the generation of excess pore fluid pressure. Time is also a factor that should be considered as the state of disequilibrium as a result of overpressure will change over time depending on the evolution of the system, unless a state of zero effective permeability is achieved, which is difficult to maintain in the water phase over

geological time (Deming, 1994; Swarbrick, 1999). The distribution and magnitude of overpressure will, therefore, change over time as a result of fluctuations in overpressure accumulation and overpressure dissipation associated with leakage.

Permeability is the property responsible for controlling fluid flow through a rock. Fluid retention is largely due to low permeability in non-reservoir rocks such as shales and evaporites and may lead to overpressure. The properties of a rock such as the grain size and shape control the permeability of the rock. A rock with a low permeability makes it a suitable seal or barrier to flow. Watts (1987) defines a seal as rock which impedes the natural upwards migration of buoyant hydrocarbons, however, no rock is 100% sealing over geological time. The permeability of a rock is defined by the equation that expresses Darcy's law and relates flow rate of a given fluid per unit of time, along a known flow path across which there is a specific pressure drop:

Equation 1.6

$$Q = \frac{kA\Delta P}{\mu L}$$

Where Q is the volume rate of flow, k is permeability, L is the length scale, ΔP is the pressure drop across the length scale, μ is the viscosity of the fluid and A is the area across which flow takes place.

There are a variety of mechanisms that generate overpressure within a source stratigraphic succession for mud volcanism, which can be divided into three categories: 1) An increase in compressive stress via disequilibrium compaction (vertical compression via burial) and/or tectonic compression (horizontal compression) resulting in a reduction in pore volume; 2) A change in the volume of the pore fluid or rock matrix (i.e. aquathermal pressuring, diagenesis, a build-up in gas pressure); 3) Fluid movement and/or buoyancy (Osborne and Swarbrick, 1997; Swarbrick, 1999). The two primary causes of submarine mud volcano formation are thought to be high sedimentation rates and lateral tectonic compression, hence why mud volcanoes are frequently observed in convergent plate settings and areas with high sedimentation rates (Milkov, 2000). Mud volcanoes have also been observed to display a spatial and

genetic relationship with oil and gas fields, which may provide evidence for hydrocarbon potential and the relationship between hydrocarbons and the generation of overpressure (Guliyev et al., 1996; Etiope et al., 2004b; Etiope et al., 2002; Hedberg, 1980; MacDonald et al., 2000). The mechanisms that could potentially contribute to the generation of overpressure are discussed below.

1.3.1.1 Disequilibrium compaction

At any given depth in a sedimentary basin the vertical load due to overlying sediments (overburden stress) is a combination of effective stress and fluid pressure as stated above (Equation 1.2). As sediments are buried the vertical load increases, which in most cases results in compaction. This process reduces the pore volume and forces out formation fluids. For example, Sandstones deposited at porosities around 39-49% (Lundegard, 1992) compact to porosities of 15-25% at depths of 2-3km (Osborne and Swarbrick, 1997). The expulsion of fluids during compaction strongly depends on sedimentation rate, lithology and stratigraphy. Sandy sediments generally have high permeability and hydraulic conductivity, which allows pore fluids to dissipate quickly even during loading (Berndt, 2005).

In contrast to sandstones, clays typically have low permeability but may have porosity in the range of 65-80% at deposition and will be compacted at great depths of 4-km where porosity can be reduced to as little as 5-10% of the rock volume (Sclater and Christie, 1980; Kopf, 2002; Osborne and Swarbrick, 1997). Under slow burial conditions, normal compaction of sediments occurs where there is a state of equilibrium between the overburden and reducing pore fluid volume. This results in an increase in pore fluid pressure with depth that follows a hydrostatic pressure gradient (Figure 1.7). However, as burial continues, the permeability of the sediment decreases until what is known as the fluid isolation depth is reached, where fluid will start to be retained within the succession (Osborne and Swarbrick, 1997).

Rapid burial may similarly result in unusually high fluid retention. During rapid burial, the rapid expulsion of fluids would be required in response to increasing

overburden stress in order to maintain a hydrostatic state of equilibrium. If pore fluids cannot be expelled rapidly enough, the pore fluid pressure will rise above the hydrostatic gradient, which results in undercompaction, a greater porosity than expected at a certain depth and overpressuring (Osborne and Swarbrick, 1997; Swarbrick, 1999; Maltman and Bolton, 2003). In pressure vs depth plots, this will be displayed as pore fluid pressure increasing along a pressure-depth path that is parallel to the lithostatic pressure gradient (Figure 1.7). No rock is entirely impermeable though and so some fluids will continue to escape resulting in the pore fluid pressure rising sub-parallel to the lithostatic gradient.

1.3.1.2 Tectonic stress

Within a basin where no lateral compression occurs, horizontal stresses would be equal to or less than vertical stresses (Osborne and Swarbrick, 1997). Despite a change in the direction of maximum compressive stress, lateral compression can increase pore fluid pressure in the same way as vertical stress in disequilibrium compaction (Osborne and Swarbrick, 1997). Mud volcano systems are often located within anticlines, within areas of regional compression where there is an increase in lateral stress on the source stratigraphic succession for mud volcanism (Fowler et al., 2000; Yusifov and Rabinowitz, 2004; Roberts, 2010; Graue, 2000). For example, mud volcanoes onshore Trinidad are especially developed along ramp anticline crests where fluids migrate through hydraulic fracture systems (Deville and Guerlais, 2009). The build-up of overpressure due to tectonic processes can be very rapid; however, rapid pressure decrease could also occur if large volumes of fluid were to escape up fault planes and fractures (Sibson, 1990; Osborne and Swarbrick, 1997).

1.3.1.3 Aquathermal expansion (Temperature increase)

If a body of water is contained within a sealed vessel and is above 4°C, the internal pressure rises rapidly if heated (Osborne and Swarbrick, 1997). To generate

overpressure via aquathermal expansion, the rock system must be close to perfectly sealed and it must maintain a constant volume as temperature rises. Due to leak-off, the conditions required for aquathermal pressuring will rarely be met. The volume of expansion that aquathermal pressuring produces is actually relatively small and may rapidly dissipate by fluid flow, even where the sealing rock has a very low permeability (Daines, 1982; Osborne and Swarbrick, 1997). It is, therefore, thought to be unlikely that aquathermal expansion represents a primary mechanism for the generation of overpressure.

1.3.1.4 Diagenetic transformations

There are numerous diagenetic transformations that have the potential to result in the generation of overpressure including, dehydration due to the transformation of smectite-to-illite and gypsum-to-anhydrite and also diagenesis without dehydration. Smectite is a common detrital mineral in shale and contains abundant interlayered water in its crystal structure (Osborne and Swarbrick, 1997). It is thought that the water released during the dehydration of Smectite may result in overpressuring, as some of the interlayed water molecules are arranged in a denser packing than that of ordinary water (Bertoni and Cartwright, 2015; Osborne and Swarbrick, 1997). Smectite dehydration is likely to occur only under conditions of high effective stress. However, it is thought that the development of overpressure in low-permeability shale would actually inhibit smectite dehydration (Osborne and Swarbrick, 1997). The volume of fluid released via this process is also thought to be small (Osborne and Swarbrick, 1997). These factors cast doubt on the viability of this mechanism to generate significant overpressure and suggest that smectite dehydration is unlikely to be a primary source of overpressure.

The transformation of gypsum to anhydrite results in a loss of 39% of bound water and is considered to be an important mechanism for generating overpressure within evaporite units (Osborne and Swarbrick, 1997). This reaction ensues at 40-60°C, however, as it occurs during shallow burial it is unlikely to be responsible for

overpressure at depth (Osborne and Swarbrick, 1997). This mechanism may have some relevance within the study area for this research as it contains a thick and regionally extensive unit of evaporites at variable depth (See Chapter 3).

Diagenesis can have a significant impact on the porosity and permeability of sedimentary rocks due to the effect of cementation. In a closed system, the growth of cement in the pores of a rock can reduce the pore volume and potentially increase pore-fluid pressure (Osborne and Swarbrick, 1997). Mineral precipitation may also reduce a rock's porosity and permeability slowing the escape of overpressured fluid produced via other mechanisms and in some cases cement may produce a diagenetic seal (Tigert and Al-Shaieb, 1990). However, there is the potential for dissolution of minerals within a rock which could increase the pore volume and could result in a reduction in pore fluid pressure. For either of these processes to be effective fluid must not escape from the rock.

1.3.1.5 Hydrocarbon generation

There are two main sources of methane, which include biogenic due to the bacterial production of gas and thermogenic, due to leakage from deeper gas sources (Dia et al., 1999). At temperatures ranging from 120 – 180°C almost complete thermal cracking from oil to lighter gaseous hydrocarbons (i.e. methane) occurs (Hunt, 1979). The change from kerogen to liquid hydrocarbons, gas, residue and by products, produces a volume expansion of up to 25%, which within a closed system could result in the generation of overpressure (Meissner, 1978; Osborne and Swarbrick, 1997). In order for kerogen maturation to result in overpressuring on a basin wide scale, there must be a thick aerially extensive and mature source rock with high organic carbon content present, otherwise there will only be local spots of overpressure generation (Osborne and Swarbrick, 1997).

Methane gas can also be generated biogenically within sediments that are shallowly buried, at temperatures of <80°C or released via the melting of gas hydrates (Barker, 1987; Osborne and Swarbrick, 1997; Hunt, 1979). The migration and

accumulation of hydrocarbons may result in a localised build-up of pore fluid pressure, due to the lower density of hydrocarbons in comparison to formation waters (Cartwright and Santamarina, 2015; Osborne and Swarbrick, 1997). An increase in overpressure may, however, impede further kerogen maturation (Osborne and Swarbrick, 1997). This brings into question the potential for kerogen maturation as a valid primary source of overpressure. However, methane gas is commonly observed in association with mud volcanoes. For example, gas analysis from sediment and water samples from mud volcanoes within the Nile Deep Sea Fan have been documented to contain methane of a thermogenic origin and other hydrocarbons (Dupre et al., 2005; Huguen et al., 2009; Loncke et al., 2004; Pierre et al., 2014; Prinzhofer and Deville, 2011; Dupré et al., 2014; Charlou et al., 2003). It has been suggested by Milkov et al. (2003) that the concentration of methane in gas from mud volcanoes varies from 0% to 99% with an average of 86.2% and a median of 94.1%.

1.3.2 Liquefaction

In order for a conduit to facilitate the upwards migration of sediments, the sediments must be in a semi-liquid phase, due to the inclusion of fluids and gas (predominantly water and methane), which produces a mud slurry. A state such as this could be achieved via the process of liquefaction. Liquefaction occurs when the pore fluids temporarily sustain the entire stress exerted on the sediment and so there is no internal friction or cohesion between grains (Judd and Hovland, 2007). This can be achieved via an increase in pore fluid pressure within a succession, which results in a reduction in effective stress. When effective stress is reduced to zero, the overburden will cease to be matrix supported but will in fact be supported by the pore fluids. This can occur when the upward force of the flowing fluids equals the buoyant weight of the grains and can allow the sediments to flow like a liquid (Judd and Hovland, 2007; Lowe, 1975).

The mechanisms for generating overpressure discussed above may contribute to the increase in pore fluid pressure and reduction in effective stress that is required

for liquefaction. It is clear that in some cases seismicity (Earthquakes) can have a significant impact on pore fluid pressure as seismic waves attempt to compact a succession, which can cause a sudden increase in overpressure (Mellors et al., 2007). This sudden increase in overpressure could result in a significant reduction in effective stress to zero and result in liquefaction and potentially trigger mud volcanism (Davies et al., 2008; Mellors et al., 2007; Kopf, 2002; Deville and Guerlais, 2009). However, the eruption of a mud volcano does not have to be related to seismicity despite being linked in some cases (Deville and Guerlais, 2009). In the example of mud volcanoes observed in Trinidad by Deville and Guerlais (2009) it was found that they displayed no correlation between eruption and seismic events, therefore, suggesting that the local pressure regime is responsible for the frequency of mud volcano activity.

1.3.3 Buoyancy

A secondary driving force behind the mobilisation of sediment is the buoyancy of the fluid and sediment slurry, which is a function of the bulk density contrast (Judd and Hovland, 2007). The bulk density (p_{bulk}) is defined as the density of the whole succession which is comprised of the rock matrix and pore fluids and is represented as;

Equation 1.7

$$p_{bulk} = \frac{[M_{\text{mineral}} + M_{\text{liquid}} + M_{\text{gas}}]}{V}$$

Where *M* is the mass and *V* is the volume. A succession that is undercompacted and has retained a lot of pore fluids or within which fluids are accumulating, may have a low bulk density when compared to an overlying succession that is normally compacted (Judd and Hovland, 2007). Conditions such as these are thought to exist within a source stratigraphic succession for mud volcanism. In a case such as this, the bulk density will decrease with depth, which results in a density inversion represented as;

Equation 1.8

$$BF_{parent} = (p_{parent} - p_{os}) \times g \times h_{parent}$$

Where BF_{parent} is the buoyancy of the source stratigraphic succession, p_{parent} is the bulk density of the parent bed, p_{os} is the bulk density of the overlying succession, g is the acceleration due to gravity and h_{parent} is the vertical thickness of the source stratigraphic succession.

The bulk density contrast between a source stratigraphic succession that is undercompacted and a more dense overburden will create gravitational instability and could present an additional driving force behind the ascent of mud in combination with overpressure (Kopf, 2002; Dimitrov, 2002; Brown, 1990). The ascent of a body of muddy sediments (i.e. mud diapirs), has previously been thought to be driven upwards potentially by bulk density contrasts alone (Judd and Hovland, 2007; Brown, 1990; Kopf, 2002). In order for this mechanism to be viable, the buoyancy force exerted by the sediment must be greater than the lithostatic pressure exerted by the overlying sedimentary succession (Judd and Hovland, 2007). Once the body of muddy sediment ascends, a reduction in pore fluid pressure may allow gases to come out of solution, resulting in a decrease in density (Judd and Hovland, 2007). It is, however, thought that in the majority of cases gravitational instability alone is not sufficient for mud volcanism and large overpressuring of the parent body is required (Dimitrov, 2002). Some mud volcanoes have previously been interpreted to originate from the crest of diapirs (Guliyev et al., 1996; Brown, 1990; Dimitrov, 2002; Milkov, 2000), however, there are many examples of mud volcanoes that are not connected with diapirs (Dimitrov, 2002; Reiche et al., 2014; Roberts et al., 2010).

1.4 Seal Bypass Systems

Seal bypass systems are large scale geological structures which breach a sealing system above a reservoir allowing fluid and gas to flow through it (Cartwright, 2007). The presence of a seal bypass system can severely reduce the sealing capacity of a cap rock and their orientation can be either vertical or horizontal. They invoke cross-strata fluid migration allowing fluids to bypass impermeable lithologies and the surrounding rocks pore network. If pore pressure is sufficiently high to cause mechanical failure of an overlying seal, the resulting fractures may produce a path for fluid, gas and other

Seal Bypass System	Setting	Dimensions	Seismic expression
Faults: trap defining	Any tectonically active setting commonly seismogenic in character	Variable, but lengths commonly greater than 5 km	Systematic offsets of stratal reflections
Faults: supratraps	Faults embedded in sealing sequence, generally not lined to basement	Usually <10 km in length, <1 -2 km vertical extent	Systematic offsets of stratal reflections
Intrusion: sand	Mainly in deep-water basins; various tectonic settings; very fine-grained seals	Aperture: centimetres to meters; height: meters to 1 km; length: meters to 10 km	Discordant amplitude anomalies, localised forced folding
Intrusions: mud	Mainly in tectonically active basins, commonly with highly overpressured deeper sequences	Aperture: centimetres to meters; height: meters to 1 km; length: meters to 10 km	Cylindrical conduits with amplitude anomalies distributed adjacent to or within the conduit
Intrusion: salt	Within salt basins	Height: tens of meters to kilometres; width: tens of meters to kilometres	Geometries range from diapirs to walls to fault-controlled intrusions
Intrusion: Igneous	In volcanic margin basins and other magmatically active settings	Height: tens of meters to kilometres; width: tens of meters to kilometres	Discordant amplitude anomalies, localized forced folding, and hydrothermal pipes
Pipes: dissolution	Underlain by carbonate or evaporite sequences	Height: tens of meters to kilometres; width: tens of meters to kilometres	Cylindrical or steeply conical zones of intense disruption of stratal reflections, localized sag folding
Pipes: hydrothermal	In volcanic margin basins and other magmatically active settings; associated with magmatic intrusions into basin fill sequences	Height: tens of meters to several kilometres; width: tens of meters to 1–2 km	Cylindrical or steeply conical zones of intense disruption of stratal reflections typically developed directly above igneous intrusions and commonly linked to sea-floor mounds
Pipes: blowout	Various basin types, but commonly where there are overpressured intervals at depth	Height: tens of meters to 1–2 km; width: tens to hundreds of meters	Cylindrical or steeply conical zones of intense disruption of stratal reflections typically developed directly above localized breach points of underlying fluid source interval; linked to pockmarks; distributed amplitude anomalies are common
Pipes: seepage	Various basin types, but commonly where there are overpressured intervals at depth	Height: tens of meters to 1–2 km; width: tens to hundreds of meters	As for blowout pipes, but no link to pockmarks

Table 1.1 A summary of the various types of seal bypass system from Cartwright et al. (2007).

materials to migrate through (Cartwright et al. 2007). There are several types of seal bypass systems that can be separated into three varieties. These are: 1) fault and fracture related; 2) intrusion related and; 3) pipe related, all of which are summarised in Table 1.1 (Cartwright et al. 2007). Mud volcano conduits are discussed above in section 1.2. Other seal bypass systems that are relevant to this study are discussed below.

1.4.1 Faults and fractures

Faults and fractures are the most commonly found and efficient bypass system for the migration and flow of entrapped fluids, including hydrocarbons (Cartwright et al., 2007; Aydin, 2000; Løseth et al., 2009). The damage zones of some faults are more permeable than their host sequences and can be major flow routes irrespective of their specific history of rupture and displacement. It is in these cases that faults may act as cross strata migration routes on a semi-permanent basis. They are most likely to act as valves for fluids during active rupture events. However, many fault zone rocks are characterised by lower permeability than their hosting succession (Cartwright et al., 2007; Knipe, 1997). Evidence from ore deposits, however, make it hard to dispute that faults act as fluid flow pathways (Cartwright et al., 2007). Clustering of small gas related amplitude anomalies in seismic data that are stacked vertically in footwall or hanging wall traps along single faults may also suggest fluid flow along the fault plane (Heggland, 1997) (Figure 1.8).

Faults commonly have lengths >5 km and can cross thick sealing sequences (Figure 1.8). They, therefore, have the potential to act as conduits for long range vertical fluid transmission (Hooper, 1991) (Figure 1.8). If a reservoir were to come into contact with an active fault, that fault could be exploited as a preferential pathway for large amounts of fluid migration. On some occasions pockmark craters can be found above the upper tips of faults planes as an indication of leakage. Although less directly observed, mud mounds or mud diapirs are thought to form above fault planes, which has previously been suggested as evidence that fault planes could be exploited by

significant fluid and sediment flux (Berryhill et al., 1987; Cartwright et al., 2007; Loncke et al., 2004; Davies et al., 2011; Mazzini et al., 2009) (Figure 1.9).

Aydin (2000) states that a fracture is a structure defined by two surfaces or a zone across which a displacement discontinuity occurs. Hydraulic fractures are thought to form in high fluid pressure environments resulting in vertical fracture dikes, horizontal fracture sills or a combination of the two creating a fracture network (Hubbert and Willis, 1972; Secor, 1969). The fracture orientation is dictated by a combination of the state of stress and abnormal fluid pressure, which initiates fracturing (Mandl and Harkness, 1987). Once initiated, hydraulic fractures are capable of cutting through impermeable cap rock as much as a few kilometres vertically and tens of kilometres horizontally (Mandl and Harkness, 1987; Davies et al., 2012; Fisher and Warpinski, 2011). Fracture dikes and sills may act as conduits for hydrocarbon migration flow (Cartwright and Santamarina, 2015; Aydin, 2000; Cartwright et al., 2007). Hydrocarbon entrapment could ensue should fractures not fully bypass an impermeable lithology. Fracture flow presents a potential leakage mechanism found above small parts of a trap and can have a high flow rate, which can drain a hydrocarbon filled trap over a small amount of geological time (Roberts and Nunn, 1995).

Fractures are far too small to be imaged on 3D seismic data, despite being able to bypass thick sealing lithologies. However, in the event that the fracture is a leaky fracture, it may produce a line of seismic anomalies such as reflection discontinuities that are observable in seismic profile and reveal the fracture to be a conduit (Løseth et al., 2009). Despite the challenges of observing hydraulic fractures using seismic data, their relationship with the formation of mud volcanoes is supported by the observation of fracture networks associated with mud volcano conduits (Roberts et al., 2010; Morley, 2003; Morley et al., 1998). It is thought that the seal bypass systems of fluid escape pipes, mud volcano conduits and sand injections may all share a common first phase in their formation, which involves high fluid overpressure opening a hydraulic fracture through low permeability sediments (Arntsen et al., 2007; Cartwright et al., 2007; Løseth et al., 2009; Løseth et al., 2011; Cartwright and Santamarina, 2015).

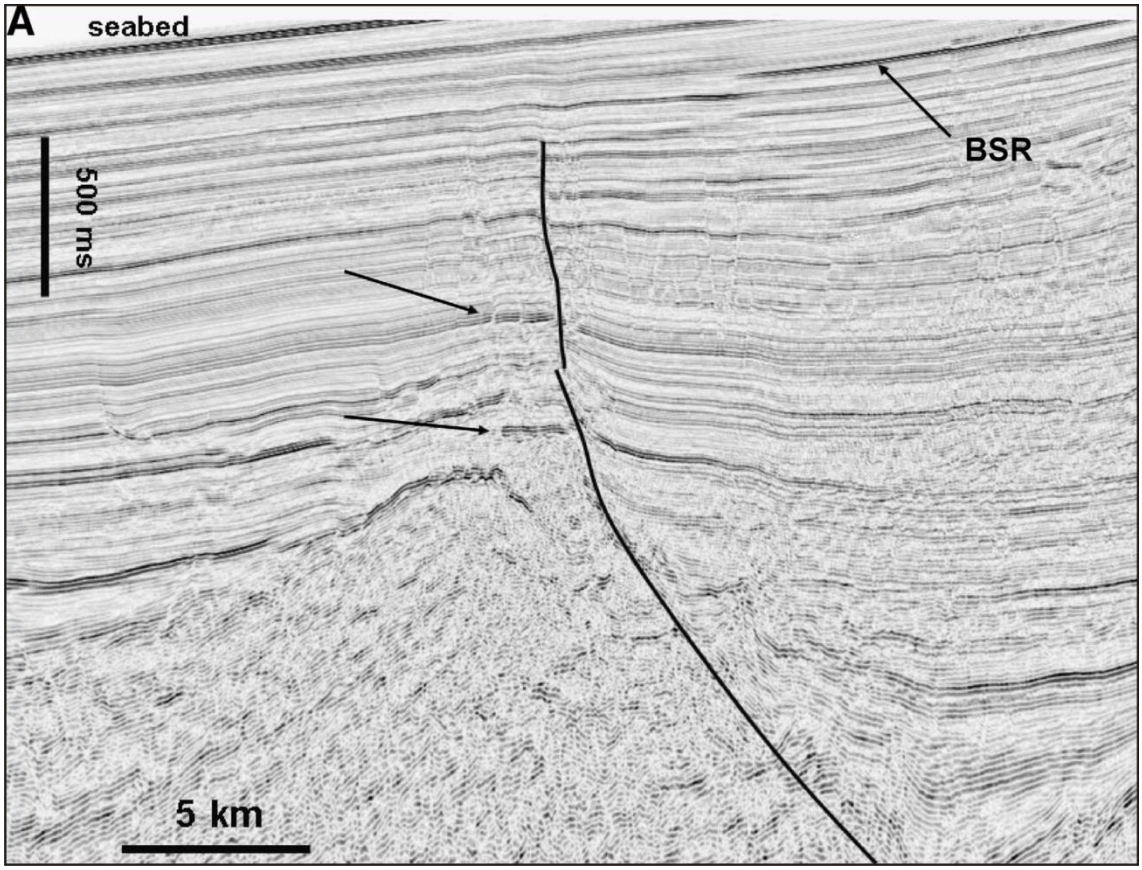

Figure 1.8 A seismic profile that illustrates hydrocarbon leakage associated with faults. Leakage from the crestal region of a large tilted fault block is expressed as vertically distributed amplitude anomalies (pointed to by arrows) in the footwall to this major trap-defining fault. A bottom simulating reflection (BSR) associated with local development of gas hydrates can be seen near the top of the profile (From Cartwright et al. (2007)).

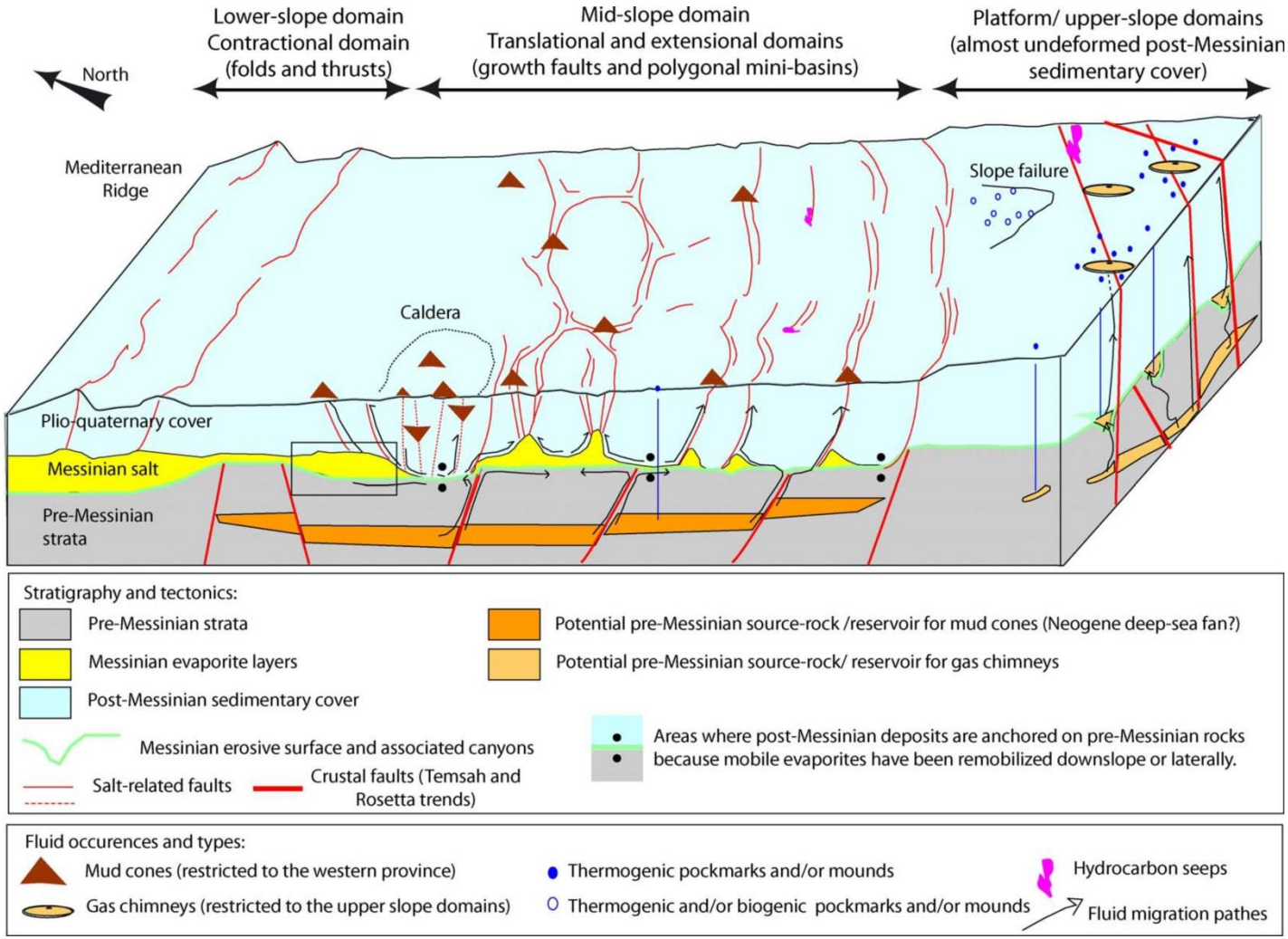

Figure 1.9 A block diagram summarizing the most common settings of fluid escape in the NDSF. It has been interpreted that fluids have migrated along deep crustal faults and fluid and mud have migrated along thin skinned faults, which are salt-related and result in the formation of mud volcanoes above the fault plane (From Loncke et al. (2004)).

1.4.2 Fluid escape pipes

Fluid escape pipes are defined as vertical to sub-vertical pathways of focused fluid venting from an underlying source region (Cartwright and Santamarina, 2015; Hustoft et al., 2007; Moss and Cartwright, 2010a) (Figure 1.10). Fluid escape pipes are widely considered to form via the catastrophic breaching of top seals to shallow gas reservoirs in a highly dynamic process involving the formation of hydraulic fractures, under elevated pore fluid pressure (Løseth et al., 2001; Berndt et al., 2003; Hustoft et al., 2007; Judd and Hovland, 2007; Ligtenberg, 2005; Cartwright et al., 2007; Løseth et al., 2009). They tend to be localised at natural leak-off points for overpressured pore fluids, for example the crest of structures, above gas reservoirs or at the updip limits of aquifers (Cartwright et al., 2007). An alternative suggestion to the formation of some fluid escape pipes involves subsurface volume loss via a mechanism such as the dissolution of either carbonate or evaporites, which results in a pipe-shaped collapse geometry (Bertoni and Cartwright, 2005; Cartwright et al., 2007; Cartwright and Santamarina, 2015; Sun et al., 2013).

Fluid escape pipes are characterised by zones of seismic disruption, attenuation, and localised enhanced amplitude on 3D seismic data, that are aligned in vertical to sub-vertical columnar structures, with a circular to elliptical form (Hustoft et al., 2007; Moss and Cartwright, 2010a; Løseth et al., 2001) (Figure 1.10). It has been suggested that in many cases, the columnar disturbance zones that characterises fluid escape pipes are formed by the propagation of hydraulic fractures, which facilitates the ascent of fluids (Løseth et al., 2001). Within a pipe that is comprised of a vertical zone of hydraulic fractures, dilated fractures would greatly increase the bulk permeability from the low background values of low permeability stratigraphy (i.e. mud dominated sediments), therefore, allowing fluids to bypass the pore network (Berndt, 2005; Cartwright et al., 2007).

The tallest fluid escape pipes identified thus far are close to 2000 m in vertical extent (Moss and Cartwright, 2010a; Moss and Cartwright, 2010b) while pipes of >1000 m are relatively common (Løseth et al., 2001). The large vertical extent of fluid

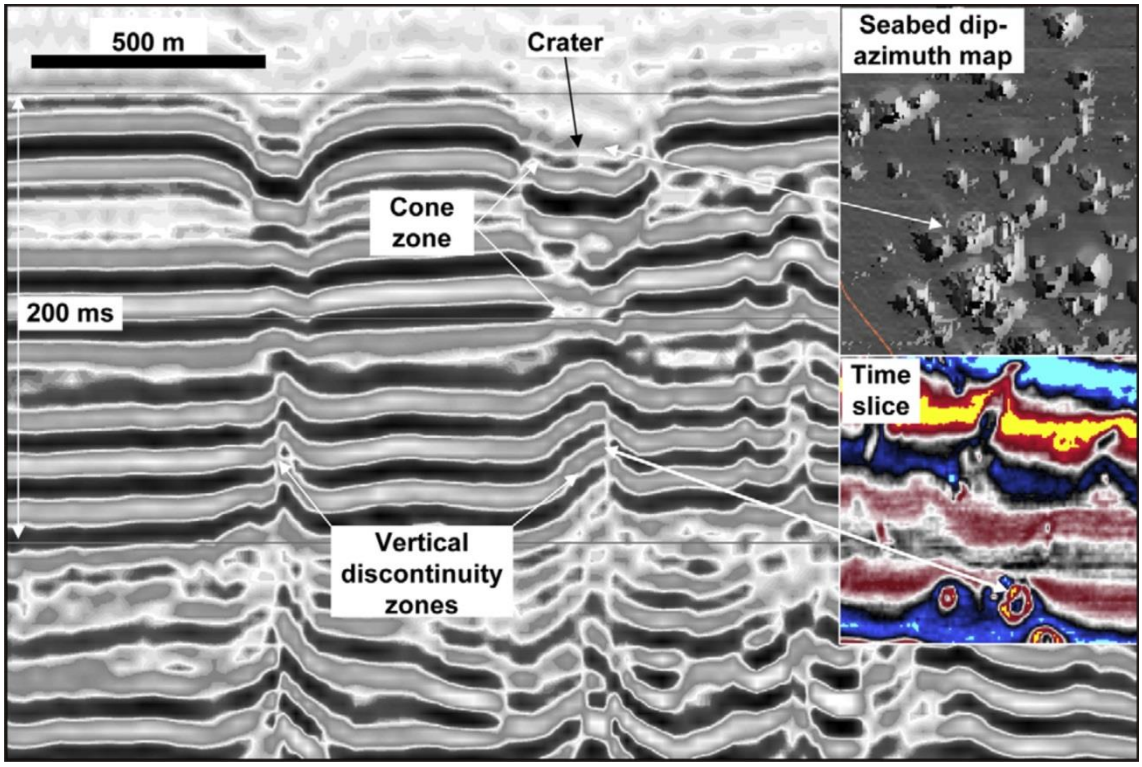

Figure 1.10 An example of fluid escape pipes and seabed craters in seismic profile, dip-azimuth map and time slice. The seismic profile displays a depression at the seafloor that defined the craters and underlying vertical zones of discontinuity that are typical of fluid escape pipes. The dip-azimuth map is of the seabed showing the craters appear to form in clusters. The time slice shows that the pipes leading up to the craters are circular to elliptical (From Løseth et al. (2009))

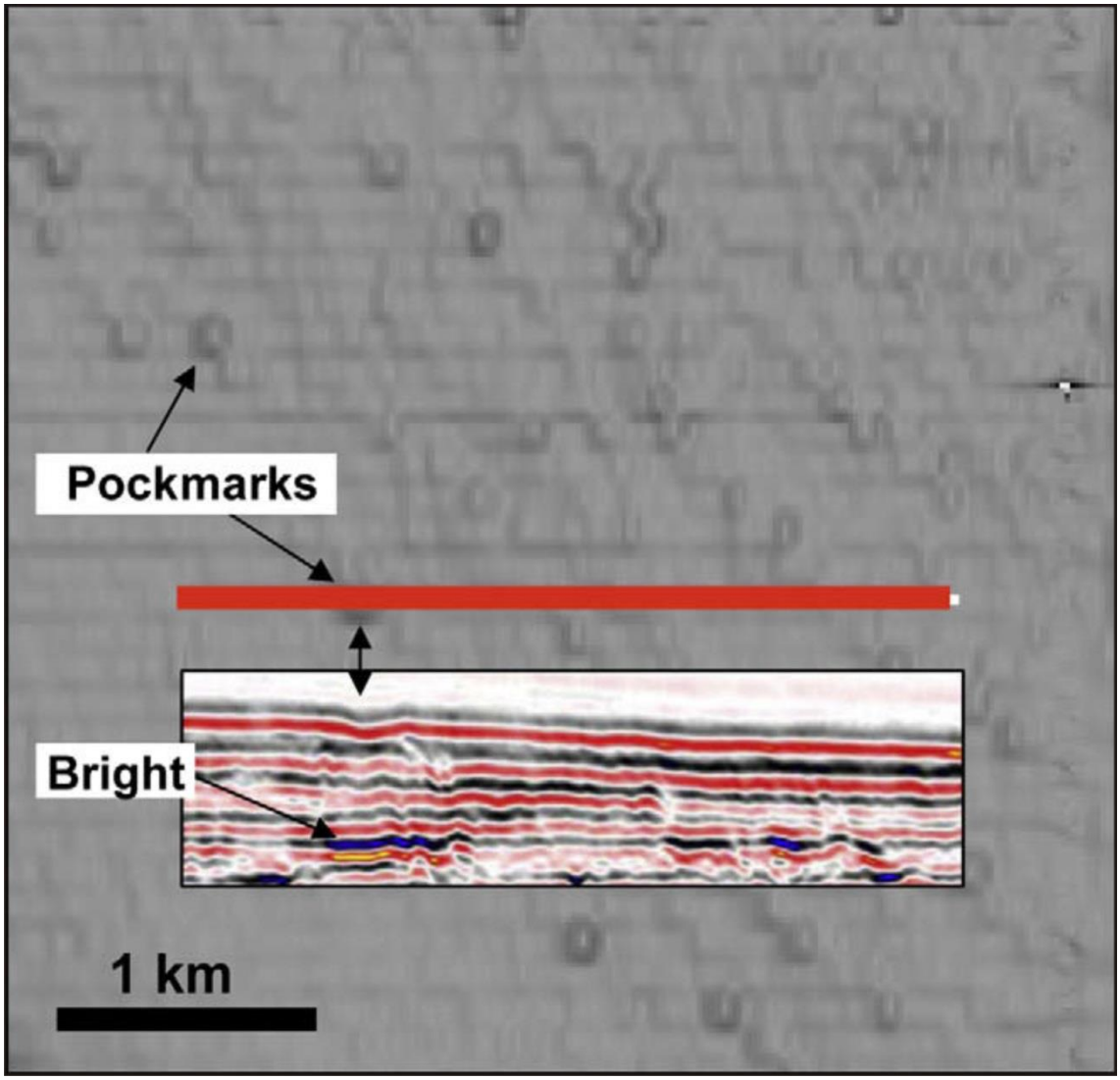

Figure 1.11 A seafloor map that displays numerous circular depressions that have been interpreted as pockmarks. These pockmarks are clearly displayed in seismic profile. High amplitude anomalies beneath the pockmark are observable in seismic profile and have been interpreted as a shallow gas accumulation that is feeding the pockmark with gas (From Løseth et al. (2009)).

escape pipes means they pose an important component of vertical fluid flow in sedimentary basins (Berndt, 2005; Cartwright, 2007). They rarely occur in isolation, but more typically in clusters (Løseth et al., 2001; Van Rensbergen et al., 2007; Gay et al., 2007; Davies and Clarke, 2010; Hustoft et al., 2010; Moss and Cartwright, 2010b). They are also commonly observed in alignments that are either linear and follow faults, structural or topographic highs, buried scarps or pinch outs (Løseth et al., 2001; Hustoft et al., 2010; Moss and Cartwright, 2010a; Moss and Cartwright, 2010b), or curvilinear following the shape of underlying channel sand bodies (Davies, 2003; Gay et al., 2007; Gay et al., 2006).

Fluid escape pipes can frequently be distinguished on the basis of their association with surface or paleo pockmarks, craters or mud mounds (Berndt, 2005; Hovland and Judd, 1988; Cartwright et al., 2007; Løseth et al., 2009; Løseth et al., 2001) (Figure 1.10 and Figure 1.11). Fluid escape pipes are commonly associated with methane migration and so represent an important component of the secondary migration of methane and indeed oil to oceans and atmosphere (Cartwright et al., 2007; Huuse et al., 2010; Cathles et al., 2010). Fluids that escape from focused fluid flow related features at the seafloor, such as pockmarks and mud volcanoes, may affect climate change (Berndt, 2005; Svensen et al., 2004) and aid in the prediction of hydrocarbon migration patterns in the subsurface (MacDonald et al., 2002).

Pockmarks were first discovered in the Northern North Sea in the 1970's (Hovland and Judd, 1988; King and MacLEAN, 1970). They are shallow seabed depressions of a few to tens of metres deep and typically several tens of meters in diameter (Figure 1.11). Their shape can be circular, elliptical or composite as a result of individual pockmarks merging together (Figure 1.11). Generally they are formed in soft, fine grained seabed sediments due to the escape of fluid and gas into the water column (Hovland and Judd, 1988; Løseth et al., 2009).

Craters can also be observed in association with fluid escape pipes, much like pockmarks. However their size is of several hundreds of metres in diameter and several tens of metres deep. On occasions they occur in clusters or elongated above underlying faults, just as pockmarks do (Figure 1.10). It is interpreted that they are

structures formed from violent and episodic gas blowouts and leaking hydrocarbons (Løseth et al., 2001; Løseth et al., 2011). Over time the depressions of pockmarks and craters can be infilled with sediment which can be seen using 3D seismic data (Heggland, 1998; Løseth et al., 2009).

It has previously been suggested that fluid escape pipes may represent an early stage of the evolutionary sequence that could ultimately lead to the development of conduits for mud volcanoes, because the theoretical conditions for formation are similar in both cases (Cartwright et al., 2007; Karakin et al., 2001; Cartwright and Santamarina, 2015). The potential link to mud volcano conduits is evident from the similarities of scale and seismic expression of some fluid escape pipes and mud volcano conduits. It is possible that the different outcomes could be controlled by differences in the source layer of fluids, with regards to whether there is sufficient flux of gas-saturated mud to reach the surface and build a constructional mud volcano (Cartwright et al., 2007; Cartwright and Santamarina, 2015). If a pipe terminates at a mound that is comprised of extruded sediment, then there is a strong case for the pipe feeding the mound representing a conduit for the primary stage for development of a sedimentary volcano (Cartwright, 2007; Huuse et al., 2010). It has also been suggested that the consistently convex deformation of pipe interiors may suggest a collapse of the pipe interior, perhaps analogous to caldera collapse observed in mud volcano conduits (Deville et al., 2003; Evans et al., 2008).

1.5 Direct Hydrocarbon Indicators (DHIs)

Direct hydrocarbon indicators (DHIs) is a term used to define the specific responses that are observed in seismic data, which are directly indicative of the presence of hydrocarbons (Barry and Shugart, 1974; Brown et al., 2004; Millahn et al., 1979). The formation of mud volcanoes and fluid escape pipes is thought to often be intimately related with the presence of hydrocarbons (Pierre et al., 2014; Dupré et al., 2014; Huguen et al., 2009; Milkov, 2000; MacDonald et al., 2000; Berndt, 2005; Kopf and Behrmann, 2000; Charlou et al., 2003; Cartwright et al., 2007; Huuse et al., 2010).

An understanding of the DHIs that may be observed in 3D seismic data in association with these fluid flow features is, therefore, important.

Variations in acoustic impedance are directly reflected in amplitude (See 2.2.1 and 2.2.3 of Chapter 2) and so a contrast in acoustic impedance results in a high amplitude reflection (Brown et al., 2004; Hart, 1999). An acoustic impedance contrast and increase in amplitude can occur when hydrocarbons are present, so in some cases, high amplitudes can in fact be indicators for the presence of hydrocarbons (Bacon et al., 2007; Løseth et al., 2009). Amplitude anomalies are, however, poor indicators of gas saturation. Even small CO_2 saturations produce a significant drop in P-wave velocity. The implications of this are that even a low gas saturated reservoir will display similar seismic amplitude to that of a high gas saturated reservoir of economic value (Bacon et al., 2007). Any amplitude anomalies identified at a target level seen to correlate with overlying or underlying changes should be treated as suspicious.

A DHI in seismic data can be displayed as a number of seismic anomalies that could be indicative of the presence of hydrocarbons. Identifying their presence is particularly important within the hydrocarbon industry to reduce the risk of drilling into hazardous shallow gas during hydrocarbon exploration and as a pointer for migration pathways and/or deeper hydrocarbon reserves. Typical examples include amplitude anomalies found on the top reservoir reflector showing conformance to the structure. Another example is a flat spot, which is a horizontal reflector due to a gas-oil or oil-water contact that cross cuts the bedding-plane reflectors.

The most common type of leakage related anomaly is any lateral variation along a reflection such as increases or decreases in amplitude, continuity, frequency and AVO (amplitude versus offset). These anomalies are often found in groups or clusters forming patterns, textures and shapes. Using 3D seismic data it is possible to map 3D shapes and the spatial distribution of leakage related seismic anomalies (Løseth et al., 2009). Various amplitude anomalies and patterns that could be considered DHIs are summarised in Table 1.2. Several different DHIs that could potentially be identifiable in 3D seismic data in association with mud volcanoes and mud volcano conduits are described below.

Amplitude anomaly	Definition
Bright spots or high amplitude anomaly	Local increase in positive or negative amplitude along a reflection from any reason.
Amplitude blanking and dip spots	Local decrease in positive or negative amplitude along a reflection or in a zone for any reason.
V-shaped bright	High amplitude V-shaped reflection in seismic profile that is discordant to the reflections from depositional surfaces. Seldom more than 2-3 km wide.
Flat spot	Relatively flat seismic reflection with an angle to the stratigraphic reflections.
Phase reversal	Phase shift of 180° along a continuous reflection, so that a peal becomes a trough and vice versa.
AVO	Amplitude variation with offset.
Reduced continuity	Local reduction of continuity of seismic reflections in contrast with adjacent areas.
Increased continuity	Local increase of continuity of seismic reflections.
Reduced frequency	Local decrease in frequency
Bottom simulating reflectors (BSR)	High amplitude reflection that is often parallel to the seabed and associated with gas hydrates.
Mounds	Positive structure of any shape rising above the regional datum of a reflection. The reflection pattern below the mound can be of any type.
Push down	Apparent down-bending produced by a local, shallower low-velocity region
Pull up	Apparent uplift produced by a local, shallower high-velocity region.

Table 1.2 A table of descriptions of amplitude anomaly and anomalous pattern terms from analysis of seismic data. An amplitude anomaly is defined as a local increase or decrease of seismic reflection amplitude (Modified from Løseth et al. (2009)).

1.5.1.1 Amplitude blanking/Dim spot

Amplitude blanking (also known as 'acoustic voids', 'acoustic transparency', 'blank zones', 'wipe-outs', 'white zones', 'dim spot' and 'dim zone') is defined as a localised reduction in seismic amplitude and reflection continuity relative to adjacent areas, as a result of a reduction of acoustic impedance between layers (Judd and Hovland, 2007; Løseth et al., 2009) (Figure 1.12). One possible reason for the formation of areas of amplitude blanking is that the energy is attenuated (absorbed and scattered) by gas bubbles, which results in chaotic reflections. This acoustic transparency is often observed close to the seabed and is generally vertical in orientation and sometimes displayed as a thin and vertical 'columnar disturbance' (Judd and Hovland, 2007) (Figure 1.13). Examples of this can be seen in plumes, fault zones and fluid escape pipes (Figure 1.13). The presence of fluid escape features such as fluid escape pipes, pockmarks, intra sedimentary domes and mud volcanoes could in some cases be considered to be an indirect indicator of hydrocarbons (Cartwright et al., 2007; Hovland and Judd, 1988; Judd and Hovland, 2007). The margins of the acoustic turbidity are referred to as the 'gas front'. Acoustic turbidity is most common in soft, fine grained sediments but it is important to be aware that similar effects can be caused by other lithologies such as gravel beds (Hovland and Judd, 1988).

1.5.1.2 Enhanced Reflections (gas brightening)

Enhanced reflections are identifiable in 3D seismic data as coherent reflections that display significantly higher amplitude over a portion of their length (Judd and Hovland, 2007). It has previously been interpreted that these high amplitudes are caused by minor accumulations of gas, likely within thin, moderately porous sediment layers (Judd and Hovland, 2007). The presence of gas produces a large negative impedance contrast, which results in large-amplitude and phase-reversal reflections, which are the shallow equivalent of bright spots (Hovland and Judd, 1988) (Figure 1.12).

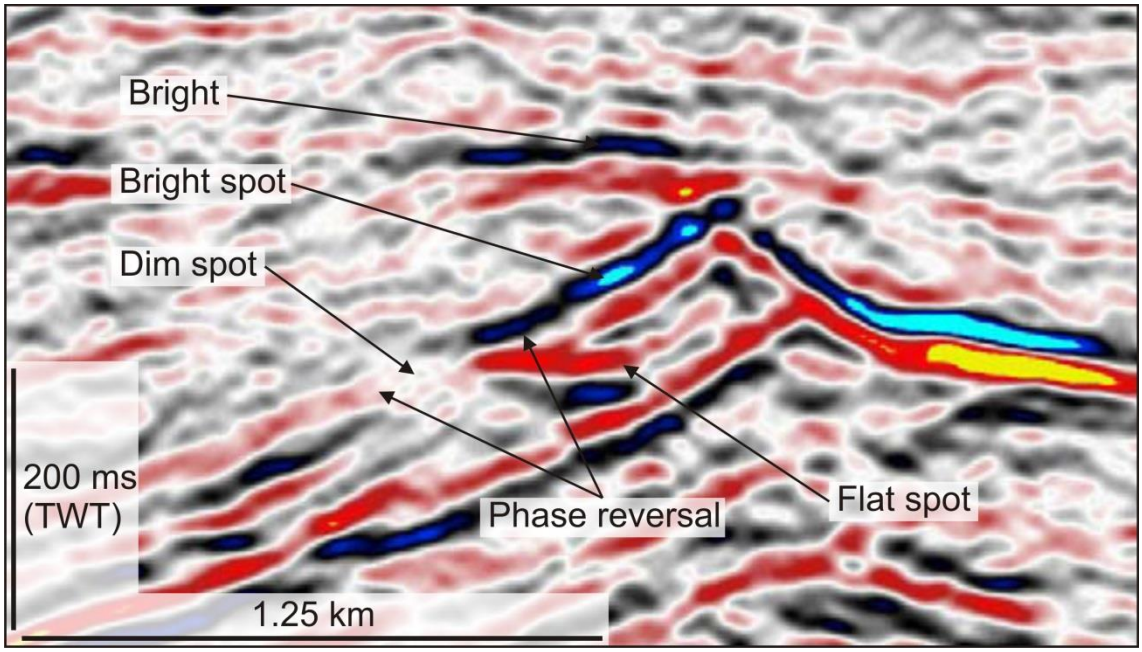

Figure 1.12 A seismic profile that displays a bright spot, dim spot and flat spot, all of which are indicative of the presence of hydrocarbons. An increase in amplitude and continuity in the cap rock above the reservoir further confirms this (Modified from Løseth et al. (2009))

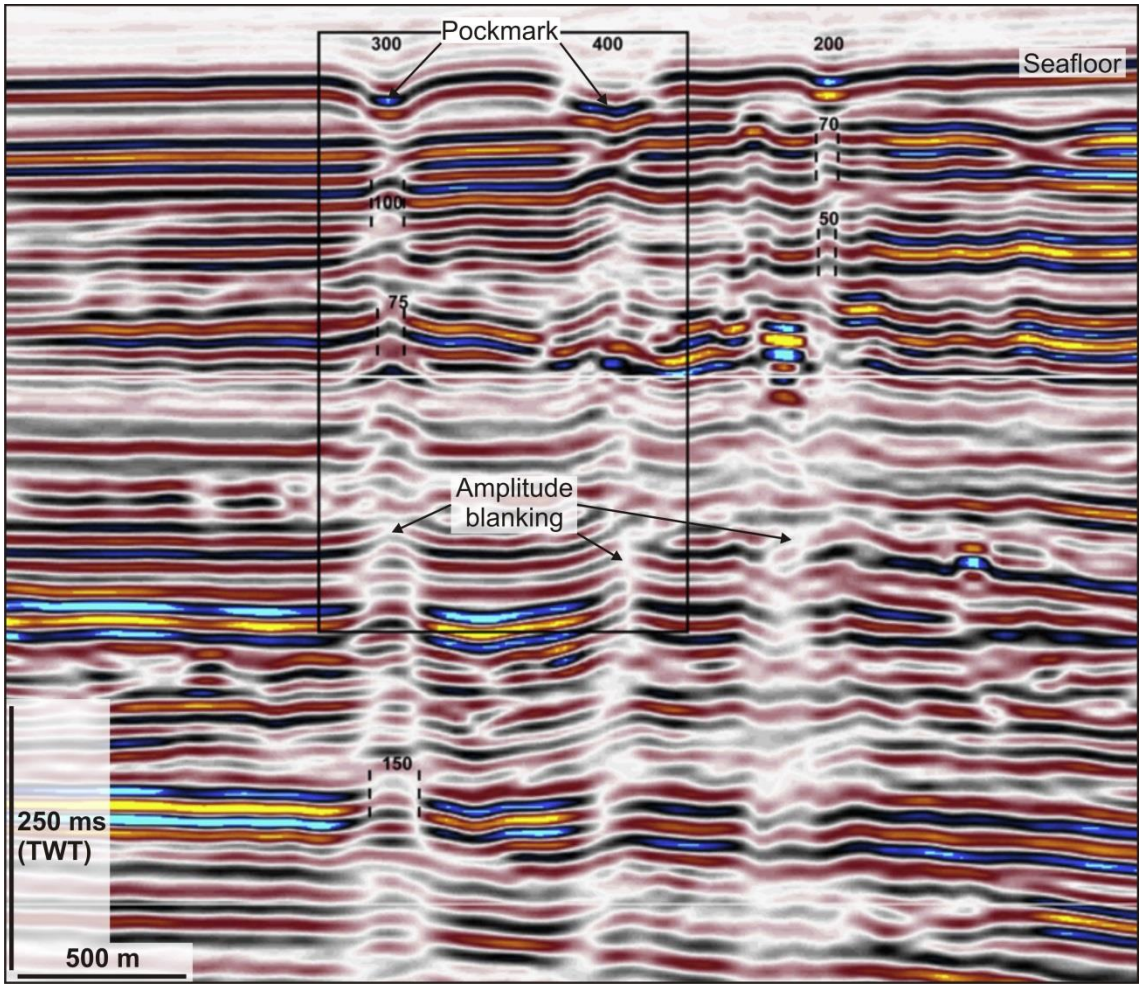

Figure 1.13 A seismic profile that displays pockmarks at the seafloor with underlying zones of amplitude blanking that are thin and vertical and columnar in shape (Modified from Løseth et al. (2011)).

1.5.1.3 Pull-up and push-down

Push-down is identifiable on coherent reflections and thought to often occur below units of gas bearing sediments. If the gas bearing zone is thick enough it will produce the illusion that the sediments are sagging when in actual fact what is displayed is a seismic artefact. This effect is produced by a reduction in acoustic velocity through gas in the overlying sediment and results in an increase in two-way travel time of the p-waves, despite the sediments being horizontal (Hovland and Judd, 1988). Pull-up is also a seismic artefact that is the result of the opposite effect to that described above, where p-waves travel through a high velocity zone, which results in a decrease in two-way travel time (Judd and Hovland, 2007).

1.5.1.4 Bright Spots

Bright spots are displayed as discontinuous and high amplitude, negative phase sections of a reflection that is observable in 3D seismic data (Figure 1.12) (Judd and Hovland, 2007). They are amplitude anomalies that are caused by a strong decrease in acoustic impedance at the top of a reservoir charged with hydrocarbons (Figure 1.12) (Schroot and Schüttenhelm, 2003). Gas charged sediments result in a reduction in acoustic velocities, which contrast with overlying water saturated sediments of faster acoustic velocities. This strong acoustic impedance contrast, therefore, produces a high amplitude reflection which is easily identified on 3D seismic data (Judd and Hovland, 2007). Bright spots are often observed in association with fluid escape features such as fluid escape pipe and their effect diminishes with depth and is stronger with gas than oil (Hovland and Judd, 1988; Schroot and Schüttenhelm, 2003; Løseth et al., 2009).

1.5.1.5 Flat spots

A flat spot is a coherent reflection that occurs at the gas-water interface in a hydrocarbon reservoir (Schroot and Schüttenhelm, 2003; Judd and Hovland, 2007; Brown et al., 2004). Gas or oil filled and water filled sediments form a contrast in acoustic impedance, resulting in a distinct acoustic anomaly, which is often orientated horizontally unless the overlying gas produces a 'pull-down' effect. If the reservoir and hydrocarbon column is of a sufficient thickness, the base of the gas or oil phase will display a positive impedance contrast in seismic profile. The height of the gas column can be estimated based on the distance between the flat spot at the base of the gas accumulation and an associated overlying bright spot at the top (Hovland and Judd, 1988).

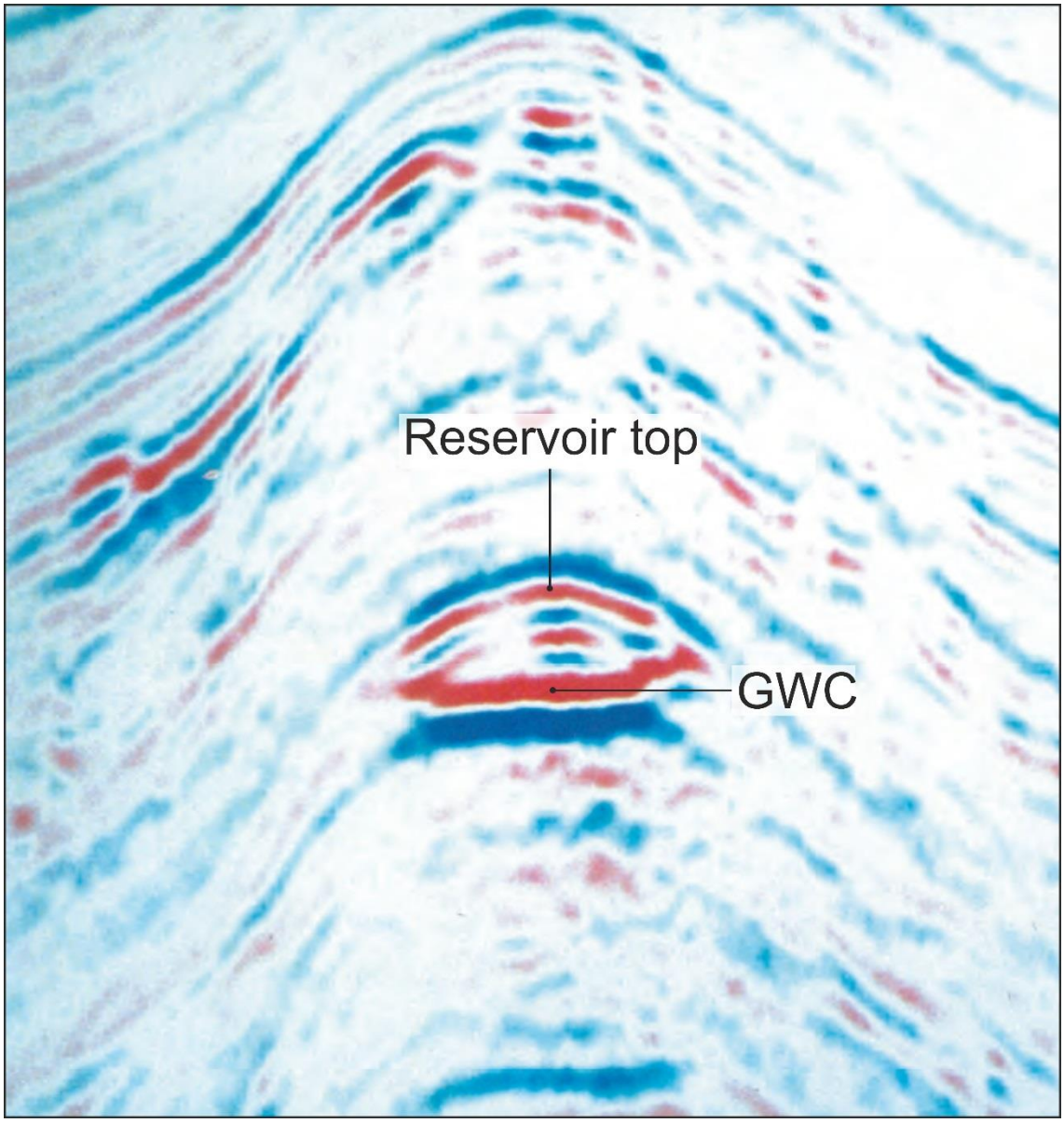

Figure 1.14 A classic example of a flat spot from the Gulf of Mexico. A flat and positive reflection (red) defines the gas water contact (GWC). The bright spot directly above defines the top of the reservoir (Modified from Brown et al. (2004)).

1.6 Project aims

In recent years there has been a significant increase of studies that involve the analysis of a variety of subject matter associated with mud volcanoes in a variety of settings (Calves et al., 2010; Davies et al., 2007; Deville and Guerlais, 2009; Deville et al., 2010; Dimitrov, 2002; Dupré et al., 2014; Etiope et al., 2002; MacDonald et al., 2000; Roberts et al., 2010; Rudolph et al., 2011; Davies and Stewart, 2005). Very few studies, however, have focused on the volumetric and distributional analysis of mud volcanoes. Few 3D seismic studies have provided a detailed description of mud volcano conduits or had the opportunity to discuss how a mud volcano conduit, such as those within this study, have been able to bypass a thick succession of sealing evaporites. With regards to the Eastern Mediterranean and fluid flow associated with the Messinian Salinity Crisis, there are numerous documented examples of fluid flow associated with overpressure release during the early stages of the Messinian Salinity Crisis (Bertoni and Cartwright, 2015; Bertoni et al., 2013; Frey-Martnez et al., 2007; Lazar et al., 2012). However, despite being implied by Bertoni and Cartwright (2015), there has until now been very little evidence for overpressure and fluid release in association with the later stages of the Messinian Salinity Crisis such as its climax (Lazar et al., 2012).

The specific project aims are noted below:

1. Describe the seismic expression and geometry of the mud volcanoes within this study area using 3D seismic data.
    - Describe a previously undiscovered suite of giant mud volcanoes, which display an irregular geometry (Chapter 4)
    - Described the seismic characteristics and geometry of a large number of mud volcanoes found throughout the Pliocene to Recent Succession of the study area (Chapter 5).
2. Examine the spatial distribution of mud volcanoes and fluid escape pipes and understand the controls on their locations.
    - Analyse the controls on the location of a suite of giant mud volcanoes (Chapter 4).

- Analyse the spatial distribution of numerous small and conical mud volcanoes and investigate the mechanisms that control their location (Chapter 5).
- Analyse the spatial distribution of fluid escape pipes in relation to mud volcanoes and the numerous top and base-salt depressions within the study area (Chapter 6).
- Discuss the reasons for the extensive mud volcanism within the region of the Eastern Mediterranean where this data is located (Chapter 7).

3. Identify the source stratigraphic layer for fluid and mud within this study area.
    - Discuss the observable evidence for the source of mud feeding the giant mud volcanoes in combination with viable mechanisms for mud volcanism (Chapter 4).
    - Analyse the evidence for a source stratigraphic succession based on depletion and volumetric analysis (Chapter 5).
    - Analyse numerous mud volcano conduits and fluid escape pipes in order to ascertain their root zone and the stratigraphic successions they transect (Chapter 6).
4. Analyse a large number of mud volcano conduits and fluid escape pipes.
    - Discuss evidence for a connection between the giant mud volcanoes and the source stratigraphic succession (Chapter 4).
    - Describe the seismic expression and geometry of the mud volcano conduits and fluid escape pipes and discuss the potential mechanisms driving their formation based on these observations (Chapter 6).
5. Discuss the impact that mud volcanism and fluid escape has had on the mobile Messinian evaporites succession.
    - Analyse the impact that localised gravitational loading of evaporites by mud volcanoes has had on the mobile succession (Chapter 4 and Chapter 5).
    - Analyse the impact that the ascent of fluids and mud have had on dissolution of the evaporites and the formation of conduits through salt (Chapter 4 and Chapter 5 and Chapter 6).

6. Propose a model for the mobilisation and depletion of the source stratigraphic succession.
    - Discuss the way in which the area of the source stratigraphic succession that is depleted during mud volcanism becomes liquefied and is mobilised (Chapter 7).

1.7 Thesis outline

This chapter (Chapter 1) has presented an introduction and overview of the main research topics that are discussed in this thesis. The seismic interpretation method and methods of spatial and statistical analysis that are used within the results of this thesis are presented in Chapter 2. The geological setting of the Eastern Mediterranean with particular focus on the western province is presented in Chapter 3. The descriptions, analysis and discussion presented in Chapter 4, Chapter 5 and Chapter 6 comprise the main results chapters for this thesis. Chapter 4 is focused on the analysis of a suite of giant mud volcanoes identified directly on top of the Messinian evaporite succession. Within Chapter 5 a large number of small and conical mud volcanoes are described. The examination of these mud volcanoes includes the analysis of their distribution, dimensions, volumetrics and association with localised depressions within sedimentary successions. Chapter 6 involves the analysis of mud volcano conduits and fluid escape pipes. The mechanisms behind their formation and the bypassing of a 'sealing' evaporite succession will also be discussed. Chapter 7 will summarise the findings from the previous chapters and address unanswered questions about the depletion zone and process of remobilisation for these mud volcanoes. Discussion points will be drawn from the previous chapters to address the wider implications regarding mud volcanism within this study area and other regions. The main conclusions are listed in Chapter 8 and the appendix (on CD) contains spreadsheets of data collected from all the mud volcanoes and fluid escape pipes, and images of them all can also be found.

Chapter 2

2 Data and methodology

2.1 Introduction

The results presented in this thesis are based on the interpretation of three-dimensional (3D) seismic data and quantitative analysis of numerous key geological features and successions that are of interest here. The dataset and methodologies used in this thesis are similar to those that might be used within oil companies during the exploration of hydrocarbons. The aims of this chapter are to 1) outline the datasets used in this thesis; 2) Provide an synopsis of the seismic method; 3) describe the parameters of the seismic survey; 4) briefly explain the various methods of interpretation, analysis and seismic attributes; 5) describe the volumetric and Geographical Information System techniques and spatial statistics used throughout this thesis; 6) discuss the limitations of the seismic survey.

2.2 Seismic data

The dawn of 3D seismic technology has allowed the seismic interpreter to map and view subsurface horizons, structures and features at a higher level of detail and quality than was previously possible. This has led to many fascinating results and helped advance the research of subsurface geology (Cartwright and Huuse, 2005). A 3D seismic data set can provide detailed information of the subsurface often to a resolution of only a few tens of meters (Cartwright and Huuse, 2005). A single exploration 3D cube supplied by Statoil has been used to conduct this research. The data includes pre-stacked time migrated and pre-stack depth migrated seismic and velocity data.

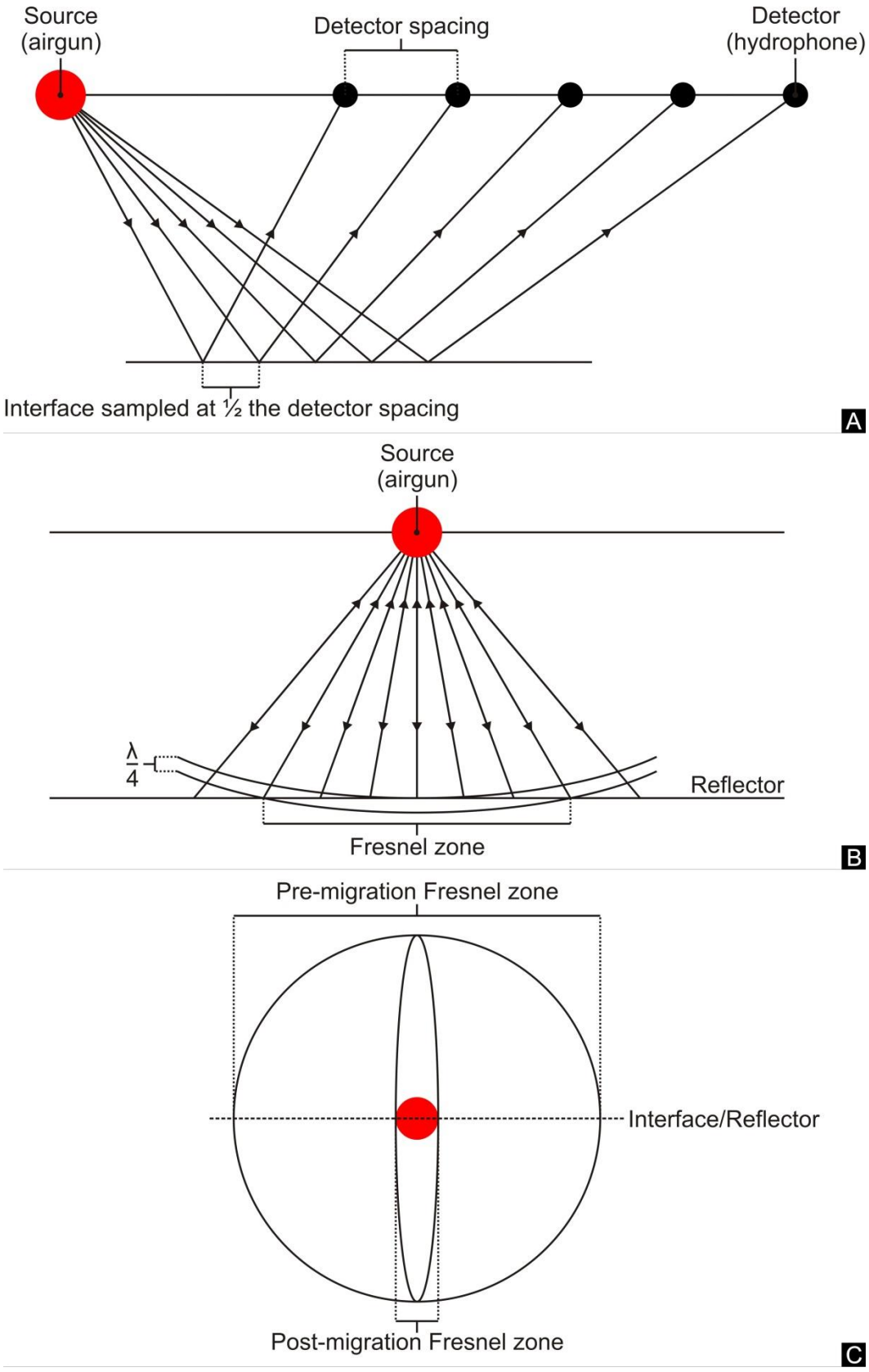

Figure 2.1 Horizontal resolution and defining the Fresnel zone. A: The horizontal resolution of a seismic survey is governed in part by the horizontal sampling, which is half the detector spacing. B: Energy emitted from the seismic pulse is returned to the source from all points of a reflector. The region of the reflector from which energy is returned within half a wavelength of the initial reflection arrival is referred to as the Fresnel zone. C: The width of the Fresnel zone controls the resolution and 3D migration reduces the size of the Fresnel zone (Adapted from Brown et al. (2004).

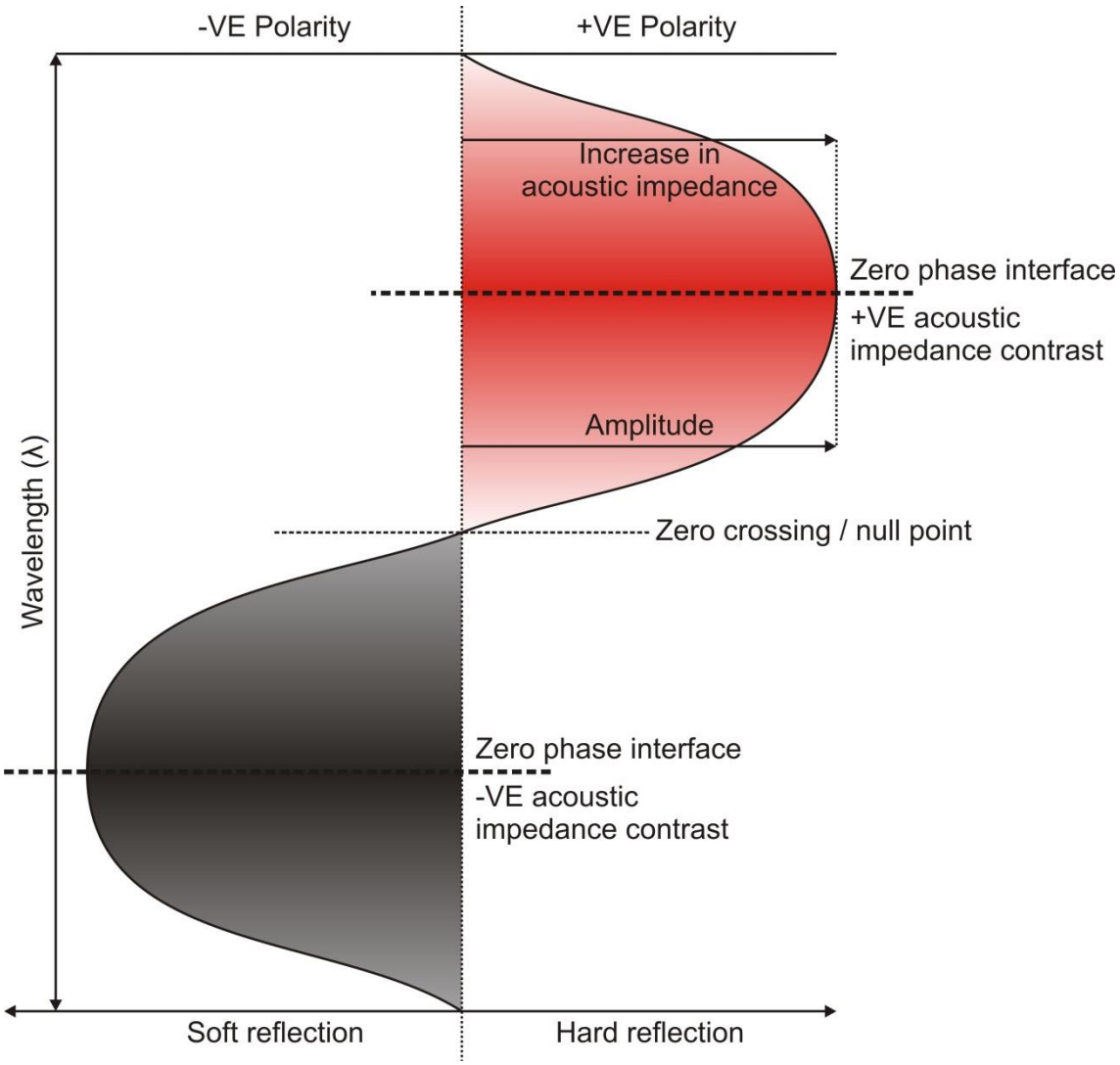

Figure 2.2 Schematic of a seismic wave, illustrating the conventions of polarity and phase used in this research. (Adapted from Hart (1999))

2.2.1 3D seismic data acquisition

In offshore 3D seismic acquisition, an acoustic pulse is generated by an airgun towed by a survey vessel. This acoustic pulse generates compressional waves (p-waves) that travel down through the water column and through the subsurface (Figure 2.1). These p-waves are reflected off geological boundaries back towards the surface. These boundaries are formed by subsurface impedance contrasts due to changes in physical properties (Hart, 1999; Bacon et al., 2007). At the surface the p-waves are received by an array of hydrophones (detectors) towed further behind the survey vessel that record the amplitude and two-way-travel time (TWT) for the p-wave to and from an acoustic impedance contrast (Figure 2.1) (Hart, 1999; Bacon et al., 2007). P-wave velocity through rock varies according to numerous factors including composition, porosity, fluid content, elastic modulus and density (Rider, 1986).

The seismic data in this thesis is displayed in zero phase SEG (Society of Exploration Geophysicists) normal polarity; therefore, an increase in acoustic impedance corresponds with a peak in the seismic wavelet, which is symmetrical with the peak corresponding to the zone of maximum energy (Evans., 1997; Brown., 2004) (Figure 2.2). The data used is referred to as zero-phase because the displayed wavelet is symmetrical with the peak corresponding to the zone of maximum energy (Brown et al., 2004) (Figure 2.2). P-waves that are reflected from an interface of positive downwards impedance contrast will correlate with a peak on the wavelet (red wave in Figure 2.2). In contrast, p-waves that are reflected from an interface of negative downwards impedance contrast will correlate with a trough (black wave in Figure 2.2). The amplitude of the wave (the height of either a peak or trough) corresponds to the magnitude of impedance contrast (Figure 2.2). The acoustic impedance (Z) is calculated via the formula;

Equation 2.1

$$Z = pV$$

Where p is the density of the rock unit and V is the p-wave velocity.

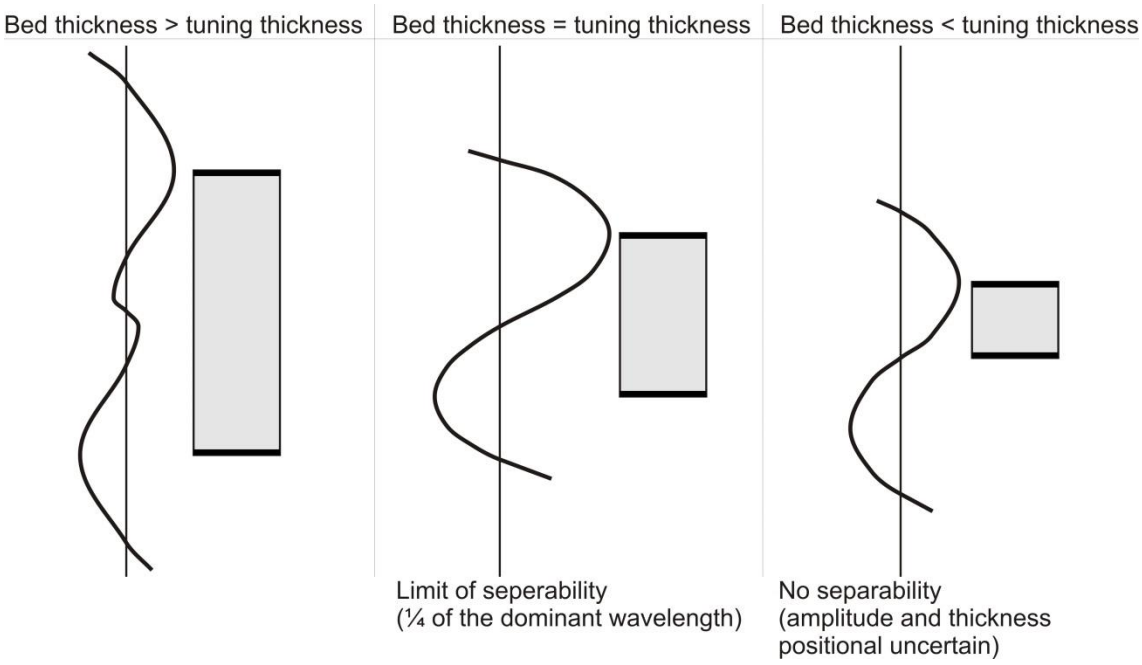

Figure 2.3 Tuning thickness. Resolution of the reflections from the top and bottom of a bed is dependent on the interaction of closely spaced wavelets (adapted from Brown et al. (2004)).

The recognition and accuracy of interpretation of a geological feature using 3D seismic data is heavily influenced by the resolution of the seismic data, which varies both vertically and horizontally. P-wave velocity generally increases with depth as the compaction and the age of the rock increases. The dominant frequencies decreases with depth, as high frequencies are more quickly attenuated, which results in an increasing wavelength and a decrease in the resolution of the seismic data (Brown et al., 2004). The vertical resolution is typically ¼ of the dominant wavelength (λ) of the seismic pulse (Figure 2.3). The limit to the visibility of the reflection of a bed is dependent on the thickness of the bed relative to the tuning thickness. The tuning thickness is the bed thickness at which it is no longer possible to distinguish between two reflections (Figure 2.3). This means that at a spacing of less than ¼λ, reflections will undergo constructive interference and result in a single high amplitude reflection. A spacing greater than ¼λ will result in a reflection being seismically resolved as two separate reflections (Brown et al., 2004) (Figure 2.3).

Two factors that govern the horizontal resolution of seismic data are spacing of the detector (hydrophone) and the width of the Fresnel zone. The spacing of the hydrophones determines the spacing of the depth estimates from which the subsurface interface is reconstructed (Figure 2.1). The horizontal sampling will be equivalent of half the detector spacing, in the example of a flat lying reflector (Kearey et al., 2009). The Fresnel zone is defined by the energy returned to the detector within half a wavelength of the initial arrival (Kearey et al., 2009) (Figure 2.1). It Is within this zone that the reflected waves interfere constructively to give the reflected signal (Kearey et al., 2009) (Figure 2.1). The migration of seismic data attempts to effectively focus the spread of energy within the Fresnel zone, in order to remedy inaccuracies caused by reflections that have been misplaced due to variations in dip and removes reflection patterns from points and edges (Brown et al., 2004).

2.2.2 El Dabaa 3D survey parameters

Seismic interpretation was performed on a high resolution 3D survey covering an area of ~4300 km^2 encompassed within an area ~6500 km^2. The binset dimensions

of 12.5 x 6.25 m yield a lateral resolution of c.25 m throughout the interval of interest, whilst vertical seismic resolution is ~3 m at the seabed (Frequency – 125 Hz; Velocity – 1520 m/s), ~8 m within the Pliocene to Recent succession (Frequency – 60 Hz; Velocity – 1800 m/s) and ~30 m at the Top Messinian (Frequency – 35 Hz; Velocity – 4400 m/s) (See section 3.5 for description of sedimentary succession).

2.2.3 Seismic interpretation

The results that are presented within this thesis are derived from the mapping of 3D seismic data using Schlumberger's GeoFrame Version 4.0.4.2 and Petrel 2013 seismic interpretation and visualisation software. Mapping has been primarily focused on several regionally extensive and some none regionally extensive Horizons and features such as the numerous mud volcanoes within this study area.

The process of mapping involves the creation of a 3D surface of stratigraphic and structural features via seismic picking of a particular reflection. Through the use of the seismic interpretation software stated above, it is possible to track a series of inlines and crosslines via manual picking and auto-tracking, which will produce a grid of interpretation that covers an area of interest. The inlines and crosslines are spaced at an increment that is appropriate for the surface that is been mapped, based on its complexity and the level of detail that is desired, in order to ensure a sufficient level of accuracy to the final mapped surface. Heavily deformed and complex Horizons may require a finer increment between inlines and crosslines to limit the potential for error in the mapped surface. Arbitrary lines can also be mapped where necessary to aid in the picking of a Horizon.

The grid of interpretation that has been mapped can provide seed points for automated horizon tracking, which consists of a series of algorithm operations that automatically attempt to identify the seismic phase and amplitude similar to the seed points that were manually interpreted. The gaps within the interpreted grid are filled in by the algorithm operations, which results in a complete surface. An alternative approach to fill the gaps in the interpreted grid is the process of interpolation. This

operation is comparatively simple in that it does not attempt to locate and join reflections of a similar seismic phase and amplitude and instead simply directly connects the seed points. In order to ensure the interpolated surface is accurate, the increment between the inlines and crosslines must be suitably small enough for a given reflection to ensure an accurate representation of the surface. Interpolation is most appropriate for complex surfaces where automated horizon tracking is difficult and ineffective.

The resultant surface produced via automated horizon tracking or interpolation display changes in either TWT or depth, depending on whether the Horizon has been mapped within the pre-stack time migrated (PSTM) or pre-stack depth migrated (PSDM) volumes. Within this project, both time and depth maps are particularly useful in providing information regarding prominent changes in relief and various geological features and structures. Seismic attributes employed within this research include:

- **Dip**: Dip is a measurement of variations in gradient. Time-dip magnitude is a time-derived attribute that measures changes in the Horizons gradient by comparing the time value between adjacent points. Dip maps such as these are useful for highlighting surface morphology and structures such as faults.
- **Amplitude**: Seismic amplitude is a measure of the distance between the maximum displacement of a wave at the crest of a reflection, whether either a positive or negative, to the point at which there is no displacement, also known as the null point (Figure 2.2). An amplitude measurement is the product of the energy of the incidence wave and the acoustic impedance contrast between the material above and below and even along Horizon variation. Variation in the acoustic impedance and hence amplitude can be caused by numerous factors, including changes in lithology, porosity, fluid content, the continuity of bedding, bed thickness and geometry (Brown et al., 2004; Hart, 1999). Amplitude maps can be informative when analysing for the presence of and margins of structures and sedimentary features that could be displayed as various amplitude patterns and linear or areal features. Fluid flow related indicators such as acoustic turbidity, amplitude attenuation, enhance reflections, pull-up, push-down, bright spots and flat spots can be observed as

changes to the background reflectivity of a hosting succession (Judd and Hovland, 2007). The amplitude of the host succession is directly related to the degree to which these indicators related to fluid flow can be observed.

- **Variance**: The analysis of variance is undertaken using a time sliced cube. A variance profile or time slice highlights areas of discontinuities in the reflections of a succession and is free of interpretational bias as no actual interpretative picking of a Horizon is required (Brown et al., 2004). Variance uses a set of mathematical calculations similar to correlation to compare adjacent waveforms (Brown et al., 2004). Variance is highly effective in identifying and mapping the 3D nature of faults as a result of the discontinuity produced by the fault zone. This type of analysis is, therefore, also excellent for identifying and mapping the margins and 3D geometry of conduits such as fluids escape pipes, which are characterised as an area of discontinuity.

The analysis of isopach maps is used frequently throughout this project. An isopach map shows either the time thickness or thickness in meters (depending on whether the reference horizons are time or depth migrated) between two horizons. In the context of this research, the analysis of isopach maps in combination with seismic profiles can provide important information regarding areas of anomalous increases in thickness associated with mud emplacement or areas of anomalous thinning associated with the withdrawal of salt or fine grained sediment. Isopach maps are also used during the process of measuring the volume of a sedimentary succession or within a mud volcano. The analysis of isopach maps is used in Chapters 3, 4, 5, and 7.

2.3 GIS

Numerous horizons that have been mapped within the seismic interpretation software described above were exported as x, y, z in meters files. The x, y, z data is then delimited and saved as a Data file (*.dat) using Golden Software's 3D visualization software Surfer 11. The Data file can then be imported into Global Mapper v13 where it is gridded as an elevation grid from 3D point data. The grid can then be exported in the elevation grid format Arc ASCII Grid. In this format the seismically derived horizon

can finally be imported and displayed into ArcMap 10.1 Geographic Information System (GIS). Mud volcanoes and pipe co-ordinates that have been tabulated in Microsoft Excel 2010 were also imported into ArcMap as x and y data points. Additional quantitative and geometrical information recorded from seismic data such as mud volcano thickness, area and volume could then be joined to the attribute databases of the mud volcano data points. The information within these databases and the tools within the ArcMap 10.1 GIS software made it possible to perform a variety of spatial analysis of the mud volcanoes and pipes, based on the statistics that were recorded from them.

2.3.1 Spatial and statistical analysis

All of the spatial statistics used within this research were done using the analytical tools available within ArcMap 10.1 GIS. The tools used are the Average Nearest Neighbour Analysis (Rn), Ripley's K function multidistance cluster analysis (Ld), Kernel density and Voronoi polygons.

2.3.1.1 Average Nearest Neighbour Analysis

The Nearest Neighbour Index (Rn) is a value given as a ratio of the observed mean distance to the expected mean distance for a hypothetical random distribution of points (mud volcanoes) in order to determine whether their distribution is random or dispersed or clustered (Mitchell, 2005; Clark and Evans, 1954; ESRI, 2013a) (Figure 2.4). The expected distance is calculated as the average distance between neighbouring points in a hypothetical random distribution using the same number of mud volcanoes as the observed and the same area. The distance between each mud volcanoes centre and the central point of its nearest neighbour is measured and then an average of all these nearest neighbour distances is calculated to give the average observed mean distance. The average nearest neighbour ratio is then calculated by

dividing the observed average distance by the expected average distance. The Rn value is calculated via the formula;

Equation 2.2

$$Rn = \frac{\overline{D}(Obs)}{0.5\sqrt{\frac{a}{n}}}$$

Where D(Obs) is the mean observed nearest neighbour distance, n is the number of mud volcanoes and a is the aerial extent of mud volcano coverage in the study area.

A ratio of 1 signifies a random distribution and a ratio of <1 is clustered. The nearer to 0, the more clustered the distribution. A ratio > 1 signifies a regular distribution. In order to determine whether there is a pattern to the distribution of mud volcanoes, the Z score is calculated. The Z score (Z) is a test of statistical significance, which evaluates for a normal distribution of the nearest neighbour distances. Very high or very low Z scores indicate that it is very unlikely that the observed pattern has occurred by chance. A Z score is a measure of the standard deviation away from the mean;

Equation 2.3

$$Z = \frac{\overline{D}(Obs) - 0.5\sqrt{\frac{a}{n}}}{SE}$$

Where SE is the standard error as below;

Equation 2.4

$$SE = \frac{0.26136}{\sqrt{n^2 / A}}$$

Where A is the aerial extent of mud volcano coverage in the study area (Mitchell, 2005; Moss, 2010; ESRI, 2013a).

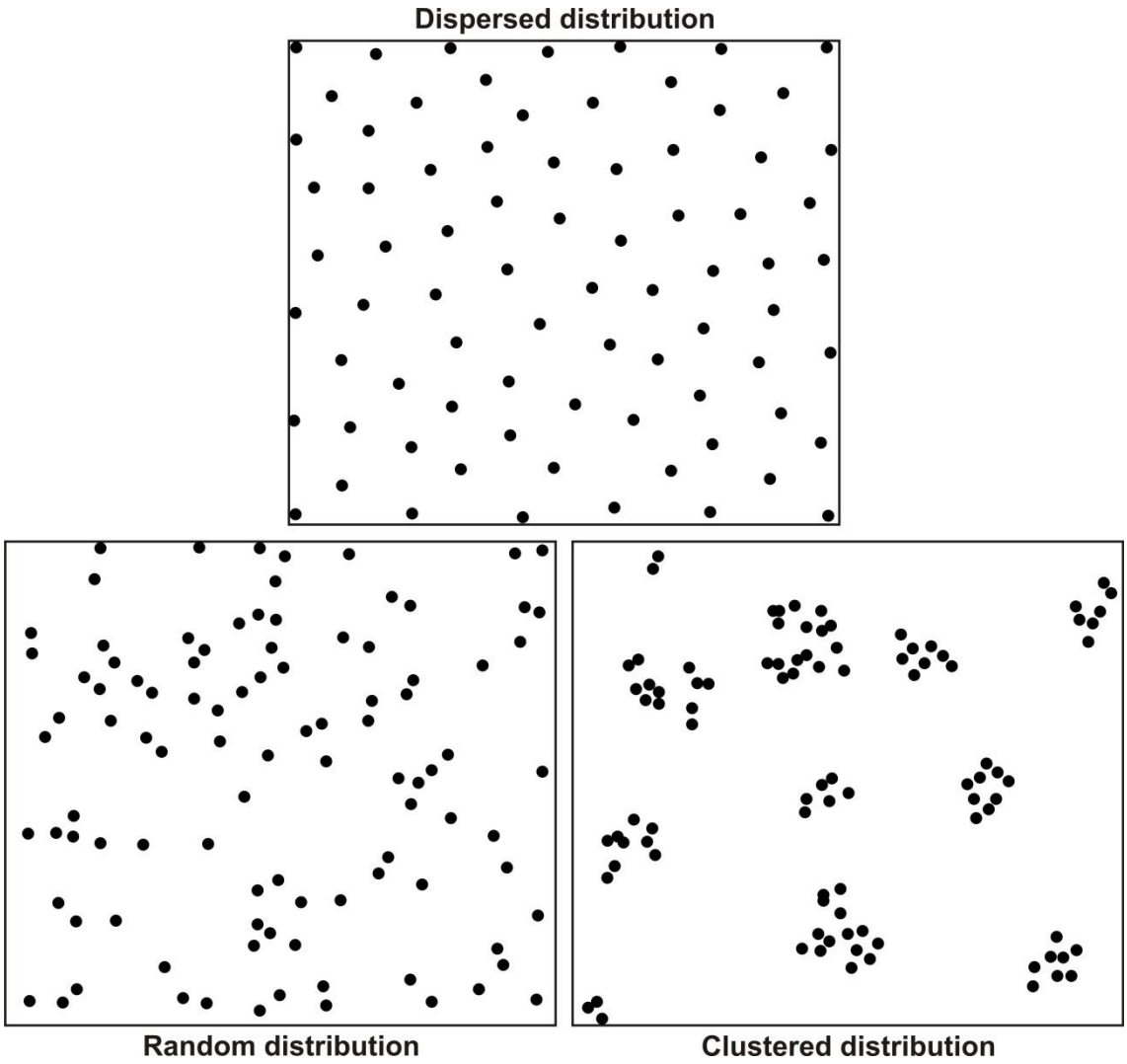

Figure 2.4 Schematic representation of spatial distribution patterns, ranging from a dispersed distribution, to random distribution, to clustered distribution.

2.3.1.2 Ripley's K

Ripley's K is a form of second order statistics. In contrast to the Nearest Neighbour Index the K function includes all neighbouring mud volcanoes within a given distance rather than the distance to each mud volcanoes nearest neighbour. The K function summarizes spatial dependence (feature clustering or feature dispersion) of a range of distances (ESRI, 2013d) (Figure 2.4). Ripley's K, therefore, demonstrates how the spatial clustering or dispersion of mud volcanoes changes when the neighbourhood size changes (ESRI, 2013d). As the neighbourhood size increases, each mud volcano will typically have more neighbours. If the average number of mud volcanoes for a particular neighbourhood distance is greater than the average concentration of features throughout the study area, the distribution would be considered to be clustered at that distance (ESRI, 2013d; Mitchell, 2005). The formula for Ripley's K is given as;

Equation 2.5

$$K(d) = \frac{A}{n^2} \sum_{i \neq} \sum_{j} I_{ij} d_{ij}$$

Where the value of the *K* statistic at distance (*d*) *K*(*d*) is the measured distance between points (*I*, *j*), the weight for the pair (*Iij*), the area (*A*) and the number of points (*n*). The weight (*I*) equals one if the neighbouring point is within the distance of the target point or 0 if it is not.

The K value is transformed using a variation of the K function (*L(d)*), in order to reduce the size of the K value as distances increase (Mitchell, 2005). The equation for this transformation is as follows;

Equation 2.6

$$L(d) = \sqrt{\frac{A \sum_{i \neq} \sum_{j} I_{ij} d_{ij}}{\pi n (n-1)}}$$

When interpreting K function results, if the observed K value is larger than the expected K value for a particular distance, then the distribution is more clustered at

that distance (ESRI, 2013d; Mitchell, 2005). Conversely, when the observed K value is smaller than the expected K value, the distribution is more dispersed than a random distribution at that distance (ESRI, 2013d; Mitchell, 2005).

The confidence envelope for this analysis is constructed by distributing points randomly in the study area and calculating K for that distribution, each random distribution of which is called a permutation (ESRI, 2013d).The number of permutations selected can be loosely translated to confidence levels (i.e. 9 for 90%; 99 for 99%; 999 for 99.9% confidence. 999 permutations was selected for this analysis in Chapter 5, which resulted in the random distribution of points 999 times for each iteration. After the distribution of points 999 times for each distance, the K value that deviated above and below the expected K value by the greatest amount defines the confidence envelope. The lower margin of the confidence envelope is called the LwConfEnv and the upper margin is called the HiConfEnv. When the observed K value is greater than the HiConfEnv value, spatial clustering for that distance is statistically significant. When observed K value is lower than the LwConfEnv value, spatial dispersion is statistically significant (ESRI, 2013d; Mitchell, 2005).

2.3.1.3 Kernel density

Kernel density has been used to calculate the density of mud volcano data points within a neighbourhood around each point. This function calculates a magnitude per output raster cell from these points using a kernel function (Silverman, 1986; ESRI, 2013c). The default raster cell size is used in this analysis, which is calculated as the shorter of the width or height of the output extent in the output spatial reference (the study area), divided by 250. Based on the dimensions of the study area used in this project, the output raster cell size is calculated as 265.81 m^2.

A circular neighbourhood, referred to here as a kernel surface, is generated around each data point that is located central of the kernel surface. The magnitude value that is calculated is greatest at the centre of the kernel surface where it is equal to 1. The calculated value diminishes with increasing distance from the data point,

eventually equalling zero at the margins of the kernel surface. The density within an output raster cell is calculated by adding the values of all kernel surfaces that overlie the centre of the raster cell. The density within all the output raster cells within the project area is calculated (ESRI, 2013c).

The radius of the kernel surface that is used should be large enough that at least some points fall within the neighbourhood, but not so large that the output raster that is produced is too generalized (ESRI, 2013c). Increasing the radius of the kernel surface may incorporate more data points, however, these points will be further from the centre of the kernel surface and this number will be divided by a larger area when calculating density (ESRI, 2013c). The resulting output of this spatial analysis is a smooth kernel surface that displays changes in the density of mud volcanoes throughout the study area and will highlight any clusters due to an increase in density.

2.3.1.4 Voronoi polygon

Voronoi tessellations proportionally divide a distribution of points, in this case mud volcanoes, into cells or Voronoi polygons (Okabe et al., 2009; Moss, 2010). Each polygon contains only a single mud volcano point and is unique in that any location within that polygon should be closer to its related point than to any other point within another polygon (ESRI, 2013b). Voronoi polygons are used in proximity analysis. For example, within this thesis they are used to ascertain whether there is spatial ordering to the distribution of mud volcanoes.

2.3.1.5 Chi-square test

In order to analyse the distribution patterns of the mud volcano volume data, a Chi-Square test was used in Chapter 5. The chi-square test measures the degree of uniformity in the data and the goodness-of-fit test was also used to compare the observed data with a Poisson distribution and Negative Binomial model. The Poisson

distribution test measures the degree of randomness in the data and the Negative Binomial test indicates the degree of clustering.

The purpose of a chi-square test is to statistically evaluate the difference between an observed and expected frequency in each cell (bin), scaled by the expected frequency. The expected frequency is calculated as the total number of points (mud volcanoes), divided by the number of cells (the number of bins). Each bin represents a range of volume values, which increase by 0.105 km^3 from one bin to the next and results in a total of 32 bins. The chi-square test (X^2) analyses the goodness of fit of the observed distribution to that of an expected uniform distribution, given by;

Equation 2.7

$$X^2 = \sum_{i=1}^{k} \frac{(O_i - E_i)^2}{Ei}$$

Where Oi is the observed number of points in cell i, and Ei is the expected number of points in cell i (Davis and Sampson, 2002; Cochran, 1952). This test is variable with k-32 degrees of freedom (df), where k is the number of estimated parameters that define a theoretical distribution.

A modified Poisson distribution (Davis and Sampson, 2002) can be used to test the randomness of a distribution. This analysis is used here to test for randomness to the distribution of mud volcano volumes. This modified distribution will analyse the frequency of mud volcanoes volumes across the whole range of bins of given volumes to predict the probability (P) of occurrence of a particular number of mud volcanoes per bin (x), calculated by;

Equation 2.8

$$P(x) = e^{(-\lambda A)} \frac{(\lambda A)^x}{x!}$$

Where *e* is approximately equal to 2.71828 (*e* is the base of the natural logarithm system), λA is the mean number of mud volcanoes per bin, *x* is the number of mud volcanoes. The goodness-of-fit of the Poisson model to the observed results can then be tested using the chi-square test. The expected frequency for this test is obtained by

multiplying the Poisson probability by the number of bins (T). The parameters that have been used for the Poisson model have also been used to calculate the variance in mud volcanoes per bin (S^2), which is given by;

Equation 2.9

$$S^2 = \frac{\sum_{i=1}^{T}(x_i - m/T)^2}{T-1}$$

A negative binomial distribution has been used to test whether the volume values of the mud volcanoes are of a clustered distribution. This test considers the number of mud volcanoes (*x*), the probability of the occurrence of a mud volcano in a particular bin (*p*) and the degree of clustering of the data (*k*) (Davis and Sampson, 2002). The degree of clustering of the data is estimated by;

Equation 2.10

$$k = \frac{(m/T)^2}{S^2 - (m/T)}$$

With k calculated, it is then possible to calculate the probability (*p*) by;

Equation 2.11

$$p = \frac{(m/T)}{k}$$

The probability of the occurrence (PO) of mud volcanoes per bin based on the degree of clustering and probability is given by;

Equation 2.12

$$PO = \frac{1}{(1+p)^k}$$

The estimated number of mud volcanoes per bin is obtained by multiplying the probabilities of the occurrence by the number of bins. The goodness-of-fit of the binomial model to the observed results can then be tested using the chi-square test.

2.3.1.6 Volumetric analysis

One aspect of the mud volcano analysis within this thesis is focused on their geometrical statistics. Due to the generally conical shape of the mud volcanoes described in Chapter 5, their volumes are calculated using the equation for the volume of a cone:

Equation 2.13

$$V = \frac{1}{3}\pi r^2 h$$

Where V is volume, r is radius and h is height. The research conducted in this thesis will focus on detailed description and the analysis of a large range of statistics that have been collected such as volume, in order to produce a comprehensive analysis of all the mud volcanoes within this study area.

2.4 Potential sources of error and limitations

Throughout this thesis numerous qualitative and quantitative measurements have been recorded with a full appreciation that these measurements are limited by the resolution of the data and potentially any errors in the data. Although the quality of this seismic survey is high, there are specific areas such as around the edges of the data where there is a decrease in quality. This makes taking measurements from some mud volcanoes problematic when they are located at the edge of the data.

Acoustic and amplitude anomalies can be found within the seismic data, which can result in poor imaging that can make interpretation challenging and potentially impact the accuracy of seismic picking and measurements taken from seismic data. Velocity pull-up and push-down can result from increases or decreases in interval velocities and from lateral facies variations. For example, a feature or layer with a high seismic velocity such as evaporites that is surrounded by rock with a low seismic velocity could cause what appears to be a structural high beneath as a result of velocity pull-up. In contrast, a layer or feature with low seismic velocity such as fluid escape pipes or mud volcano conduits that are surrounded by rock with a higher

seismic velocity causes what appear to be a structural low beneath as a result of velocity push-down. This effect introduces a potential source of error within this research when measuring the relief associated with certain depressions, and measuring and describing the dimensions of some fluid escape pipes and mud volcano conduits. Seismic migration should reduce the magnitude of effects such as this, however an influence by velocity anomalies will inevitably still remain (Brown et al., 2004). Further specifics on various seismic artefacts and amplitude related anomalies, some of which may be associated with the presence of gas, may also affect the accuracy of interpretation are discussed in Chapters 4, 5 and 6

Chapter 3

3 Geological Setting

3.1 Introduction

The 3D seismic cube used in this research is located from the Western Province of the Eastern Mediterranean, within the Egyptian passive margin (Figure 3.1). The study area is located between the deep basin and lower continental slope region offshore Egypt, where extension associated with gravitational collapse is prevalent, and within the catchment area of the present day Nile Deep Sea Fan (NDSF) (Figure 3.2). Rather than using several seismic cubes from various settings, this research has been conducted using a single seismic cube, and so only a single geological setting section is required for this thesis. The aims of this chapter are to: (1) describe the geographical setting; (2) describe the regional geodynamics; (3) describe the regional geology of the Eastern Mediterranean with a focus primarily on the Western Province and Nile deep see fan (NDSF) and; (4) describe the seismic stratigraphy of the study area.

3.2 Geodynamic setting

The Egyptian continental margin is considered a passive margin, the formation of which is inferred to have initiated through rifting between Jurassic to Early Cretaceous times (Figure 3.2 and Figure 3.3) (Dolson et al., 2005). The modern day Eastern Mediterranean is characterised by a combination of active thin and thick skinned crustal tectonics which are the product of a complex interaction of various tectonic plates and microplates (McKenzie, 1970; Sage and Letouzey, 1990; Mascle et al., 2000; McClusky et al., 2000). These tectonic interactions produce several geodynamic features surrounding the region (Figure 3.4) including:

1. The very slow, near aborted Suez Rift in the southeast, initiated in the Eocene (Figure 3.3 and Figure 3.4) (Loncke et al., 2004; Mascle et al., 2000);

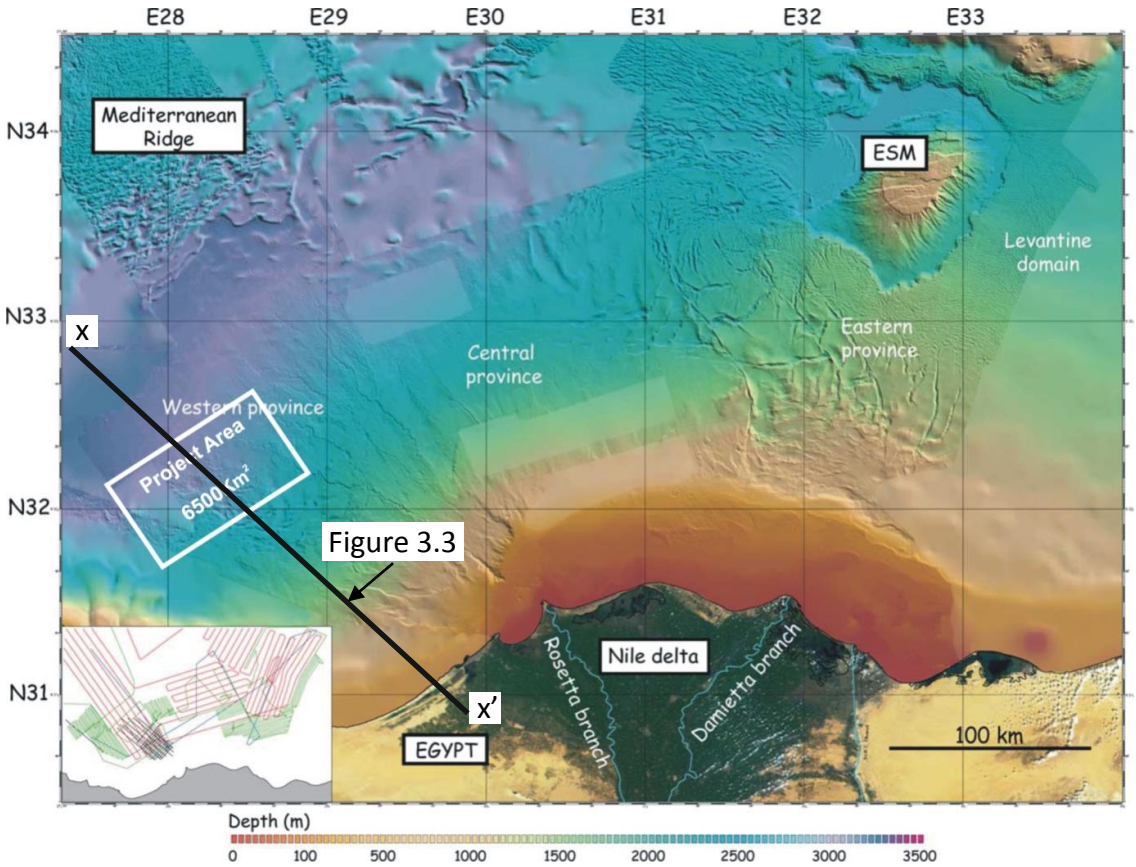

Figure 3.1 A location and bathymetric map of the present day Nile Deep Sea Fan. The location of the study area is highlighted by the white rectangle The line of section (X – X') for Figure 3.2 is displayed. ESM - Eratosthenes Seamount (Modified from (Loncke et al., 2006).

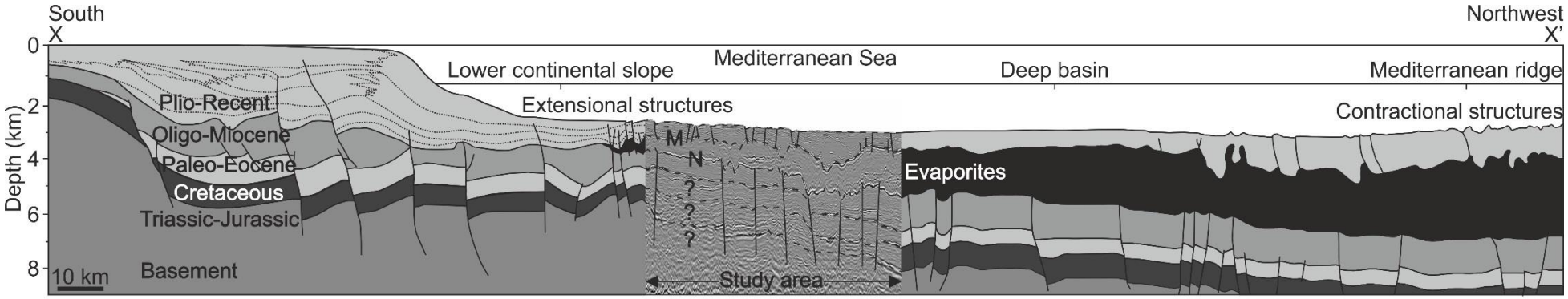

Figure 3.2 Sequence stratigraphic overview that extends from the Nile Delta, through the study area, and to the Mediterranean ridge. The section blends line profiles with a seismic profile through the study area and interpretively connects stratigraphic sequences identified in the literature, with prominent reflections of a correlatable depth in the seismic profile. The line of section (X – X') is displayed in Figure 3.1. M – Horizon M; N – Horizon N; ? – uncertainty in stratigraphic sequence correlation (Modified from Vandré et al. (2007) and Lofi et al. (2011)).

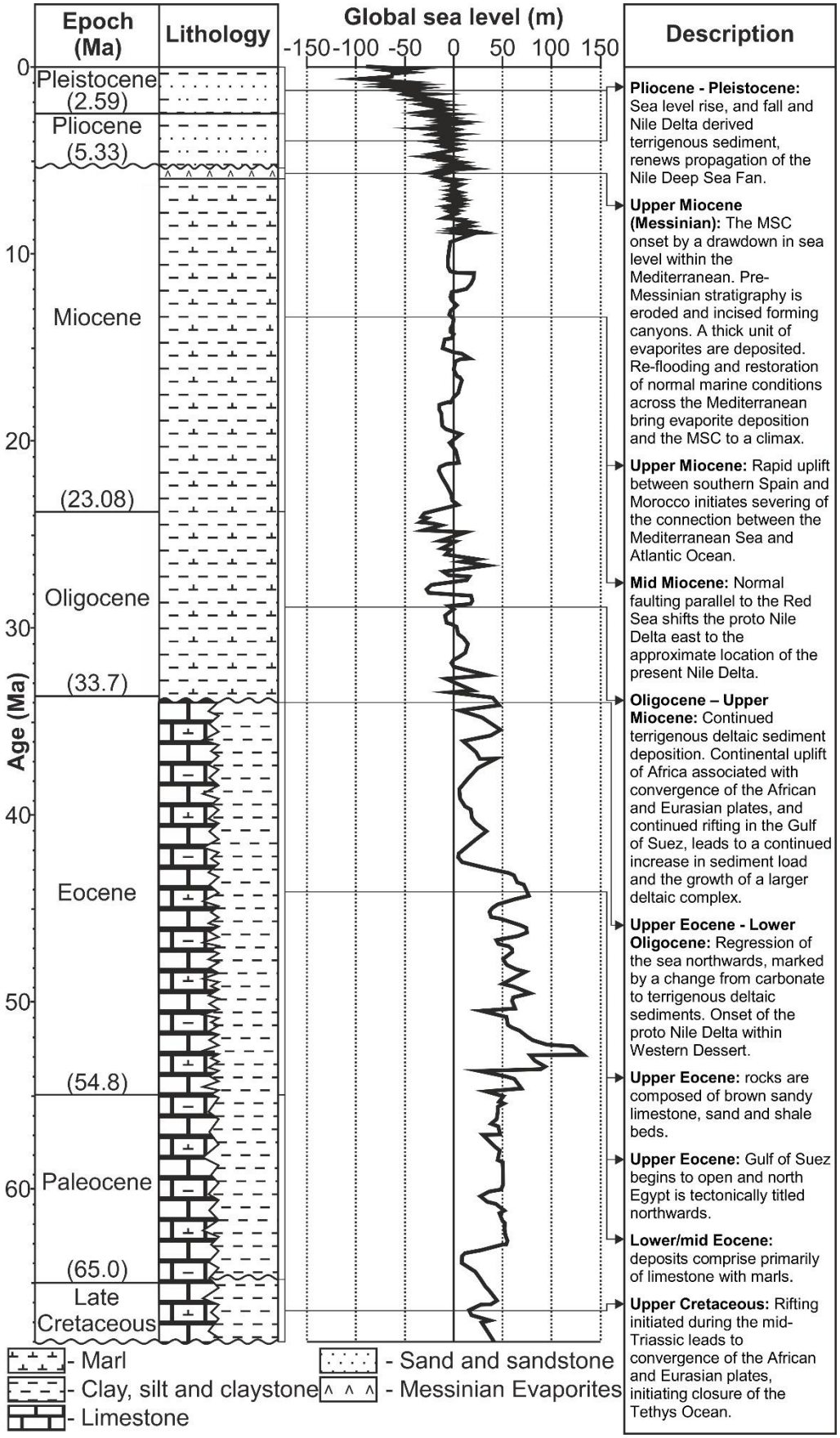

Figure 3.3 A conceptual stratigraphic chart, global sea level curve and description of key events during the geological history of this study area and the wider Eastern Mediterranean (Modified from Bertoni and Cartwright (2005) and Miller et al. (2005))

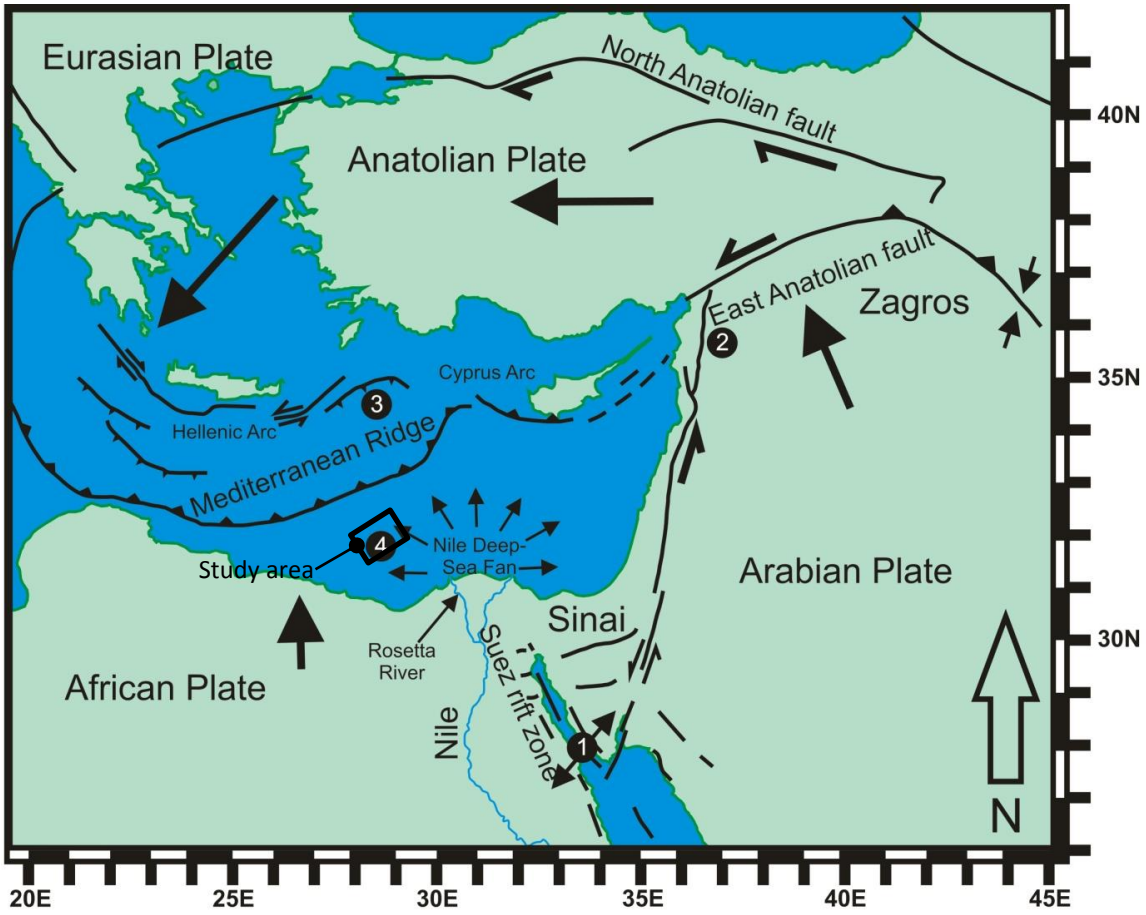

Figure 3.4 Tectonic framework of the Eastern Mediterranean. The larger black arrows are indicative of relative plate motions. Numbers 1-4 correspond with numbers 1-4 in the text. (Modified from Loncke et al. (2006) and Mascle et al. (2000).

2. The Dead Sea/Levant and East Anatolian Fault zones in the east and northeast which are related to the transcurrent motion of the Arabian plate with respects to Africa (Figure 3.4) (Loncke et al., 2006; Loncke et al., 2004; Ducassou et al., 2007);
3. The Mediterranean ridge to the North, where the Eastern Mediterranean has been influenced by subduction/collision of Africa beneath Aegea-Anatolia along the eastern Hellenic and Cyprus arcs (Figure 3.2 and Figure 3.4) (Loncke et al., 2006; Sage and Letouzey, 1990; Loncke et al., 2004; Ducassou et al., 2007; McClusky et al., 2000);
4. The Egyptian margin, which is a passive margin of Mesozoic age that may have been partially reactivated during the Miocene rifting of the Suez-Red Sea Rift system. Sediments from the NDSF overlie the former Egyptian passive margin (Figure 3.2 and Figure 3.4) (Loncke et al., 2006; Mascle et al., 2000; Loncke et al., 2004).

3.3 Basin Formation, stratigraphy and the evolution of the NDSF

The Eastern Mediterranean has a complex tectonic history. The evolution of the Mediterranean Sea was initiated by the opening of the Tethys Ocean in the Early-Late Triassic (Morelli, 1978; Hirsch et al., 1995; Dupre et al., 2007). From the middle/late Triassic to early Cretaceous, successive episodes of rifting (Hirsch et al., 1995) formed NE-SW oriented marine sedimentary basins in Northern Egypt (Figure 3.2 and Figure 3.3). Convergence of the African and Eurasian plates (Figure 3.4) in the Upper Cretaceous initiated the closure of the Tethys Ocean and the formation of the Alpine chain between the two plates (Figure 3.3) (McKenzie, 1970; Sage and Letouzey, 1990).

There are primarily two structural regimes within the study region of this research: (1) regional basement tectonics which are associated with the Rosetta Fault system as a result of rifting during the evolution of the margin (Aal et al., 2000) and; (2) gravity driven tectonics linked to downslope spreading of the

Messinian evaporites, which have heavily impacted the morphology of the continental slope (Figure 3.2) (Gaullier et al., 2000; Loncke et al., 2006; Cartwright and Jackson, 2008). Two major fault trends are found offshore the Nile, the Temsah trend which is oriented NW-SE and the Rosetta trend running NE-SW and ENE-WSW (Loncke et al., 2004; Aal et al., 2000).

Within northern Egypt, outcrop studies have found lower to mid Eocene deposits to be comprised primarily of limestone with marls (Figure 3.3) (Salem, 1976; Said, 1962). In contrast, the upper Eocene rocks are composed of brown sandy limestone, sand and shale beds, similar to the overlying Oligocene terrigenous section (Figure 3.3) (Salem, 1976; Said, 1962). The change from carbonate in the lower and Mid Eocene, to terrigenous deltaic sedimentation in the upper Eocene, combined with a limited extent of upper Eocene rocks, is considered strong evidence for the regression of the sea towards the north in the late Eocene (Figure 3.3) (Salem, 1976; Said, 1962). The change to primarily terrigenous sediments continued from the late Eocene to the Oligocene and through to the Miocene (Figure 3.3). Within the Levant Basin to the far east where well data extends as deep as late Cretaceous sediments , the upper Eocene to mid/late Miocene sediments are predominantly clay, silt, claystone and marl (Figure 3.3) (Bertoni and Cartwright, 2005).

The transition to terrigenous sediments in the late Eocene to early Oligocene, occurred as the Gulf of Suez began to open and northern Egypt was tectonically tilted northwards towards the Mediterranean, which resulted in large volumes of clastics entering the basin through deep canyons (Figure 3.3) (Dolson et al., 2005). This change from carbonates to deltaic sedimentation in the upper Eocene, combined with a limited extent of upper Eocene rocks is considered as evidence for the regression of the sea towards the north and the onset of the proto-Nile Delta in the Eocene, within the Western Desert, to the west of the modern day NSDF location (Figure 3.3) (Said, 1962; Salem, 1976; Barber, 1981). This paleo delta is a predecessor of the modern day Nile delta, however, on a much smaller scale. Gradual mega-continental uplift of Africa throughout the Cenozoic and the associated rifting in the Gulf of Suez led to a continual increase in sediment

load to the proto-Nile Delta, which has built out an increasingly larger deltaic complex through time (Figure 3.2 and Figure 3.3) (Barber, 1981).

Within the Western Desert, the Oligocene section is comprised of fluviomarine or deltaic facies, which are associated with pro-delta sediments and were deposited during a time of northward deltaic propagation over an immature shelf (Salem, 1976). Along the modern day Mediterranean coast line, Oligocene and lower Miocene facies are characterised by abnormally high sand content and are represented by slope fan or turbidity sediments, as well as shale and limestone (Salem, 1976). Similar to the modern day seafloor, the Oligocene and Neogene deposits also dip gently and regionally increase in thickness toward the north (Figure 3.2) (Salem, 1976). The Afiq, El Arish and Ashod canyon exists as prime examples of areas of preferential erosion by submarine channels and later depositional infill, starting in the early Oligocene and continuing until the mid-Miocene when the slope collapsed as a result of large scale sliding, which ultimately led to the incision of the shelf in the late Miocene (Figure 3.3) (Druckman et al., 1995; Bertoni and Cartwright, 2006).

Mid-Miocene normal faulting parallel to the Red Sea shifted the proto-Nile delta system from its earlier position in the Western Desert to approximately its present location (Figure 3.3) (Barber, 1981; Salem, 1976). From this point on, the proto-Nile Delta began to flow along a course similar to the present day, forming a thick deltaic sequence accumulation near the site of the modern Nile Delta (Salem, 1976). By the Tortonian, the proto-Nile had established a substantial delta complex which was later severely eroded during the drawdown of the Mediterranean during the Messinian Salinity Crisis (MSC) (Figure 3.3) (Ryan and Cita, 1978; Hsü, 1978; Rizzini et al., 1978; Barber, 1981). For reference and discussion within subsequent chapters, it is important to state now that the Tortonian interval is the interval located directly beneath the Messinian evaporites and that the precise stratigraphy of this interval lacks nearby well calibration. However, by extrapolation from other well calibrated pre-Messinian successions in the Levant Basin (Bertoni and Cartwright, 2005) and at outcrop in Sicily (Grasso et al., 1982), it is most likely to comprise a marly to muddy interval.

7.8 Ma, rapid uplift of up to 5mm/yr^{-1} between southern Spain and Morocco began to sever the connection between the Mediterranean Sea and the Atlantic Ocean, until eventually the two became entirely disconnected at the end of the Miocene (5.9Ma) (Figure 3.3) (Barber, 1981; Duggen et al., 2003). As a result there was a fall in sea level of between 800-1500m within the Mediterranean Sea (Bertoni and Cartwright, 2007b; Druckman et al., 1995; CIESM, 2008). Prominent sub-aerial erosion during the desiccation of the Mediterranean, led to incision of valleys and canyons along the basins margins (Figure 3.3) (Barber, 1981; Rizzini et al., 1978; Druckman et al., 1995; Bertoni and Cartwright, 2006). The drawdown in sea level led to the onset of the MSC throughout the entire Mediterranean Basin (Hsü, 1978; Ryan, 1978), which abruptly interrupted normal marine sedimentation (Bertoni and Cartwright, 2007b).

A continued restriction of oceanic water during the Messinian caused partial isolation of the Mediterranean Basin, which led to the deposition a thick sequence of evaporites, which reach thicknesses as great as 3 km in some deep basins (Figure 3.3) (Bertoni and Cartwright, 2007b; Hsü et al., 1977; Clauzon et al., 1996; Krijgsman et al., 1999; Hsü et al., 1973; Ryan and Cita, 1978; Ryan, 1978; Sage and Letouzey, 1990; Aal et al., 2000; Dupre et al., 2007; Barber, 1981; Rizzini et al., 1978; Druckman et al., 1995; Bertoni and Cartwright, 2006). The evaporites were deposited at exceptional sedimentation rates of c. >4 cm/yr over a period of 600 kyrs and form a wedge shaped interval geometry which regionally thins up dip to the north and becomes thicker down dip to the south (Figure 3.2) (CIESM, 2008). The upper Messinian is characterised by a formation only a few tens of meters thick, and is composed of thick layers of Anhydrite interbedded with thin layers of clay, which is known as the Rosetta Anhydrite. The upper limits of this formation can be recognised by the appearance of Lower Pliocene marine clays and is well developed only in areas north of the delta and offshore (Figure 3.3) (Rizzini et al., 1978).

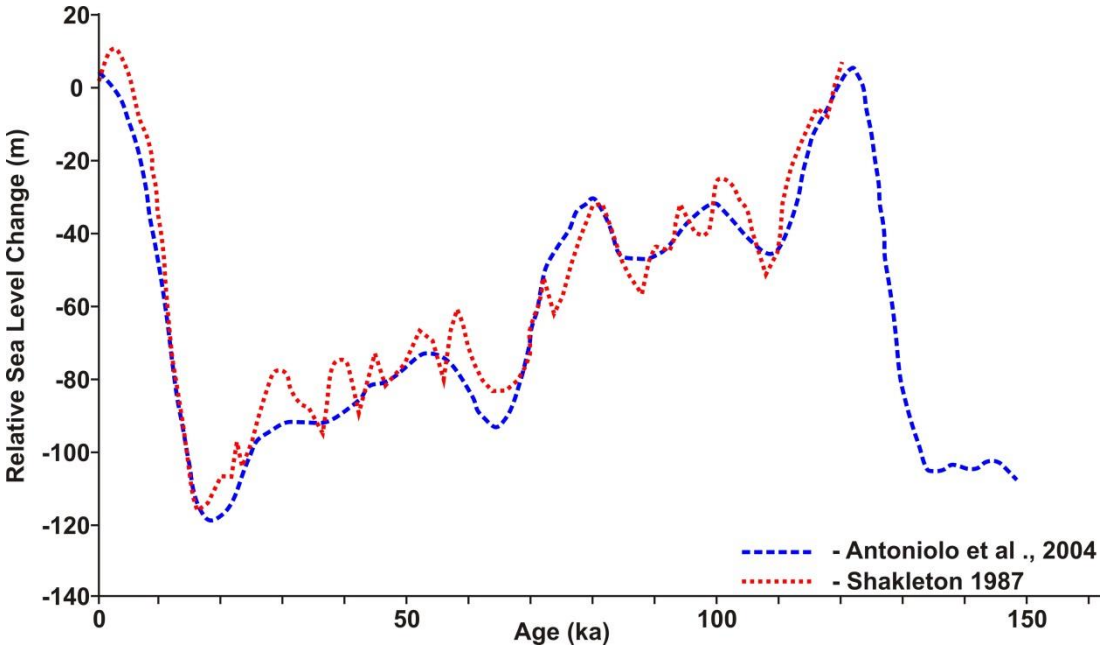

Figure 3.5 Eustatic sea level change. The graph displays relative sea level change (m) since the Pleistocene) based on planktonic and benthonic 18O data from Shackleton (1987) (red dotted line) and data from Argentarola Cave spelothems in Italy, from Antonioli et al. (2004) (blue dashed line) (Modified from Moss (2010)).

The restoration of normal marine conditions across the Mediterranean Basin in the Pliocene (5.33 Ma) brought an end to evaporite deposition in the area (Hsü et al., 1977; McKenzie, 1999; Bertoni and Cartwright, 2007b). Sea level rise and subsequent fall during the Pliocene and Pleistocene (Figure 3.3 and Figure 3.5) and an abundant supply of terrigenous sediment, sourced from the Nile Delta, resulted in renewed propagation of the NDSF ~3.8 Ma (Figure 3.2) (Dolson et al., 2001; Mascle et al., 2006; Ross and Uchupi, 1977; Salem, 1976). The NDSF has continued to propagate throughout Pliocene to Recent times and the current shelf edge marks the maximum seaward extension of the deltaic system (Figure 3.2 and Figure 3.3).

The modern NDSF is now a large sedimentary wedge that covers c. 100,000 km^2 and extends northwards towards the Mediterranean ridge and Eratosthenes Seamount (Figure 3.2 and Figure 3.4) (Ross and Uchupi, 1977; Ryan and Cita, 1978). It drapes a segment of much older passive margin, the total thickness (including post Miocene deposits) of which is believed to be in excess of 9-10 km (Aal et al., 2000; Mascle et al., 2006). The post-salt overburden of the Pliocene to Recent succession exceeds 3 km in many regions of the Eastern Mediterranean and is clay-dominated and has been rapidly deposited (Dupre et al., 2007; Loncke et al., 2002; Loncke et al., 2004). The rapidity of deposition of this unit is thought to be a viable mechanism for developing significant overpressure in deeply buried sediments, which is considered to be evident within the Eastern Mediterranean by the major fluid and sediment remobilisation in the area (Frey-Martínez et al., 2006; Loncke et al., 2004). The Pliocene to Recent interval of the southern deep water region is characterised by N-S oriented linear turbidite channels, which originate from the Nile Delta and can be mapped over some 120 km (Aal et al., 2000). These channels are typically aggradational with seismic facies and compaction features indicating gross reservoir thickness of more than 100 m (Aal et al., 2000).

After the deposition of the Messinian evaporites and thick sedimentary overburden, salt tectonics became very active within the Eastern Mediterranean (Figure 3.2). When subjected to abnormally high strain rates, similar to other rock, salt fractures; however, under typical geologic strain rates most evaporites deform

viscoelastically (Hudec and Jackson, 2007; Weijermars et al., 1993; Quirk et al., 2012; Strozyk et al., 2012). Gravitational loading of the evaporites by Pliocene to Recent sediments and down slope gravitational collapse resulted in syn-sedimentary deformation, which is currently still active (Figure 3.2) (Dupre et al., 2007; Cartwright and Jackson, 2008; Loncke et al., 2002; Gaullier et al., 2000). This region is considered to be tectonically mature due to the structural pattern of the salt and the impact of these kinematics, which are particularly prominent within the middle and lower Nile fan of the western and eastern provinces, where MTDs, growth faults, salt diapirs and crestal grabens are common (Dupre et al., 2007; Garziglia et al., 2008; Loncke et al., 2009; Dimitrov, 2002). Syn-sedimentary deformation also includes up dip thinning of the evaporites and subsequent thin skinned extension of the post salt overburden (Dupre et al., 2007; Cartwright and Jackson, 2008; Loncke et al., 2002; Gaullier et al., 2000; Loncke et al., 2004). Within the upper slope, the Messinian evaporites are almost absent entirely. The strongly tectonized Pliocene to Recent succession of the NDSF, is thought to be particularly susceptible to fluid migration to the seafloor (Dimitrov, 2002).

Several basins within the eastern Mediterranean are karstic, with depressions created from Messinian evaporite dissolution (Camerlenghi and Cita, 1987). Bertoni and Cartwright (2005) suggested that subjacent dissolution at the base of the evaporites, within the Levant basin, led to collapse of weakly lithified overburden and deformation in the form of a series of centric extensional faults. Subjacent dissolution was thought to occur where the evaporites act as an effective seal for upward migration of deep fluids from clastic pre-evaporite deposits, therefore, undersaturated fluids migrate along the base of the evaporites. This resulted in subjacent dissolution of soluble evaporites, which has been interpreted to have formed circular and localised dissolution structures (Bertoni and Cartwright, 2005).

3.4 Sub-regions and physiography of the Eastern Mediterranean and NDSF

Spanning from east to west across the eastern Mediterranean and Nile Delta, there are 4 provinces distinguished by their contrasting morphostructural patterns , influenced by the Messinian Paleo geography (Huguen et al., 2009). These are the Levantine, Eastern, Central and Western provinces (Figure 3.1). There are two main branches of the Nile River that feed the Nile Delta. The Rosetta branch feeds the western delta and slope and the Damietta branch feeds the eastern and central delta (Dolson et al., 2005).

The Levantine province is located east of the Eratosthenes seamount (Figure 3.1). The seafloor surface in this region is characterised by gentle folds, which are the result of progressive gliding of Pliocene to Recent sediments that overlie the Messinian evaporites. The evaporite unit within this area is relatively thin in comparison to other regions of the Eastern Mediterranean, and the sedimentary succession that overlies is but a few hundred meters in thickness. This sedimentary succession is dissected by a few channels some of which are alleged to have originated from the Levantine coast (Loncke et al., 2004).

The Eastern province is defined by a NW-SE oriented tectonic corridor that is > 200 km long and almost 100 km wide. This corridor is bounded on both sides by zones of linear and narrow faults and contains numerous small collapse basins within the upslope region (Gaullier et al., 2000; Mascle et al., 2000; Loncke et al., 2002; Loncke et al., 2009; Loncke et al., 2006). These basins weld to pre-Messinian stratigraphy as a result of salt withdrawal. Within the midslope, uncollapsed depocenters are bound by crestal grabens and the Messinian evaporite succession progressively increases in thickness downslope, where curved salt ridges and a wedge of short-wavelength folds have formed (Loncke et al., 2002; Loncke et al., 2004; Loncke et al., 2009). The Eratosthenes seamount (Figure 3.1) defines the eastern margin of the NDSF (Robertson, 1998). It is has a distinguished flat top and gullied slopes which are the result of significant erosion during the MSC. E-W trending faults deform the structures surface and are thought to result from

bending and uplift, during subduction processes near the Cyprus arc (Sage and Letouzey, 1990; Loncke et al., 2009). Within the easternmost part of this region, the presence of the Eratosthenes Seamount has had a significant influence on the structural evolution of the NDSF. The Eratosthenes Seamount has served as a buttress in limiting and deflecting the north-eastward advance of the allochthonous Messinian evaporites, which has also resulted in further complications to the deformation pattern of the overlying Pliocene to Recent sedimentary succession (Loncke et al., 2009; Loncke et al., 2006). The eastern slope region of the NDSF is steeper than in the other provinces and is dominated by rapid Pliocene to Pleistocene sedimentation in a growth fault province (Loncke et al., 2004).

In contrast to the other sub-regions of the Eastern Mediterranean, the central province is not characterised by prominent canyons or deep-sea channels. The seafloor in this region is primarily defined by a chaotic surface, which is interpreted to have formed via repeated sediment instabilities (MTDs) (Loncke et al., 2002; Loncke et al., 2009; Newton et al., 2004). These instabilities have led to the covering and dislocation of channels of Pleistocene age (Aal et al., 2000) within the post-salt succession. In this region, most of the growth faults that root within the evaporite unit are thought to have been sealed, except towards the east where a 150 km long E-W trending belt of still active growth faults run along the upper continental slope (Loncke et al., 2009). Within this province, the base of the slope is bound by a series of contractional folds, which have formed as the result of halokinesis.

The El Dabaa project area, which is where the 3D seismic cube used in this research is from, is located within the Western province and covers an area of 6500Km^2. Recent studies in the Western Province document that recently abandoned and active channel-levee systems, fluid seepage constructions and mass transport deposits are the primary architectural elements controlling the slope evolution in the area (Dupre et al., 2007; Garziglia et al., 2008; Loncke et al., 2009).

The Western province is intensely cut by the Rosetta active channel-levee system (Huguen et al., 2009; Ducassou et al., 2007), which extends across a c. 80

km wide continental shelf, from its origin of the Rosetta branch of the Nile Delta. As such, the modern day Western Province is in part characterised by a network of meandering levee channels and is the most active province in terms of turbidite deposits. The Pliocene to Recent succession hosts a series of recently abandoned and active well-ramified channel-levee systems, through which turbidite sediments have been and are still transported up to 300 km from the shelf edge. Toward the north, channel-levee systems and distal lobes are gradually incorporated into the Mediterranean Ridge accretionary prism (Huguen et al., 2009; Huguen et al., 2001; Loncke et al., 2002; Loncke et al., 2009).

There are several types of fluid escape features within the Western province, in particular there are a large number of mud volcanoes which vary in shape and size however have similar seismic characteristics. Within the El Dabaa study area there are as many as 400 mud volcanoes found throughout the region, many of which are still active with mud cones visible at the surface, while others are buried and inactive. It has previously been suggested by Loncke et al. (2004) that growth faults embedded in pre-Messinian layers may present potential conduits for fluid migration. Loncke et al. (2004) has also suggested that the distribution of mud volcanoes over time is intimately linked to the regional structure and salt tectonics. This has been thought to dictate not only growth fault emplacement but the regional pressure regime (Loncke et al., 2004). Halokinesis has caused thinning of the salt and thickening of the post salt overburden, which will elevate overpressure within deep fluid reservoirs (Loncke et al., 2004).

Several of the mud cones at the surface have a depressed centre, which forms crater like topographic features. Most are scattered around the seafloor, however, some are found within two caldera like subdued depressions named the Menes caldera and small caldera (Loncke et al., 2004; Huguen et al., 2009). The Menes caldera is a large circular seafloor depression of about 8km in diameter. It has steep walls on all sides other than its northern margin and a basin floor depth of about 3020m and it is clearly visible on Bathymetric maps (Huguen et al., 2009). 3D seismic data shows the extent of the mud volcanism and deformation within the caldera extends far beyond that of its seafloor expression. The southern edge has

many active normal faults due to underlying salt movement (Huguen et al., 2009; Loncke et al., 2004). Within the Caldera, there are three well defined mud cones that are visible at the seafloor named Mykerinos, Cheops and Chephren (Huguen et al., 2009).

Up dip towards the Nile delta, downslope gravitational sliding of the post Messinian evaporite overburden has produced active growth faults which promote fluid migration to the seafloor (Loncke et al., 2004; Dimitrov, 2002). Core studies have shown that the present day marine domain of the Nile primarily consists of clays and silts, with secondary sandy, carbonate and sapropelic deposits (Loncke et al., 2009). Western Province sedimentation rates are very high, with average rates as high as 32 cm/1000 yr for the last 58,000 years within the offshore extension of the Rosetta branch (Dolson et al., 2001).

3.5 Seismic Stratigraphy

The seismic stratigraphy of the study area will be described within this section. In the absence of nearby well-calibration, it is difficult to detail the precise lithologies and age of the subsurface succession within this study area. It is, however, possible to describe the seismic facies of the various successions.

3.5.1 Unit 1A and Unit 1B

This succession comprises reflections of variable amplitude (Figure 3.6). In some parts of the basin these reflections display considerable lateral continuity and in other appear discontinuous where seismic artefacts shroud the reflections. These units are deep within the pre-salt section of the succession and so seismic artefacts including amplitude attenuation and scattering result in migration smiles and often poor quality imaging (Figure 3.6). Unit 1A and Unit 1B are divided by a continuous and high amplitude and positive reflection (Figure 3.6). Large basement faults that

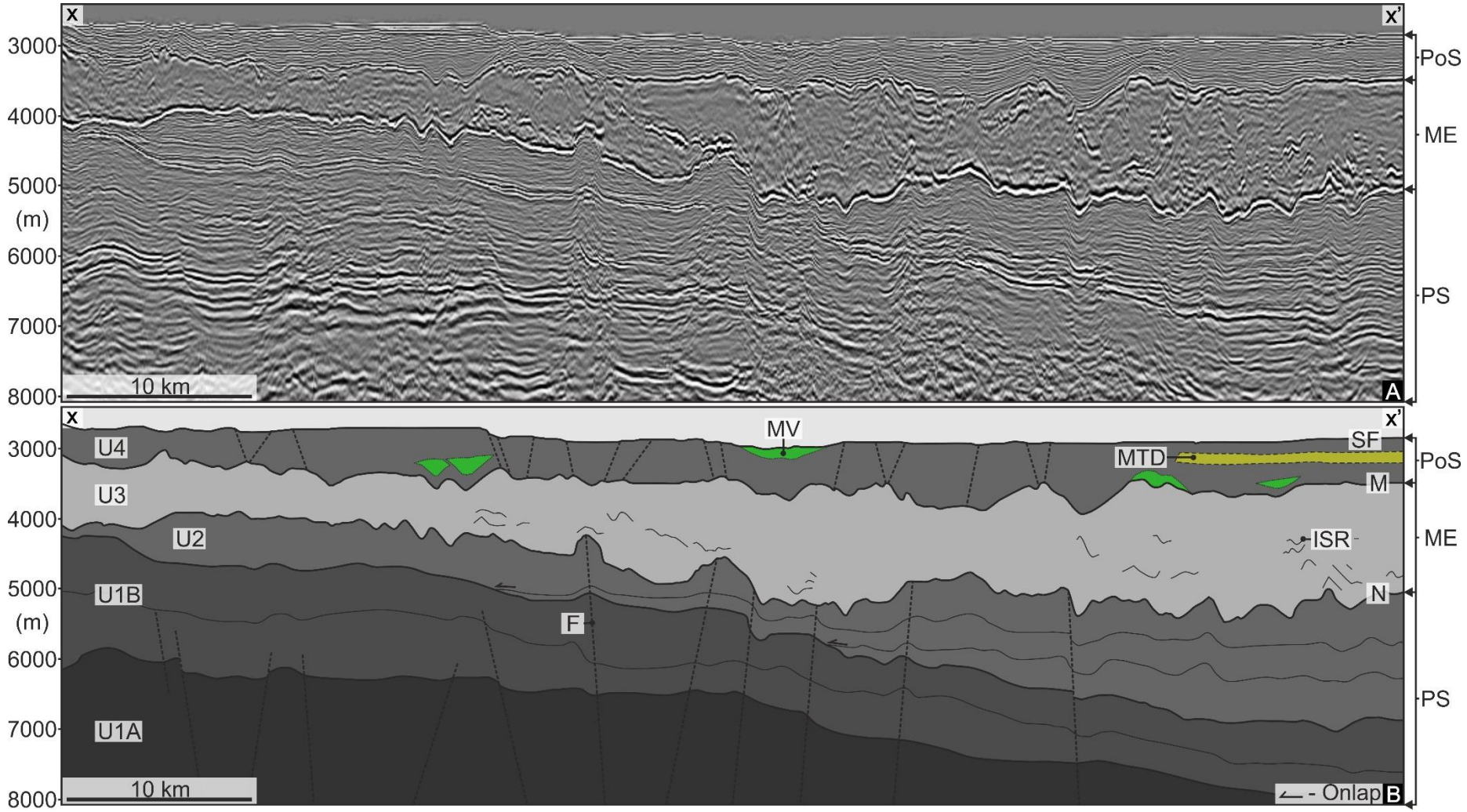

Figure 3.6 Seismic stratigraphy of the study area. A: An un-interpreted PSDM seismic profile through the study area (line of section in Figure 3.6). B: An interpretation of the seismic stratigraphy within the study area. PS – Pre-salt; ME – Messinian evaporites; PoS – Post-salt; SF – Seafloor; M – Horizon M; N – Horizon N; F – Fault; MV – Mud volcano; MTD – Mass transport deposit; ISR – Intra-salt reflection.

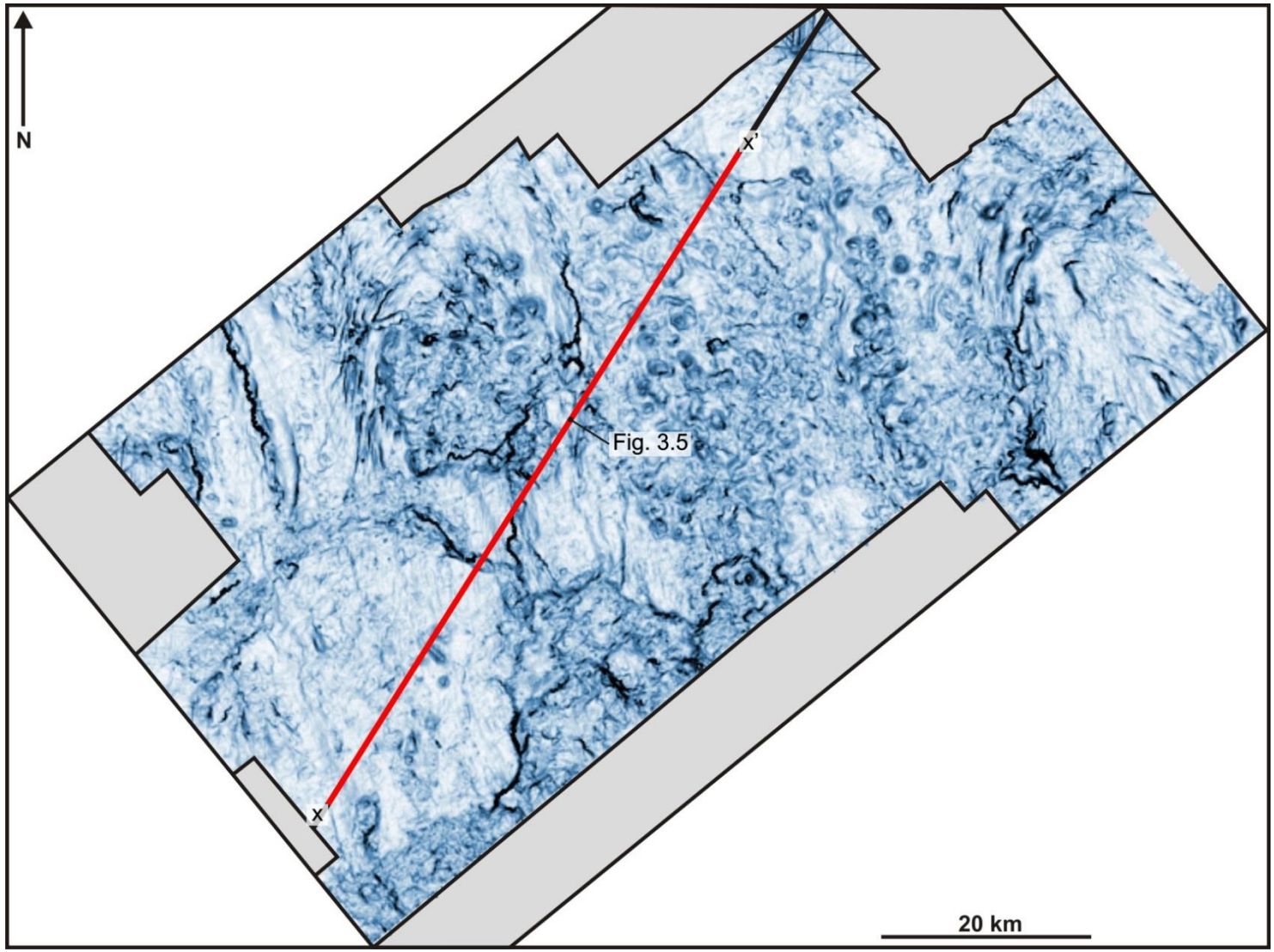

Figure 3.7 Dip map of the base of the evaporites (Horizon N). The line of section for Figure 3.6 is displayed. Some of the linear and black structures that are visible are correlatable with pre-salt faults visible in Figure 3.6.

transect through these units display a horst and graben structure (Figure 3.2 and Figure 3.6). It is possible that this graben structure is associated with the successive episodes of rifting during the Triassic that are discussed above (Morelli, 1978; Hirsch et al., 1995; Dupre et al., 2007). Some of these faults have also propagated several kilometres up towards the base of the evaporite succession (Figure 3.6 and Figure. 3.6). The majority of the research within this project is focused on the succession above Unit 1B where the imaging quality is improved.

3.5.2 Unit 2

Unit 2 displays wedge shaped geometry and increases in thickness towards the northeast (Figure 3.6 and Figure 3.8). The top of this unit is characterised by a regionally correlatable, high amplitude reflection of negative polarity (Figure 3.6). This represents the basal reflection of the evaporite succession within this study area, known as Horizon N, which demarcates the onset of the MSC 5.9 Ma (Bertoni and Cartwright, 2007b; Duggen et al., 2003). It can, therefore, be inferred that the sediments at the top of unit 2, immediately beneath the evaporite succession, are at youngest Tortonian in age. The reflection of Horizon N undulates and display several localised and large sub-circular to irregularly shaped depressions (Figure 3.9). Several pre-salt faults that are observable in seismic profile (Figure 3.6) have clearly propagated to Horizon N and can be seen as linear structural features within a dip map of the Horizon N (Figure 3.6).

The bounding reflection between the base of Unit 2 and the top of unit 1b is a thick and regionally consistent positive and high amplitude reflection, which is difficult to identify in some areas where seismic artefacts result in poor imaging (Figure 3.6). The basal surface of the succession is c. 3700 m at its most elevated towards the south of the study area and is c. 7650 m at its deepest part. At its thickest the unit is c. 2800 m in the northeast of the study and thins significantly towards the southwest where the thickness of the succession reaches as little as c. 200 m (Figure 3.8).

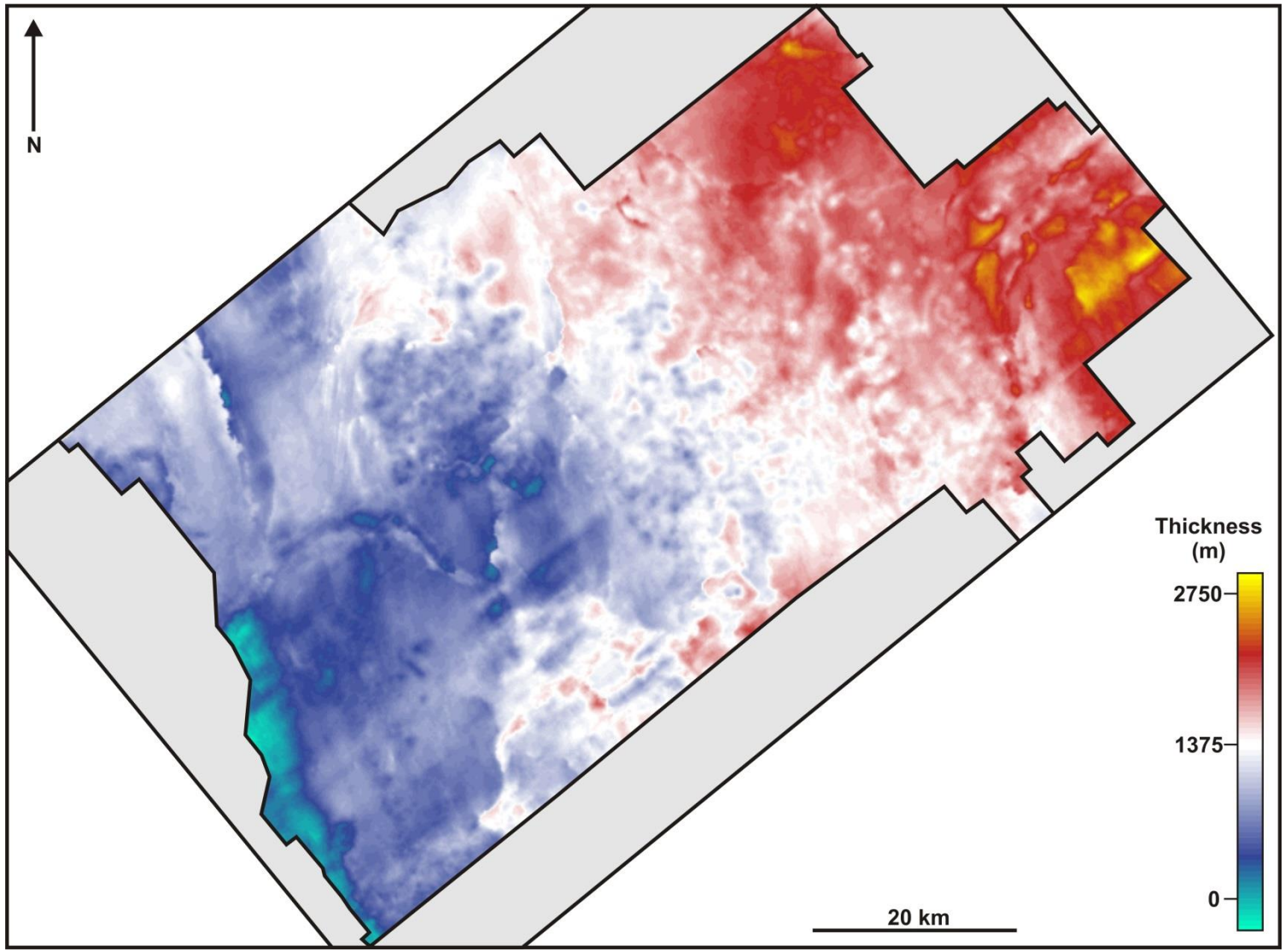

Figure 3.8 An isopach map unit 2 (U2). The unit generally increases in thickness towards the Northeast. The map has a mottled appearance associated with areas of localised and anomalous thinning.

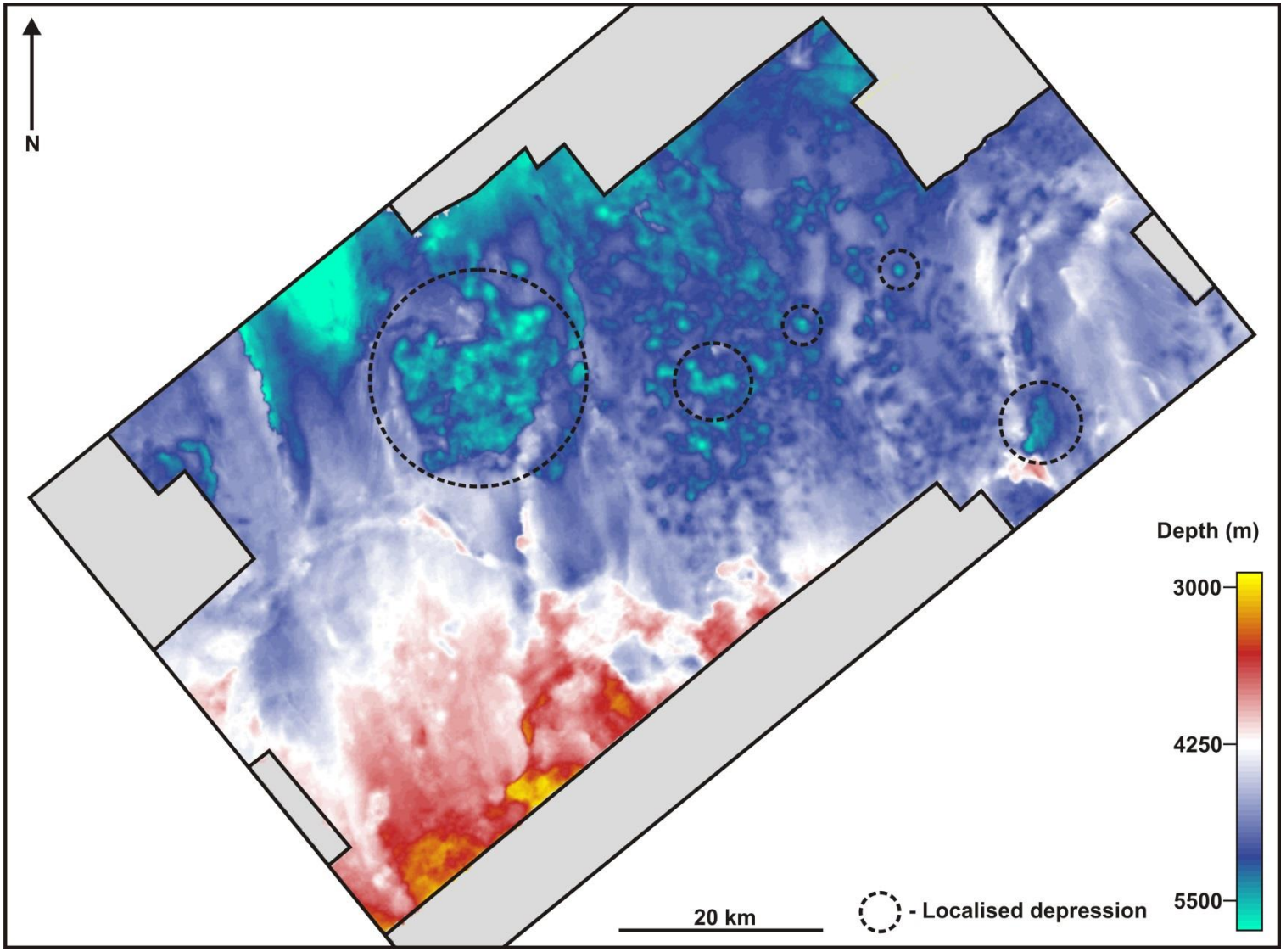

Figure 3.9 A depth map of the base of the evaporites (Horizon N). The map displays a generally northward dipping direction and localised areas of anomalous depression, some examples of which have been highlighted (black dashed circle).

This succession is generally comprised of a coherent reflective depositional unit, with variable amplitude, and high lateral continuity and frequency seismic facies, which is typical of hemipelagic deposits. The reflections within this unit display generally greater coherence and continuity towards the base of the succession and exhibit a decrease in amplitude and continuity towards its upper bounding reflection (Figure 3.6). The reflections within and towards the base of this unit can clearly be observed to onlap the basal reflection of the succession (Figure 3.6).

3.5.3 Unit 3 – Messinian evaporites

Unit 3 is comprised of reflections that are of predominantly transparent, discontinuous and chaotic seismic facies, typical of halite, such as that described by Bertoni and Cartwright (2007b) within the Levant Basin (Figure 3.6). This unit is regionally extensive across the Mediterranean and is comprised of evaporites (Bertoni and Cartwright, 2005; Grasso et al., 1982; Barber, 1981). The evaporite succession is observable as a thick wedge that increases in thickness towards the North and dips in a northward direction within this study area (Figure 3.10 and Figure 3.10).

A regionally correlatable, high amplitude and positive reflection is visible at the top of the unit (Figure 3.6). This reflection marks the top of the evaporites and is known as Horizon M, which demarcates the climax of the MSC 5.33 Ma (Ryan, 1978; Bertoni and Cartwright, 2007b; Duggen et al., 2003). As described above, the basal reflection of the evaporites is identifiable as another regionally correlatable reflection called Horizon N, which demarcates the onset of the MSC 5.9 Ma (Bertoni and Cartwright, 2007b; Duggen et al., 2003) (Figure 3.6). This unit of evaporites is, therefore, Messinian in age (**Error! Reference source not found.**). Other than the seafloor, the reflections of Horizon M and N are the most continuous and high amplitude reflection within this study area. Similar to the above description of Horizon N, Horizon M undulates and display several large sub-circular to irregularly shaped depressions (Figure 3.10). The formation of the depressions will be discussed within the subsequent chapters.

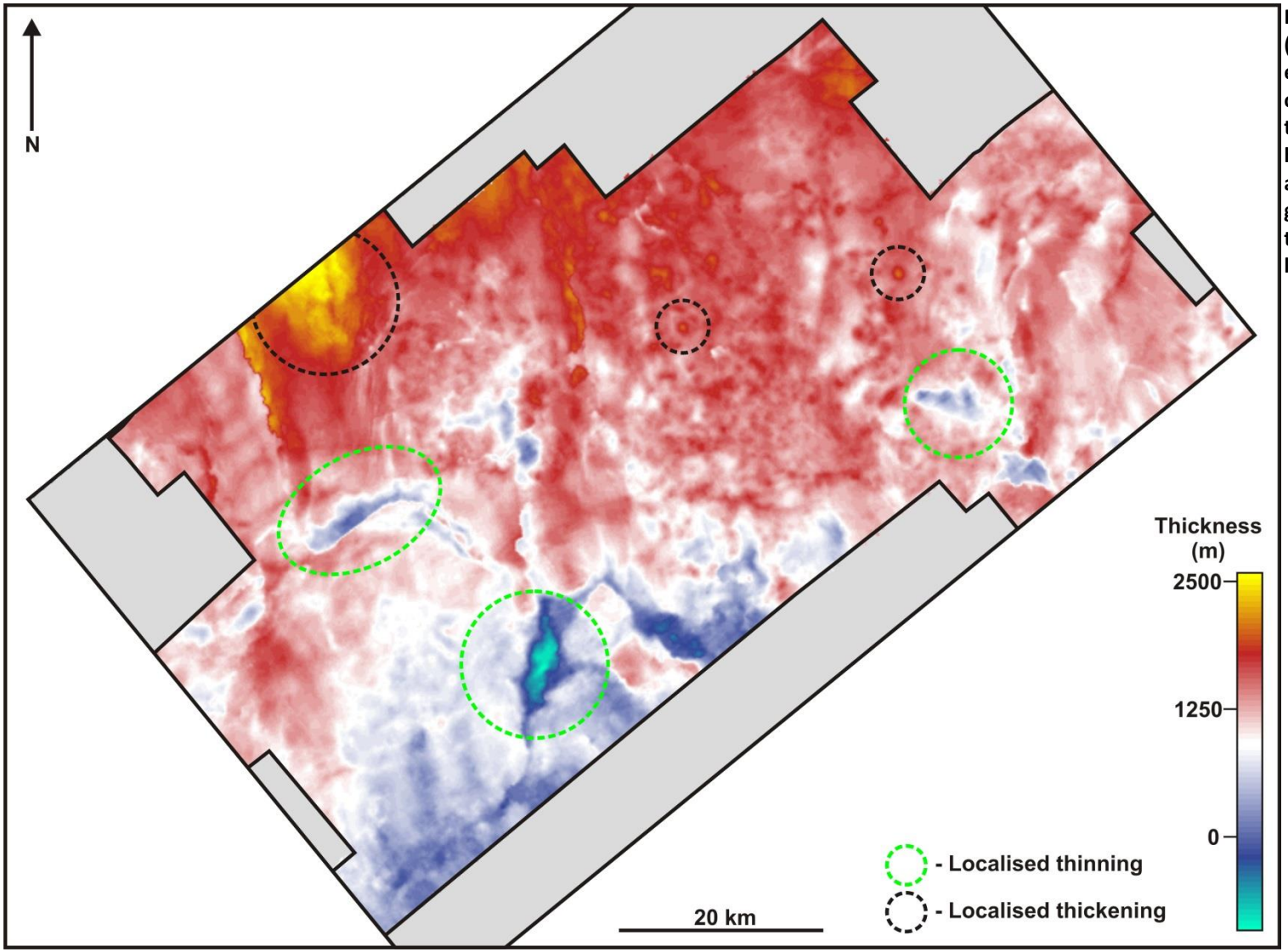

Figure 3.10 An isopach map of unit 3 (U3), the Messinian evaporites evaporite succession. There is an overall increase in the thickness of the unit towards the north and highlighted areas of localised and anomalous thinning (circle with green dashed line) and increased thickness (circle with back dashed line).

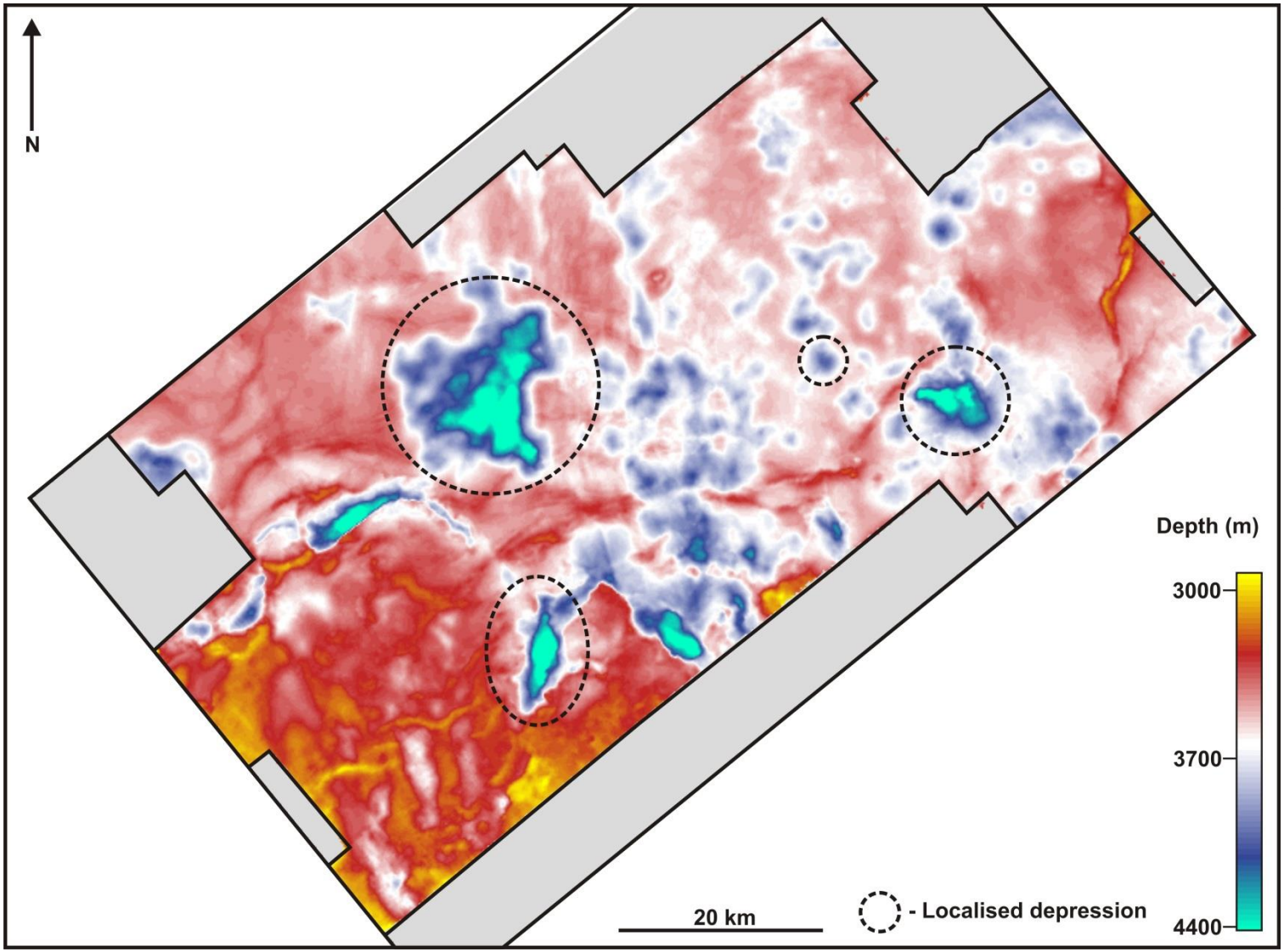

Figure 3.11 A depth map of the top of the evaporite succession (Horizon M). The surface has a general northerly dip direction and displays numerous localised and anomalous depressions, some examples of which have been highlighted (circle with black dashed line).

Towards the base of the evaporite unit, in some parts of this study area localised and high amplitude reflections with moderate continuity can be seen, which could be indicative of heterogeneities within the salt (Figure 3.6). The Messinian evaporite unit is known to include intercalations of clastic deposits in other parts of the Eastern Mediterranean (Bertoni and Cartwright, 2007a; Roveri et al., 2014). These areas of greater continuity and higher amplitude within the evaporite succession are localised features rather than regionally extensive reflections.

Within this study area, both Horizon M and N can be observed at various depths below sea level. Horizon M ranges from c. 2950 m at its most elevated, to a depth of c. 4880 m at its deepest (Figure 3.10). Horizon N ranges from c. 3050 m at its most elevated, to a depth of c. 6050 m at its deepest (Figure 3.9). At its thickest the Messinian evaporite unit reaches a maximum thickness of c. 2440 m (Figure 3.10). In contrast, this succession thins so significantly within some regions of the study area that its upper and basal surfaces converge, resulting in a connection between the pre and post-salt successions (Figure 3.10).

3.5.4 Unit 4 – Pliocene to Recent succession/post-salt overburden

Unit 4 is a regionally consistent aggradational unit, the upper surface of which dips in a NW direction and displays an overall increase in thickness towards the east (Figure 3.11). The base of this unit is very clearly defined by the regionally correlatable and high amplitude reflection of Horizon M (Figure 3.6). The top of the unit is defined by the high amplitude and positive reflection of the seafloor (Figure 3.6). As stated above, Horizon M demarcates the climax of the MSC 5.33 Ma, therefore, the age of unit 4 ranges from Pliocene to Recent.

The depth of the seafloor beneath sea level ranges from c. 2450 m at its most elevated, to c. 3050 m at its deepest. It is characterised by faults, a channel and a levee complex found within the northeast of the study area and a large number of fluid escape features, including mud volcanoes and pockmarks, which will be described and discussed in greater detail in subsequent chapters (Figure 3.12 and Figure 3.14). The

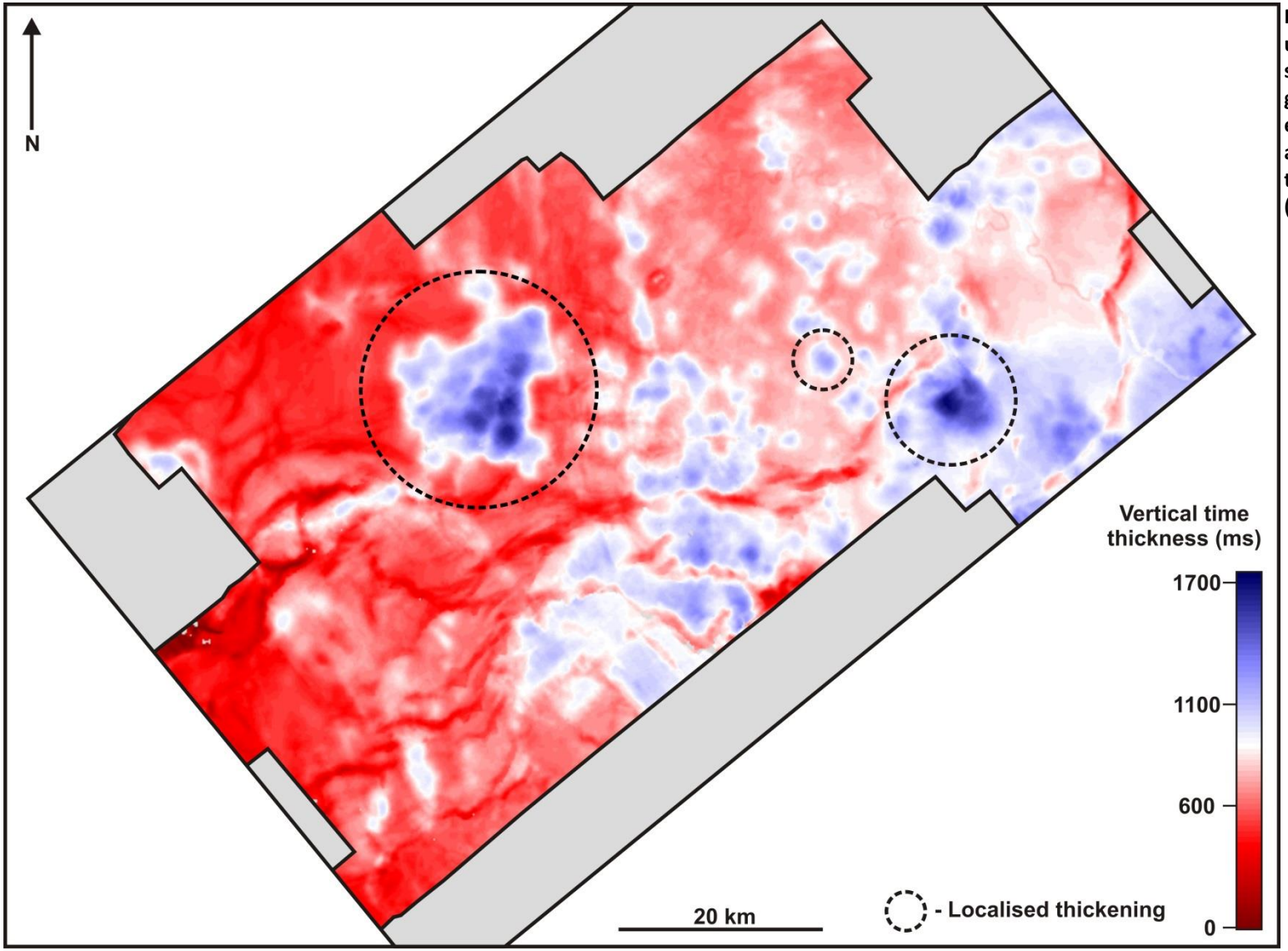

Figure 3.12 An isopach map of the unit 4 (U4), the Pliocene to Recent succession. The succession generally increases towards to the east. Examples of areas of localised and anomalous increases in thickness have been highlighted (circles with black dashed line).

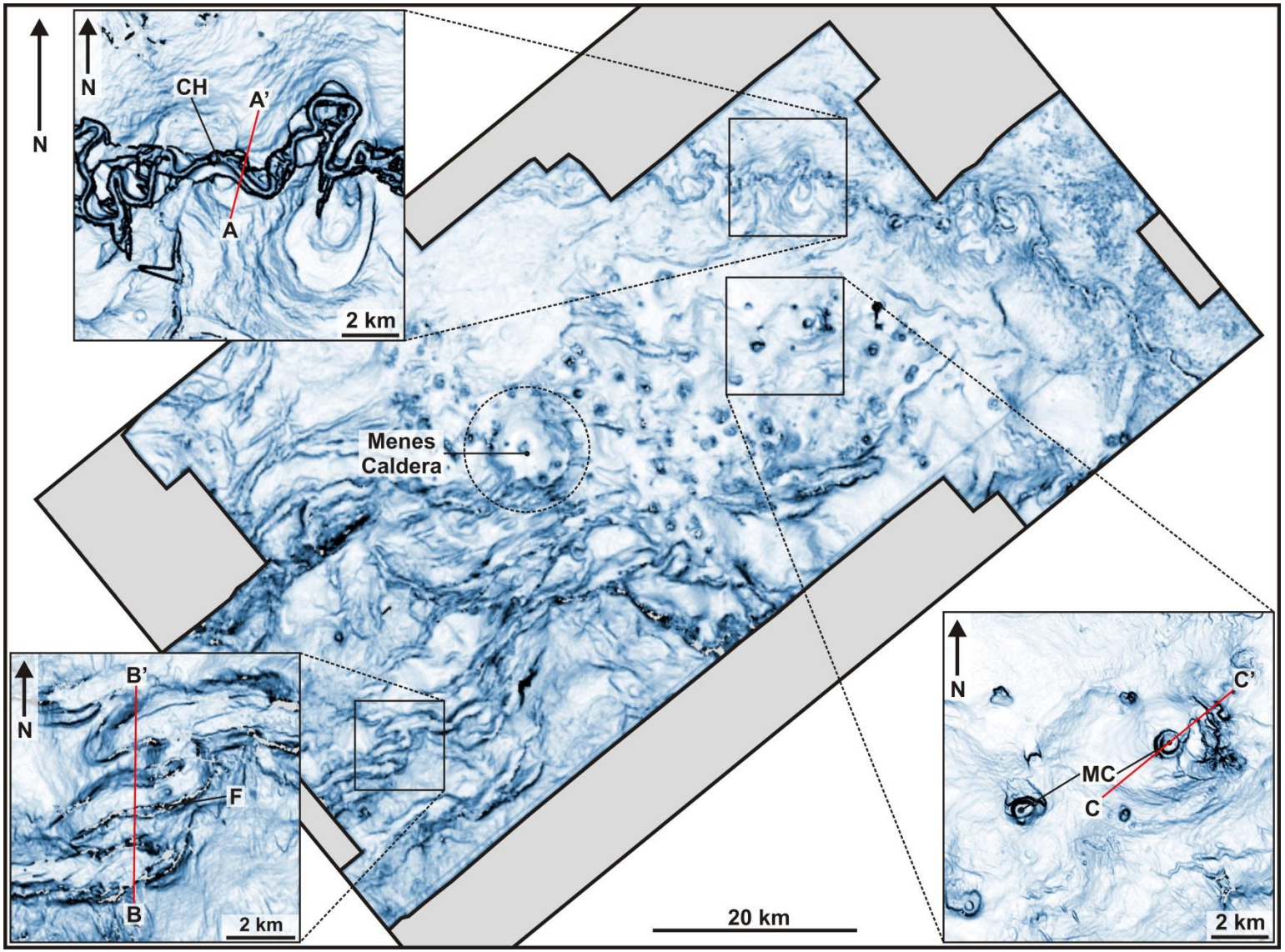

Figure 3.13 Seafloor time-dip map. Channels, faults, mud volcanoes and the Menes caldera are highlighted. The lines of section for the seismic profiles in Figure 3.14 are displayed. CH – Channel; F – Fault; MC – Mud cone.

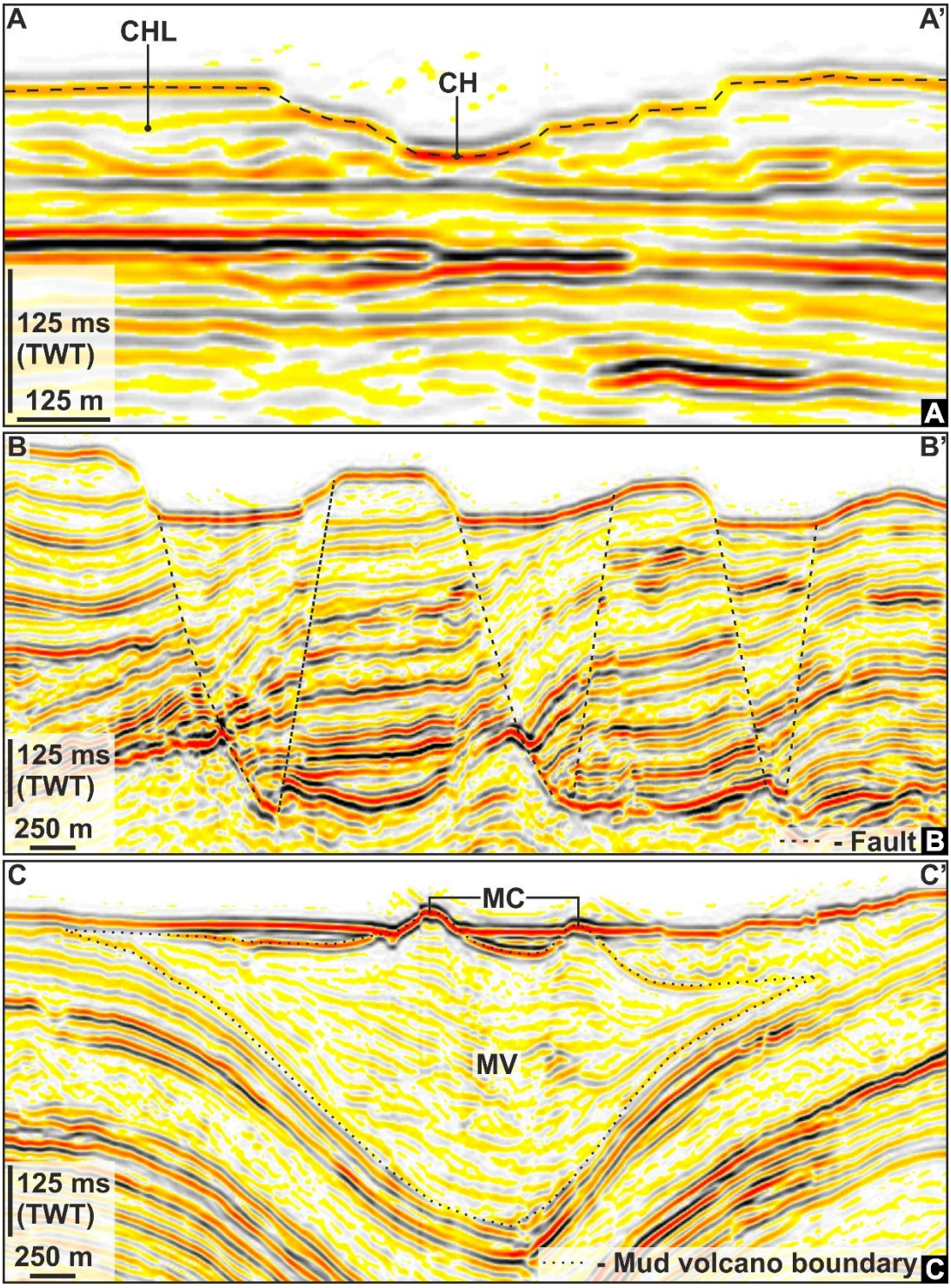

Figure 3.14 Seismic profiles through seafloor features. A: Seismic profile through a channel and channel levees at the seafloor. B: Seismic profile through faults within the Pliocene to Recent succession that propagate to the seafloor. C: Seismic profile through a mud volcano that displays a mud cone at the seafloor. The lines of section for these seismic profiles are displayed in Figure 3.12. CH – Channel; CHL – Channel levees; MV – Mud volcano; MC – Mud cones.

Pliocene to Recent succession predominantly comprise of a coherent reflective depositional unit, with variable amplitude, and high lateral continuity and frequency seismic facies, which similar to as observed in unit 2 is typical of hemipelagic deposits. The Pliocene to Recent succession exhibits numerous localised and sub-circular to irregularly shaped areas of anomalous thickening (Figure 3.11). At its greatest two-way-time thickness, the post-salt overburden is c. 1700 ms and at its thinnest it is as little as c. 50 ms (Figure 3.11). It is within this stratigraphic unit that the majority of geological features described within this thesis are observed.

A large number of mud cones associated with mud volcanoes can be observed at the seafloor (Figure 3.12 and Figure 3.14). As well as the numerous mud cones described at the seafloor there are also hundreds of buried paleo mud cones throughout the post-salt overburden (Figure 3.6), which are described in Chapter 5. Other fluid escape features within this study area include a large number of fluid escape pipes with pockmarks at their upper termination, which are described in Chapter 6. Similar to the mud volcanoes, as well as pockmarks that are visible at the present day seafloor, many can also be observed buried throughout the post-salt overburden.

West of the centre of the study area, a prominent sub-circular depression that is c. 8 km in diameter can be observed at the seafloor (Figure 3.12). This seafloor depression has been previously documented and been named as the Menes Caldera and is thought to comprise a highly active area of mud volcanism and brine seepage (Huguen et al., 2009; Pierre et al., 2014; Mascle et al., 2014; Dupré et al., 2014). The seafloor depression is also spatially correlatable with a localised area of increased thickness of the Pliocene to Recent succession and a base-salt depression (Figure 3.9 and Figure 3.11). The Menes caldera and the geometry of the underling succession associated with the seafloor depression are described in greater detail in Chapter 5.

A mass transport deposit can be observed buried in the northeast of the study area (Figure 3.6), which is described in detail in Chapter 5. Widespread slope instability in this region has been suggested to be related to changes in sediment supply, sea level change, earthquakes or the circulation of gas rich fluids within subsurface

sediments (Loncke et al., 2004; Garziglia et al., 2008; Loncke et al., 2009). The seafloor channel and levee complex observed in the northeast of the study area displays a NW-SE orientation (Figure 3.12). This channel is characterised by a typical bowl shape and sloping levees at the flanks in seismic profile (Figure 3.14A). The levees comprise a chaotic but very high amplitude seismic facies and the concave reflection of the channel is high amplitude. It is possible that this channel and levee system is a branch of the Rosetta channel system discussed above.

A large number of faults can be observed within the post-salt overburden (Figure 3.12 and Figure 3.14). Faulting is present throughout the study area, however, there is a particularly high frequency of faults within the southwest, the majority of which strike in a NE-SW orientation (Figure 3.12). Some of these faults display throw of 10s to 100s of meters. They can be observed displacing the reflection of Horizon M but correlatable displacement has not been observed at horizon N, which suggests that these faults detach within the evaporite unit.

3.6 Hydrocarbon potential and exploration history

The main source rocks within the NDSF region are found in either Upper Cretaceous black shales, Oligocene/Miocene gas rich sediments and even in Pliocene sapropels with very high TOC values (Loncke et al., 2004). Potential reservoirs are localised in Miocene distal terrigenous deposits or in reefal limestones and Pliocene channel complexes (Loncke et al., 2004). Pliocene targets have been readily identified by direct hydrocarbon indicators (DHIs) in seismic data, which have enabled a sustained industry success rate of 90% (Dolson et al., 2005). Thermogenic hydrocarbon accumulations have been discovered in Pliocene to Pleistocene deep-water channel and basin-floor turbidite sands, Upper Miocene fluvial and/or turbidite sands and in pre-salt distal turbidites (Aal et al., 2000).

Likely gas origins within the NDSF are thought to be related to: (1) deep sourced thermogenic or biogenic fluid migration towards the seabed (Aal et al., 2000; Samuel et al., 2003; Loncke et al., 2004); (2) shallow sourced fluid (gas) generation

(Gontharet et al., 2007a); (3) a combination of both thermogenic and biogenic fluid in the form of microbial and thermogenic methane(Vandré et al., 2007).

In 2011, Shell relinquished its vast Northeast Mediterranean (NEMED) licence in Egypt's deep water Nile delta. In 10 years of exploration, the company made two gas discoveries named La52-1 and Kg45-1 but decided against pursuing them because of "challenging economics" (Economist, 2011). Blocks 11, 12 and 13 of that licence are located as little as c. 55 km northeast of the El Dabaa survey area (Figure 3.15). In 2012 these blocks were auctioned off by the Arab Republic of Egypt Ministry of Petroleum and Mineral Resources and the Egyptian Natural Gas Holding Company, whom at the time publically released technical reports on these areas. These technical reports include information on various Pliocene and Messinian play concepts, including details on the source, reservoir, trap and seal.

For the Pliocene plays, basal Pliocene shale allegedly provide an effective source rock for biogenic gas and high porosity and permeability sands within slope turbidite channel complexes represent the reservoir rocks. The basal Pliocene shale referred to in these reports is accompanied by a seismic profile (Figure 3.16). Structural traps such as three way dip closure are the main trapping style identified, while thick interbedded shales have good sealing capacity. Oligocene to Miocene terrestrial and marine deposits and sands within channel/levee systems below and in between the Rosetta Anhydrite are considered the main source and reservoir rocks for the Messinian plays (Figure 3.17). The Rosetta Anhydrite acts as an effective seal and the main traps include structural traps such as a four way dip closure and partial stratigraphic traps (EGAS, 2012a; EGAS, 2012b; EGAS, 2012c).

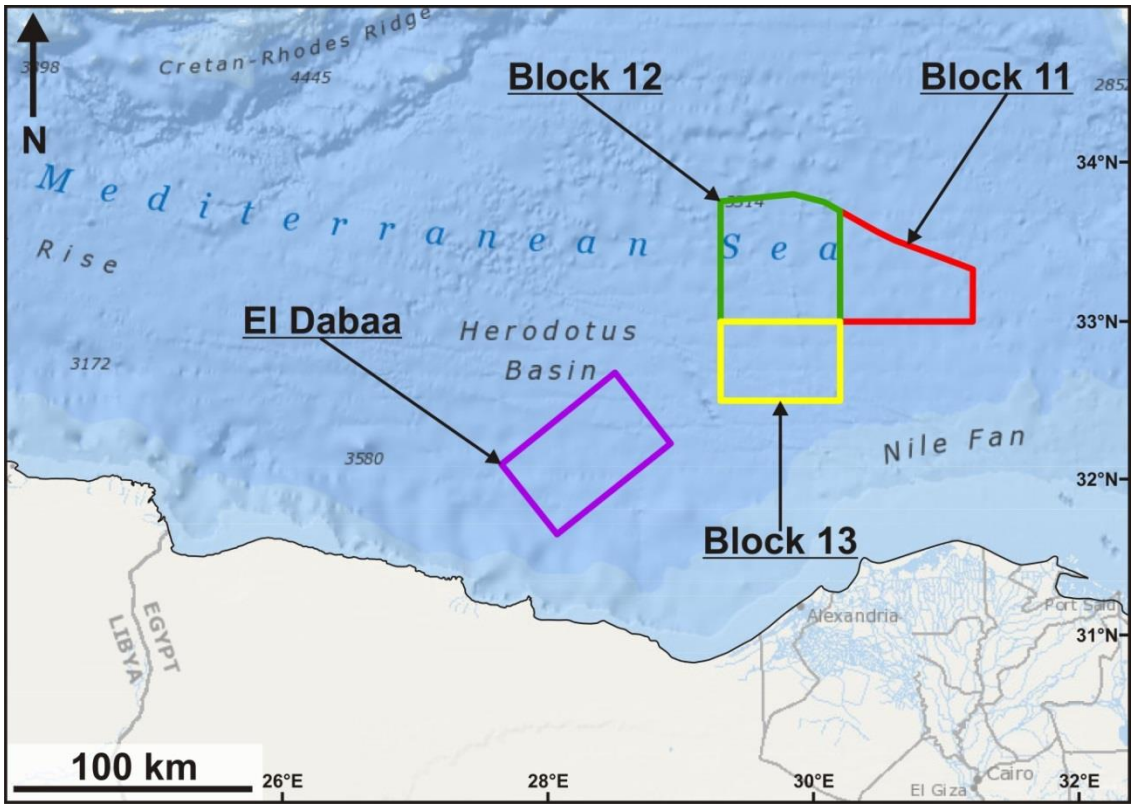

Figure 3.15 Exploration blocks. A location map of offshore Egypt and the Nile delta showing the geographical position of the El Dabaa survey area and the relinquished blocks 11, 12 and 13 from Shell's NEMED licence. The El Dabaa survey area and Block 13 to the NE are separated by a mere 55km.

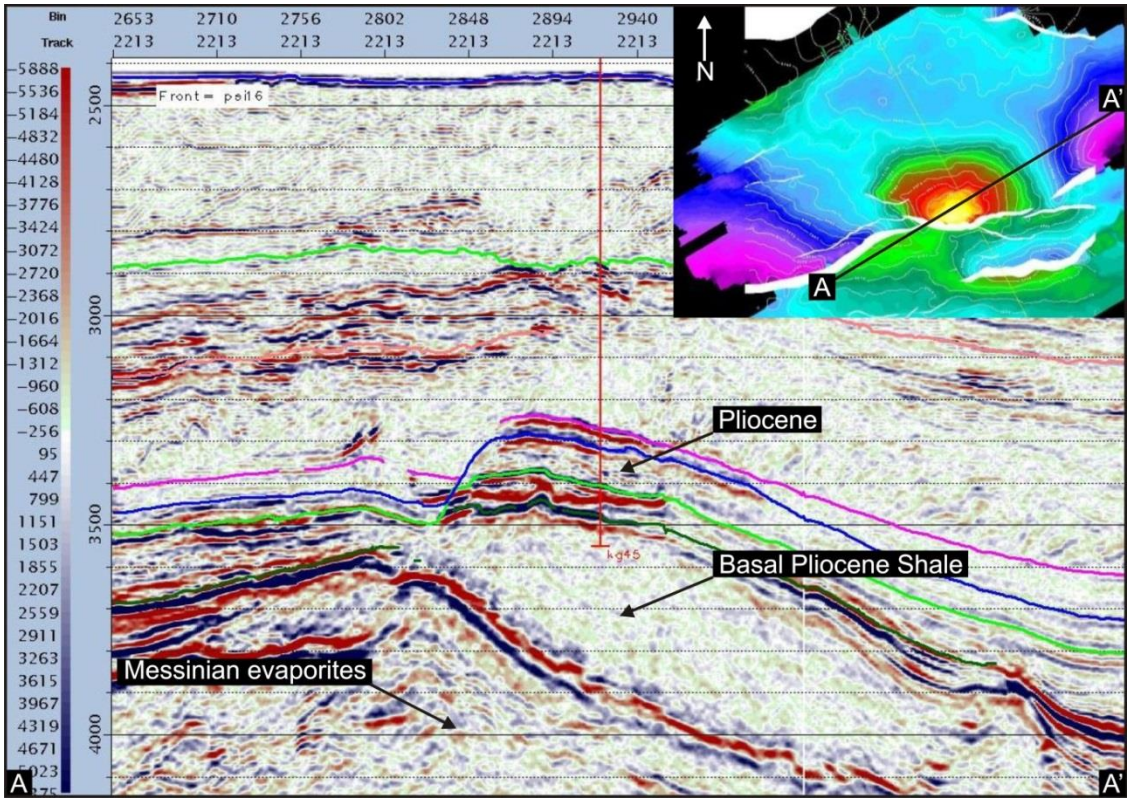

Figure 3.16 Basal Pliocene shale. A map from Shell's relinquished NEMED licences showing the line of section for the above seismic profile through one the basal Pliocene shale. These basal Pliocene shales were described as an excellent source rock for Biogenic gas. Image modified from (EGAS, 2012c).

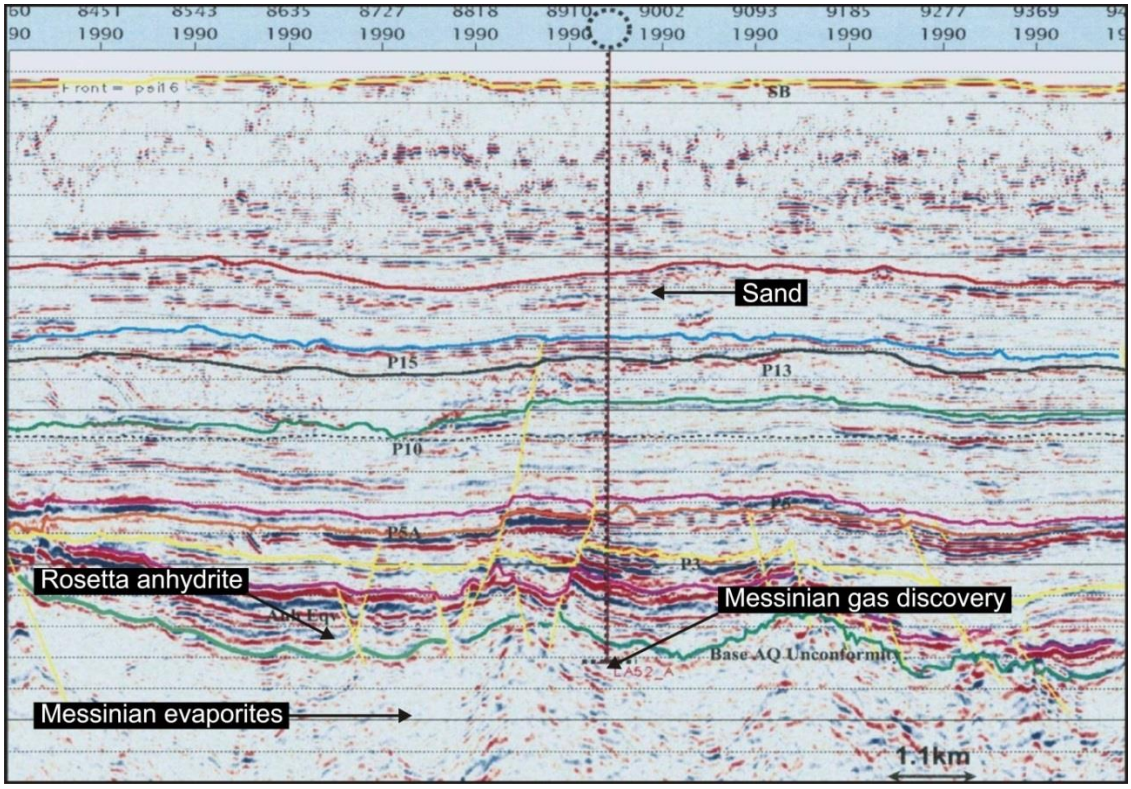

Figure 3.17 Messinian gas discovery. A seismic profile from Shell's relinquished NEMED licences showing a Messinian gas discovery and the Rosetta anhydrite at the top of the Messinian evaporite sequence, which is considered to create an effective seal. (Image modified from (EGAS, 2012a).

Chapter 4

4 Giant mud volcano formation within the Western slope of the Nile Cone

4.1 Abstract

A three dimensional seismic survey located on the western slope of the Nile Cone, is used within this chapter to interpret a suite of giant lensoid bodies emplaced onto the upper surface of the c. > 1 km thick Messinian evaporite succession. The convergence of the bounding reflections of these lensoid bodies, their isopach distribution, relief at their upper surface and the stratal geometries of the bodies and underlying and overlying deposits leads to the conclusion that these are giant mud volcanoes. These giant mud volcanoes all erupted at the end of the Messinian Salinity Crisis, the largest of which has a volume of over c. 116 km^3. The source of these extruded bodies is in the pre-Messinian stratigraphy, and implies massive remobilisation and intrusion through the thick evaporite layer. It is argued here that the huge mud fluxes and timing of eruption was primed and triggered by high overpressure in the pre-salt sediments generated through their rapid burial and loading during the Messinian Salinity Crisis and catastrophic re-flooding during its immediate aftermath. These interpretations combined with the stratal position of the giant mud volcanoes demonstrate the potential for a major phase of highly focused fluid and mud expulsion and venting of overpressure at the climax of the Messinian Salinity Crisis. The absence of internal stratigraphy and interdigitation at the margins results in a single body form, which implies that they were extruded in a single eruptive phase. Drawing analogy with extrusive fluxes measured for the modern Lusi eruption in Indonesia, implies the potential for an eruptive period of several millennia.

4.2 Introduction

Mud volcanoes are one of the most impressive natural hydrodynamic structures formed via fluid, gas and sediment extrusion (Hovland and Judd, 1988; Kopf, 2002). They are widely developed in highly mobile tectonic belts and in some intra-plate settings (see Kopf, 2002). They are particularly prevalent in settings that experience rapid sedimentation, thrust loading or active horizontal tectonic compression (Milkov, 2000). Previous studies within the western province of the Eastern Mediterranean, which is located on the Egyptian passive margin, have already identified extensive mud volcanism at the surface, predominantly via observations from bathymetric maps, piston cores and sonar data (Loncke et al., 2004; Giresse et al., 2010; Dupré et al., 2010; Huguen et al., 2009) (Figure 4.1). However, document analyses of the vast number of mud volcanoes that are buried within the region is relatively limited (Dupré et al., 2014; Mascle et al., 2014; Pierre et al., 2014).

With the use of 3D seismic data, it has been possible to identify several types of fluid escape structures within the Western province of the Eastern Mediterranean. This includes over 300 conically shaped mud volcanoes, which are the primary focus in Chapter 5 and so will be described and discussed in greater detail at a later point. As well as numerous conical mud volcanoes, a small number of irregularly shaped and very large mud volcanoes, which are of an order of magnitude larger by volume than the smaller and conical mud volcanoes, have also been observed within this study area. It is these giant mud volcanoes that will be the focus of this chapter. Measurements of their size will be based on maximum diameter, thickness, area and volume. Other mud volcanoes of significantly large volumes have been identified within other sedimentary basins including the Mediterranean Ridge (Kopf et al., 2001) and also the South Caspian Basin where Davies and Stewart (2005) documented the discovery of allegedly the largest mud volcano yet described, which has a volume of c. 22.5 km^3 (Figure 4.2).

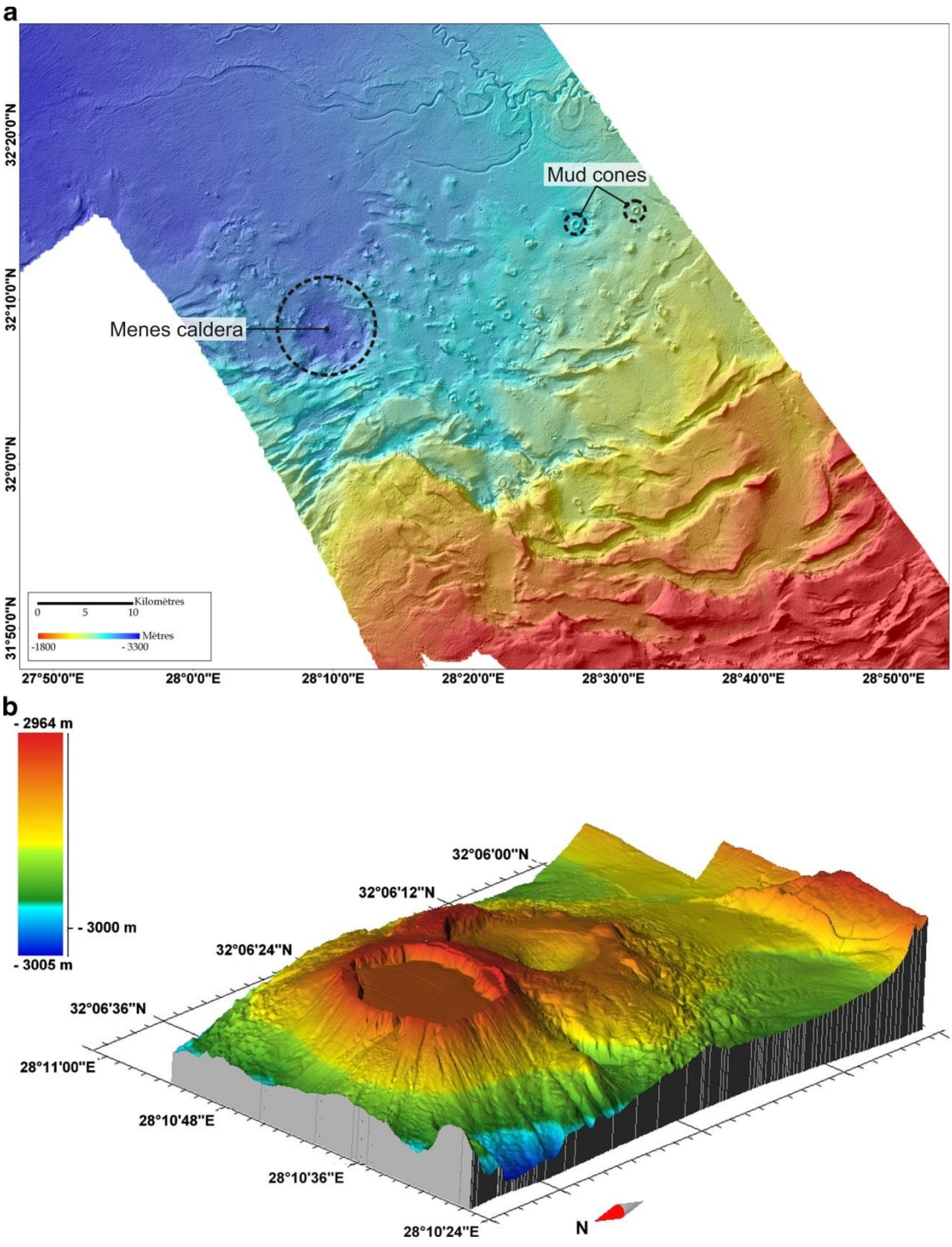

Figure 4.1 An example of recent research on mud volcanoes within this study area. a: A map of the seafloor within the western province of the Eastern Mediterranean. The map is characterised by numerous mud cones and the seafloor depression of the Menes caldera. b: a seafloor map of two mud cones that are located within the Menes caldera. (Modified from Mascle et al. (2014))

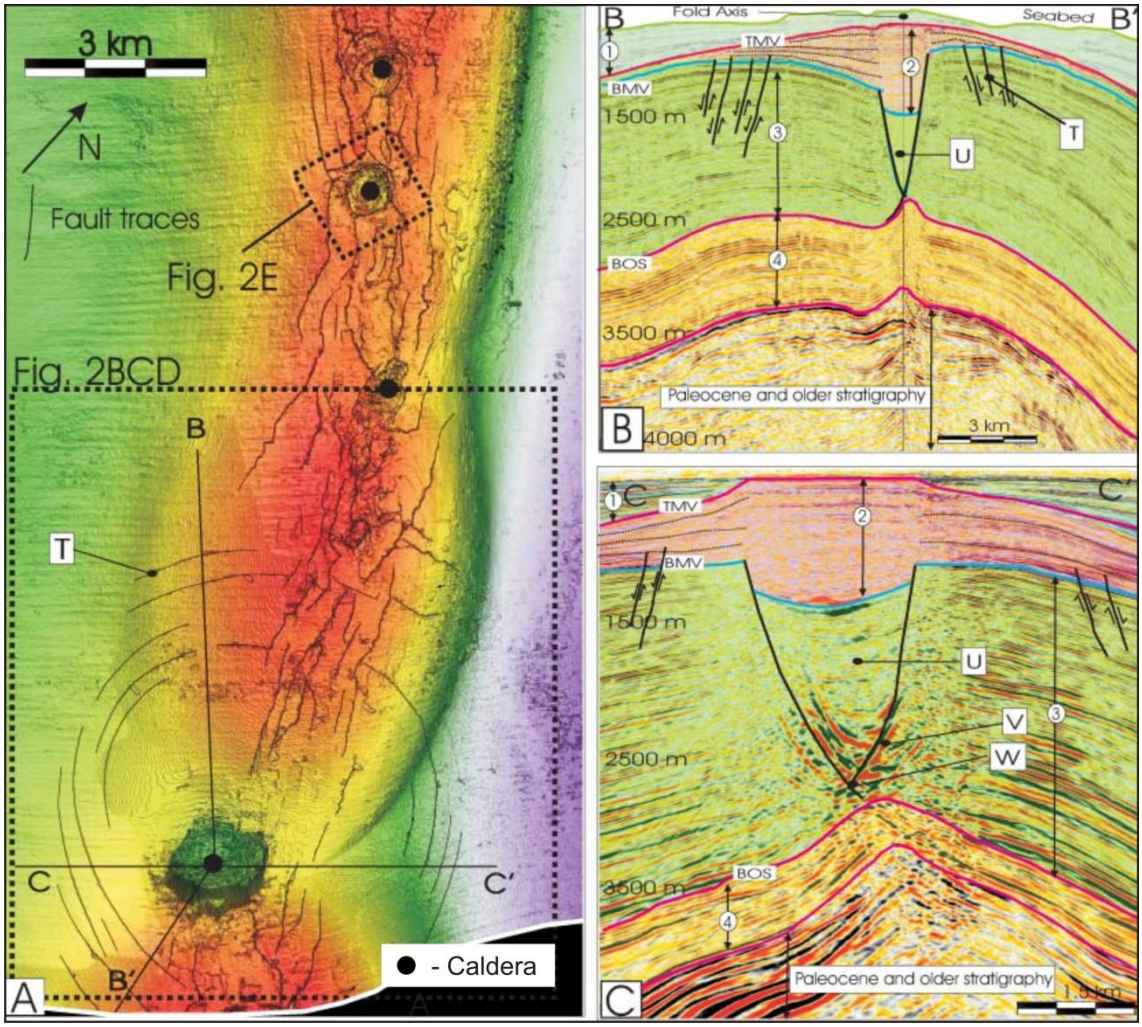

Figure 4.2 Largest mud volcano yet described, South Caspian Basin. A: Map of the basal surface of the mud volcano (red= high; purple = low) showing the location of four calderas and the location of the mud volcano in Figure 4.2B and Figure 4.2C, within the dashed box. B: Seismic profile through the mud volcano in Figure 4.2A. C: A seismic profile through the mud volcano in Figure 4.2, perpendicular to the profile in Figure 4.2B. T – Concentric planar normal fault; U – Downward tapering cone; TMV – Top mud volcano; BMV – Base mud volcano; V – High amplitude dipping reflections (Modified from Davies and Stewart (2005)).

Over recent years, compelling evidence has been presented for extensive fluid venting events that are associated with the Messinian Salinity Crisis (Bertoni and Cartwright, 2015; Bertoni et al., 2013; Lazar et al., 2012). Giant pockmarks have been observed and described at the base of the Messinian evaporites, within the Levant Basin (Bertoni et al., 2013; Lazar et al., 2012). These pockmarks have been interpreted as related to large-scale methane venting at the onset of the Messinian Salinity Crisis as a response to water unloading (Bertoni et al., 2013; Lazar et al., 2012). These observations and interpretation pose a key question, is there evidence for other similar large-scale venting events associated with other stages of the Messinian Salinity Crisis, within the Eastern Mediterranean?

4.2.1 Aims and scope

The giant mud volcanoes and smaller and conical mud volcanoes described within this thesis are both formed via the ascent of fluids and mud through a lithological succession, until eventually they are extruded over the seafloor and form constructional mud volcanoes of varied morphology (Dimitrov, 2002; Kopf, 2002; Milkov, 2000). Other similarities that can be observed include the convergence of the top and basal reflections of the extruded bodies, which forms a morphology that is lensoid. They also display comparable seismic facies, which comprise low amplitude and discontinuous reflections internally and high amplitude reflections that define their margins.

Despite the similarities, there are significant differences between the giant mud volcanoes and smaller and conical mud volcanoes that have resulted in them being divided into two separate mud volcano types. The conical geometry of the smaller mud volcanoes contrasts with the irregular shape of the giant mud volcanoes. Size by volume is one of the most significant differentiating factors because; the giant mud volcanoes are generally several orders of magnitude larger. The giant mud volcanoes also cover a greater area and are thicker than the smaller and conical mud volcanoes. The one caveat to these contrasting characteristics is LB5 (described in section 4.3.2.5),

which is of a volume similar to some of the mud volcanoes described in Chapter 5. LB5, however, is analysed within this chapter with the giant mud volcanoes because of another significant differentiating factor, which is the stratigraphic position and timing of the formation of the mud volcano. All of the mud volcanoes descried in this chapter, including LB5, share the same regionally correlatable reflection as the basal reflection of their extruded body. The timing of their formation was, therefore, synchronous, which indicates that they may also share the same forming mechanisms.

In this chapter, using 3D seismic data I present a study based on a suite of giant mud volcanoes from the El Dabaa study region offshore Egypt (See section 3.2 of Chapter 3 for location) that were erupted at the end of the Messinian Salinity Crisis. The Messinian Salinity Crisis and events in the immediate aftermath, notably the sudden re-flooding during the Zanclean have recently been invoked as having exerted a major influence on the development of overpressure in basins in the Mediterranean region (Bertoni and Cartwright, 2015; Bertoni et al., 2013). Hence the documentation of large volume mud mobilisation at this time could potentially have major implications for our wider understanding of such a major environmental crisis.

The pre-stack time migrated 3D seismic data used in this study has a spatial resolution of c.25 m throughout the Pliocene to Recent. The velocity data used is based off pre-stack depth migrated data and is effective in showing the boundary between two units of contrasting p-wave velocity. This means that it is possible to clearly image the giant mud volcanoes within this study area. It is, therefore, possible to: (1) identify and analyse the geometry and seismic expression of the giant mud volcanoes; (2) take accurate measurements of their dimensions.

The aims of this chapter are to:

1. Describe the seismic characteristics and geometry of a suite of lensoid bodies.
2. Present compelling evidence that these lensoid bodies are in fact the product of surface eruption and, therefore, giant mud volcanoes.
3. Ascertain the source stratigraphy of mud and fluid.
4. Propose a model that explains the mechanisms and timing of formation of the giant mud volcanoes.

5. Place their occurrence in the wider genetic context of the basin pore pressure history linked to the Messinian Salinity Crisis.
6. Described the relationship between the giant mud volcanoes and the undulating top and base of the evaporites.

This study is primarily based on quantitative and semi quantitative analysis and description of these giant mud volcanoes. The primary foci of this chapter is, the extrusive and constructional bodies of these giant mud volcanoes and the implications that their stratigraphic position has with regards to timing and basin hydrodynamics, when married with key events in the geological history of the Eastern Mediterranean. Basin hydrodynamics here refers to the changes in pore fluid pressure within the sedimentary basin.

The accurate interpretation of the margins of these giant mud volcanoes is an important part of their analysis and is crucial for the conclusions that will be drawn in this chapter. There are, however, several factors that make the interpretation of their margins challenging at times. The Pliocene to Recent succession within this region of the Eastern Mediterranean is tectonically mature (as stated in section 3.3 of Chapter 3), which has resulted in growth faults, salt pillows and crestal grabens within this study area (Dupre et al., 2007; Garziglia et al., 2008; Loncke et al., 2009; Dimitrov, 2002). The impact of these kinematics on the giant mud volcanoes is that numerous faults have propagated through and partially compartmentalised them, resulting in a highly deformed lensoid body. Significant amplitude attenuation and disruption of the seismic reflections beneath the central region of these mud volcanoes can make interpreting their basal bounding reflection problematic.

The internal reflections of the giant mud volcanoes are of a low amplitude and discontinuous seismic facies, similar to the underlying Messinian evaporites (Figure 4.3). This means that their appearance is relatively similar in seismic profile and that interpreting the boundary between the base of the giant mud volcanoes and the top of the salt can be problematic, especially in areas where the seismic reflectors are disrupted and attenuated. To ensure the interpretation of the margins of these mud volcanoes is accurate, they have been iteratively mapped using pre-stack time

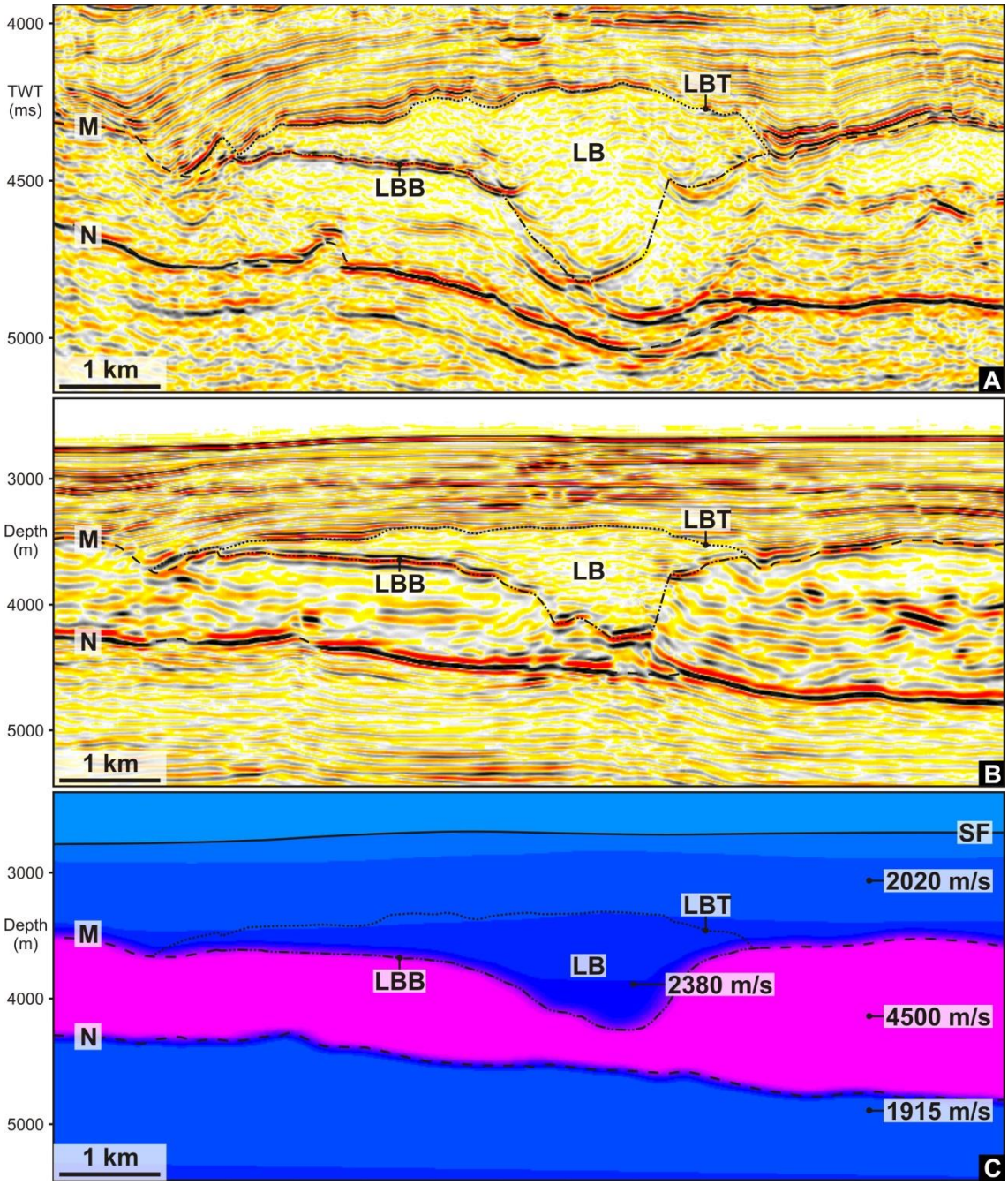

Figure 4.3 PSTM, PSDM and velocity profiles through a lensoid body. A: PSTM seismic profile through a lensoid body. B: PSDM seismic profile through a lensoid body. C: Velocity profile through a lensoid body. SF – Seafloor; LB – Lensoid body; LBT – Lensoid body top; LBB – Lensoid body base; M – Horizon M; N – Horizon N.

migrated data, with constant reference to the pre-stack depth migrated and velocity data (Figure 4.3). The velocity data is based off the pre-stack depth migrated data and the contrast in velocity between the giant mud volcanoes and the Messinian evaporites clearly defines the boundary between the two (Figure 4.3).

The seismic picking of the mud volcanoes below has been conducted primarily on the pre-stack time migrated data, as it is the volume within which these mud volcanoes are displayed most clearly and, therefore, enables the maximum extent of these mud volcanoes to be interpreted. The images displayed in the figures within this chapter represent those that best display the true seismic expression of these giant mud volcanoes. The regional geology of the study area is presented in Chapter 3.

4.3 Results

4.3.1 Observations from three-dimensional seismic data

Preliminary analysis of seismic profiles revealed that the top-salt and base-salt reflections of Horizon M and Horizon N are highly irregular within this study area. Horizon M and N are regionally extensive reflections that correlate with the onset of the Messinian Salinity Crisis (5.9 Ma) and its climax (5.33 Ma) respectively (discussed in section 3.5.3 of Chapter 3). Based on this observation, initial seismic picking focused on the regional mapping and interpretation of these two undulating reflections.

Mapping of Horizon M throughout the study area revealed numerous large, circular to irregular depressions greater than c. 1000 m deep (Figure 4.4), while mapping of Horizon N similarly revealed large depression up to c. 800 m and mounded areas of relief up to c. 700 m (Figure 4.5). The Pliocene to Recent succession that overlies the top of the Messinian evaporites predominantly comprises a highly coherent reflective depositional unit, with variable amplitude, and high lateral continuity and frequency, which is considered typical of hemipelagic deposits (Figure 4.6). In a small number of instances, these large top-salt depressions are observed to

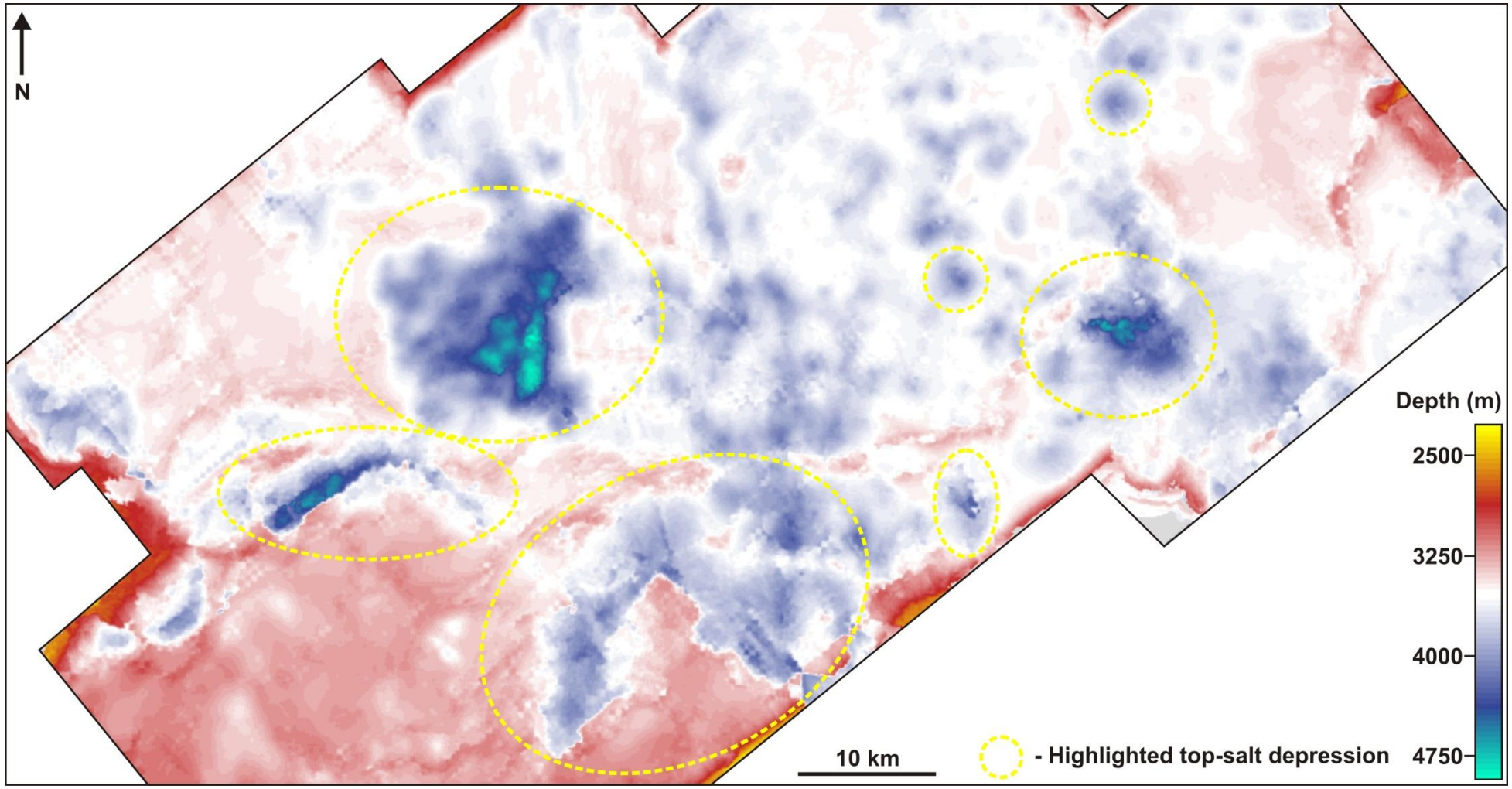

Figure 4.4 Depth map of the top-salt (Horizon M). The depth map displays numerous large and irregular shaped depressions (blue), some of which have been highlighted by circle/ellipses with yellow dashed lines.

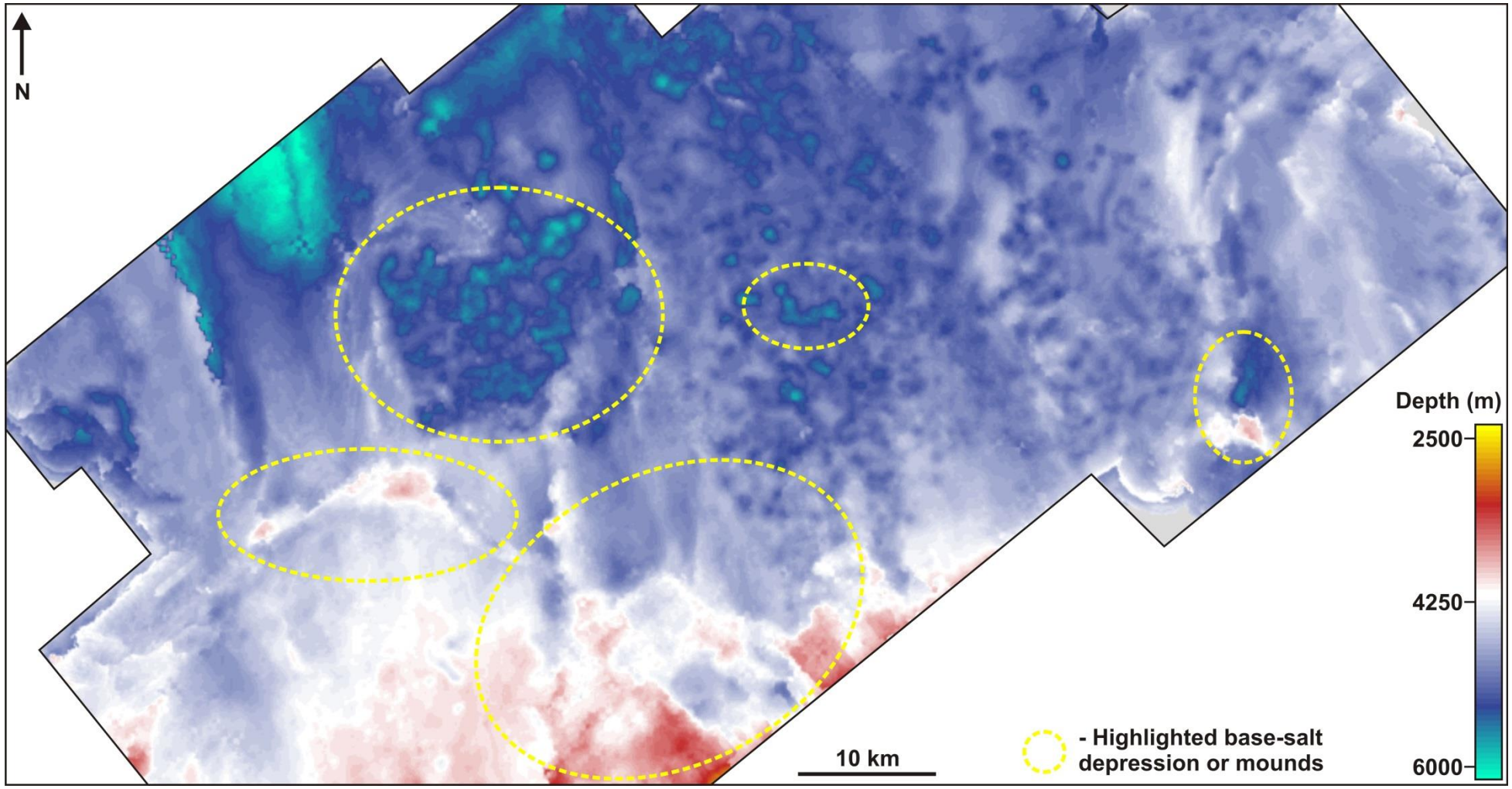

Figure 4.5 Depth map of the base-salt (Horizon N). The depth map displays numerous large and irregular shaped depressions (white-blue) and mounds (white-red), some of which have been highlighted by circle/ellipses with yellow dashed lines.

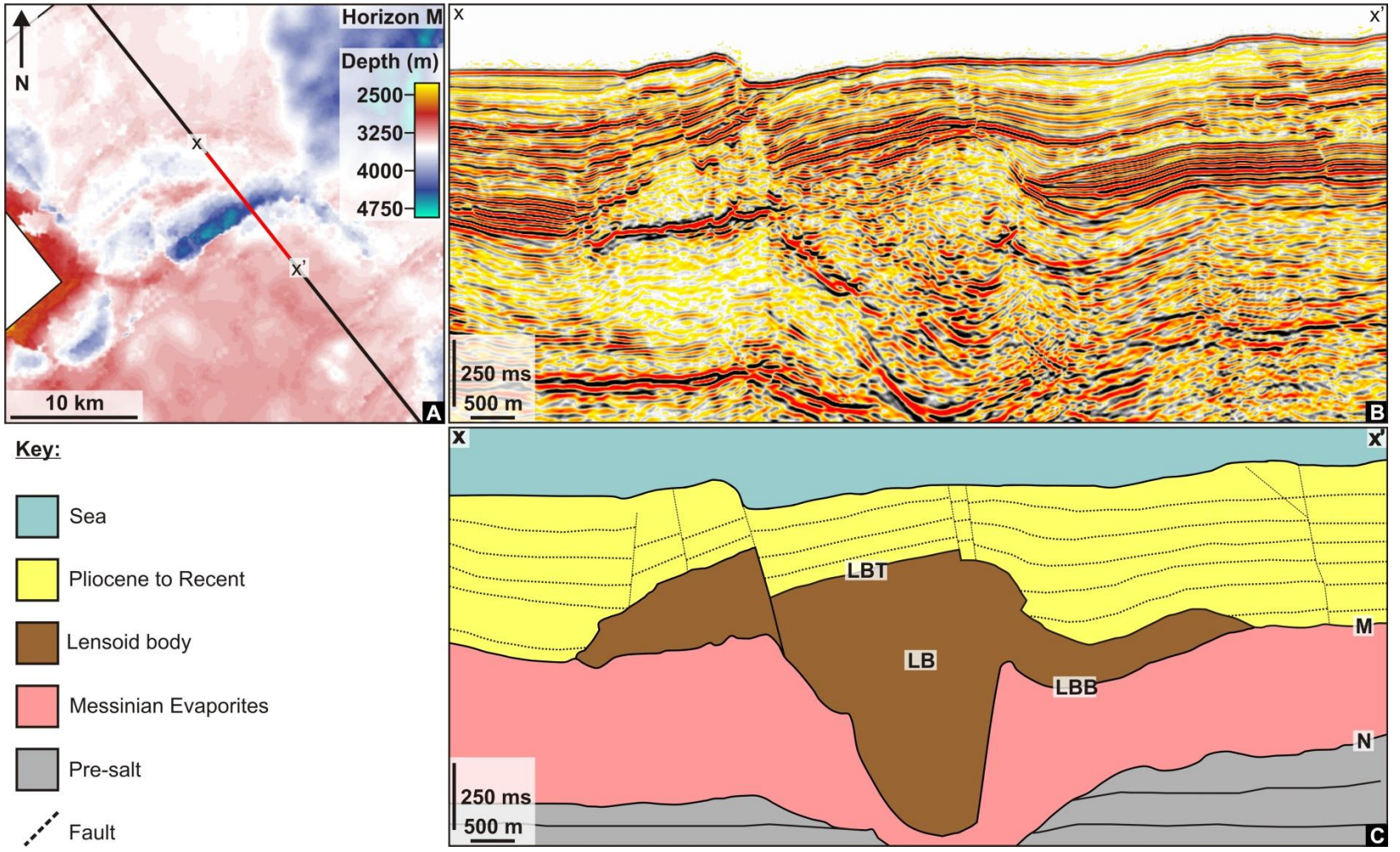

Figure 4.6 A lensoid body in seismic profile. A: A depth map of the top-salt (Horizon M) displaying a large and irregular shaped depression and the line of section for Figure 4.6B. B: A seismic profile through the depression displayed in Figure 4.6A. C: A cartoon profile of the seismic profile in Figure 4.6B, showing interpretation of the main successions based on contrasts in seismic facies. LB – Lensoid body; LBT – Lensoid body top; LBB – Lensoid body base; M – Horizon M; N – Horizon N.

be overlain by seismic facies comprising reflections that are chaotic to discontinuous, low frequency, and generally low amplitude with localised high amplitude anomalies (Figure 4.6). These seismic facies contrast with those of the hemipelagic deposits that overlie the top of the evaporites across the majority of the study area. This difference prompted an investigation into why there was this contrast above some top-salt depressions.

High amplitude and continuous reflections of the hemipelagic deposits overlie the low amplitude and discontinuous seismic facies of the anomalous lithology that is described above (Figure 4.6). This contrast in seismic facies means that the boundary between these two lithologies is clearly visible. The upper surface of the anomalous lithology is defined by a continuous and negative reflection, which signifies a reduction in acoustic impedance across the interface (Figure 4.6). The interface between the base of the anomalous lithology and the underlying Messinian evaporites produces a high amplitude and positive red reflection, which signifies an increase in acoustic impedance. This reflection is in fact the regionally correlatable reflection of Horizon M (Figure 4.6). Importantly, seismic interpretation of these two reflections revealed that the upper negative reflection of the anomalous lithology converges by onlap or downlap with its basal surface, which is Horizon M (Figure 4.6). This means that this lithology is not regionally extensive and forms a lensoid body that sits directly on top of the Messinian evaporites.

4.3.2 Seismic expression and geometry of the lensoid bodies

Qualitative and semi-quantitative analysis was carried out on five lensoid bodies that have been interpreted directly overlying Horizon M. The areas of Horizon M that they overlie are characterised by irregular and enclosed depressions that are up to 400m deep and > 20 km long. Based on measurements taken using 3D seismic data, the lensoid bodies that are situated within these depressions exhibit variable maximum thickness (660 m to 1190 m), widths (3.27 km to 28.60 km) and volumes (1.25 km^3 to 116 km^3). Their geometry in planform varies from circular to irregular.

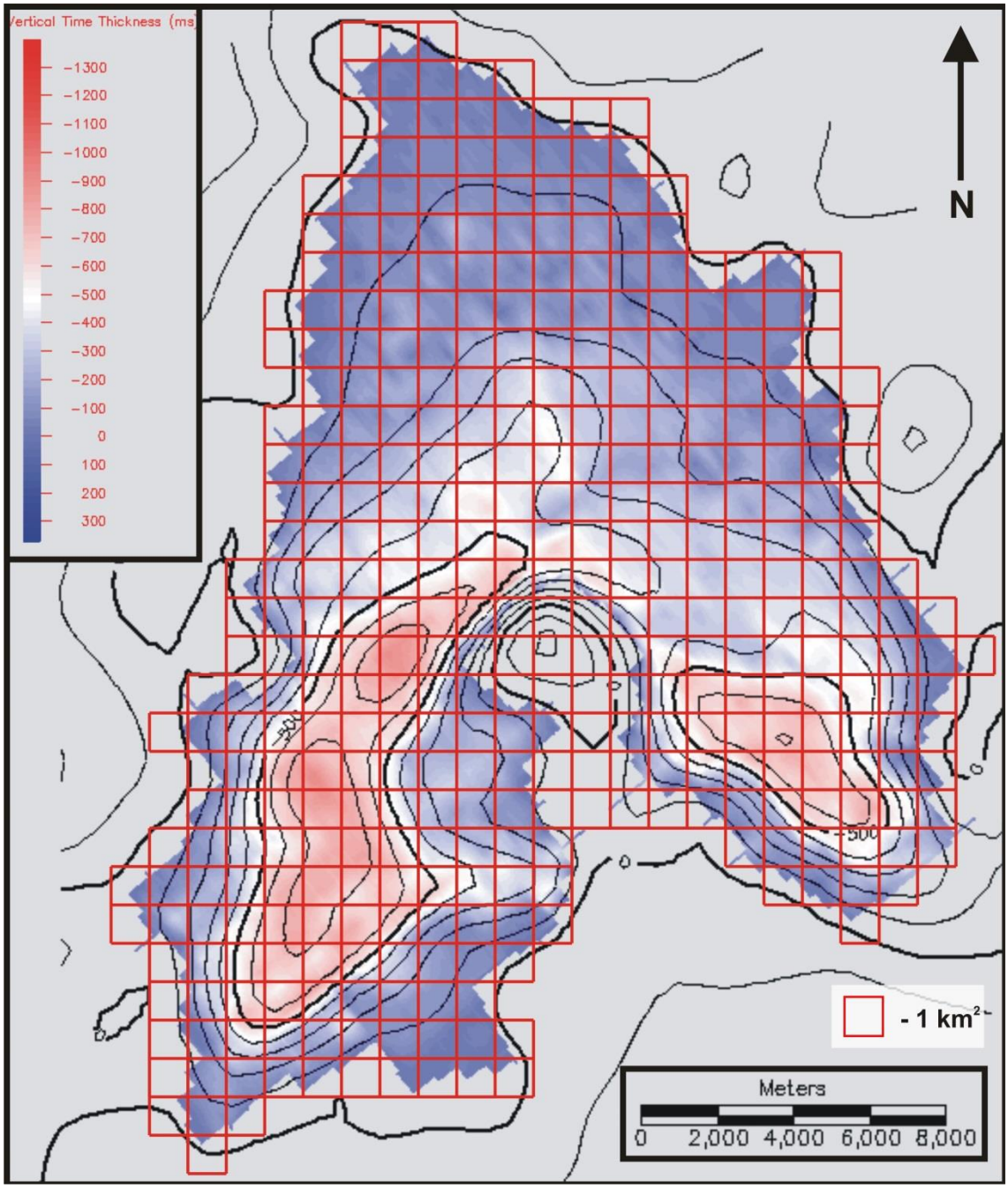

Figure 4.7 Isopach map LB1, overlain by contours and a grid comprised of 1 km^2 boxes. The contours and grid can be used to calculate the volume of LB1 in each 1 km^2 and be combined to give the total volume of the lensoid body. Location of LB1 can be seen in Figure 4.8.

They exhibit their greatest thickness centrally and decrease in thickness towards their margins, where their upper and lower surface converge (Figure 4.8).

The various dimensions of these lensoid bodies (width, thickness, area and volume) are measured and recorded from 3D seismic data. Accurately measuring the volume of these lensoid bodies is very important as it is used here as means to quantify the size of a lensoid body. In order to measure their volume, firstly the upper and basal bounding reflections were picked using seismic interpretation software (see section 2.2.3 of Chapter 2). By combining these two mapped reflections it was possible to produce a contoured isopach map of the mud edifices. Exporting these two horizons to Golden Software Surfer 11 made it to produce 3D models and to calculate the volume of space between the two horizons, therefore, giving the total mud edifice volume for each mud edifice. The full extent of the upper and basal reflections of the lensoid bodies is most clearly resolved within the pre-stack depth migrated. These surfaces were, therefore, picked within this volume and then depth converted using average interval velocities calculated using velocity data. In order to ensure that the volume calculated using Surfer 11 was accurate, another method of volume calculation was also used. This involved gridding the mud edifices contoured isopach map in boxes of $1km^2$ in area and combining them with the contours to calculate the volume of each cube and, therefore, eventually the entire edifice (Figure 4.7).

The high amplitude reflection of Horizon M clearly defines the boundary between the Messinian evaporites and the overlying lensoid bodies (Figure 4.3 and Figure 4.6). However, the seismic facies of the lensoid bodies and Messinian evaporites appear relatively similar in seismic profile (Figure 4.3 and Figure 4.6). It could be interpreted that the lensoid bodies are stratigraphically linked to the main evaporitic depositional systems. Importantly, the velocity data clearly shows that the lensoid bodies have a significantly lower average velocity than the evaporites (Figure 4.3C). The velocity contrast clearly defines a prominent boundary between the lensoid bodies and the underlying salt (Figure 4.3C). This argues strongly against these lensoid bodies being comprised of salt. The lensoid bodies are described in more detail below, to further expand on and clarify these interpretations.

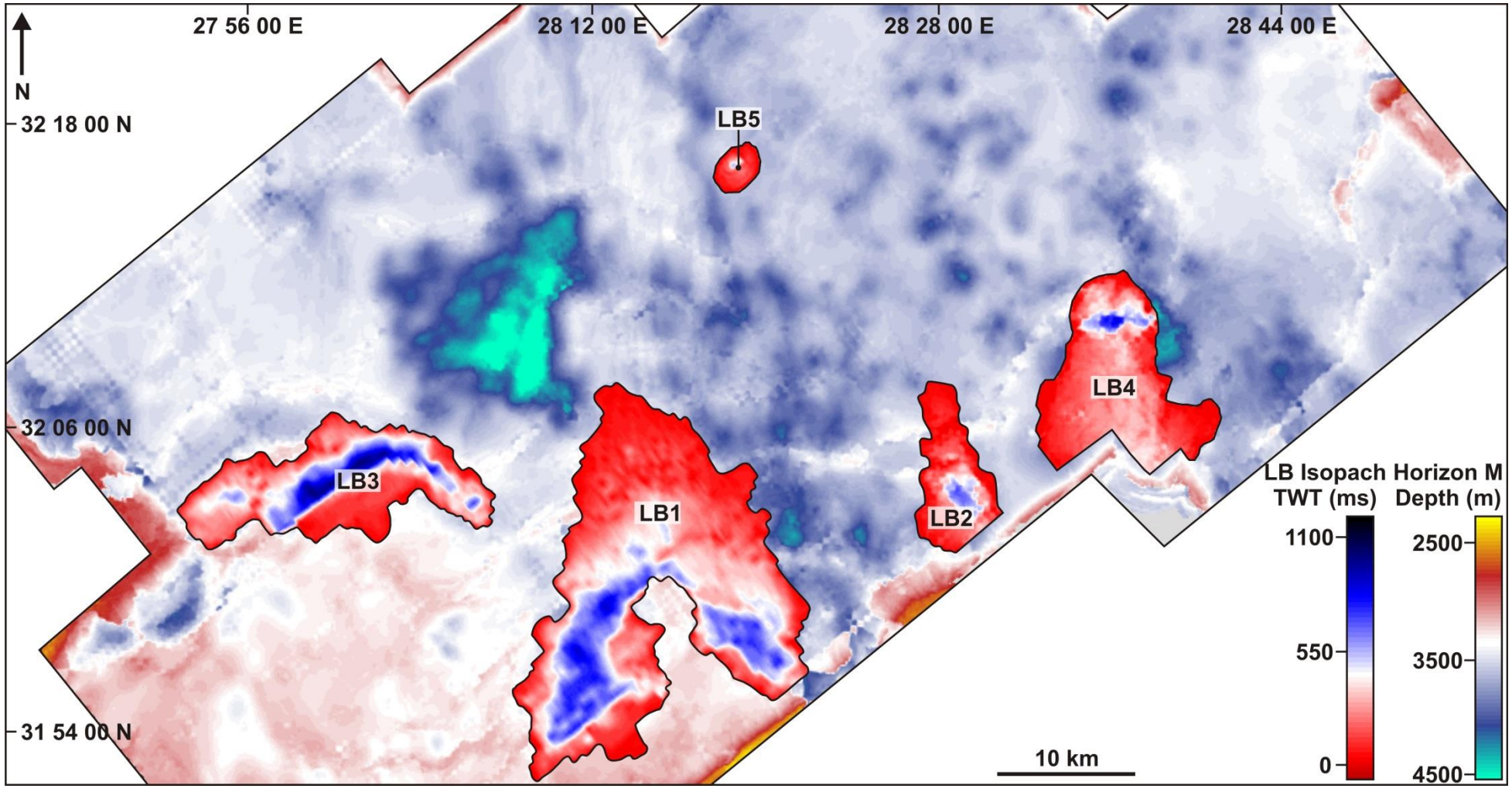

Figure 4.8 Lensoid body locations. A Depth map of top-salt (Horizon M), which has been overlain by an isopach map of the lensoid bodies. The isopach map displays the location of the lensoid bodies, the geometry in planform of the lensoid bodies and thickness variation within the bodies. LB – Lensoid body.

4.3.2.1 Lensoid Body 1 (LB1)

LB1 is located within the south central part of the study area at longitude 28.24401 E and latitude 32.01514 N (Figure 4.8). It has an asymmetrical shape in seismic profile, extends across a large section of Horizon M and appears heavily deformed by faults (Figure 4.9). It is the largest of the lensoid bodies in the study area with a maximum thickness of 900m, a depositional relief of up to 300 m , an area of 315 km^2 with an irregular, almost triangular planform, and a volume of 116 km^3 (Figure 4.10C). The overall form is asymmetric while a central ridge, which is the thickest part of the feature, separates a more gently 1.56° dipping upper surface towards the northern flank from a steeper 3.43° southern flank (Figure 4.10C). This upper bounding reflection of the lensoid body converges with basal bounding reflection, which is also the reflection of Horizon M (Figure 4.10B). The southeast margin of LB1 is clipped by the margins of the data. What has been clipped is away from LB1s thick central ridge and the lensoid body has already thinned significantly. Only a small fraction of its overall volume is, therefore, thought to have been unaccounted for.

Horizons M and N are both highly irregular beneath LB1. Horizon N hosts several depressions and an irregular ridge of relief directly beneath the lensoid body (Figure 4.11C), which is correlatable with the thickest areas of the lensoid body seen in Figure 4.10C. Horizon M displays a large depression beneath the lensoid body (Figure 4.11D), which is also correlatable with the thickest areas of the lensoid body seen in Figure 4.10C. The thickness of the evaporite succession decreases significantly where there is relief at Horizon N and a depression at Horizon M (Figure 4.11E). The reflections of the base of the lensoid body and Horizon N converge in some areas directly beneath LB1, which results in complete salt removal and a connection between LB1 and the pre-salt (Figure 4.11A and Figure 4.11E). This geometry can be seen clearly in a velocity profile due to the contrast in velocity between LB1, the evaporites and the pre-salt (Figure 4.11B). This connection has geometry in plan form which is visible as an irregularly shaped area of increased discontinuity in variance (Figure 4.12C).

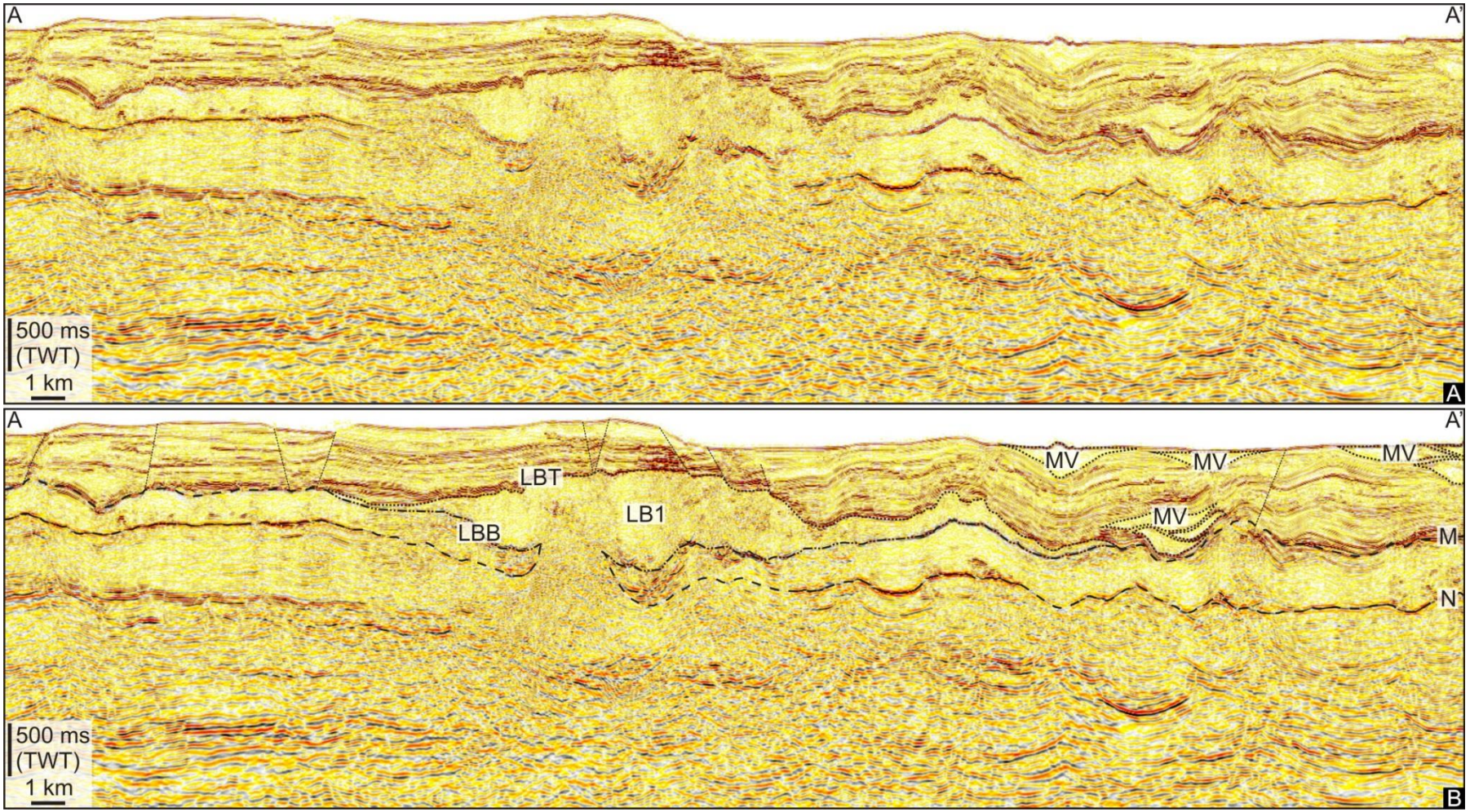

Figure 4.9 Seismic profile of lensoid body 1. A: An uninterpreted seismic profile through Lensoid body 1. B: The same seismic profile as in Figure 4.9A, showing the interpretation of Horizon M and Horizon N and the location of Lensoid body 1 and numerous mud volcanoes. LB1 – Lensoid body 1; LBT – Lensoid body top; LBB – Lensoid body base; MV – Mud volcanoes; M – Horizon M; N – Horizon N.

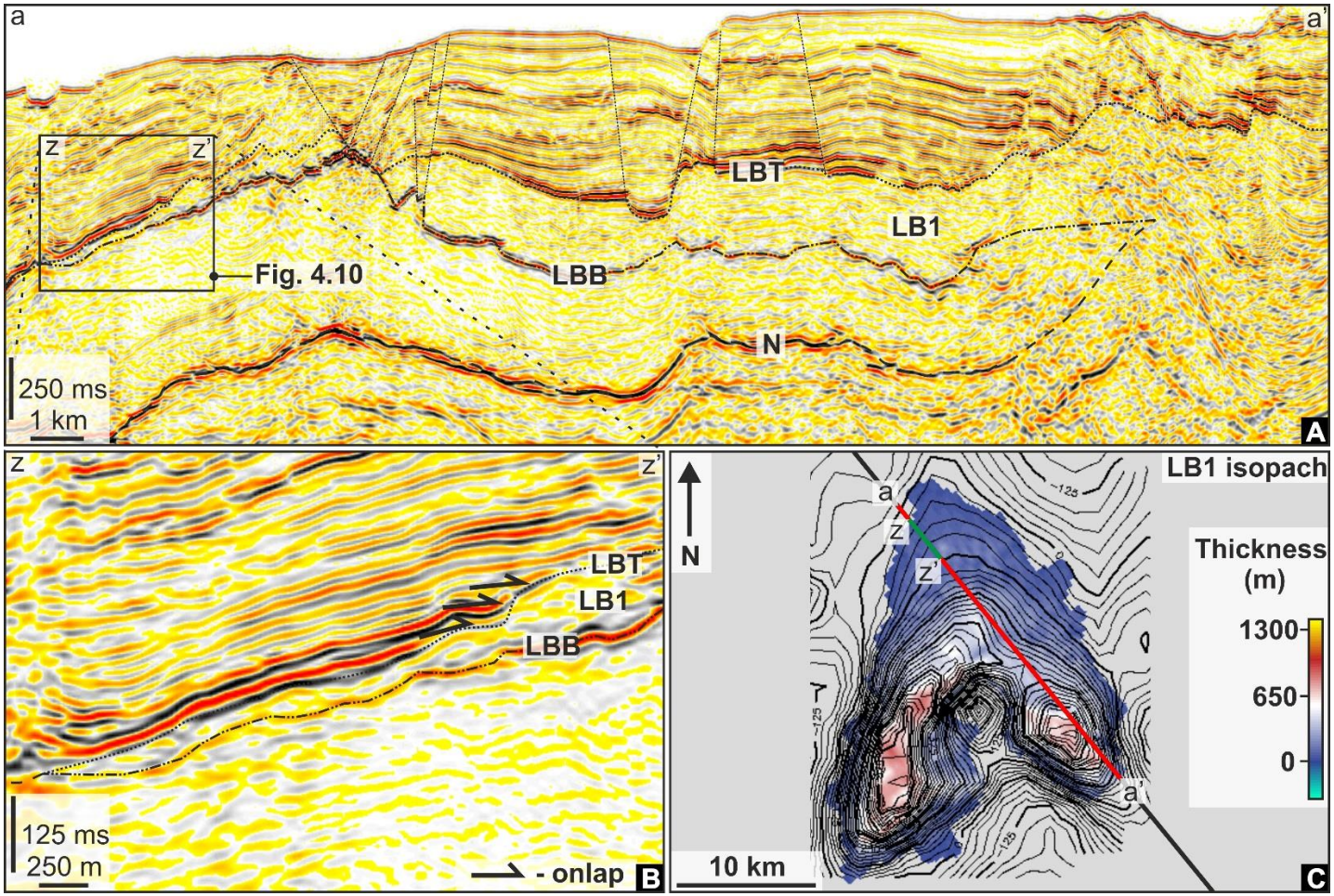

Figure 4.10 Interpretation of Lensoid body 1 and onlap. A: A seismic profile through Lensoid body 1, displaying an interpretation of the lensoid bodies top and basal reflections. B: A seismic profile through the margin of lensoid body 1, showing the convergence of the top and basal reflections. Reflections of hemipelagic deposits onlap onto the top reflection of the lensoid body. C: An isopach map of Lensoid body 1 and the line of section for Figure 4.10A and Figure 4.10B. LB1 – Lensoid body 1; LBT – Lensoid body top; LBB – Lensoid body base; N – Horizon N.

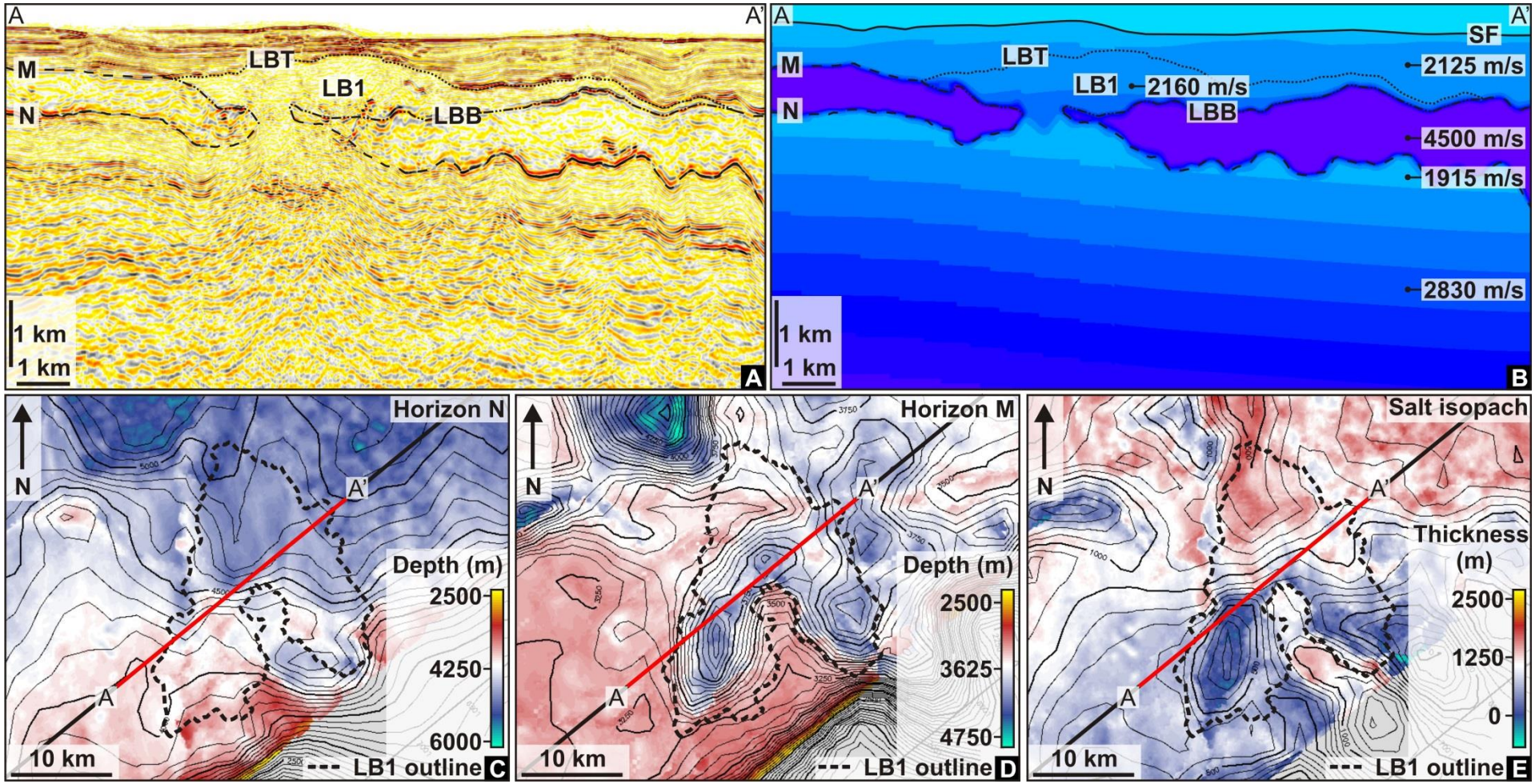

Figure 4.11 PSDM profile through Lensoid body 1 and interpretation of the evaporites. A: A seismic profile through Lensoid body 1. B: A velocity profile through Lensoid body 1. C: A depth map of Horizon N beneath Lensoid body 1. D: A depth map of Horizon M beneath Lensoid body 1. E: An isopach map of the salt underlying Lensoid body 1. LB1 – Lensoid body 1; LBT – Lensoid body top; LBB – Lensoid body base; M – Horizon M; N – Horizon N; SF - Seafloor.

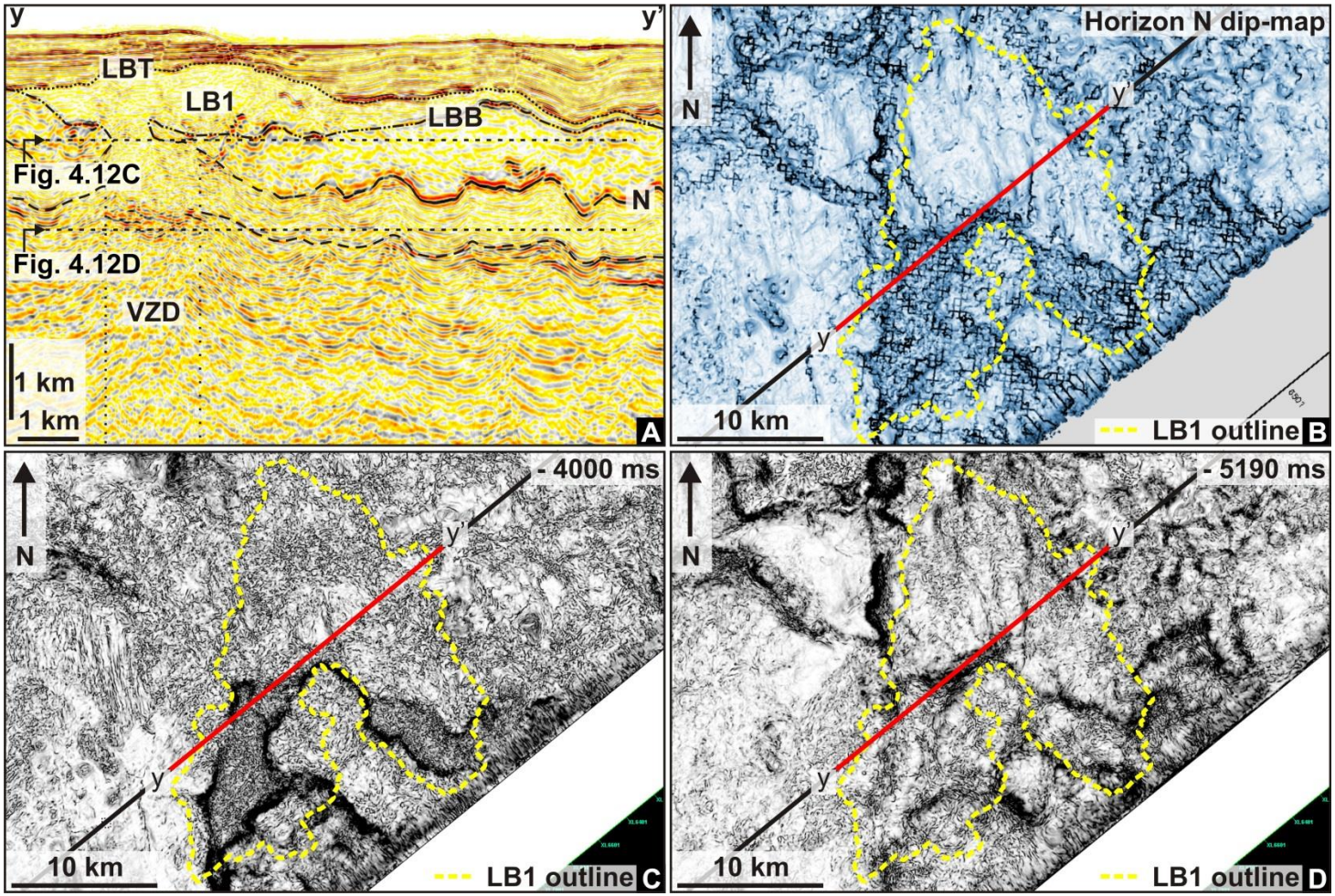

Figure 4.12 Pre-salt connection and structure beneath Lensoid body 1. A: A seismic profile through Lensoid body 1. B: A dip map of Horizon N beneath Lensoid body 1. C: A variance slice of the connection between the pre-salt and Lensoid body 1. D: A variance slice of the pre-salt beneath Lensoid body 1. LB1 – Lensoid body 1; LBT – Lensoid body top; LBB – Lensoid body base; VZD – Vertical zone of disruption; N – Horizon N.

The data quality is poor beneath Horizon N, particularly beneath the region where there is a connection between LB1 and the pre-salt (Figure 4.12A). Tracking a pre-salt reflection which is of high amplitude and continuity shows that there is a change in the reflection angle and stratigraphic position across this vertical zone of disruption (Figure 4.12A). Changes in gradient along Horizon N reveal pre-salt structures which display some linearity beneath LB1, where LB1 and the pre-salt converge (Figure 4.12B). A correlatable structure can also be observed deeper within the pre-salt via variance slice (Figure 4.12D).

4.3.2.2 Lensoid Body 2 (LB2)

LB2 is located in the East central region of the study area Northeast of LB1 at longitude 28.47415 E and latitude 32.06930 N (Figure 4.8). This lensoid body extends over Horizon M and is heavily deformed by faults, which display throw of up to c. 250 m and result in a very irregular top and basal reflection to the lensoid body (Figure 4.13). LB2 is the fourth largest of the lensoid bodies with a maximum thickness of thickness of 730 m, depositional relief of up to 350 m, an area of 46 km^2 and a volume of 11 km^3 (Figure 4.14C). This lensoid body has also been clipped by the margins of the data, similar to LB1, which means the full geometry and size is unfortunately unknown. The lensoid body is irregular in shape and has a nearly triangular planform, similar to LB1 (Figure 4.14C). LB4 displays an asymmetric form overall and is thickest at its centre dipping most gradually 2.92° to the north and a steeper 3.92° to the west (Figure 4.14C). The gently dipping top reflection of the lensoid body eventually converges with its basal reflection at the margins of the structure and reflections of the hemipelagic deposits clearly onlap onto its upper surface (Figure 4.14B).

Horizon M and N both display an irregular geometry beneath LB2 (Figure 4.15A), similar to the example of LB1 (Figure 4.11). Horizon M exhibits a large depression of up to 440 m (Figure 4.15D), which is correlatable with the thickest part of LB2 (Figure 4.14C). Horizon N clearly undulates within the area underlying LB2 (Figure 4.15A), however, there is not a pronounced depression or build-up of relief

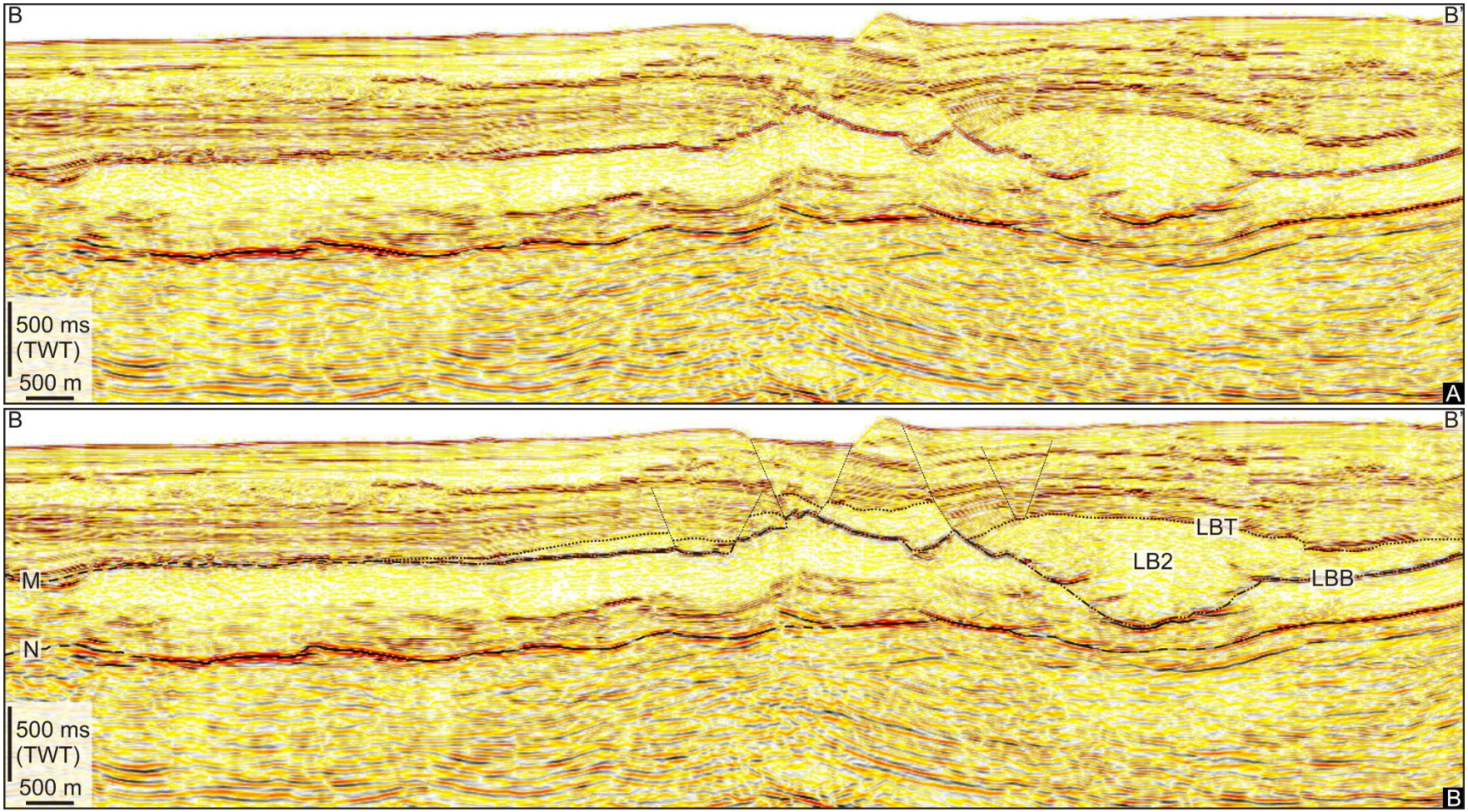

Figure 4.13 Seismic profile of lensoid body 2. A: An uninterpreted seismic profile through Lensoid body 2. B: The same seismic profile as in Figure 4.13A, showing the interpretation of Horizon M and Horizon N and the location of Lensoid body 2. LB2 – Lensoid body 2; LBT – Lensoid body top; LBB – Lensoid body base; M – Horizon M; N – Horizon N.

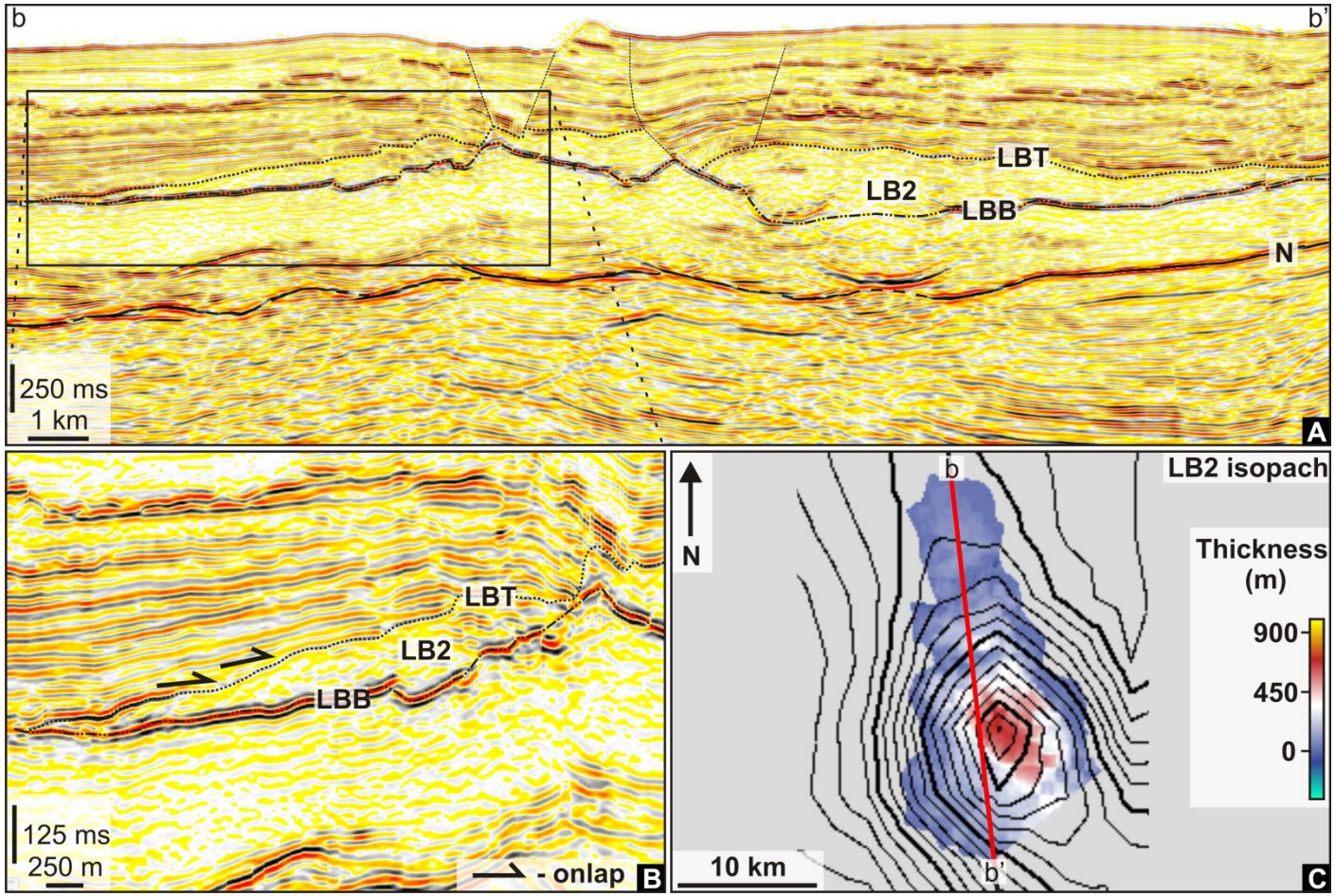

Figure 4.14 Interpretation of Lensoid body 2 and onlap. A: A seismic profile through Lensoid body 2, displaying an interpretation of the lensoid bodies top and basal reflections. B: A seismic profile through the margin of lensoid body 2, showing the convergence of the top and basal reflections. Reflections of hemipelagic deposits onlap onto the top reflection of the lensoid body. C: An isopach map of Lensoid body 2 and the line of section for Figure 4.14A. LB2 – Lensoid body 2; LBT – Lensoid body top; LBB – Lensoid body base; N – Horizon N.

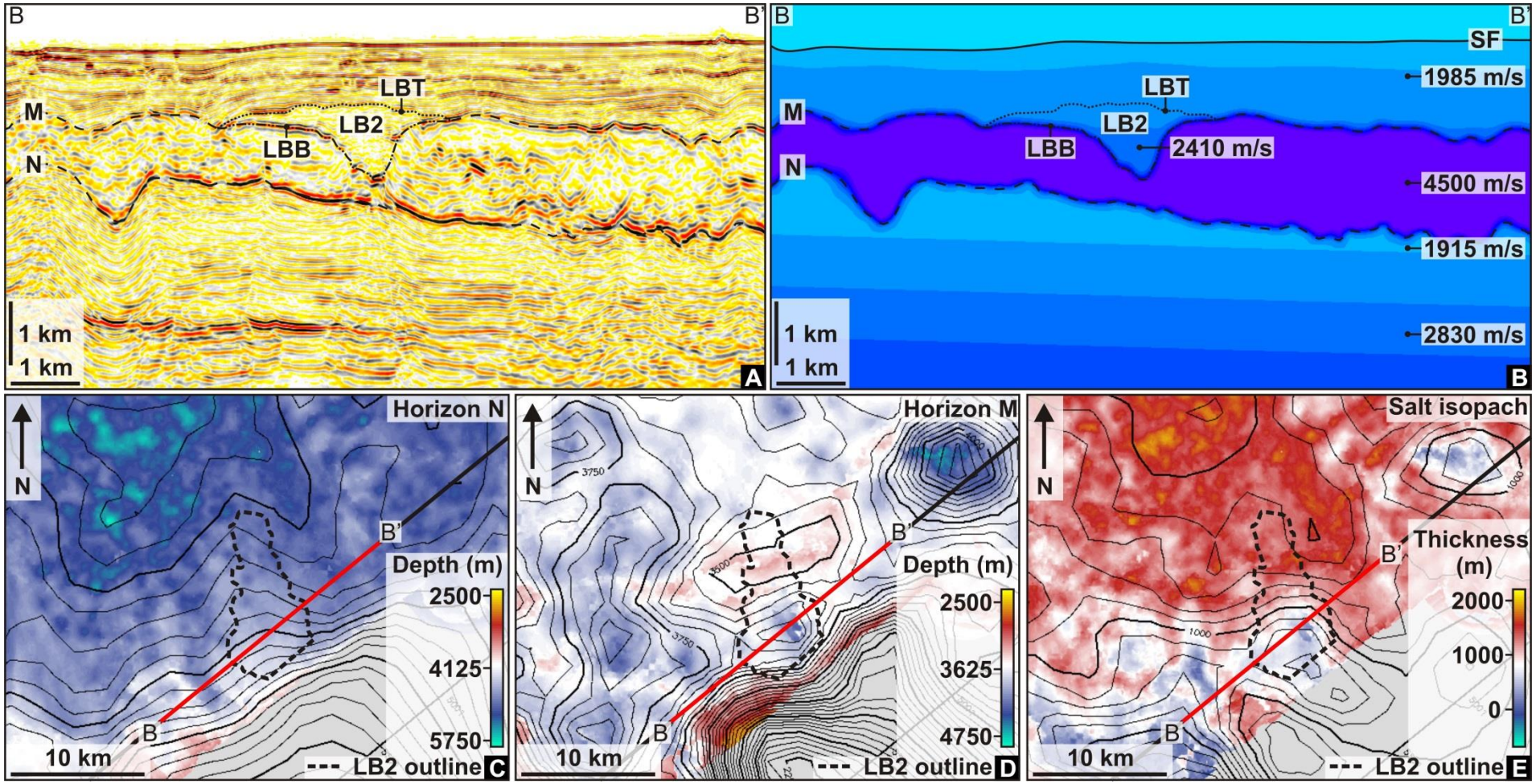

Figure 4.15 PSDM profile through Lensoid body 2 and interpretation of the evaporites. A: A seismic profile through Lensoid body 2. B: A velocity profile through Lensoid body 2. C: A depth map of Horizon N beneath Lensoid body 2. D: A depth map of Horizon M beneath Lensoid body 2. E: An isopach map of the salt underlying Lensoid body 2. LB2 – Lensoid body 2; LBT – Lensoid body top; LBB – Lensoid body base; M – Horizon M; N – Horizon N; SF – Seafloor.

directly beneath the lensoid body (Figure 4.15C), in contrast to LB1 (Figure 4.11C). The salt locally thins beneath LB2, which is correlatable with the observed top-salt depression (Figure 4.15E). There is, however, no clear connection between the lensoid body and the pre-salt in contrast to the example of LB1 (Figure 4.11). This is clearly demonstrated by the velocity profile which shows that the salt has thinned significantly beneath LB2, but that some still remains (Figure 4.15B). No linear pre-salt structure could be observed beneath LB2 (Figure 4.15A).

4.3.2.3 Lensoid Body 3 (LB3)

LB3 is located within north westerly region of the study area at latitude of 32.08393 N and longitude of 28.00300 E (Figure 4.8). LB3 is also located on top of Horizon M, however, relative to the previous two examples, the flanks of the lensoid body do not extend a large distances across Horizon M away from the centre of the lensoid body (Figure 4.17A and Figure 4.17C). LB3 is the second largest of the lensoid bodies with a maximum thickness of 1190 m, which makes it the thickest of the lensoid bodies, relief of up to 450 m, an area of 122 km^2 and a volume of 52 km^3. It displays an asymmetric form with an elongated, almost linear shape, which is as great as c. 20 km long and trends in an E-W orientation (Figure 4.17C). A prominent central ridge forming the thickest part of the body separates steeply sloping sides ranging from 2.56° on the southern flank, to 9.54° at the northeast (Figure 4.17C). The angle of LB3s upper bounding reflection is consistently steeper than the previous two examples. The reflection of the upper surface converges with the lensoid bodies basal reflection at is margins and its upper bounding reflection is clearly onlapped by the reflections of hemipelagic deposits (Figure 4.17B).

Horizon M displays a large depression with relief as great as c. 500m (Figure 4.18A and Figure 4.18D) directly beneath the thickest part of LB3 (Figure 4.17C). This depression displays E-W orientated linearity (Figure 4.18D), which is correlatable with the E-W orientated ridge of maximum thickness observed in an isopach of LB3 (Figure 4.17C). Horizon N undulates beneath LB3 and similar to LB1 a build-up of relief can be

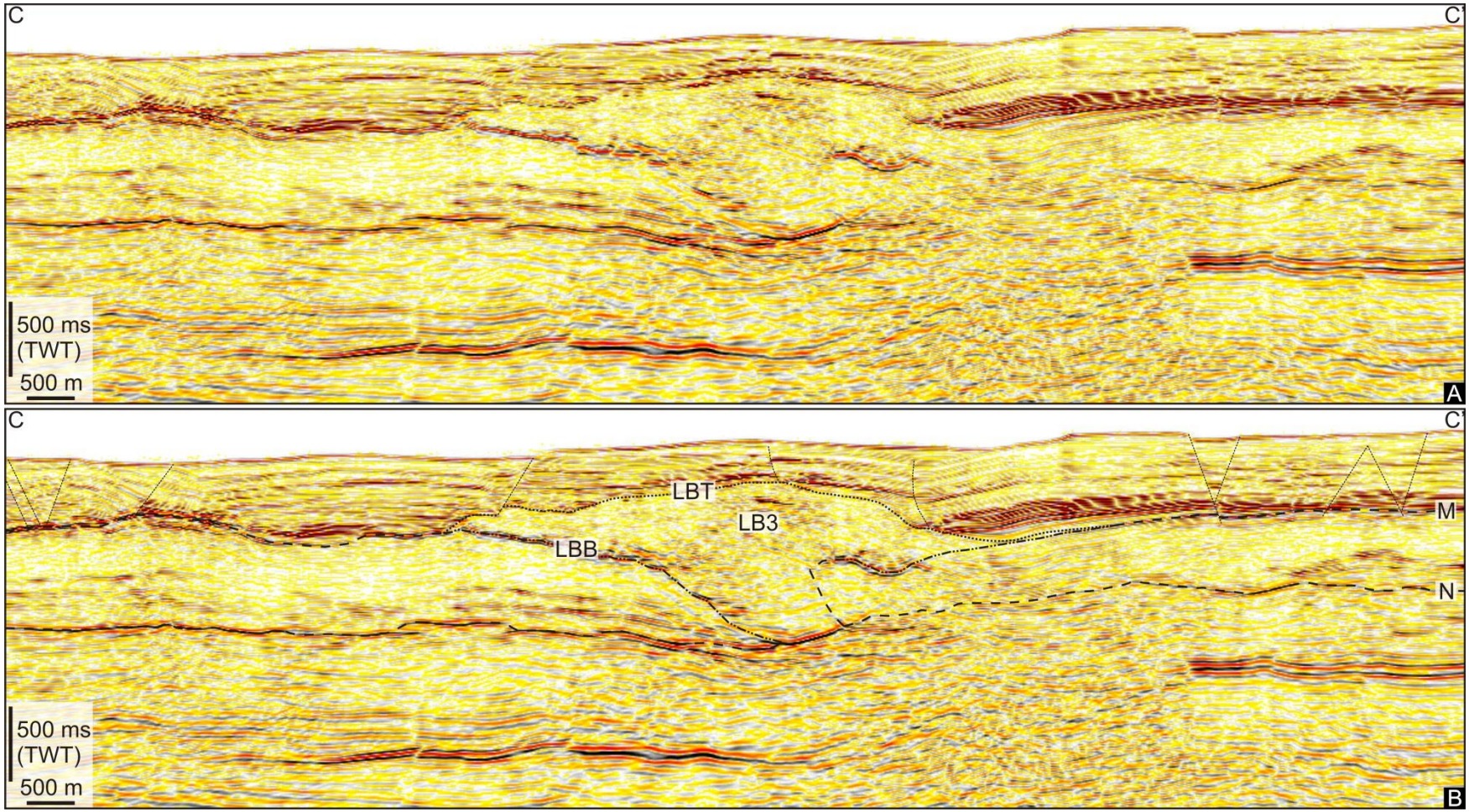

Figure 4.16 Seismic profile of lensoid body 3. A: An uninterpreted seismic profile through Lensoid body 3. B: The same seismic profile as in Figure 4.16A, showing the interpretation of Horizon M and Horizon N and the location of Lensoid body 3. LB3 – Lensoid body 3; LBT – Lensoid body top; LBB – Lensoid body base; M – Horizon M; N – Horizon N.

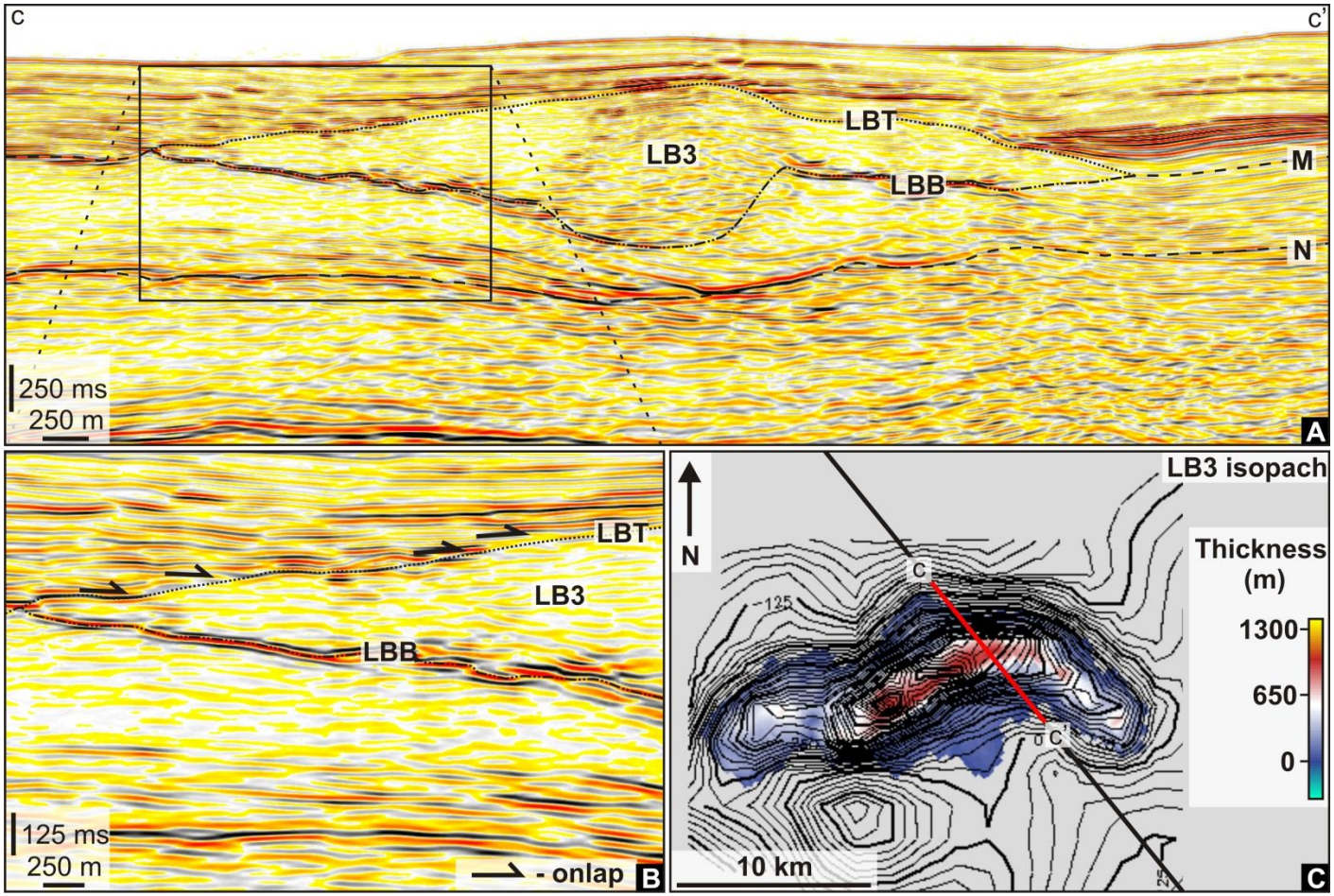

Figure 4.17 Interpretation of Lensoid body 3 and onlap. A: A seismic profile through Lensoid body 3, displaying an interpretation of the lensoid bodies top and basal reflections. B: A seismic profile through the margin of lensoid body 3, showing the convergence of the top and basal reflections. Reflections of hemipelagic deposits onlap onto the top reflection of the lensoid body. C: An isopach map of Lensoid body 3 and the line of section for Figure 4.17A. LB3 – Lensoid body 3; LBT – Lensoid body top; LBB – Lensoid body base; N – Horizon N.

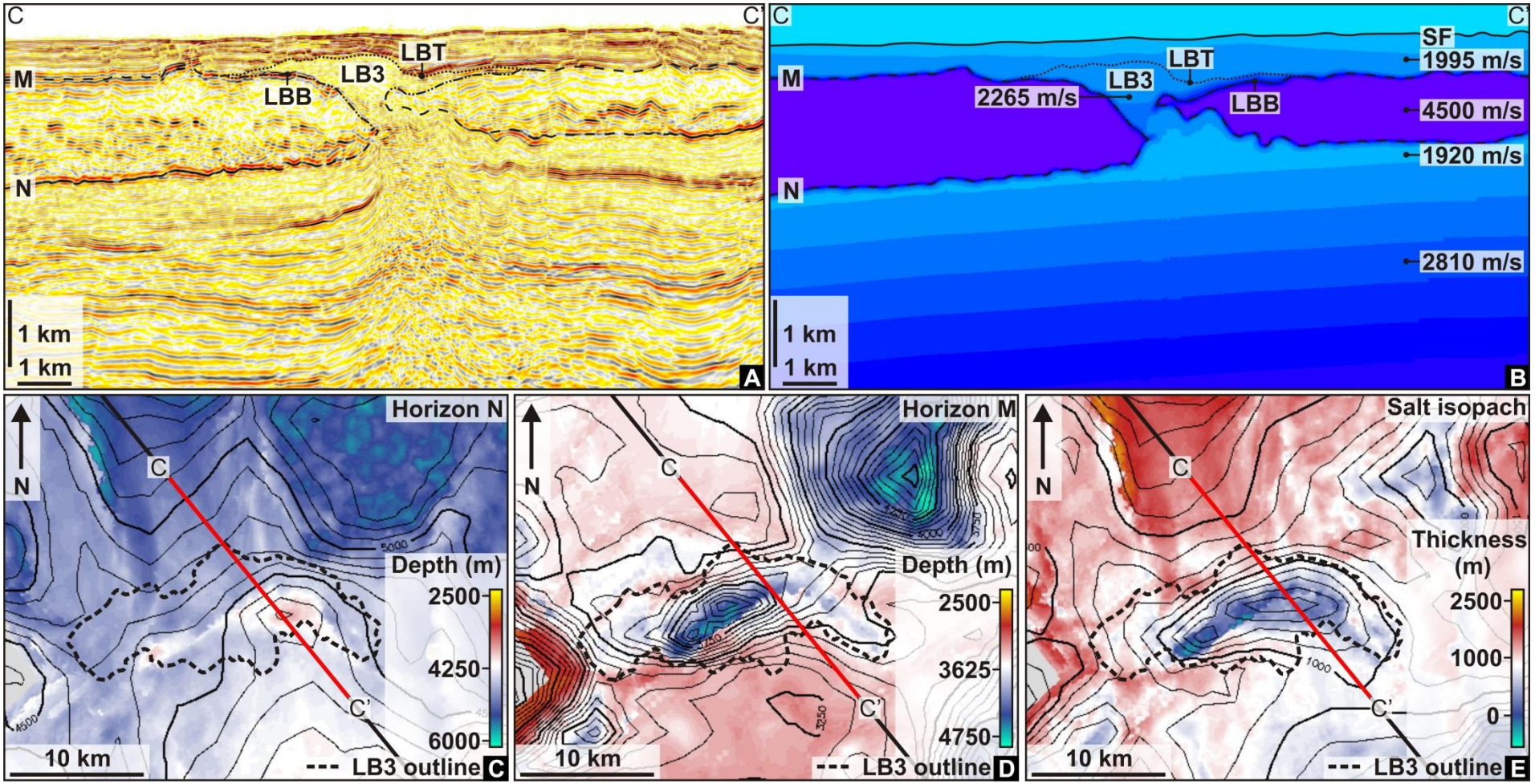

Figure 4.18 PSDM profile through Lensoid body 3 and interpretation of the evaporites. A: A seismic profile through Lensoid body 3. B: A velocity profile through Lensoid body 3. C: A depth map of Horizon N beneath Lensoid body 3. D: A depth map of Horizon M beneath Lensoid body 3. E: An isopach map of the salt underlying Lensoid body 3. LB3 – Lensoid body 3; LBT – Lensoid body top; LBB – Lensoid body base; M – Horizon M; N – Horizon N; SF – Seafloor.

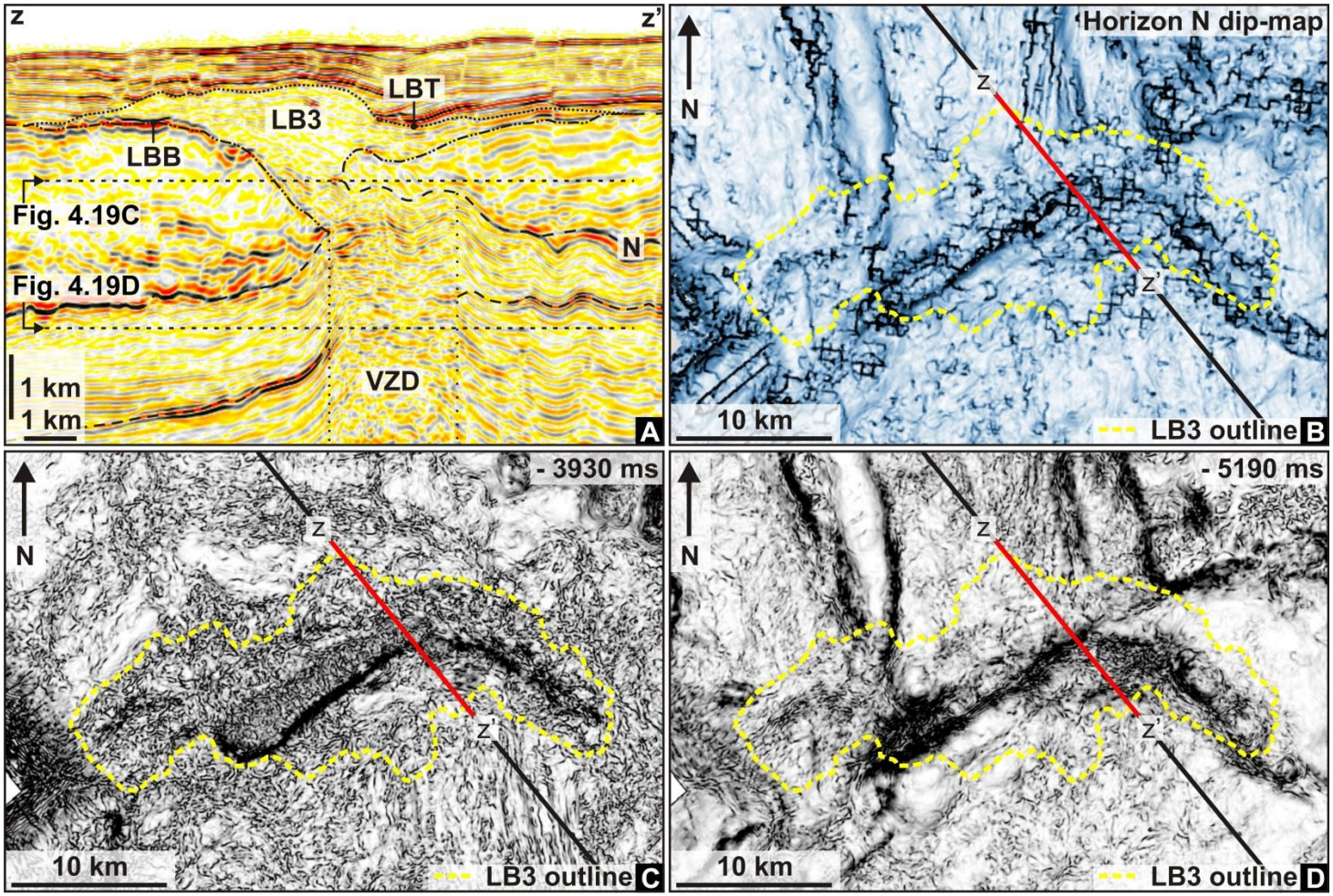

Figure 4.19 Pre-salt connection and structure beneath Lensoid body 3. A: A seismic profile through Lensoid body 3. B: A dip map of Horizon N beneath Lensoid body 3. C: A variance slice of the connection between the pre-salt and Lensoid body 3. D: A variance slice of the pre-salt beneath Lensoid body 3. LB3 – Lensoid body 1; LBT – Lensoid body top; LBB – Lensoid body base; VZD – Vertical zone of disruption; N – Horizon N.

observed directly beneath the lensoid body (Figure 4.18A and Figure 4.18C). This build-up of relief is prominent and localised and displays a similar linear trend to that observed in the lensoid body that directly overlies (Figure 4.18C and Figure 4.17C). The build-up of relief at Horizon N and depression at Horizon M directly beneath LB3, result in a localised area of decreasing salt thickness (Figure 4.18E). Complete salt removal can be observed where there is a connection between LB3 and the pre-salt (Figure 4.18B), similar to as was observed in LB1. This connection has an irregular and E-W orientated linearity which is observable in variance data as an area of increased discontinuity relative to the host successions background continuity (Figure 4.19C).

A vertical zone of disruption to the reflections of the pre-salt succession can be observed underlying the build-up in relief exhibited at Horizon N (Figure 4.19A). Picking of a continuous and high amplitude reflection within the pre-salt succession shows that there is a significant change in the dip and the depth of reflections across the vertical zone of disruption (Figure 4.19A). Structural features that have correlatable geometry to the overlying lensoid body can be seen along Horizon N in dip map (Figure 4.19B). Discontinuity with similar geometry can also be observed in variance data within the pre-salt (Figure 4.19D). It is, however, important to state that pre-salt data quality is poor, particularly beneath these lensoid bodies. These observations are very similar to those of LB1 (Figure 4.12).

4.3.2.4 Lensoid Body 4 – LB4

LB4 is located within the eastern region of the study area at latitude of 32.14085 N and longitude of 28.60079 E (Figure 4.8). Despite poor data quality towards the centre of the lensoid body, improved imaging towards its margins clearly shows that LB4 lies directly on top of Horizon M (Figure 4.20). It is the third largest of the lensoid bodies with a maximum thickness of 1010 m, depositional relief of 280 m, an area of 105 km^2 and a volume of 36 km^3. The lensoid bodies shape is characterised as irregular, asymmetric and has a triangular/rectangular planform (Figure 4.21C). It is thickest towards its central region and its upper surface has a slope angle of 3.57° to

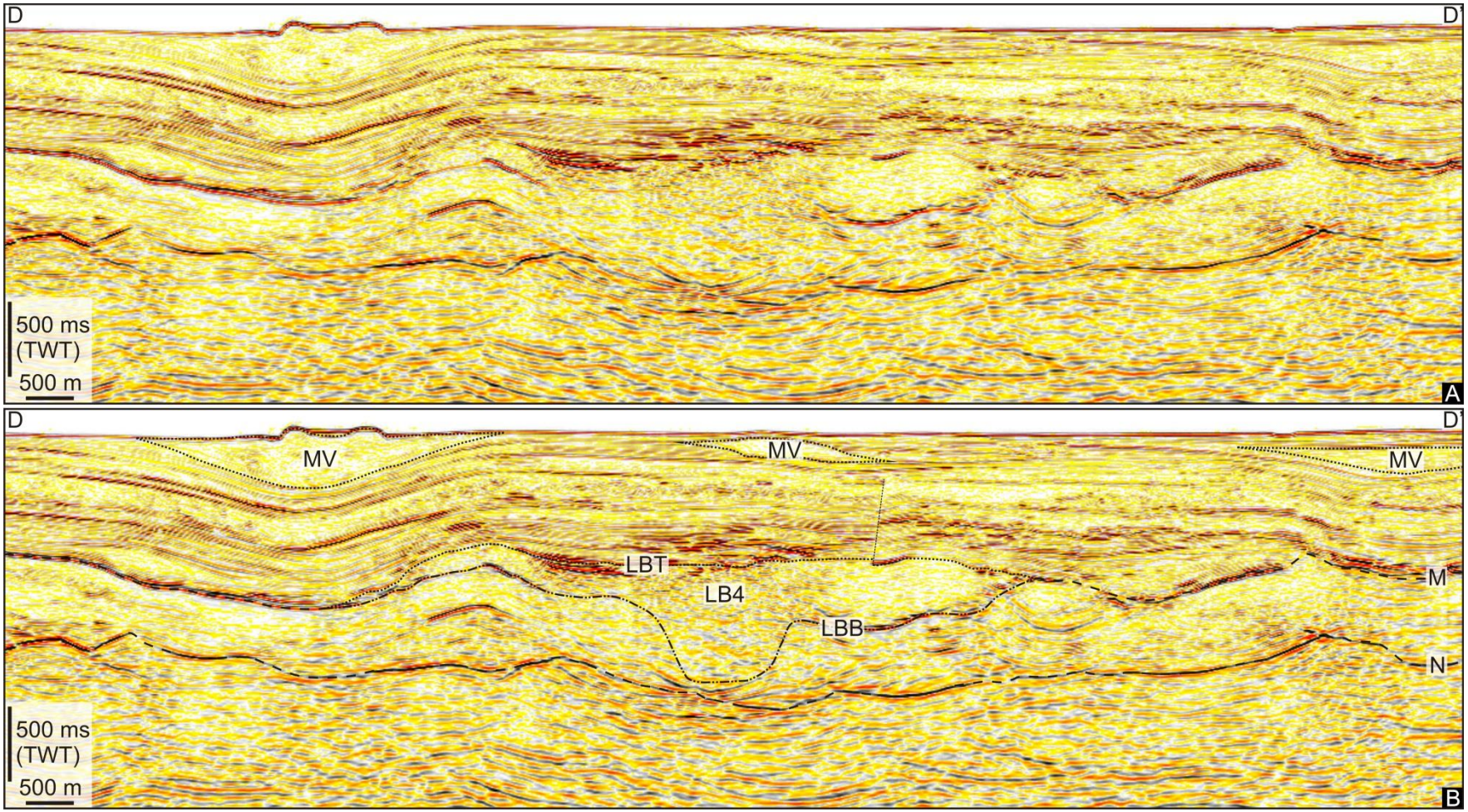

Figure 4.20 Seismic profile of lensoid body 4. A: An uninterpreted seismic profile through Lensoid body 4. B: The same seismic profile as in Figure 4.20A, showing the interpretation of Horizon M and Horizon N and the location of Lensoid body 4 and several mud volcanoes. LB4 – Lensoid body 4; LBT – Lensoid body top; LBB – Lensoid body base; MV – Mud volcanoes; M – Horizon M; N – Horizon N.

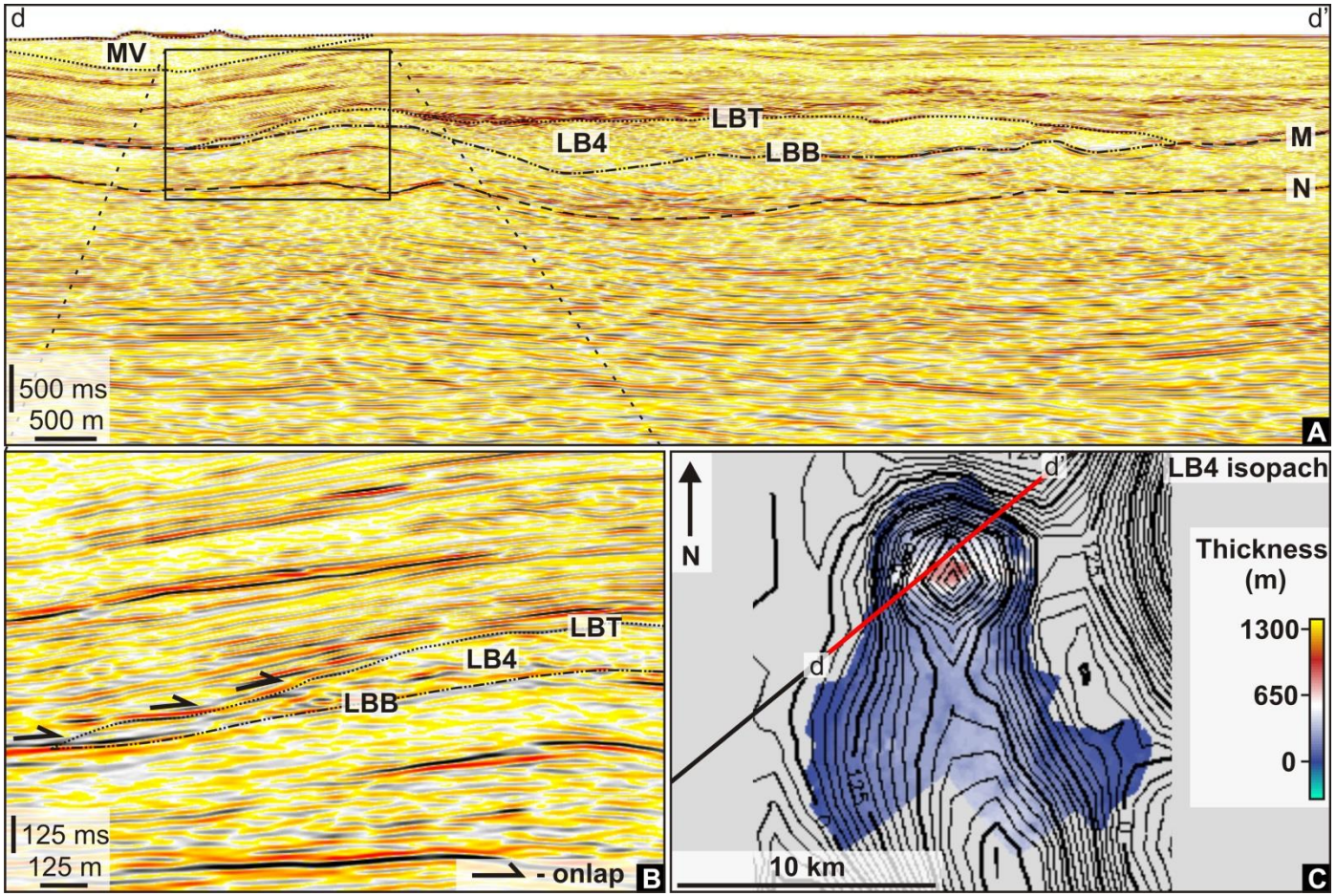

Figure 4.21 Interpretation of Lensoid body 4 and onlap. A: A seismic profile through Lensoid body 4, displaying an interpretation of the lensoid bodies top and basal reflections. B: A seismic profile through the margin of lensoid body 4, showing the convergence of the top and basal reflections. Reflections of hemipelagic deposits onlap onto the top reflection of the lensoid body. C: An isopach map of Lensoid body 4 and the line of section for Figure 4.21A. LB4 – Lensoid body 4; LBT – Lensoid body top; LBB – Lensoid body base; N – Horizon N.

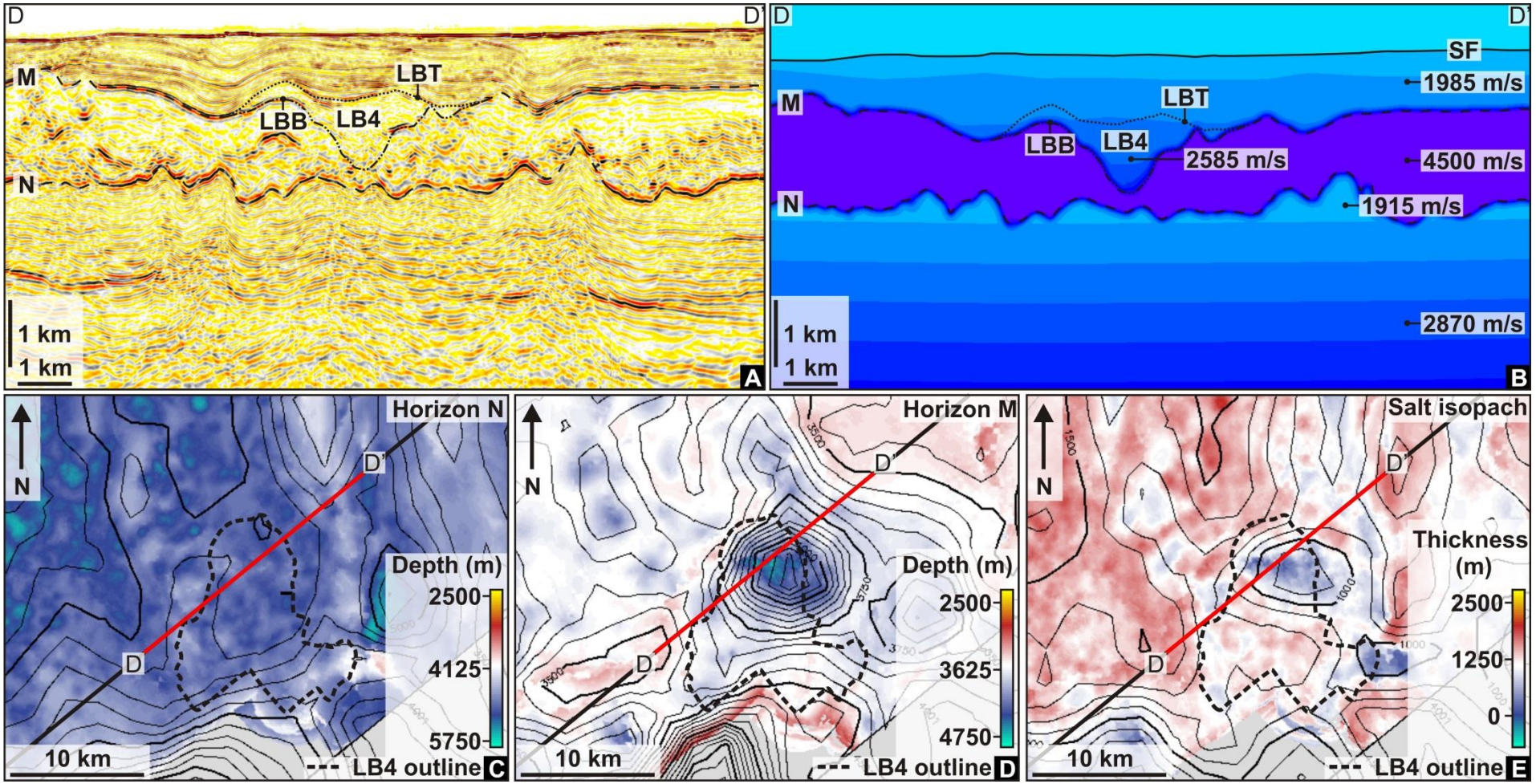

Figure 4.22 PSDM profile through Lensoid body 4 and interpretation of the evaporites. A: A seismic profile through Lensoid body 4. B: A velocity profile through Lensoid body 4. C: A depth map of Horizon N beneath Lensoid body 4. D: A depth map of Horizon M beneath Lensoid body 4. E: An isopach map of the salt underlying Lensoid body 4. LB4 – Lensoid body 4; LBT – Lensoid body top; LBB – Lensoid body base; M – Horizon M; N – Horizon N; SF – Seafloor.

the southwest and has a greater dip angle of 8.83° to the Northeast (Figure 4.21C). Downlap of the upper bounding reflection of LB4 onto its basal bounding reflection is clearly visible at the margins of the lensoid body (Figure 4.21B). Reflections of hemipelagic deposits onlap onto the upper surface of the lensoid body, similar to all previous examples (Figure 4.21B). The south side of the mud volcano is clipped by the margins of the seismic data area, which means it is unfortunately not possible to determine the full extent and size of the lensoid body (Figure 4.21C).

A large top-salt depression with relief as great as c. 750m is correlatable with the thickest region of LB4 (Figure 4.21C and Figure 4.22D). Horizon N undulates beneath LB4, however, there is no observable build-up in topography in contrast to LB1 and LB3 (Figure 4.22A and Figure 4.22C). Numerous small depressions can be observed at the base of the evaporites directly beneath LB4 (Figure 4.22C). No structural features can be observed within the pre-salt beneath LB4, in contrast to LB1 and LB3 (Figure 4.22A). The evaporite succession thins considerably beneath LB4, however, despite the large top-salt depression there is a relatively thin layer of salt beneath this depression and no clear connection with the pre-salt (Figure 4.22B and Figure 4.22E).

4.3.2.5 Lensoid Body 5 (LB5)

LB5 is located within the north to central region of the study area at latitude of 32.28446 N and longitude of 28.30696 E (Figure 4.8). It has a total volume of 1.25 km^3 and is the smallest of the group of lensoid bodies to have developed immediately on top of Horizon M (Figure 4.23). It also exhibits a maximum thickness of 650 m, relief of up to 250 m and an area of 7.87 km^2. Other than being the smallest of the five lensoid bodies, additional ways in which it contrasts with the other lensoid bodies is in its geometry in planform, which is circular to elliptical rather than irregular (Figure 4.24C). Similar to the previous examples though, LB5 is thickest centrally (Figure 4.24C). Its upper bounding reflection dips steeply to the southwest at 14.74° and steeper yet towards the northwest at 16.49°. This results in LB5 thinning toward its margins where

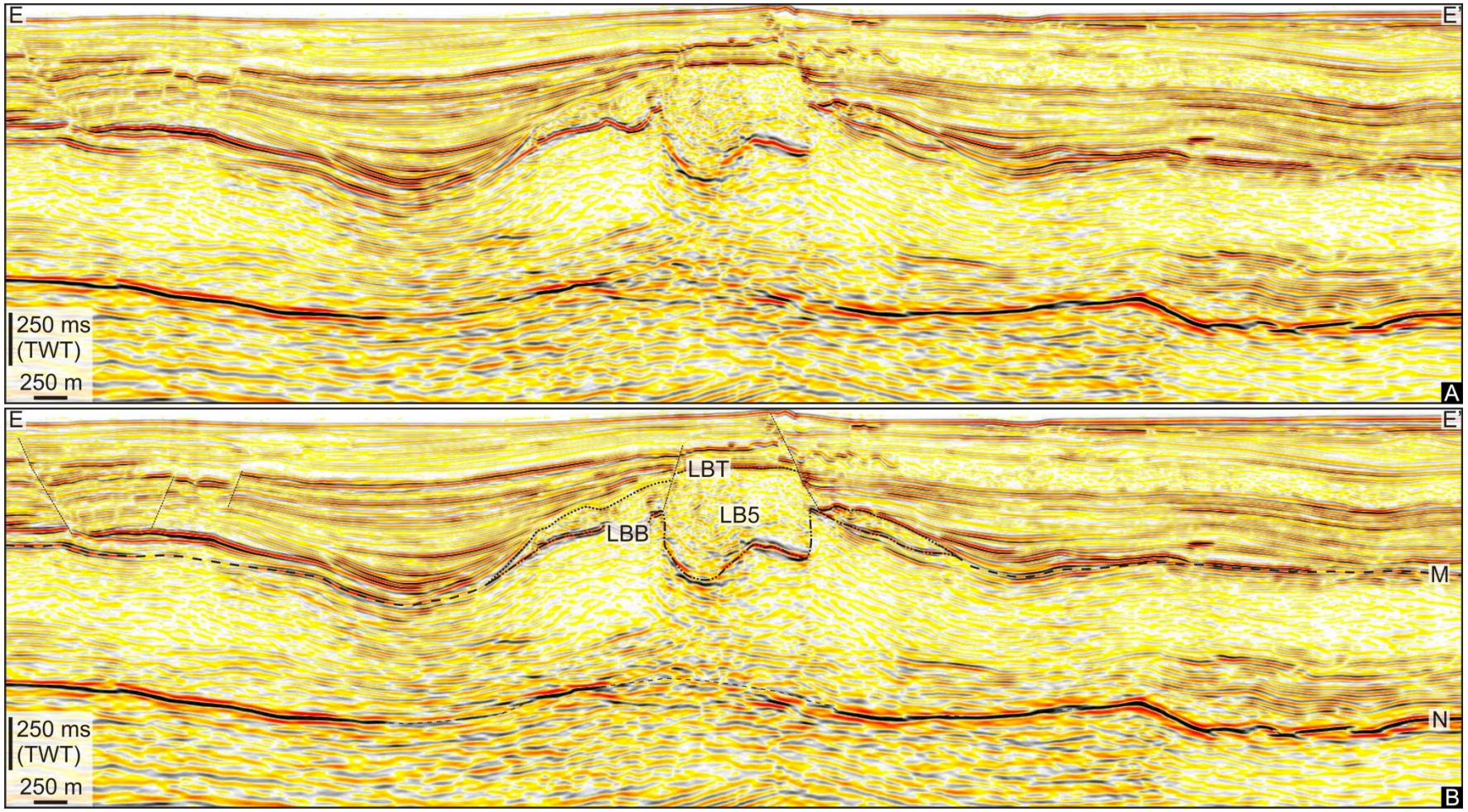

Figure 4.23 Seismic profile of lensoid body 5. A: An uninterpreted seismic profile through Lensoid body 5. B: The same seismic profile as in Figure 4.23A, showing the interpretation of Horizon M and Horizon N and the location of Lensoid body 5. LB5 – Lensoid body 5; LBT – Lensoid body top; LBB – Lensoid body base; M – Horizon M; N – Horizon N.

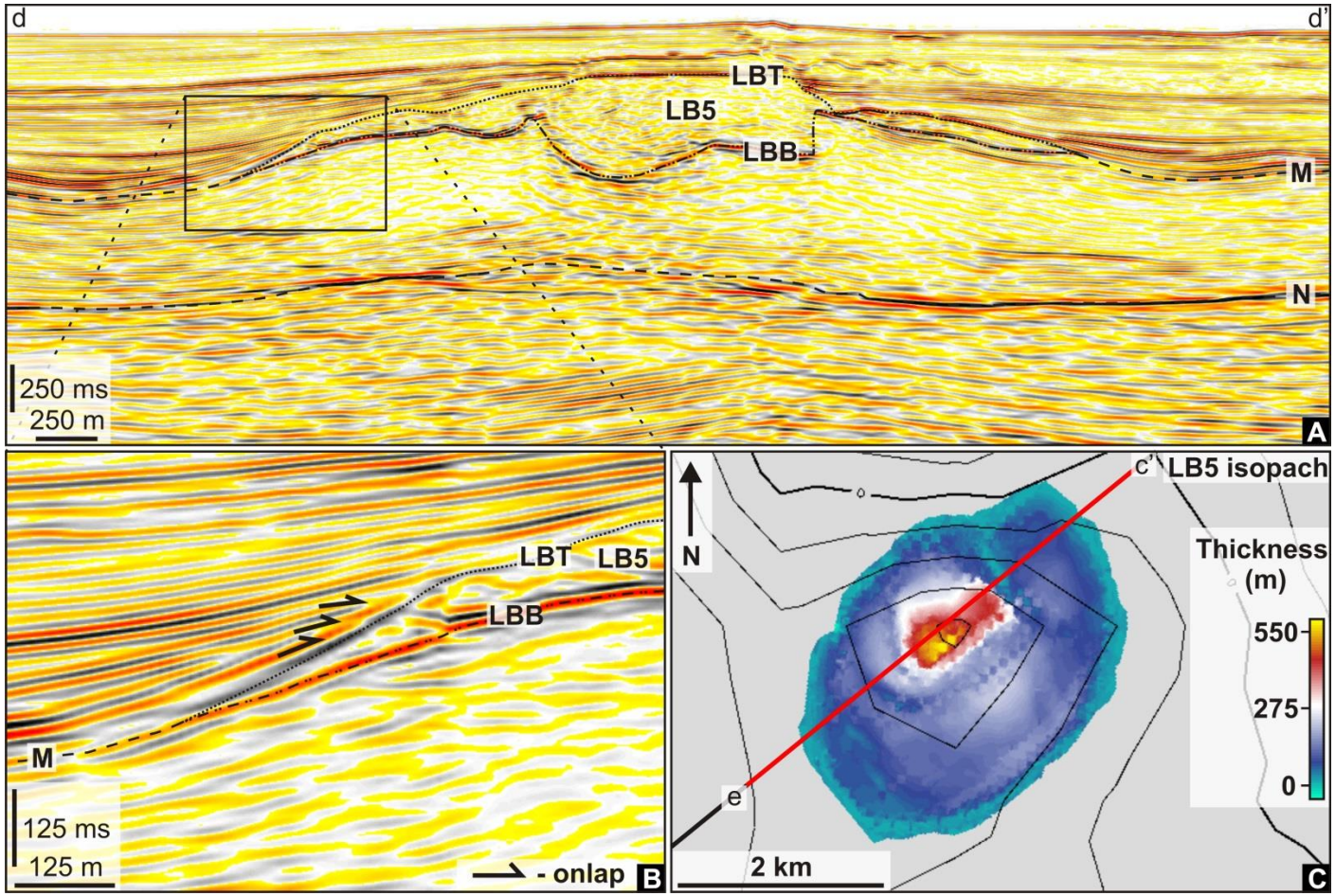

Figure 4.24 Interpretation of Lensoid body 5 and onlap. A: A seismic profile through Lensoid body 5, displaying an interpretation of the lensoid bodies top and basal reflections. B: A seismic profile through the margin of lensoid body 5, showing the convergence of the top and basal reflections. Reflections of hemipelagic deposits onlap onto the top reflection of the lensoid body. C: An isopach map of Lensoid body 5 and the line of section for Figure 4.24A. LB5 – Lensoid body 5; LBT – Lensoid body top; LBB – Lensoid body base; N – Horizon N.

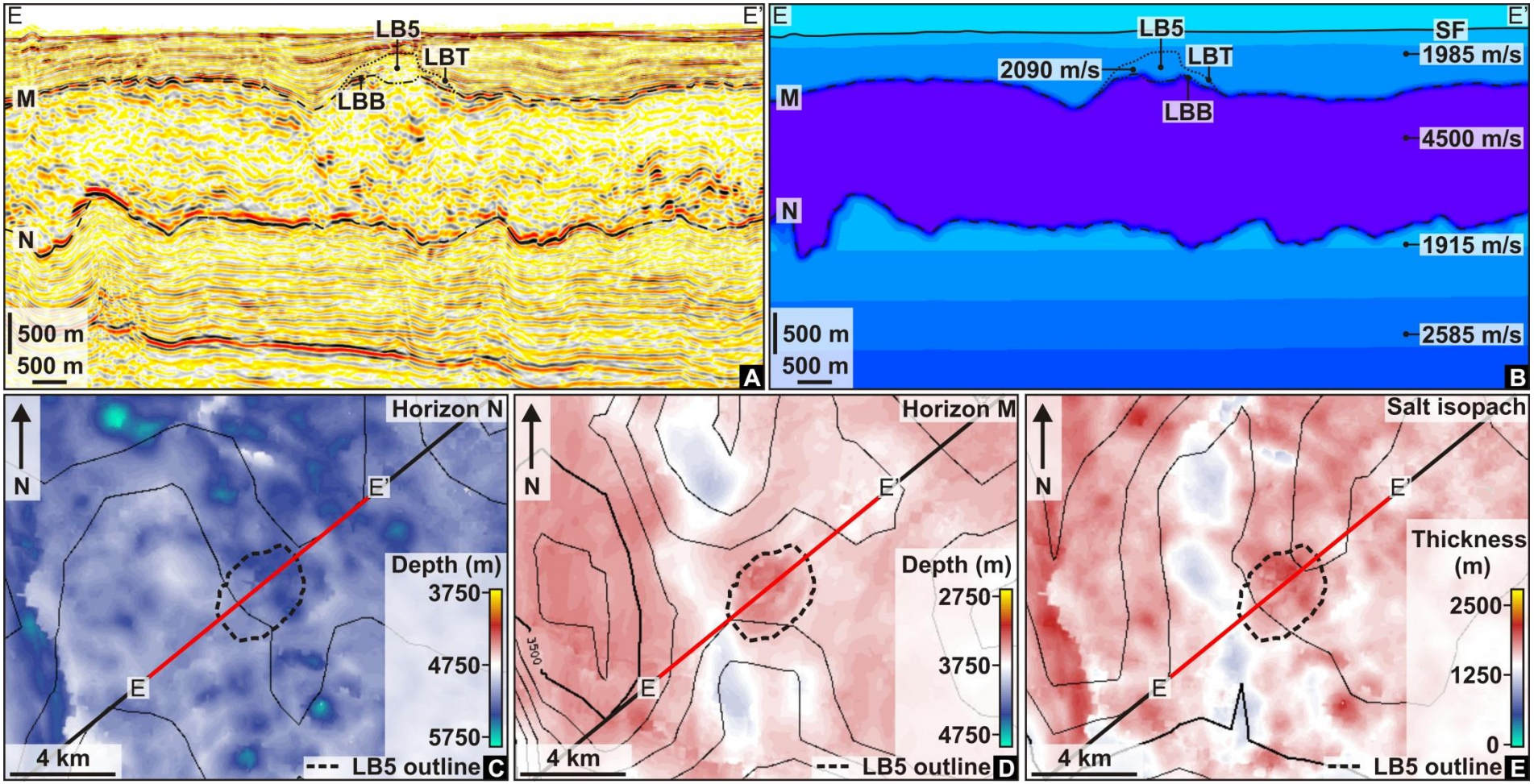

Figure 4.25 PSDM profile through Lensoid body 5 and interpretation of the evaporites. A: A seismic profile through Lensoid body 5. B: A velocity profile through Lensoid body 5. C: A depth map of Horizon N beneath Lensoid body 5. D: A depth map of Horizon M beneath Lensoid body 5. E: An isopach map of the salt underlying Lensoid body 5. LB5 – Lensoid body 5; LBT – Lensoid body top; LBB – Lensoid body base; M – Horizon M; N – Horizon N; SF – Seafloor.

its upper and lower bounding reflections converge and reflections of hemipelagic deposits onlap the upper surface (Figure 4.24B). The upper surface of LB5 dips at a significantly greater angle than all four of the other lensoid bodies described here.

Underlying LB5 there is only a very small depression that can be observed at the top of the evaporite succession (Figure 4.25A and Figure 4.25D) and it correlates with the thickest area of the overlying lensoid body (Figure 4.24C). A depression at the base of the evaporites can be observed underlying LB5 (Figure 4.25C). The thickness of the evaporite succession does not vary significantly beneath the LB5 in contrast to all the previous lensoid bodies described Figure 4.25E. There are also no pre-salt structures that can be observed beneath LB5 in contrast to those observed in LB1 and LB3.

4.3.3 Summary and interpretation

The lensoid bodies described in section 4.3.2 are notable for: (1) the geometry of their upper and lower bounding surfaces, which converge to form an isolated lensoid body; (2) their isopach distribution, which display maximum thickness centrally and a reduction in thickness with increasing proximity to the margins of the feature; (3) the relief observed at the upper surface of the lensoid bodies, which is onlapped by the reflections of the hemipelagic deposits; (4) the downlap of the upper surface onto Horizon M and the significant extent of Horizon M that they directly overlie. Based on these observations, an interpretation can be made that these lensoid bodies represent a type of constructional mound. Constructional mounds with similar enclosed perimeters are frequently found to comprise carbonate sediments or volcanic rocks, however, both these interpretations can be rejected due to the sub-2500 m/s p-wave velocity of the bodies (Rider, 1986). It is also unlikely that these lensoid bodies are submarine fans since they are completely isolated and unconnected to any potential feeder system. Contourite bodies can be isolated and exhibit similar baselap and onlap geometries, however, they are universally found to be internally stratified (Faugères et al., 1999).

An alternative explanation of these lensoid bodies is that they are in fact mud volcanoes. This interpretation would explain the general lack of internal stratification and is also supported by the recognition of > 350 smaller and conical mud volcanoes at stratigraphically younger levels within the study area (See Chapter 5) and other documented examples of these mud volcanoes, predominantly from seafloor studies (Loncke et al., 2004; Huguen et al., 2009; Dupré et al., 2010; Dupré et al., 2014; Mascle et al., 2014; Pierre et al., 2014). In contrast to these younger mud volcanoes, the lensoid bodies are generally significantly larger and do not exhibit the classic conical geometry that is commonly associated with mud volcanoes (Evans et al., 2007). Their geometry and gross volume is similar in some aspects to large extruded and tabular 'mud pies' (sensu Kopf (2002)), similar to those described from the nearby tectonically active central Mediterranean Ridge by Kopf et al. (2001). LB5 represents the one exception in that its geometry and volume are more closely comparable to the small and conical mud volcanoes discussed in Chapter 5, however, its upper bounding surface downlaps onto Horizon M similarly to the other four lensoid bodies. The observations of a lack of internal stratification and the appearance of a single body may have significant implications with regards to the episodicity of these mud volcanoes and which will be discussed in section 4.3.3 below.

The volumes of mud that are recorded to have been extruded during the formation of these mud volcanoes are exceptional in their scale. The onlap relationship between the upper surface of the mud volcanoes and the surrounding hemipelagic deposits demonstrates that the extrusion of such large volumes of mud has clearly built topography (Figure 4.10 and Figure 4.24). Top-salt depressions display a strong correlation with areas of anomalous thinning of the underlying evaporites (Figure 4.11 and Figure 4.22). The descriptions here of a striking spatial correspondence between the depressions of Horizon M and areas of anomalous thinning of the Messinian evaporites and the lensoid bodies, argues powerfully that the lensoid bodies grew with commensurate displacement or removal of mobile evaporites that underlie the LBs by a process of downbuilding (Jackson, 1995). The reflections of the hemipelagic deposits that onlap the upper surface of the mud volcanoes show no evidence of downsagging associated with subsidence of the mud volcanoes and top-salt. This suggests that

subsidence and the formation of these top-salt depressions occurred before the deposition and onlap of the hemipelagic deposits onto the upper surface of the mud volcanoes. The potential mechanisms for the displacement or removal of the Messinian evaporites will be discussed in section 4.4.3 below.

The reflection of Horizon N and immediate pre-salt stratigraphy are observed to have been elevated above the regional datum beneath LB1 and LB3, however, not beneath the other lensoid bodies (Figure 4.12 and Figure 4.19). These features are characterised as localised areas of relief as great as c.500m within the pre-salt, which internally comprise a chaotic seismic facies (Figure 4.12 and Figure 4.19). The description of the structures combined with their spatial correspondence to overlying mud volcanoes is indicative that they are mounds or ridges, similar to those observed in other sedimentary basins (Brown, 1990; Van Rensbergen et al., 1999). Diapiric features such as these form via the forceful movement of a more or less plastic body from an area of greater pressure to an area of lower pressure (Kopf, 2002). It is commonly believed that in many cases mud volcanoes can often form directly above diapiric features such as these (Brown, 1990; Dimitrov, 2002; Guliyev et al., 1996; Milkov, 2000). An interpretation could be made that these mounds are associated with the extrusion of LB1 and LB2 due to the observation that their geometry in planform is correlatable with the overlying lensoid bodies. Pre-salt structures observed in dip map and variance slices combined with the observation of a change in the angle and depth of reflections across these structures could be interpreted as indicative of pre-salt faults. Based on the descriptions above for LB1 and LB3, the geometry in plan form of these faults appear to be correlatable with the geometry in planform of the pre-salt mud ridges and lensoid bodies that directly overlie and these features may all, therefore, be intimately associated.

A potentially important observation is that in all the examples presented above, the thick pre-salt section comprises sediments with anomalously low p-wave velocity (<2000m/s) for their burial depth of 3-4km (Figure 4.11B and Figure 4.25B). This velocity is not only significantly lower than the Messinian evaporite succession but also lower than that of the shallower Pliocene to Recent succession. This inversion in

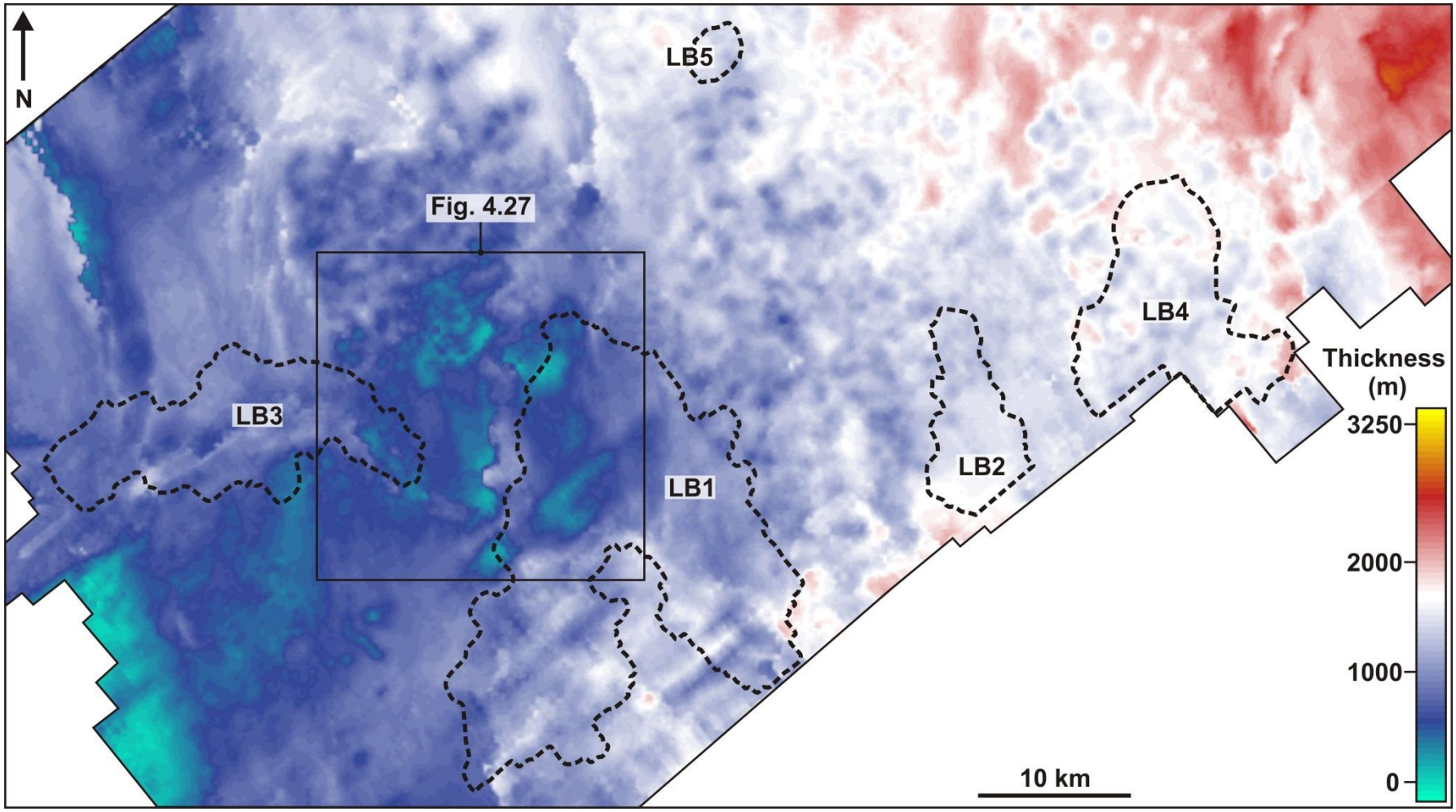

Figure 4.26 Immediate pre-salt isopach map. An isopach map of the unit directly underlying the evaporite succession also showing the location of all five lensoid bodies. The light blue areas in particular represent areas of anomalous thinning. LB1 – Lensoid body 1; LB2 – Lensoid body 2; LB3 – Lensoid body 3; LB4 – Lensoid body 4; LB5 – Lensoid body 5.

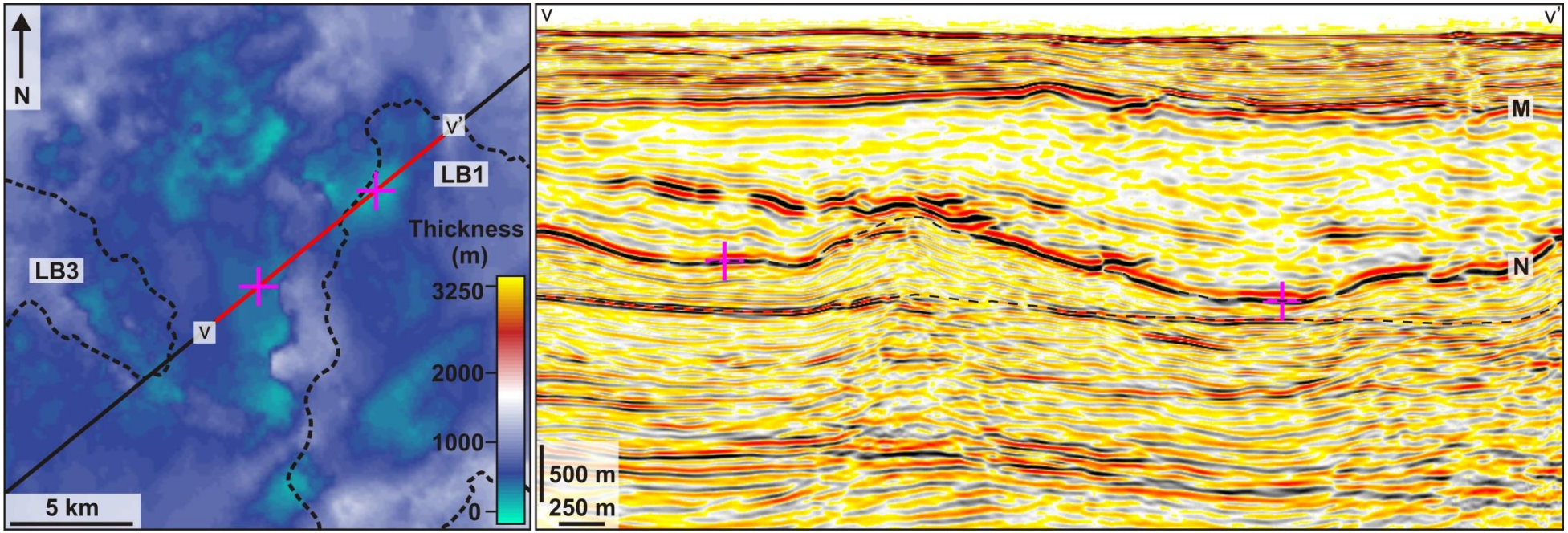

Figure 4.27 Anomalous thinning of the immediate pre-salt. A: An isopach map of the immediate pre-salt succession within a small region of the study area, showing areas of anomalous thinning. B: A seismic profile through the areas of anomalous thinning displayed in Figure 4.27A, which displays depression along Horizon N which correlate with thinner sections of the immediate pre-salt succession. LB1 – Lensoid body 1; LB3 – Lensoid body 3; M – Horizon M; N – Horizon N.

velocity could be interpreted as indicative of a significant degree of undercompaction (Magara, 1978). The observation was made that Horizon N undulates and displays numerous depressions, but how do these depressions influence the thickness of the pre-salt? Areas of anomalous thinning in close spatial association with these lensoid bodies can be observed within the immediate pre-salt (Figure 4.26). These areas of anomalous thinning are correlatable with the depressions observed along Horizon N which, therefore, suggests that there has been removal of material from the immediate pre-salt (Figure 4.27). The potential for undercompaction of the pre-salt and its viability as a source layer will be discussed below.

4.4 Discussion

4.4.1 Source of mud and fluids

The high resolution seismic data from this study has revealed a suite of mud volcanoes, which are of an exceptional scale and directly overlie the top of the Messinian evaporites. The individual volumes of the largest three bodies (LB1 – 116 km^3, LB3 – 52 km^3, LB4 – 36 km^3) far exceed the largest previously identified and described single mud volcano, which has been mapped using 3D seismic data within the South Caspian Basin and documented to have a volume of 22.5 km^3 (Davies and Stewart, 2005). These mud volcanoes are, therefore, amongst the largest documented thus far. The identification of these very large extrusive and constructional mud volcanoes poses the question; from which stratigraphic unit/units have the fluids and mud that feed these mud volcanoes been sourced? Correctly identifying the source of mud and fluids is a potentially critical interpretation in order to understand the possible mechanisms required to form these giant mud volcanoes.

A simple but important observation to make is that the giant mud volcanoes are observed here to have formed directly on top of the Messinian evaporites. The mud and fluid source must, therefore, be at least pre-Pliocene. A source within the

evaporite succession can be ruled out due to the lack of fine-grained sediment within a succession thought to comprise predominantly of halite, due to its seismic facies (Bertoni and Cartwright, 2007b). The giant mud volcanoes interval velocity also precludes any significant component of evaporitic source material. Another critical observation in ascertaining the source of mud and fluids is the clear connection that can be seen in some cases between a mud volcano and the pre-salt. The connection described here is most clearly defined in cross-sections through the giant mud volcanoes using the velocity data (Figure 4.11B). This connection potentially represents the conduit that links the extruded mud volcanoes and source stratigraphy. These observations clearly indicate that the source of fluids and mud for these giant mud volcanoes is within the pre-salt.

Drawing comparison to the smaller and conical mud volcanoes within this study area could provide supporting evidence for the source of fluids and mud for the giant mud volcanoes. In Chapter 5, it is discussed that there is a volumetric balance and clear spatial relationship between the top-salt and base-salt depressions and the overlying small and conical mud volcanoes. The potential for the formation of these depressions, due to pre-salt sediment withdrawal is discussed within section 5.6.4. Analysis of the conduits for those mud volcanoes and their root zones, also results in the interpretation of a pre-salt fluid and mud source within Chapter 6. Depressions at the base of the evaporites and even anomalous thinning of the immediate pre-salt unit have also been observed in close proximity to the giant mud volcanoes described here and could, therefore, similarly be interpreted as indicative of a pre-salt source. This interpretation is supported by the low velocity (<2000 m/s) that has been observed within the first 1000 m of the sub-salt section, which is anomalously low for its present day burial depth of between 3 and 5km and potentially undercompacted (Magara, 1978). The precise stratigraphy of the immediate pre-salt interval lacks nearby well calibration, but by extrapolation from other well calibrated pre-Messinian successions in the Levant Basin (Bertoni et al., 2013) and at outcrop in Sicily (Grasso et al., 1982), it is most likely to comprise a marly to muddy interval of mid-late Miocene age.

The above interpretations are further substantiated by the documentation of piston core samples from mud volcanoes at the seafloor within this study area, which

reportedly contain rock clasts of up to Cretaceous in age (Dupré et al., 2014; Mascle et al., 2014; Giresse et al., 2010). Pre-salt withdrawal and mobilisation of overpressured Tortonian shales within the immediate pre-salt has also been previously interpreted within this study area (Bentham et al., 2006). It is possible that the mud and fluid components that fed these mud volcanoes could be derived from more than one single interval, or each sourced from different intervals in the pre-salt (c.f. Mazzini et al. (2012)). These interpretations imply that a large volume of mud, mobilised from the pre-salt, somehow crossed a > 1000 m thick layer of evaporites prior to extrusion on the top-salt surface. An interpretation such as this challenges the general belief that thick evaporite sequences represent almost impermeable barriers to upward fluid migration (Downey, 1984; Cartwright et al., 2007).

4.4.2 The Genesis of giant mud volcanoes

The enormous scale of the giant mud volcanoes within this study area and the interpretation of a pre-salt fluid and mud origin raise important questions, regarding the mechanisms involved in the ascent of fluids and mud from the pre-salt succession and the genesis of these giant mud volcanoes. A key question that has not yet been discussed is: what is the timing of emplacement of these mud volcanoes? Ascertaining the time at which these mud volcanoes formed is certain to be of critical importance in understanding the mechanisms involved in the formation of these giant mud volcanoes. Unfortunately there is no direct well calibration of the key seismic markers. The identification of Horizons M and N is, however, straightforward since these regionally important surfaces are correlatable across the entire Eastern Mediterranean (Barber, 1981; Bertoni and Cartwright, 2005; Ryan and Cita, 1978). The downlap of the upper surface of the mud volcanoes with Horizon M, which is regionally correlatable with the end of the Messinian Salinity Crisis, implies that to the limits of vertical resolution, all five of the mud volcanoes described here have been emplaced synchronously and that their formation coincided with the end of the Messinian Salinity Crisis.

Establishing the timing of emplacement of the mud volcanoes naturally leads to the question, what factors preconditioned this region for such extreme eruptive fluxes at the end of the Messinian Salinity Crisis? It is generally believed that high overpressure within a sedimentary layer is a critical precursor to the formation of a mud volcano (Kopf, 2002; Osborne and Swarbrick, 1997; Milkov, 2000; Deville and Guerlais, 2009; Dimitrov, 2002). Evidence of widespread overpressure in pre-Messinian sediments at the time of the Messinian Salinity Crisis, has been mounting in the last few years from descriptions of mud mobilisation, cold seep and pockmark formation and shallow-level mud laccolith intrusion (Frey-Martnez et al., 2007; Lazar et al., 2012; Bertoni and Cartwright, 2015; Bertoni et al., 2013).

There are numerous mechanisms for generating overpressure within a sedimentary basin, which include disequilibrium compaction, tectonic compression and volume changes due to aquathermal expansion, mineral diagenesis and hydrocarbon generation, as discussed in section 1.3.1 of Chapter 1 and section 6.4.2 of Chapter 6 (Osborne and Swarbrick, 1997; Swarbrick, 1999). Generating overpressure via tectonic compression can be ruled out here, due to the fact that this study area is located within a passive margin that is not tectonically active. Aquathermal expansion and mineral diagenesis are two mechanisms that are considered to be of secondary importance, as it is commonly thought that they are unlikely to generate significant overpressure (Osborne and Swarbrick, 1997) (See section 6.3.2.1 of Chapter 6). There is the potential for a build-up of gas pressure associated with the generation of hydrocarbons within this study area, which will be discussed at length in section 6.3.2.1 of Chapter 6.

The Messinian evaporites are known to have been deposited within the Eastern Mediterranean over a time span of 600 kyrs, which is exceptionally rapid deposition for a unit which reaches thicknesses > 1 km in this study area, as stated in section 3.3 of Chapter 3 (Hsü et al., 1977; McKenzie, 1999; Bertoni and Cartwright, 2007b; Duggen et al., 2003). The deposition of Messinian evaporites is known to have occurred at exceptional sedimentation rates of c. >4 cm/yr (CIESM, 2008). The rapid deposition of Messinian evaporites could, therefore, represent a form of disequilibrium compaction, which in some sedimentary basins has been documented

as a vital mechanism for generating overpressure during the formation of mud volcanoes (Milkov, 2000).

When sediments are deposited within marine conditions, considerable amounts of seawater can be trapped within pore spaces, therefore, on deposition clays can have porosity of up to 80% (Kopf, 2002). Under normal burial conditions, fluids within sediment pore spaces are expelled as the unit becomes loaded by sediments that are being deposited. The unit will remain hydrostatically pressured and, therefore, maintain a state of equilibrium (Kopf, 2002; Osborne and Swarbrick, 1997). In contrast, where fluids cannot be expelled from the sediment pore spaces fast enough due to the rapidity of deposition, the pore fluid pressure can rise and the sedimentary sequence can become overpressured (Osborne and Swarbrick, 1997).

Rapid burial of pre-Messinian marly muds beneath 'sealing' evaporites, could lead to a state of undercompaction and unusually high porosity and fluid retention (Milkov, 2000). With fluids within the pre-Messinian succession unable to escape, loading produces a vertical direction of compressive stress on the undercompacted layer. This would lead to an elevation in pore fluid pressure, particularly within the immediate pre-salt, which could result in significant overpressure generation during early burial (Osborne and Swarbrick, 1997; Deville and Guerlais, 2009; Kopf, 2002). This metastable condition would have persisted until a critical fluid pressure for hydraulic fracture of the overlying evaporites seal occurred.

A secondary driving force that should also be considered in the upward flow of plastic mud is the reaction to buoyancy. Buoyancy forces can have an impact on mud remobilisation and volcanism as a result of the bulk density contrast between an undercompacted and fluid rich and overpressured mud at depth and a sedimentary overburden of greater density (Brown, 1990; Kopf, 2002). The density of mud can be as little as c. 1800 kg/m^3 when undercompacted (Rider, 1986). Evaporites are generally considered to be of low density relative to other lithologies at depth (Hudec and Jackson, 2007; Rider, 1986). However, salt is incompressible and is deposited at its maximum density of c. 2200 kg/m^3, which is a relatively high density for a newly deposited succession (Hudec and Jackson, 2007; Rider, 1986). The density of the

Messinian evaporites could potentially have been of a greater density on deposition than the underlying mud. The bulk density contrast between the mud and evaporites has the potential to generate gravitational instability and present an additional driving force behind the ascent of mud (Kopf, 2002; Brown, 1990). Bulk density contrasts such as this are often thought to one of the driving forces behind the formation of mud diapirs (Judd and Hovland, 2007) (Figure 4.28A). It is, however, important to state that buoyancy forces alone are generally considered insufficient to drive mud volcanism and another mechanism such as the generation of overpressure is thought to be required (Kopf, 2002; Dimitrov, 2002).

While rapid salt deposition may have caused significant overpressure within the pre-salt stratigraphy, a trigger is still required to cause liquefaction and extensive mud volcanism. Since the mud volcanoes described in this chapter are all emplaced at the end of the Messinian 5.33Ma (CIESM, 2008), it seems most plausible that the source layer achieved this critical condition for mud mobilisation at this time. The Messinian Salinity Crisis came to its climax when Atlantic waters flooded through the Gibraltar Strait refilling the Mediterranean during the Messinian or Zanclean flood (Garcia-Castellanos et al., 2009). Recent modelling of this re-flooding event argues that 90% of the refilling occurred in a sudden flood spanning a few months to two years, with peak sea level rise rates of >10m a day (Garcia-Castellanos et al., 2009).

The critical trigger for mud remobilisation could, have been provided by the almost instantaneous (<2 years) loading of an estimated 1-2 km water column during the Zanclean Flood event at 5.33 Ma (Barber, 1981; Druckman et al., 1995; Garcia-Castellanos et al., 2009). This would explain the correlation between Horizon M and the base of these mud volcanoes. Such rapid refilling of the Mediterranean would almost instantaneously increase the overburden stress, which would have a massive impact on the fluid pressure of the already overpressured pre-Messinian sediments. The dramatic addition of vertical load and a concomitant reduction of effective stress could potentially result in liquefaction, leading to seal failure of the evaporites and extrusion of the mobilised liquefied mud at the surface (Judd and Hovland, 2007). The mechanisms with the greatest potential for bypassing the Messinian evaporites include hydraulic, fracturing, dissolution and stoping and are discussed at length in section

6.4.2 of Chapter 6. Breaching of the Messinian evaporites then led to a massive release in pre-salt overpressure and the ascension of a significant volume of fluid and mud (Figure 4.28B).

If these giant mud volcanoes do in fact signify a massive overpressure release event at the end of the Messinian Salinity Crisis, is it possible that other fluid escape features exist at the top of the evaporites in other basins? Basal Pliocene shales were described in section 3.6 of Chapter 3 from Shell's relinquished Northeast Mediterranean licence in Egypt's deep water, Nile Delta. These basal Pliocene shales were described as efficient source rocks. This features display seismic facies which comprise chaotic to discontinuous, low frequency and generally low amplitude reflection (Figure 3.8). The base surface is of a positive polarity and is a reflection that appears to also be shared by the top of the evaporites (Horizon M) (Figure 3.8). The top surface is of a negative polarity and clearly downlaps onto the base surface (Figure 3.8). This shows that the feature is not regionally extensive and appears to be lensoid. The seismic characteristics of this feature and its stratigraphic position show a strong resemblance to the giant mud volcanoes described here. Taking into consideration the close geographical relationship between the survey areas (c. 55 km), it is possible that the basal Pliocene shales discovered by Shell are in fact giant mud volcanoes, similar to those described within this chapter. Pockmarks have also been interpreted at the top of the evaporites, further to the east within the Levant basin (Lazar et al., 2012).

The extraordinary examples of overpressure release and mud extrusion presented here should not be regarded in isolation. These interpretations further contribute to the mounting argument for a major phase of highly focused fluid expulsion and venting of overpressure from the pre-salt succession at the end of the Messinian Salinity Crisis, within basins around the Mediterranean (Bertoni and Cartwright, 2015; Lazar et al., 2012). The giant mud volcanoes observed within this study area demonstrate the massive scale of this overpressure release event, which was evidently significant enough to lead to the formation and now discovery of some of the largest mud volcanoes documented thus far. The primary requirement to form a mud volcano on this scale would appear to be a thick layer of highly undercompacted fine-grained sediment, and extreme priming and triggering mechanisms.

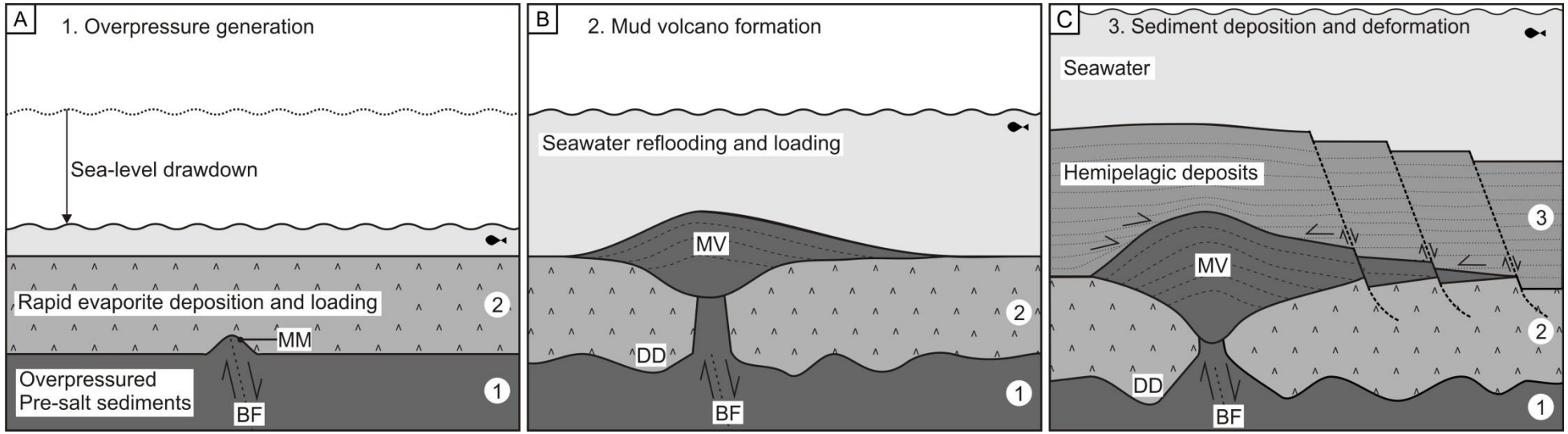

Figure 4.28 Model for giant mud volcano genesis. A: Sea-level drawdown and rapid evaporite loading during the Messinian Salinity Crisis primes the pre-Messinian sediments for mud extrusion. Buoyancy via bulk density contrast between the overpressured pre-salt and evaporite succession drives the formation of a mud mound. B: Sudden and rapid loading of seawater triggers liquefaction of pre-salt sediments which leads to seal failure and the extrusion of liquefied mud. Underlying basement faults appear to play a key role in the extrusion location and base-salt depressions form due to depletion of pre-salt sediments. C: Pliocene-Recent hemipelagic deposits drape and onlap the mud volcano. Gravitationally driven extensional faulting and the localised loading and salt dissolution influence the final form of the mud volcano and Pliocene-Recent interval. MV – Mud volcano; DD – Depletion depression; BF - Basement faults; MM – Mud mound; 1 – Oligo-Miocene; 2 – Messinian evaporites; 3 – Pliocene-Recent.

4.4.3 Giant mud volcano geometry and flux

The geometry and seismic characteristics of these giant mud volcanoes contrasts with what may be considered the typical geometry of a mud volcano, which include: their irregular and varied shape in planform, the lack of interdigitation at the mud volcanoes horizontal margins and their unusually large volume. Other than their exceptionally large volume what other reasons may there be for the irregular shape of these giant mud volcanoes?

It is well documented that faults have the potential to act as preferential pathways for fluid migration (Cartwright et al., 2007; Hooper, 1991). Fluid migration along faults has been shown to heavily influence the location of pipes and pockmarks and even mud volcanoes in other sedimentary basins, such as the Lusi mud volcano (Mazzini et al., 2009; Davies et al., 2008; Mazzini et al., 2007; Gay et al., 2006). Similar to the Lusi mud volcano, it is possible that fluids could be drained from various deeper layers within the pre-salt succession, due to fluid migration along potentially exploitable fault zones such as those identified here within the pre-salt, which could present preferential pathways for fluid migration (Mazzini et al., 2009). As stated above, the potential for fluid origins deeper than the immediate pre-salt are evident from geochemical analysis of samples from mud volcanoes at the surface within the study area (Giresse et al., 2010).

The striking spatial and geometrical correlation between the pre-salt faults and mud mounds and lensoid bodies argues powerfully that at least in the example of LB1 and LB2, the pre-salt faults have had a strong impact on the final geometry of both the mud mounds and the giant mud volcanoes. Mud ridges that form directly above fault planes have previously been invoked as evidence for linking fault planes to significant fluid flux (Cartwright et al., 2007; Berryhill et al., 1987). The formation mud mounds such as these are potentially a function of overpressure within the pre-salt succession and buoyancy forces produced by bulk density contrasts between the pre-salt and the overlying evaporite succession, which could have been locally enhanced by the

addition of migrating fluids along pre-salt faults (Van Rensbergen and Morley, 2003; Brown, 1990; Judd and Hovland, 2007) (Figure 4.28A).

Another factor to consider in the formation of such irregular mud volcanoes is the impact that their extrusion directly on top of a unit of mobile evaporites may have had on their final morphology. The upper surface of the thick Messinian evaporites will undoubtedly have been relatively flat after deposition, which contrasts with the undulation and large depression observed along the present day top-salt reflection of Horizon M. The strong correlation between top-salt depressions, thinning of the evaporites and the overlying giant mud volcanoes presents strong evidence that these top-salt depressions are associated to the formation of the giant mud volcanoes (Figure 4.28A).

In order to form areas of anomalous thinning such as those observed here requires the removal and or withdrawal of salt from the Messinian succession. The significant gravitational load that is applied on the salt by the mud volcano that directly overlies has the potential cause the withdrawal of salt away from the area of elevated load, due to the mechanical properties of salt that allow it to behave somewhat like a fluid over geological time (Hudec and Jackson, 2007). Alternatively or potentially in combination with gravitational loading, the ascent of hot fluids through the evaporite succession during the formation of the giant mud volcanoes could result in the dissolution of the evaporites as observed in other parts of the Mediterranean (Bertoni and Cartwright, 2005), provided the migrating fluids are not already supersaturated. The lack of a classical conical shape could, therefore, in part be rationalised by the iterative process of construction and collapse that would be expected with concurrent flow and/or removal of the underlying salt during the formation of these giant mud volcanoes. It is also possible that the relief built-up at the upper surface of these mud volcanoes is not a prominent as it could have potentially been, due significant volume of mud having subsided as result of the removal/withdrawal of evaporites (Figure 4.28C).

The Pliocene to Recent succession, including the giant mud volcanoes, has been heavily deformed faults associated with the thin skinned gravity tectonics (Gaullier et al., 2000; Loncke et al., 2006; Cartwright and Jackson, 2008) (Figure 4.29A). The throw

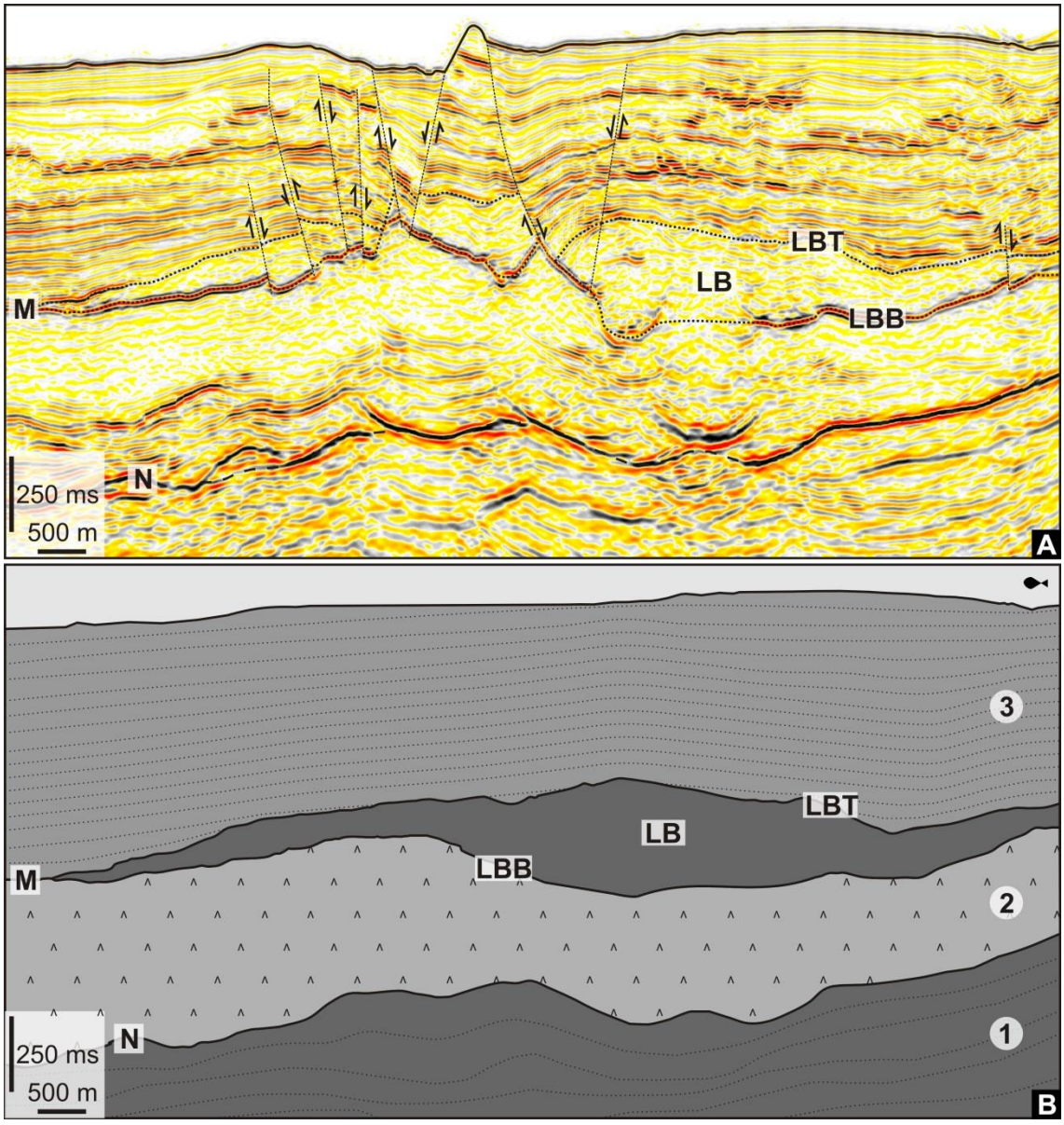

Figure 4.29 Lensoid body reconstruction. A: A seismic profile through LB2 showing significant throw and displacement of the lensoid body across faults within the Pliocene to Recent succession. B: A cartoon reconstruction of what the lensoid body may have looked like prior thin skinned deformation. The reconstruction attempts to compensate for the throw over the faults within the Pliocene to Recent succession. LB – Lensoid body; LBT – Lensoid body top; LBB – Lensoid body base; M – Horizon M; N – Horizon N; 1 – Pre- Messinian succession; 2 – Messinian evaporites; 3 – Pliocene to Recent succession.

over these faults has also contributed to the irregular geometry of the upper and basal bounding reflections of the giant mud volcanoes (Figure 4.28C). Reconstruction of a giant mud volcano was undertaken in an attempt to demonstrate its un-deformed form (Figure 4.29). The reconstruction compensates for the throw over the faults within the Pliocene to Recent succession and shows that prior to deformation, the geometry of these mud volcanoes was less complex and more comparable in seismic profile to what would be considered the classic geometry of a mud volcano (Davies and Stewart, 2005) (Figure 4.29). The basal bounding surface and the upper bounding surfaces are no longer as irregular or undulating and the upper surface slopes more gradually, until converging with the basal surface at the mud volcanoes margins (Figure 4.29).

Another intriguing contrast to other documented mud volcanoes is that in each example described within this chapter, the geometry of the extruded and constructional mud volcano is a single edifice. The extrusion of mud during the formation of a mud volcano is generally thought to occur during cyclic phases of activity including catastrophic events and periods of relative quiescence, which is characterized by moderate activity (Deville and Guerlais, 2009). The frequency and length of eruptions is dictated by changes in the local pressure regime of the primary source (Deville and Guerlais, 2009). Mud volcanoes observed in other basins tend to display interdigitation with basinal sediments, which results in a Christmas tree geometry (Deville et al., 2003; Deville and Guerlais, 2009). The upper and lower bounding reflections of the giant mud volcanoes described here converge onto a single seismic reflection, with no evidence of any internal stratification or interdigitation with the hemipelagites of the Pliocene to Recent succession. These are important observation because they contrast with the seismic characteristics that would be expected from a mud volcano that has been episodically extruded and implies that the extrusion of these mud volcanoes was a single phase event (Evans et al., 2007; Deville and Guerlais, 2009; Kopf, 2002). An alternative explanation could be that the lack of interdigitation in these mud volcanoes is due to formation during a period of low sedimentation, however, the lack of internal stratification maintains the argument for of a single episode of extrusion (Deville and Guerlais, 2009; Evans et al., 2007).

If these mud volcanoes were indeed formed in a single episode of extrusion, is it possible to place any constraints on the likely duration of the eruptive period? This is a challenging problem to solve due to the lack of well calibration and without knowing the eruptive flux of each mud volcano. Using average sedimentation rates for the Pliocene to Recent interval of 200 m/Ma, and a seismic resolution limit of 10 m, it is possible to estimate that the maximum thickness of background sedimentation that could have been concurrent with eruption to be 40 m, yielding a maximum duration of 200 kyrs. It must be emphasised this is only a crude estimate, based simplistically on a longer term average measure of sedimentation rate.

An alternative approach to the timing question is to estimate what the eruption time would be for a mud volcano with volumes similar to those measured here, based on the eruptive flux from a known protracted mud volcano. An eruption flux such as this could be derived from well constrained values of the presently active Lusi mud eruption in Indonesia, which has been estimated to have a flux of 10^4 m^3/day (3652420 m^3/year) (Mazzini et al., 2012). Applying this flux to the $116x10^9$ m^3 volume of LB1, for example, the eruption would have lasted for approximately 30 kyrs. In this context, even with the uncertainties in dating, the scale of these latest Messinian eruptions is clearly orders of magnitude greater than many other documented mud volcanoes, and shows the potential for long-lived mud volcanism in single eruptive episodes (Davies and Stewart, 2005). Recent modelling suggests that the eruptive flux of the Lusi mud volcano is decreasing, and that this catastrophic eruption could terminate by the mid-2030s (Davies et al., 2011). However, potential for long-lived mud volcanism is societally relevant, due to the significant geological hazard and disruption that long-lived extrusion of a mud volcano such as Lusi could pose.

4.5 Conclusion

A suite of five lensoid bodies that lie directly on top of the top surface of the Messinian evaporites within the El Dabaa study region, offshore Egypt, have been identified. Analysis of these lensoid bodies focused on their seismic characteristics, geometrical form and stratal relationship with overlying and underlying deposits. The

images and description of the lensoid bodies presented here build a strong argument that they are in fact the product of surface expulsion, which has formed giant mud volcanoes. The scale of these giant mud volcanoes rank them amongst the largest mud volcanoes to have been documented and described thus far. Further key outcomes from the descriptive analysis are as follows:

- Observations such as a clear connection between mud volcanoes and the pre-salt results in the interpretation that the source of fluids and mud are pre-salt.
- The immediate pre-salt presents a viable candidate as the primary source of mud. Fluids could potentially also be sourced from various deeper pre-salt layers.
- The interpretation of a pre-salt fluid and mud source implies significant fluid and sediment remobilisation that has bypassed a >1000 m thick layers of evaporites and challenges the general belief that thick evaporite sequences represent almost impermeable barriers to upward fluid migration.
- All five of the mud volcanoes described here have been emplaced synchronously directly on top of the upper surface of the Messinian evaporites succession. There formation, therefore, coincided with the end of the Messinian Salinity Crisis.
- Calibration between distant well data in the Levant basin and outcrop studies in Sicily indicates that the immediate pre-salt sediments comprise a marly mud.
- Rapid burial of pre-Messinian marly muds beneath 'sealing' evaporites (deposited within 600 kyrs), could have led to a state of undercompaction and unusually high porosity and fluid retention. Loading of the pre-Messinian sediments beneath a thick unit of evaporites resulted in significant overpressure generation.
- The bulk density contrast between the overpressured mud and evaporites has the potential to generate gravitational instability and present an additional driving force behind the ascent of mud.
- The almost instantaneous (<2 years) loading of an estimated 1-2 km water column during the Zanclean Flood event at 5.33 Ma presents a critical trigger for mud volcanism.

- The timing of the re-flooding event at the end of the Messinian Salinity Crisis would explain the correlation between Horizon M and the base of these mud volcanoes.
- The interpretation of these giant mud volcanoes contributed to the mounting evidence of a major phase of overpressure release from the pre-salt succession at the end of the Messinian Salinity Crisis, within the Eastern Mediterranean.
- Localised gravitational loading of the Messinian evaporites by the giant mud volcanoes that overly and dissolution of the evaporites within the ascending fluids has resulted in prominent and localised thinning of the Messinian evaporites and top-salt depressions.
- A single extrusive body to these mud volcanoes implies that their eruption was a single phase event.
- Estimates for the potential eruptive duration of these mud volcanoes implies the potential for long-lived mud volcanism on the order of several millennia.

Chapter 5

5 The spatial distribution and volumetrics of a large mud volcano province offshore Egypt

5.1 Abstract

This chapter documents and describes through the use of 3D seismic data, a field of up to 386 mud volcanoes located at various depths within the post-salt overburden of the El Dabba study region, offshore Egypt. These mud volcanoes share many similarities in their seismic expression and overall geometrical form; however, they display significant variation in their dimensions. The analysis of base-salt depressions and thinning of the pre-salt succession show that they are spatially related to the location of overlying mud volcanoes. These observations combined with volumetric balance calculations between the pre-salt and mud volcanoes and documented analysis of core samples from these mud volcanoes are indicative of a pre-salt fluid and mud origin. Statistical and spatial analysis of the location of the mud volcanoes shows that those within this study area are statistically clustered and preferentially form in close spatial relation to each other. Various controls dictate the overpressure regime within the pre-salt, which results in areas of localised and elevated overpressure and clusters of mud volcanoes. The interpretation of the mud volcanoes within this study area demonstrate that mud volcanism has occurred within the region for approximately the last 5.3 Myrs. It is suggested here that this region should be considered as among the largest mud volcano provinces in the world, due to the scale of mud volcanism that has been observed.

5.2 Introduction

Focused fluid migration and sediment remobilisation are common and important processes in many sedimentary basins, and are expressed in a variety of large-scale fluid escape features including fluid expulsion pipes and mud volcanoes (Cartwright et al., 2007; Berndt, 2005). Mud volcanoes form via the ascent of mud and overpressured pore fluids from deeper sedimentary layers to the seafloor or surface (Gontharet et al., 2007b; Hovland and Judd, 1988; Brown, 1990; Dimitrov, 2002). They represent the product of an extremely efficient mechanism for dewatering rapidly buried and overpressured clay-rich sedimentary sequences (Kopf and Behrmann, 2000). The precise location and distribution of mud volcanoes is thought to be associated with the generation of overpressure. They are, therefore, of importance within the oil and gas industry as their presence could be indicative of overpressure, which presents a significant drilling hazard. Overpressure such as this can be generated in settings such as where there is rapid sediment loading and the generation of hydrocarbons, both of which are setting often associated with the formation of mud volcanoes (Kopf, 2002; Milkov, 2000).

Previous studies within the Western Province of the Eastern Mediterranean have documented the presence of mud volcanoes at the seafloor through bathymetric maps, side-scan sonar and submersible studies (Prinzhofer and Deville, 2011; Giresse et al., 2010; Loncke et al., 2004; Gontharet et al., 2007b; Dupre et al., 2005; Dupré et al., 2010; Dupre et al., 2007; Huguen et al., 2009; Huguen et al., 2004). Loncke et al. (2004) identified more than 150 sub-circular and conical features within the Western Province, with diameters ranging between 100 - 1000 m and elevations from 10 – 60 m. These observations provide a robust record of present seafloor geometry and mud volcanoes. However, little is known about any buried mud volcanoes or the history of mud volcanism within the area. It is, therefore, currently unclear as to when mud volcano formation began in the area, how the frequency of volcanism has change over time, and what the spatial distribution and controls on mud volcano location are. With the use of 3D seismic reflection data from the El Dabaa survey, it is possible to detect active mud volcanoes at the surface and inactive and buried mud volcanoes. Identification of these mud volcanoes provides an important and complete record of

the eruptive history of the area and potentially the dissipation of long lived overpressure or newly generation of overpressure.

5.2.1 Aim/scope

In Chapter 4, several large mud volcanoes deposited directly on top of the Messinian evaporite succession were identified and described. Prior to their extrusion there is no evidence for mud volcanism within the study area. However, hundreds more mud volcanoes albeit of a comparatively smaller scale can be found to post-date their emplacement. Using 3D seismic data it is possible to observe the entire extruded and constructional body of these mud volcanoes. The regions of the world with the greatest abundance of mud volcanoes known to date are the Mediterranean ridge and Tethyan belt which spans from the south of Greece over the Black and Caspian Sea into Azerbaijan, the Crimea and Tanan Peninsular, Iran, Turkmenisten, the Makran coast, Trinidad and the Barbados ridge (Kopf, 2002). The number of mud volcanoes that have been observed within the El Dabaa study area is comparable in magnitude to those observed within these other regions (Kopf, 2002; Milkov, 2000). Therefore, it is suggested here that the mud volcanoes of the El Dabaa study area should also be considered as among the largest mud volcano provinces known in the world.

In this chapter, a study is presented of the mud volcanoes from the El Dabaa study region offshore Egypt using high resolution 3D seismic data. The data quality of the survey area is very high with a spatial resolution of c.25 m throughout the interval of interest. This means that the 386 mud volcanoes within the survey area are very well imaged, which makes it possible to: (1) accurately identify, pick and catalogue the locations of all mud volcanoes; (2) document their range of dimensions and acoustic characteristics.

The aims of this chapter are to:

1. Understand the controls on the spatial and temporal distribution of mud volcanoes within the study area.

2. Explore how the dimensions of the mud volcanoes, particularly their volume, have changed over time to provide insights into changes in basin hydrodynamics and overpressure.
3. Understand the origin of base-salt and top-salt depressions and investigate any possible relationship between these depressions and the emplacement of mud volcanoes.
4. Analyse and discuss evidence for the source of mud and fluids and the potential trigger mechanisms for mud volcanism.

This study is primarily based on quantitative and semi-quantitative analysis and description of mud volcano geometry and distribution. The geometric information used here (diameter, max thickness, slope angle, volume etc.) was calculated using pre-stack time-migrated 3D seismic reflection data. Kernel density, nearest neighbour index, Ripley's K and Voronoi polygon spatial statistics and chi-square tests were utilised in the analysis for this chapter. For greater detail on these types of analysis and the 3D seismic data used see Chapter 2. Chapter 6 will focus more specifically on the conduits feeding the mud volcanoes and how the mud slurry may have migrated through what is considered to be a world class seal in the form of a thick wedge of evaporites. The wider contextual interpretation of this extraordinary mud volcano province will be discussed in Chapter 7.

5.3 Results

5.3.1 Geometry

The exceptionally large number of present-day and paleo-mud volcanoes within the El Dabaa study area exhibit a broad spectrum of geometrical forms, and are found at a range of depths. The 3D cube covers an area of ~4300 km^2 and contains an extensive mud volcano field with over 386 observed mud volcanoes which are

stratigraphically constrained to the Pliocene to Recent interval. Many of the mud volcanoes are found at the surface, although the majority are buried.

Geometrically these mud volcanoes are recognisable as circular to elliptical and conical lensoid features that are thickest at their centre and thin out towards their flanks (Figs. 5.4D and 5.6D), similar to those described in Dimitrov (2002). Many have clearly built positive topography in the form of a mud cone with slope angles ranging from 5° – 30° (Figs. 5.5 and 5.8). In some cases the interpretation of paleo-cones is more problematic if deformation of the mud volcano has occurred. Deformation including folding, faulting and tilting sometimes results in a more irregular geometry in planform and cross-section (Figs. 5.6 and 5.7). The degree of deformation imparted upon the mud volcanoes tends to increase with depth through the Pliocene to Recent interval, and also includes the general flattening strain associated with burial and compaction.

A typical example of a relatively un-deformed mud volcano that is observable at the surface is presented in Figure 5.1 and Figure 5.2. The volcano has built topography, which is expressed at the seafloor as a mud cone, with a connecting mud flow, within an irregular-circular depression (Figure 5.1A). The features visible at the seafloor are but a fraction of the overall volumetric expression, of the volcano of mud beneath, as demonstrated by the seismic profile in Figure 5.2. The top surface of the volcano is uneven and overall slopes away from the central mud cone. The top surface and base surface converge at the flanks of the mud volcano, forming a lensoid body (Figure 5.1A and Figure 5.2). The base surface has steep, inward sloping sides, which form a central depression (Figure 5.1C). Top and base surface slope angles for all mud volcanoes range from 0.6° - 4.4° and 1.1° - 30.4° respectively. The thickness of the volcano increased towards its centre, which results in an area of maximum thickness that is located centrally (Figure 5.1D and Figure 5.2). The thickness of the mud volcano decreases towards its flanks, and the geometry in planform is circular to elliptical, which results in an overall conical shape (Figure 5.1D and Figure 5.2). A depression and downsagging of reflections can be observed beneath the mud volcano (Figure 5.2). Reflections of the hosting Pliocene to Recent succession onlap part of the upper bounding surface of the mud volcano (Figure 5.2).

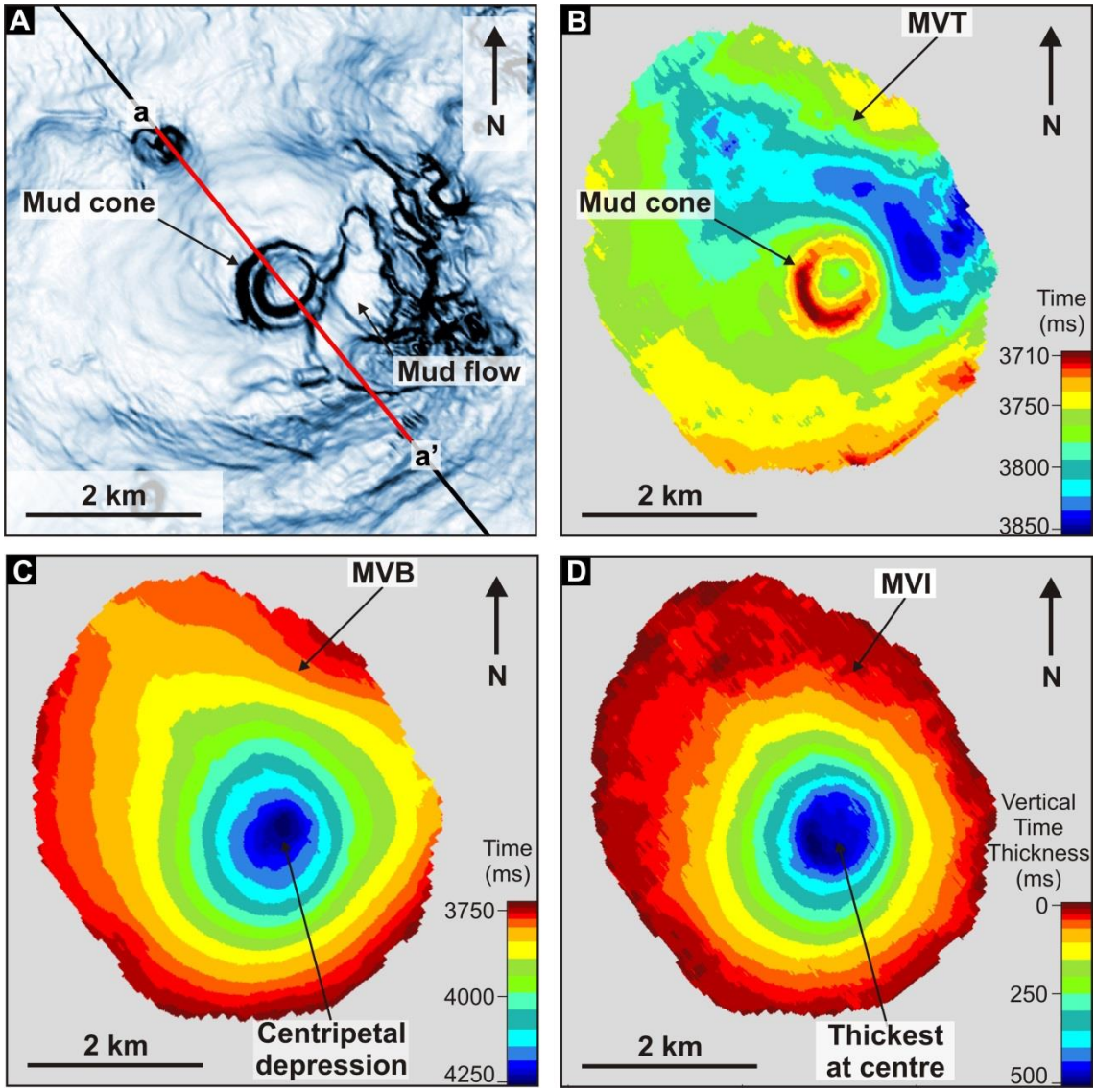

Figure 5.1 Mud volcano geometry. A: A Seafloor dip map showing a mud cone at the surface and the line of section for Figure 5.2. The mud volcano has produced topography in the form of the mud cone. B) A time map of the mud volcanoes top surface showing the increase in relief at the mud cone. C: A time map of the mud volcanoes base surface showing that it is deepest at its centre and is conical. D) A time isopach map of the mud volcano produced from the top and base surfaces, which shows that the mud volcano is circular to elliptical, is thickest at the centre and thins out towards the flanks. MVT – Mud volcano top; MVB – Mud volcano base; MVI – Mud volcano isopach.

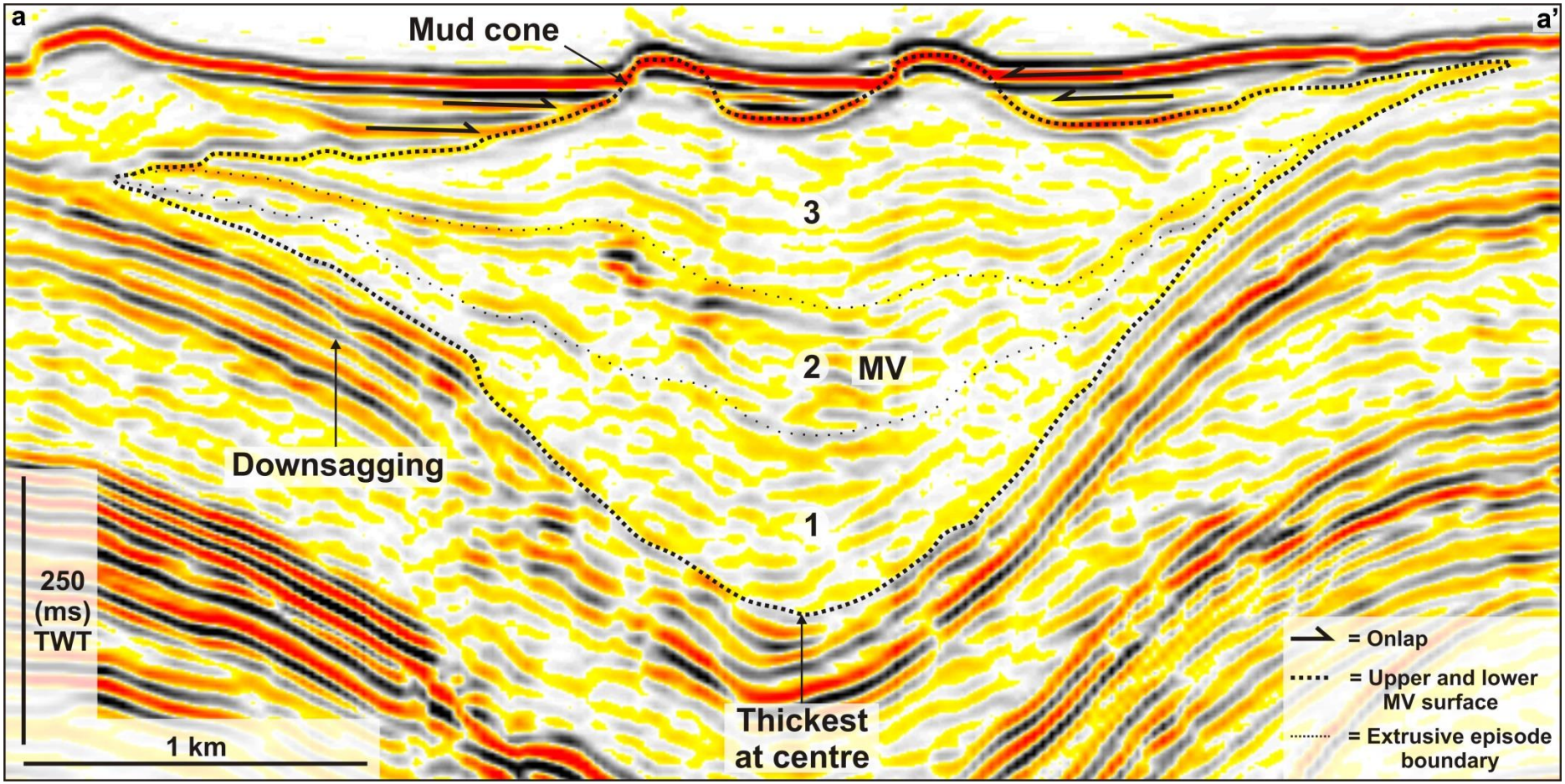

Figure 5.2 Mud volcano geometry seismic profile A: A seismic profile through the mud volcano displayed in Figure 5.1. The mud volcano has a conical shape and has produced a mud cone at the seafloor and is thickest at its centre. Reflections downsag beneath the mud volcanoes, while others onlap onto the volcanoes top surface provides evidence for partial burial. Some continuous internal stratification is suggestive of episodicity. Potential episodes are numbered 1 to 3 in order of formation. MV – Mud volcano.

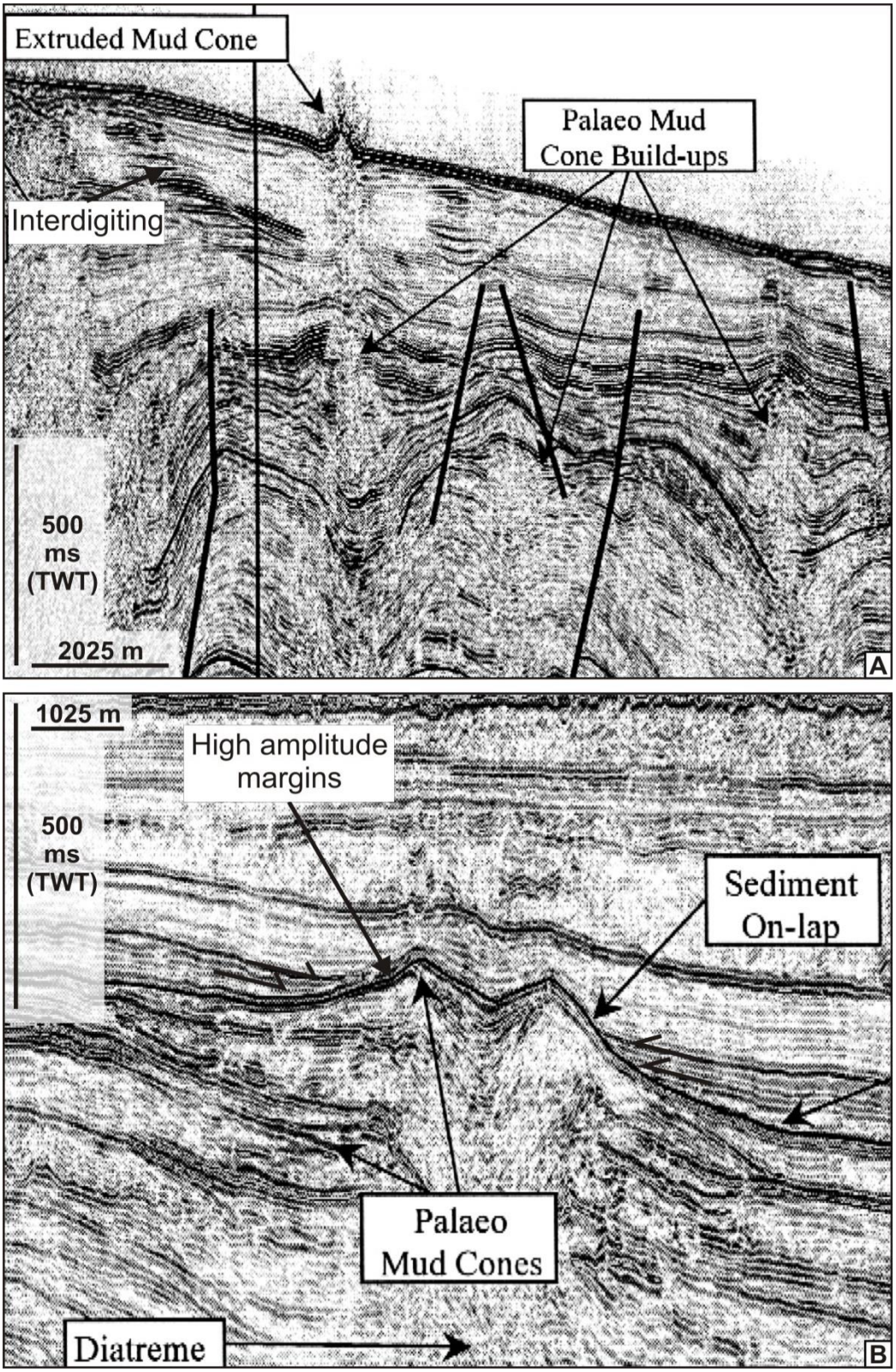

Figure 5.3 Mud volcanoes from Shah Deniz, South Caspian Sea. These mud volcanoes have high amplitude margins and internal seismic facies that comprise of reflections that are generally chaotic to discontinuous, low frequency and low amplitude. A: Buried mud volcanoes and a mud volcano at the surface that exhibits interdigiting with the host rock and has formed a mud cone at its upper surface. B: A mud volcano with a well preserved mud cone onlapped by later sediment deposition. (Images modified from Fowler et al., 2000).

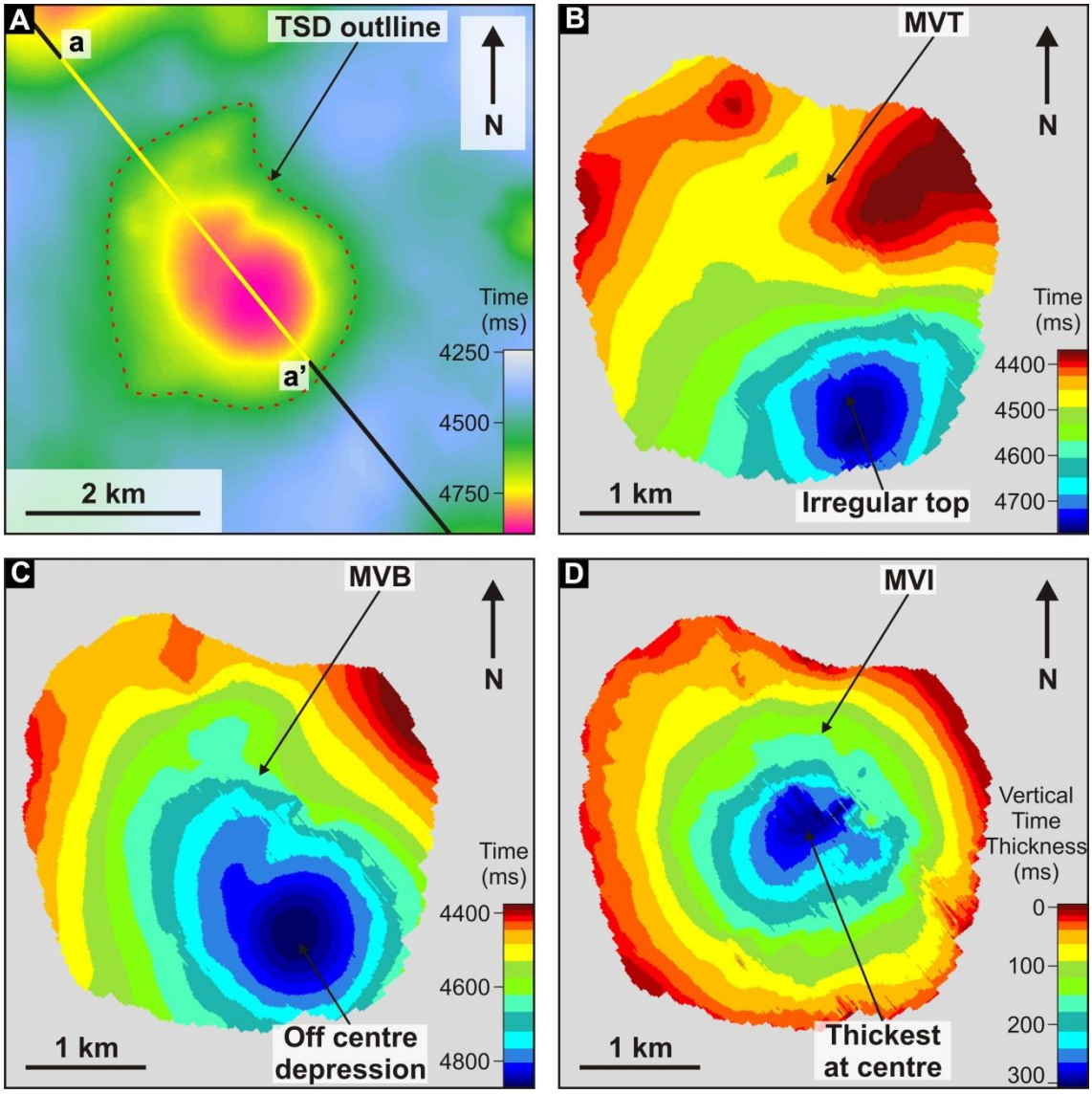

Figure 5.4 A: Deformed mud volcano geometry. A: A time map of the top-salt showing a depression that is related to the location of an overlying paleo mud volcanoes and the line of section for Figure 5.5. B) A time map of the mud volcanoes top surface showing and irregular surface that slopes towards the SSE. The mud volcano has clearly been deformed. C: A time map of the mud volcanoes base surface showing that it is deepest at an off central point towards its SSE flank. D) A time isopach map of the mud volcano produced from the top and base surfaces shows that while irregular the mud volcano has a sub-circular shape and despite the irregularity of its surfaces is thickest at the centre and thins towards the flanks. TSD – Top-salt depression; MVT – Mud volcano top; MVB – Mud volcano base; MVI – Mud volcano isopach.

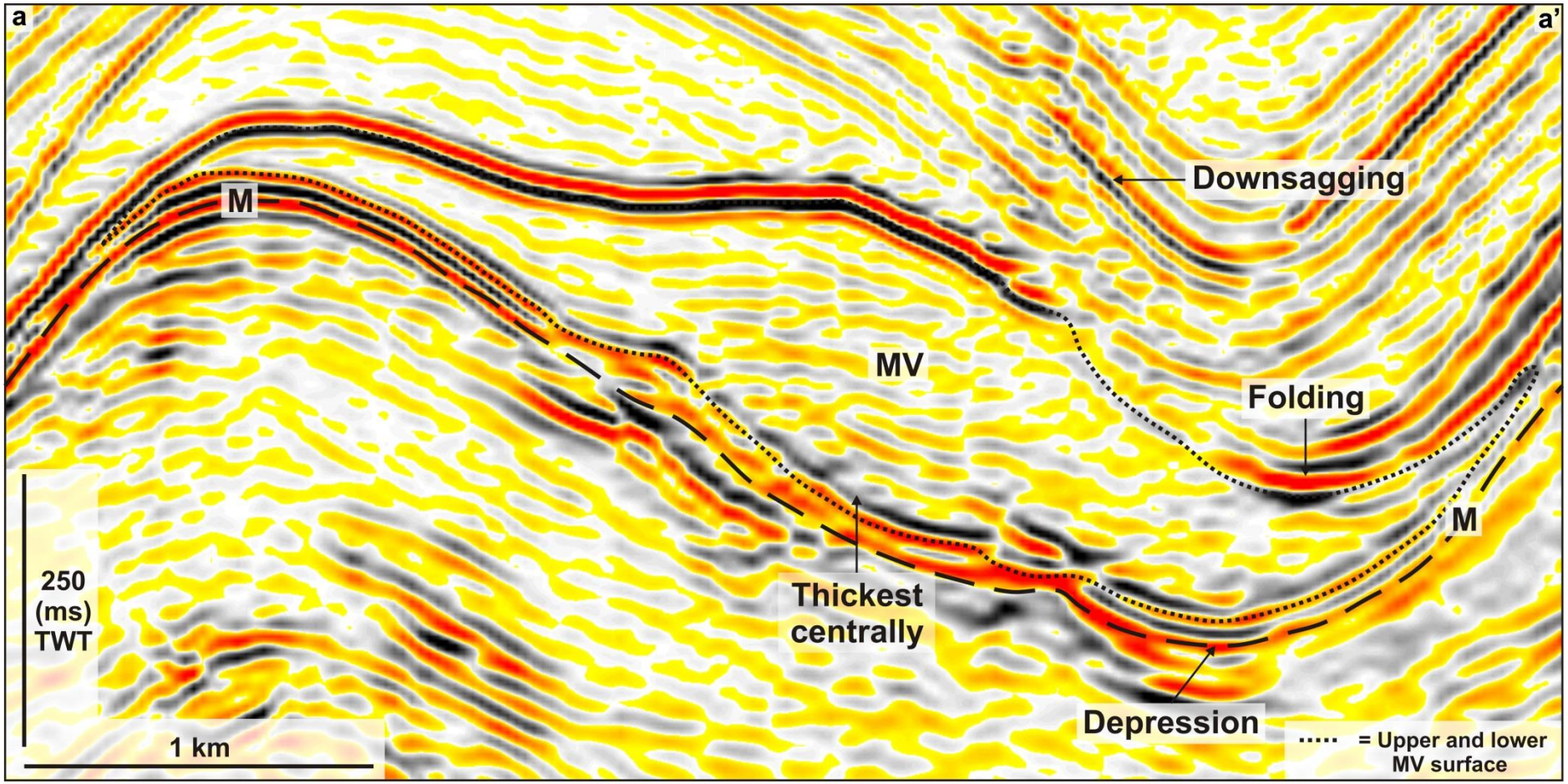

Figure 5.5 A: A seismic profile through the mud volcano displayed in Figure 5.4. The mud volcano has been significantly deformed and the deepest part of the volcano is found towards its south east flank which can be seen to coincide with a top-salt (Horizon M) depression. Despite the deformation the thickest part of the mud volcano is found centrally, similar the mud volcano in Figure 5.5. M = Horizon M; MV – Mud volcano.

An example of a mud volcano that is located just above Horizon M and has subsequently been buried, tilted and folded is presented in Figure 5.4 and Figure 5.5. Some aspects of the appearance of this mud volcano contrast with the example presented in Figure 5.1 and Figure 5.2 due to deformation. The location of this more deformed mud volcano partially overlies a top-salt depression (Figure 5.4A). The upper and lower surface of the mud volcano displays geometry that is irregular and slopes towards the SSE (Figure 5.4B and Figure 5.4C), which contrast with the examples in Figure 5.1. Despite the irregular upper and lower bounding surfaces, the thickness of the mud volcano increases towards its centre and decreases in thickness towards its margins (Figure 5.4D and Figure 5.5). The upper surface of this mud volcano downlaps onto its basal surface margins of the feature and forms as single lensoid body (Figure 5.5). The geometry in planform of the mud volcano is circular to elliptical and its overall form is conical (Figure 5.4 and Figure 5.5). Its geometry is, therefore, similar to previously described mud volcano, despite initial contrast in appearance.

The onlap relationships observed at the margins of the mud volcano examples presented above is indicative that they have built-up topography and that they are partially and even fully buried (Figure 5.2 and Figure 5.3). A similar observation has also been made in other buried mud volcanoes such as those within the South Caspian Basin (Fowler et al., 2000) (Figure 5.3). Mud volcanoes are generally believed to form episodically and their extrusion history is believed to be dependent on the hydrodynamic conditions of the source layer, which provides the flow of mud (Brown, 1990; Dimitrov, 2002; Deville and Guerlais, 2009). The frequency of eruption is essentially controlled by the local pressure regime within the sedimentary pile (Deville and Guerlais, 2009). Some mud volcanoes such as those found onshore Trinidad display phases of activity including catastrophic events followed by periods of relative quiescence characterised by moderate activity (Higgins and Saunders, 1974; Deville and Guerlais, 2009). Mud and gas flows expelled are much reduced during quiescent phases (Deville and Guerlais, 2009).

Episodicity in the flux of a mud volcano can result in interdigitation between the mud volcano and the sediments of the hosting succession at the margins of a mud volcano, similar to the examples presenting in Figure 5.3, from the South Caspian Sea.

The mud volcanoes within this survey area show little indication for episodicity, such as interdigitation (Figure 5.2 and Figure 5.5) with the host hemipelagic deposits and it appears that their extrusion has produced a single conically shaped body. There is however continuity in some internal reflections, suggestive of stratification which may be indicative of some degree of episodicity in their formation (Figure 5.2 and Figure 5.5).

5.3.2 Seismic expression

Despite the observed differences in the geometry of the mud volcanoes within this study area, they all display similar seismic characteristics which are distinctive (Figure 5.2 and Figure 5.5). Examples of the seismic characteristics of mud volcanoes, further to those displayed above can also be seen in Figure 5.6. They are characterised by high amplitude top and base reflections (Figure 5.6). These bounding reflections contrast with their internal seismic facies, which comprise reflections that are generally chaotic to discontinuous, low frequency and low amplitude, with some continuous stratification and amplitude anomalies (Figure 5.6). Their internal reflections also contrast with the high amplitude and continuous seismic facies of the hosting Pliocene to Recent aged hemipelagic deposits (Figure 5.6). This description is similar to that of other mud volcanoes described from the Central Mediterranean Ridge and Nile deep-sea fan which have been described as “acoustically transparent” (Huguen et al., 2004; Giresse et al., 2010). Other examples of mud volcanoes with similar geometries and seismic characteristics are found within Shah Deniz in the South Caspian Sea (Fowler et al., 2000) (Figure 5.3).

Localised amplitude anomalies are often observed within these mud volcanoes (Figure 5.7). They are defined as very high amplitude and negative reflections (black) that are bound above and below by very high amplitude and positive reflections (red), which is typical of a soft reflection (Figure 5.7). The margins of these amplitude anomalies are abrupt and correlate with the horizontal margins of a zone of amplitude attenuation within underling conduits that will be described in

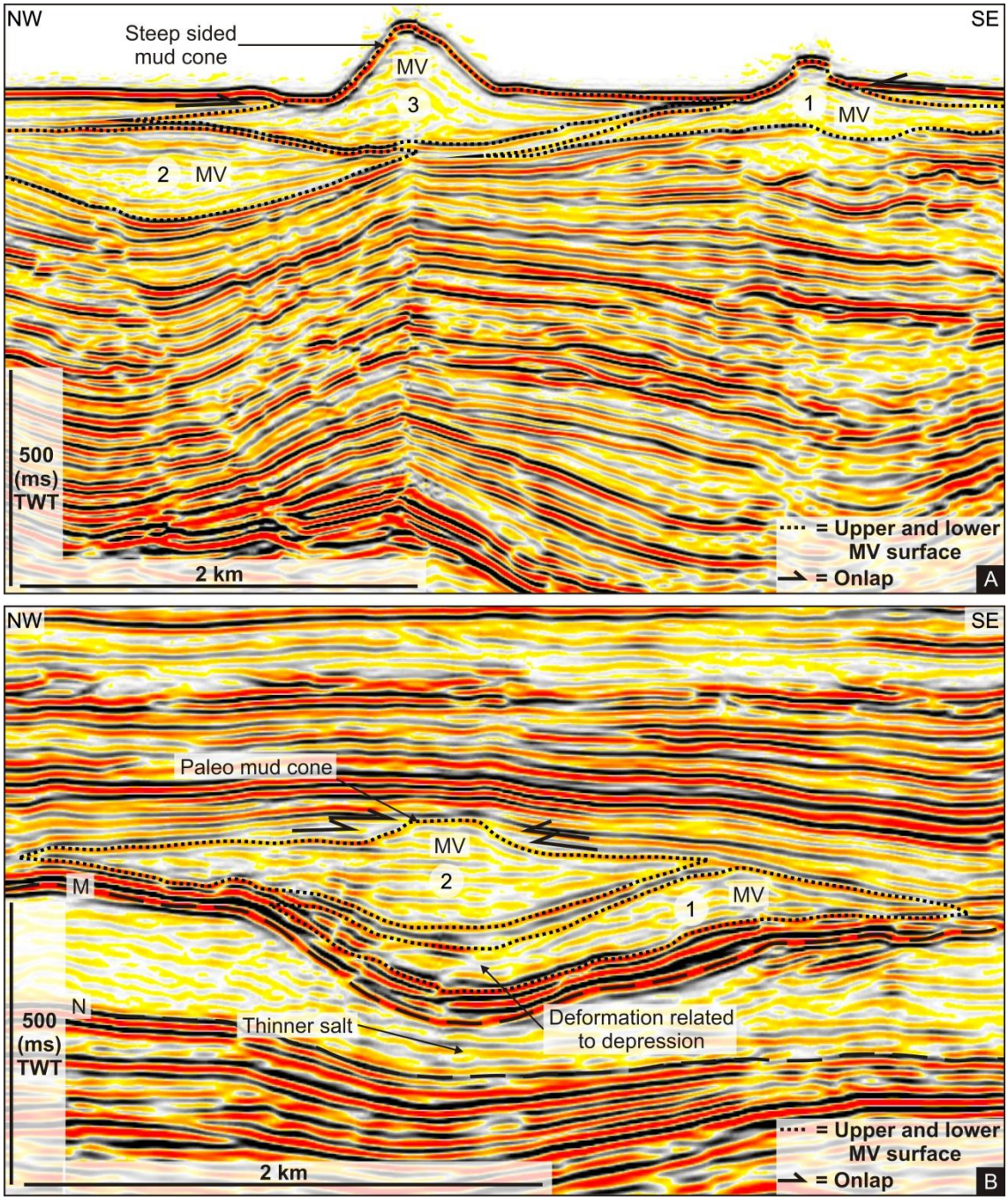

Figure 5.6 Mud volcanoes with varying geometry and key seismic characteristics. In the seismic profiles the mud volcanoes are numbered in order of formation. A) Three mud volcano near the seafloor. B) Two mud volcanoes just above Horizon M. MV – Mud volcano.

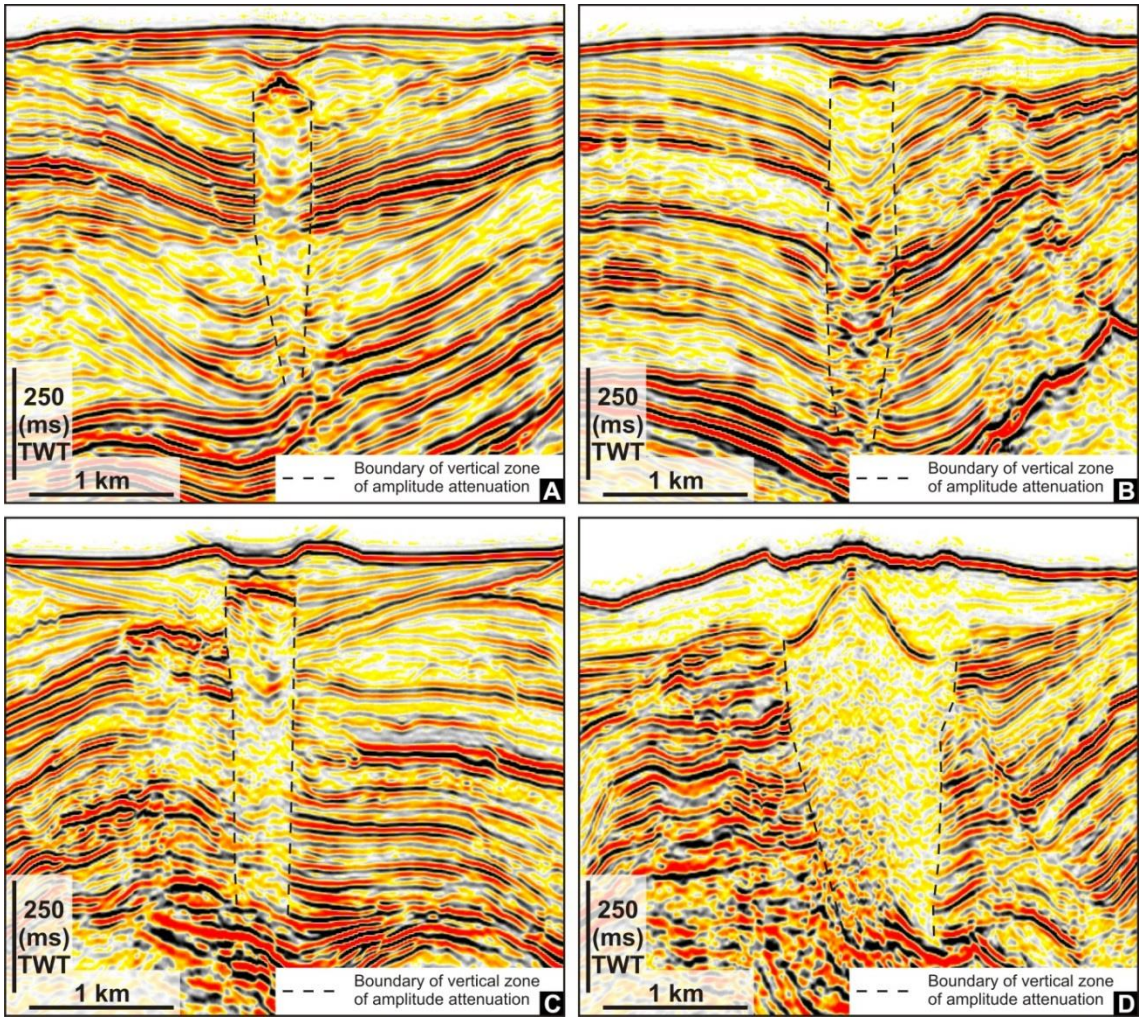

Figure 5.7 Amplitude anomalies associated with mud volcanoes. A-D: four examples of high amplitude soft reflections at the centre of the mud volcano and a vertical zone of amplitude attenuation beneath the overlying soft reflection, both of which have abrupt margins.

detail in Chapter 6 (Figure 5.7). Attenuation of reflections with depth within the volcano can make identifying the base of the volcano and its conduit difficult. Amplitude anomalies such as those described here are sometimes associated with the presence of gas and often occur through scattering and absorption of acoustic energy within gas charged sediments, resulting in vertical zones of reduced seismic signal (Judd and Hovland, 1992).

The deformation imparted on a mud volcano can result in it being more challenging to interpret. An example of a deformed mud volcano has been described above from Figure 5.5. A mud volcano that has been significantly deformed and is overlain by another mud volcano can be seen in the example displayed in Figure 5.6B. The upper and lower surface of the deformed mud volcano in this example slopes towards the NW and its deepest part is correlatable with a underlying top-salt depression, which is correlatable with the centre of a more recently formed mud volcano that overlies and is un-deformed (Figure 5.6B). Despite the contrast in geometry between the deformed and un-deformed mud volcanoes, their seismic characteristics are clearly similar and as previously discussed their overall form is lensoid, which means their interpretation remains relatively straight forward (Figure 5.4 and Figure 5.5). The mud volcanoes are very well imaged throughout the Pliocene-Recent interval even with increasing depth. This has allowed for seismic picking and documentation of the varied dimensions of all mud volcanoes within this study area (See supplementary data for Chapter 5 in the appendices).

5.3.3 Recent mud volcanism

The geometry of the present day seafloor has been significantly influenced by a large number of mud volcanoes, distributed across a range of bathymetry, from 2500 m to 3300 m. In a gross sense, the area can be divided into three distinct domains based on the dominant geological features that characterise them. These domains include a growth fault dominated region to the west (Domain A), a channel/levee region to the east (Domain C) and a central fluid escape region which contains the

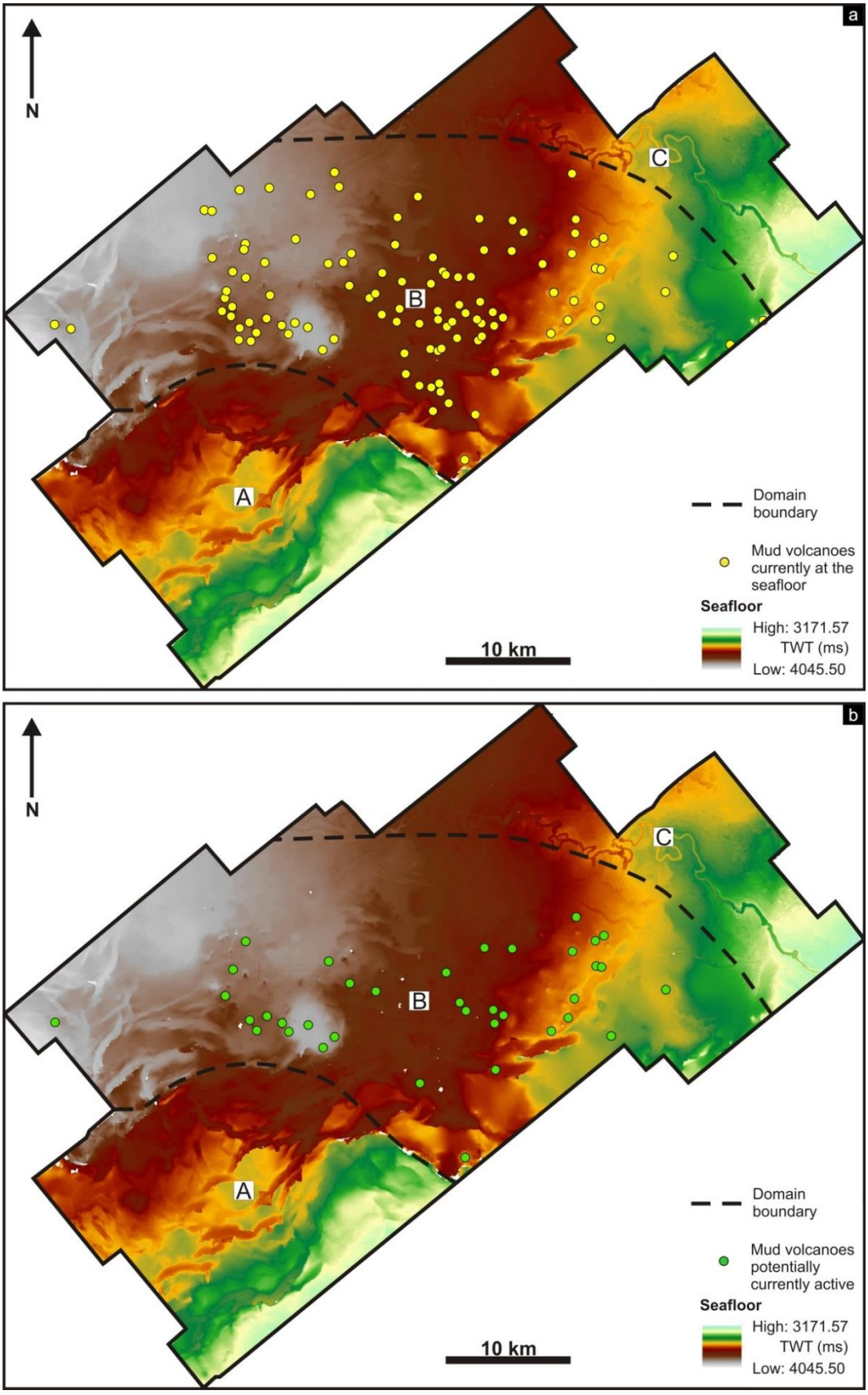

Figure 5.8 Active and inactive seafloor mud volcanoes A: Time attribute map of the seafloor showing the location of all mud volcanoes currently at the seafloor within the study area. B: Time attribute map of the seafloor showing all mud volcanoes currently at the seafloor and show no evidence of burial so are interpreted to currently active. A = Domain A (Growth fault domain); B = Domain B (Fluid escape feature domain); C = Domain C (Channel levee domain).

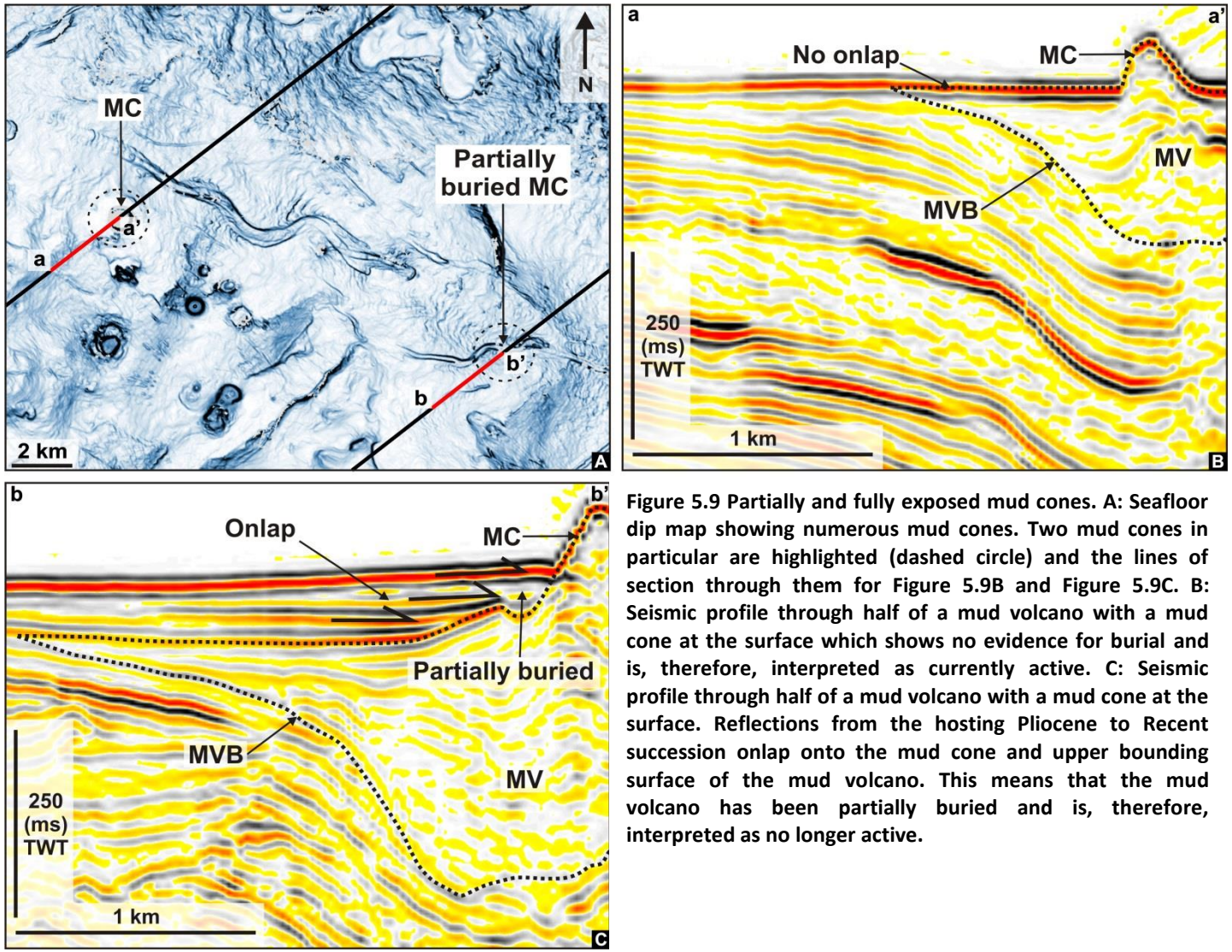

Figure 5.9 Partially and fully exposed mud cones. A: Seafloor dip map showing numerous mud cones. Two mud cones in particular are highlighted (dashed circle) and the lines of section through them for Figure 5.9B and Figure 5.9C. B: Seismic profile through half of a mud volcano with a mud cone at the surface which shows no evidence for burial and is, therefore, interpreted as currently active. C: Seismic profile through half of a mud volcano with a mud cone at the surface. Reflections from the hosting Pliocene to Recent succession onlap onto the mud cone and upper bounding surface of the mud volcano. This means that the mud volcano has been partially buried and is, therefore, interpreted as no longer active.

majority of the mud volcanoes that are seen at the surface (Domain B) (Figure 5.8). These mud volcanoes are invariably characterised by a mud cone, which produces a prominent circular positive topographic feature, with sloping sides and in some cases a depressed centre (Figure 5.8). Mud cones are formed when mud of moderate to high viscosity is emitted from a central feeder or conduit, onto the seabed over a period of time, resulting in a mud mass build up in the shape of a cone like structure (Fowler et al., 2000; Kopf, 2002).

There are 110 mud volcanoes exposed at the seafloor, however, not all of them are currently active (Figure 5.8). Some mud volcanoes are fully exposed and show no signs of burial, while some show evidence of partial burial through the onlapping of reflections, interpreted to be hemipelagic deposits, onto the mud cone and top surface (Figure 5.9). 77 mud volcanoes show evidence for burial and the remaining 37 mud volcanoes show no evidence of burial via onlap onto the volcanoes upper bounding surface or mud cone (Figure 5.8). Those 37 mud volcanoes that show no evidence for burial are interpreted as currently active. All but two of these mud volcanoes are found within Domain B of the survey area (Figure 5.8). Many fully buried mud volcanoes also exhibit a mud cone and reflections of the host succession clearly onlap the feature similar to that which is observed in some more shallowly buried mud volcanoes (Figure 5.6B and Figure 5.9C).

5.3.4 Distribution

5.3.4.1 Temporal distribution

The mud volcanoes within this study area are stratigraphically restricted to within the Pliocene to Recent succession and can be found at a multitude of depths throughout this stratigraphic unit ranging from a seafloor depth of 3100 m, to as deep as 6120 m subsea, i.e. just above the evaporites (Figure 5.11). In order to examine the distribution of mud volcanoes vertically through the Pliocene to Recent interval, a small number of key marker horizons that are regionally continuous within the

succession were mapped over the entire study area. The purpose of the regional mapping was to assess whether there are particular sections of the Pliocene to Recent interval where mud volcano frequency increases or decreases.

The precise age of individual reflections within the Pliocene to Recent succession and hence age of the conical mud volcanoes within this study area are unfortunately unknown in the absence of reliable well calibration. An alternative approach to the timing question is to consider what other key marker horizons exist within the stratigraphic succession that could allow the mud volcanoes to be divided into broad phases of mud volcano formation. One key marker horizon is the high amplitude and continuous reflection of Horizon M. This regionally extensive reflection is correlatable with the end of the Messinian Salinity Crisis 5.33Ma and defines the boundary between the Pliocene to Recent succession and the underlying Messinian succession.

The Pliocene to Recent succession is primarily comprised of moderate to high amplitude reflections that generally display high lateral continuity, however, these reflections are frequently not regionally extensive and there is no present means to age them. The only surface within the Pliocene to Recent succession that could potentially be correlated with a particular age is the base of a large mass transport deposit (MTD) within the east of the study area. This prominent MTD, which will here be referred to as the El Dabaa slide, displays highly disrupted to transparent seismic facies internally. Some higher amplitude packages that show a greater degree of coherency can be observed within the MTD and it is bound by top and base reflections that are high amplitude (Figure 5.13 and Figure 5.14). The basal surface of the El Dabaa slide is uneven and in parts has a small step like geometry. The upper bounding surface is smooth by comparison. Both the upper and basal surface reflections of the EL Dabaa slide are concordant with the reflections of the underlying succession, which display numerous depressions. These depressions are spatially related to top-salt depressions (described in detail in section 5.3.6); therefore, slope failure pre-dates the formation of these depressions.

Unfortunately only a fraction of the full areal extent of the El Dabaa slide can be seen as it is cut by the limits of the survey area to the north, east and south. What can be observed of it though covers an area of 1602 km^2 with vertical thickness ranging from 70 m to 230m, an average burial depth of 415 m, and a volume of approximately 262 km^3. This data was calculated by exporting the El Dabaa slides upper and basal surface from Schlumberger's IESX software to Golden Software's Surfer 11. Within Surfer the surfaces were depth converted based on an average velocity of 1950 m/s, which was calculated using the pre-stack depth migrated velocity data, and the volume between the two surfaces was calculated. The El Dabaa slide is thickest towards the SE and thins towards the NW, dipping in a NW direction at an average angle of <1° concordantly with the hosting Pliocene to Recent succession (Figure 5.14). This dip angle is very shallow, which could be indicative that what can be seen of this MTD is closer to the toe of the larger slide, with the head scarp possibly located further to the SE near the head of the continental slope. It has a very steep western flank, which is the only margin that is visible within this study area. The average TWT interval between the seafloor and basal surface of the El Dabaa slide is approximately 400 ms.

A mere <45 km to the east of the El Dabaa study area (Figure 5.15), seven other examples of MTDs observed at different stratigraphic levels have been described by Garziglia et al. (2008). The largest of these MTDs named SL2 has a general SE to NW direction of movement and is cut by the NW limits of the survey area; therefore the full extent of the MTD is unknown (Figure 5.15). Despite this the SL2 slide has been interpreted to cover an area of approximately 5000km^2 and has an approximate volume of 500 km^3. The west and east margins of the SL2 slide, which are perpendicular to the MTDs direction of movement, display very steep slopes (Figure 5.15). The NW margin of the SL2 slide where it is cut by the limits of the data displays the MTDs area of greatest thickness and width, which suggests it is possible that the SL2 slide could extended several hundreds of kilometres down slope and cover an area of several thousand more square meters (Garziglia et al., 2008) (Figure 5.15).

Garzigilia et al. (2008) speculated that methane hydrate destabilisation due to a sea level drop of about 50 m at approximately 117 kyrs may have triggered the SL2 slide event. Hydrate formation can cement sediments and impede normal mechanical

compaction of the hydrate bearing sediments; therefore destabilisation of hydrates via dissociation or dissolution may lead to significant plastic deformation (Sultan, 2007). Garziglia et al. (2008) suggests that the inevitable decrease in hydrostatic pressure following the Eeimian high stand (120 ka) may not have been outweighed by a decrease in sea bottom water temperature, which might have led to the destabilisation of any gas hydrates present.

The SL2 slide shares many similarities to the El Dabaa slide in that it displays comparable seismic facies with few rafted blocks and its thickness varies from several tens to several hundreds of meters (Garziglia et al., 2008). The SL2 and El Dabba slide display steeply sloping sides at their western margin. Based on the seismic profiles in Garziglia et al. (2008), the SL2 and El Dabaa slide are also located at comparable TWT intervals between the seafloor and basal surface of the MTDs and the SL2 slides direction of movement appears to be oriented in the direction of the El Dabaa study area. Based on the similar characteristics between the El Dabaa and SL2 slides, their geographical position relative to each other and the SL2 slides potential to extend a significant distance further downslope, it is conceivable that the El Dabaa slide could in fact be part of the SL2 slide (Figure 5.15). If the correlation of these two MTDs is correct (Figure 5.15), it would suggest that the EL Dabaa slide formed between 117 and 105 ka (Figure 5.17).

The stratified distribution of mud volcanoes is illustrated in the seismic profiles in Figure 5.11 and Figure 5.12. It can be clearly observed that there are numerous mud volcanoes near to the base of the Pliocene – Recent succession (Figure 5.11 and Figure 5.12). The frequency of mud volcanoes appears to decreases up through the succession which results in a relatively thick interval where no mud volcanoes can be observed (Figure 5.11 and Figure 5.12). An increase in the frequency of mud volcanoes can be observed once again nearer the top of the Pliocene to Recent succession. This interpretation is also supported by the previously stated observation of 110 mud volcanoes that have been observed to be at least partially exposed at the seafloor. The basal surface of the El Dabaa slide is stratigraphically located between the two observed periods of high mud volcano frequency. In the absence of well calibration, the El Dabaa slide represents the best means to provide some constraints

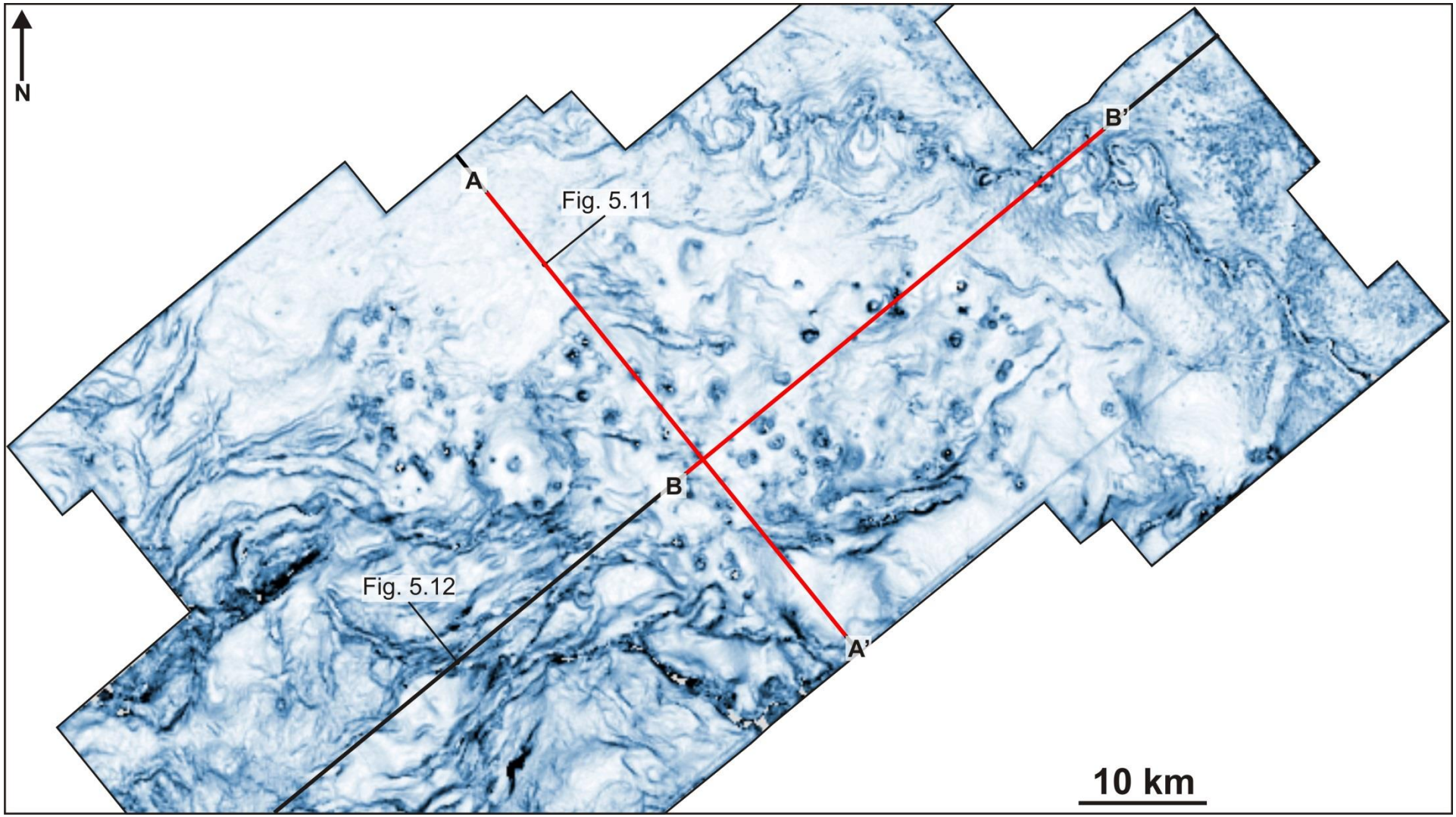

Figure 5.10 Seafloor dip map of the survey area showing the two regional lines of section used in Figure 5.11 and Figure 5.12).

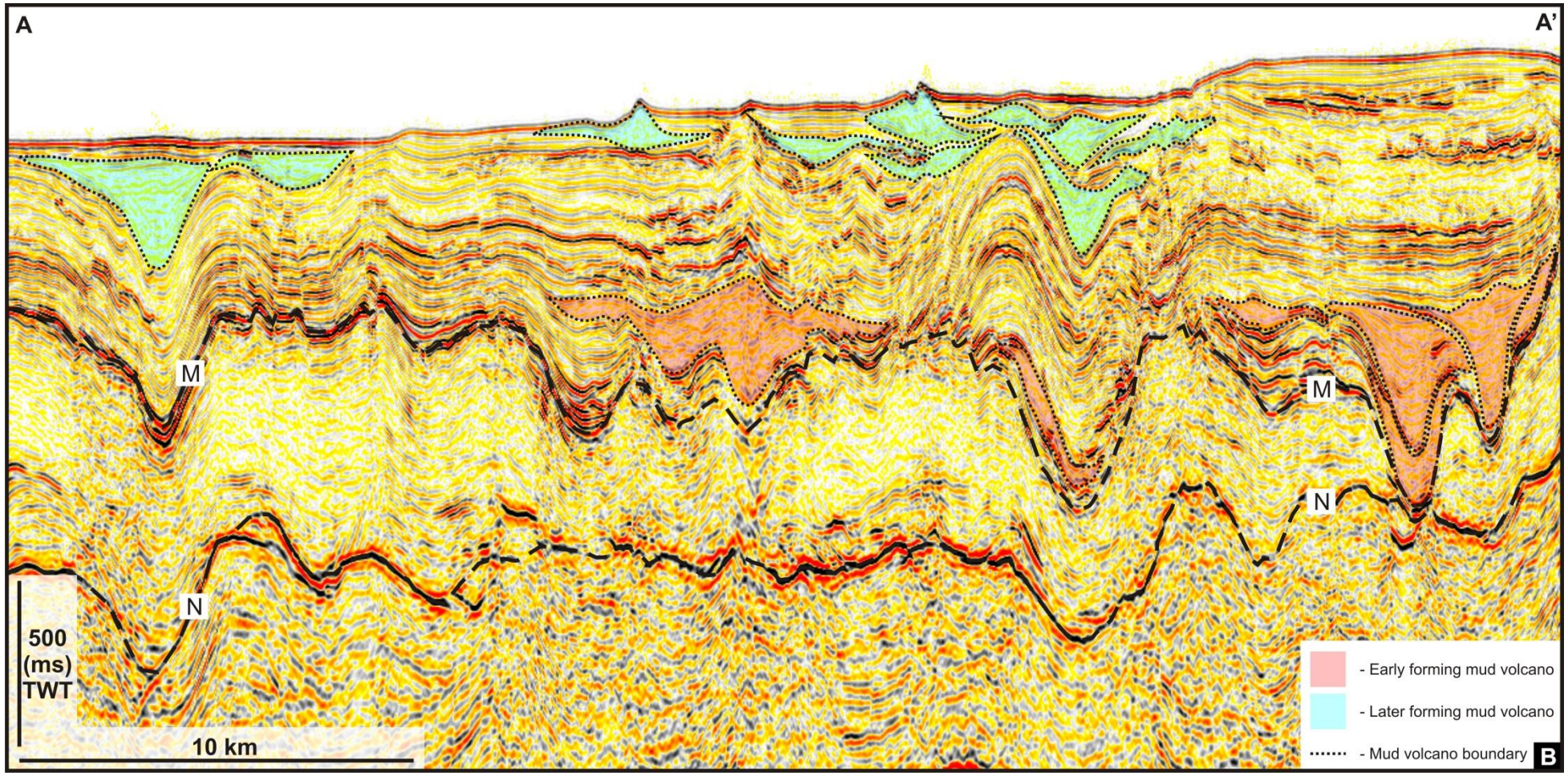

Figure 5.11 NW to SE seismic profile through the survey area highlighting the mud volcanoes. There are a large number of mud volcanoes found near the base of the Pliocene interval above Horizon M. The number of mud volcano appears to decrease vertically up through the succession until their number increases again nearer the top of the succession. This fluctuation in the frequency of mud volcanoes produces an early and a later phase of mud volcano formation, phase 1 (red) and phase 2 (blue).

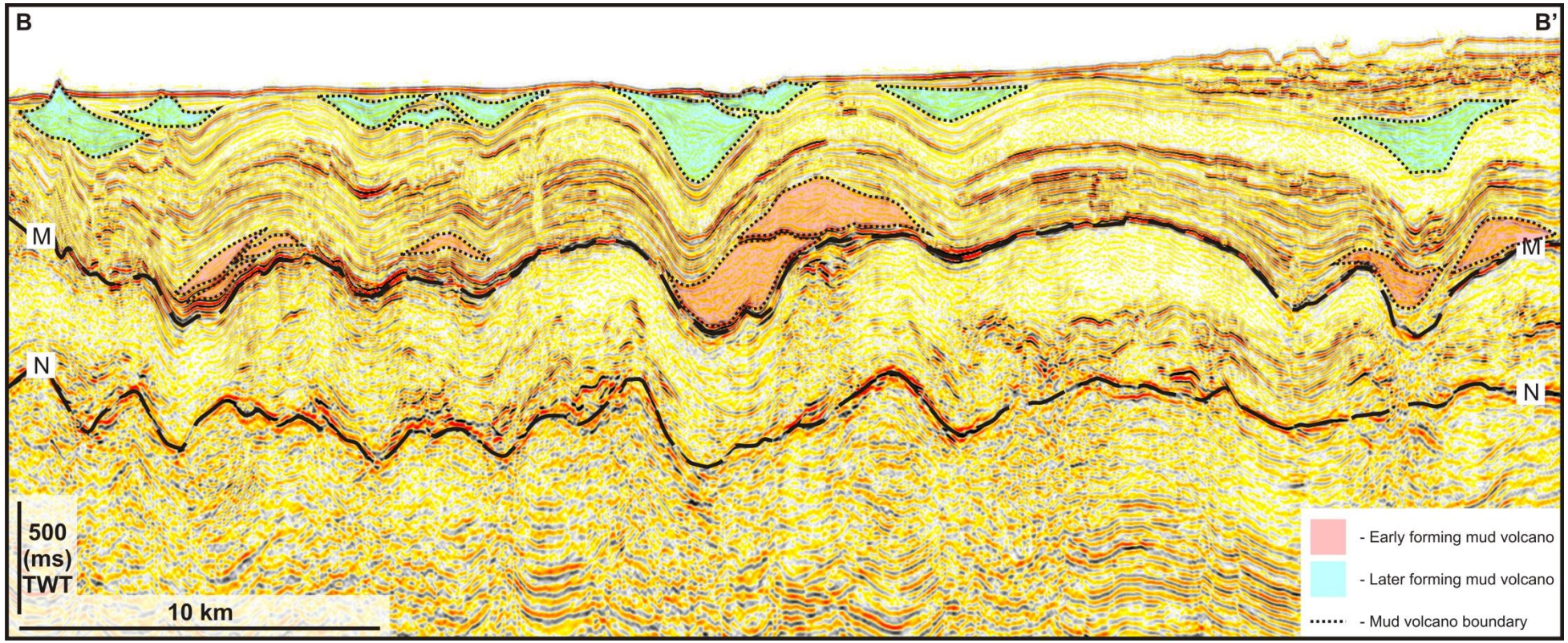

Figure 5.12 SW to NE seismic profile through the survey area highlighting the mud volcanoes. There are a large number of mud volcanoes found near the base of the Pliocene interval above Horizon M. The number of mud volcano appears to decrease vertically up through the succession before increasing again nearer the top of the succession. This fluctuation in the frequency of mud volcanoes produces an early and a recent phase of mud volcano formation, phase 1 (red) and phase 2 (blue).

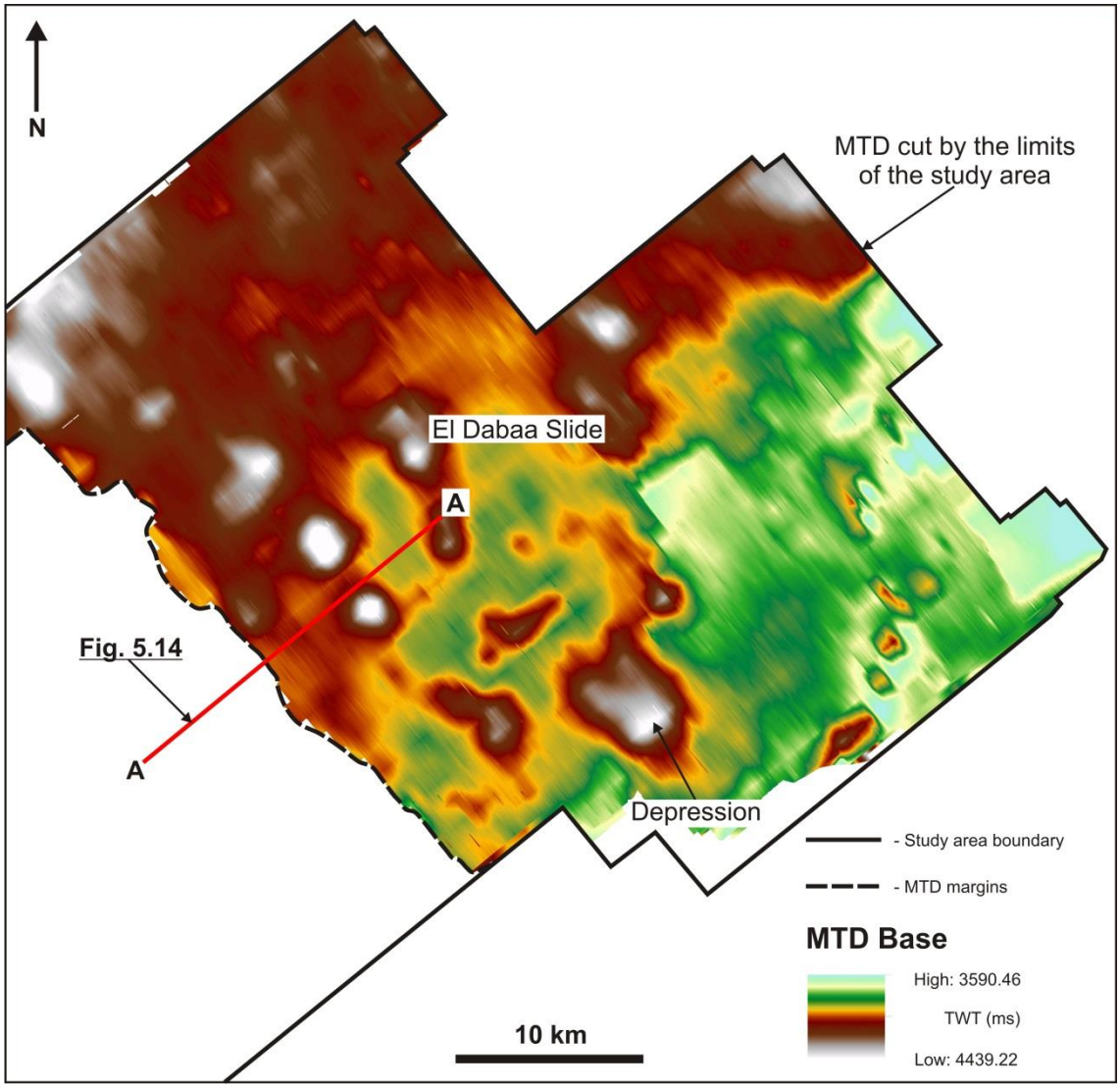

Figure 5.13 Mass transport deposit (MTD). A time map of the basal surface of the El Dabaa slide, showing the areal extent of the MTD within the study area, several depressions and the line of section for Figure 5.17. The MTD is cut by the edges of the survey area therefore the full extent of the MTD is unknown.

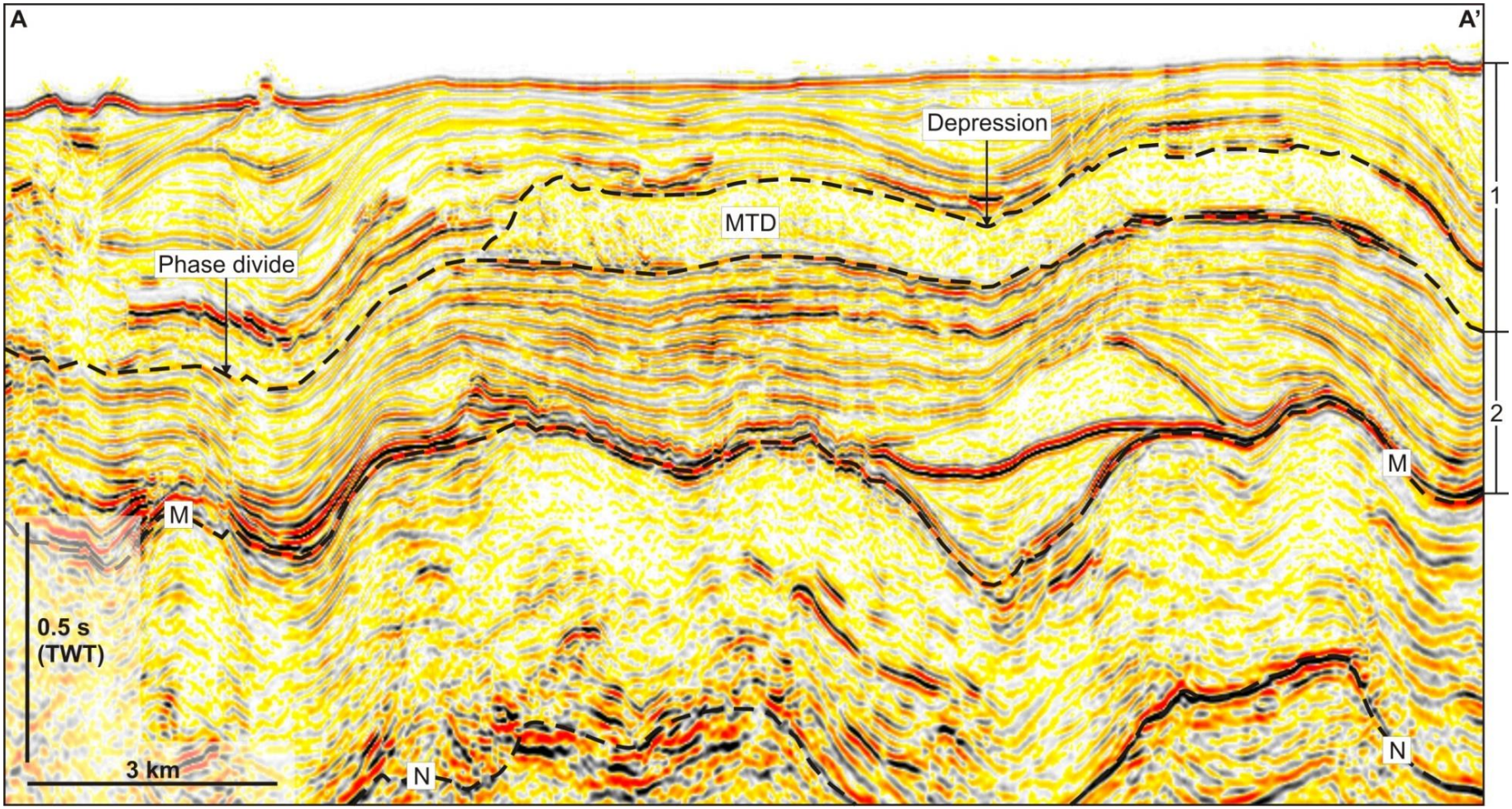

Figure 5.14 Seismic profile through the El Dabaa slide. It is seismically characterised by uneven high amplitude top and base reflectors and comprises of highly disrupted to transparent seismic facies with some higher amplitude packages. The MTD package is concordant with the underlying reflections of hemipelagic deposits and is therefore deformed into numerous depressions. The basal surface of the MTD can be correlated regionally and serves as a divide between the mud volcanoes of phase 1 and 2. 1 = Phase 1; 2 = Phase 2.

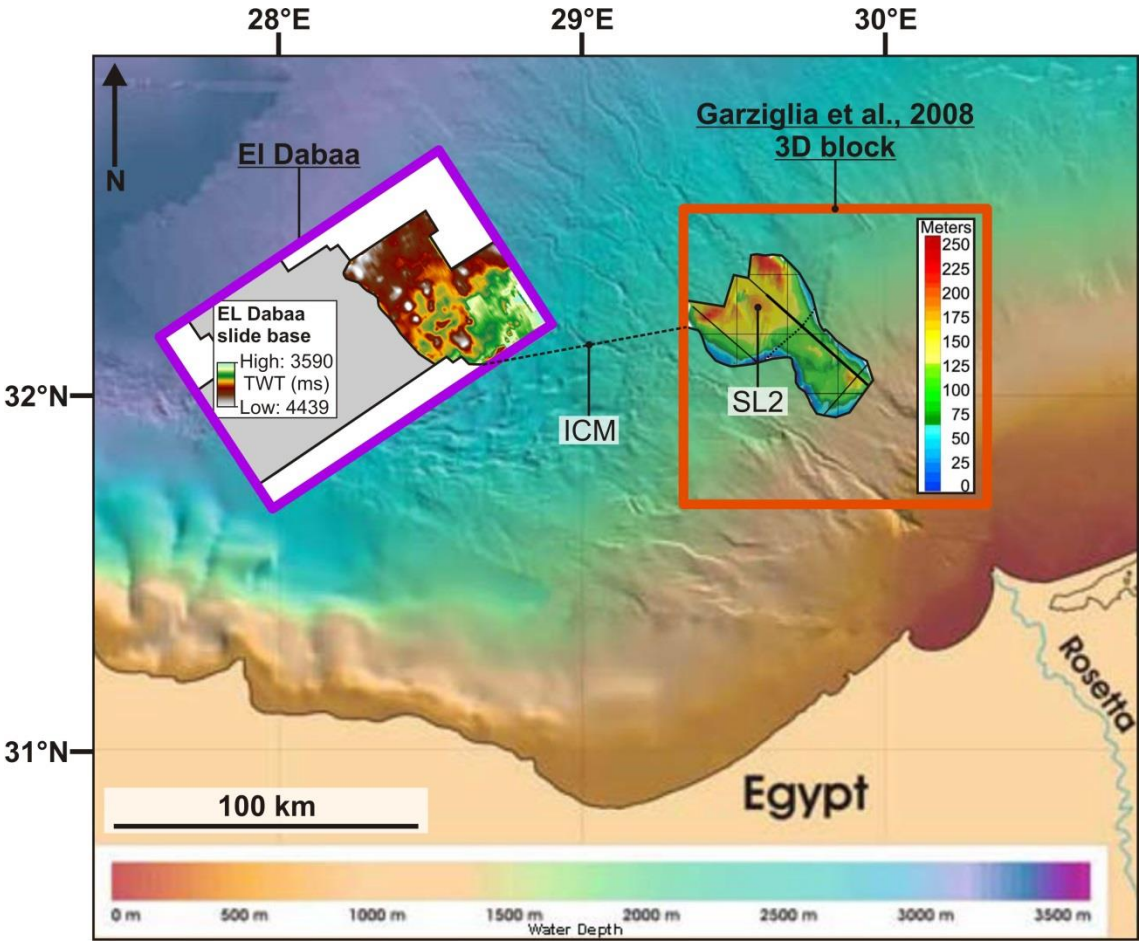

Figure 5.15 A location map of offshore Egypt and the Nile delta showing the geographical position of the El Dabaa study area and the El Dabaa slide within the study area and the survey area used in Garziglia et al. (2008) and the SL2 slide that is described by Garziglia et al. (2008). The location map shows that the two survey areas are separated by a mere 45 km and that the El Dabaa slide and southwest margin of the SL2 slide may be correlatable. ICM – Interpretive correlation of mass transport deposit (Isopach map of the SL2 landslide is modified from Garziglia et al. (2008)).

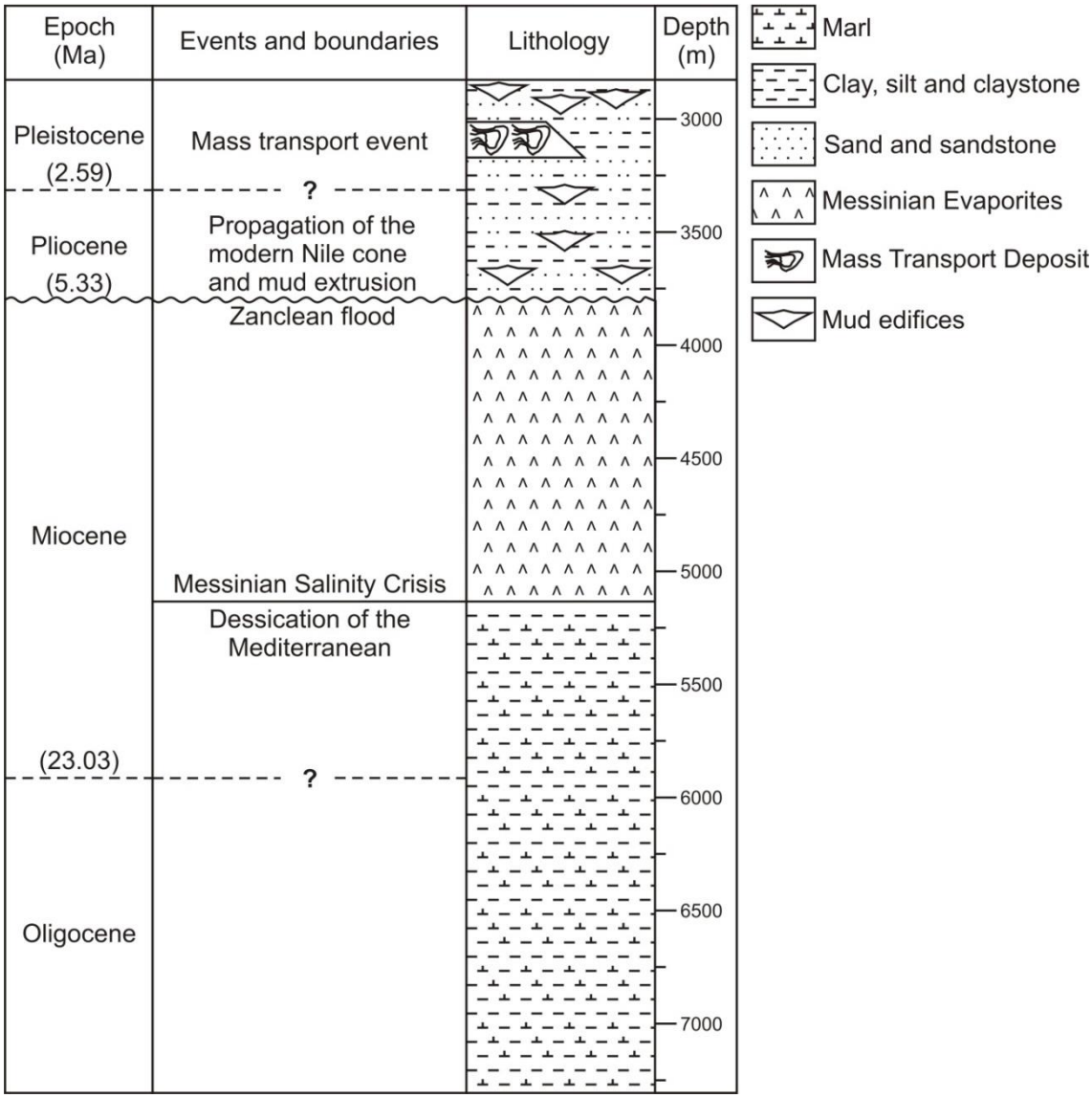

Figure 5.16 Chronostratigraphic chart of the sedimentary succession within the El Dabaa study area. Due to a lack of nearby well calibration, this chronostratigraphic chart is an approximation based on 3D seismic observations and draws inspiration from the chronostratigraphy of the Levant basin (Bertoni and Cartwright, 2005).

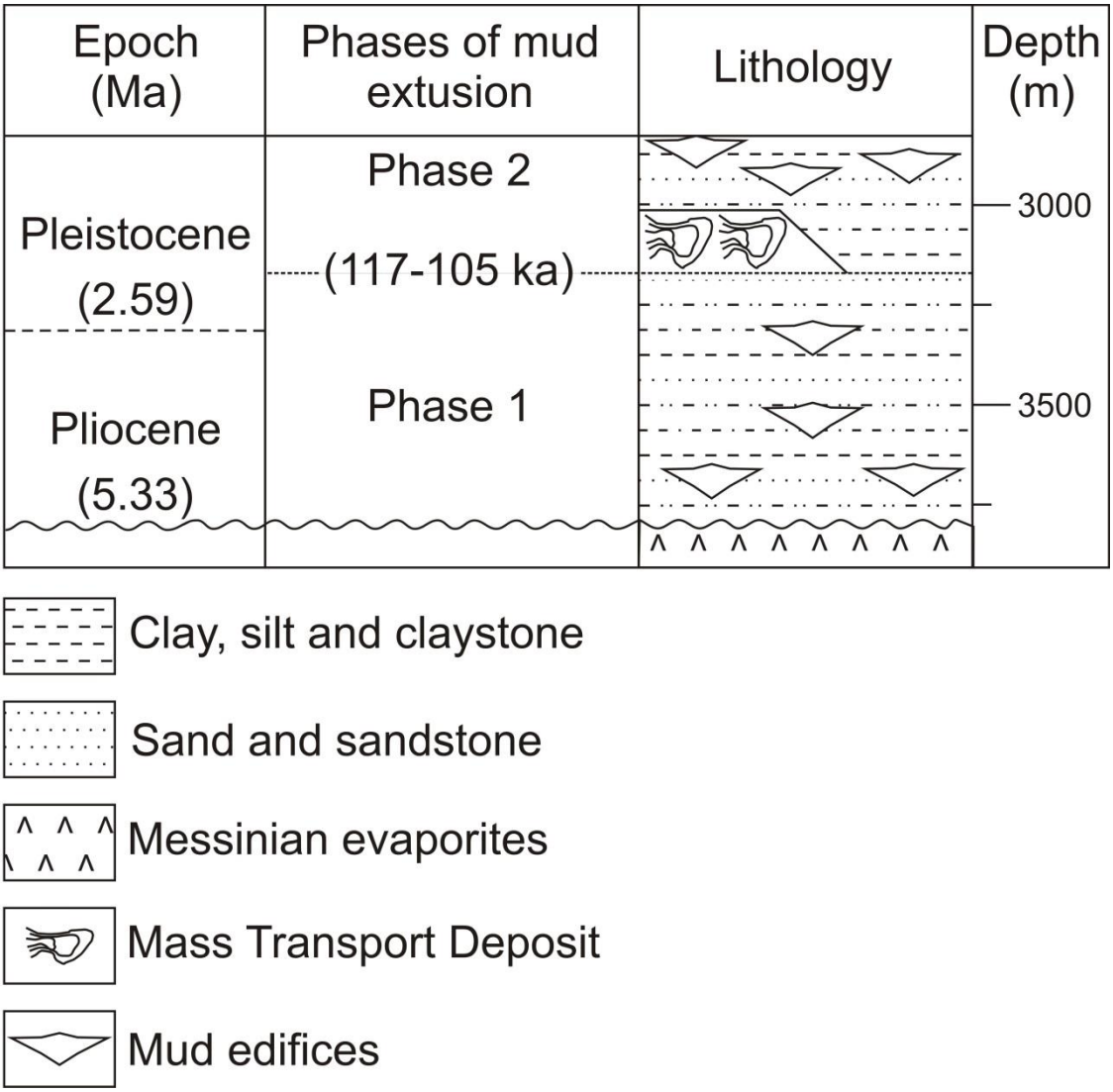

Figure 5.17 Chronostratigraphy of the Pliocene to Recent succession within the El Dabaa study area. An approximation of the chronostratigraphy of the Pliocene to Recent succession, highlighting the frequency of mud volcano formation and Phase 1 and 2.

on the timing of mud volcano formation, based on the correlation with the SL2 slide that formed 117 to 105 ka.

The basal reflection of the EL Dabaa covers a 1602 km^2 area of the 4300 km^2 study area and can be extrapolated across the entire study area. As the only reflection other than Horizon M and the seafloor that can be aged with any confidence it can be used to divide the mud volcanoes into two phases. All of the mud volcanoes located between Horizon M and the basal reflection of the El Dabaa slide range in age from Pliocene to Upper Pleistocene (Figure 5.17). These mud volcanoes comprise Phase 1 and are distributed at depths ranging from 3938 m to 6117 m, just above the top of the evaporites. Phase 1 includes the high frequency of mud volcanoes previously described near the base of the Pliocene to Recent succession (Figure 5.11 and Figure 5.12). All mud volcanoes located above the basal reflection of the El Dabaa slide range in age from Upper Pleistocene to Recent (Figure 5.17). These mud volcanoes comprise Phase 2 and are distributed at depths ranging from 4240 m, to 3148 m just beneath the seafloor. Phase 2 includes the high frequency of mud volcanoes that has been observed at the top of the Pliocene to Recent succession and at the seafloor (Figure 5.11 and Figure 5.12). The number of mud volcanoes to have formed during Phase 1 and Phase 2 are 184 and 202 respectively. If the correlation of the El Dabaa slide is correct, the time length of Phase 1 is significantly longer than Phase 2, however, a greater number of mud volcanoes have formed over the last 117 Kyrs during Phase 2 than the approximately 5.2Myrs of Phase 1 that preceded.

5.3.4.2 Spatial distribution

On a gross scale the vast majority of mud volcanoes within Phase 1 and Phase 2 are distributed within Domain B (Figure 5.18 and Figure 5.19), which is similar to the distribution of mud volcanoes currently observable at the seafloor (Figure 5.8). Of the 386 mud volcanoes, 353 are located within Domain B, while a remaining 14 and 19 are located within Domain A and Domain C respectively. The majority of these outliers are from Phase 1 (Figure 5.18) with only 6 having formed during to Phase 2 (Figure 5.19).

The density of mud volcanoes was calculated by overlaying the survey area with a grid containing cells of 1 km^2 and counting the number of mud volcanoes within each cell (Figure 5.20). Density of mud volcanoes varies over the entire survey area ranging from 0-3 mud volcanoes per km^2. This is a high density of mud volcanoes within a relatively small area in comparison to other mud volcano provinces such as offshore Barbados where 450 mud volcanoes are documented within a considerably larger area of 150,000 km^2 (Milkov, 2000).

The mud volcanoes from Phase 1 and Phase 2 appear to display a clustered distribution (Figure 5.18 and Figure 5.19). In order to quantify this observation, spatial and statistical analysis has been undertaken on the total population of 386 mud volcanoes throughout the survey area to ascertain whether they are of a dispersed, random or clustered distribution (Davis and Sampson, 2002). To determine this, first order spatial analysis in the form of the nearest neighbour index (Rn) (see section 2.3.1.1 of Chapter 2 for definition of Rn) has been used (Clark and Evans, 1954; ESRI, 2013a; Mitchell, 2005), which considers the acceptance or rejection of a null hypothesis here stated as:

H_o: There is no pattern to mud volcano distribution and are, therefore, randomly distributed (Davis and Sampson, 2002).

This analysis has been conducted on the mud volcanoes from Phase 1 and Phase 2 separately and also for all mud volcanoes. The results of this analysis show that the mud volcanoes of Phase 1 and 2 and both combined are statistically significantly clustered. The results from this test can be seen in Figure 5.21. Analysis of Phase 1 and Phase 2 separately show that the mud volcanoes from Phase 1 have a lower Rn value, which means they are clustered to a greater degree than those of Phase 2. Given the very low z-scores (see section 2.3.1.1 of Chapter 2 for definition of the z-score) there is less than 1% likelihood that these clustered patterns could be the result of random chance (ESRI, 2013a).

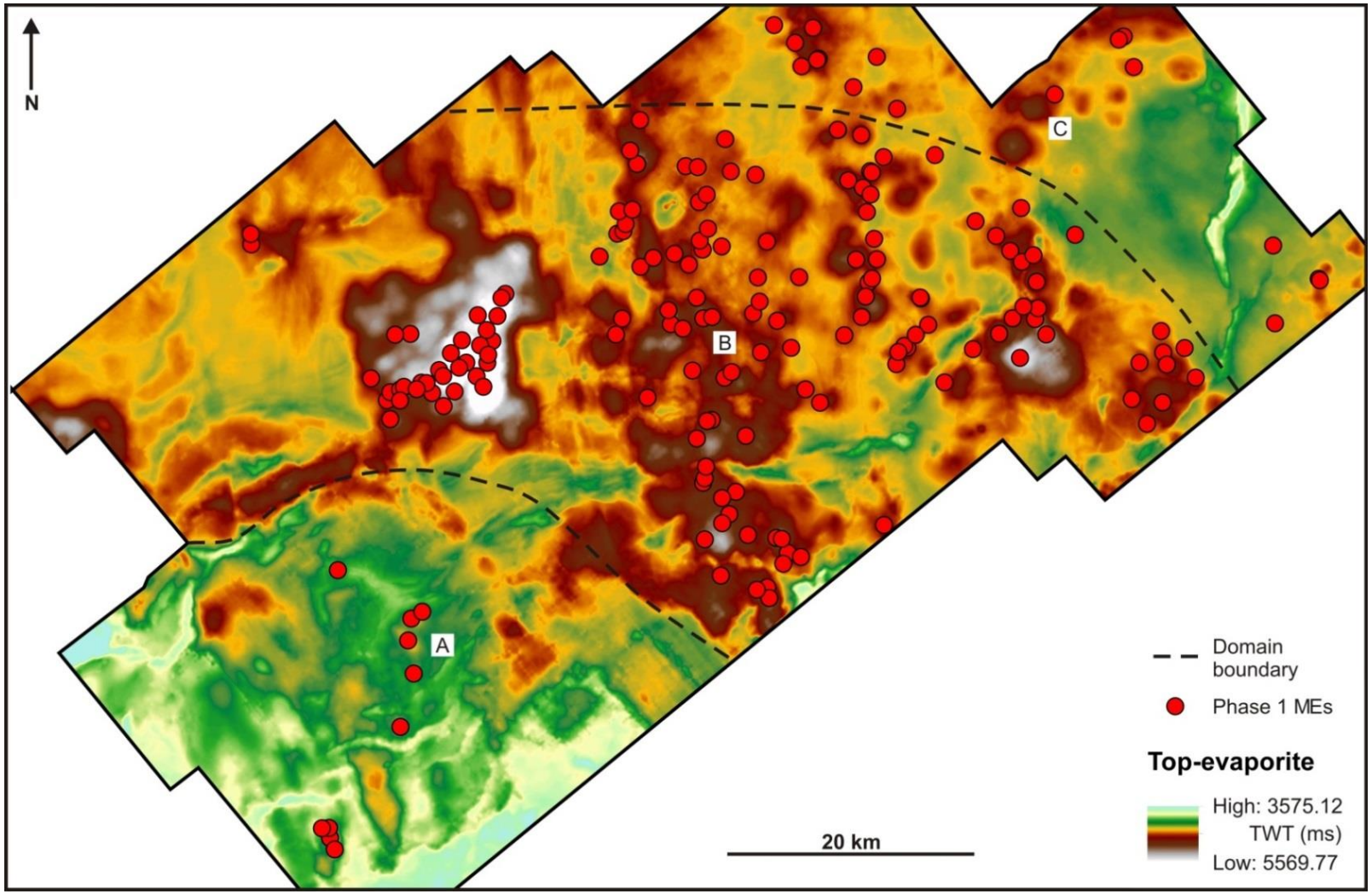

Figure 5.18 Phase 1 mud volcano distribution. Time attribute map of the top-evaporites within the El Dabaa survey area showing the location of every phase 1 mud volcano (red points) and the interpreted boundaries between domains A, B and C. The majority of mud volcanoes are found within domain B. MEs = Mud volcanoes

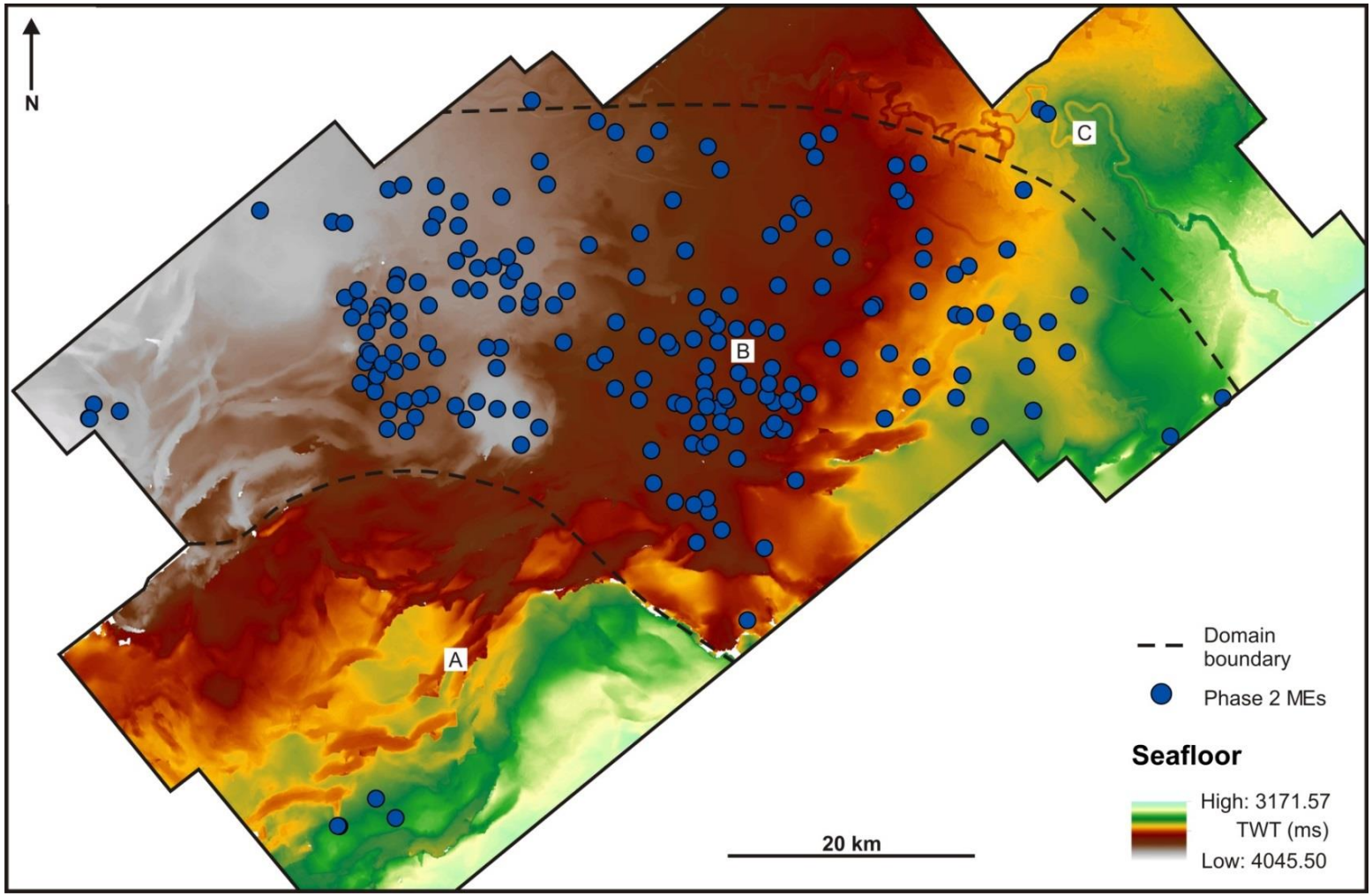

Figure 5.19 Phase 2 mud volcano distribution. Time attribute map of the top-evaporites within the El Dabaa survey area showing the location of every phase 2 mud volcano (blue points) and the interpreted boundaries between domains A, B and C. The mud volcanoes are even more limited to domain B than the phase 1 mud volcanoes. MV = Mud volcanoes

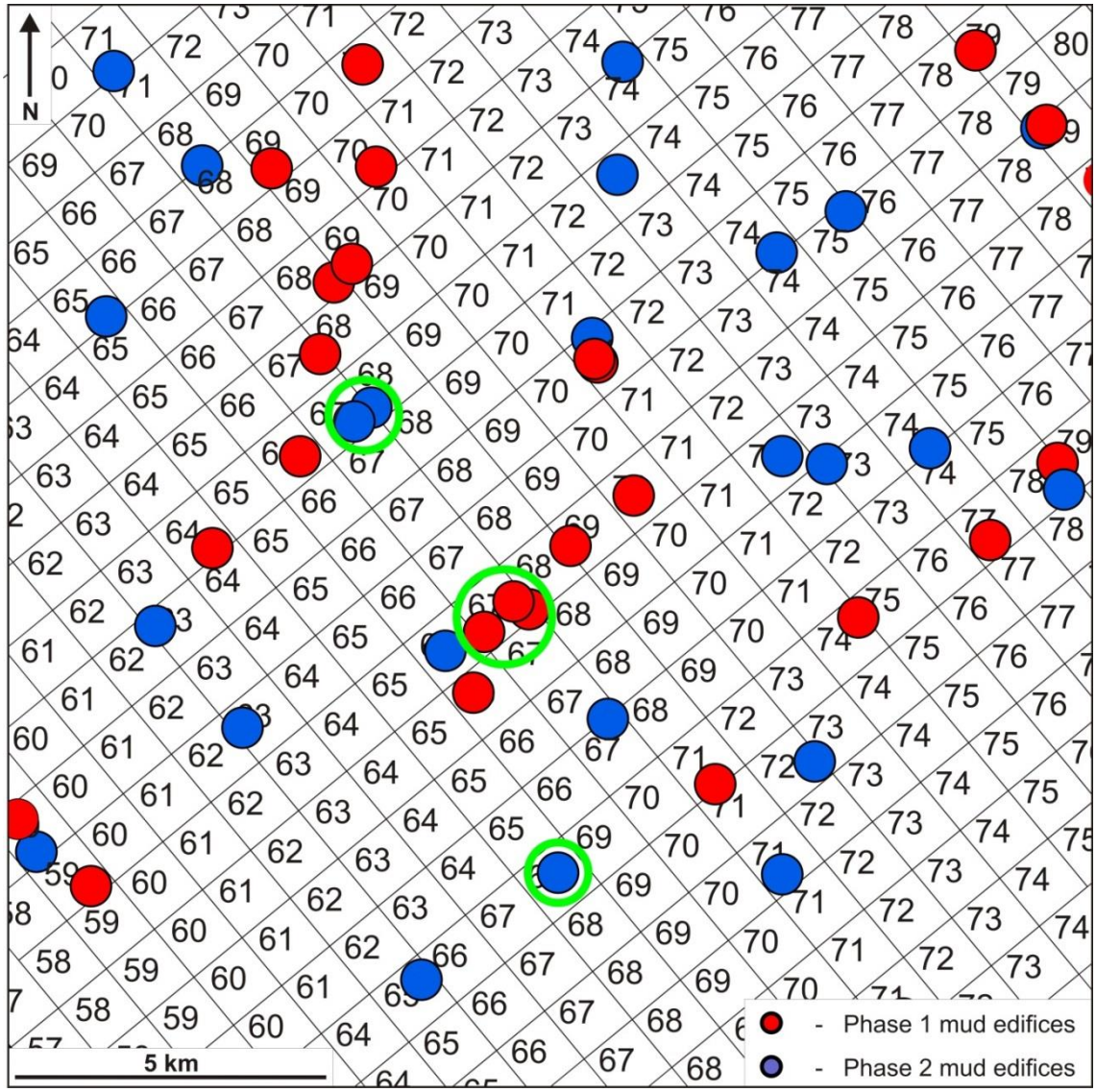

Figure 5.20 Calculating density. A grid containing cells of 1 km^2 and mud volcanoes from both phase 1 and phase 2. The number of mud volcanoes within each cell throughout the survey area was counted in order to calculate the range for mud volcano density per km^2. Densities range from 0-3 mud volcanoes per km^2 as highlighted by the green circles.

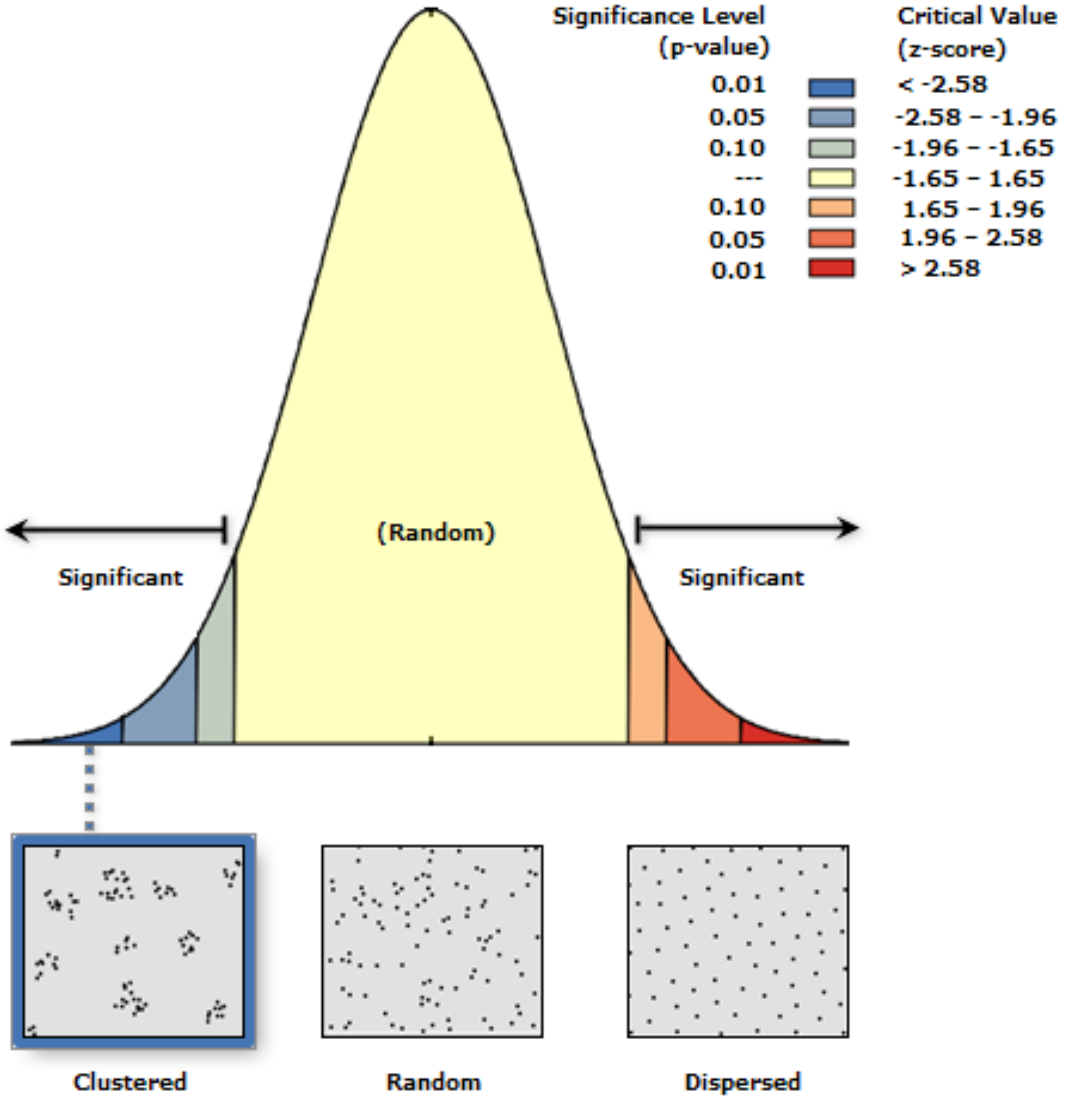

	All Mud Volcanoes	Phase 1	Phase 2
Observed Mean Distance (M):	1202.89	1451.01	1606.62
Expected Mean Distance (M):	1729.26	2423.16	2245.39
Nearest Neighbour Ratio (Rn):	0.70	0.60	0.72
z-score:	-11.44	-10.41	-7.73
p-value:	0.00	0.00	0.00
Dispersed, random or clustered	Clustered	Clustered	Clustered

Figure 5.21 Results from the nearest neighbour index (Rn) analysis. Rn values calculated are less than 1 therefore statistically proving that the distribution of mud volcanoes is clustered within the survey area. The graph demonstrates that the distribution is clustered and that the low z-scores and p-vales calculated show there is less than 1% likelihood that these patterns could be the result of random chance.

First order statistics only provide a general overview of a distribution based on average values within a single search radius, while second order statistics such as Ripley's K (described in section 2.3.1.2 of Chapter 2) look for patterns within multiple search radii (ESRI, 2013d) which in this case was set to every 1000m (Figure 5.22). This analysis shows that the observed K value (defined in section 2.3.1.2 of Chapter 2) is larger than the expected K value at multiple neighbourhoods around a mud volcano at distances between 1000 m and 31000 m (Figure 5.22). This observation means that the distribution of mud volcanoes is statistically clustered, up to a distance of 31000 m from a mud volcano. At a confidence level of 99.9% the K value is consistently greater than the HiConfEnv value (HiConfEnv is defined in section 2.3.1.2 of chapter 2); therefore, spatial clustering for that distance is statistically significant.

Kernel density calculations (see section 2.3.1.3 of Chapter 2 for description) are used here to analyse changes in the density or distribution of mud volcanoes within the study area. This analysis highlights areas where there is a change in magnitude in the spatial density of mud volcanoes, for the mud volcanoes within Phase 1 and Phase 2 (Figure 5.23 and Figure 5.24). These density maps can then be overlain to analyse whether there is a stacking relationship between the mud volcanoes that formed earlier within Phase 1 and the more recently formed mud volcanoes of Phase 2 (Figure 5.25). For this analysis the default raster cell size of 265.81 m^2 has been used, which is calculated as the shorter of the width or height of the output extent in the output spatial reference, divided by 250 (See section 2.3.1.3 of chapter 2). The neighbourhood radius has been set at 2 km in order to ensure that there is overlap in the neighbourhoods of the mud volcanoes. The value of magnitude of the neighbourhood around a mud volcano is greatest at the centre of its data point where it is equal to one. The value of magnitude diminishes at a constant gradient with increasing distance from the central point of the mud volcano, reaching zero at the margin of the neighbourhood. The density at each raster cell is then calculated as the sum of all neighbourhood values within that raster cell. The values and contour maps that are produced via this analysis, therefore, display magnitude values at varied distances away from the mud volcanoes via the addition of any neighbourhoods that overlap. The result is a map that shows variation in the magnitude of the density of mud

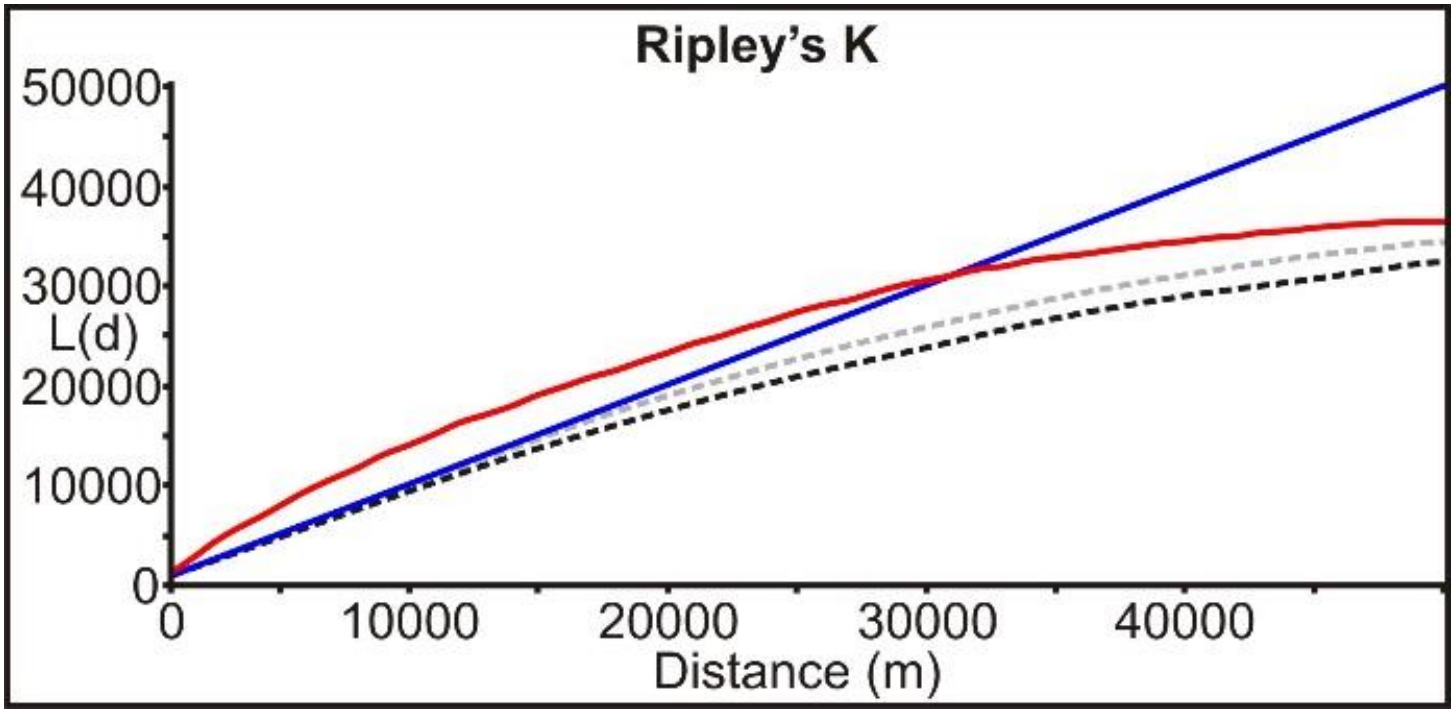

Figure 5.22 Results from the Ripley's K analysis. Observed K L(d) values (red line) greater than the expected K L(D) values (blue line) over a distance of c. 31000 m indicate that a distribution is clustered over that distance. Observed K L(d) values lower than expected K L(D) values mean the distribution is dispersed. The observed K is greater than the higher confidence envelope (grey dashed line), which means that to a confidence level of 99.9 the mud volcanoes are of a clustered distribution. The black dashed line represents the lower confidence envelope.

volcanoes and highlights in particular areas of high magnitude, which are indicative of areas where the spatial density of mud volcanoes is greatest (Figure 5.23 and Figure 5.24).

The kernel density calculations for phase 1 and phase 2 produce values ranging from 0-0.958 and 0-0.897 respectively (Figure 5.23 and Figure 5.24). The distribution of Phase 1 volcanoes produces a larger range of density values relative to Phase 2, which means that the Phase 1 mud volcanoes are more densely clustered (ESRI, 2013c). This supports the nearest neighbour spatial analysis where the mud volcanoes of Phase 1 produced a comparatively lower Rn value than the Phase 2 volcanoes and, therefore, exhibit a greater degree of clustering despite hosting fewer mud volcanoes. The green circles highlight areas where the clustering of volcanoes is significant enough to produce a value for magnitude of 0.513 and greater in Figure 5.23 and Figure 5.24. These highlighted areas display magnitude values that are greater than the median for the range of values that have been calculated and is indicative of an area of clustering of mud volcanoes. The distribution of the Phase 1 volcanoes produces 12 locations where mud volcanoes display significant clustering compared to only 9 in Phase 2 (Figure 5.23 and Figure 5.24). This shows that the volcanoes from Phase 1 can be observed more frequently in clusters than those of Phase 2.

These kernel density surfaces produce density patterns that are circular in shape where there is just a single mud volcano and irregular in shape where there is an amalgamation of neighbourhood radii, due to a clustering of mud volcanoes. The mud volcanoes and kernel surface from Phase 1 form several N-S trending clusters which produce elongated blobs that represent a N-S trend in the distribution of mud volcanoes (Figure 5.23). No similar trend is observed within the data points or kernel surface of Phase 2 mud volcanoes (Figure 5.24). The distribution of mud volcano clusters is displayed in Figure 5.25. Phase 1 mud volcanoes that are not spatially associated with any mud volcanoes that formed during Phase 2 are displayed in Box A of Figure 5.25. Mud volcanoes from Phase 2 are located in close spatial association with mud volcanoes that formed during Phase 1 within Box B (Figure 5.25). Mud volcanoes that formed during Phase 2 and are stacked directly above mud volcanoes that formed during Phase 1 are displayed in Box C (Figure 5.25).These observations

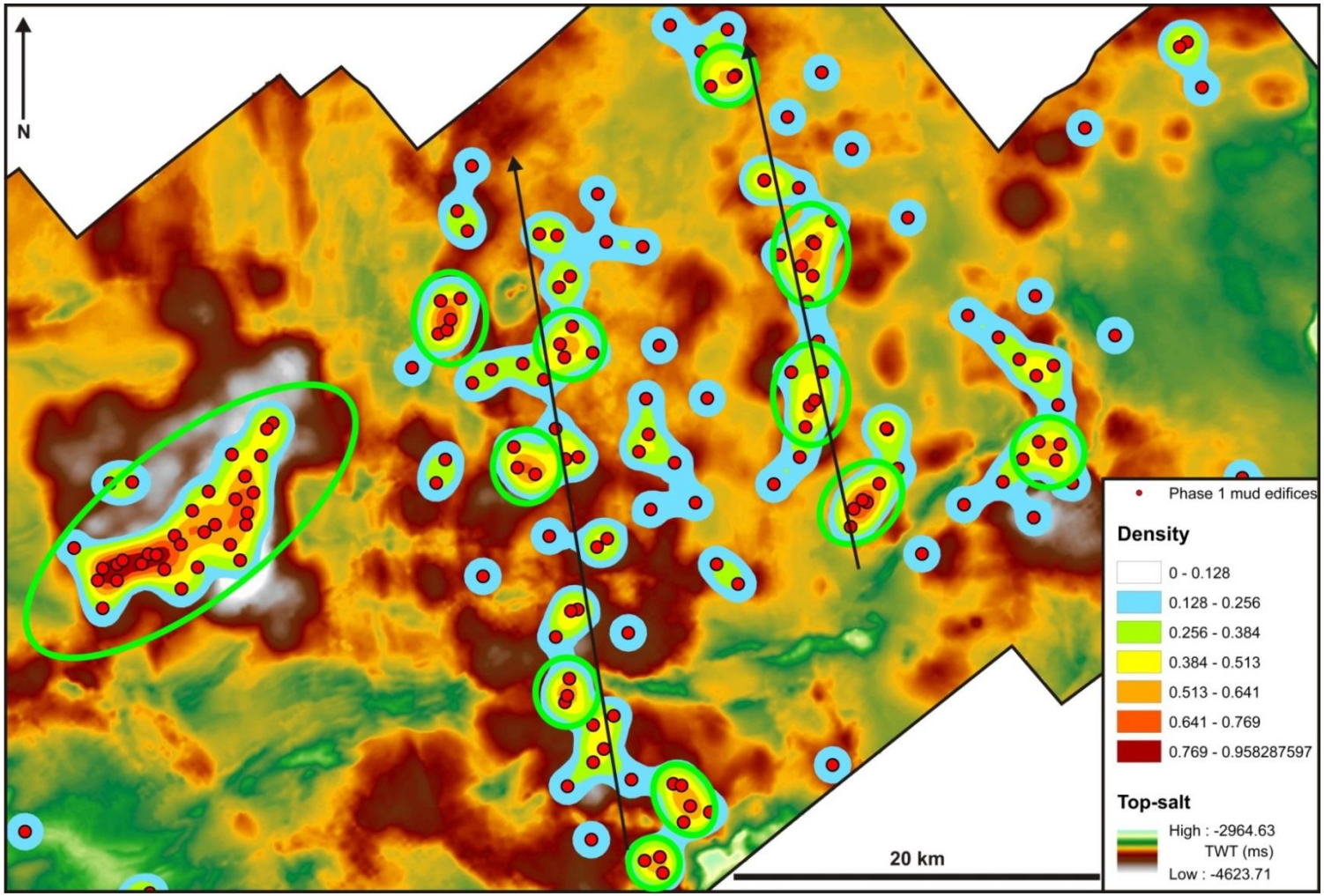

Figure 5.23 Phase 1 kernel density. The kernel surface displays several N-S trending clusters which produce elongated blobs, as highlighted by the arrows. 11 green circles highlight areas where the magnitude of density of mud volcanoes highest.

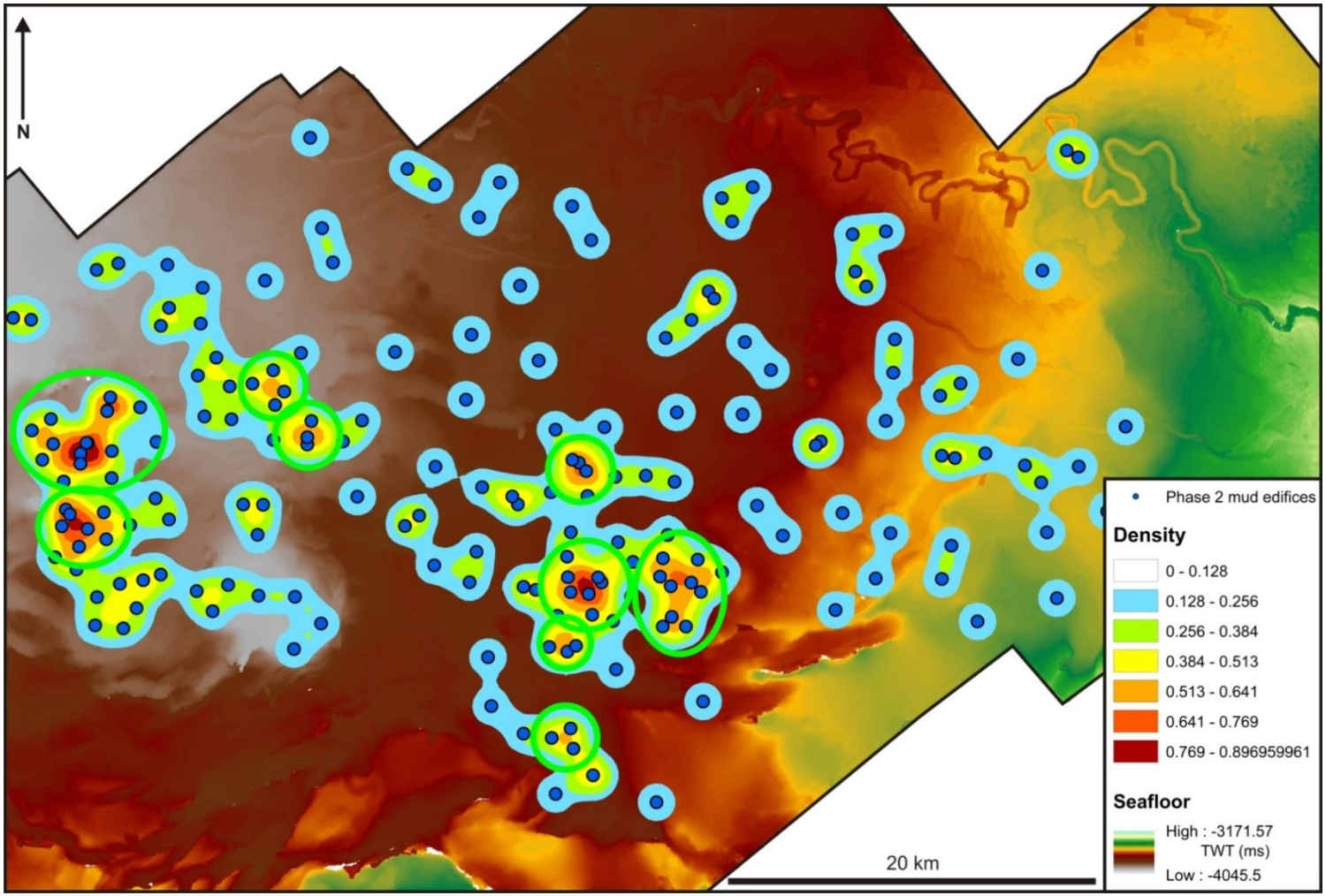

Figure 5.24 Phase 2 kernel density. 9 green circles which highlight areas where the magnitude of density of mud volcanoes highest. There are fewer clusters than in the phase 1 kernel surface despite a greater number of mud volcano.

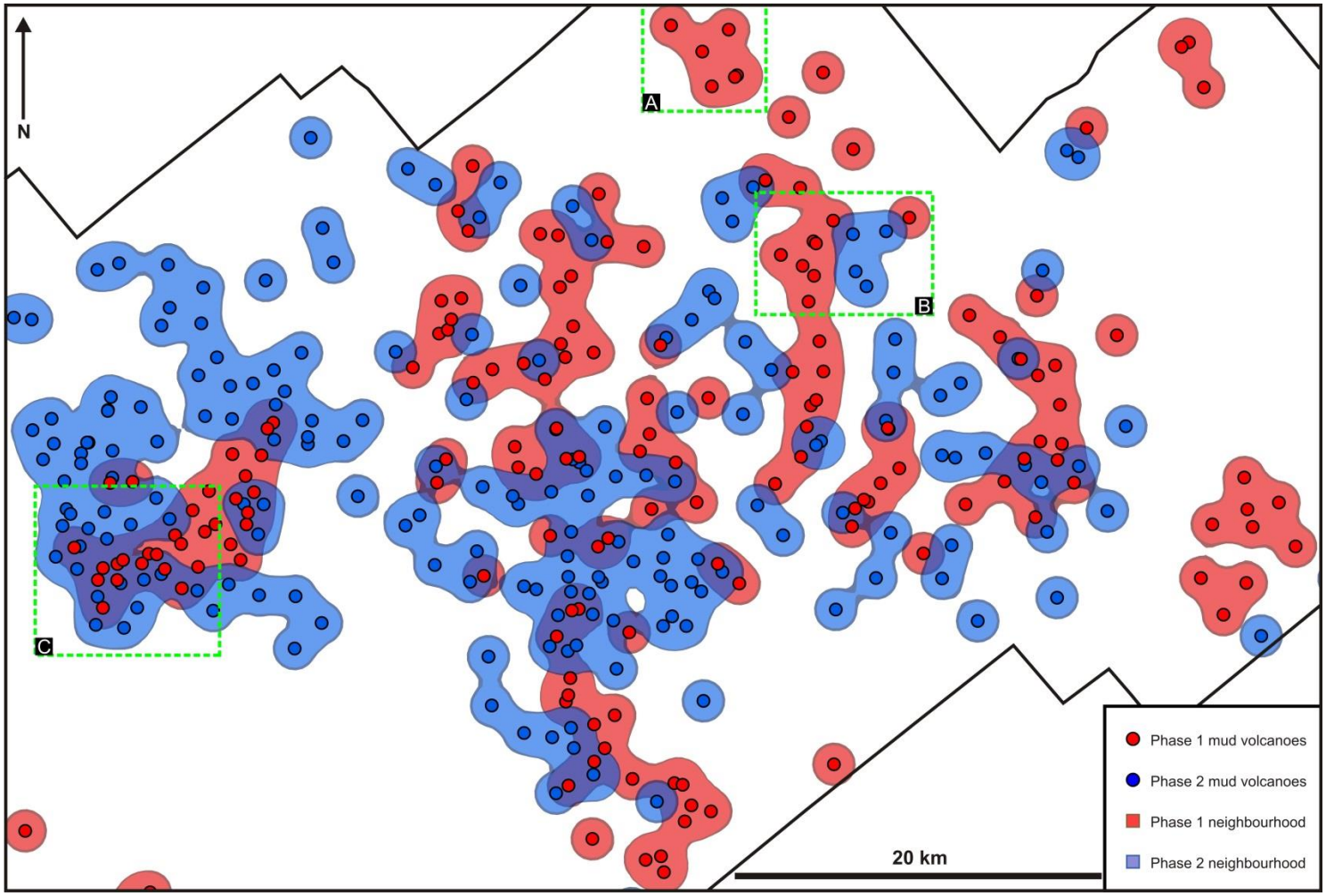

Figure 5.25 Phase 1 and 2 kernel density. Green dashed boxes highlight varying stacking trends. Box A – Phase 1 mud volcanoes isolated; Box B – Phase 2 mud volcano in close spatial association with Phase 1 mud volcanoes; Box C – Phase 2 mud volcanoes stacked above Phase 1 mud volcanoes.

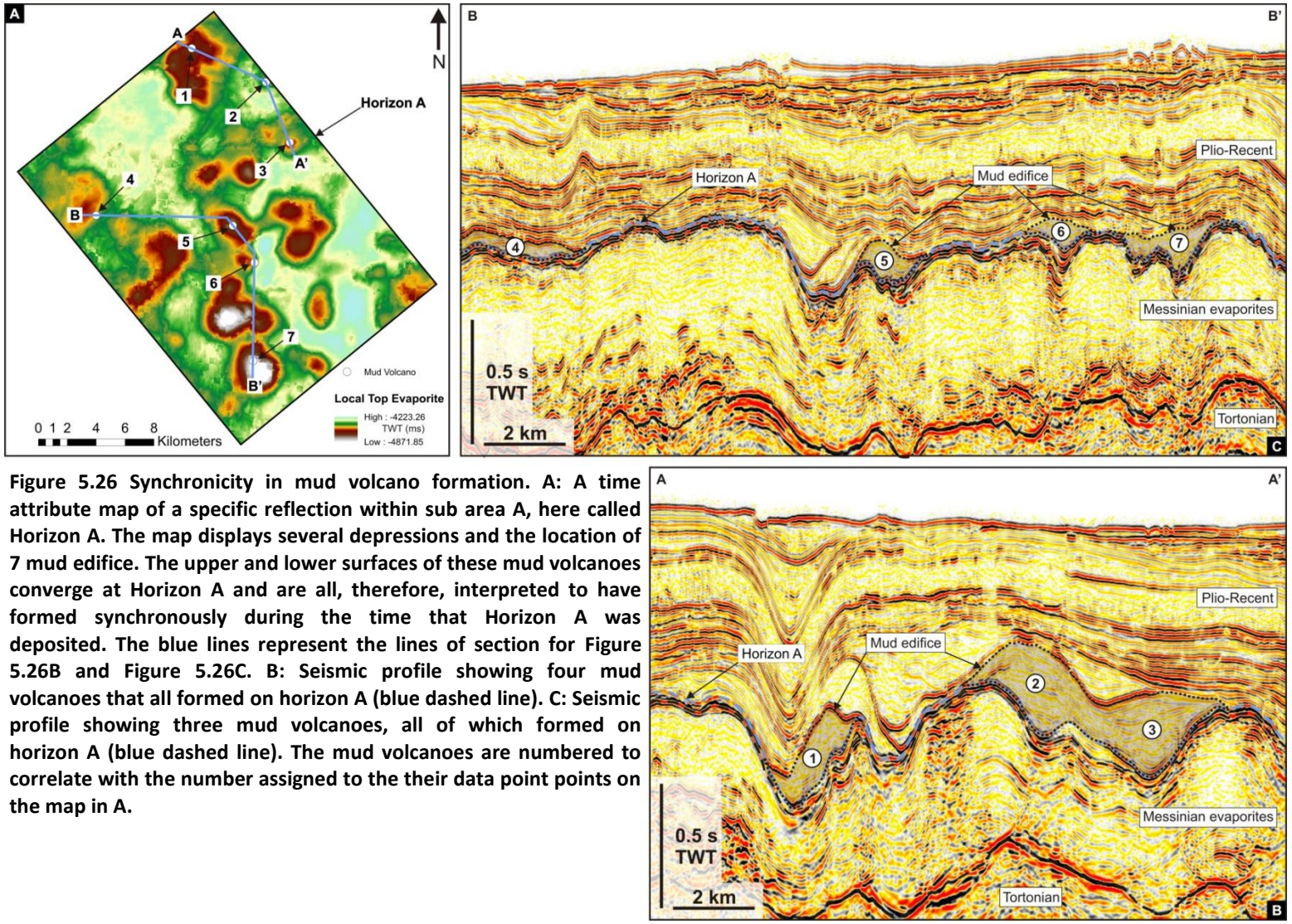

Figure 5.26 Synchronicity in mud volcano formation. A: A time attribute map of a specific reflection within sub area A, here called Horizon A. The map displays several depressions and the location of 7 mud edifice. The upper and lower surfaces of these mud volcanoes converge at Horizon A and are all, therefore, interpreted to have formed synchronously during the time that Horizon A was deposited. The blue lines represent the lines of section for Figure 5.26B and Figure 5.26C. B: Seismic profile showing four mud volcanoes that all formed on horizon A (blue dashed line). C: Seismic profile showing three mud volcanoes, all of which formed on horizon A (blue dashed line). The mud volcanoes are numbered to correlate with the number assigned to the their data point points on the map in A.

indicate that there may be a spatial relationship between the location of recently formed mud volcanoes and the location where pre-existing mud volcanoes formed, resulting in some cases in the stacking of mud volcanoes.

An important question to consider is did any of the mud volcanoes within these phases erupt at approximately the same time? If two or more mud volcanoes were to form at the same time, the reflection at which their top and base surfaces converge would be the same. Mapping of a single reflection within the Pliocene – Recent succession within a sub-area of the study area, here named sub-area A, shows that some mud volcanoes are distributed along the same laterally continuous reflection (Figure 5.26). The example seen in Figure 5.26 shows a single reflection, here referred to as Horizon A, which covers an area of 430 km^2 and is located just above the top-salt reflection of Horizon M. The entire Pliocene-Recent interval within this 430 km^2 area is host to 60 mud volcanoes, 7 of which can be seen to have formed along Horizon A (Figure 5.26). The upper bounding reflection of these 7 mud volcanoes can all be observed to downlap onto the reflection of Horizon A, which is also their basal bounding reflection. This suggests that within this relatively small area these mud volcanoes have formed synchronously within a similar window of time, which could be indicative of a shared trigger mechanism.

5.3.5 Dimensions

A large number of mud volcanoes (386) have been mapped within the study area, a slightly larger number of which (202) have been mapped within the interval of Phase 2 compared to Phase 1 (184). The various types of dimensions recorded from the mud volcanoes within this survey area are displayed in a schematic representation in Figure 5.27. These dimensions vary significantly from one mud volcano to another (Table 5.1). The full range of statistics recorded for mud volcanoes from Phase 1, Phase 2 and combined can be found in Table 5.1. Since the geometry of most mapped volcanoes approximate a circle (Figure 5.1 and Figure 5.4) the area has been measured using the max radius (Table 5.1). Due to the geometry of these mud volcanoes of a

circular planform and overall conical shape, the equation for calculating the volume of a cone (See section 2.3.1.6 of Chapter 2) has been used to calculate the volumes of these mud volcanoes (Table 5.1). The mud volcanoes from Phase 2 cover a smaller area and have a smaller max thickness compared to those of Phase 1.

When recording the parameters of deformed mud volcanoes, their deformation was taken into account and the measurements recorded are based on a restored undeformed version of the volcano. Potential errors are based on; (1) how well the margins of the volcano are imaged, (2) vertical resolution, and (3) any irregularities in the overall conical shape of the mud volcano, from which the use of the formula to calculate the volume of a cone is based on. An error of +/- 10% is considered a reasonable estimate. Interpretive error is based on unbiased picking of the line that intersects the crest of the volcanoes to gain maximum thickness and diameter.

Plots of diameter and maximum thickness of the mud volcanoes from Phase 1 and Phase 2 mud volcanoes have been constructed to analyse whether there is a scaling relationship between the two dimensions (Figure 5.28 and Figure 5.29). The plots for Phase 1 and Phase 2 mud volcanoes are both highly scattered although the data distribution is more tightly delimited by upper and lower boundaries in the Phase 2 plot (Figure 5.28 and Figure 5.29). This distribution of points produces low R^2 values of 0.135 for Phase 1 and a slightly greater linear relationship of 0.389 for Phase 2. The R^2 value is a measure of the goodness-of-fit of a linear regression given as a fraction between 0 and 1, as a way to measure the linear correlation between two variables, which in this case are diameter and max thickness of mud volcanoes. When choosing the appropriate type of trend line, the R^2 value is taken into account in order to have a trend line that is of the best goodness-of-fit and, therefore, produces the highest R^2 value (Davis and Sampson, 2002). Based on this reasoning a power law trend line was the most appropriate for the Phase 1 plot and the exponential for Phase 2. The high scattering of data points and low R^2 values that have been calculated indicate that there is no scaling of diameter and thickness and that the dimensions and geometry of these mud volcanoes are possibly governed by a combination of variables.

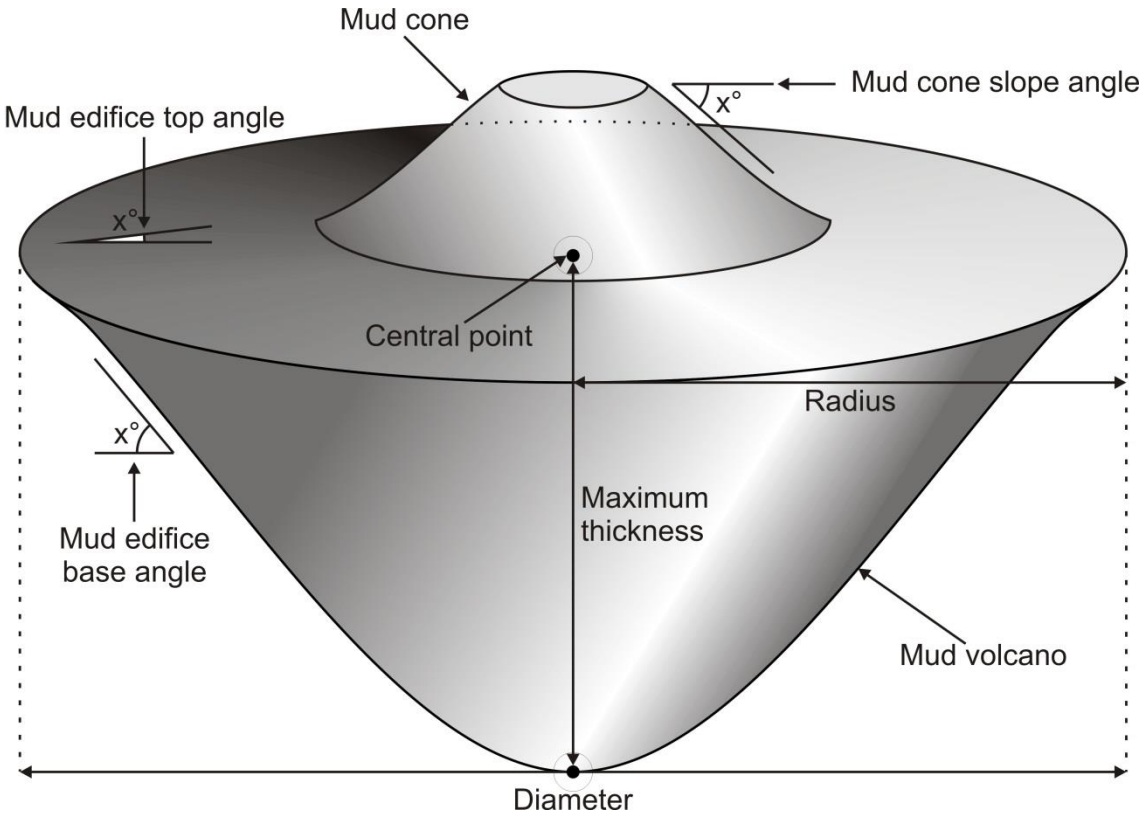

Figure 5.27 Schematic representation of a mud volcano. The diagram shows an idealised three dimensional cartoon of a mud volcano and the main measurements taken from the mud volcano such as diameter, maximum thickness and various angles.

	Phase 1				Phase 2				All			
	Min	**Max**	**Median**	**Average**	**Min**	**Max**	**Median**	**Average**	**Min**	**Max**	**Median**	**Average**
Radius (m)	665	2830	1578	1588	273	2725	1343	1224	273	2830	1438	1468
Diameter (m)	1330	5660	3155	3177	547	5350	2685	2448	547	5660	2875	2937
Thickness (m)	54	511	179	197	22	476	164	178	22	511	168	186
Depth (m)	3938	5462	4529	4560	3148	4240	3634	3563	3148	6117	4105	4354
Area (km^2)	1.4	25.2	7.8	8.6	0.2	23.3	5.7	5.3	0.2	25.2	6.5	7.5
Volume (km^3)	0.1	2.7	0.4	0.6	0.1	3.3	0.3	0.5	0.1	3.3	0.4	0.5
Total Number of MVs	184				202				386			
Total Area (km^2)	1584.1				1323.6				2907.7			
Total Volume (km^3)	113.9				93.7				207.7			

Table 5.1 Statistic of the various dimension of the mud volcanoes

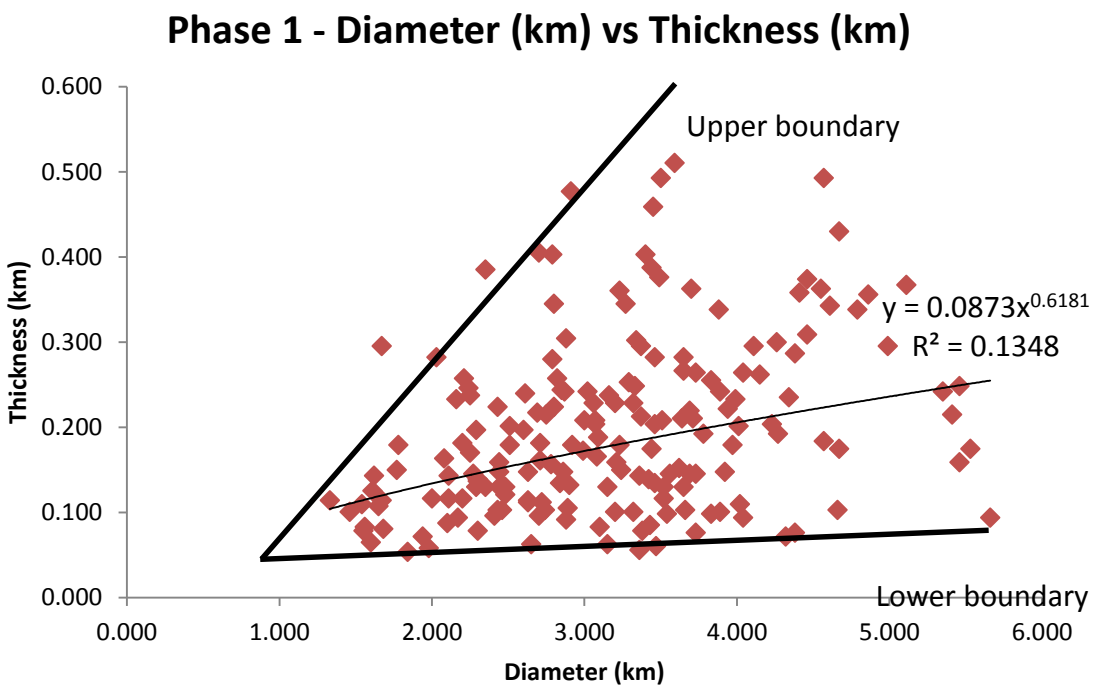

Figure 5.28 Phase 1 mud volcano diamter vs thickness. This plot shows a large scatter of points. There is no correlation between height and thickness, which implies that no scaling relationship exists between mud volcano geometries.

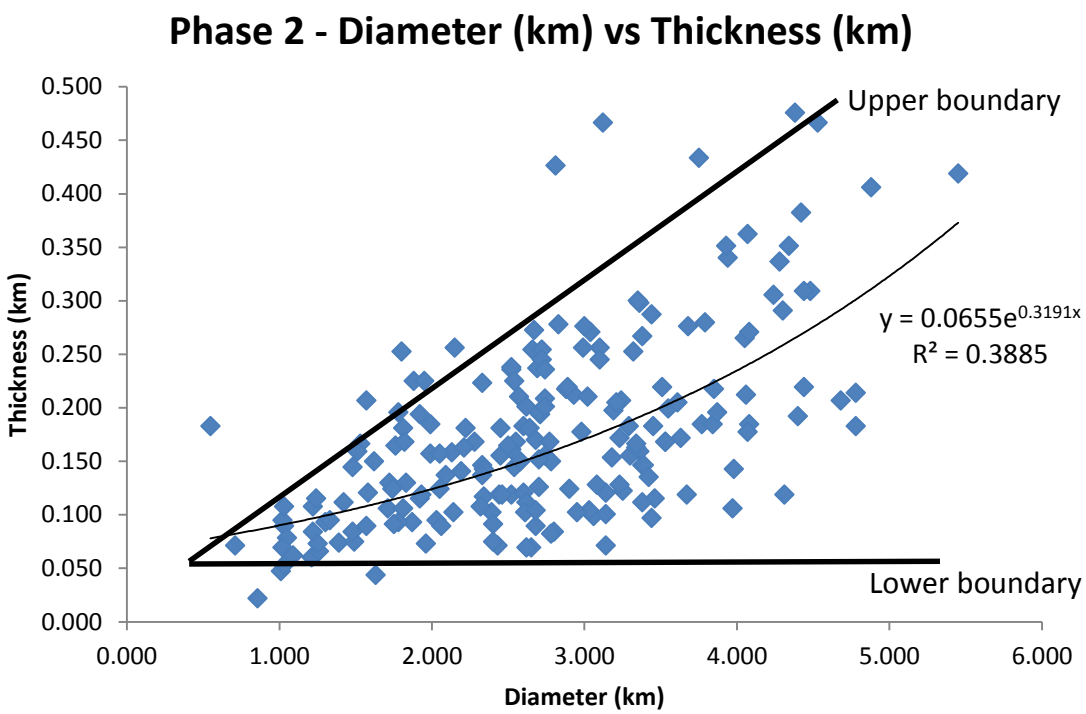

Figure 5.29 Phase 2 mud volcano diamter vs thickness. This plot shows a large scatter of points, however, the data distribution is more tightly bound than the example in Figure 5.28. There is no correlation between height and thickness, which implies that no scaling relationship exists between mud volcano geometries.

5.3.6 Depressions at Top and Base Salt

In sections 4.3.1 and section 4.4.3 of Chapter 4 it was discussed that mapping of Horizon M and N revealed numerous sub circular and irregular depressions, some of which were shown to be related to the giant mud volcanoes described. This interpretation was made by the observation of areas of localised thinning within the Messinian evaporites and thinning of the immediate pre-salt succession, in close spatial association to the overlying giant mud volcanoes and the top and base-salt depressions. A large number of top and base-salt depressions that are not related to these large mud volcanoes have also been observed and will be described and discussed here. This section aims to analyse the distribution of these top and base-salt depressions and describe their spatial relationship with the smaller and conical mud volcanoes that are discussed within this chapter. This analysis may give an insight to the region of sediment withdrawal and depletion for these mud volcanoes and to any potential impact their extrusion has had on the evaporite succession.

The majority of top and base-salt depressions observed within the study area are located within Domain B, which is also where the vast majority of mud volcanoes are located (Figure 5.30 and Figure 5.31). This indicates that these depressions and the mud volcanoes may be spatially related (Figure 5.30 and Figure 5.31). These depressions are here defined as localised areas of lower relief relative to the surrounding region, along a particular horizon. Maps that outline and highlight all of the depressions along Horizon M and N respectively have been created, based on the contoured time maps in Figure 5.30 and Figure 5.31 (Figure 5.32 and Figure 5.33). An overlay of these two maps display areas where top or base-salt depression are located independent of the other and where a top-salt depressions is located overlying a base-salt depression (represented by green area) (Figure 5.37). These depressions are generally irregular in shape and often appear to be formed via an amalgamation of depressions that merge into a larger depression. The top-salt and base-salt depressions display relief of up to 1400 m and 730 m respectively.

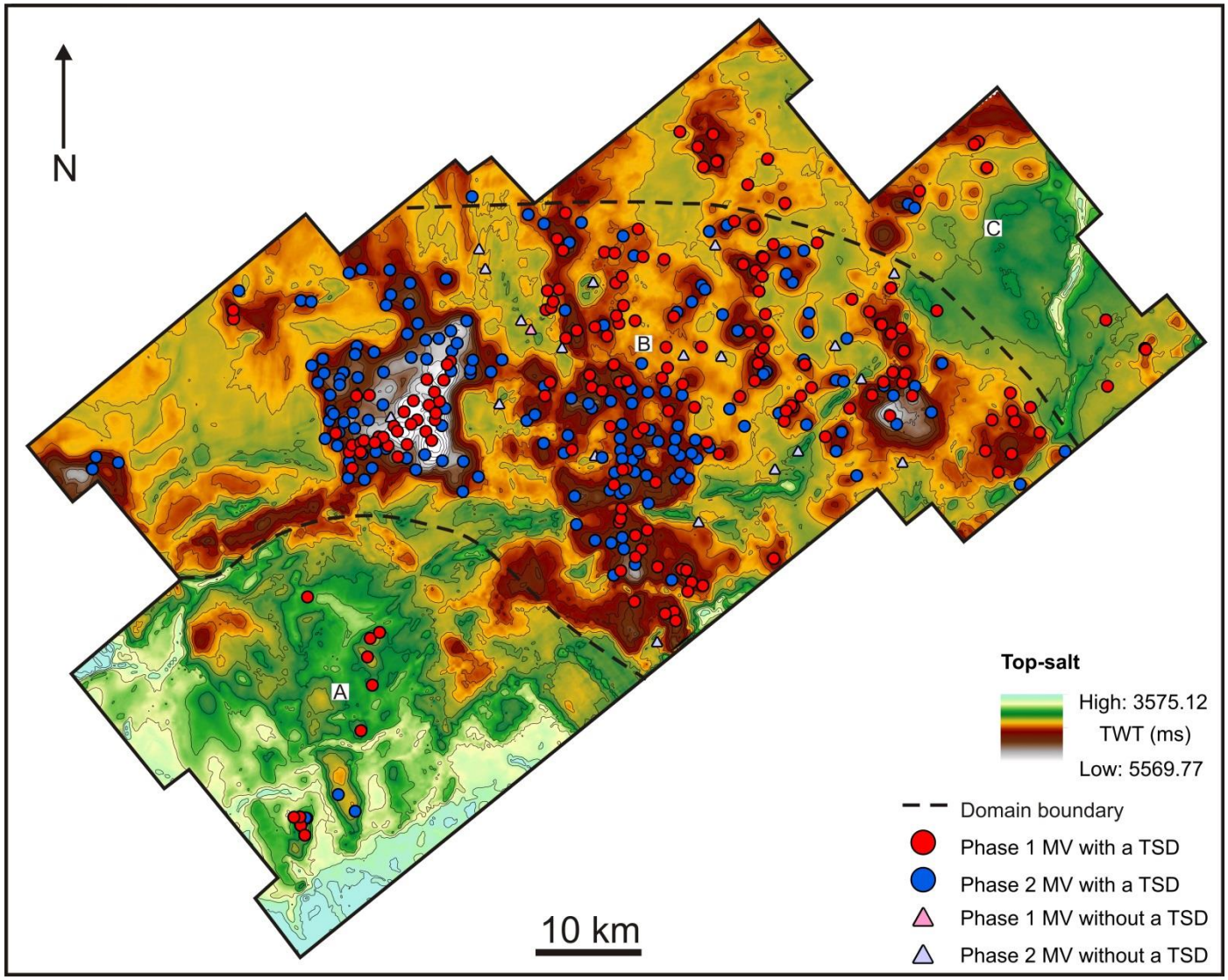

Figure 5.30 Top-salt depressions. A contoured time map of the top-salt (Horizon M) showing the vast array of top-salt depressions within the survey and how they are predominately located within the fluid escape region similar to the large field of mud volcanoes. Overlying the map are all of the mud volcanoes, divided by whether they are from phase 1 or 2 and by whether they directly overly a top-salt depression (TSD). MV – Mud volcano; A – Domain A; B – Domain B; C – Domain C.

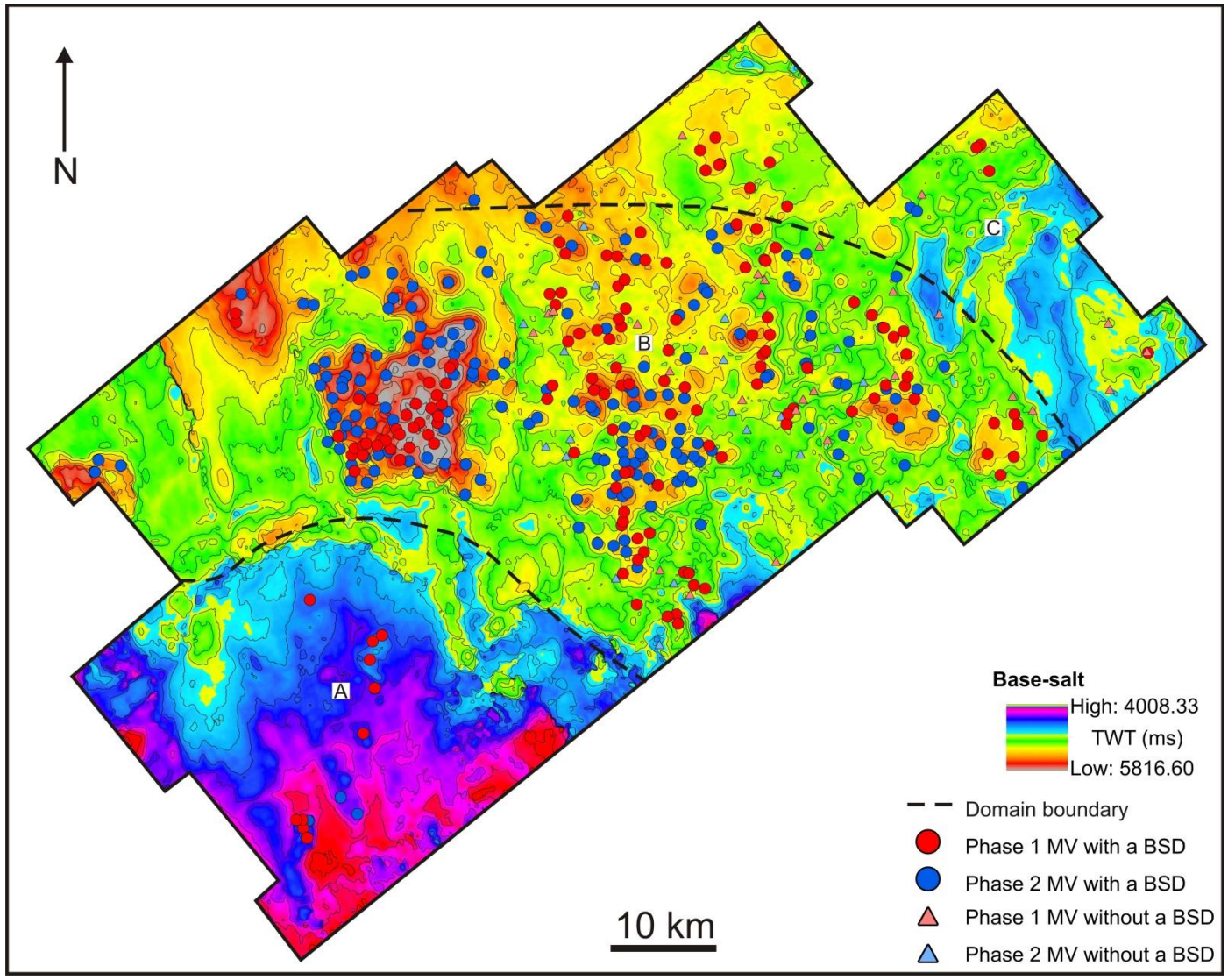

Figure 5.31 Base-salt depressions. A contoured time map of the base-salt (Horizon N) showing the vast array of base-salt depressions within the survey. Similar to the top-salt depressions they are predominately located within the fluid escape region similar to the large field of mud volcanoes. Overlying the map are all of the mud volcanoes, divided by whether they are from phase 1 or 2 and by whether they do or do not directly overly a base-salt depression (BSD). MV – Mud volcano; A – Domain A; B – Domain B; C – Domain C.

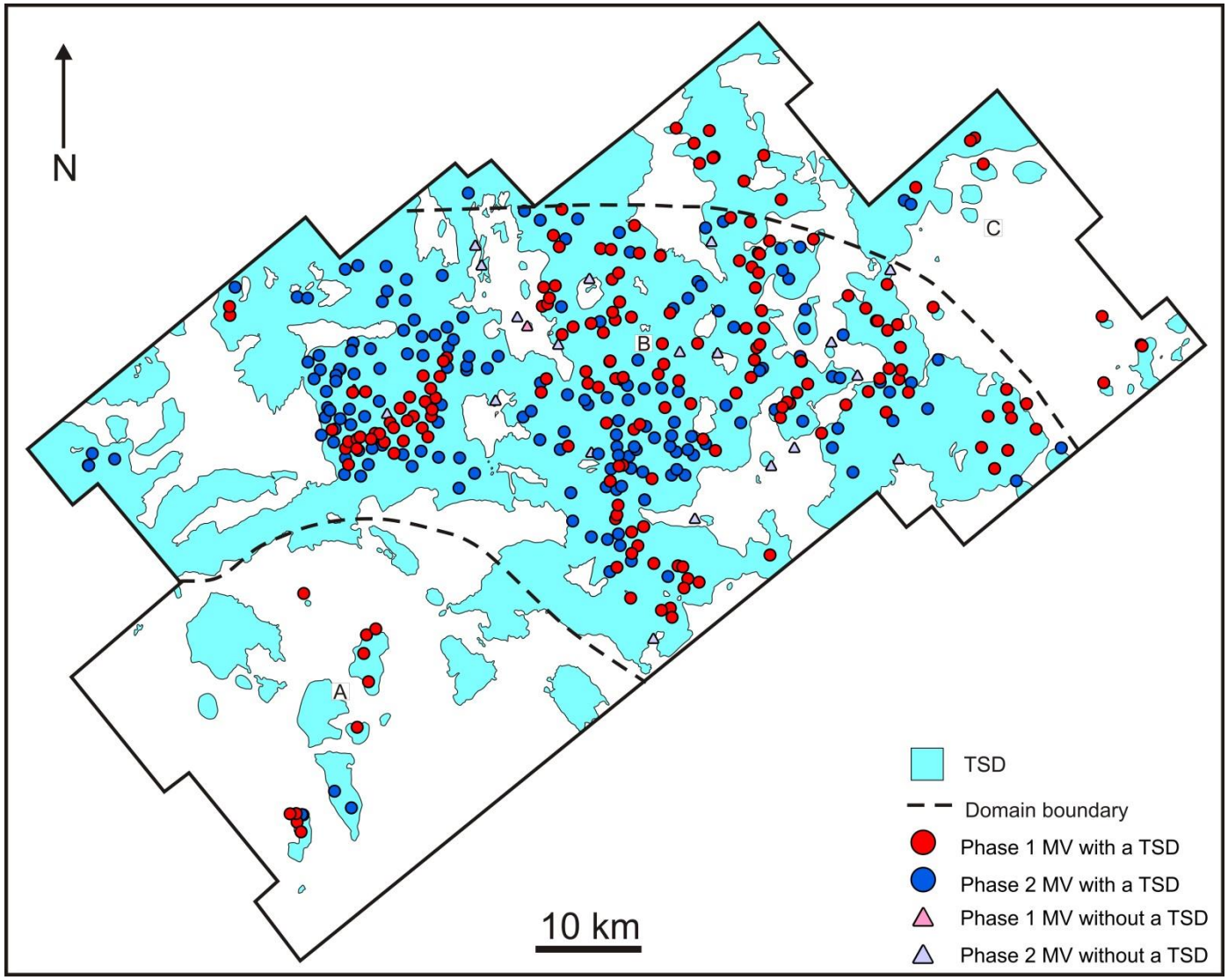

Figure 5.32 Top-salt depressions. A map showing the outlined full extent of all top-salt depressions based on the contoured time map in Figure 5.41 and seismic profiles. Overlying the outline map are all the mud volcanoes within the survey area; therefore clearly showing whether each one does or does not overly a top-salt depression (TSD). Of the 386 mud volcanoes 183 and 182 mud volcanoes from phase 1 and 2 respectively overly a TSD. 1 and 20 mud volcanoes from phase 1 and 2 do not overly a TSD. MV – Mud volcano; A – Domain A; B – Domain B; C – Domain C.

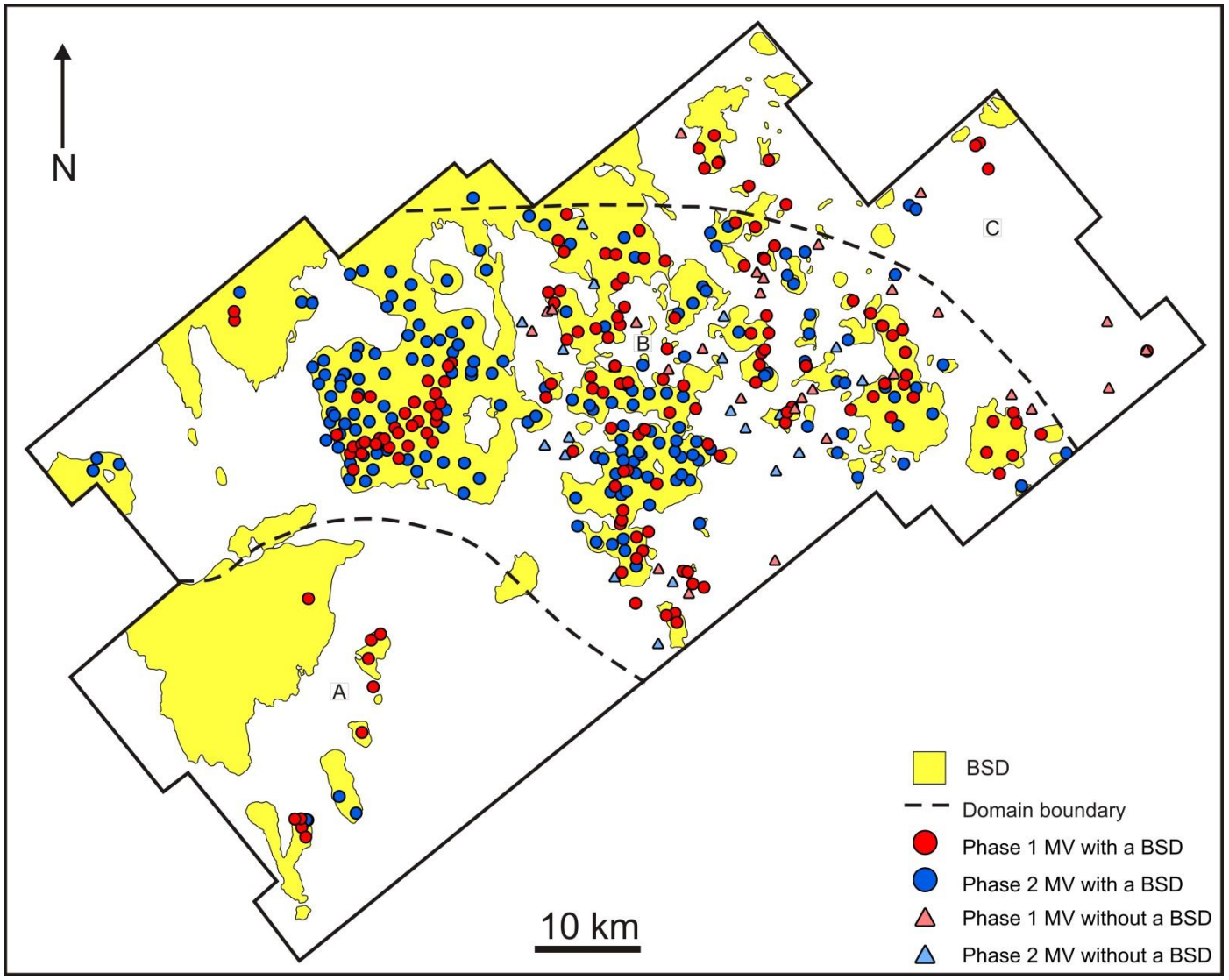

Figure 5.33 Base-salt depressions. A map showing the outlined full extent of all base-salt depressions based on the contoured time map in Figure 5.31and seismic profiles. Overlying the outline map are all the mud volcanoes within the survey area; therefore clearly showing whether each one does or does not overly a base-salt depression (BSD). Of the 386 mud volcanoes 156 and 182 mud volcanoes from Phase 1 and 2 respectively overly a BSD. 28 and 20 mud volcanoes from phase 1 and 2 do not overly a BSD. **MV – Mud volcano; A – Domain A; B – Domain B; C – Domain C.**

An example of a base-salt depression in seismic profile can be seen in Figure 5.35A, the location of which is displayed in Figure 5.34. Horizon N is not concordant with the reflections of the immediate pre-salt succession, which are truncated by the reflection of the depression at Horizon N, in the example displayed in Figure 5.35A. The depression produces a large bowl shape in seismic profile and reflections of the evaporite succession onlap onto the inner sides of the depression (Figure 5.35A). This particular depression has an irregular geometry in planform, is up to 400 m deep and greater than 15 km wide (Figure 5.34 and Figure 5.35A). There is a slight depression at Horizon M directly over the depression but generally the top and base-salt surfaces are not concordant with one another and the evaporite interval increases in thickness within the depression (Figure 5.35A).

An example of a different base-salt depression in seismic profile is displayed in Figure 5.35B. This depression displays an irregular and elongated geometry in plan form (Figure 5.34). In this example, Horizon M and the intra salt reflections are not concordant with Horizon N, and the evaporite interval is thicker within the pre-existing depression, similar to Figure 5.35A (Figure 5.35B). The reflections of the immediate pre-salt succession are not truncated by the base-salt depression but are in fact concordant, which contrast with the example in Figure 5.35A (Figure 5.35B). A very clear and abrupt displacement of Horizon N can be seen at the location of the depression (Figure 5.35B). The observed linearity of this depression and the displacement of Horizon N suggest that this depression is controlled by pre-salt faults. The throw between the footwall and the hanging wall of the fault has resulted in the formation of a half graben mini-basin.

The truncation of pre-salt reflections against the localised depression in (Figure 5.35A) is indicative of erosion and highlights an area of incision that is characterised by sloping sides and a curved base. The stratal relationship between the onlapping evaporites and depression suggests that the formation of the depression pre-dates evaporite deposition. These observations indicate that the timing of formation of this erosional depression is correlatable with the onset of the Messinian Salinity Crisis, which is known to be associated with a period of drawdown in sea level and major canyon incision (Barber, 1981; Druckman et al., 1995).

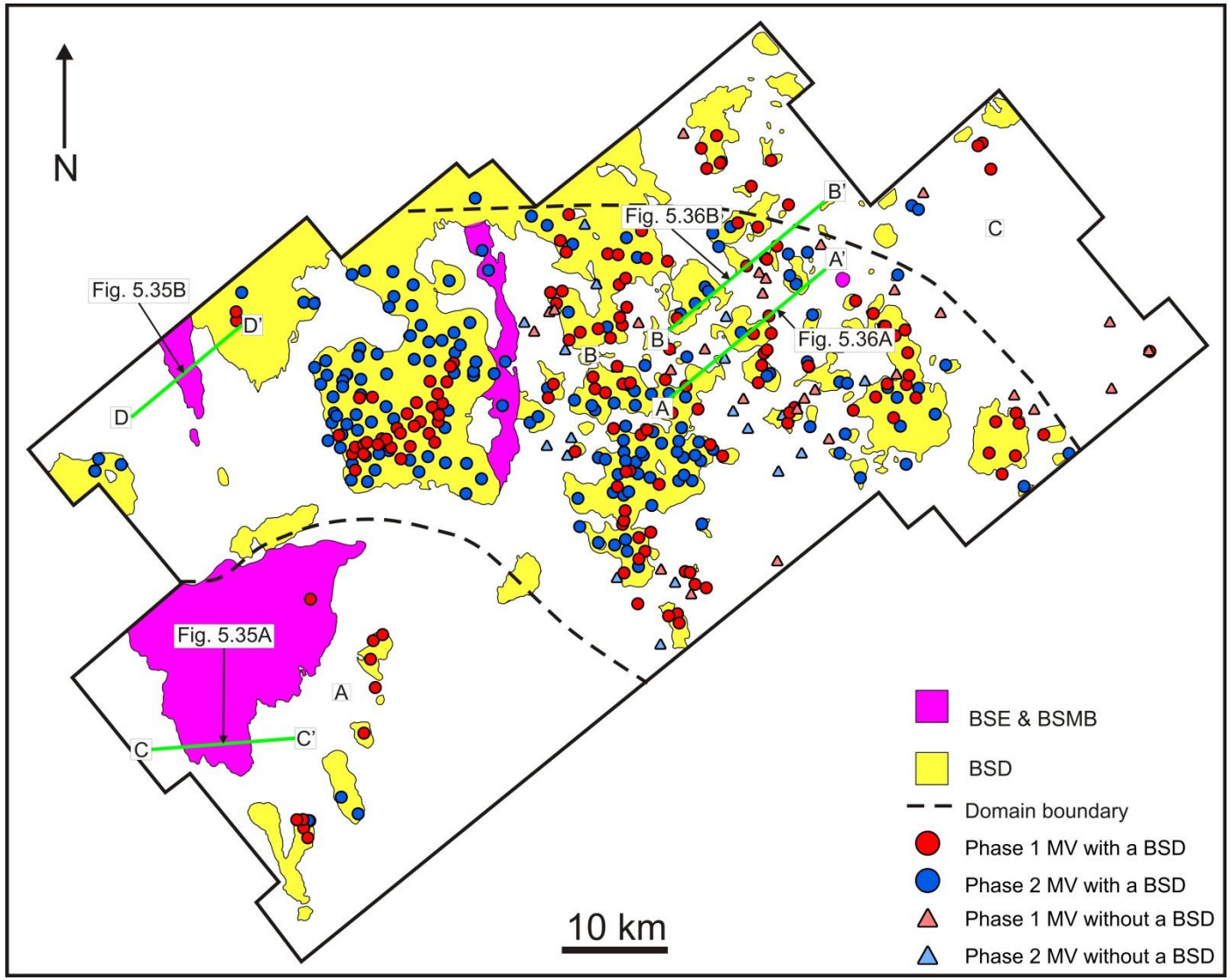

Figure 5.34 Pre-salt withdrawal or removal. A map showing the outline of all base-salt depressions. The depressions have been colour coded:
(1) Yellow - the depression is interpreted to be due to depletion and therefore represent the drainage areas of the overlying mud volcanoes;
(2) Purple – are formed through erosion or are associated with faulting.
BSD – Base-salt depletion. BSE&BSMB – Base-salt erosion and base-salt mini basin. The green lines represent the lines of section for Figure 5.35A, Figure 5.35B, Figure 5.36A, Figure 5.36B. MV – Mud volcano; A – Domain A; B – Domain B; C – Domain C.

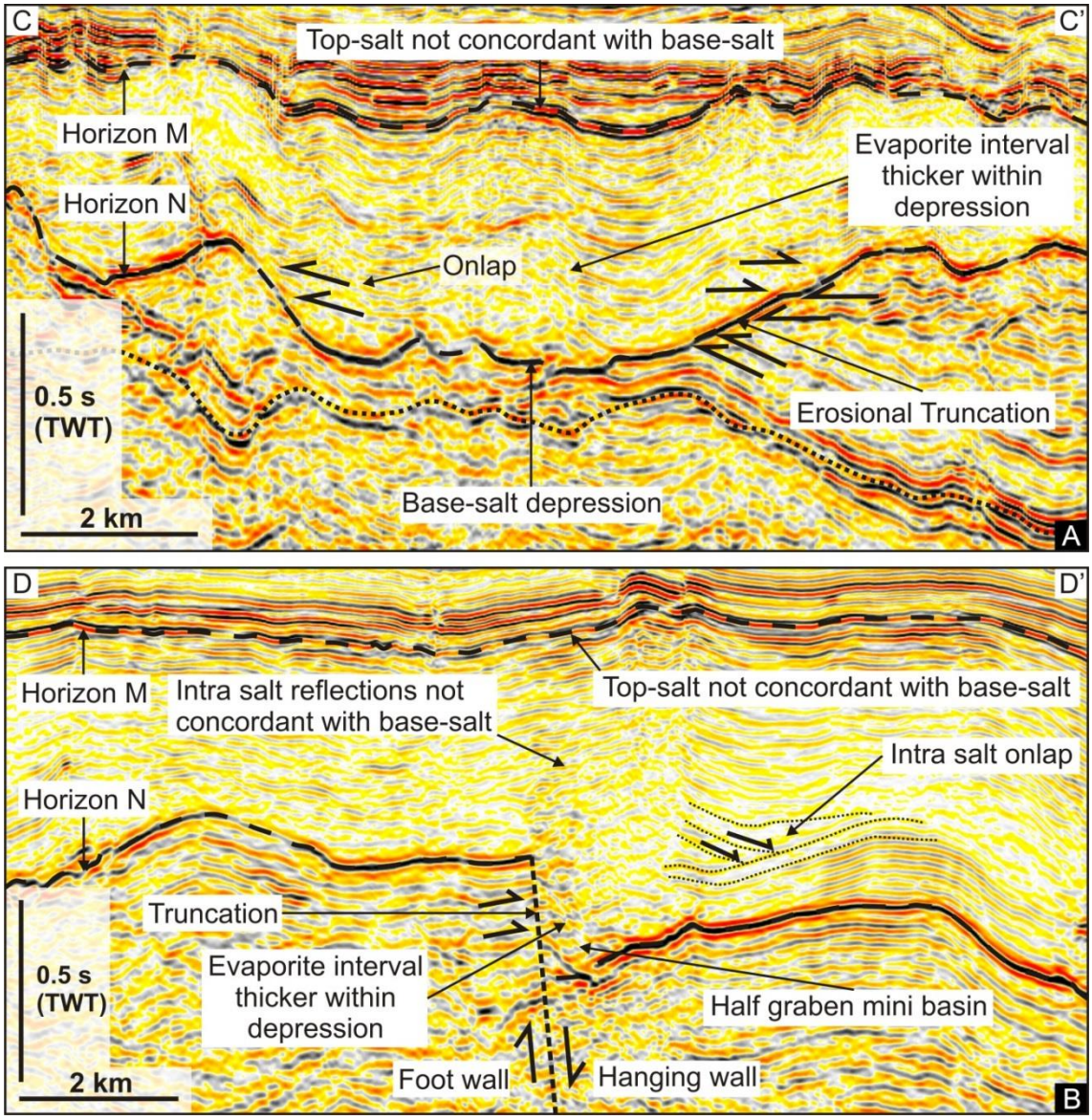

Figure 5.35 Depressions associated with the removal of pre-salt sediments and throw across a pre-salt fault. The lines of section for A and B are displayed in Figure 5.34.

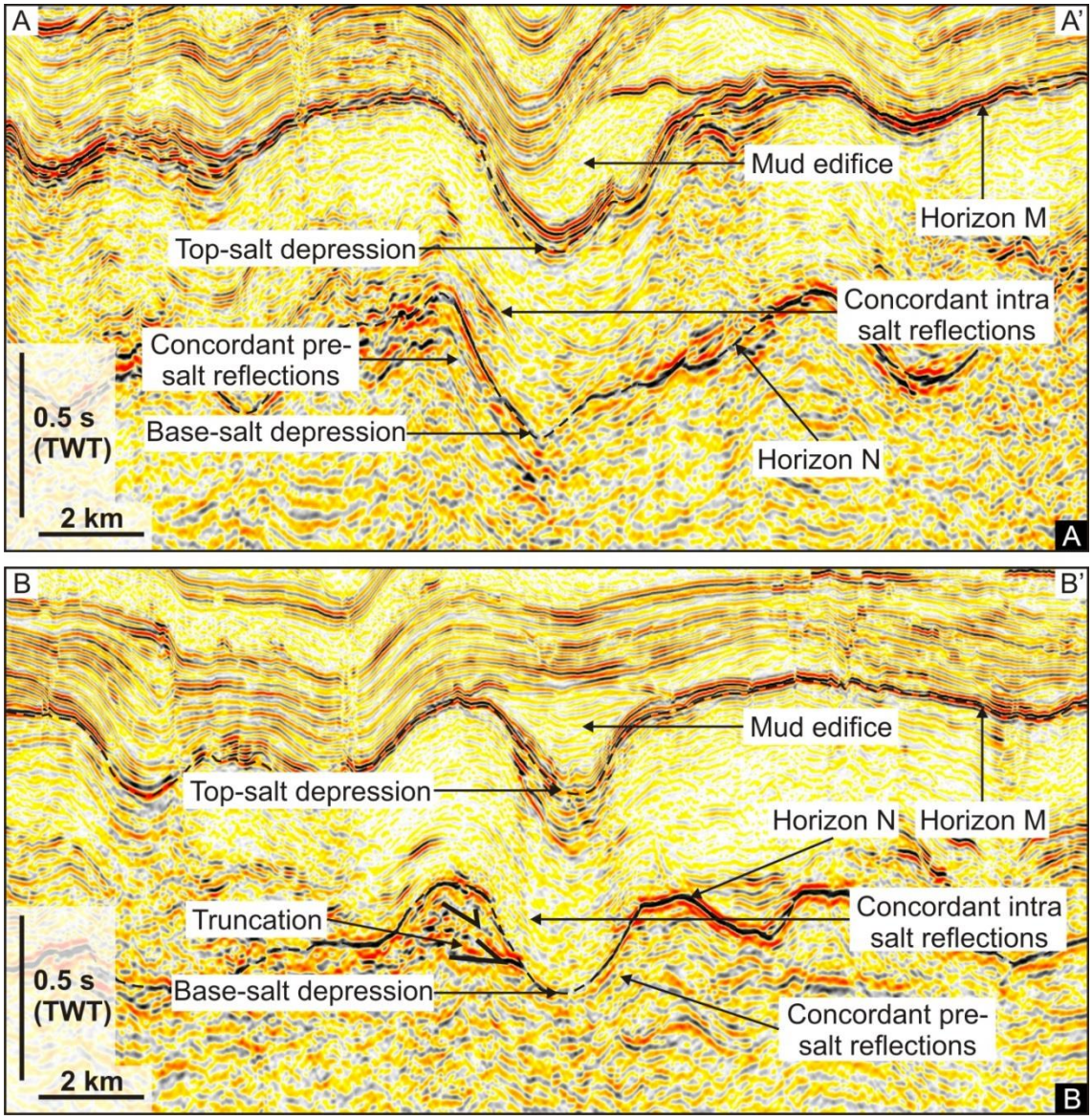

Figure 5.36 Depressions associated with the withdrawal of pre-salt sediments. The lines of section for A and B are displayed in Figure 5.34.

The description of the geometry of the depression in Figure 5.35A, its stratal relationship with reflections of the pre-salt and evaporite succession and the timing of its formation are all indicative that this erosional feature is a canyon (sensu Druckman et al. (1995)). It is interpreted here that its formation is correlatable with early stages of the Messinian Salinity Crisis, during which the pre-salt succession was eroded and infilled later by the deposition of Messinian evaporites. In support of this interpretation, it is well documented that in other parts of the Eastern Mediterranean the Oligo-Miocene unit has been incised by canyon development during the desiccation of the Mediterranean at the beginning of the MSC (Hsü et al., 1973; Bertoni and Cartwright, 2006; Barber, 1981; Buchbinder and Zilberman, 1997). A prime example can be found further towards the east within the Levant basin where other base-salt canyons have been identified and observed overlying other older Oligo-Miocene canyon systems (Afiq, El Arish and Ashod canyons); therefore suggesting these systems acted as preferential sites of erosion in the earliest stages of the MSC (Bertoni and Cartwright, 2006).

Two examples of large base-salt depressions that contrast with the previous two examples are displayed in Figure 5.36. In both examples, mud volcanoes can be observed overlying a base-salt and top-salt depression (Figure 5.36). The top and base-salt reflections are generally concordant with each other, as are some of the more continuous intra salt reflections that can be observed within the evaporites succession (Figure 5.36). The observation of concordant intra salt reflections is notable because it may be expected that these reflections would onlap onto the depression if the sedimentary sequence had been deposited after the formation of a depression. The concordance of the reflections, therefore, implies that the depression formed after the deposition of the overburden. Some reflections within the immediate pre-salt are truncated by the depression at Horizon N; however, some reflections also display a change in angle towards the depression and some slight concordance with Horizon N (Figure 5.36). The change in angle of reflections towards base-salt depression and the partial concordance of pre-salt reflections contrast with the examples in Figure 5.35.

The observations made from the base-salt depressions in Figure 5.36 contrast with those of the base-salt depressions in Figure 5.35 and argue against their

formation via the removal/erosion of pre-salt sediment formed during canyon incision or giant pockmark formation (Bertoni et al., 2013; Bertoni and Cartwright, 2006). Another factor to take into consideration is that if the base-salt depression had been formed via erosive process prior to evaporite deposition, then the top-salt surface would probably be flatter and result in a localised increase in salt thickness, similar to as observed in Figure 5.35.

The observed stratal relationships combined with the spatial relationship between these depressions and the overlying mud volcanoes builds a strong argument for sediment withdrawal from within the pre-salt succession. The observed base-salt depressions could, therefore, be interpreted to represent the zone of sourcing/depletion for the overlying mud volcanoes. Based on these observations, the depressions outlined and colour coded yellow in Figure 5.34 represent the depression are interpreted to be associated with depletion. The depressions that are colour coded purple are interpreted to be associated with the removal of pre-salt sediment via erosive processes (Figure 5.34). A significant number of the base-salt depressions within this study area are, therefore, interpreted to be associated with pre-salt sediment withdrawal, the majority of which are spatial related to overlying mud volcanoes and are predominantly located within Domain B (Figure 5.34).

An important observation to be made with regards to the analysis of the location of mud volcanoes is that, frequently the reflections of the hemipelagic deposits and top-salt (Figure 5.30 and Figure 5.32) and base-salt (Figure 5.31 and Figure 5.33) are depressed beneath (Figure 5.36). In order to analyse this relationship on a regional scale, time maps of Horizon M and Horizon N, which also contain data points of every mud volcano within the survey areas have been created (Figure 5.30 and Figure 5.31). By using the contours on these maps and via constant reference to seismic profiles, maps that clearly display the outline of all top-salt and base-salt depressions and the location of all the mud volcanoes has been created (Figure 5.32 and Figure 5.33). These two maps have also been overlain, in order to analyse the stacking relationship between mud volcanoes and underlying top-salt and base-salt depressions (Figure 5.37).

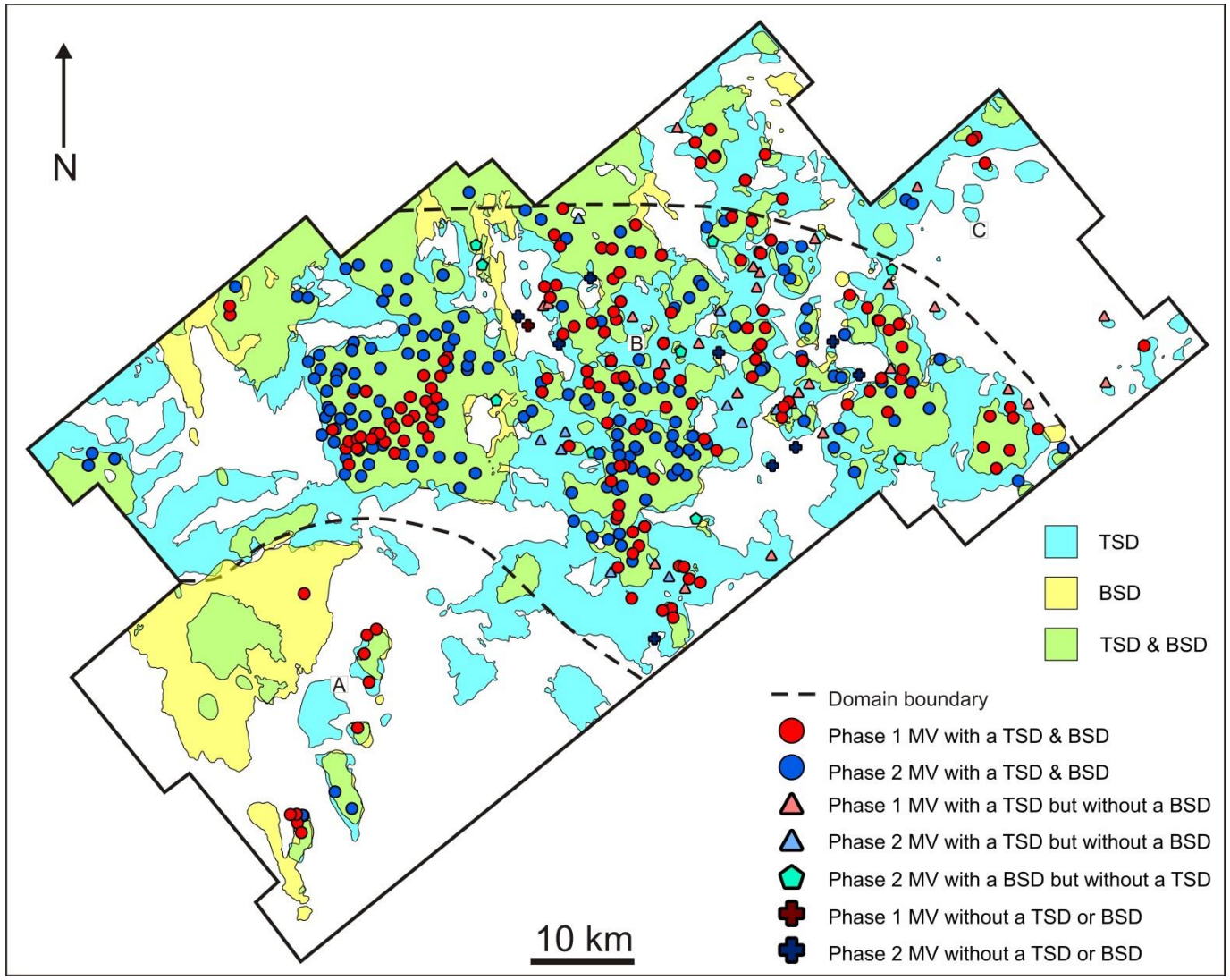

Figure 5.37 Top and base-salt depressions. A map showing the outlined full extent of all base-salt depressions (Yellow) and top-salt depressions (Blue). There is a strong spatial relationship between the two types of depression frequently resulting in top-salt depressions directly overlying base-salt depressions (Green). The location of mud volcanoes within the survey area also frequently overly both top-salt and base-salt depressions. This shows that mud volcano formation is likely related to the location and formation both top and base-salt depressions. MV – Mud volcano; A – Domain A; B – Domain B; C – Domain C.

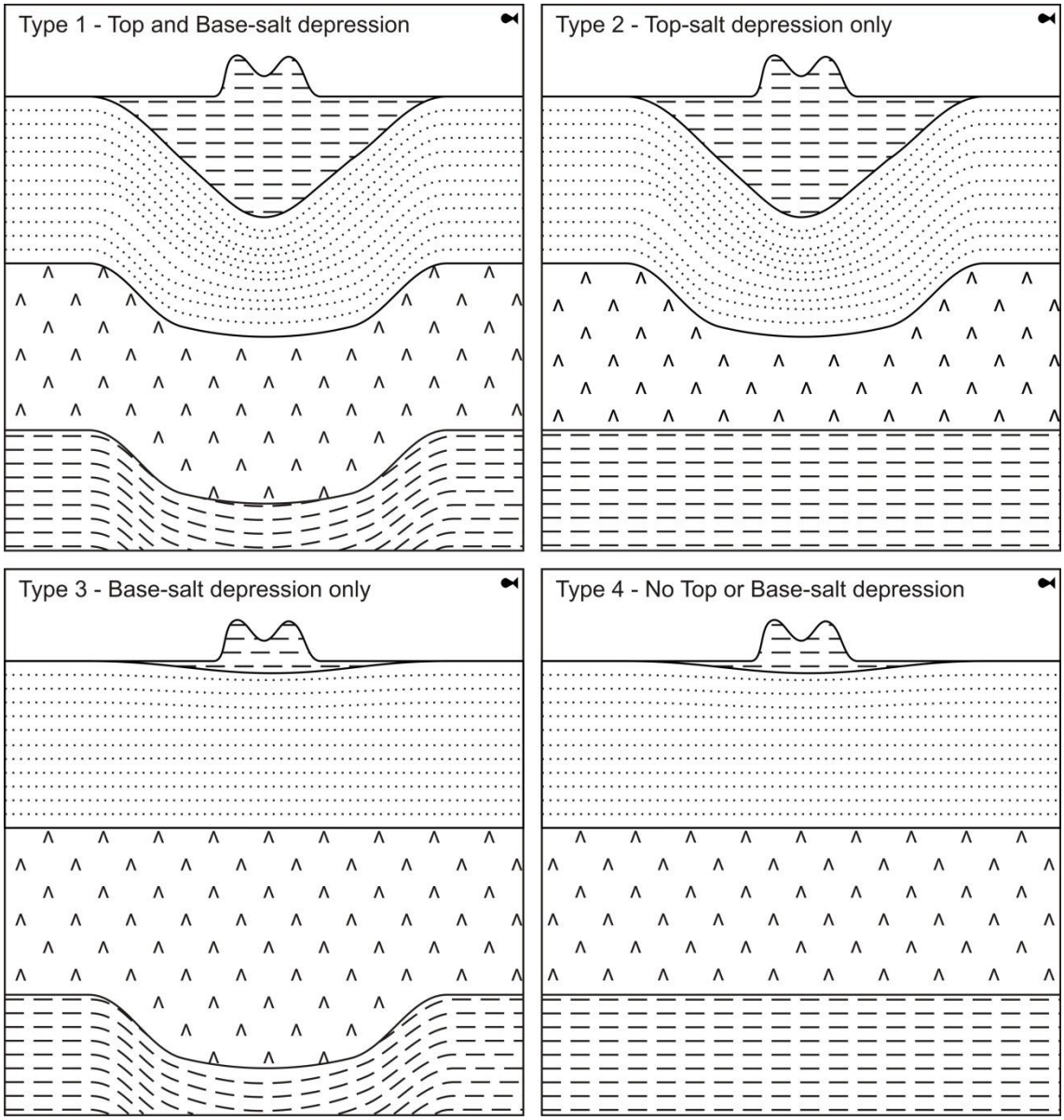

Figure 5.38 Schematic representation of various types of depression related to overlying mud volcanoes. Type 1 - a mud volcano with both a top and base-salt depression beneath. Type 2 - a mud volcano with a top-salt depression beneath it but no base-salt depression. Type 3 a mud volcano with a base-salt depression beneath it but no top-salt. Type 4 - a mud volcano with neither a top or base-salt depression beneath it.

	Total Number of MVs	Type 1	Type 2	Type 3	Type 4
Phase 1	184	156	27	0	1
Phase 2	202	173	11	9	9
All	386	327	38	11	10

Table 5.2 Depressions and mud volcanoes. The data in this table summarises the statistical comparison of the relationship between the survey areas mud volcanoes and the underlying top and base-salt depressions. Type 1 - a mud volcano with both a top and base-salt depression beneath. Type 2 - a mud volcano with a top-salt depression beneath it but no base-salt depression. Type 3 a mud volcano with a base-salt depression beneath it but no top-salt. Type 4 - a mud volcano with neither a top or base-salt depression beneath it. The vast majority of mud volcanoes fulfil the criteria of type one meaning that the formation of most mud volcanoes is intrinsically related to the formation of top and base-salt depressions.

The relationship between the mud volcanoes and horizon M and N can be divided into four different types (Figure 5.38); (1) Type 1 - a mud volcano with both a top and base-salt depression beneath; (2) Type 2 - a mud volcano with a top-salt depression beneath but no base-salt depression; (3) Type 3 which exhibits a mud volcano with a base-salt depression beneath but no top-salt; and (4) Type 4 - a mud volcano with neither a top or base-salt depression beneath it.

The results of this analysis (Table 5.2) shows that of a possible 386, 327 (85%) of the mud volcanoes within the survey area overly a combined top and base-salt depression. There is a very strong correlation between the location of mud volcanoes and depressions. This analysis in combination with the interpretation of sediment withdrawal having had a significant influence on the base-salt geometry is indicative that the formation of these mud volcanoes has had a significant influence on the development of top and base-salt depressions within this study area.

There are large portions of the study area where top and base-salt depressions can be found juxtaposed vertically. However it is clear that Horizon M and N are not entirely coincident with each other as seen for example in Figure 5.39. Frequently, top-salt depressions cover a far greater area than base-salt depressions (Figure 5.39). Underlying base-salt depressions tend to be located relatively centrally with respect to top-salt depressions and are smaller areally but with a similar shape. The area covered by the overlying mud volcanoes is also very similar (Figure 5.39).

Analysis of salt isopach maps displays localised thinning of the evaporites in regions where there are several mud volcanoes a combination of top-salt and base-salt depression (Figure 5.40A). This means that where mud volcanoes have formed, evaporites have either been removed or withdrawn. It is very difficult to distinguish the mode of salt thinning. Similarly an isopach map of the immediate pre-salt interval within the same location shows significant thinning (Figure 5.40B). This area of thinning of the pre-salt is correlatable to the overlying top-salt and base-salt depression (Figure 5.39) and localised thinning of the evaporite succession (Figure 5.40B). These observations in combination with the previously described stratal relationships between the base-salt depression and pre-salt reflections (Figure 5.36) is

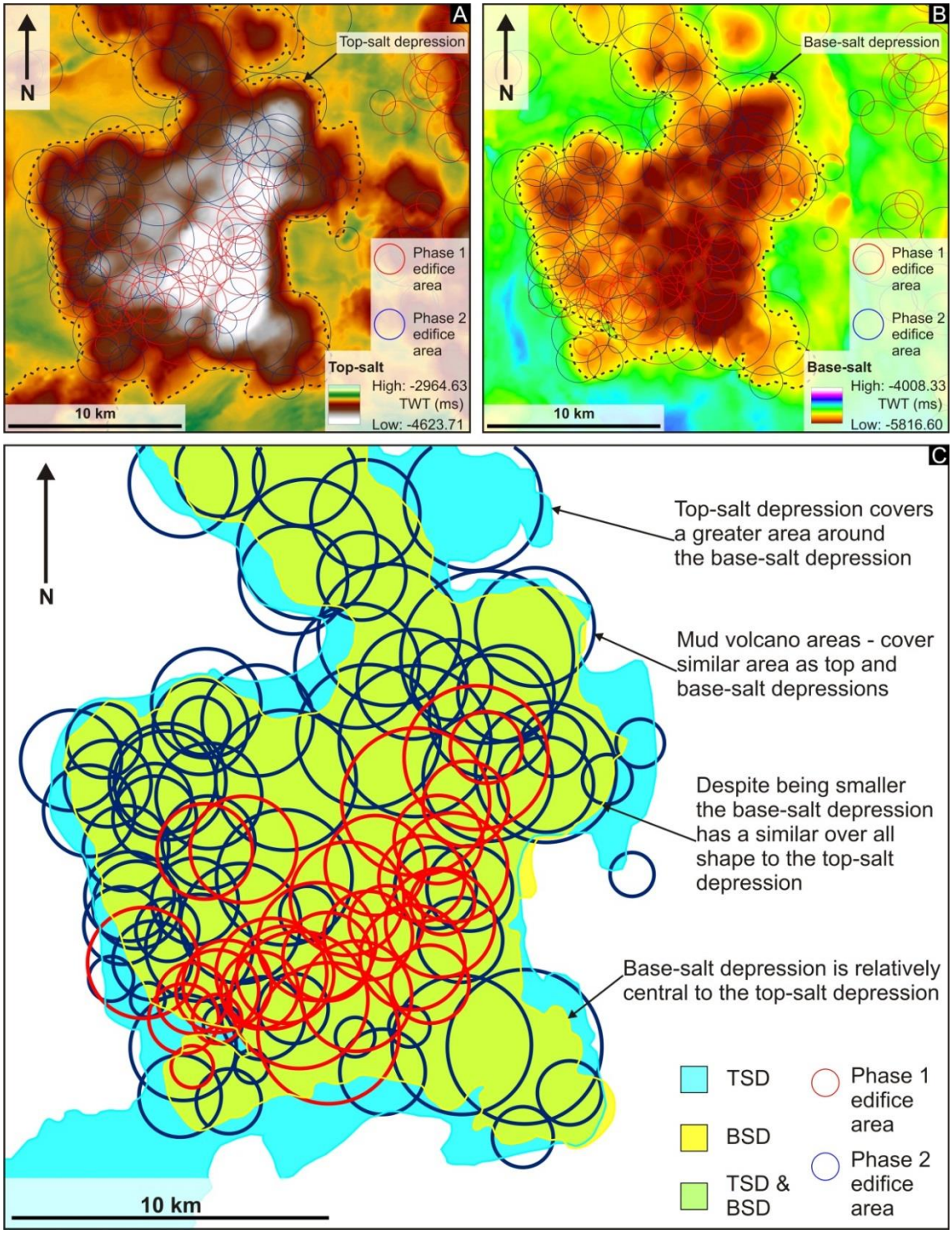

Figure 5.39 Spatial extents of top and base-salt depressions in the Menes area. A: Outline of top-salt depression overlain by mud volcanoes. The circles represent the area of the mud volcanoes which are calculated here based on radius measurement that have been recorded. B: Outline of base-salt depression overlain by mud volcanoes C: A maps showing top-salt depressions (TSD) (Blue), base-salt depressions (BSD) (Yellow), where the two overly (Green) and where the area covered by overlying mud volcanoes.

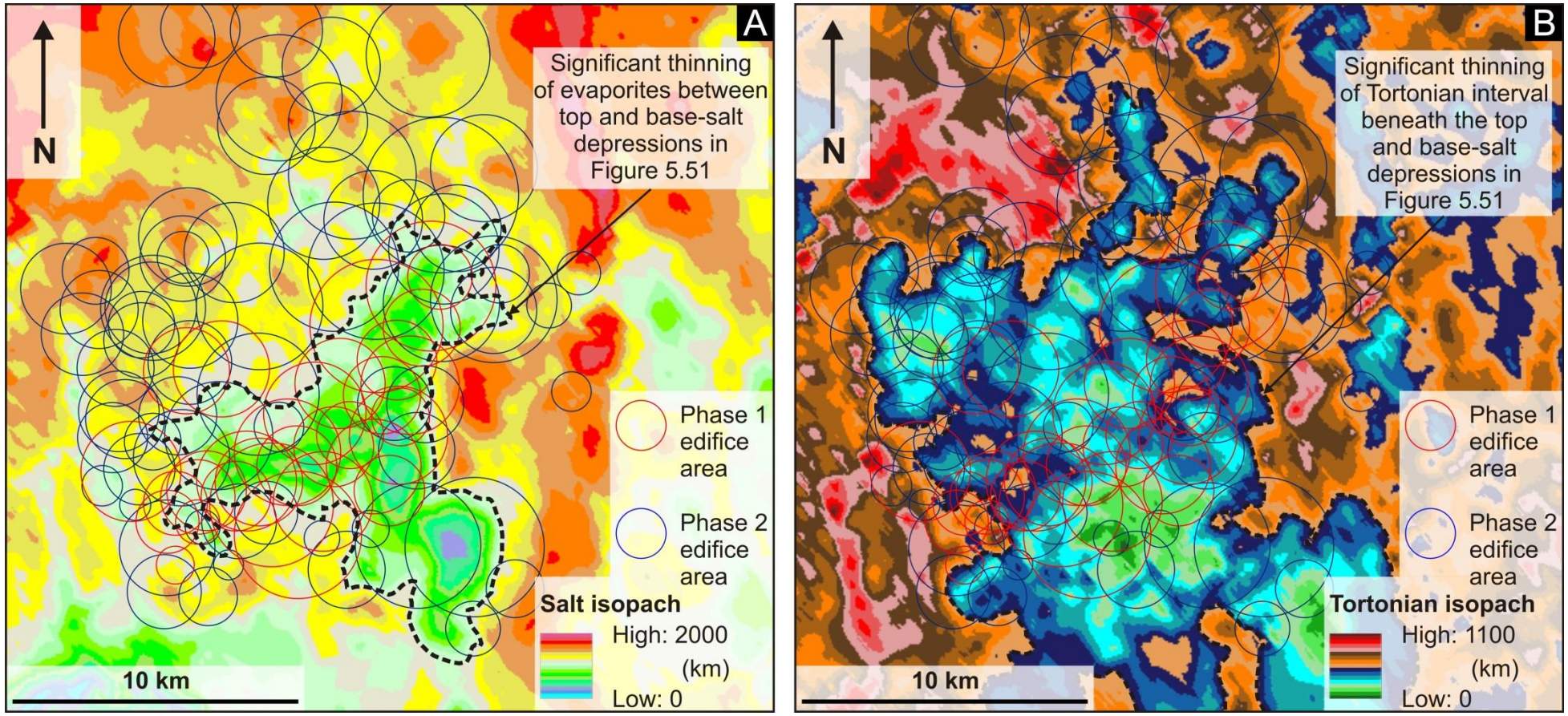

Figure 5.40 Thinning of the Messinian evaporites and immediate pre-salt interval. This analysis focuses on the Menes area similar to Figure 5.39. A. Salt-isopach map overlain by mud volcanoes, showing an area of significant thinning that has been outlined. B: Isopach map of the immediate pre-salt succession overlain by mud volcanoes, showing an area of localised thinning that has been outlined.

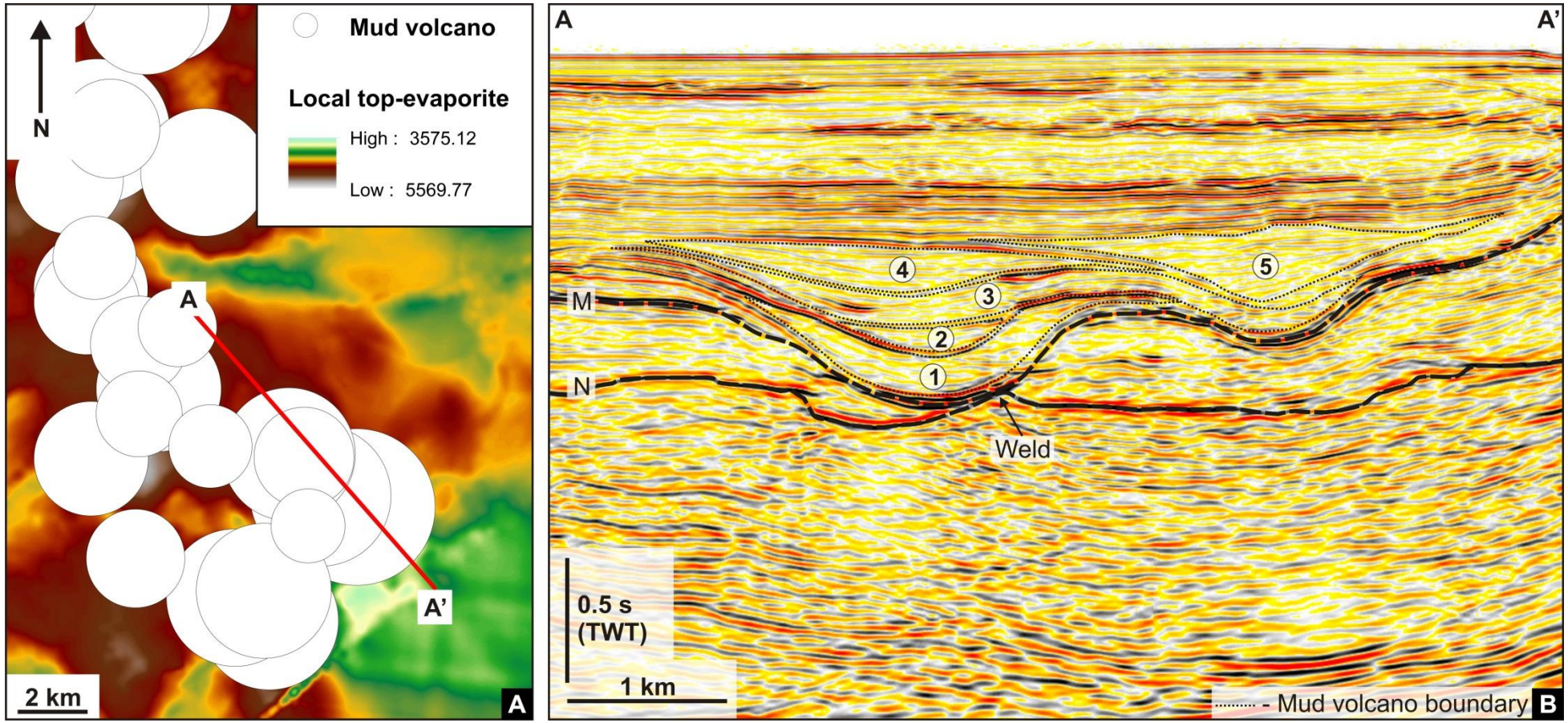

Figure 5.41 Volcano stacking and salt welding A: Time attribute map of top-evaporites showing a cluster of mud volcanoes. The area of each circle has been calculated based on their radius. The red line represents the line of section for Figure 5.41B. B: Seismic profile through the mud volcanoes in A showing several mud volcanoes stacked one above the other and a top-salt depression beneath them which welds with the base-salt. The mud volcanoes are numbered 1-5 based on order of formation.

strongly indicative of sediment withdrawal from the immediate pre-salt associated with fluid and sediment mobilisation from the unit during the formation of overlying mud volcanoes.

In some areas multiple mud volcanoes are clustered and stacked one above the other resulting in a large top-salt depression and thinning of the evaporites beneath. An excellent example of this is presented in Figure 5.41, which clearly shows five volcanoes, four of which are stacked one on top of the other. They are not precisely stacked, which means that the central points of these mud volcanoes are not vertically aligned. Despite this the combined effect of the stacking pattern has produced the bulk of the fill for a large depression, which is most pronounced at Horizon M. The evaporites beneath this large depression have thinned so significantly that it has resulted in a weld between the top-salt and base-salt. This is considered the extreme end member in the spectrum of salt depression geometries associated with mud volcanoes.

Some areas of pronounced mud volcano clustering and stacking are spatially related to a combination of crudely concordant seafloor and top-salt depressions, as exemplified in the maps in Figure 5.42 and Figure 5.43. These depressions are characterised by downsagging of reflection, most clearly observed in the reflections of Horizon M and the reflection of the Pliocene-Recent succession that underlie the mud volcanoes. Linear-arcuate faults which are predominantly outward dipping can be observed on the margins of the depressions, particularly on south facing side (Figure 5.42 and Figure 5.44). The internal structure of these features primarily comprise of numerous mud volcanoes that have infilled the depression associated with the 'downsagging' hemipelagic deposits (Figure 5.43 and Figure 5.44).

One of the most prominent seafloor features within the study area is the Menes Caldera which can be seen in Figure 5.42. The Menes Caldera has previously been described as an area of active fluid escape within a large circular depression almost 8 km wide, which is heavily fault controlled, particularly on its southern edge (Huguen et al., 2009; Dupré et al., 2014; Pierre et al., 2014) (Figure 5.42 and Figure 5.43). Typically caldera diameters range from 2 - 50 km and downsag can be a common

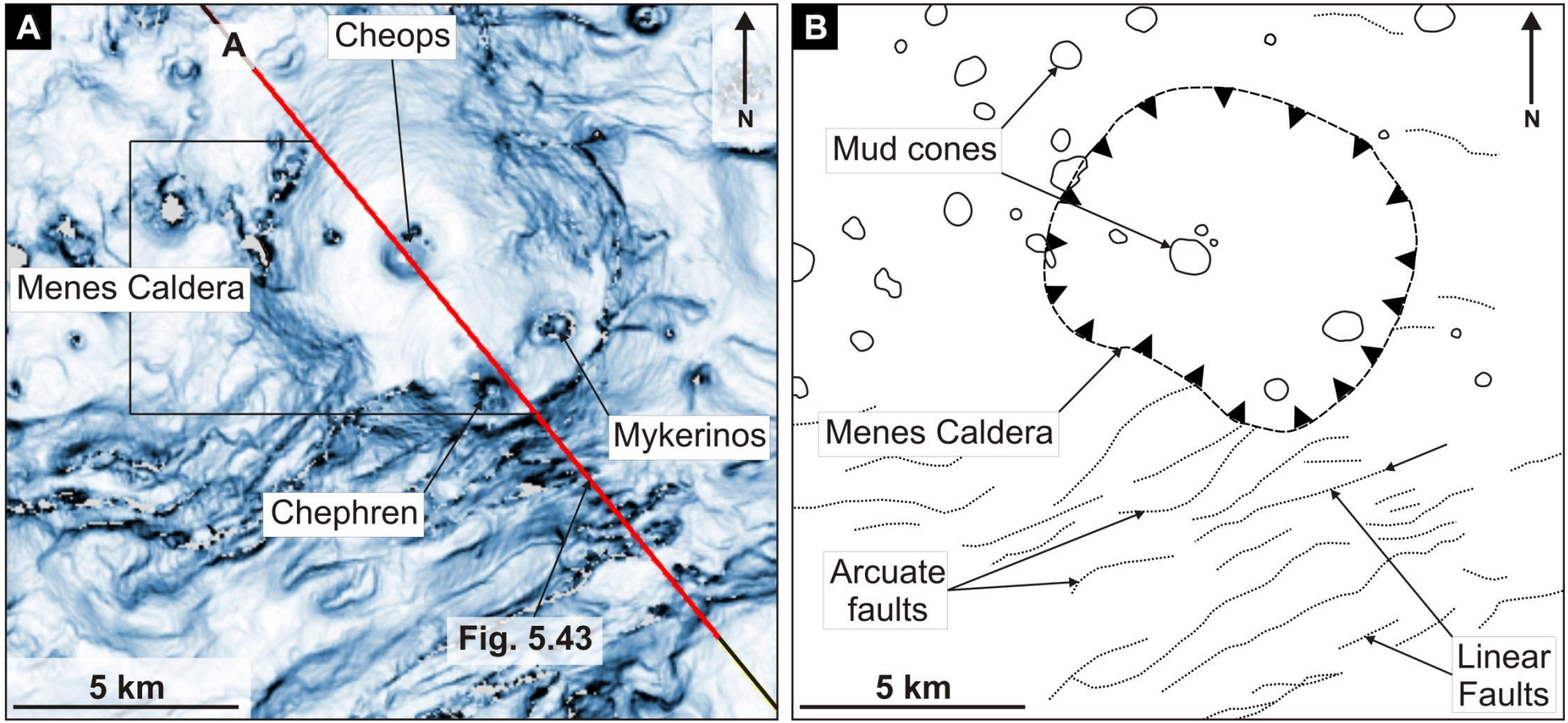

Figure 5.42 Seafloor caldera. A: A time-dip map of the seafloor showing a seafloor depression approximately 8 km in diameter. Within the seafloor depression there are three mud cones named Cheops, Chephren and Mykerinos. The red line shows the line of section for Figure 5.43. B: A schematic representation of the seafloor and features in Figure 5.42A highlighting the specific limits of the depression, various mud cones at the surface and numerous linear-arcuate faults around the depression particularly on the south facing side.

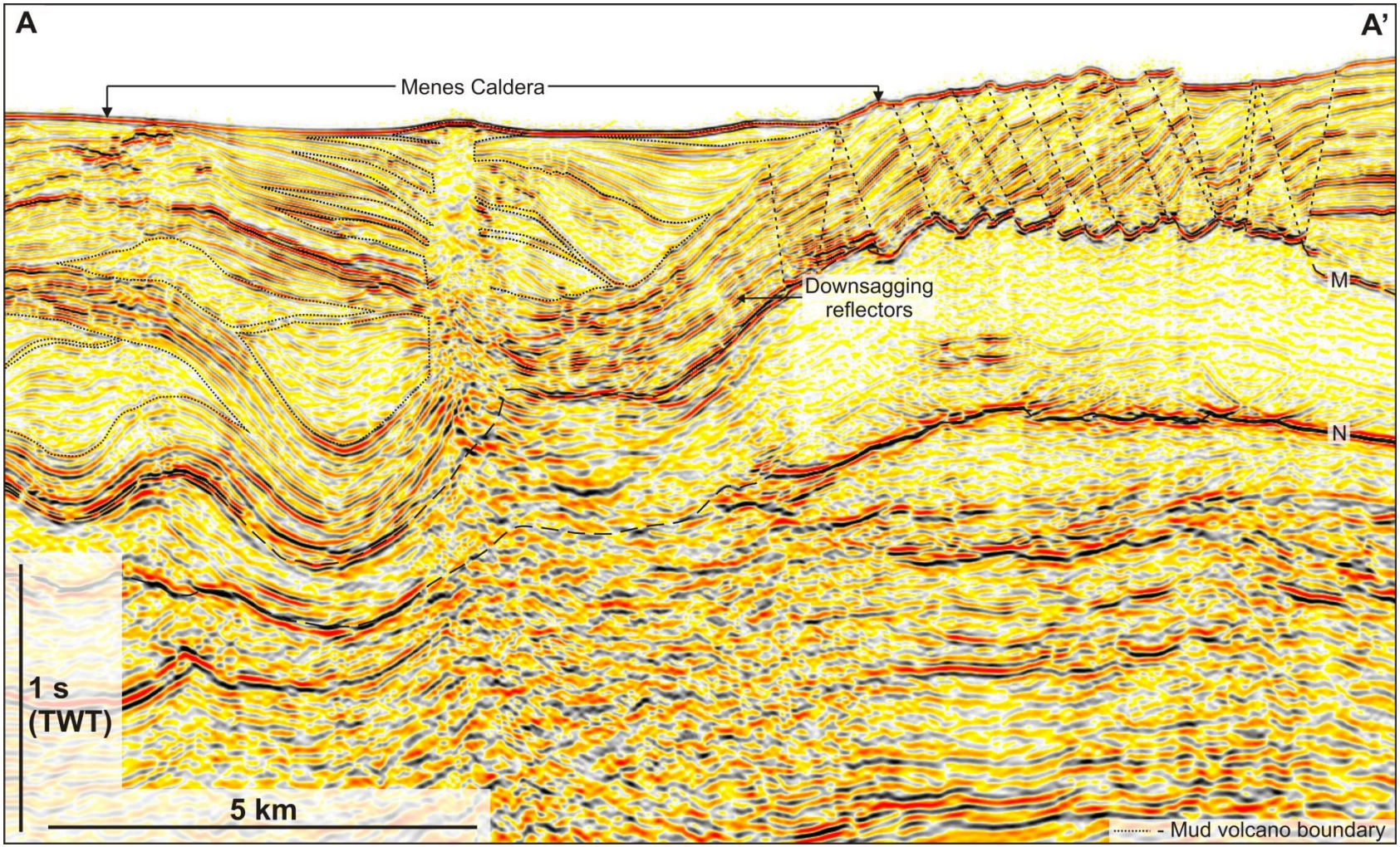

Figure 5.43 Caldera seismic profile. A seismic profile through the seafloor depression seen in Figure 5.42 the extent of which has been highlighted in the profile. Beneath the seafloor depression there is a high concentration of mud volcanoes and reflections of the hemipelagic deposits downsag beneath the depression. Faults observed in the Figure 5.42 can be seen to be normal and predominantly outward dipping.

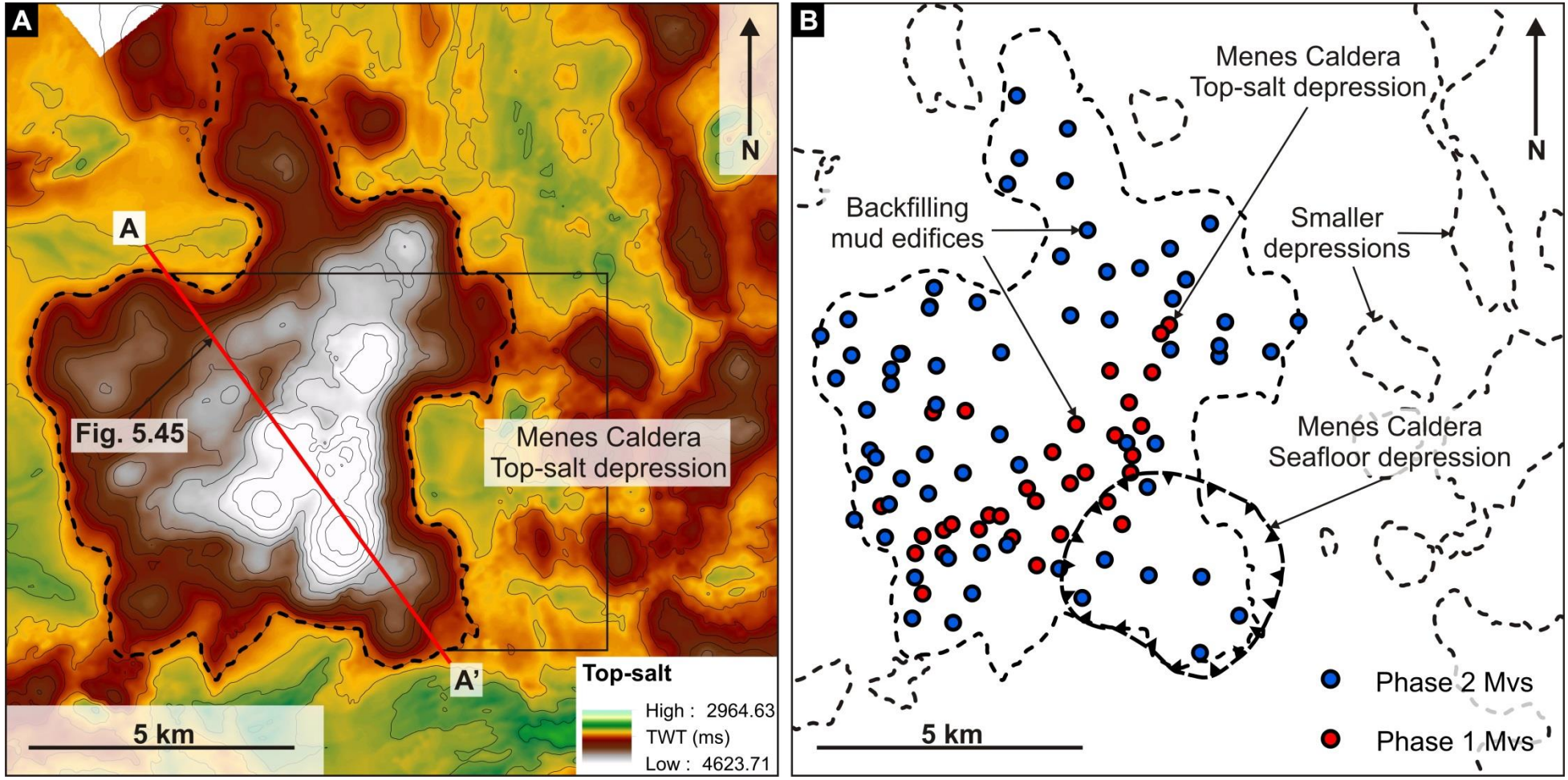

Figure 5.44 Top-salt caldera. A: A time map of the top-salt showing a large depression as great as 20 km wide beneath the Menes seafloor caldera. The red line represents the line of section for Figure 5.45. B: A schematic representation of the top-salt depression highlighting the specific limits of the top-salt depression in relation to the seafloor depression. All the mud volcanoes identified within the confines of the top-salt depression have been overlain, of which there are 98.

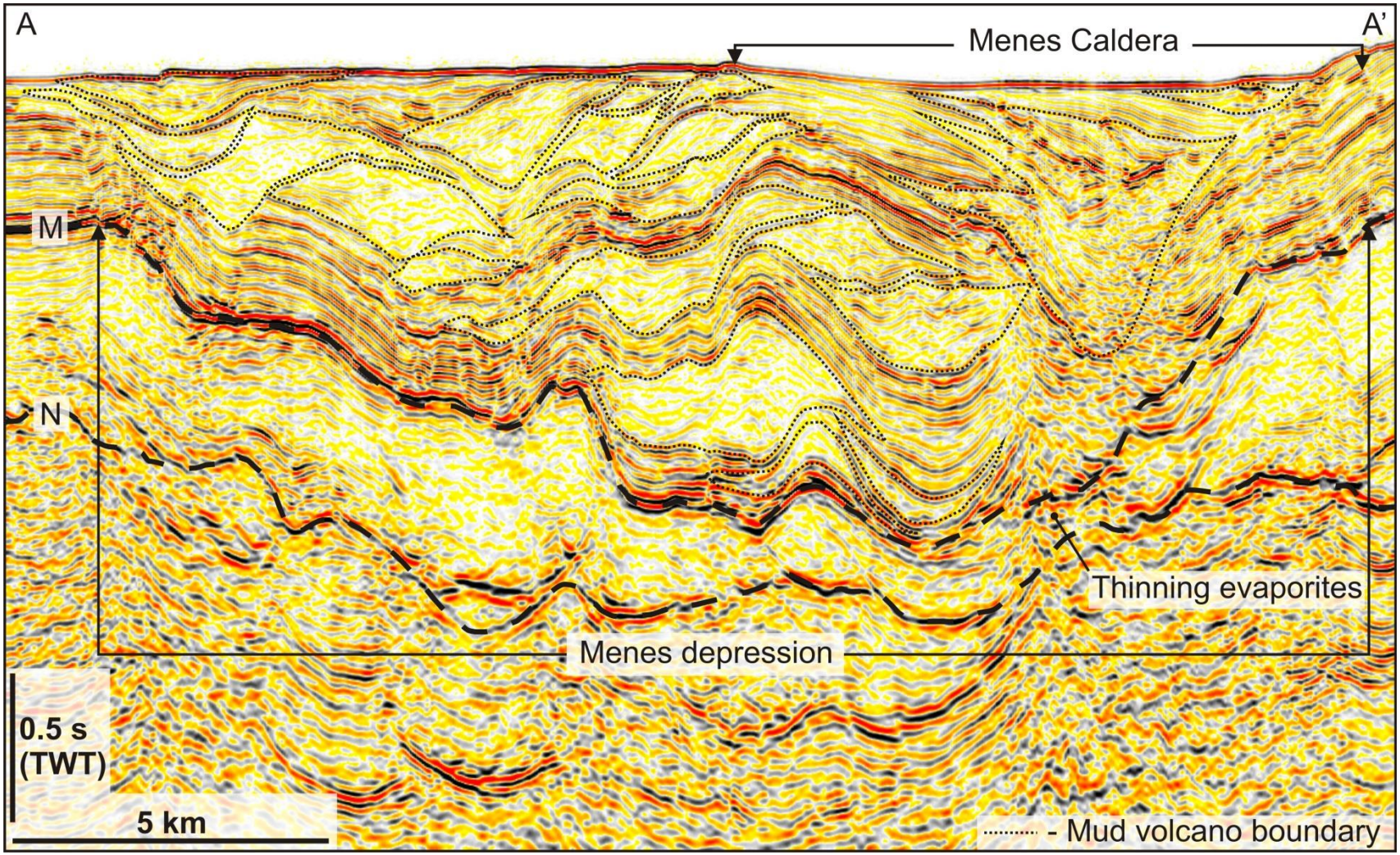

Figure 5.45 Seismic profile through the Menes Caldera. Demonstrates the difference in scale between the seafloor depression and top salt depression of the Menes Caldera. Numerous mud volcanoes have infill the depression and thinning of the evaporites is clearly visible beneath, particularly where the top-salt is at its deepest.

cause of the concentric-arcuate faulting because it causes radial extension near the margin of subsidence (Branney, 1995). Within the Menes Caldera there are three mud cones that can be identified at the modern day seafloor and have been named Cheops, Chephren and Mykerinos (Huguen et al., 2009) (Figure 5.42). Analysis of this caldera using 3D seismic data has revealed that the seafloor expression of this caldera and the three mud volcanoes at the seafloor represent but a fraction of the calderas full extent (Figure 5.44 and Figure 5.45). The subsurface beneath the seafloor depression of the Menes caldera is characterised by a large top-salt depression, up to 20 km wide and relief as great as 1400 m, here referred to as the Menes depression (Figure 5.44 and Figure 5.45). This large depression has been infilled by as many as 98 mud volcanoes, which have a cumulative volume of c. 67.93 km^3 (Figure 5.44 and Figure 5.45). The density of mud volcanoes within the Menes area is exceptionally high and has clearly had a significant impact on the Messinian evaporites beneath (Figure 5.44 and Figure 5.45). The full extent of mud volcanism and subsidence within the Menes area would appear to be significantly greater than previously recognised (Huguen et al., 2009; Dupré et al., 2014; Dupre et al., 2005; Giresse et al., 2010).

5.3.7 Volumetric Analysis

The substantial variability in geometry of the mud volcanoes within this study area results in a large range of calculated volumes for mud volcanoes. The mud volcanoes of Phase 1 exhibit volumes ranging from 0.1 km^3 to 2.7 km^3 with an average of 0.6 km^3, a median of 0.4 km^3 and a total extruded volume of 113.9 km^3 (Table 5.1 and Figure 5.46). By comparison the mud volcano volumes of phase 2 have a greater range from 0.1 km^3 to 3.3 km^3; however the average of 0.5 km^3 and median of 0.3 km^3 are comparatively smaller (Table 5.1 and Figure 5.46). The total extruded volume from phase 2 is 93.735 km^3, which when compared to the total extruded volume of phase 1 is significantly smaller, despite phase 2 hosting a greater number of mud volcanoes. This is an important observation because the dating of Phase 1 and Phase 2 suggests that the time span of Phase 1 is in all likelihood much longer than Phase 2. If the dating is even slightly accurate, these results imply that the number of mud volcanoes

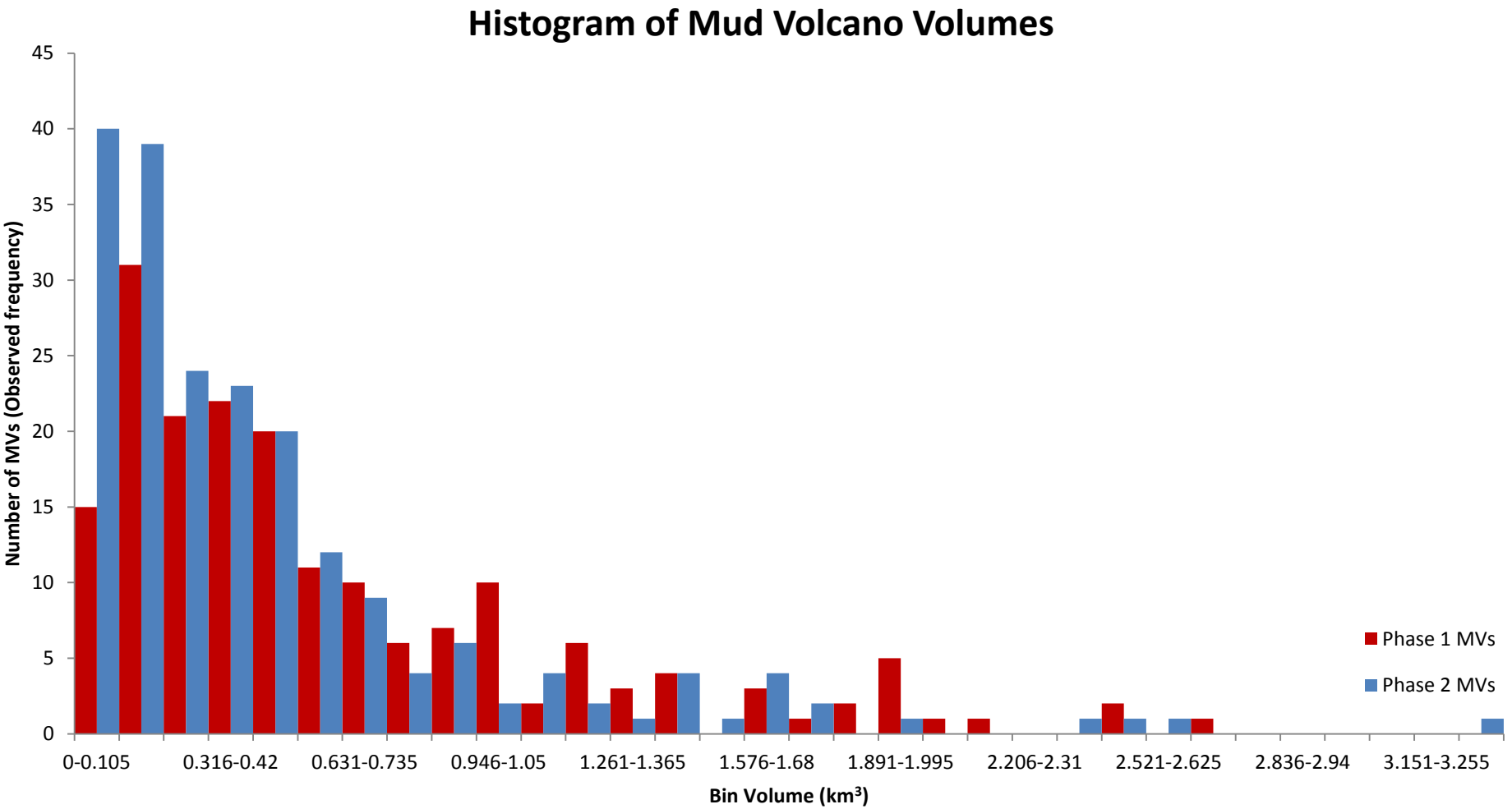

Figure 5.46 Histogram of mud volcano volumes. The histogram shows the frequency of mud volcanoes, within a range of bins each one increasing by a volume of 0.105 km^3, for each phase 1, phase 2. The frequency within bins decreases as volume increases.

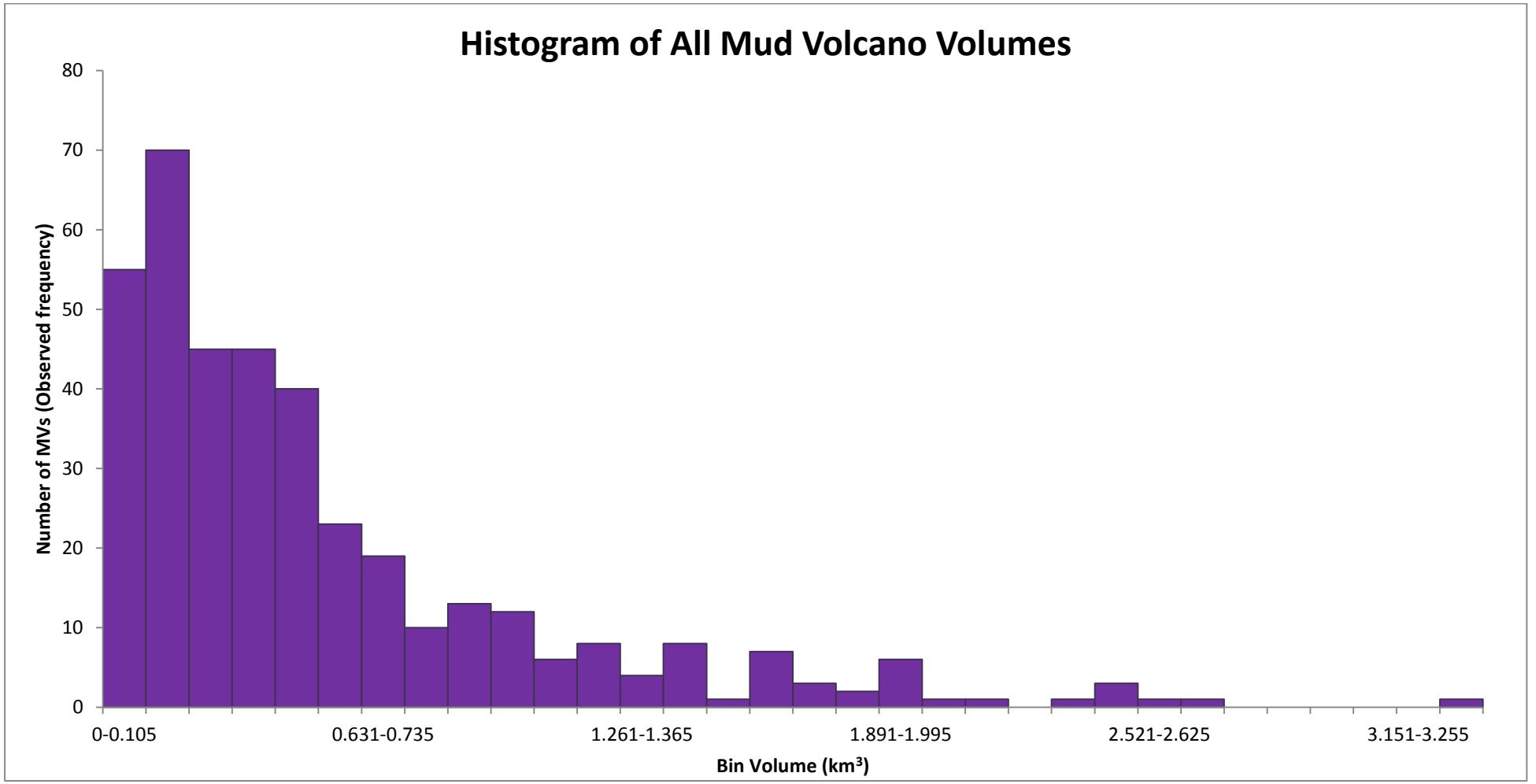

Figure 5.47 Histogram of all mud volcano volumes. The histogram shows the frequency of mud volcanoes, within a range of bins each one increasing by a volume of 0.105 km³, for all mud volcanoes within the study area. The frequency within bins decreases as volume increases.

that form within this study area has increased since the Upper Pleistocene but that they are on average of a smaller size. The total extruded volume of mud from phase 1 and 2 combined has been calculated as 207.7 km^3 (Table 5.1 and Figure 5.47).

To analyse the distribution of volume sizes, the goodness-of-fit chi-square (X^2) test, Poisson and Negative Binomial models were used (See section 2.3.1.5 of Chapter 2 for description). These tests focused on all the mud volcanoes throughout the survey area. Prior to running these tests the mud volcanoes were divided into bins based on their volumes ranging from 0 to 3.36 km^3, increasing at an increment of 0.105 km^3 per bin, resulting in a total of 32 bins (Figure 5.47). The chi-square test considers the acceptance or rejection of a null hypothesis (Davis and Sampson, 2002) here stated as:

H_o: The distribution of mud volcano volume values is uniform

The expected frequency (See section 2.3.1.5 of Chapter 2) for this test is 12.06 mud volcanoes per bin and the observed frequencies range from 0 to 70 per bin. For df (degrees of freedom) =32, the critical value of chi-square at a significance level of 1% is 53.486. The X^2 value was calculated as 58031749.86 which greatly exceeds the critical value; therefore the null hypothesis can be rejected meaning that volume size distribution is not uniform. Knowing that the distribution is non-uniform eliminates one possibility but does not provide any indication as to the actual nature of the distribution (Davis and Sampson, 2002).

In order to determine whether mud volcano volumes are randomly distributed, the observed frequencies were compared with a Poisson distribution model (Figure 5.48). The goodness-of-fit between the observed data and that of a Poisson distribution are analysed using a chi-square test which considers the acceptance or rejection of a null hypothesis here stated as:

H_o: The distribution of mud volcano volume values is random

The observed frequency range, degrees of freedom and critical value of chi-square at a significant level of 1% all remain the same as the previous test for uniform distribution. An X^2 value of 38849.027 once again greatly exceeds the critical value. The null hypothesis can therefore be rejected, meaning that the mud volcano volume

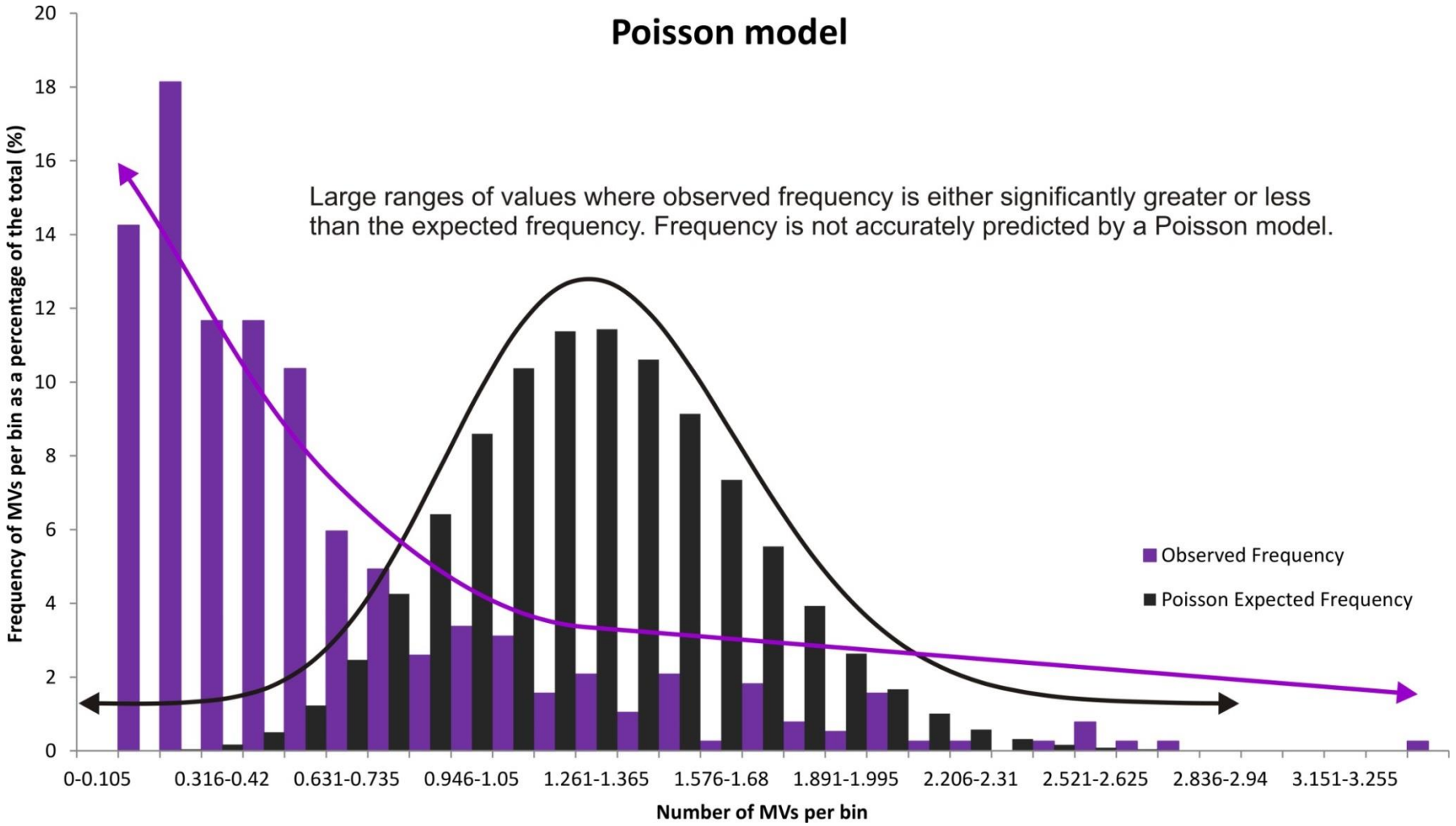

Figure 5.48 Poisson model random distribution. The observed fequency (Purple) and expected frequency (Black) based on a Poisson model. The distribution model does not provide a good fit displaying significant disparity between the frequencies, showing the data is not random.

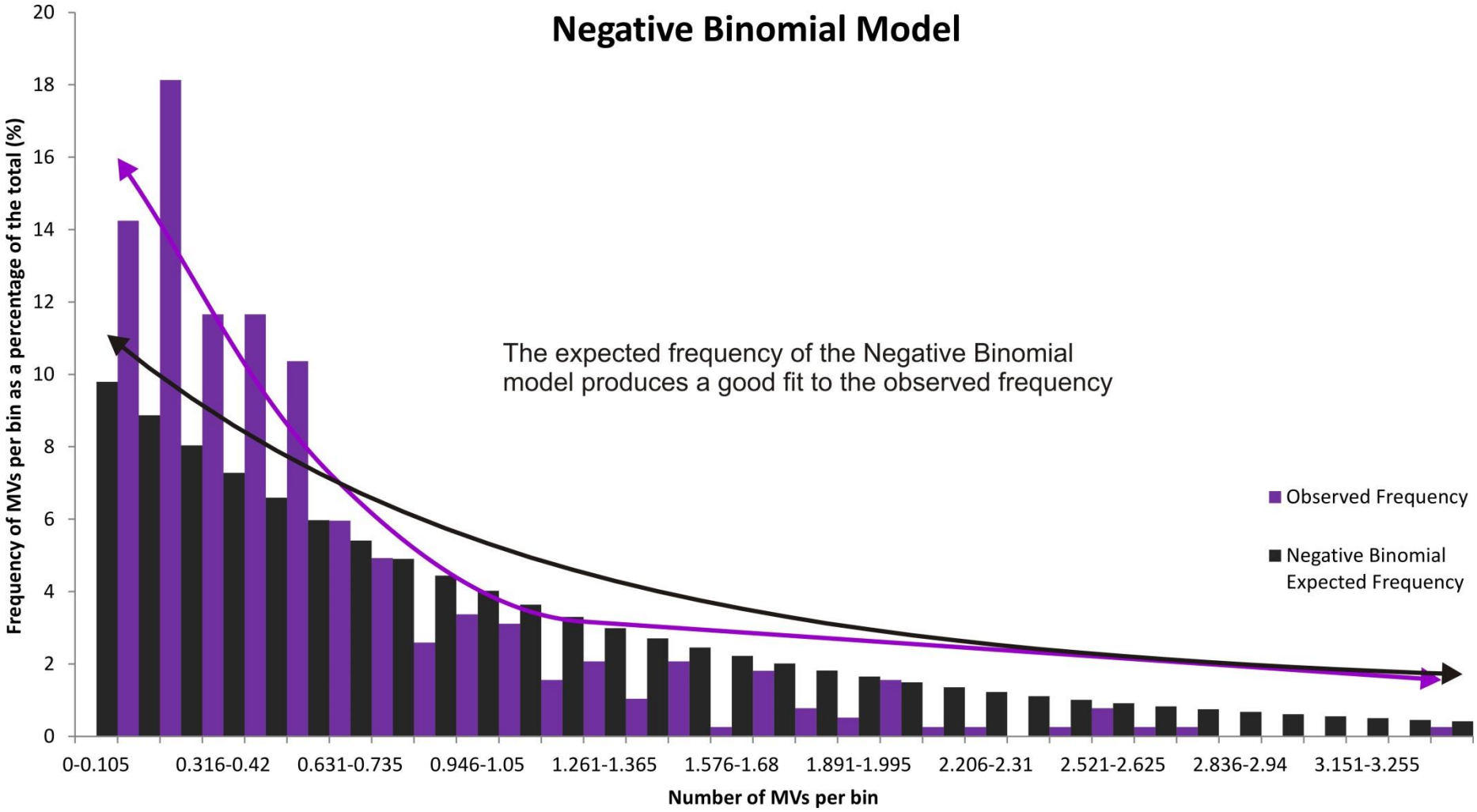

Figure 5.49 Negative Binomial model clustered distribution. The observed fequency (Purple) and expected frequency (Black) based on a Negative Binomial model. The Negative Binomial distribution provides a good fit to the observed frequencies showing that the data is of a clustered distribution with the greatest frequencies found in smaller values.

values are not of a random distribution. The graphical representation of the data in Figure 5.48 shows a histogram of the observed frequencies and expected frequencies based on the Poisson model, further showing the disparity between the two frequencies and unsuitability of the Poisson model to describe the distribution of mud volcano volume values.

A remaining possibility for the distribution of data is that of a clustered distribution, which is usually tested for using a Negative Binomial model (Davis and Sampson, 2002). This test analyses the goodness-of-fit of the observed frequencies with those of an expected using a negative binomial model (Figure 5.49). The results are again calculated using a chi-square test which considers the acceptance or rejection of a null hypothesis here stated as:

H_o: The distribution of volume values of mud volcanoes is clustered

Once again the observed frequency range, degrees of freedom and critical value of chi-square at a significane level of 1% all remain the same as the previous two tests for uniform and random distribution. The X^2 value was calculated as 48.822 which in contrast to the previous two tests is less than the critical value of chi-square 53.486 at a significance level of 1%. Consulting the table of chi-square reveals that the X^2 value actually accepts the null hypothesis to a significance level of 2.5% where the critical value is 49.480. The negative binomial test is, therefore, accepted as the appropriate test and shows that the volume values of mud volcanoes are of a clustered distribution.

An alternative analysis of the distribution can be acquired via comparison of the estimated mean number of mud volcanoes per bin (em) and variance (s^2). By calculating the ratios for em/s^2 values lower than 1 are indicative of clustered patterns, equal to 1 indicate the pattern is random and greater than one are representative of a uniform pattern. A ratio of 0.11 was calculated which further supports the results from the Negative Binomial test that the distribution of mud volcano volumes is clustered. The graphical representation of the data in (Figure 5.49) shows a histogram of the observed frequencies and expected frequency's based on the negative binomial model. While the histogram shows that there is still some disparity between the two

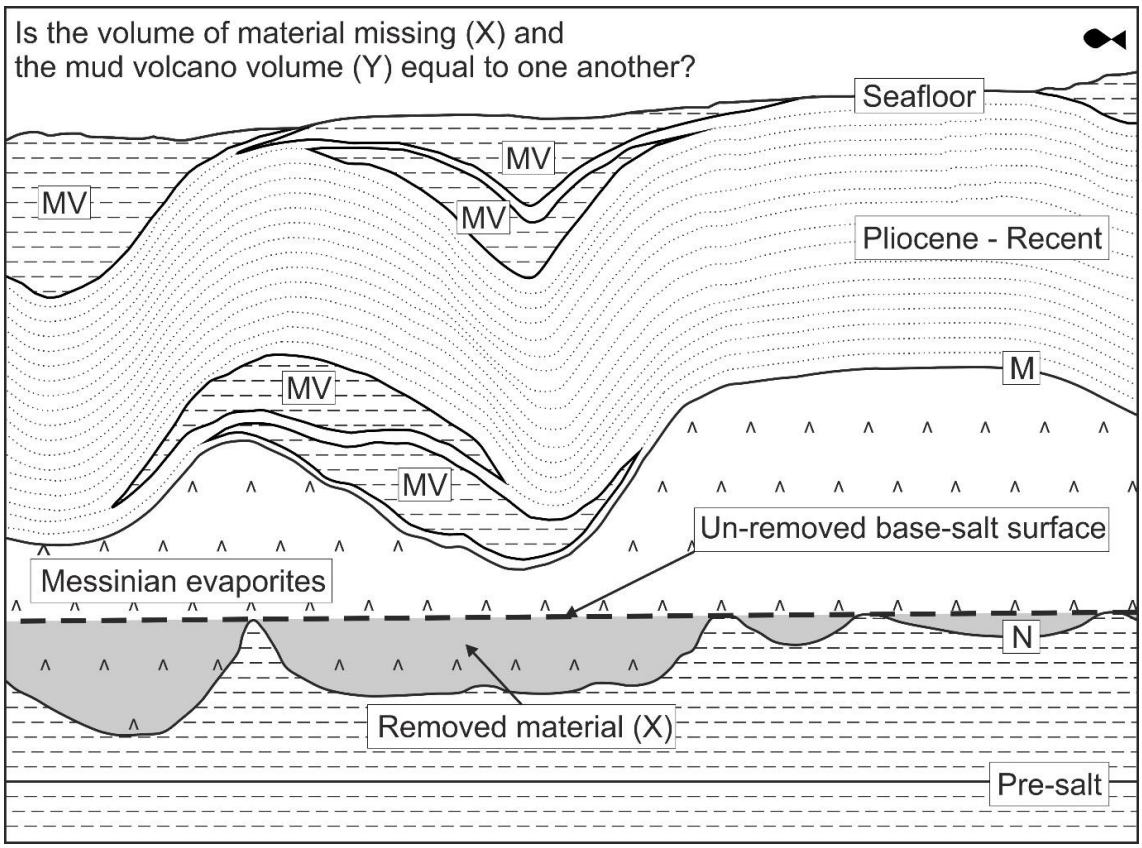

Figure 5.50 Volumetric balance cartoon. The cartoon demonstrates the balance between sediment removed from immediate pre-salt interval and the volume of the overlying mud volcanoes..

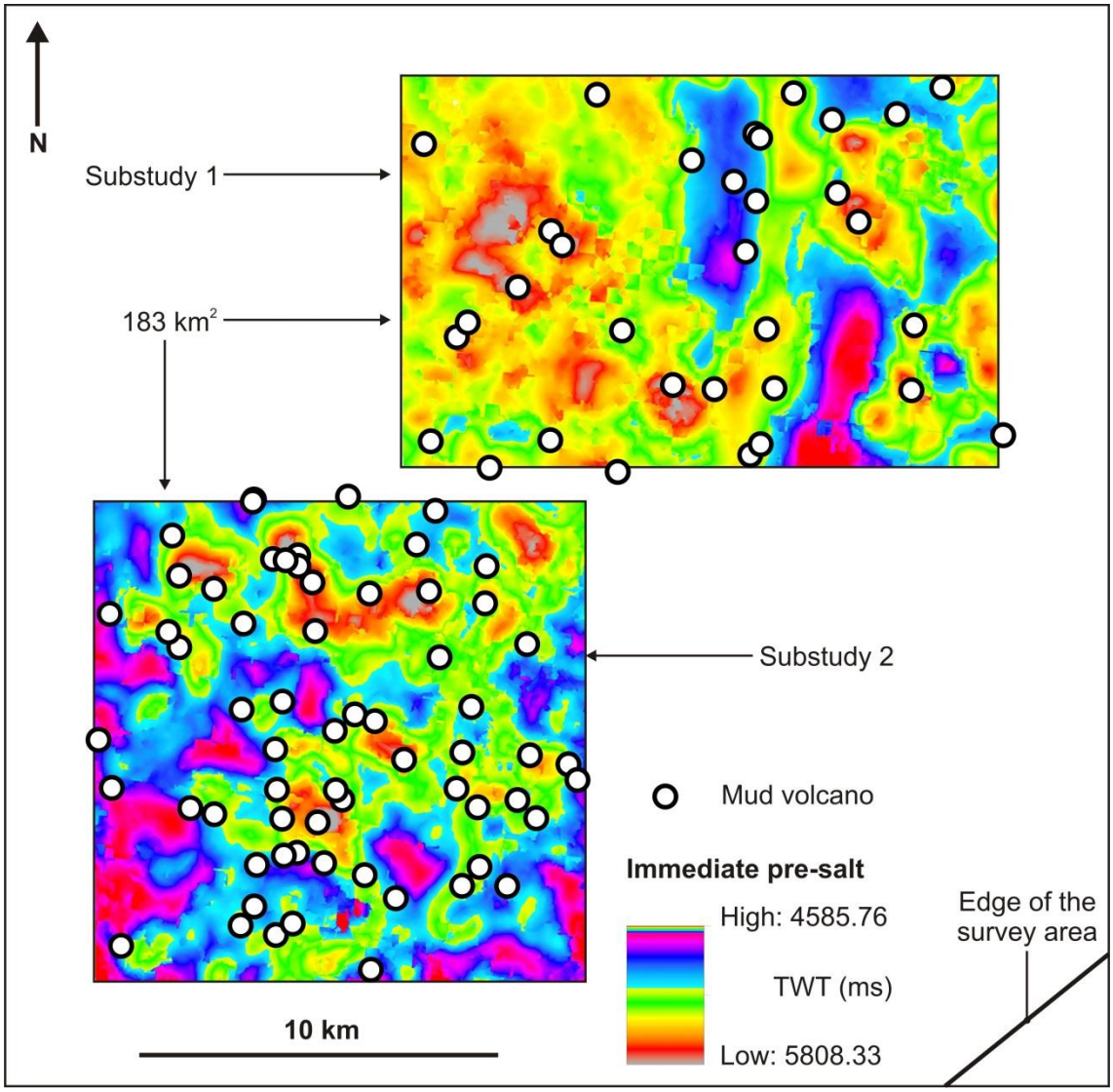

Figure 5.51 Volumetric balance substudy location. Shows the two substudies used for volumetric balance analysis between the volume of sediment missing within the immediate pre-salt succession and the overlying mud volcanoes. Substudy 1 contains 33 mud volcanoes and substudy 2 contains 64 and each covers an area of 183 km^2.

frequencies, the overall trends are similar and their distributions are statistically well matched.

In Chapter 4, it was argued that a suite of giant mud volcanoes that are irregularly shaped erupted synchronously at the end of the Messinian Salinity Crisis. The origin of their mud was interpreted to have been sourced predominantly from the immediate pre-salt due to: (1) their stratigraphic position directly ontop of the evaporite succession; (2) an observed connection between the pre-salt and the giant mud volcanoes; (3) anomalous thinning of the immediate pre-salt in close spatial relation to giant mud volcanoes; (4) anomalously low velocities within the first 1000 m of the pre-salt. The observations and interpretation made with regards to the source succession for the giant mud volcanoes in Chapter 4 raises the question, are the smaller and conical mud volcanoes sourced from the same stratigraphic interval?

In section 5.3.6 it is suggested that the stratal relationship of some base-salt depressions and their close spatial relationship with overlying mud volcanoes could be interpreted as indicative of sediment withdrawal from the immediate pre-salt. If this is true, is it possible to quantify the volume of sediment withdrawal from the immediate pre-salt interval and is that volume correlatable with the volumes calculated in the overlying mud volcanoes (Figure 5.50)? To undertake this analysis two substudies are used within areas where there are base-salt depressions previously interpreted to be associated with sediment withdrawal from the pre-salt (Figure 5.34 and Figure 5.51). These two substudies are here named substudy 1 and substudy 2 (Fig. 5.37). Each substudy covers an area of 183 km^2 and hosts 33 and 64 mud volcanoes respectively. Seismic picking was first focused on Horizon N and the base of the immediate pre-salt succession, in order to produce an isopach map within the two substudies (Figure 5.51). A horizon that is geometrically representative of an un-depleted base-salt was also constructed, based on parts of Horizon N that do not exhibit a depression (Figure 5.50).

To calculate the volume of sediment removed from the immediate pre-salt succession, firstly the volume between the base of the immediate pre-salt interval and the un-depleted base-salt horizon was calculated. The volume between the base of the

immediate pre-salt succession and Horizon N was then calculated. Finally the volume of sediment removed is calculated as the difference in volume between the two intervals. This volume can then be compared to the calculated total volume of extruded mud from the mud volcanoes found within each substudy. For substudy 1 the depleted volume and extruded volume were calculated as 22.6 km^3 and 26.4 km^3 respectively, and 21.1 km^3 and 25.1 km^3 respectively for substudy 2. In both substudies the depleted volumes and extruded volumes are similar.

An initial steep increase in the observed frequency of mud volcanoes within the smaller volume bins can be observed in the cumulative frequency plot in Figure 5.52. At approximately 0.525 there is an inflection point at which the curve begins to flatten (Figure 5.52). Despite a volume range of 0.01 km^3 to 3.3 km^3, of the 386 mud volcanoes 255 have a volume less than 0.525km^3 (Figure 5.52). This analysis confirms that the distribution of volume values for mud volcanoes are clustered predominantly in favour of smaller values, specifically <0.525. Frequency decreases as volume increases, resulting in a lesser frequency of mud volcanoes towards the upper end of the range that exhibit relatively large volumes (Figure 5.52). This leads to an important question, is there spatial ordering of mud volcanoes based on the location of pre-existing mud volcanoes of a relatively large volume?

In order to analyse whether mud volcanoes preferentially form at the maximum distance possible from previously formed mud volcanoes that are of a significantly large volume, Voronoi polygons were constructed. A mud volcano that exhibits a significantly large volume is here considered as >0.525 km^3 based on the inflection point observed from the cumulative frequency plot in Figure 5.52. Voronoi polygons were constructed for all the mud volcanoes with a volume >0.525 km^3 that formed during Phase 1 because the timing of their formation is certain to pre-date the formation of the Phase 2 mud volcanoes (Figure 5.53). The implications of this analysis are that if mud volcanoes forming during Phase 2 were to be positioned on the boundaries of the Voronoi polygon, there may be spatial ordering to their distribution. This would mean that mud volcano formation has occurred at the maximum possibly distance from the location and depletion zone of pre-existing mud volcanoes of a

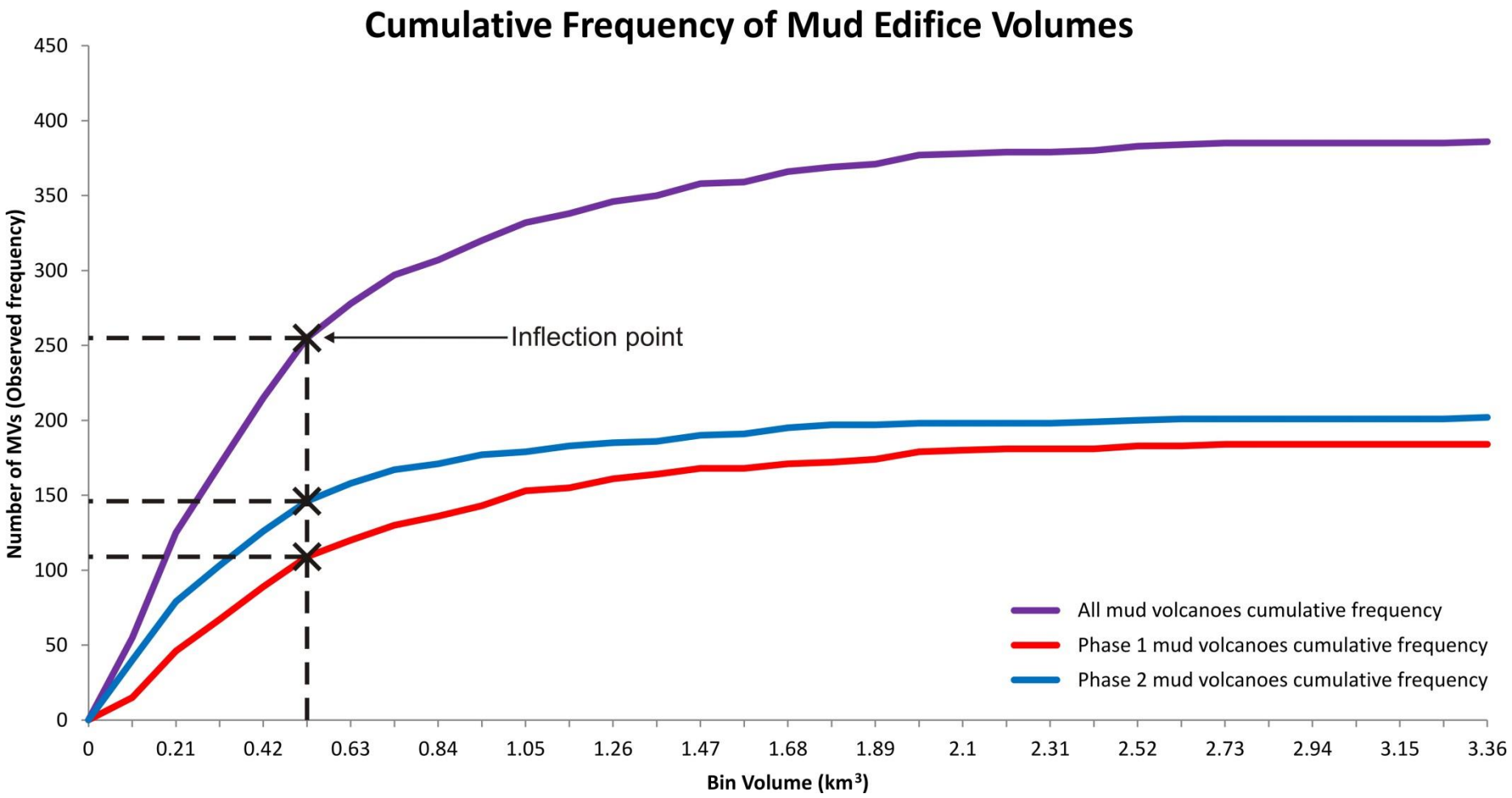

Figure 5.52 Cumulative frequency. Cumulative frequency plots for mud volcanoes of phase 1 and 2 and for all mud volcanoes. All plots display an initial steep increase in the observed frequency of mud volcanoes within the smaller volume bins. At approximately 0.525 there is an inflection point at which the curve begins to flatten out. The frequency significantly decreases for volcano sizes over 0.525 km^3.

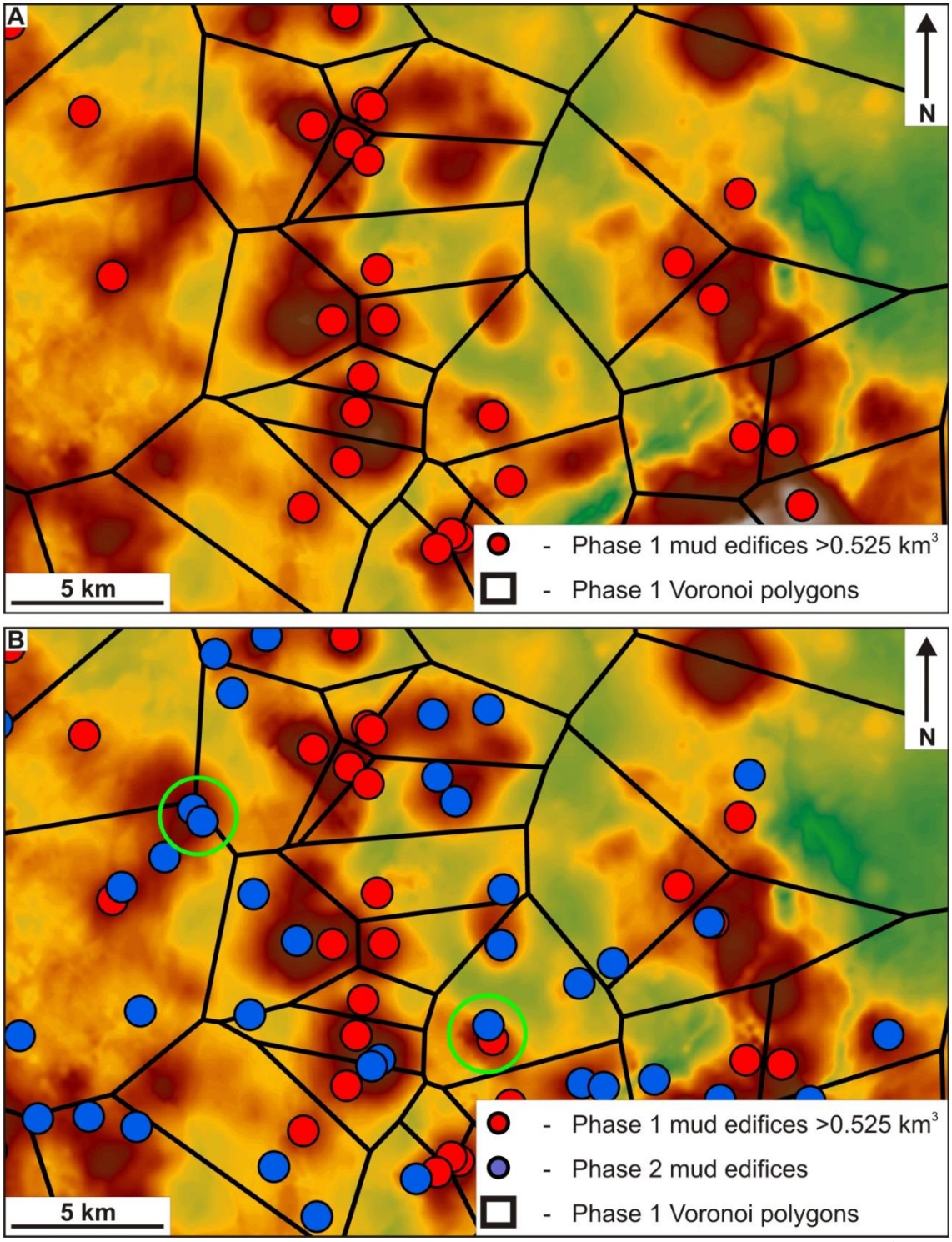

Figure 5.53 Volume Voronoi polygons. A: Phase one mud volcanoes of volume >0.525 km^3 with Voronoi polygons. Polygon lines are constructed based on the greatest distance from a mud volcano, while still being closer to that mud volcano than its nearest neighbour. B: Phase 2 mud volcanoes plotted with the phase 1 mud volcanoes and their Voronoi polygons. Green circles highlight that phase 2 mud volcanoes are found both on the lines of and within the phase 1 polygons. This shows that there is no spatial ordering based on pre-existing phase 1mud volcanoes.

significant volume. The hypothesis is stated as:

H: There is no spatial ordering for the distribution of mud volcanoes based on the volume of prior existing mud volcanoes.

The results shows that mud volcanoes emplaced during phase 2 have formed both equidistantly and within Voronoi polygons. This means that there is no spatial control between the location of more recently formed mud volcanoes of phase 2 in relation to the location of the pre-existing mud volcanoes from phase 1 with volumes >0.525 km^3; therefore agreeing with the hypothesis.

5.3.8 Summary

The El Dabaa survey area hosts an expansive mud volcano field with an exceptionally high concentration of buried and active mud volcanoes, predominantly located within a domain that is characterised by fluid escape. Important observations and interpretations that have been made thus far include:

1) The mud volcanoes within this study area are characterised as single lensoid bodies which exhibit varied dimensions. They are identifiable as circular to elliptical features that display an overall conical geometry and exhibit similar seismic characteristics to one another in seismic profile.
2) Of the 386 mud volcanoes that have been identified, 110 can be observed at the seafloor, 37 of which display no stratal relationship at their upper surface with the hosting hemipelagic deposits, which is indicative that they are currently active.
3) Correlation of the El Dabaa slide with the SL2 MTD described in Garziglia et al. (2008), allows the mud volcanoes to be divided into two phases, the durations of which can be aged. Phase 1 is significantly longer than Phase 2; however, Phase 2 contains more mud volcanoes than Phase 1. If the correlation of the El Dabaa slide is accurate, it suggests that the frequency of mud volcano formation has increased since the Upper Pleistocene to Recent.

4) Statistical analysis of the spatial distribution of mud volcanoes within this study area shows that they are statistically clustered.
5) Cluster analysis of Phase 1 and Phase 2 clusters of mud volcanoes displays a close spatial relationship between the two phases and even stacking of the Phase 2 clusters above Phase 1 clusters. Clusters of mud volcanoes of Phase 1 can also be observed not in spatial association with mud volcanoes of Phase 2.
6) Numerous mud volcanoes can be observed along the same seismic reflection, which indicates that their formation occurred within a similar period of time.
7) There is no scaling between the diameter and thickness of mud volcanoes, which suggests a combination of other factors control the final geometry of these mud volcanoes.
8) Variability in the stratal relationships between depressions at Horizon N and reflections of the immediate pre-salt succession and Horizon M differentiates base-salt depressions as formed either via erosion, deep structural controls or the withdrawal of sediments from the pre-salt succession.
9) A strong correlation is observed between base-salt depressions that are interpreted to be formed via sediment withdrawal and overlying top-salt depression and mud volcanoes.
10) Calculations of potential pre-salt sediment withdrawal when compared to the volume of sediment calculated within overlying mud volcanoes are found to be relatively similar.
11) Anomalous thinning of the evaporite succession and the immediate pre-salt succession, beneath areas of combined base and top-salt depressions and mud volcanoes, further supports the interpretation that the immediate pre-salt succession is the primary source layer.
12) The distribution of volume values of mud volcanoes is best matched to a Negative Binomial model and statistically demonstrates that the volume values of mud volcanoes are of a clustered distribution, with the greatest frequencies observed in small volumes.
13) Vononoi polygon analysis demonstrates that there is no spatial control that can be observed with regards to the formation location of mud volcanoes, relative to the location of prior formed mud volcanoes of a relatively large volume.

5.4 Discussion

5.4.1 Mud volcano formation and geometry: Source of fluids

The geometry of mud volcanoes within the El Dabaa survey area vary significantly, but what are the controlling factors that influence the differences in their morphology and how does this compare to other mud volcano fields? For example, it was observed in section 5.3.5 that there is very little correlation between mud volcano diameter and thickness (Figure 5.28 and Figure 5.29). A slightly stronger correlation is evident for Phase 2 mud volcanoes but generally the results produce a scattered distribution and a low R^2 value. Therefore an increase in diameter is not always matched by an increase in the thickness of a mud volcano.

Similar results to this have been observed in the South Caspian Basin, offshore Azerbaijan where Yusifov and Rabinowitz (2004) described numerous mud volcanoes within an offshore mud volcano field. A vast range of areas and heights were recorded which also produced plots with a high degree of scattering (Figure 5.54). Yusifov and Rabinowitz (2004) similarly found that mud volcanoes may have great areal extent yet have very low relief or vice versa, and concludes that these differences in morphology are due to the relationship between pressure, material supply and conduit width. This interpretation is supported by Kopf (2002) who states that mud volcano geometry is largely influenced by viscosity, while Cartwright (2007) postulates that conduit geometry is one of the most important controls on the flux and morphology of a mud volcano. A mud slurry of high fluid content and, therefore, low viscosity typically produces a mud volcano with a large diameter, shallow slope angles and smaller thickness relative to one with a higher viscosity mud slurry (Brown, 1990; Kopf, 2002). A constant viscosity could possibly lead to results where the diameter and thickness are more closely in proportion with each other. This suggests that fluid content and therefore viscosity of the mud and/or conduit geometry may vary within the survey area. A detailed analysis of conduit geometry will be undertaken in Chapter 6.

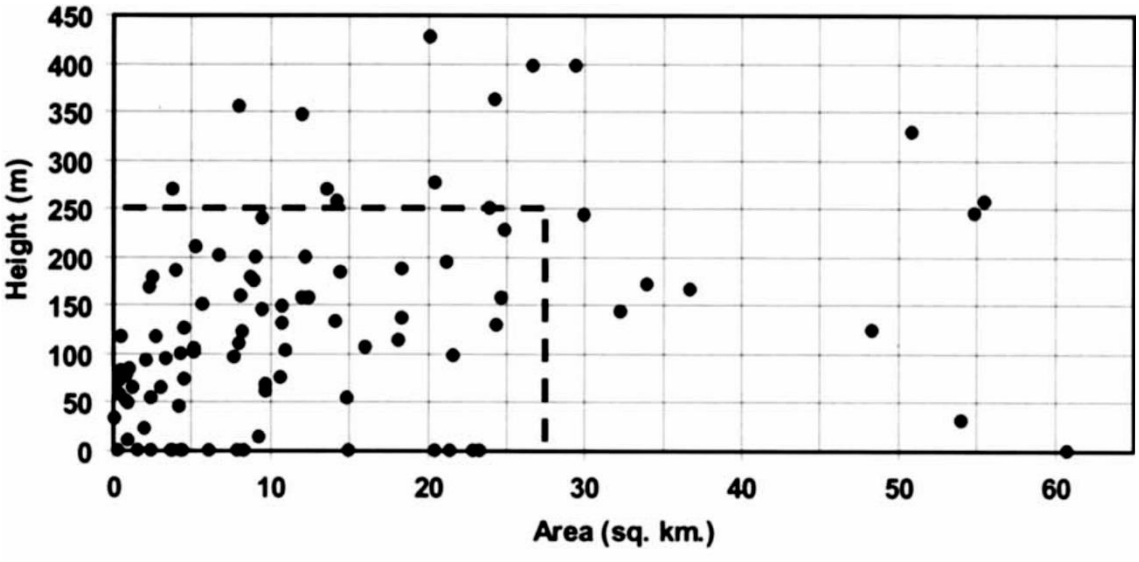

Figure 5.54 Area vs Height of mud volcanoes from Azerbaijan. The plots are highly scattered, similar to the diameter vs thickness plots in Figure 5.28 and Figure 5.29. Image taken from Yusifov and Rabinowitz (2004).

The El Dabaa mud volcano field is spatially extensive and, therefore, requires a fluid source or multiple fluid sources that are of similar or greater areal extent. The potential for significant undercompaction and fluid retention within the immediate pre-salt succession was discussed in section 4.4.2 of Chapter 4. Barber (1981) states that the onset of the proto-Nile Delta occurred as early as the Eocene. When newly deposited, clays can have porosity of up to 80% or more (Kopf, 2002), therefore, the rapidly deposited organic rich fine grained sediments of the Nile Deep Sea Fan would have been ideal for initially high water contents and could have been prone to early overpressure generation. High pore fluid retention within the immediate pre-salt succession could reasonably be expected considering the rapid rate of evaporite deposition, the regional extent of the evaporites and their low permeability (Bertoni and Cartwright, 2015). Loading this interval and subsequent elevation of pore fluid pressure would have produce a metastable condition that could have persisted within numerous parts of the study area, until a critical fluid pressure for pressure and fluid bleed-off via hydraulic fracturing was achieved (Kopf, 2002). Undercompaction and rapid loading are, therefore, considered here to be a potential important mechanism behind overpressure generation in the source interval for the mud volcanoes within this El Dabaa field.

It is pertinent to ask, is it possible that there may be other sources of fluid that could have contributed pore fluids to the already overpressured immediate pre-salt succession? It is important to note that nannofossil analysis of cores taken from mud volcanoes within the this study area found clasts as old as Cretaceous in age in the mud breccia's extruded from mud volcanoes at the seafloor (Giresse et al., 2010). This suggests that there could indeed be multiple sources of fluid and sediment feeding these mud volcanoes, potentially from deeper stratigraphic layers than the immediate pre-salt succession (Giresse et al., 2010). A similar interpretation of multiple fluid sources has also been made for the Lusi mud volcano in Indonesia (Mazzini et al., 2009; Mazzini et al., 2007; Tanikawa et al., 2010). The precise age and stratigraphic location of all secondary fluids is unfortunately not possible to determine. Further research into hydrocarbon plays and fluid sources within this specific region may be

needed to fully understand the relationship between fluid location and a generative mechanism for overpressure.

The formation of mud volcanoes is generally believed to be intimately associated with the generation of buoyant hydrocarbons as it can play a key role in pressure generation within the source region (Hedberg, 1980; Charlou et al., 2003; Dimitrov, 2002; Kopf, 2002; Wilford, 1967; Humphrey, 1963; Stamatakis et al., 1987). Shallow amplitude anomalies and acoustic disturbance have been commonly observed within the extruded body of these mud volcanoes. The high amplitude and soft reflection of the amplitude anomalies, combined with their abrupt margins and zone of amplitude attenuation beneath, the margins of which are correlatable with the overlying amplitude anomaly, could be interpreted as potentially indicative of shallow gas (Figure 5.7). If there is pre-salt hydrocarbon generation within this basin, the thick Messinian evaporites would present a suitable seal for any upwards migrating fluids and result in their trapping within the immediate pre-salt succession. The addition and accumulation of fluids (methane) within the immediate pre-salt succession could potentially elevate pore fluid pressure and contribute to the bulk density contrast between the immediate pre-salt succession and overlying evaporite, therefore, assisting in driving mud remobilisation (Hedberg, 1980; Charlou et al., 2003; Dimitrov, 2002; Kopf, 2002; Wilford, 1967; Humphrey, 1963; Stamatakis et al., 1987; Brown, 1990; Judd and Hovland, 2007).

Numerous other amplitude anomalies that are interpreted as direct hydrocarbon indicators are also discussed in section 6.3.4 of Chapter 6, in relation to fluid escape pipes within the study area. Evidence of active hydrocarbon plays a mere 55 km to the northeast within Shell's relinquished NEMED blocks could be considered indicative of the potential for hydrocarbon generation within this study area, considering their geographical relationship (EGAS, 2012a; EGAS, 2012b; EGAS, 2012c) (See section 3.6 of Chapter 3). Documented analysis of core samples have been found to comprise a strongly gas saturated mousse-like mud breccia characterised by a strong oil and hydrogen sulphide smell and brine sample analysis found them to be hot, methane-rich, oily and hydrocarbon-rich (Pierre et al., 2014; Dupré et al., 2014; Huguen et al., 2009). These finding strongly support the interpretation that the mud

volcanoes within this study area are associated with hydrocarbon generation and that their identification could be considered an indirect indicator for active hydrocarbon plays within this regions of the Eastern Mediterranean.

5.4.2 Trigger events for mud volcanism

Possible triggering events for mud volcanism include earthquakes, hydrostatic pressure variation caused by waves and tides, changes in eustatic sea level, sediment loading and unloading and steam/hydrothermal fluid injection (Judd and Hovland, 2007). There is no evidence for any magmatic activity in the survey area or in nearby sectors of the continental slope shelf and the study area is within c. 3 km water depth, therefore, making it unlikely that hydrothermal or wave and tidal influences played a role. Large scale sliding events are observed 45 km to the east by Garziglia et al. (2008) and a MTD similar to the ones described in that area could represent a source of rapid loading. The El Dabaa slide post-dates all Phase 1 mud volcanoes and only fractionally encroaches on Domain B, however there is a significant increase in mud volcano formation after the emplacement of the El Dabaa slide during Phase 2. It remains possible that the rapid loading effect by the El Dabaa slide may have had an impact on pore fluid pressure within the pre-salt in order to trigger mud volcanism.

A rapid increase in sea level at the climax of the MSC and the loading effect of the water column were attributed as the primary trigger for the giant mud volcanoes described in the Chapter 4. There have only been relatively modest eustatic changes in the study area since the Zanclean flood, typically of < 100m (Antonioli et al., 2004; Shackleton, 1987) (See Figure 3.4 of section 3.3 of Chapter 3). A general falling trend in sea level during the late Pleistocene and reached its lowest level at c. 18,000 Ma (Antonioli et al., 2004; Shackleton, 1987). A significant fall in eustatic sea level could potentially reduce hydrostatic pressure, which could promote hydraulic fracturing and/ capillary migration in buoyant overpressured fluids (Judd and Hovland, 2007), such as those trapped beneath the evaporite succession within this study area. Eustatic variation such as this has previously been proposed as a potential trigger mechanism

for the formation of numerous chronostratigraphically dated pockmarks within the Egyptian passive margin by Moss (2010). A similar mechanism has also been proposed for early Messinian pockmark formation within the Levant basin, during the drawdown of the Mediterranean at the onset of the MSC (Bertoni et al., 2013). The mud volcanoes within this study area lack chronostratigraphic dating so it is difficult to correlate and falls or increases in sea level with mud volcano formation, however, similar eustatic variation could also present a plausible trigger mechanism. Eustatic variation has also resulted in periods of rapid increases in sea level (See Figure 3.4 of section 3.3 of Chapter 3), particularly between c. 18,000 yr ago and the present. Rapid increases in sea level could potentially present a mechanism for rapid loading and, therefore, increase overpressure within the pre-salt stratigraphy which could lead to hydraulic fracturing, which will be discussed in greater detail in Chapter 6.

Earthquakes are not uncommon within the Egyptian passive margin as it is located within the tectonically active region of the Eastern Mediterranean. It is a complex tectonic setting and has been affected by many earthquakes in recent and historical times (El-Sayed et al., 2004). Low magnitude earthquakes (M_s = 6) are known to have occurred offshore Egypt during the Quaternary (El-Araby and Sultan, 2000; El-Sayed et al., 2004). These earthquakes are also considered to be one of the contributing triggering mechanisms for the MTD's described by Garziglia et al. (2008). Earthquakes cause sediments to compact and reduce in volume which can create a significant increase in pore fluid pressure, which generates overpressure if pore fluids and buoyant gases have been retained beneath a seal (Gluyas and Swarbrick, 2009). It is, therefore, argued here that generation of overpressure and liquefaction due to earthquakes presents one of the most plausible triggers for widespread mud volcano formation within this region.

The potential for synchronicity in the timing of mud volcano formation has been demonstrated by numerous mud volcanoes having formed along the same reflection. This observation suggests that some of the mud volcanoes were emplaced at exactly the same time or within a maximum of 200 kyrs, which is based on average sedimentation rates for the deposition of a single seismic reflector within the study area (as discussed in section 4.4.3 of Chapter 4). Simultaneous formation over a large

area suggests that the trigger for mud volcano formation must have triggered several at one time. In the case of an earthquake, for numerous mud volcanoes to form during a similar small time window would require a single earthquake event of sufficient magnitude or several earthquakes in quick succession, in order to cause liquefaction. It is well documented that ground shaking events can reduce effective stress within a uncompacted sedimentary succession to zero, resulting in the grains within the succession becoming temporarily suspended in pore fluids (Judd and Hovland, 2007; Brown, 1990; Davies et al., 2008). The observation of mud volcanoes located at numerous stratigraphic levels could imply that the mechanism for generating overpressure must have occurred several times. These topics and questions will be addressed in greater detail in Chapter 7.

5.4.3 Source of mud and its relationship to the spatio-temporal distribution and extruded volumes of mud volcanoes

Mud volcanoes within the survey area have formed within a window of approximately 5.3 my, starting soon after the end of the MSC and continuing to present day. In Chapter 4, it was argued that the formation of the first mud volcanoes to have formed within this study area are directly associated with the release of overpressure at the end of the Messinian Salinity Crisis, which was generated via the rapid deposition of the Messinian evaporites. Persistent mud volcano emplacement since the end of the MSC to the present day argues that the immediate pre-salt succession has remained overpressured throughout the Pliocene to Recent and that the basin is to this day in an overpressured state. In section 5.3.4.1, the mud volcanoes within the Pliocene to Recent succession were divided into two phases of extrusion (Phase 1 and Phase 2) that have been aged based on the only reflection within the Pliocene to Recent succession that can be dated with any confidence, which is the base of the El Dabaa slide. The observation of mud volcanoes at various stratigraphy levels within the Pliocene to Recent succession and increases and decreases in their frequency up through the succession, raises the question as to the origin of cyclicity in

the frequency of emplacement and potentially volume of mud volcanoes within this study area?

The distinction of numerous mud volcanoes at various levels within the Pliocene to Recent succession could be suggestive of a fundamental cyclicity in the pressure generative process. For example, a decrease in the volume of mud extruded during mud volcano formation could be considered indicative of a decrease in overpressure within the source layer, which could be due to mobilisation and drainage of sediment and pore fluids. To increase the volumes of extruded mud again would, therefore, require a recharging mechanism of the source layer in order to elevate overpressure, similar to that observed in groups of mud volcanoes from regions such as Trinidad and Azerbaijan (Dia et al., 1999; Mellors et al., 2007). This could be achieved through hydrocarbon generation, fluid migration and further accumulation beneath the sealing evaporites resulting in an in increase pore fluid pressure within immediate pre-salt succession. The decrease in the frequency of mud volcanoes observed within the upper part of Phase 2 could potentially be attributed to depletion and depressurising of the source interval during the early parts of Phase 2. It is, therefore, possible that the observed increase in the frequency of mud volcanoes during Phase 1 could be the result of a recharging mechanism within the pre-salt.

Observational and statistical analysis of the mud volcanoes within the survey area has found that they are significantly clustered and that clusters from phase 2 mud volcanoes have formed in close spatial relation to pre-existing clusters from phase 1. This suggests that there are preferential areas for mud volcano formation within the study area. This raises the question, what factors have influenced the location for the formation of these mud volcanoes in order for their distribution to be clustered?

As with pockmark formation, the main processes that comprise the formation and location of mud volcanos are the driving forces of overpressure generation and buoyancy, seal failure and subsequent emplacement following the ascent of fluidised mud through the lithological succession (Judd and Hovland, 2007). Overpressure is commonly attributed to tectonic compression, rapid sediment loading such as the rapid deposition of the Messinian evaporites, and fluid (methane) generation at a

greater rate than it can be released (Osborne and Swarbrick, 1997; Swarbrick, 1999). It is commonly believed that the spatial position of seal failure and, therefore, location of mud volcano formation is situated at the point of maximum overpressure and where there are sub seismic heterogeneities in the seal, such as pre-existing fractures, permeability contrasts or localised small scale doming (Judd and Hovland, 2007). This would suggest that there are specific mechanisms, within the areas where mud volcanoes are distributed, that locally increase overpressure within the immediate pre-salt succession relative to those where mud volcanoes are not found. Possible mechanisms for increasing overpressure include fluid migration and addition of buoyant hydrocarbons.

It is possible that the clustered spatial distribution of mud volcanoes is related to deeper pre-salt basinal features such as the position of isolated sand bodies within the pre-salt succession, hydrocarbon generation and structural controls. Faults have the potential to act as conduits for fluid migration (Cartwright, 2007) and could, therefore, influence the location of overlying mud volcanoes, similar to what has been observed in mud volcanoes such as the Lusi mud volcano in Indonesia (Mazzini et al., 2009; Davies et al., 2008; Mazzini et al., 2007). Fluids could migrate along faults via a dilatancy/fluid diffusion model also known as seismic pumping (Scholz et al., 1973). Alternatively faults could act through a passive role as permeable conduits for percolating fluids (Sibson et al., 1975).

Mud volcanoes have also been known to be spatially confined to above large anticlinal structures (Kholodov, 2002). In the instance of syn-sedimentary growth of an anticlinal structure with alternating rigid and plastic sedimentary layers, the folding and subsequent pressure rise could result in the injection of plastic material into the anticlines arch zone and lead to diapiric breakthrough and extrusion of mud breccia onto the surface (Kholodov, 2002). However within the El Dabaa survey area no underlying anticlinal features have been observed within the pre-salt stratigraphy in relation to mud volcanoes. The top of the immediate pre-salt succession, which is interpreted to be the primary source of mud, in fact exhibits large depressions beneath the mud volcanoes rather than any anticlinal geometry.

Isolated sand bodies have the potential for greater porosity and permeability than their surrounding country rock and can therefore present a preferential location for migrating fluids and entrapment. Deltaic sediment input from the proto Nile Delta throughout the Oligocene to Miocene produced areas of high sand content in the form of slope fan, turbidite and channel/levee deposits which may provide suitable isolated pre-salt sand bodies (Salem, 1976). Although the immediate pre-salt within this study area is here interpreted to primarily comprise an interval of marly mud as previously discussed (Bertoni and Cartwright, 2005; Grasso et al., 1982), there may also be lithological variation within this interval. Cores from recent mud volcanoes within the Menes Caldera recovered samples with high sand/silt content (Huguen et al., 2009) which is indicative of sediment inclusion from facies of predominantly sand/silt content within the ascending mud.

Overpressure can be built up either uniformly throughout a fluid source or within localised pockets also referred to as “cells”, the limits of which are variable and are determined by changes in permeability (Moss and Cartwright, 2010b). A triggering event of sufficient magnitude such as an earthquake could cause localised overpressure generation in sand bodies which are surrounded by facies of a lower permeability. This could result in fluid from these sand bodies to migrate vertically until they are impeded by the sealing evaporites and accumulate within the immediate pre-salt succession. The addition of migrating fluids, to an already overpressured succession would locally further elevate overpressure and could explain the specific location and clustered spatial distribution of mud volcanoes.

Does the location of pre-existing mud volcanoes influence the location of later forming mud volcanoes? During mud volcano formation, fluid and sediment from the pre-salt succession are drawn into the conduit, creating a drainage areas which is unique to each isolated or group of mud volcanoes based on sub seismic changes in permeability, level of overpressure and supply of fluid and sediment. Once the fluids and mud from the source layer (or layers) have been sufficiently depleted and pressure has returned to hydrostatic, a drainage area of insufficient fluid, sediment and pressure will remain. Within the catchment of this drainage area further mud volcano formation will not be possible. The absence of any significant spatial ordering of mud

volcanoes due to the location or volume of pre-existing mud volcanoes shows that depletion of fluid, sediment and pressure within these drainage areas has not been sufficient for mud volcano formation to cease. There is therefore a high probability that future mud volcanoes will form above pre-existing drainage areas near pre-existing mud volcanoes. In these areas there is a proven supply of fluid, sediment and level of overpressure adequate for mud volcano formation which presently shows no evidence of discontinuing.

The lack of specific mechanisms to generate additional buoyancy is one explanation for why some parts of the survey area contain fewer mud volcanoes but what are some other reasons influencing their absence? Erosive base-salt features observed within the survey area such as the submarine canyon represent confined areas of incision and downcutting of the top Oligo-Miocene seismic reflections by Horizon N. Considering the compelling evidence that the immediate pre-salt succession is the primary source of mud in this region, it stands to reason that removing large portions of this interval through erosional events would result in fewer mud volcanoes within those specific areas.

The regional structure of the area is also likely to have had a direct impact on the mud cone distribution (Loncke et al., 2004) in relation to the generation of overpressure due to the thickness of the evaporites and post salt overburden. The evaporites and Pliocene to Recent interval are not of a uniform thickness throughout the region and so the gravitational load applied cannot be constant. In up dip areas where the evaporitic wedge is thinner and thin skinned gravitational collapse of the post-salt overburden has resulted in thinning of the Pliocene to Recent succession, the effects of loading on pore fluid pressure will be significantly reduced. It could therefore be argued that the pre-salt succession within Domain A is most likely in a comparatively lower state of overpressure due to a lesser loading effect.

5.4.4 The impact of mud volcano formation on salt and subsidence

Having argued from a number of separate lines of evidence that the immediate pre-salt is the primary source of mud, it is then far more understandable that a large proportion of the base-salt depressions are indeed related to depletion via formation of the overlying mud volcanoes. How then are the top-salt depressions related to mud volcano formation? An argument could be made for a process whereby depressions are formed as a result of subsidence due to the removal of an underlying supporting remobilised material, similar to as argued for the modern day Lusi mud volcano (Istadi et al., 2009; Fukushima et al., 2009). This process involves down-sagging of the salt and overlying stratigraphy coinciding with depletion of the immediate pre-salt succession which produces base-salt depressions during mud volcano formation. The observed downsagging of intra salt reflections above depletion induced base-salt depressions further suggests that the salt has simultaneously subsided in response to depletion. The depression created is subsequently and concurrently infilled with remobilised mud breccia resulting in the formation of one or several mud volcano with a total volume similar to that which was depleted from the immediate pre-salt succession (Stewart, 1999). These features can occur not just as a single circular feature but as a more complex partially overlapping composite structure (Branney, 1995). It has been observed though that the top-salt depressions cover a larger area than the base-salt depressions. This raises the question, are there alternative combined processes other than subsidence influencing the top-salt depressions?

Thinning of the evaporite interval has been observed associated with top and base-salt depressions with overlying mud volcanoes, but what are the processes behind the subtraction of evaporites? One contributing factor could be removal via dissolution within the pore fluids of migrating mud breccia. This could result in a dissolution sag which has clearly been observed at the top-salt (Stewart, 1999), similar to circular dissolution features observed within the Levant Basin, offshore Israel (Bertoni and Cartwright, 2005). This interpretation is supported by various examples of brine pools often associated with evaporite dissolution (Warren, 1999) within the

eastern Mediterranean, such as the brine filled depressions within the Tyro and Bannock Basin (De Lange et al., 1990), or those associated with mud volcanoes such as the Napoli, Milano, Maidstone and Moscow mud volcanoes located within the Olimpi field, south of Crete on the Mediterranean ridge (Charlou et al., 2003). Other large hypersaline brine lakes have even been identified associated with the mud volcanoes of the Menes caldera found within this survey areas (Huguen et al., 2009). In each case these brine pools have been interpreted to be produced via dissolution of Messinian evaporites within rising fluids. This interpretation combined with the observed decreases in evaporite thickness indicates that dissolution is a major contributing factor in the removal of evaporites and further enhancing the scale of the top-salt depressions.

Another possible contributing process is gravitational loading where the localised erupted mud generates localised gravitational loading of the Messinian evaporites. The mechanical properties of salt lead it to behave somewhat like a fluid and deform viscoelatically under typical geologic strain rates over geological time (Hudec and Jackson, 2007).Applying sufficient vertical pressure (σ1) in the form of extruded mud breccia could cause horizontal salt flow or "salt expulsion" perpendicular to the pressure direction (σ3) (Hudec and Jackson, 2007). As no evaporites are actually removed through this process, the evaporites thin beneath the point of gravitational loading however the volume of the entire unit should be maintained (Bertoni and Cartwright, 2005). It is possible that neither dissolution nor gravitational loading are solely responsible for thinning the evaporites and enhancing the area of top-salt depressions, but more likely a combination of the two.

5.5 Conclusion

A large number of mud volcanoes have been identified within the 4300 km^2 El Dabaa 3D seismic survey offshore Egypt. They have formed within this region for approximately the last 5.3 Myrs and continue to form and actively extrude mud over the present day seafloor. The 386 mud volcanoes that are described within this chapter comprise a dense and extensive mud volcano field. Due to the exceptional

scale of mud volcanism within the El Dabaa study area, it is suggested here that this region should be considered as among the largest mud volcano provinces in the world. Further key outcomes of the analysis within this chapter are as follows:

- The mud volcanoes within this study area are identifiable as crudely conical features which display varied dimensions and geometry. An increase in the dimension of diameter is not correlatable with an increase in thickness. Other controlling factors such as viscosity of the extruded mud and conduit geometry possess the greatest potential to impact the geometry of mud volcanoes.
- Pore fluids within the immediate pre-salt succession, which is potentially undercompacted, presents a significant fluid source. However, analysis of samples from mud volcanoes within this area indicates that fluids have also been sourced from deeper within the basin, potentially from multiple sources.
- There are numerous indications for the active generation of hydrocarbons within this study area, which have the potential to accumulate and generate overpressure beneath the 'sealing' evaporites, within the immediate pre-salt succession.
- Potential triggers for the emplacement of mud volcanoes include a reduction in hydrostatic pressure or loading due to eustatic variation and liquefaction caused by ground shaking events.
- Synchronicity in the formation of some mud volcanoes along a singular reflection within the post salt stratigraphy is potentially indicative of a shared trigger mechanism.
- The frequency of mud volcano formation has varied over time and has increased significantly since the Upper Pleistocene to Recent. This could be considered indicative of a recharge mechanism and hence an increase in overpressure within the pre-salt since the Upper Pleistocene.
- The mud volcanoes within this study area are statistically proven to be significantly clustered. Localised controls within the pre-salt have the potential to result in the formation of mud volcanoes in a clustered distribution. These include localised areas of increased overpressure associated with isolated sand bodies, hydrocarbon generation and structural controls.

- The volumes of fluid and mud extruded during the formation of these mud volcanoes and the subsequent depressurising of the source interval has as of yet not been significant enough to result in the spatial ordering of mud volcanoes.
- There is a strong correlation between the location of mud volcanoes and underlying base-salt depressions. This observation combined with the conduit analysis from Chapter 6 is indicative that the source of mud that feeds these mud volcanoes is predominantly withdrawn from a local area directly beneath the mud volcanoes.
- The withdrawal of mud from the immediate pre-salt succession has resulted in the subsidence of the overburden. This contributes in part to the observed top-salt depressions. Mud infills the depression that forms progressively at the seafloor as more and more mud is withdrawn and the overburden subsides.
- Localised gravitational loading and dissolution of the mobile evaporites have had a significant impact on the formation and areal extent of top-salt depressions.

Chapter 6

6 Seal Bypass in an evaporite basin by mud volcano conduits.

6.1 Abstract

This chapter documents and describes the varied seismic characteristics and geometry of a large number of mud volcano conduits and fluid escape pipes that are interpreted using 3D seismic data, from the El Dabaa study region, offshore Egypt. The mud volcano conduits and fluid escape pipes share many similarities in both their seismic expression and geometry, which is crudely cylindrical. Analysis of these conduits in combination with documented evidence from piston cores, brine pools and venting gas within this study area, indicate that the source of fluids and root zone for these conduits is pre-salt. The similarities between the mud volcano conduits and fluid escape pipes suggest that the formation of one conduit type could be analogous to the formation of the other. A conceptual model for the formation of these mud volcano conduits is proposed that involves high overpressure within the pre-salt and bypassing of the Messinian evaporites via hydraulic fracturing and dissolution and stoping processes. The interpretation of direct hydrocarbon indicators from seismic data in combination with documented examples of methane-rich and oily hydrocarbon hot brines and mud samples, argue strongly for the generation of hydrocarbons within the pre-salt.

6.2 Introduction

A mud volcano conduit is a seal bypass system that connects a source stratigraphic unit and an extrusive and constructional mud volcano (Roberts et al., 2010; Stewart and Davies, 2006; Cartwright et al., 2007). The majority of research to date on mud volcanoes using 3D seismic data has primarily focused on the extrusive mud volcano, while comparatively mud volcano conduits and the processes behind their formation are poorly understood, in part due to lower quality imaging (Davies and Stewart, 2005; Roberts et al., 2010). There are several different models for mud volcano conduits which include large diapirs (Brown, 1990), steep mud injections or diatremes (Pickering et al., 1988; Robertson and Kopf, 1998; Clari et al., 2004) and narrow vertical pipes (Graue, 2000; Roberts et al., 2010; Kopf, 2002).

Narrow and vertical pipe-like structures have been documented as mud volcano conduits within various sedimentary basins, where mud volcanoes lie at the upper terminus of localised steep discontinuities (Figure 6.1) (Fowler et al., 2000; Graue, 2000; Stewart and Davies, 2006; Reiche et al., 2014). Pipes are the expression of focused fluid flow, most often through low permeability stratigraphy such as predominately fine grained sedimentary successions that have been deposited on continental slopes of either active or passive continental margins (Figure 6.2) (Berndt, 2005; Moss and Cartwright, 2010a; Løseth et al., 2001; Hustoft et al., 2007). Fluid escape pipes with heights greater than 1000 m are relatively common (Løseth et al., 2001; Moss and Cartwright, 2010a). Their large vertical extent means that they potentially offer a conduit which facilitates a large component of vertical fluid flow in sedimentary basins (Berndt, 2005; Cartwright, 2007).

Evaporites have been traditionally viewed as virtually impermeable barriers to fluid flow (Downey, 1984; Warren, 1999; Gluyas and Swarbrick, 2009). This, however, is a view that has recently been challenged due to growing evidence of numerous fluid escape features, associated with both fluid and sediment, bypassing thick evaporitic successions (Reiche et al., 2014; Davison, 2009; Schoenherr et al., 2007; Bertoni and Cartwright, 2015). Within the Eastern Mediterranean alone, various fluid flow related features including dissolution collapse (Bertoni and Cartwright, 2005),

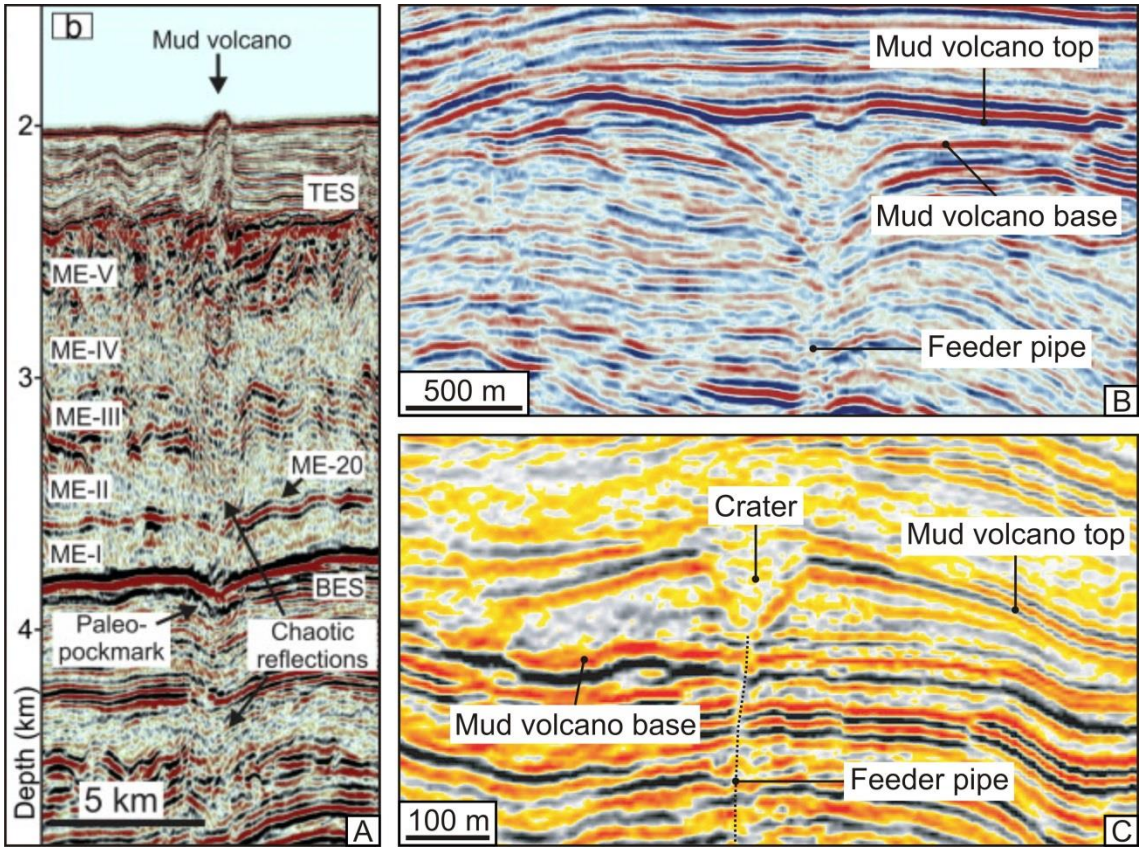

Figure 6.1 Documented examples of mud volcano conduits that are pipe-like. A: Seismic profile of a pipe-like vertical area of acoustic disruption feeding a mud volcano at the seafloor (Image from Reiche et al. (2014)). B and C: Two seismic profiles of buried mud volcanoes from the South Caspian Basin. Both mud volcanoes appear as lensoid features with a feeder pipe (conduit) directly beneath their centre (Images from Stewart and Davies (2006)).

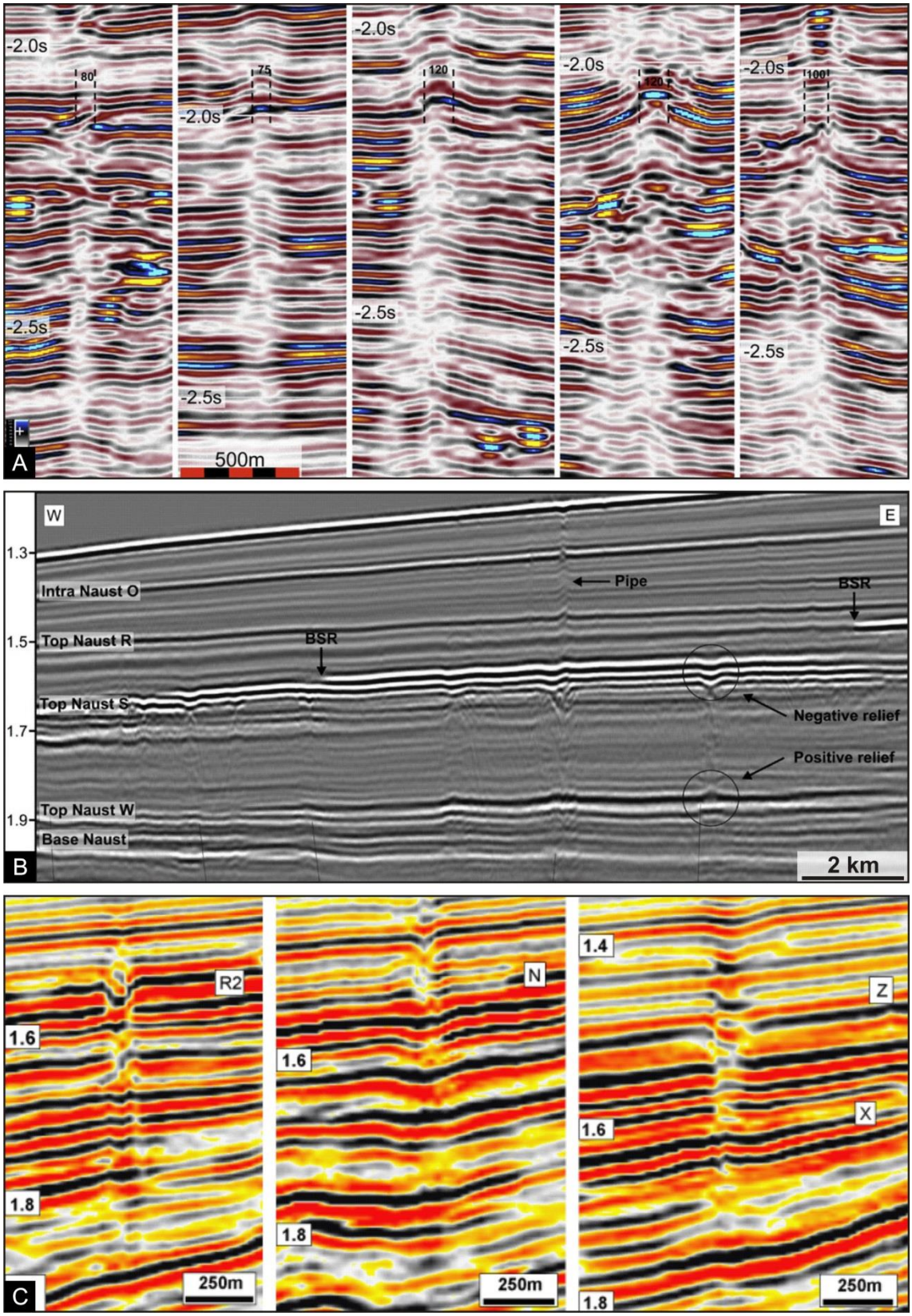

Figure 6.2 Document examples of fluid escape pipes. A, B and C all show examples of fluid escape pipes characterised by a vertical zone of discontinuity and attenuation, with concave or convex internal reflection geometry. The examples in A are from the Niger Delta (Løseth et al., 2011), the pipes in B are from the mid-Norwegian margin (Hustoft et al., 2007) and the examples in C are from offshore Namibia (Moss and Cartwright, 2010a).

gas chimneys (Bowman, 2011), fluid escape pipes (Eruteya et al., 2015), mud volcanoes (Figure 6.1A) (Reiche et al., 2014; Giresse et al., 2010) and pockmarks (Lazar et al., 2012), have all been interpreted to be associated with fluids of a pre-salt origin. The possibility that there are seal bypass systems that allow for deeply sourced fluids and sediment to migrate through thick evaporite sequences is one of the underlying themes of this thesis and is directly addressed in this chapter.

6.2.1 Aim/Scope

In Chapter 4 and 5, a strong case was presented for a pre-salt fluid and sediment origin. The vast majority of mud volcanoes within this study area directly overlie base-salt depressions, which are correlatable with areas of anomalous thinning of the immediate pre-salt unit. Volume calculations and comparisons between the mud volcanoes and base-salt depressions found similar sediment volumes within the volcanoes and potentially missing from the immediate pre-salt. Velocity data readings show an inversion in p-wave velocity within the immediate pre-salt and could be considered indicative of overpressure. A visible connection between giant mud volcanoes and the pre-salt was also documented.

Possibly the most compelling evidence for a pre-salt origin resides in the observation that many of these mud volcanoes formed directly on top of, or one or two reflections above the top-salt reflection of Horizon M, and there are no signs of depletion within the post-salt sedimentary succession (Figure 6.3). Although this study area lacks nearby well calibration, it is unlikely that there is a large source of overpressured fine grained sediment within the evaporite succession, which is as expansive as the area where mud volcanoes have formed. A more plausible solution is that the mud and fluids have been sourced from deeper than the evaporite succession. These observations in combination with those stated above build a convincing argument for a pre-salt fluid and sediment origin.

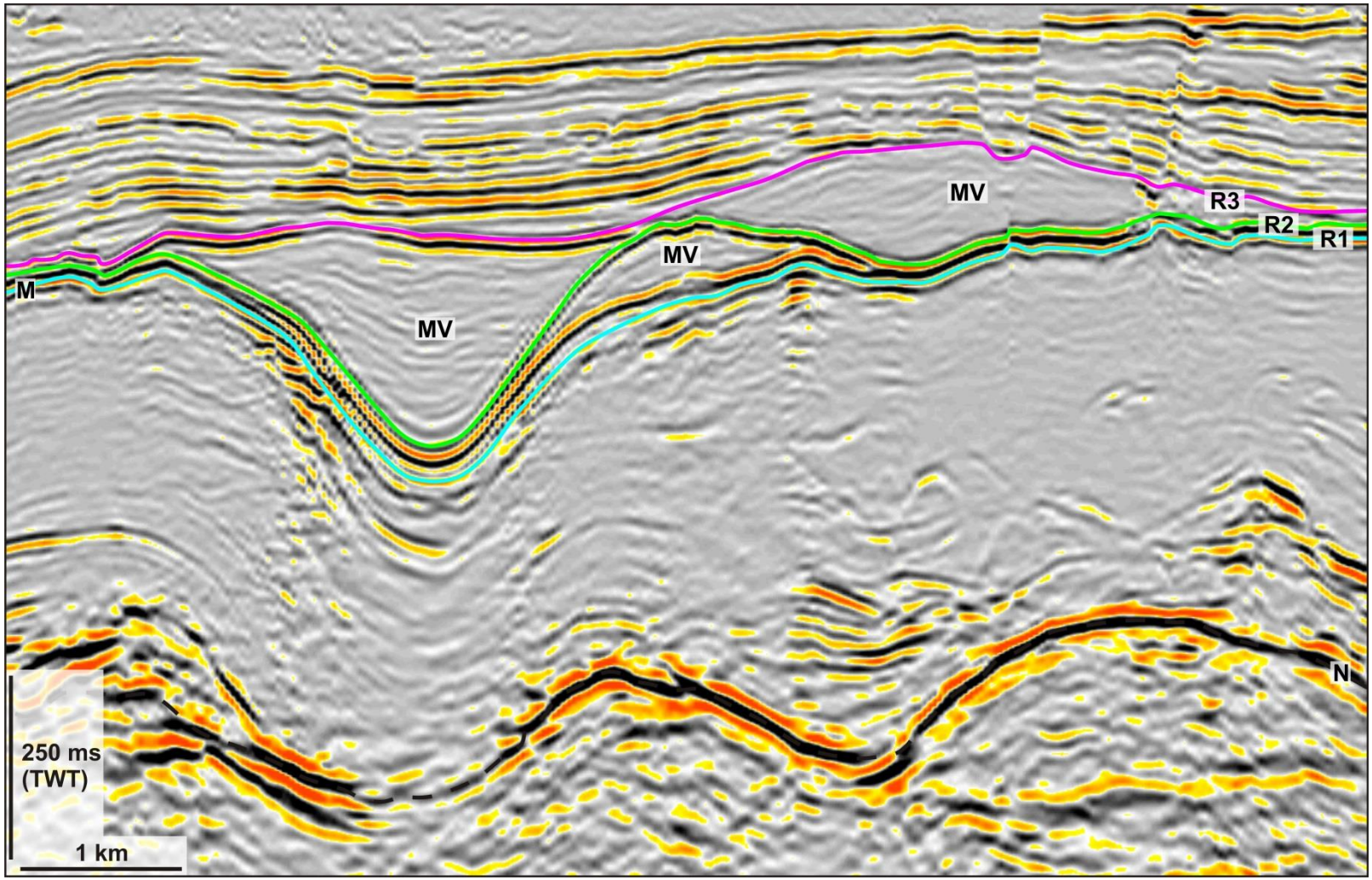

Figure 6.3 Seismic profile of mud volcanoes one or two reflections above Horizon N. M – Horizon M; N – Horizon N; R1 – Reflection 1 (also Horizon M); R2 – Reflection 2; R3 – Reflection 3; TWT – Two way time.

Until this point, within this thesis the conduits that feed these mud volcanoes and the potential breaching mechanisms in order to bypass the thick evaporite unit have not been fully explored. In this chapter, using 3D seismic data I present a study of mud volcano conduits and fluid escape pipes from the El Dabaa study region offshore Egypt (See section 3.2. of Chapter 3 for location). The data quality of the survey area is very high, with a spatial resolution of c.25 m throughout the Pliocene to Recent, which is the primary interval of interest. This means that there are a large number of mud volcano conduits and fluid escape pipes that are very well imaged. It is, therefore, possible to: (1) identify and analyse the varied geometry and seismic characteristics of the mud volcano conduits and fluid escape pipes; (2) accurately identify, measure and catalogue the location of all pipes within the survey area.

In seismic profile, mud volcano conduits and fluid escape pipes share very similar seismic characteristics and geometry. They appear as steep vertical to sub vertical zones of discontinuity, disruption and attenuation and even complete loss of coherence (Figure 6.4 and Figure 6.5) (Moss and Cartwright, 2010a; Stewart and Davies, 2006; Fowler et al., 2000; Løseth et al., 2011). These zones of acoustic disruption have localised circular to elliptical planform geometry, which varies up the vertical extent of the structure (Figure 6.6 and Figure 6.7) (Løseth et al., 2001; Hustoft et al., 2007). The 3D geometry is most closely comparable to that of a columnar structure that is pipe-like. Isolated high amplitude anomalies can be observed within and sometimes adjacent to these conduits. Amplitude anomalies such as these can in some cases be inferred as due to gas or cemented zones (Gay et al., 2007; Hustoft et al., 2007). Greater detail of the seismic expression and geometry of these mud volcano conduits and fluid escape pipes is given below.

Despite the similarities in seismic expression and geometry of these mud volcano conduits and fluid escape pipes, they are distinctly different based on the structures that overlie their upper terminus. Overlying the mud volcano conduits is an extruded mud volcano and in contrast, overlying the fluid escape pipes is a pockmark (Figure 6.4 and Figure 6.5). The difference between the two end members at the upper terminus of these conduits implies that some conduits have been exploited by predominately fluids and others have been exploited by a mud slurry.

The aims of this chapter are to:

1. Describe the seismic characteristics and geometry of these mud volcano conduits and fluid escape pipes and compare them to other documented examples.
2. Present the evidence for the mud volcano conduit and fluid escape pipes root zones.
3. Explain the potential mechanisms for the formation of the mud volcano conduits and fluid escape pipes.
4. Propose a model for seal failure and mud volcano conduit and fluid escape pipe propagation through the thick Messinian evaporites within the Eastern Mediterranean.
5. Understand the controls on the distribution of fluid escape pipes and why some pipes are not associated with mud remobilisation.

This study is primarily based on qualitative and semi quantitative analysis and description of conduits for fluid and mud migration. The key focus is primarily on how large amounts of fluid and mud have migrated through a thick wedge of "sealing" evaporites. Identifying these conduits is at times challenging as one cannot always be clearly observed feeding all the extrusive mud volcanoes, and they are less easily observed within the Messinian evaporites due to imaging issues related to seismic artefacts (Figure 6.4 and Figure 6.5). The effect of seismic artefacts can be poor seismic migration, velocity 'pull up' or 'push down', scattering and attenuation, low signal to noise ratios, reflected refractions, un-collapsed diffractions and complex multiples, all of which make imaging the true geometry and particularly the base of these conduits complicated. Poor data quality can also be associated with gas charged sediments, which can cause significant velocity anomalies and distortion to the seismic signal that potentially extends beyond the root zone of the pipe (Granli et al., 1999; Arntsen et al., 2007).

Interpreting the root zone of a conduit is important as it can give an indication as to where the migrating fluids and sediments have been sourced from and what the fluid composition is (Huuse et al., 2010; Moss and Cartwright, 2010a; Cartwright and

Santamarina, 2015). Recently there has been an increase in documented examples of fluid escape pipes for which the feeding fluids have been interpreted as sourced from the pre-salt in the Eastern Mediterranean and therefore bypassed the Messinian evaporites (Bertoni and Cartwright, 2015; Bowman, 2011; Eruteya et al., 2015). Interpreting the exact stratigraphic layer of the root zone of these mud volcano conduits and fluid escape pipes is, however, difficult to determine with full confidence for several reasons that will be described below.

The conduits presented here represent some of the best imaged within the survey area. The variance slices that are displayed were chosen as those that best display the planform margins of these fluid escape pipes and mud volcano conduits at a range of levels up their height and are not shrouded by other background discontinuities. The geometric information used in this chapter (width and height) was calculated using pre-stack time-migrated and pre-stack depth-migrated 3D seismic reflection data. The regional geological context is presented in Chapter 3.

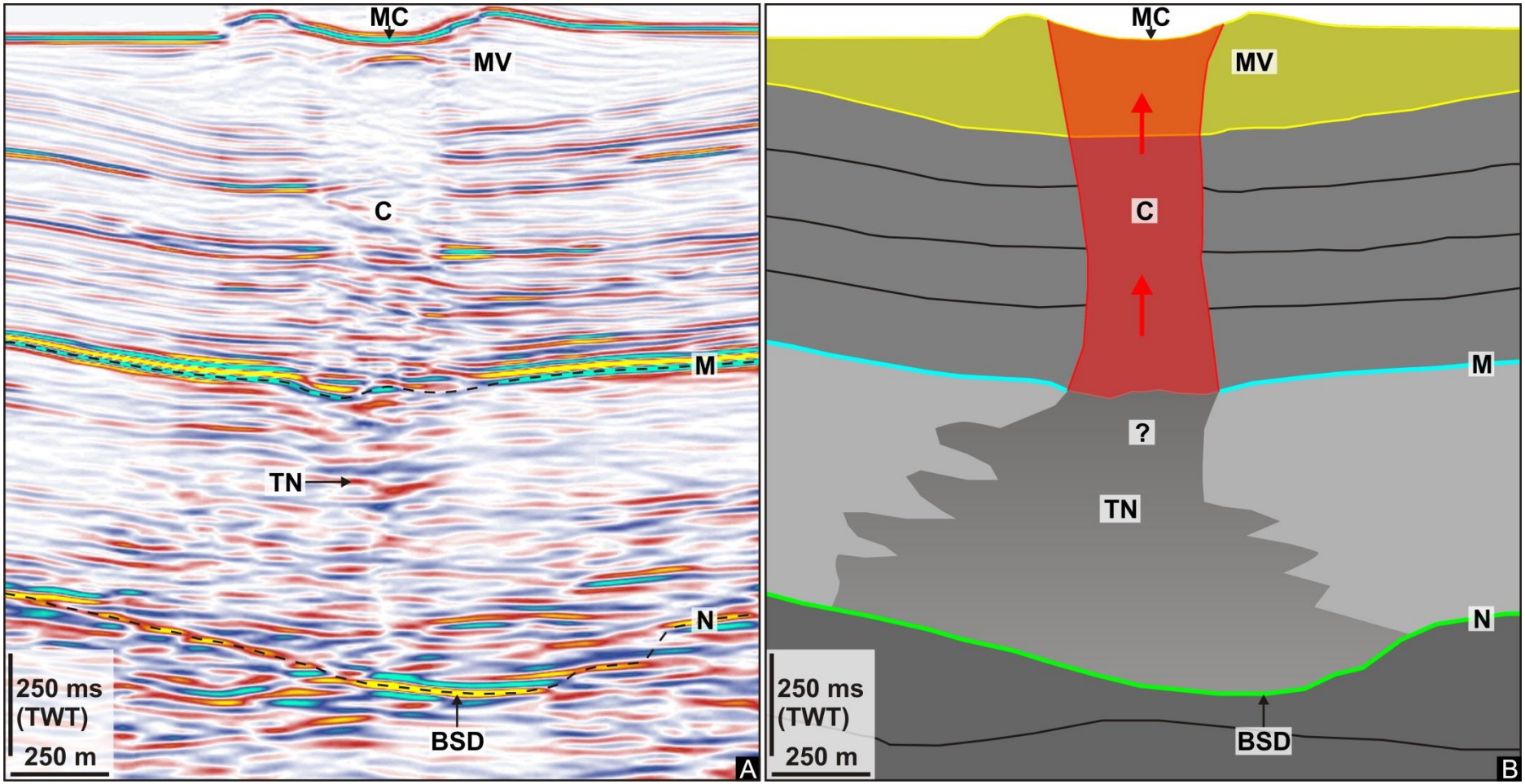

Figure 6.4 A seismic profile and cartoon showing the seismic characteristics of a mud volcano conduit within this study area. A: Seismic profile through a mud volcano conduit that has a mud volcano at its upper terminus. B: A simplified cartoon of the seismic profile in Figure 6.4A. The cartoon highlights the main features observed within the seismic profile, with particular focus on the mud volcano system. The root zone of the mud volcano conduit cannot be observed. C – Conduit; MV – Mud volcano; MC – Mud cone; TN – Trail of noise; BSD – Base-salt depression; M – Horizon M; N – Horizon N; TWT – Two way time.

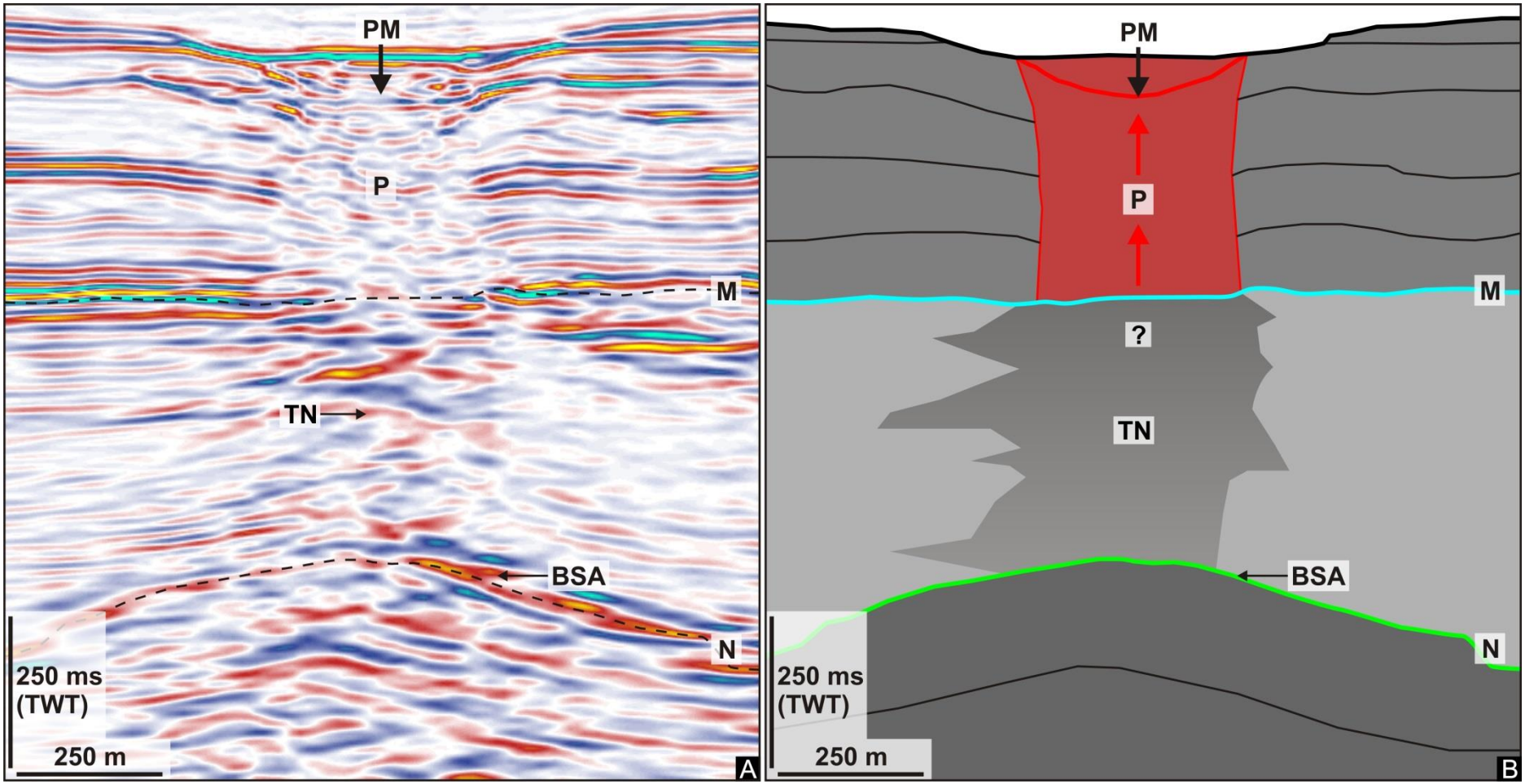

Figure 6.5 A seismic profile and cartoon showing the seismic characteristics of a fluid escape pipe within this study area. A: Seismic profile through a fluid escape pipe. B: A simplified cartoon of the seismic profile in Figure 6.5A. The cartoon highlights the main features observed within the seismic profile, with particular focus on the fluid escape pipe. The root zone of the fluid escape pipe cannot be observed. P – Pipe; PM – Pockmark; TN – Trail of noise; BSA – Base-salt anticline; M – Horizon M; N – Horizon N; TWT – Two way time.

6.3 Results

6.3.1 Seismic characteristics and geometry of mud volcano conduits and fluid escape pipes

Qualitative and semi-quantitative analysis was carried out on a large number of mud volcano conduits and fluid escape pipes from the El Dabaa study area. The ~4300 km^2 that the 3D seismic cube covers contains 386 small conical mud volcanoes, (As described in Chapter 5) 93 of which display evidence of a conduit, and 77 fluid escape pipes. These conduits display a variety of geometrical forms and dimensions. Based on measurements taken using 3D seismic data, the widths of the mud volcano conduit range from c. 40 – 525 m and the widths of the fluid escape pipe range from c. 75 – 665 m. These widths are calculated as the distance from one margin of the vertical zone of discontinuity to the other. It is important to take into consideration that these measurements may be partially artefactual.

The upper limit of these mud volcano conduits and fluid escape pipes both terminate at various levels within the Pliocene to Recent succession and form varied structures. The upper limit of the mud volcano conduits always terminate in extruded mud volcanoes located at a range of depths, from 3150 m at the seafloor to as deep as 6120 m subsea. In section 5.3.1 of Chapter 5, their geometry was described as circular to elliptical, conical lensoid features that are thickest at their centre and thin out towards their flanks and have built topography. In all examples the upper terminus of the mud volcano conduit is in line with the thickest part of a mud volcano which has a mud cone or depression at the centre of its upper surface (Figure 6.4). In contrast, the upper limit of the fluid escape pipes do not terminate in mud volcanoes but in circular to sub-circular depressions (Figure 6.5) that will be described in greater detail below.

The high amplitude and continuous seismic facies of the Pliocene to Recent succession allow for high quality imaging of the mud volcano conduits and fluid escape pipes. In seismic profile, within this succession these conduits stand out from the background reflectivity as a clear vertical zone of disrupted seismic signal,

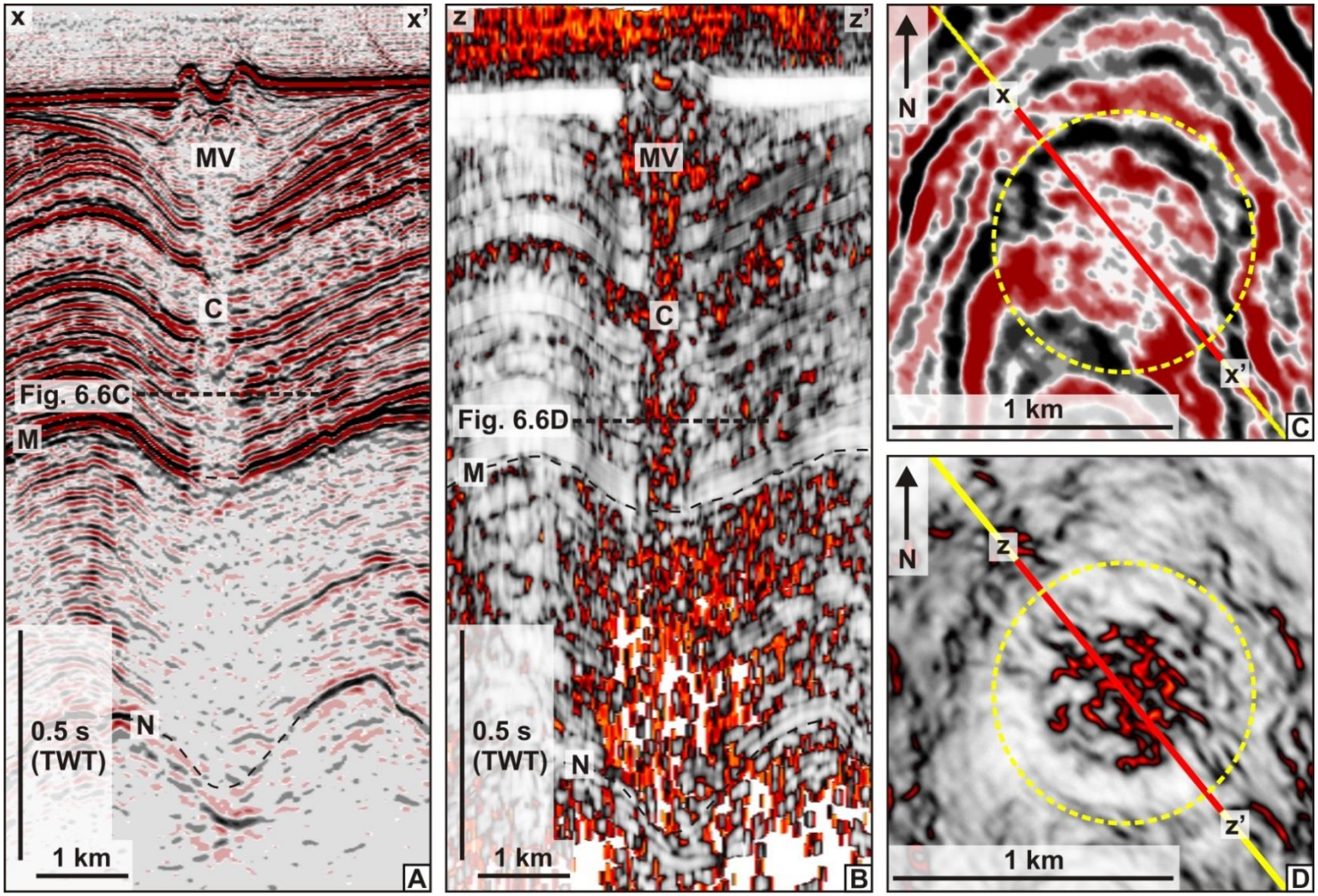

Figure 6.6 Mud volcano conduit geometry. A: Seismic profile through a mud volcano and conduit. B: Variance profile of the same mud volcano and conduit as in Figure 6.6A. C: Time slice through the conduit in Figure 6.6A. D: Variance slice through the conduit in Figure 6.6B. MV – Mud volcano; C - Conduit; M – Horizon M; N – Horizon N; TWT – Two way time. (The seismic profile and variance slice are both 5 times vertically exaggerated here)

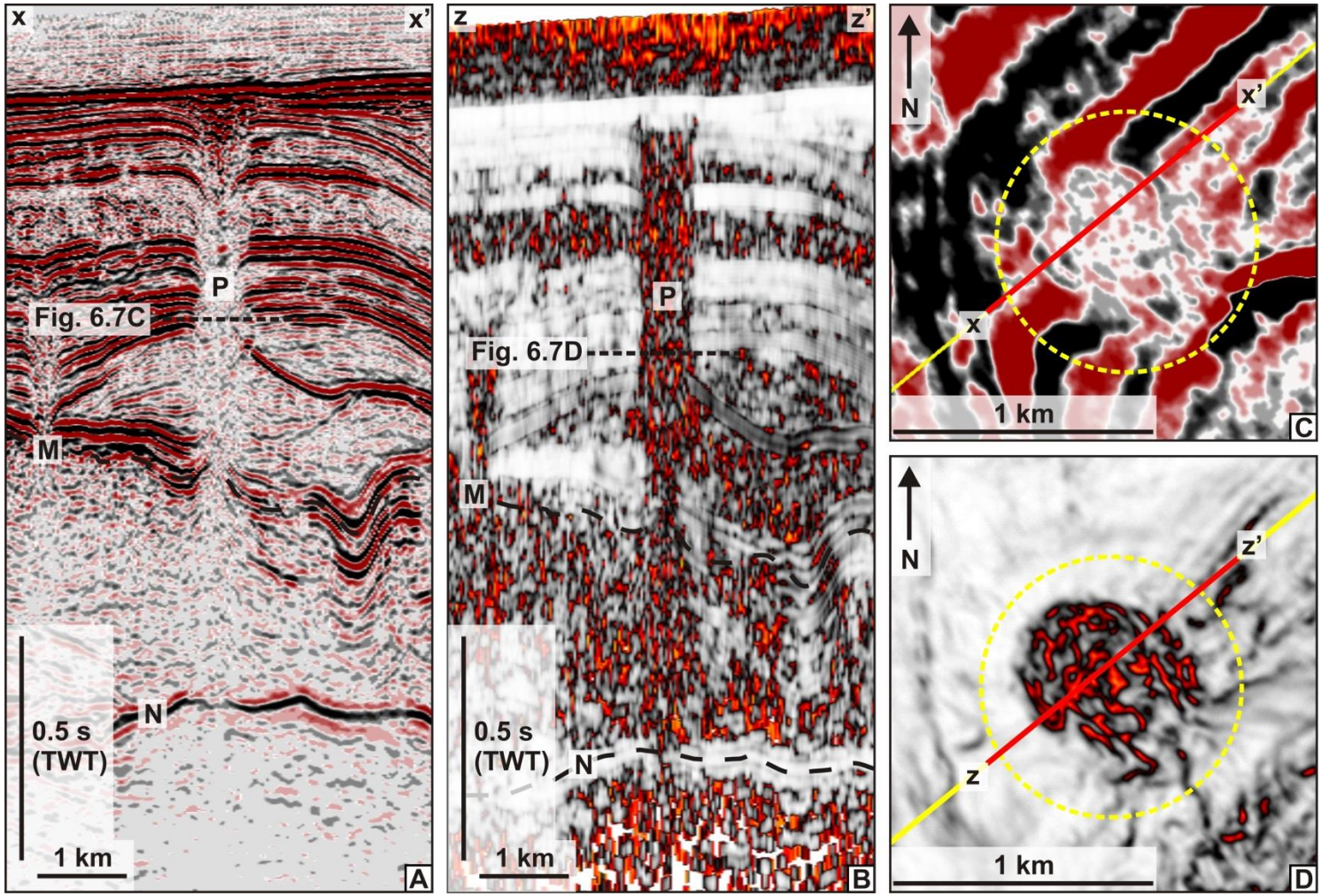

Figure 6.7 Fluid escape pipe geometry. A: Seismic profile through a fluid escape pipe. B: Variance profile of the same fluid escape pipe as in Figure 6.7A. C: Time slice through the fluid escape pipe in Figure 6.7A. D: Variance slice through the fluid escape pipe in Figure 6.7B. P – Pipe; M – Horizon M; N – Horizon N; TWT – Two way time. (The seismic profile and variance slice are both 5 times vertically exaggerated here)

lower amplitude and breaks in the continuity of the reflections of the host succession (Figure 6.6A and Figure 6.7A). In variance profile, they are displayed as clearly defined vertical zones of discontinuity (Figure 6.6B and Figure 6.7B). These vertical zones of discontinuity can be traced upwards from Horizon M for several hundreds of meters to the conduits upper terminus (Figure 6.6 and Figure 6.7). Above the upper terminus, there is no longer any reflection discontinuity or disruption in association with the underlying conduit. Time slices through these conduits displayed a circular to elliptical area of decreased amplitude (Figure 6.6B and Figure 6.7B); however the margins of these zone of reduced amplitude are poorly constrained and so do not accurately define the planform geometry of the conduit. Variance slices are useful for this type of analysis as they highlight any discontinuities within the data (Figure 6.6D and Figure 6.7D). They are therefore effective in defining the margins of these conduits as being circular to elliptical (Figure 6.6D and Figure 6.7D), provided the variance slice is within an area of the host succession that contains few other discontinuities that could shroud the conduit.

In contrast to the Pliocene to Recent succession, the evaporites are a predominantly low amplitude and discontinuous seismic facies with a low signal to noise ratio. Data quality within the evaporite succession and pre-salt also becomes progressively poorer due to increasing depth and the challenges of imaging within and beneath salt (O'Brien and Gray, 1996; Muerdter and Ratcliff, 2001). It is, therefore, difficult to confidently identify any disruption or true breaks in the continuity of reflections within the evaporites that would define a mud volcano conduit or fluid escape pipe (Figure 6.6 and Figure 6.7). In seismic profile, vertical zones of noise can in cases be traced across the evaporitic unit from Horizon N, to the base of a vertical zone of discontinuity (Horizon M) in the Pliocene to Recent succession (Figure 6.4 and Figure 6.5). It is important to bear in mind though that these trails of noise could be seismic artefacts due to the overlying zone of acoustic disruption of the conduit or even due to the presence of gas.

Presented below are further detailed descriptions of the mud volcano conduits and fluid escape pipes. Interpretation is primarily restricted to the Pliocene to Recent succession (From Horizon M to the seafloor) where these conduits are more easily

observed and accurately defined. The descriptions are based on observations made from seismic profiles, surface mapping and variance slices. The planform geometry of the mud volcano conduits and fluid escape pipes has been interpreted at multiple intervals up the conduit via iterative mapping between time and variance slices and seismic and variance profiles. The variance slices that are presented here represent the points along the conduit at which imaging of the planform geometry is clearest. Any errors in interpretation are associated with imaging quality at the margins and with increasing depth.

6.3.2 Mud volcano conduits

Within this section, three different examples of mud volcano conduits are presented. These three conduits have been selected as examples that most clearly display the seismic expression and geometry of these conduits, both in seismic profile and variance slices. They were also chosen as the examples that best display the variety in seismic expression and geometry (height and width) of the mud volcano conduits within this study area. The location of these conduits is displayed in Figure 6.8.

A mud volcano conduit can be observed extending from 4608 ms TWT at Horizon M to 4122 ms TWT in the example in Figure 6.9. It is interpreted based on clear disruption and breaks in the continuity of reflections within a vertical zone (Figure 6.10A and Figure 6.10B). The height of this conduit from Horizon M to its upper terminus is c. 535 m and its width ranges from c. 150 m to 260 m. Its upper limit terminates in a mud volcano that is buried (Figure 6.9). A small amount of discontinuity can be observed along Horizon M in seismic profile (Figure 6.9). The evaporites are predominantly transparent beneath Horizon M and there is a trail of noise that transects the evaporite succession from Horizon N to the break in continuity at Horizon M (Figure 6.10A). The geometry of the conduit in plan form is defined by a circular area of disruption and discontinuity (Figure 6.10C and Figure 6.10D). The planform area of the conduit is smallest nearer Horizon M (Figure 6.11F and

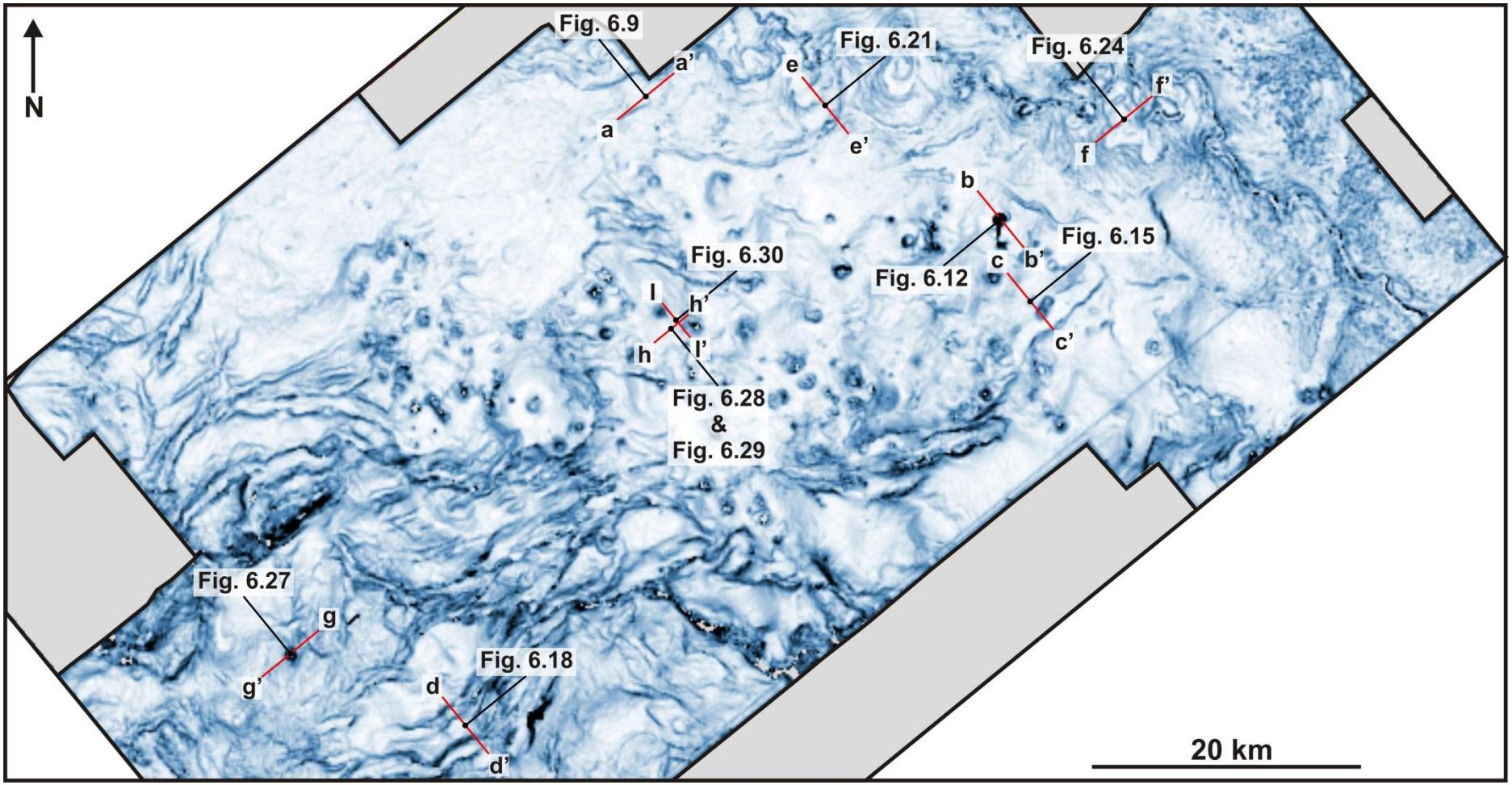

Figure 6.8 A seafloor map showing the location of the seismic profiles that are used in the upcoming examples of mud volcano conduits, fluid escape pipes and amplitude anomalies.

Figure 6.11G) and increases slightly upwards towards its upper terminus (Figure 6.11E and Figure 6.11C). The geometry of the conduit in planform is consistently elliptical up its entire vertical extent (Figure 6.11H). There is only very slight variation in the lateral position of the margins with height (Figure 6.11H). Horizon M and Horizon N both display localised and depressed geometry directly beneath the conduit (Figure 6.10E and Figure 6.10F).

Clear disruption and breaks in the continuity of reflections from 4504 ms TWT at Horizon M to 3880 ms TWT define the mud volcano conduit in Figure 6.12 and Figure 6.13. In contrast to the previous example (Figure 6.9), the upper limit of this conduit terminates at a mud volcano which can be observed at the present day seafloor (Figure 6.12). The height of the conduit between Horizon M and its upper terminus is c. 680 m and its width ranges from c. 330 m to 630 m. In seismic profile (Figure 6.12), there is a clear break in the continuity of the reflection of Horizon M (Figure 6.12). The evaporite succession beneath Horizon M is predominantly transparent but also displays some continuous and high amplitude reflections and a trail of noise that transects the evaporites from Horizon N to the break in continuity at Horizon M (Figure 6.13A). A circular area of disruption, discontinuity and also decreased amplitude define this conduit in planform (Figure 6.13C and Figure 6.13D). The planform area of discontinuity that delineates the margins is greatest at the base of the structure (Figure 6.14F and Figure 6.14G). The planform geometry of the margins progressively decreases with height (Figure 6.14D and Figure 6.14E). It is thinnest at its upper terminus (Figure 6.14B and Figure 6.14C). These observations also contrast with the example in Figure 6.11. Stacked interpretations of the planform margins up the height of the structure show that the planform geometry of the conduit ranges from circular to sub-circular (Figure 6.14H). There is lateral variation in the position of the planform margins of the conduit with height, which results in a sub-vertical structure (Figure 6.14H), rather than a simple idealised cylinder with a strictly vertical axis. Horizon M and Horizon N both display a depression that is localised directly beneath the conduit, similar to the previous example in Figure 6.10 (Figure 6.13E and Figure 6.13F).

In the final example, the vertical zone of discontinuity that defines the mud volcano conduit extends from Horizon M at 4600 ms TWT to the upper terminus at 3796 ms TWT (Figure 6.15 and Figure 6.16). The height between Horizon M and its upper terminus is c. 880 m, making this the tallest of the mud volcano conduits described here. Its width ranges from c. 460 m to 665 m, also making it the widest mud volcano conduit described. The upper terminus is characterised by a mud volcano that is currently visible at the seafloor (Figure 6.15), but is topographically more subdued than the example in Figure 6.12. Horizon M is the deepest reflection to display clear discontinuity in association with the vertical zone of the conduit (Figure 6.15), similar to the previous examples. The evaporite succession beneath Horizon M is predominantly transparent but also contains some heterogeneity (Figure 6.16A). Similar to the previous two examples there is a trail of noise through the evaporite succession; however, it is not as prominent here (Figure 6.16A). The geometry of the conduit in planform is characterised by a circular area of disruption, attenuation and discontinuity, similar to the previous example in Figure 6.13 (Figure 6.16). The area of discontinuity that defines the conduits planform margins is greatest nearer Horizon M (Figure 6.17F and Figure 6.17G) and decreases up the height of the conduit (Figure 6.17C and Figure 6.17E), similar to the example in Figure 6.14. It is, therefore, narrower towards its upper terminus (Figure 6.17H), similar to the example in Figure 6.12. Stacked outlines of the margins of the conduit (Figure 6.17H) show that it has circular planform geometry and exhibits the most closely vertical structure of the three examples. A top-salt and a base-salt depression can both be observed directly beneath the conduit, similar to the previous examples (Figure 6.16E and Figure 6.16F).

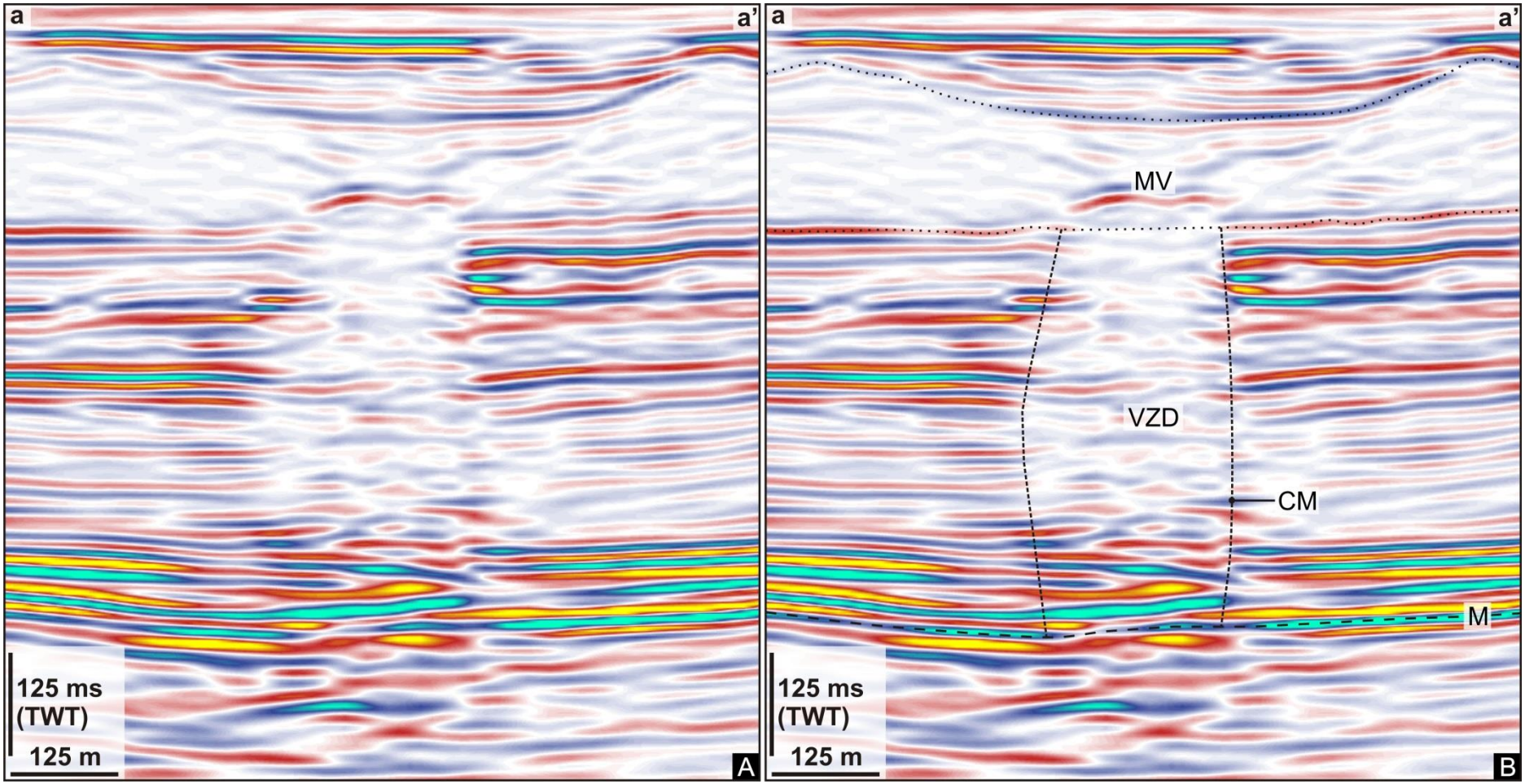

Figure 6.9 Seismic expression of a mud volcano conduit. A: An un-interpreted seismic profile through a mud volcano conduit and mud volcano. B: An interpreted profile of the mud volcano conduit and mud volcano in Figure 6.9A. MV – Mud volcano; VZD – Vertical zone of discontinuity; CM – Conduit margins; M – Horizon M; TWT – Two way time.

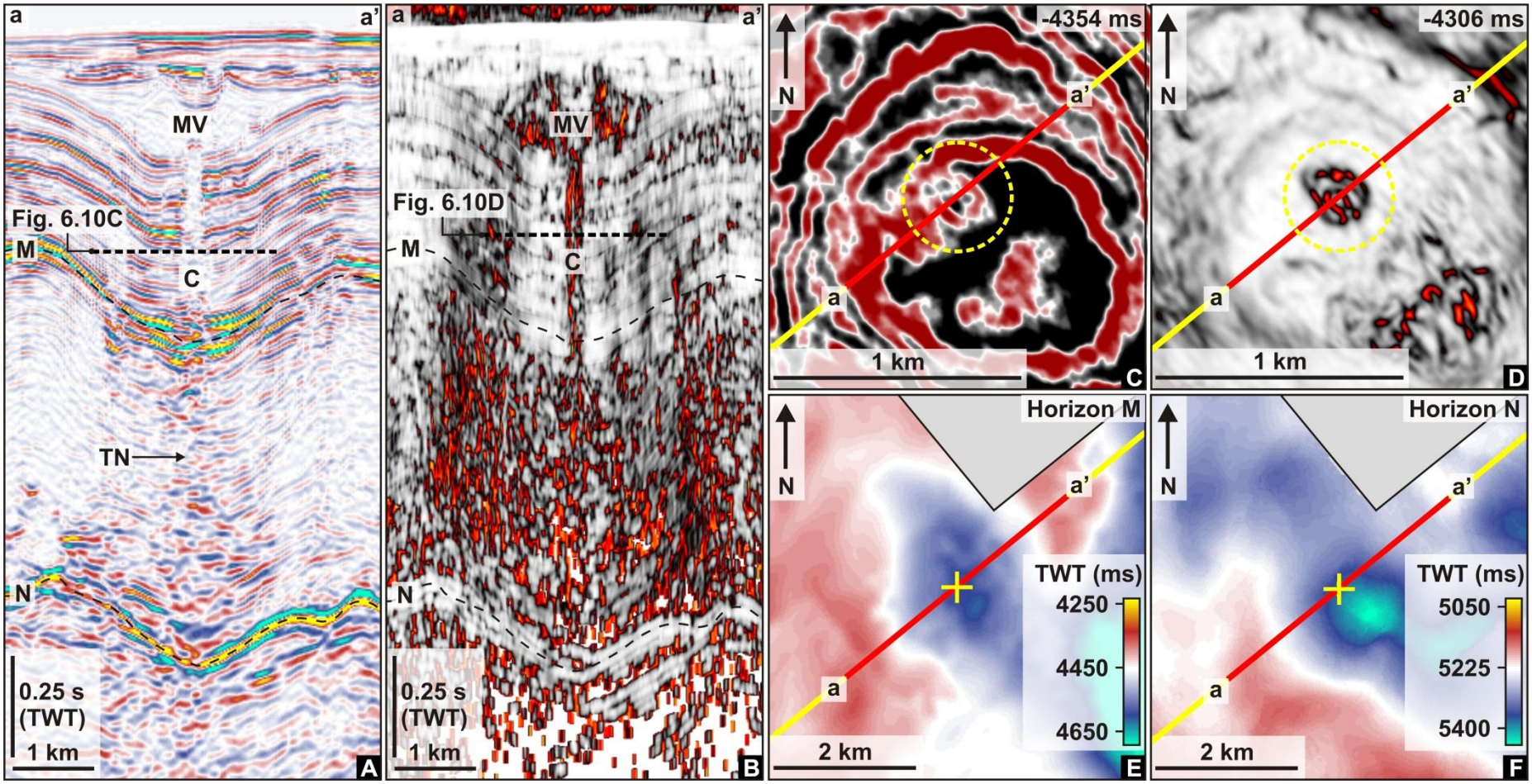

Figure 6.10 Defining a mud volcano conduit and the underlying top and base-salt geometry. A: A seismic profile through a mud volcano and mud volcano conduit. B: A variance profile through a mud volcano and mud volcano conduit. The line of section is the same as in Figure 6.10A. C: A time slice through the mud volcano conduit. D: A variance slice through the mud volcano conduit (The conduit is highlighted by the circle with a yellow dashed line in Figure 6.10C and Figure 6.10D). E: A time map of Horizon M. F: A time map of Horizon N (The yellow + marks the location of the overlying conduit in Figure 6.10E and Figure 6.10F). MV – Mud volcano; C – Conduit; TN – Trail of noise; M – Horizon M; N – Horizon N. (The seismic profile and variance slice are both 5 times vertically exaggerated here)

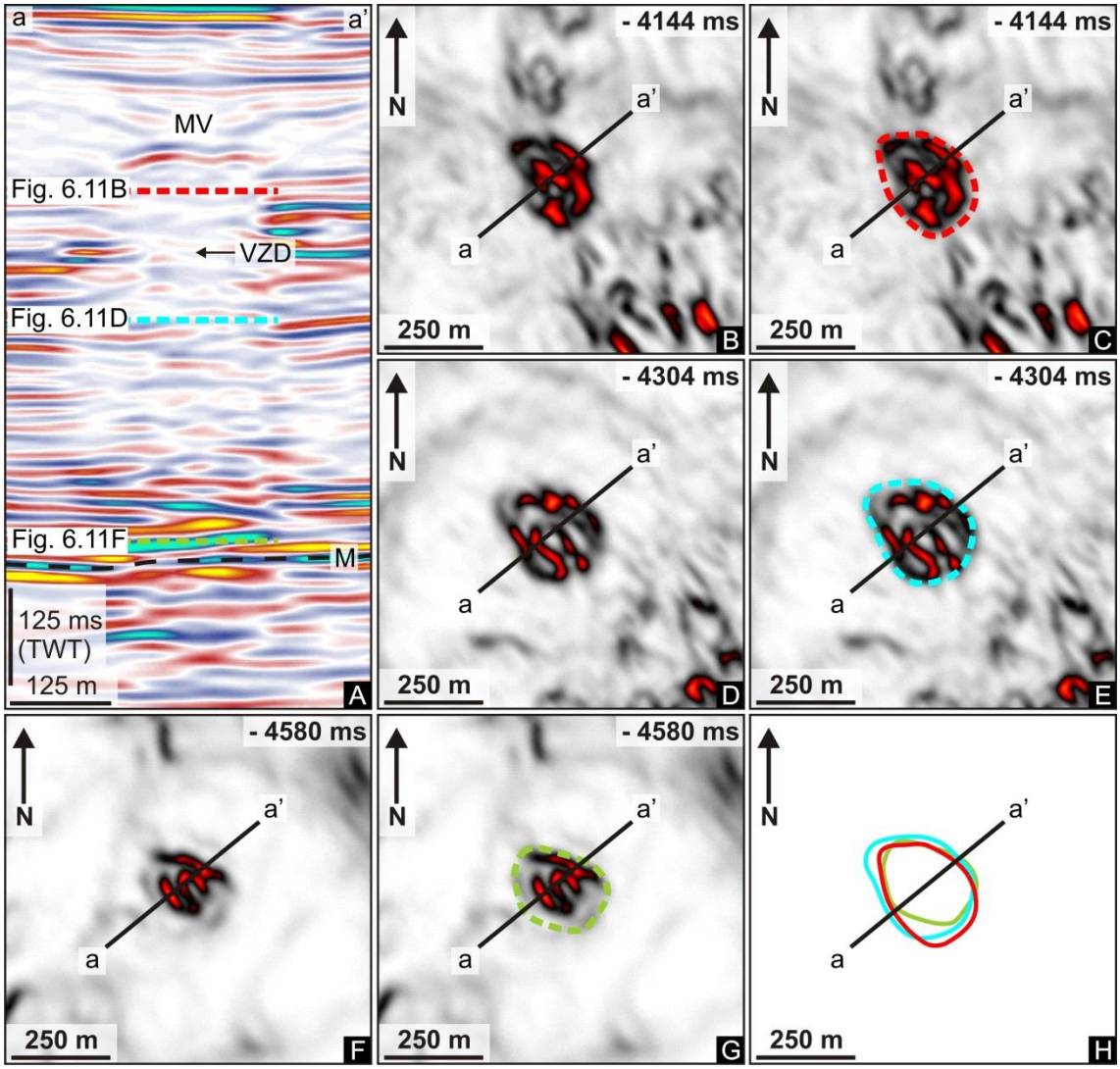

Figure 6.11 Geometry of a mud volcano conduit. A: Seismic profile through a mud volcano conduit. B: Variance profile through the mud volcano conduit in Figure 6.11A. C: Interpretation of the conduit margins from the variance profile in Figure 6.11B. D: Variance profile through the mud volcano conduit in Figure 6.11A. E: Interpretation of the conduit margins from the variance profile in Figure 6.11D. F: Variance profile through the mud volcano conduit in Figure 6.11A. G: Interpretation of the conduit margins from the variance profile in Figure 6.11F. H: Stacked outlines of the conduits margins from Figure 6.11C, Figure 6.11E and Figure 6.11G, showing the 3D geometry of the mud volcano conduit. MV – Mud volcano; VZD – Vertical zone of discontinuity; M – Horizon M; TWT – Two way time.

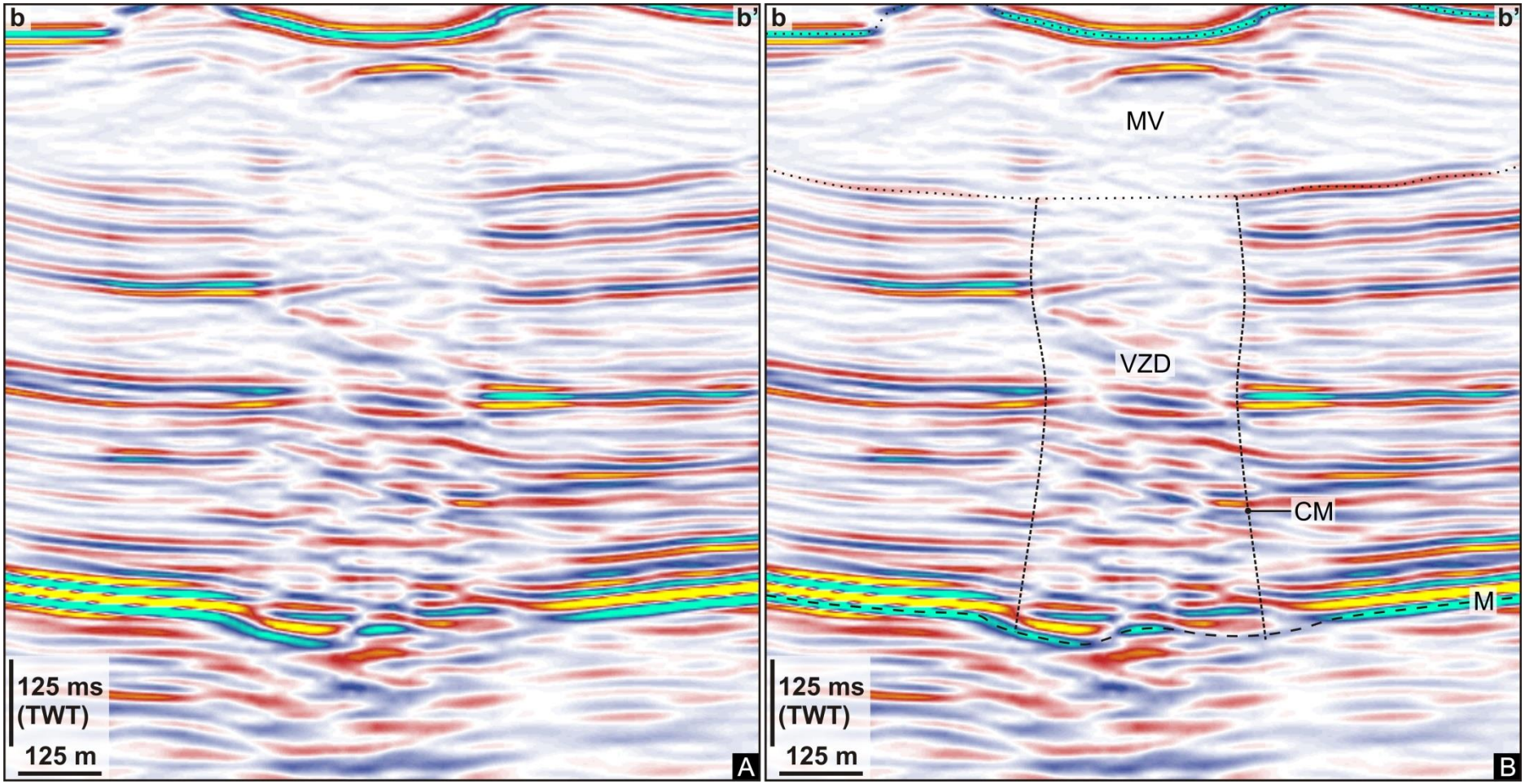

Figure 6.12 Seismic expression of a mud volcano conduit. A: An un-interpreted seismic profile through a mud volcano conduit and mud volcano. B: An interpreted profile of the mud volcano conduit and mud volcano in Figure 6.12A. MV – Mud volcano; VZD – Vertical zone of discontinuity; CM – Conduit margins; M – Horizon M; TWT – Two way time.

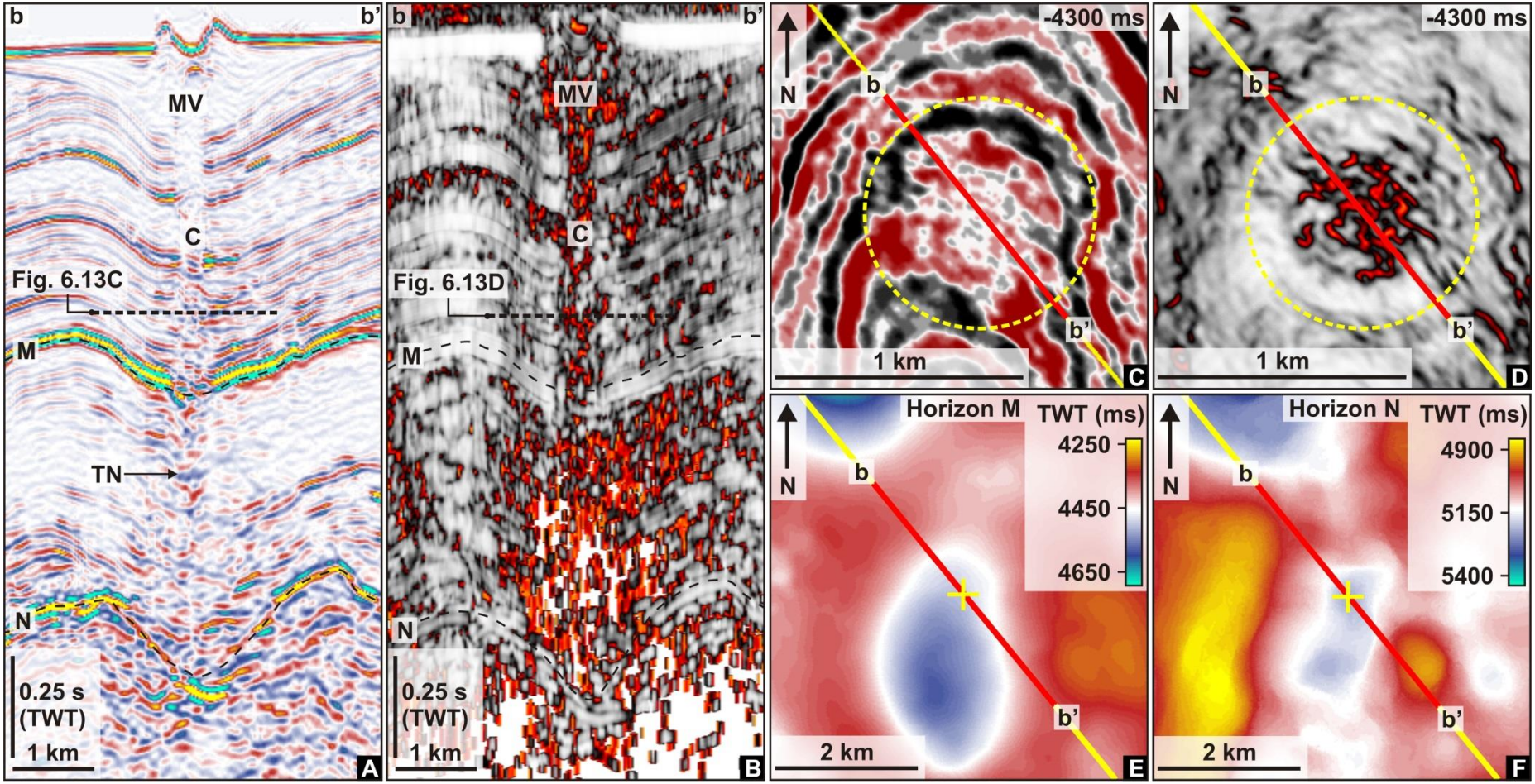

Figure 6.13 Defining a mud volcano conduit and the underlying top and base-salt geometry. A: A seismic profile through a mud volcano and mud volcano conduit. B: A variance profile through a mud volcano and mud volcano conduit. The line of section is the same as in Figure 6.13A. C: A time slice through the mud volcano conduit. D: A variance slice through the mud volcano conduit (The conduit is highlighted by the circle with a yellow dashed line in Figure 6.13C and Figure 6.13D). E: A time map of Horizon M. F: A time map of Horizon N (The yellow + marks the location of the overlying conduit in Figure 6.13E and Figure 6.13F). MV – Mud volcano; C – Conduit; TN – Trail of noise; M – Horizon M; N – Horizon N. (The seismic profile and variance slice are both 5 times vertically exaggerated here)

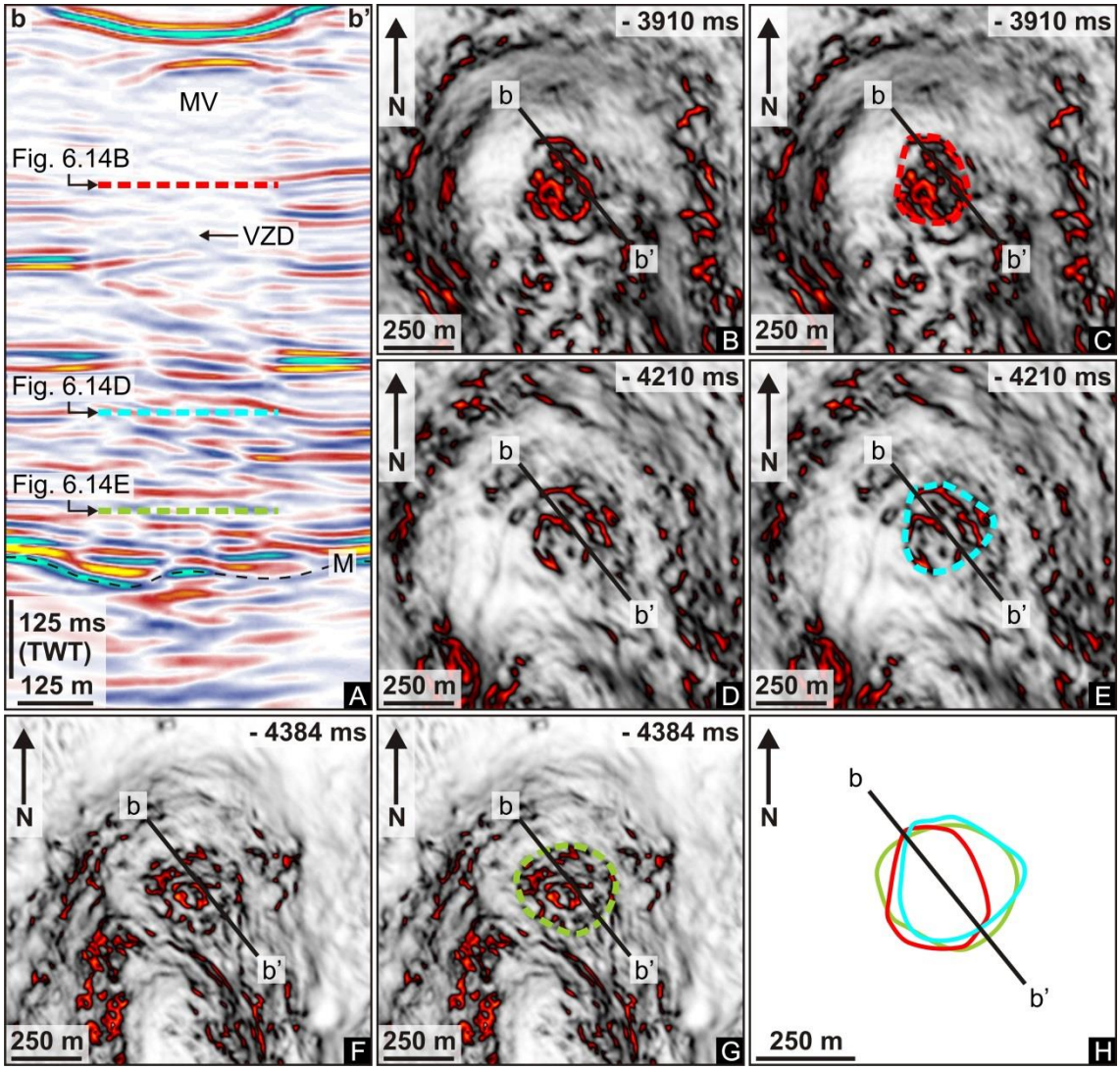

Figure 6.14 Geometry of a mud volcano conduit. A: Seismic profile through a mud volcano conduit. B: Variance profile through the mud volcano conduit in Figure 6.14A. C: Interpretation of the conduit margins from the variance profile in Figure 6.14B. D: Variance profile through the mud volcano conduit in Figure 6.14A. E: Interpretation of the conduit margins from the variance profile in Figure 6.14D. F: Variance profile through the mud volcano conduit in Figure 6.14A. G: Interpretation of the conduit margins from the variance profile in Figure 6.14F. H: Stacked outlines of the conduits margins from Figure 6.14C, Figure 6.14E and Figure 6.14G, showing the 3D geometry of the mud volcano conduit. MV – Mud volcano; VZD – Vertical zone of discontinuity; M – Horizon M; TWT – Two way time.

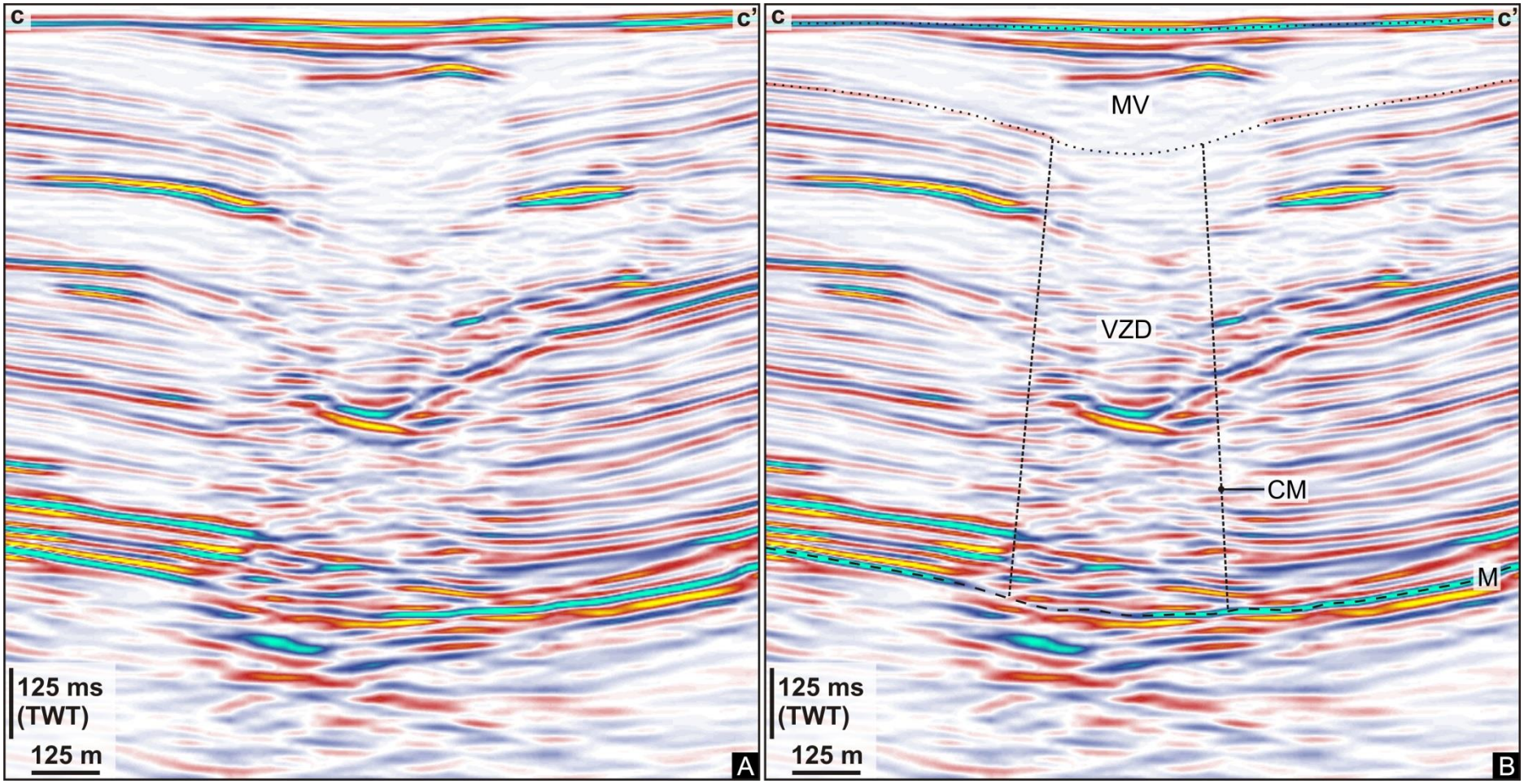

Figure 6.15 Seismic expression of a mud volcano conduit. A: An un-interpreted seismic profile through a mud volcano conduit and mud volcano. B: An interpreted profile of the mud volcano conduit and mud volcano in Figure 6.15A. MV – Mud volcano; VZD – Vertical zone of discontinuity; CM – Conduit margins; M – Horizon M; TWT – Two way time.

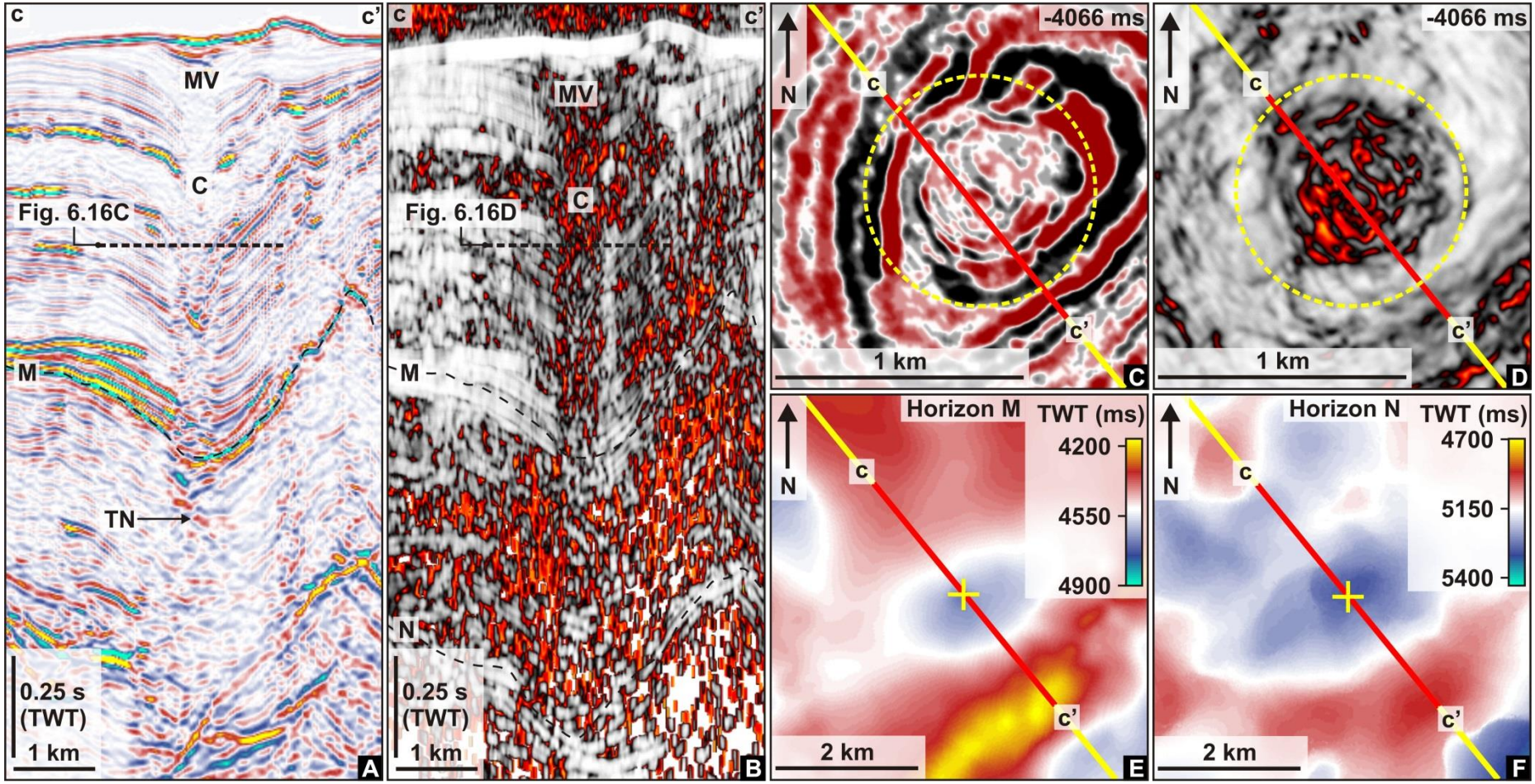

Figure 6.16 Defining a mud volcano conduit and the underlying top and base-salt geometry. A: A seismic profile through a mud volcano and mud volcano conduit. B: A variance profile through a mud volcano and mud volcano conduit. The line of section is the same as in Figure 6.16A. C: A time slice through the mud volcano conduit. D: A variance slice through the mud volcano conduit (The conduit is highlighted by the circle with a yellow dashed line in Figure 6.16C and Figure 6.16D). E: A time map of Horizon M. F: A time map of Horizon N (The yellow + marks the location of the overlying conduit in Figure 6.16E and Figure 6.16F). MV – Mud volcano; C – Conduit; TN – Trail of noise; M – Horizon M; N – Horizon N. (The seismic profile and variance slice are both 5 times vertically exaggerated here)

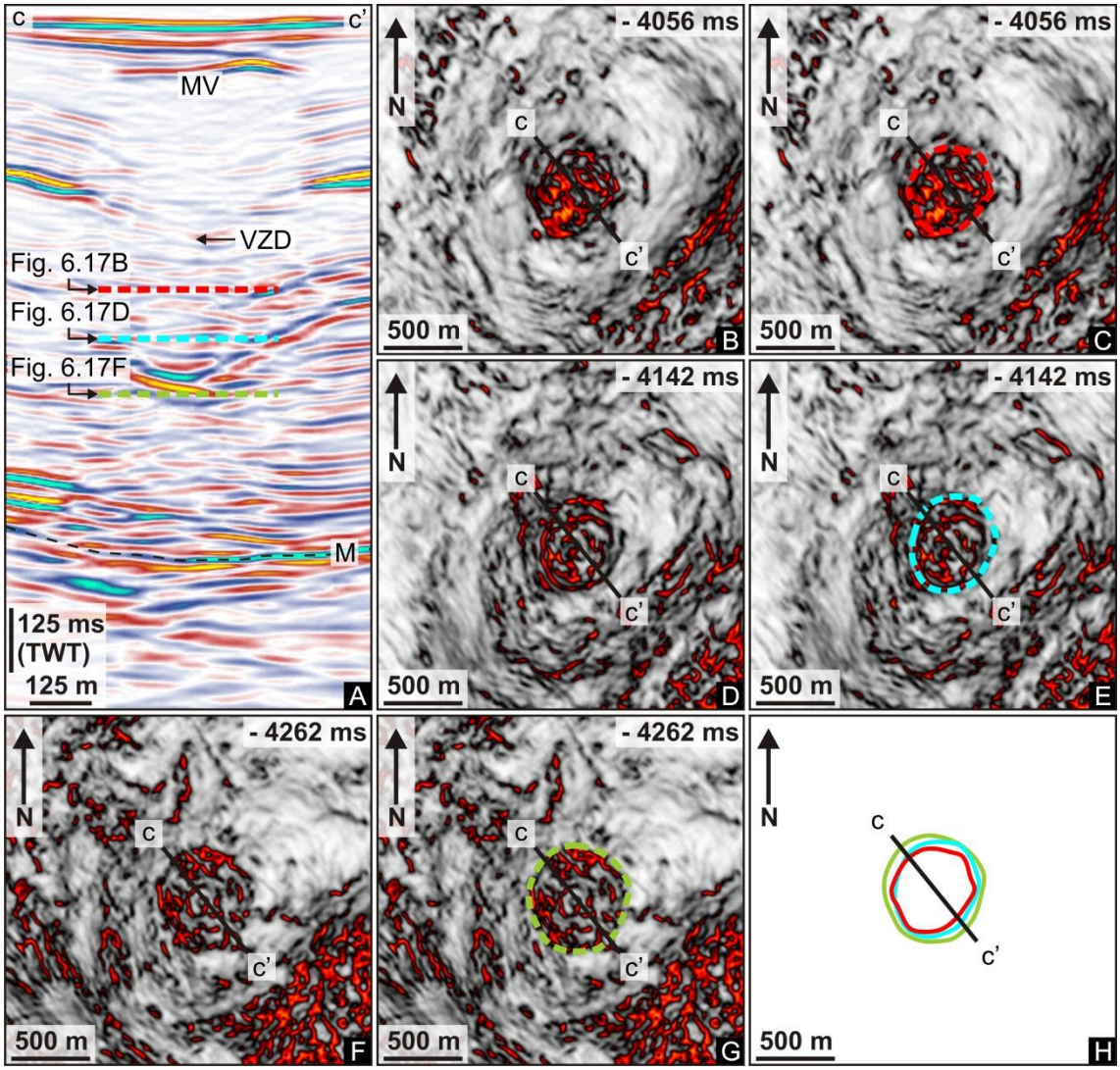

Figure 6.17 Geometry of a mud volcano conduit. A: Seismic profile through a mud volcano conduit. B: Variance profile through the mud volcano conduit in Figure 6.17A. C: Interpretation of the conduit margins from the variance profile in Figure 6.17B. D: Variance profile through the mud volcano conduit in Figure 6.17A. E: Interpretation of the conduit margins from the variance profile in Figure 6.17D. F: Variance profile through the mud volcano conduit in Figure 6.17A. G: Interpretation of the conduit margins from the variance profile in Figure 6.17F. H: Stacked outlines of the conduits margins from Figure 6.17C, Figure 6.17E and Figure 6.17G, showing the 3D geometry of the mud volcano conduit. MV – Mud volcano; VZD – Vertical zone of discontinuity; M – Horizon M; TWT – Two way time.

6.3.2.1 Summary and interpretation

The examples of mud volcano conduits presented above demonstrate that these mud volcano conduits can be reliably identified as steep zones of discontinuity, disruption and attenuation to the reflections of the host succession. The lateral margins of these conduits can be accurately defined as the edge of an area of discontinuity, within a three dimensional structure which is most closely reminiscent to a cylinder. In none of these examples, however, is the planform geometry perfectly uniform up the entire height of the structure, neither is it perfectly vertical. In all observed examples these vertical and cylindrical structures transect the host succession of the Pliocene to Recent and terminate at a mud volcano at their upper limits. The presence of a mud volcano in all examples makes defining the upper terminus of these conduits straight forward and reaffirms the interpretation that these structures are indeed mud volcano conduits.

Although imaging quality can decrease within increased depth, in all the examples presented, Horizon M is the deepest seismic reflector to show unequivocal evidence of being transected by a conduit, via breaks in the continuity of the reflection. The base of a conduit should be recognisable as the first continuous reflection to cross beneath the vertical stack of breaks in reflection continuity that defines the conduit. However, the discontinuous and predominantly transparent seismic facies of the evaporites (presumably halite (Bertoni and Cartwright, 2007b)) and seismic artefacts associated with the pre-salt make it very difficult to trace the true (i.e. geologically significant) zone of discontinuity associated with a mud volcano conduit, any deeper than Horizon M. In all examples the reflection of Horizon M and also Horizon N displayed a depressed geometry directly beneath the mud volcano conduit. Within the evaporites the data are so obscured by artefacts and imaging problems arising from the conduit zone above that it is impossible to dissemble what discontinuities might be real from those that might more realistically be artefact.

The discontinuities observed at Horizon M indicate that these mud volcano conduits have at least in part ascended through the evaporite unit. It is not possible to directly identify the root zone, whether that is within the evaporites or pre-salt.

However, this observation does strongly suggest that the conduit root zone is pre-Pliocene.

6.3.3 Fluid escape pipes

Within this section, three different examples of fluid escape pipes displayed and described in detail. Similar to the mud volcano conduits described above, these three pipes have been selected as examples that most clearly display the seismic expression and geometry of these conduits, both in seismic profile and variance slices. They were also chosen as the examples that best display the variety in seismic expression and geometry and range of termination levels of the pipes within this study area. The location of these pipes can be seen in Figure 6.8**.**

In the first fluid escape pipe example, a pipe is interpreted to extend from 4200 ms TWT at Horizon M to 4092 ms TWT (Figure 6.18). This example is defined by a clear vertical stack of disruptions to the continuity of reflections of the hosting Pliocene to Recent succession (Figure 6.19C Figure 6.19D). The height of the pipe between Horizon M and its upper terminus is 144 m and is the shortest pipe described here. Its width ranges from c. 135 m to 200 m. The upper terminus of this pipe displays a concave reflection that directly overlies the pipe (Figure 6.18). This reflection truncates underlying reflections of the Pliocene to Recent succession (Figure 6.18). A localised and sub-circular bowl shaped depression is clearly displayed in the horizon map in Figure 6.18C. This depression is deepest centrally with a maximum relief of c. 50 ms. Reflections of later deposited sediment onlap the inner side of the depression (Figure 6.18B). Above these reflections, a reflection that displays no loss in continuity or downward deflection crosses above the pipe and depression (Figure 6.18B). Approximately 200 ms directly above the upper terminus of the pipe, a stack of enhanced reflections can be seen (Figure 6.18). The margins of this amplitude anomaly display a sharp cut-off in amplitude. There is a prominent break in the continuity of Horizon M in seismic profile (Figure 6.18A). Horizon M displays a clear depressed geometry beneath the pipe (Figure 6.19E). In contrast, only a very subtle depression

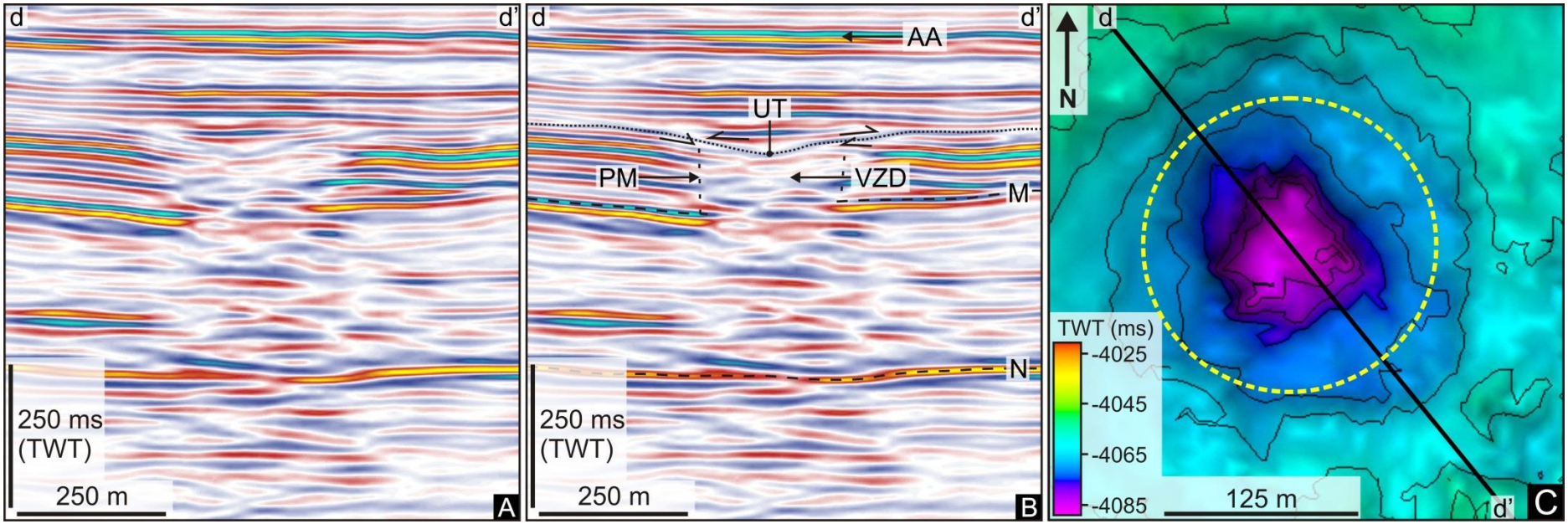

Figure 6.18 Seismic expression of a fluid escape pipe and a horizon map of its upper terminus. A: An un-interpreted seismic profile through a fluid escape pipe. B: An interpreted profile of the fluid escape pipe in Figure 6.18A. C: A TWT horizon map of the reflection of the fluid escape pipes upper terminus. VZD – Vertical zone of discontinuity; UT – Upper terminus; PM – Pipe margin; AA – Amplitude anomaly; M – Horizon M; N – Horizon N; TWT – Two way time.

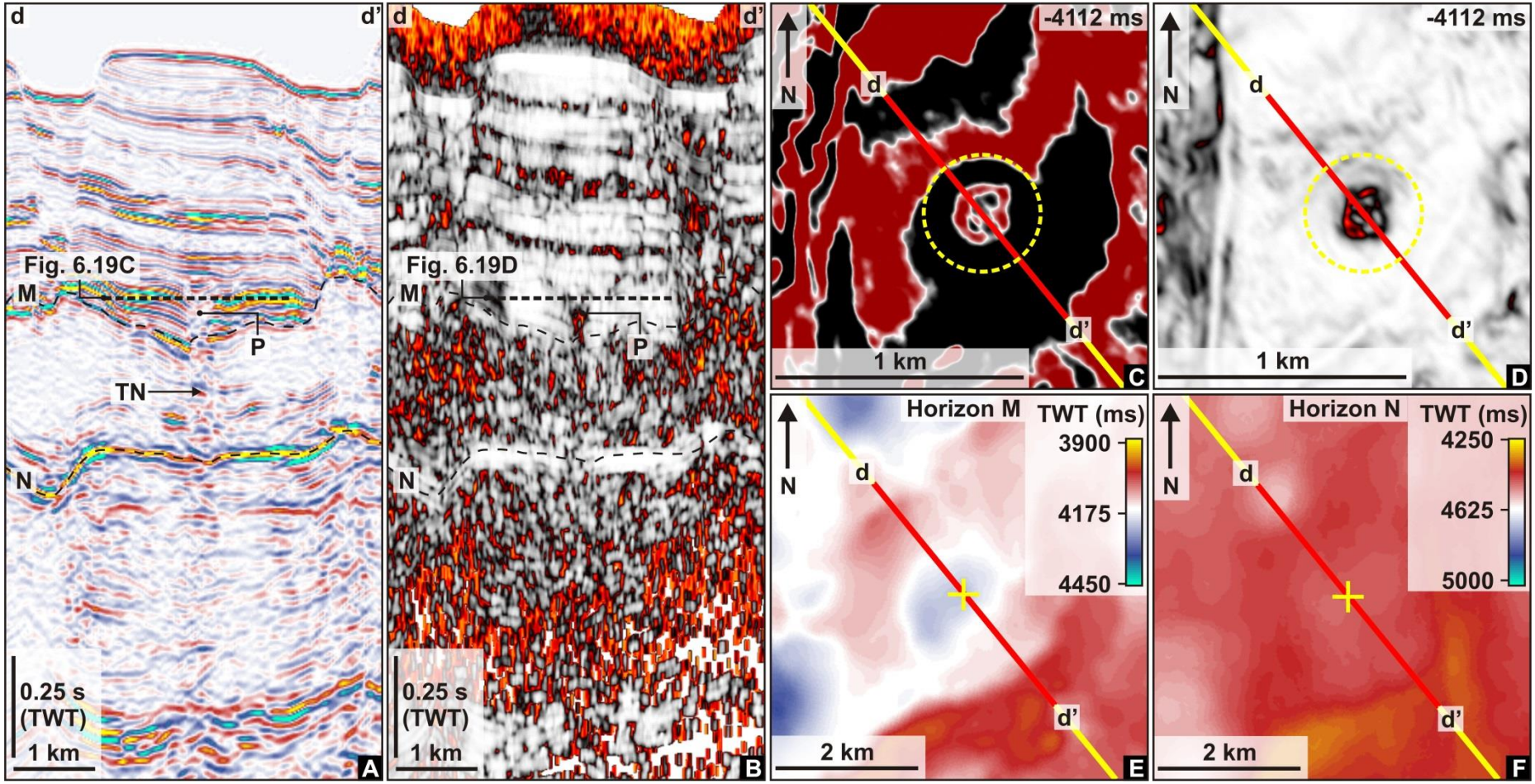

Figure 6.19 Defining a fluid escape pipe and the underlying top and base-salt geometry. A: A seismic profile through a fluid escape pipe. B: A variance profile through a fluid escape pipe. The line of section is the same as in Figure 6.19A. C: A time slice through the fluid escape pipe. D: A variance slice through the fluid escape pipe (The pipe is highlighted by the circle with a yellow dashed line in Figure 6.19C and Figure 6.19D). E: A time map of Horizon M. F: A time map of Horizon N (The yellow + marks the location of the overlying pipe in Figure 6.19E and Figure 6.19F). P - Pipe; TN – Trail of noise; M – Horizon M; N – Horizon N. (The seismic profile and variance slice are both 5 times vertically exaggerated here)

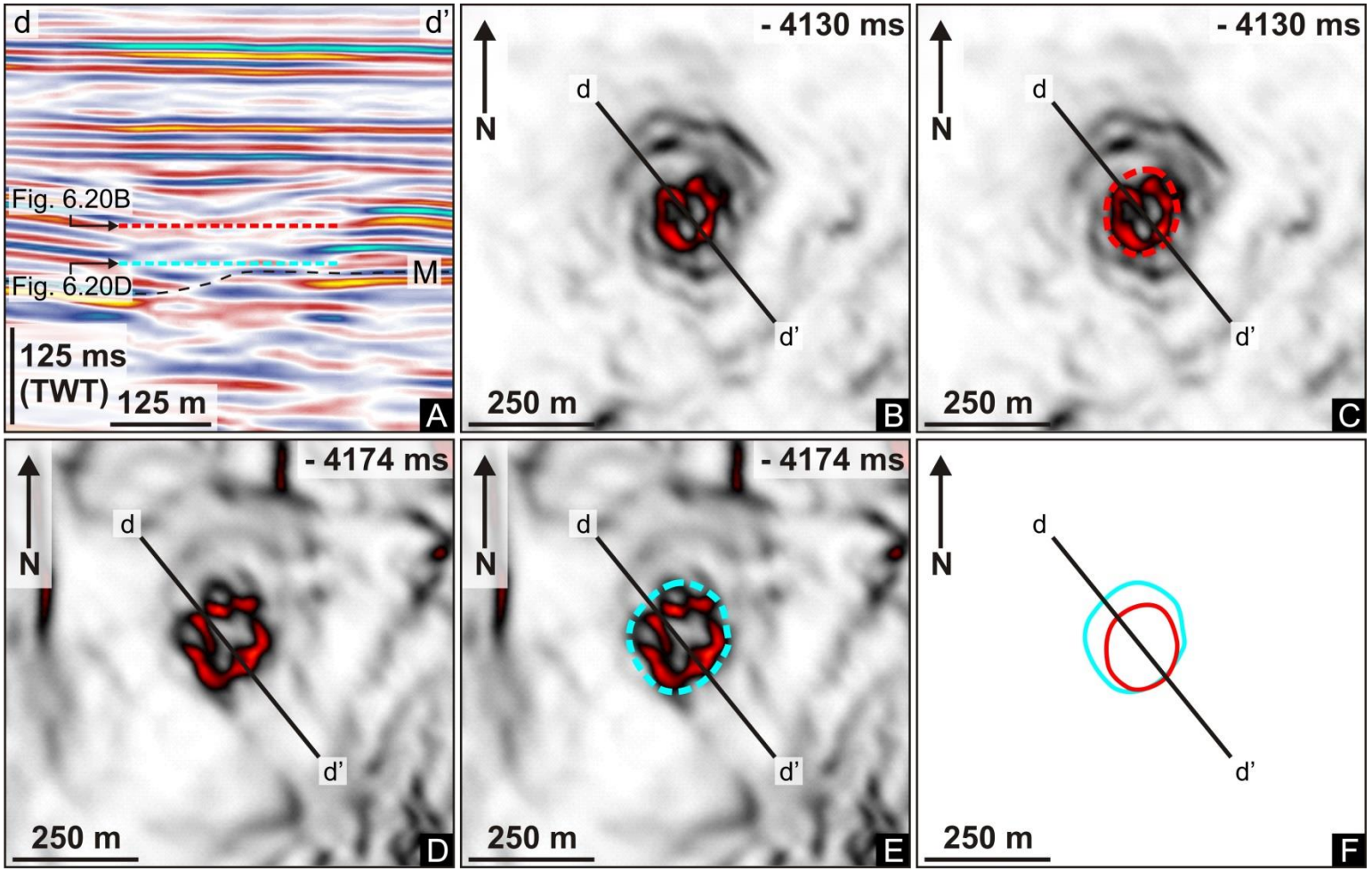

Figure 6.20 Geometry of a fluid escape pipe. A: Seismic profile through a fluid escape pipe. B: Variance profile through the fluid escape pipe in Figure 6.20A. C: Interpretation of the pipes margins from the variance profile in Figure 6.20B. D: Variance profile through the fluid escape pipe in Figure 6.20A. E: Interpretation of the pipes margins from the variance profile in Figure 6.20D. F: Stacked outlines of the pipes margins from Figure 6.20C and Figure 6.20E, showing the 3D geometry of the fluid escape pipe. M – Horizon M; TWT – Two way time.

can be observed at Horizon N beneath the pipe (Figure 6.19F). A clear trail of noise that transects the entire evaporite succession can be observed beneath the break in continuity of the reflection of Horizon M (Figure 6.19A). The geometry of the pipe in planform is characterised by a circular area of discontinuity and disruption to the reflections of the host succession (Figure 6.19C and Figure 6.19D). The geometry of the pipe in planform is circular in the deepest variance slice in Figure 6.20E. Nearer the upper terminus of the pipe, the geometry in planform is also circular but the planform area of the pipe has decreased (Figure 6.20C). This pipe is, therefore, upwards narrowing (Figure 6.20F). Stacking the interpretations of the margins demonstrates that its margins do not vertically overlie one another and the pipe and, therefore, exhibits a sub-vertical form (Figure 6.20F).

The second example of a fluid escape pipe described here is interpreted to extent from 4362 ms TWT at Horizon M to 3832 ms TWT (Figure 6.21). The example presented in Figure 6.22 is comparable to the example in Figure 6.19, in that it shares the same defining seismic characteristics. The height of the pipe between Horizon M and its upper terminus is c. 548 m and, therefore, transects a larger section of the Pliocene to Recent succession than the previously described example (Figure 6.18). Its width ranges from c. 245 m to 330 m. The upper terminus is characterised by a continuous reflection with concave geometry, which also truncates underlying reflections of the Pliocene to Recent succession (Figure 6.21B), similar to the example in Figure 6.18. A horizon map (Figure 6.21C) of this reflection shows that the depression is localised and has a planform geometry that is circular to elliptical, with maximum relief of 53 ms TWT centrally. The inner sides of this depressed reflection are onlapped by overlying reflections (Figure 6.21B). The reflection of the seafloor directly above the upper terminus of the pipe displays a localised enhancement in amplitude, which exhibits a sharp cut-off in amplitude at the margins of the anomaly (Figure 6.21B). A break in the continuity of the reflection of Horizon M is clear in seismic profile (Figure 6.21B). Neither Horizon M nor Horizon N display a clear depression directly beneath the overlying pipe (Figure 6.22E and Figure 6.22F). The evaporite succession contains a trail of noise directly beneath the pipe and numerous amplitude anomalies (Figure 6.22A). The geometry in planform and margins of the pipe

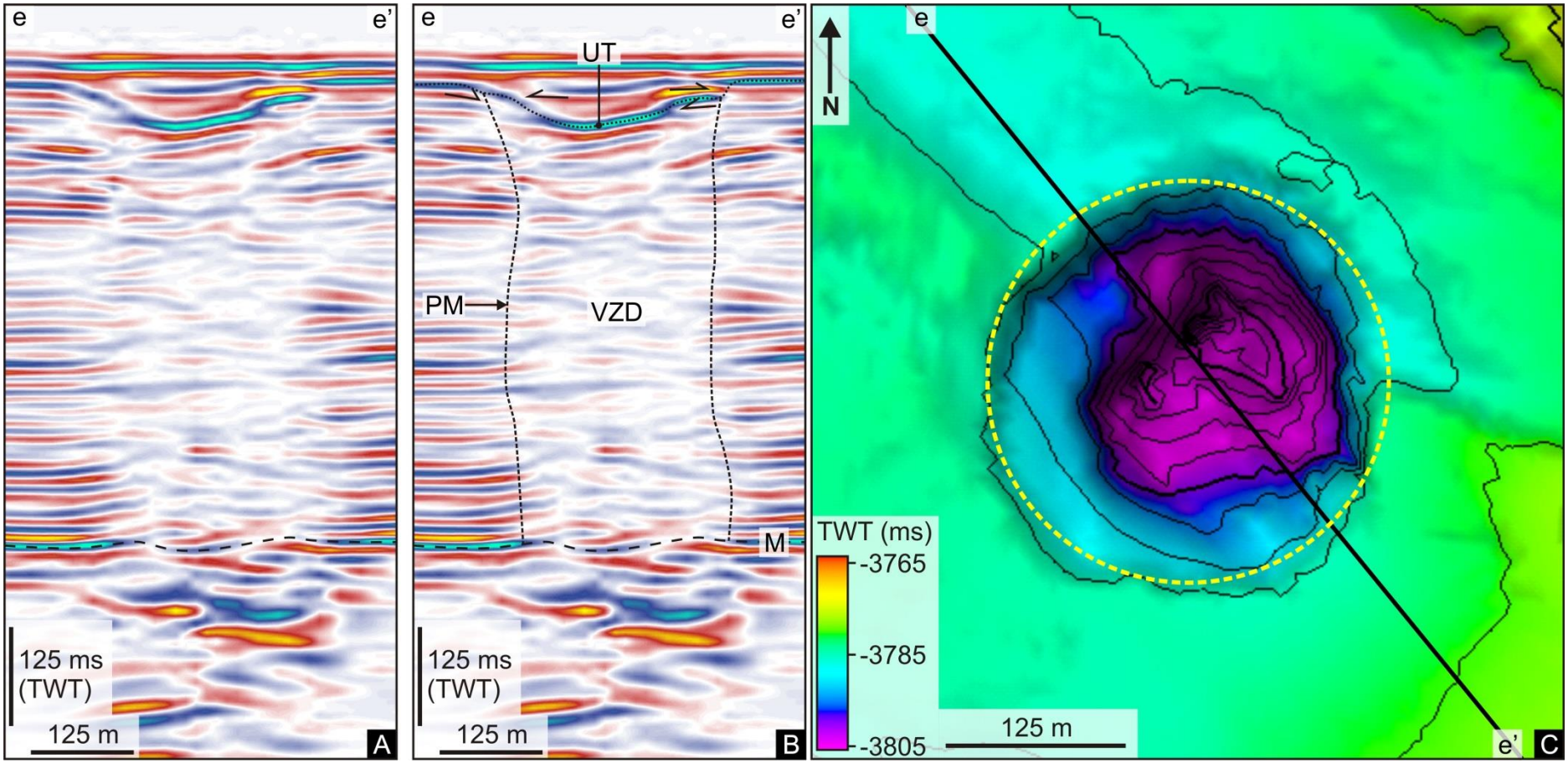

Figure 6.21 Seismic expression of a fluid escape pipe and a horizon map of its upper terminus. A: An un-interpreted seismic profile through a fluid escape pipe. B: An interpreted profile of the fluid escape pipe in Figure 6.21A. C: A TWT horizon map of the reflection of the fluid escape pipes upper terminus. VZD – Vertical zone of discontinuity; UT – Upper terminus; PM – Pipe margin; M – Horizon M; N – Horizon N; TWT – Two way time.

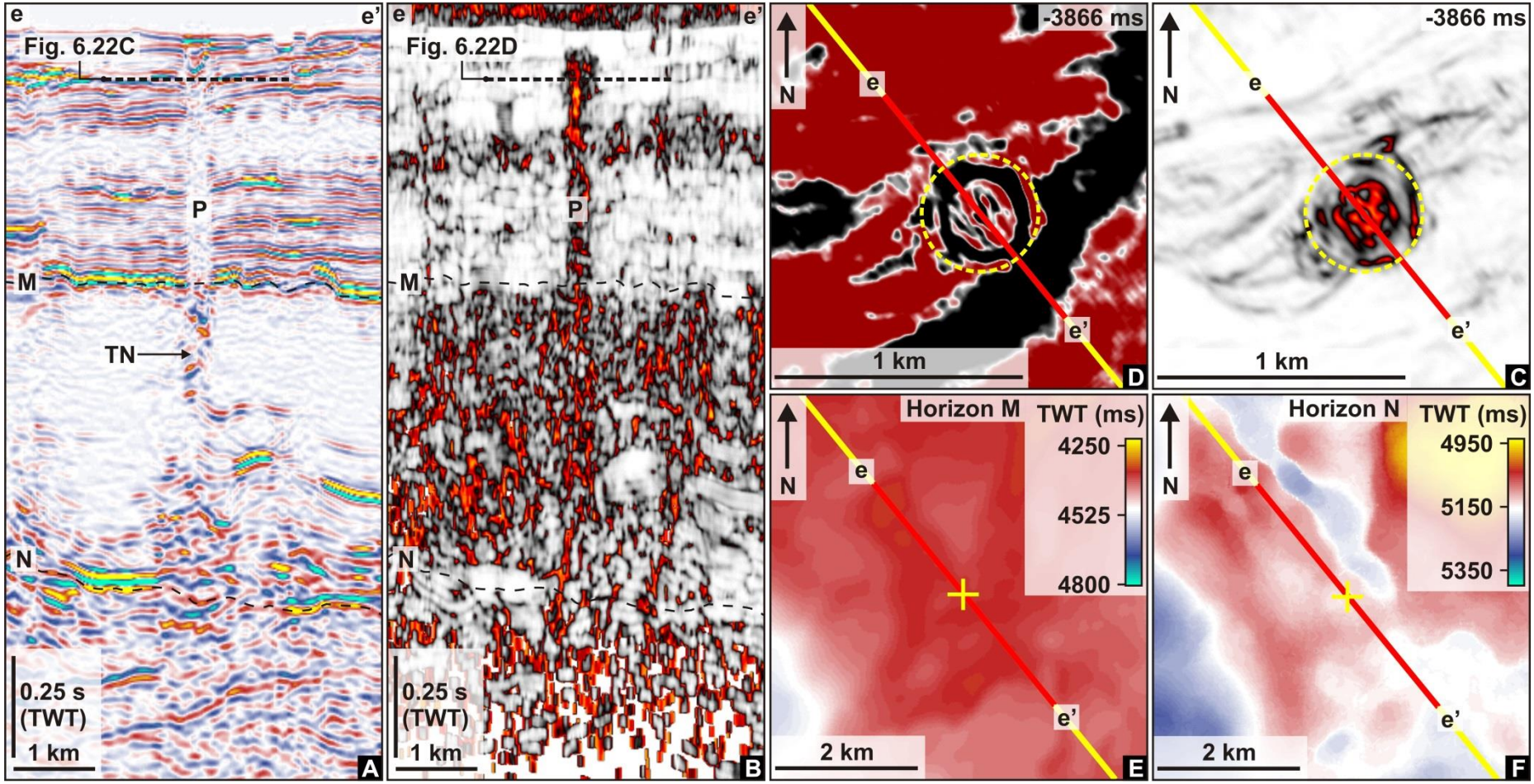

Figure 6.22 Defining a fluid escape pipe and the underlying top and base-salt geometry. A: A seismic profile through a fluid escape pipe. B: A variance profile through a fluid escape pipe. The line of section is the same as in Figure 6.22A. C: A time slice through the fluid escape pipe. D: A variance slice through the fluid escape pipe (The pipe is highlighted by the circle with a yellow dashed line in Figure 6.22C and Figure 6.22D). E: A time map of Horizon M. F: A time map of Horizon N (The yellow + marks the location of the overlying pipe in Figure 6.22E and Figure 6.22F). P - Pipe; TN – Trail of noise; M – Horizon M; N – Horizon N. (The seismic profile and variance slice are both 5 times vertically exaggerated here)

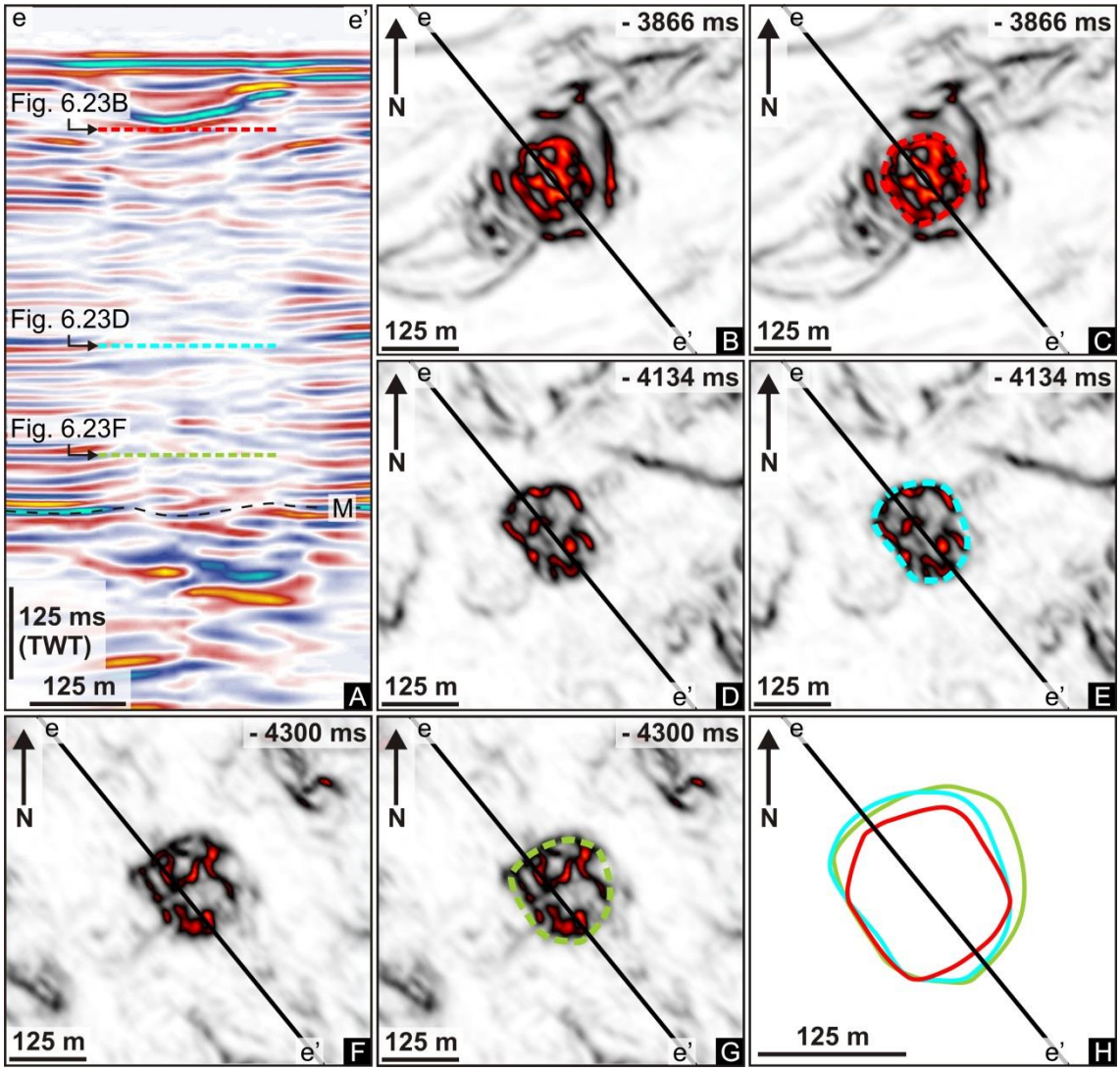

Figure 6.23 Geometry of a fluid escape pipe. A: Seismic profile through a fluid escape pipe. B: Variance profile through the fluid escape pipe in Figure 6.23A. C: Interpretation of the pipes margins from the variance profile in Figure 6.23B. D: Variance profile through the fluid escape pipe in Figure 6.23A. E: Interpretation of the pipes margins from the variance profile in Figure 6.23D. F: Variance profile through the fluid escape pipe in Figure 6.23A. G: Interpretation of the pipes margins from the variance profile in Figure 6.23F. H: Stacked outlines of the pipes margins from Figure 6.23C, Figure 6.23E and Figure 6.23G, showing the 3D geometry of the fluid escape pipe. M – Horizon M; TWT – Two way time.

are characterised by a generally circular area of disruption and discontinuity (Figure 6.22C and Figure 6.22D). A planform geometry that is circular can be observed in the variance slice near the upper terminus of the pipe (Figure 6.23C). A more sub-circular geometry in planform can be observed around the mid region on the pipe (Figure 6.23E). The pipes geometry in planform becomes more circular again nearer Horizon M (Figure 6.23G). Its overall form is sub-vertical and displays a geometry in planform that varies up the height of the structure (Figure 6.23H).

The fluid escape pipe has been interpreted to extend from 4500 ms TWT at Horizon M to its upper terminus at 3900 ms TWT (Figure 6.24). The height of the pipe between Horizon M and its upper terminus is c. 705 m and its width ranges from c. 145 m to 240 m. Similar to the two previously described examples, the upper terminus of this pipe is characterised by a circular depression that is localised and has a maximum relief of 44 ms TWT (Figure 6.24). Enhanced reflections can be seen overlying the upper terminus of this pipe also and a break in the continuity of the reflection of Horizon M is clear in seismic profile (Figure 6.24B). The location of this pipe is situated near the margins of a base-salt and a top-salt depression (Figure 6.25E and Figure 6.25F). The variance slice in Figure 6.26G shows that the planform geometry of this pipe is elliptical near Horizon M. Towards the mid region of the pipe, its planform area increases (Figure 6.26E) before decreasing again nearer its upper terminus (Figure 6.26C). Figure 6.26H demonstrates that the planform geometry of the pipe is variable up its height and that the structure is sub-vertical.

All of the examples described above display a localised depression at the upper terminus of the pipe which has been buried. The example in Figure 6.27 displays a fluid escape pipe with the same defining seismic characteristics and geometry described in the previous examples; however the depression at its upper terminus is not buried and has formed a maximum relief of 110 ms TWT at the present day seafloor. This depression displays circular to elliptical planform geometry and increases in depth towards its centre (Figure 6.27B). Similar to the previously described examples, there is a clear break in the continuity of the reflection of Horizon M (Figure 6.27A). Beneath this break in reflection continuity, a vertical trail of noise transects the evaporites from

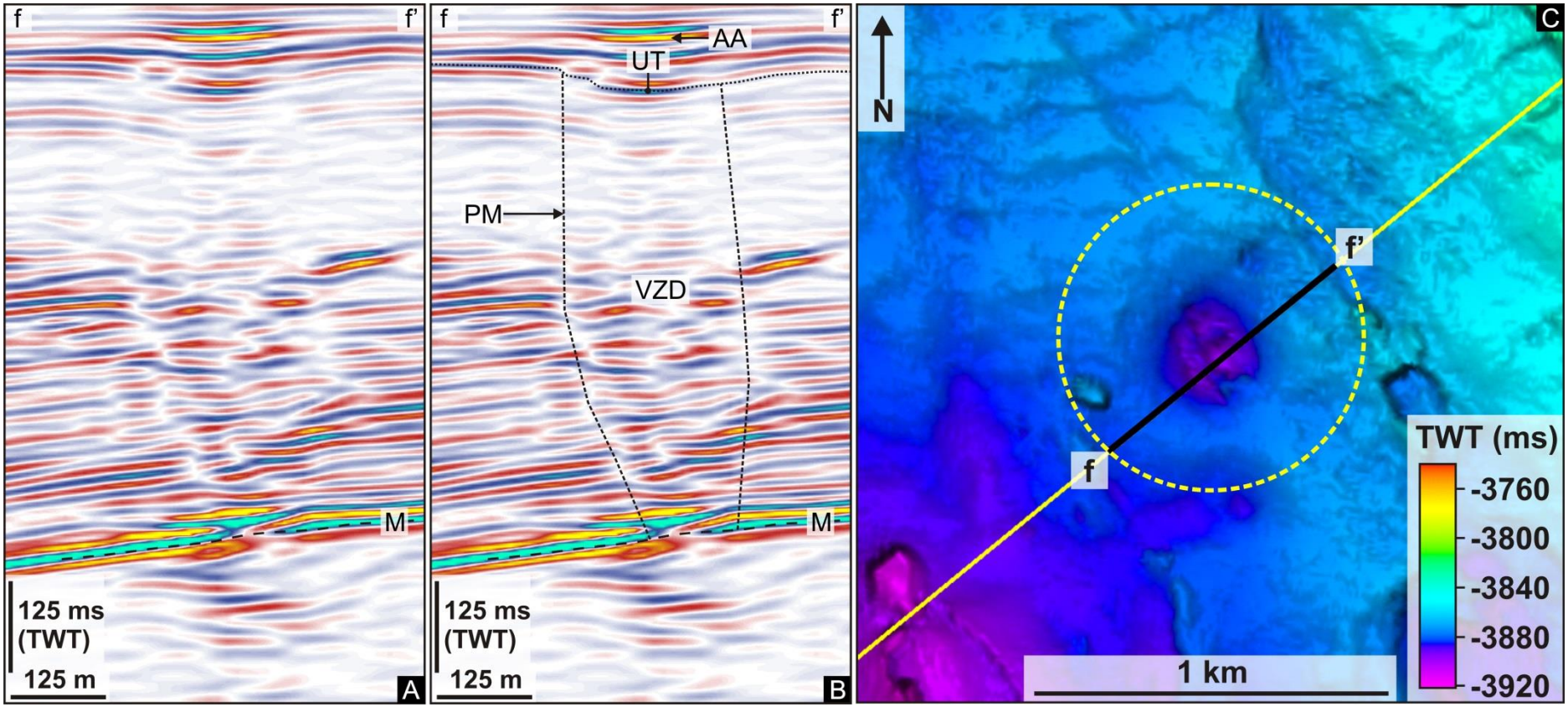

Figure 6.24 Seismic expression of a fluid escape pipe and a horizon map of its upper terminus. A: An un-interpreted seismic profile through a fluid escape pipe. B: An interpreted profile of the fluid escape pipe in Figure 6.24A. C: A TWT horizon map of the reflection of the fluid escape pipes upper terminus. VZD – Vertical zone of discontinuity; UT – Upper terminus; PM – Pipe margin; AA – Amplitude anomaly; M – Horizon M; N – Horizon N; TWT – Two way time.

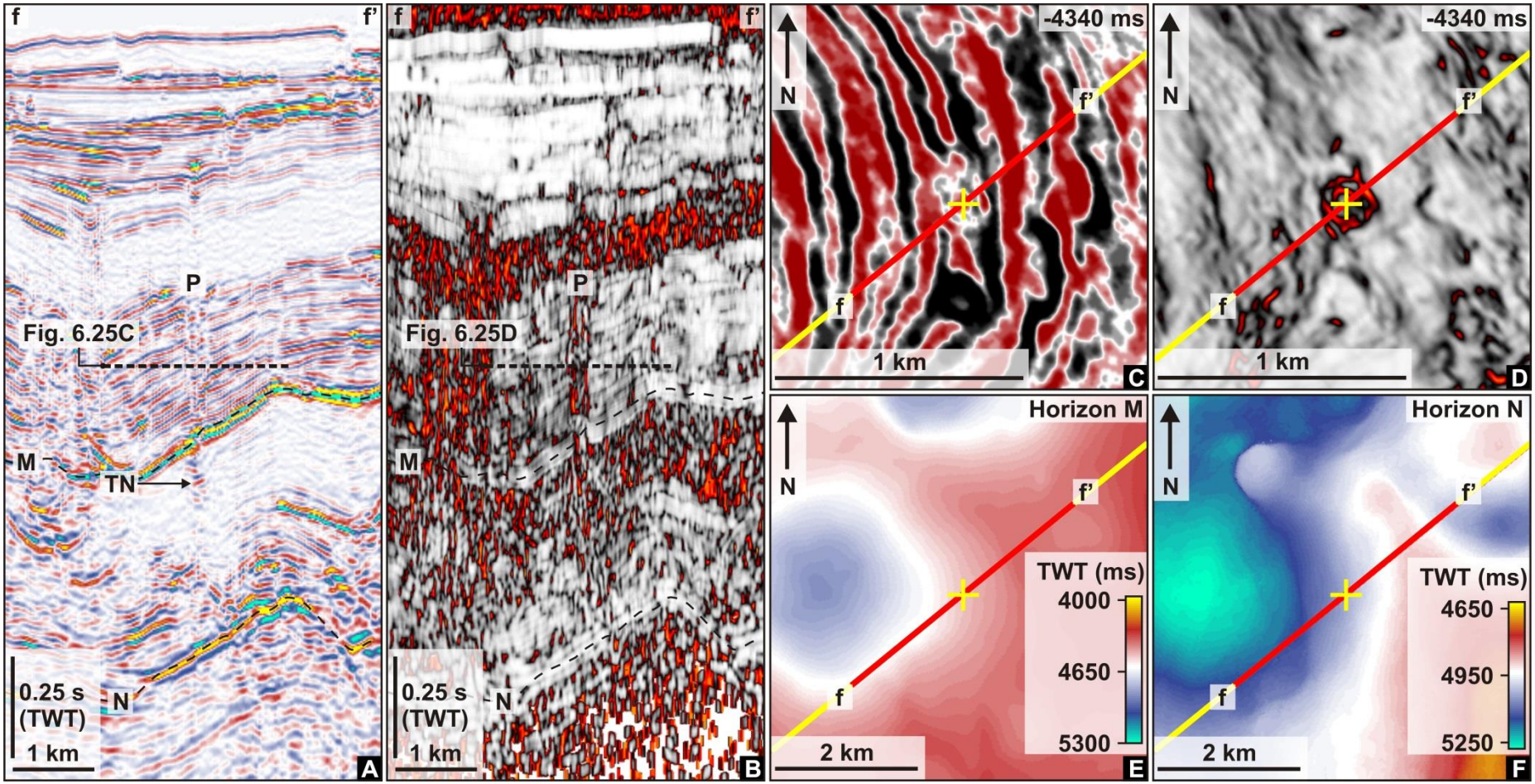

Figure 6.25 Defining a fluid escape pipe and the underlying top and base-salt geometry. A: A seismic profile through a fluid escape pipe. B: A variance profile through a fluid escape pipe. The line of section is the same as in Figure 6.25A. C: A time slice through the fluid escape pipe. D: A variance slice through the fluid escape pipe (The pipe is highlighted by the circle with a yellow dashed line in Figure 6.25C and Figure 6.25D). E: A time map of Horizon M. F: A time map of Horizon N (The yellow + marks the location of the overlying pipe in Figure 6.25E and Figure 6.25F). P - Pipe; TN – Trail of noise; M – Horizon M; N – Horizon N. (The seismic profile and variance slice are both 5 times vertically exaggerated here)

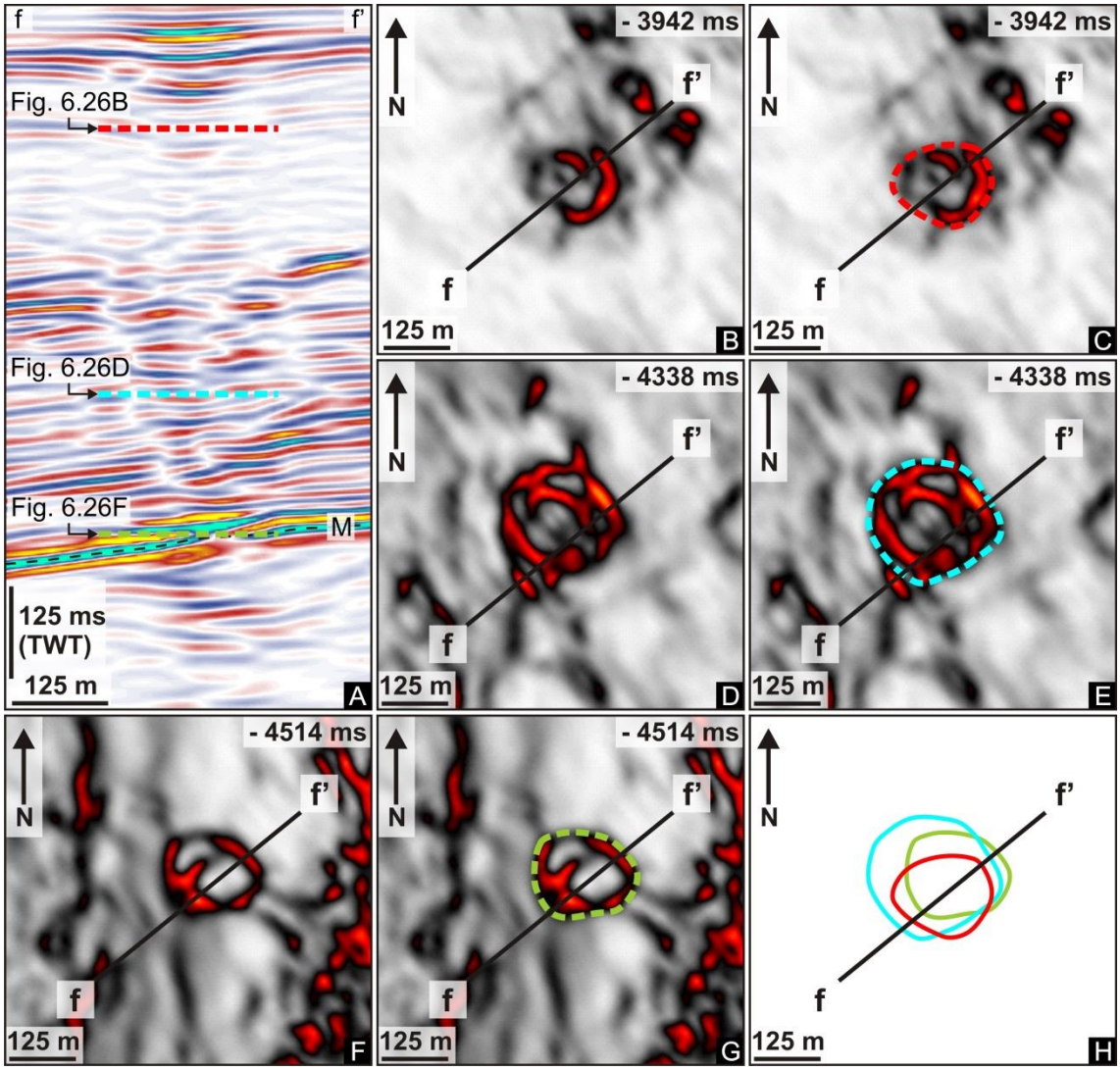

Figure 6.26 Geometry of a fluid escape pipe. A: Seismic profile through a fluid escape pipe. B: Variance profile through the fluid escape pipe in Figure 6.26A. C: Interpretation of the pipes margins from the variance profile in Figure 6.26B. D: Variance profile through the fluid escape pipe in Figure 6.26A. E: Interpretation of the pipes margins from the variance profile in Figure 6.26D. F: Variance profile through the fluid escape pipe in Figure 6.26A. G: Interpretation of the pipes margins from the variance profile in Figure 6.26F. H: Stacked outlines of the pipes margins from Figure 6.26C, Figure 6.26E and Figure 6.26G, showing the 3D geometry of the fluid escape pipe. M – Horizon M; TWT – Two way time.

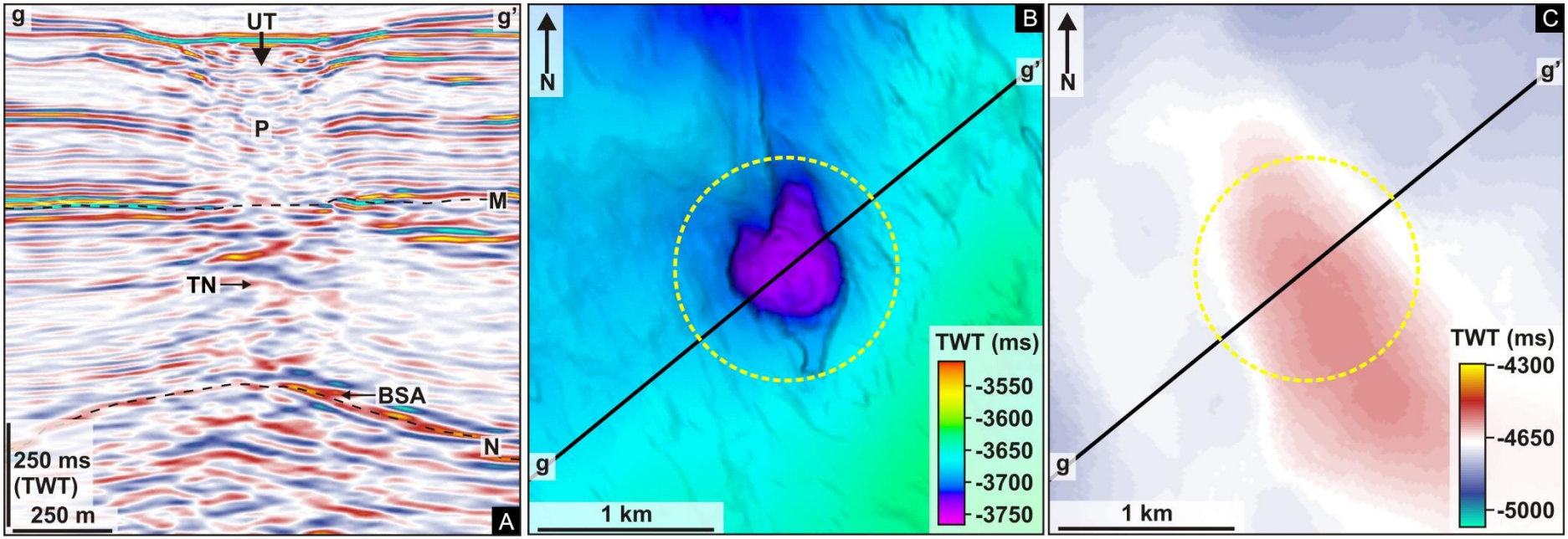

Figure 6.27 Fluid escape pipe and seafloor venting. A: Seismic profile through a fluid escape pipe. B: Time map of the seafloor showing the change in relief associated with the upper terminus of the pipe. C: Time map of Horizon N directly beneath the fluid escape pipe within the Pliocene to Recent succession and the trail of noise that transects the evaporites. P – Pipe; UT – Upper terminus; TN – Trail of noise; BSA – Base-salt anticline; M – Horizon M; N – Horizon N; TWT – Two way time.

Horizon M to Horizon N (Figure 6.27A). A Horizon map of Horizon N directly beneath the overlying fluid escape pipe displays an anticlinal geometry (Figure 6.27C).

6.3.4 Shallow amplitude anomalies

In all of the examples of fluid escape pipes described above, an amplitude anomaly was observed overlying their upper terminus. The next section will focus in greater detail on describing shallow amplitude anomalies within this study area. The colour bar used in this chapter has been modified in comparison to those used in Chapters 4 and 5. This modified colour bar is well suited to the identification and analysis of anomalies of high amplitude because it reduces the prominence of background reflectivity and allows very high amplitude reflections to stand out. In this colour scale, red/yellow is negative and blue/turquoise is positive. The highest amplitude values will be displayed as either yellow or turquois. A selection of the many shallow amplitude anomalies are described below. These were selected to allow a description of the full range of seismic characteristics observed in the survey area. Their location can be seen in Figure 6.8.

A fluid escape pipe with a stack of localised high amplitude anomalies directly above the upper terminus is displayed in the example in Figure 6.28. The bright yellow reflection between the two blue reflections is a soft reflection of high amplitude located 74 ms TWT beneath the seafloor. The margins of the amplitude anomaly are abrupt and correlate with the horizontal margins of a vertical zone of amplitude attenuation or blanking within the fluid escape pipe beneath (Figure 6.28B). A localised anomaly, which has a sub-circular shape, with a maximum width of c. 500m can be observed in a horizon map that displays amplitude of the soft reflection and hosting succession (Figure 6.28C). Its amplitude is greatest at its centre and decreases towards its margins.

A more regional-scale seismic profile of the seismic profile through the pipe in Figure 6.28 can be seen in Figure 6.29A. A larger shallow amplitude anomaly up dip of the one described in Figure 6.28 is observed 18 ms TWT beneath the seafloor (Figure

6.29A). This shallow amplitude anomaly shares all of the same seismic characteristics as the one in Figure 6.28 including a high amplitude soft reflection, a sharp cut-off in amplitude at its margins and a zone of amplitude attenuation beneath (Figure 6.29A). In contrast though, this amplitude anomaly does not directly overlie a fluid escape pipe, but, it is located up dip and in close association to the pipe in Figure 6.28. Without any obscuring elements of a fluid escape pipe directly beneath, the large area of amplitude attenuation is very clear (Figure 6.29A). Similarly, the margins of this zone of amplitude attenuation correlate with the margins of the overlying amplitude anomaly and the blanking effect decreases with depth (Figure 6.29A). The shape of this localised amplitude anomaly is irregular and it has a maximum width of 980 m (Figure 6.29B).

The final example of a shallow amplitude anomaly in Figure 6.30 shows a fluid escape pipe with a soft reflection of high amplitude overlying its upper terminus, similar to the example in Figure 6.28. This amplitude anomaly is located 40 ms TWT beneath the seafloor. Beneath the soft reflection there is also a zone of amplitude attenuation, the margins of which correlate with the margins of the soft reflection (Figure 6.30A). In contrast to the example in Figure 6.28, the underlying fluid escape pipe is not located centrally beneath the amplitude anomaly (Figure 6.30). It has a planform geometry that is irregular and extends to the southeast away from the fluid escape pipe that it overlies (Figure 6.30C). It has a maximum width of 1240 m (Figure 6.30C).

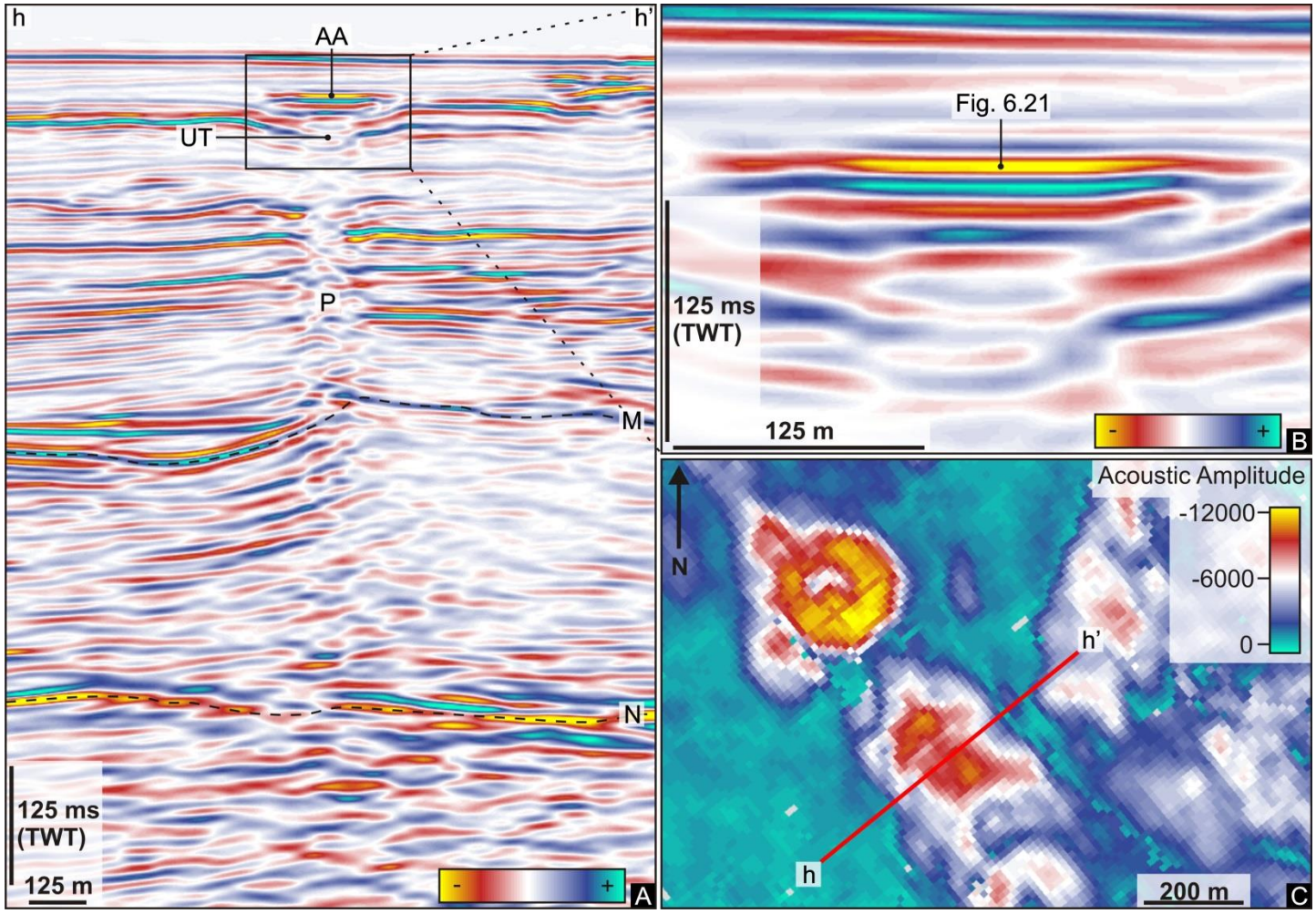

Figure 6.28 Shallow amplitude anomaly above a fluid escape pipe. A: A seismic profile of a fluid escape pipe with an amplitude anomaly overlying its upper terminus. B: A zoomed in seismic profile of the amplitude anomaly in Figure 6.28A. C: An amplitude map of the amplitude anomaly in Figure 6.28B. P – Pipe; UT – Upper terminus; AA – Amplitude anomaly; M – Horizon M; TWT – Two way time.

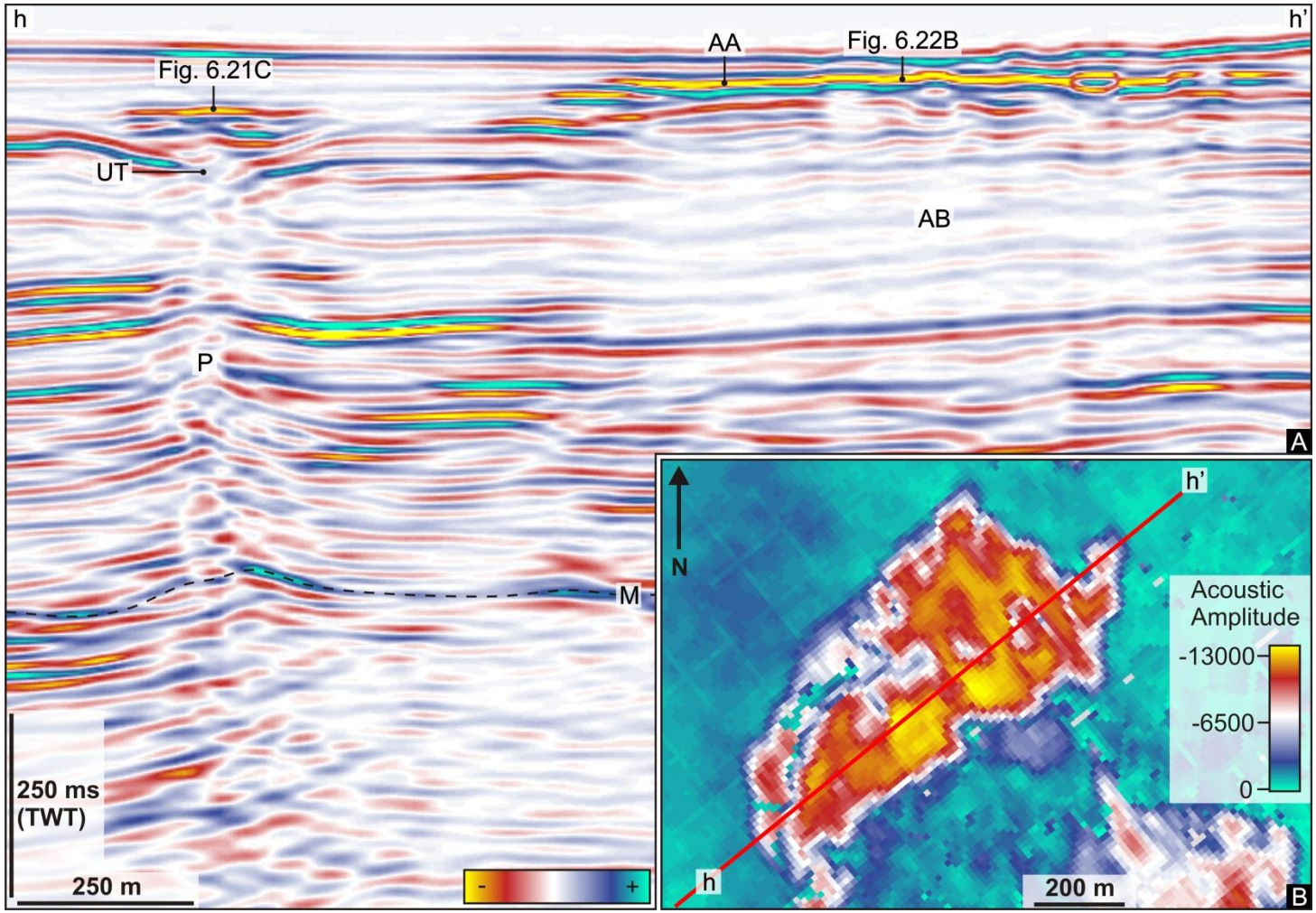

Figure 6.29 Shallow amplitude anomaly located in close association to a fluid escape pipe. A: A more zoomed out seismic profile of the fluid escape pipe in Figure 6.28A. Up dip of the upper terminus of the fluid escape pipe an amplitude anomaly is visible, beneath which there is a zone of amplitude blanking. B An amplitude map of the amplitude anomaly in Figure 6.29A. P – Pipe; UT – Upper terminus; AA – Amplitude anomaly; AB – Amplitude blanking; M – Horizon M; TWT – Two way time.

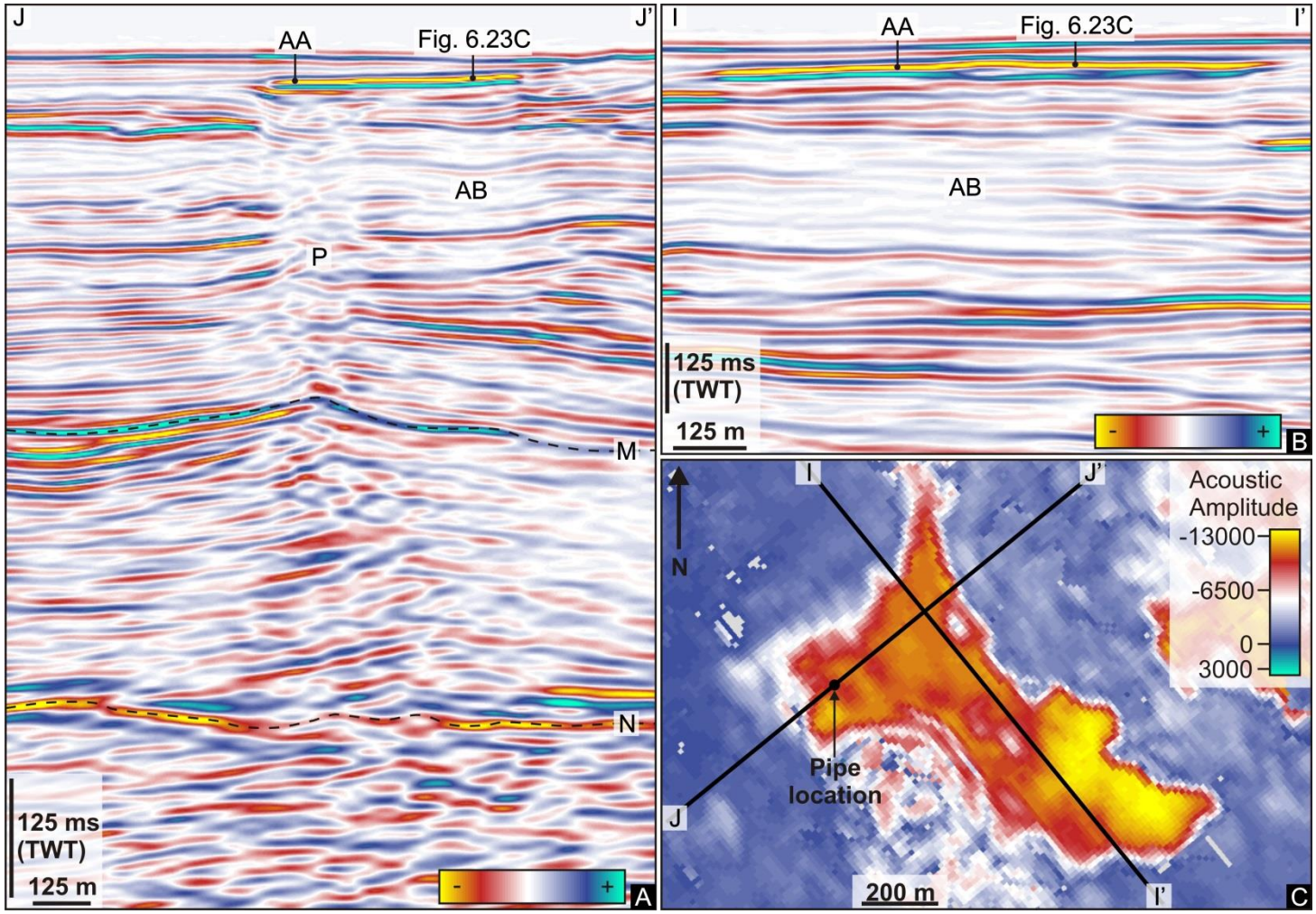

Figure 6.30 A shallow amplitude anomaly overlying a fluid escape pipe. A: A seismic profile of a fluid escape pipe with an amplitude anomaly overlying its upper terminus. B: A perpendicular line of section (Figure 6.30C) through the amplitude anomaly in Figure 6.30A. C: An amplitude map of the amplitude anomaly in Figure 6.30A and Figure 6.30B. P – Pipe; UT – Upper terminus; AA – Amplitude anomaly; AB – Amplitude blanking; M – Horizon M; TWT – Two way time.

6.3.4.1 Summary and interpretation

The features described in 6.2.3 of this chapter are interpreted as fluid escape pipes because: (1) they are vertically extensive features that transect large sections of the stratigraphic succession; (2) they are seismically expressed as a vertical zone of amplitude attenuation and breaks in the continuity of reflection of the host stratigraphy; (3) they are localised features that exhibit planform geometry that ranges from circular to elliptical.

The lateral margins of these pipes can be interpreted as the edge of a clear area of discontinuity. Variance profiles are effective in imaging these margins and demonstrate that their planform is variable up the height of the pipe, varying from elliptical, to circular, to sub circular. They are vertical to sub vertical and display a crudely cylindrical geometric form. These seismic characteristics and geometry are comparable to other documented examples of fluid escape pipes (Figure 6.2) (Berndt, 2005; Moss and Cartwright, 2010a; Løseth et al., 2001; Hustoft et al., 2007). Their defining seismic characteristics and geometry are also very similar to those exhibited by the mud volcano conduits.

In all of the examples, the deepest reflection to show a break in continuity within the pipes vertical zone of disruption is Horizon M. Additionally no continuous reflection can be observed crossing beneath the vertical stack of breaks in reflection continuity within the Pliocene to Recent succession. This means that similar to the mud volcano conduits, these fluid escape pipes have at least in part ascended through the evaporite succession. Similarly, the root zone of these pipes cannot be observed; however evidence that these pipes have transected Horizon M is indicative of a pre-Pliocene fluid origin. In contrast to the mud volcano conduits, the position of these fluid escape pipes is not always superimposed directly above either a top-salt or base-salt depression. The relationship between these fluid escape pipes and top-salt and base-salt depressions will be discussed further in section 6.2.5.

The upper terminus of these fluid escape pipes is interpreted in all cases to be characterised by a pockmark, which is defined by: (1) a reflection that crosses above

the pipe and is high amplitude, continuous and concave; (2) a bowl shaped erosional depression or crater with erosional truncation of underlying reflections characteristically seen at the margins of the crater; (3) depression geometry that is localised and elliptical, to circular, to sub-circular in planform. The observed truncation of reflections is caused by the removal of seabed sediments by the escaping fluids (Judd and Hovland, 1992). Buried pockmarks display similar geometrical and seismic characteristics to those at the present day seafloor. The onlap of reflections onto the inner side of the bowl shaped pockmarks is the result of infill of the pockmark crater (Moss and Cartwright, 2010a).

Pockmarks such as these are commonly documented in association with the upper terminus of fluid escape pipes in other basins (Moss and Cartwright, 2010a; Hustoft et al., 2009; Løseth et al., 2011; Berndt, 2005; Cartwright et al., 2007; Cathles et al., 2010). The connection of the pockmark with the upper terminus of the pipe demonstrates that there is a clear link between the formation of the pipe and the formation of the pockmark, as first described by (Løseth et al., 2001). Pockmarks are known to form at the seafloor and are universally viewed as fluid venting features resulting from vertical focused flow and expulsion of fluids from shallow reservoirs (Judd and Hovland, 2007).

The pockmarks presented here represent structures that formed during an episode of fluid venting at times that are effectively defined by the crater position (Hustoft et al., 2009; Løseth et al., 2011; Moss et al., 2012; Berndt, 2005; Cathles et al., 2010; Cartwright, 2007). The interpretation of the upper terminus of a fluid escape pipe and pockmark within the stratigraphic succession is, therefore, important in order to identify specific periods of fluid venting. The examples of fluid escape pipes and pockmarks presented above display upper terminations at various levels within the Pliocene to Recent interval. The interpretation of pockmarks ranges from those that are buried as deep as only 108 ms TWT above the top salt reflection of Horizon M, to those observed at the present day seafloor. It is clear that seafloor fluid venting has occurred at numerous intervals throughout Pliocene to Recent times. The example in Figure 6.18 represents the deepest pockmark that has been interpreted within this study.

Shallow amplitude anomalies are frequently observed in close spatial association to the upper terminations of fluid escape pipes within this study area, as demonstrated in the examples above in section 6.2.4. The amplitude anomalies described are recognisable as irregularly shaped areas of strong amplification in comparison to the background reflectivity of the Pliocene to Recent succession. They have a soft-amplitude response and have amplitude values that are an order of magnitude greater than those of the background amplitude values. These amplitude anomalies display a sharp cut-off in amplitude at their margins. The seismic characteristics described here conform to the description of seismic amplitude anomalies that are referred to as bright spots (Løseth et al., 2009; Brown et al., 2004; Foschi et al., 2014; Barry and Shugart, 1974).

Amplitude attenuation directly beneath these bright spots is here recognisable as a zone of dimming and reduced clarity in the reflections of the underlying stratigraphy. This sharp cut-off in amplitude that is observed at the margins of the bright spot is also correlatable with the margins of the underlying zones of amplitude attenuation. This argues strongly that the amplitude attenuation that is observed is related to the overlying bright spot. A dimming effect such as this could be considered to be due to the differential absorption of frequencies within gas charged layers, often observed in association with gas chimneys and other gas charged structures (Sun et al., 2012; Wu and Liu, 2009; Foschi et al., 2014). These observations are consistent with previously described examples of bright spots associated with free gas (Foschi et al., 2014; Løseth et al., 2009; Sun et al., 2012) and helps build a case that these shallow amplitude anomalies are in fact direct hydrocarbon indicators (DHI's).

6.3.5 Fluid escape pipe distribution

In Chapters 4 and 5, it was discussed that mapping of Horizon M and N revealed numerous sub-circular to irregular depressions. In Chapter 5, spatial and statistical analysis of the location of mud volcanoes relative to base-salt and top-salt depressions was undertaken. Mud volcanoes were categorised based on whether

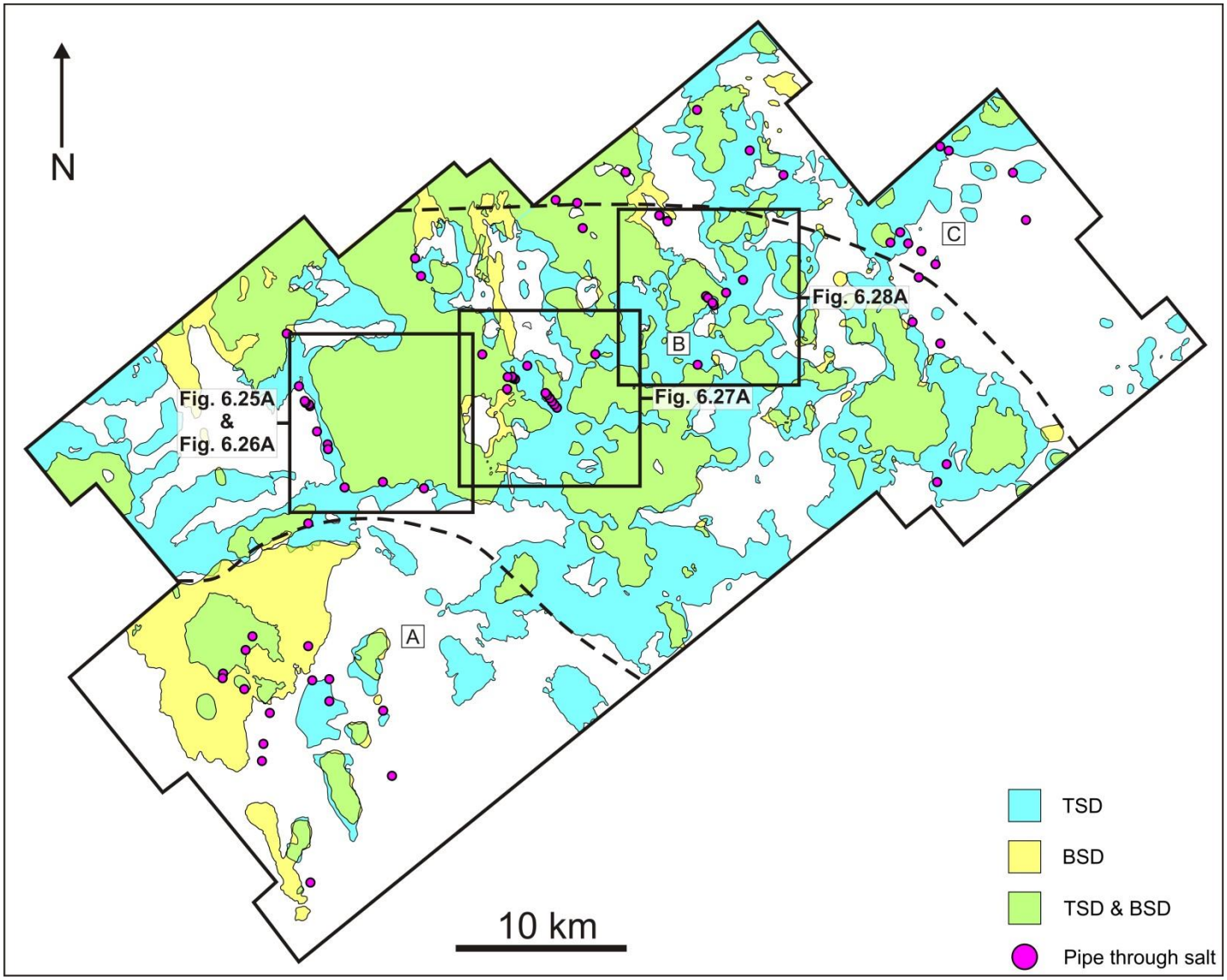

Figure 6.31 Fluid escape pipe locations and top and base-salt depressions. A map showing the outlined full extent of all base-salt depressions (Yellow) and top-salt depressions (Blue). Frequently top-salt depression directly overlie base-salt depressions (Green). The location all the fluid escape pipes observed within this study area are plotted in relation to the top and base-salt depressions. The circles on the map merely represent the location of the fluid escape pipes. The circular shape and diameter of these data points is not a reflection of their geometry. The locations of the zoomed in maps in Figure 6.32, Figure 6.33, Figure 6.34 and Figure 6.35 and displayed. TSD – Top-salt depression; BSD – Base-salt depression.

	Domain A	Domain B	Domain C
Number of pipes	15	46	16

Table 6.1 Pipes distributed within the various study area domains. Domains are divided based on criteria set in Chapters 4 and 5. Domain A: growth fault dominated region. Domain B: is fluid escape feature dominated region. Domain C: Modern channel and levee complex dominated region.

	TSD and BSD	TSD no BSD	BSD no TSD	No TSD or BSD
Number of pipes	30	23	1	23

Table 6.2 Pipe locations associated with depressions. TS and BS: A pipe with both a top and base-salt depression beneath. TS no BS: A pipe with a top-salt depression but not a base-salt depression beneath. BS no TS: A pipe with a base-salt depression but no top-salt depression beneath. No TS or BS: A pipe with neither a top or base-salt depression. TSD – Top-salt depression; BSD – Base-salt depression.

beneath them there was: (1) a top and base-salt depression; (2) a top-salt depression but not a base-salt depression; (3) a base-salt depression but not a top-salt depression and; (4) neither a top or base-salt depression. This analysis found that statistically 85% of mud volcanoes (out of 396) are found directly above both and base and top-salt depression. There is therefore a strong correlation between the location of mud volcanoes and top and base-salt depressions.

Within this section, the spatial distribution of fluid escape pipes within this study area will be described, similar to that which was previously carried out with regards to mud volcanoes in Chapter 5. Using 3D seismic data, the X and Y for the location of each pipe, of which there are 77, was recorded as the point which is at the centre of each pipe Figure 6.31. The location of fluid escape pipes will be placed contextually in relation to the top and base-salt depressions, in order to ascertain what impact, if any, the formation of fluid escape pipes has had on the pre-salt stratigraphy and evaporite succession. The distribution of fluid escape pipes and relationship with top and base-salt depression will then be compared and contrasted to the relationship observed in the location of mud volcanoes.

In Chapter 5, the study area was divided into 3 domains, Domain A, B and C, the rational for which was explained in section 5.4.3. It was observed in Chapter that Domain B contains the greatest concentration of mud volcanoes. Comparatively, both Domain A and C contain only a very small number of mud volcanoes. The 77 fluid escape pipes within this study area are distributed in a variety of configurations, from clustered and irregular patterns to linear trails which will be described below. Similarly to the mud volcanoes, the greatest number of fluid escape pipes (46 pipes) is found within Domain B (Table. 6.1).

The analysis of fluid escape pipes in relation to top and base-salt depression (Table 6.2) shows that 30 fluid escape pipes are located overlying a combined top and base-salt depression. This means that similar to as observed with the mud volcanoes, the majority of fluid escape pipes (39%) overlie a combined top and base-salt depression. This is, however, a significantly smaller proportion than was observed in mud volcanoes. Only 1 fluid escape pipe was located overlying a base-salt depression

but not a top-salt depression and 23 are located with a top-salt depression but no base-salt depression. The greatest contrast in results between the analysis of the location of mud volcanoes and fluid escapes is associated with areas where there is neither a top or base-salt depression. The analysis of the location of mud volcanoes in Chapter 5 showed that very few mud volcanoes (10) overlie neither a top or base-salt depression. The analysis here of fluid escape pipes shows that 23 pipes do not overlie either a top or a base-salt depression.

The location of fluid escape pipes in association with base and top-salt depression is analysed in greater detail in a less regional scale section of the study area in Figure 6.32. A large top-salt depression can be observed overlying a large base-salt depression and a total of 11 fluid escape pipes are interpreted in this area (Figure 6.32). All of these fluid escape pipes are situated predominantly around the periphery of these depressions and not central of them (Figure 6.32). A large top-salt depression above which several mud volcanoes overlie can be observed in seismic profile through the depression in this area (Figure 6.32B). Directly beneath this top salt depression the base-salt is also highly depressed (Figure 6.32B). The base-salt reflection of Horizon N is angled upwards towards the SW until its margins, where a convex geometry is observed (Figure 6.32B). Directly above the margin of the depression, a vertical zone of breaks in reflection continuity, disruption and low amplitude define a fluid escape pipe within the Pliocene to Recent succession. The deepest break in reflection continuity is observed at Horizon M. A trail of noise can be observed transecting the evaporites between the margin of the depression at Horizon N and the first break in the continuity of the reflection of Horizon M. A horizon map of the seafloor displays a sub-circular pockmark depression at the upper terminus of the pipe (Figure 6.32C). A similar example can be seen in Figure 6.33; however, the upper limit of this fluid escape pipe terminates in a pockmark that is buried.

Another smaller sub-region of the study area highlights a linear trail of pipe data points (Figure 6.34A). This linear trail of data points trends in a NW to SE orientation. No corresponding NW to SE linear trend of top or base-salt depressions can be observed. A clearly defined NW to SE trending zone of discontinuity can be observed in variance slice through the Pliocene to Recent interval (Figure 6.34B).

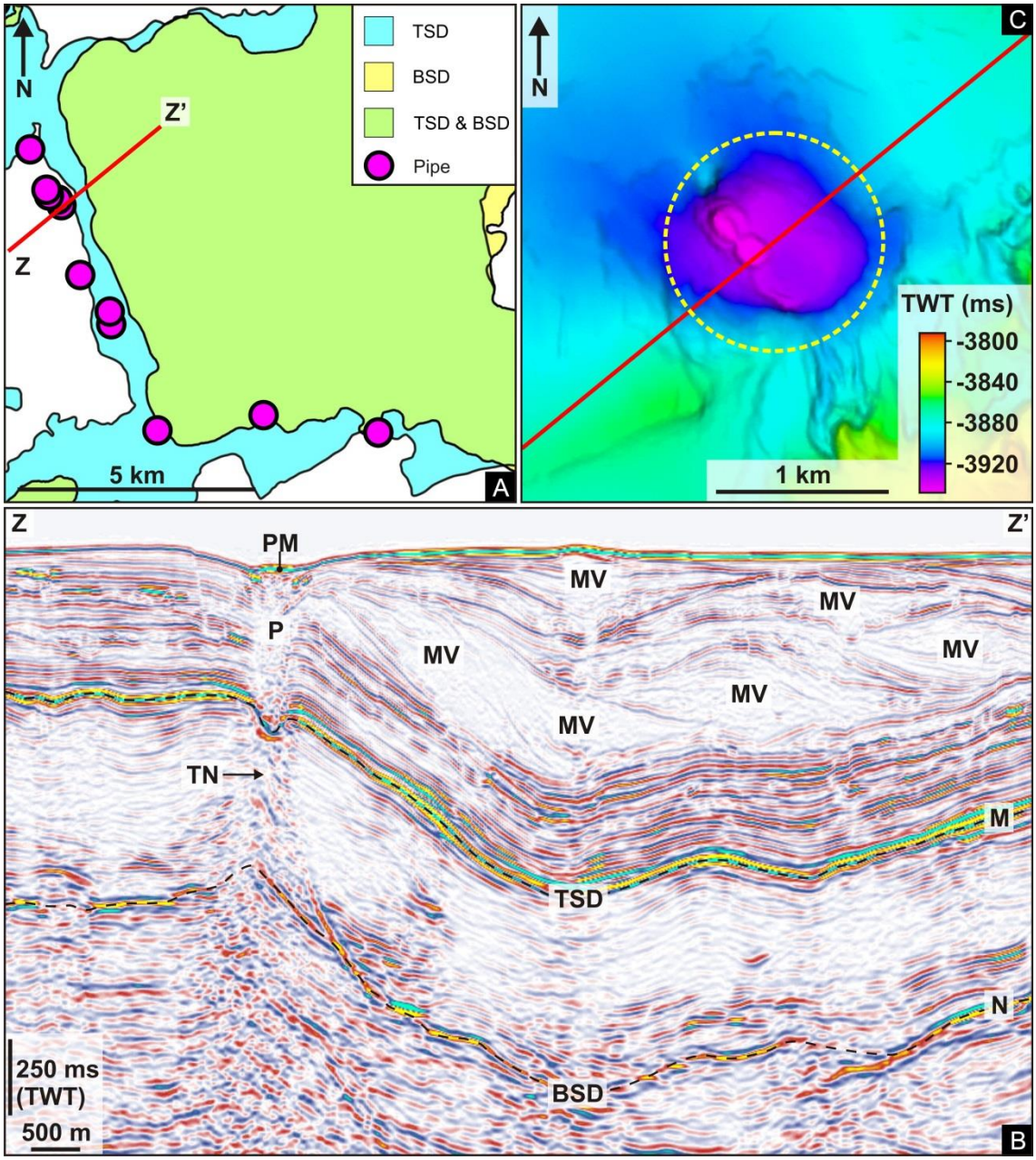

Figure 6.32 The location of fluid escape pipe in relation to top and base-salt depressions. A: A smaller region of the study area in Figure 6.31 showing location of fluid escape pipes around the periphery of top and base-salt depressions. B: A seismic profile through a fluid escape pipe showing the pipe overlying the margin of a large base-salt depression. C: A seafloor map that displays the change a change in relief associated with a pockmark at the upper terminus of the fluid escape pipe in Figure 6.32. P – Pipe; PM – Pockmark; MV – Mud volcano; TN – Trail of noise; TSD – Top-salt depression; BSD – Base-salt depression; M – Horizon M; N – Horizon N; TWT – Two way time.

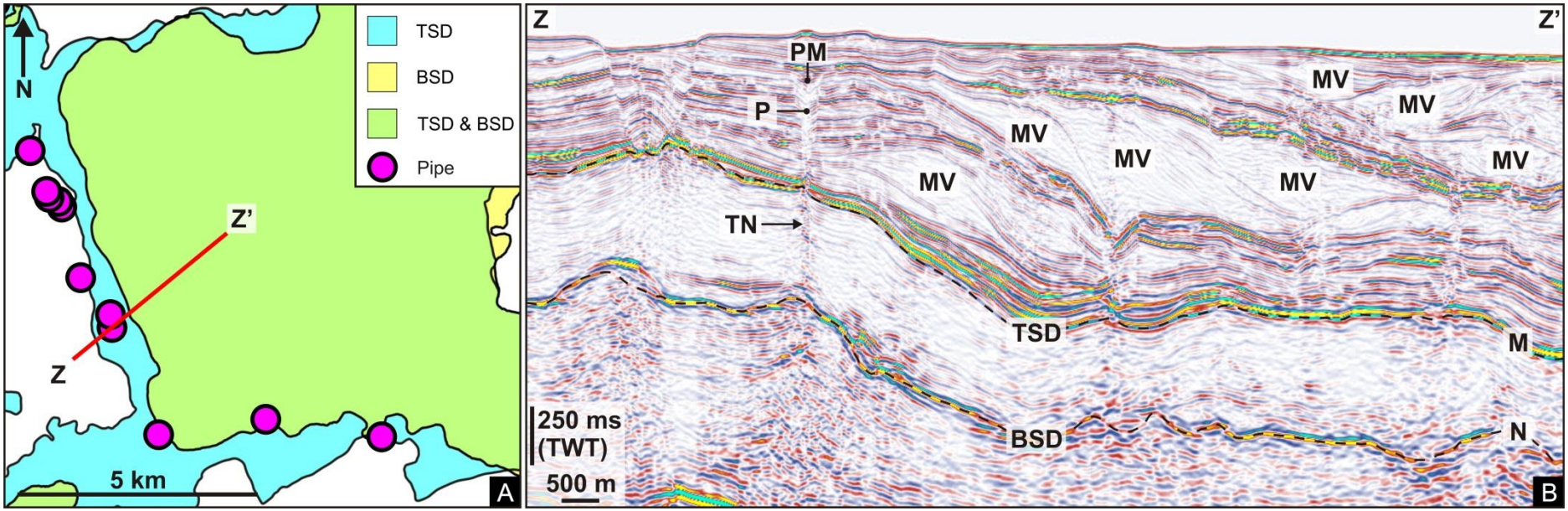

Figure 6.33 Fluid escape pipe locations in relation to top and base-salt depressions. A: A zoomed in section of the map in Figure 6.31 showing location of fluid escape pipes around the periphery of top and base-salt depressions. B: A seismic profile through a different fluid escape pipe to the one in Figure 6.32, showing the pipe overlying the margin of a large base-salt depression. P – Pipe; PM – Pockmark; MV – Mud volcano; TN – Trail of noise; TSD – Top-salt depression; BSD – Base-salt depression; M – Horizon M; N – Horizon N; TWT – Two way time.

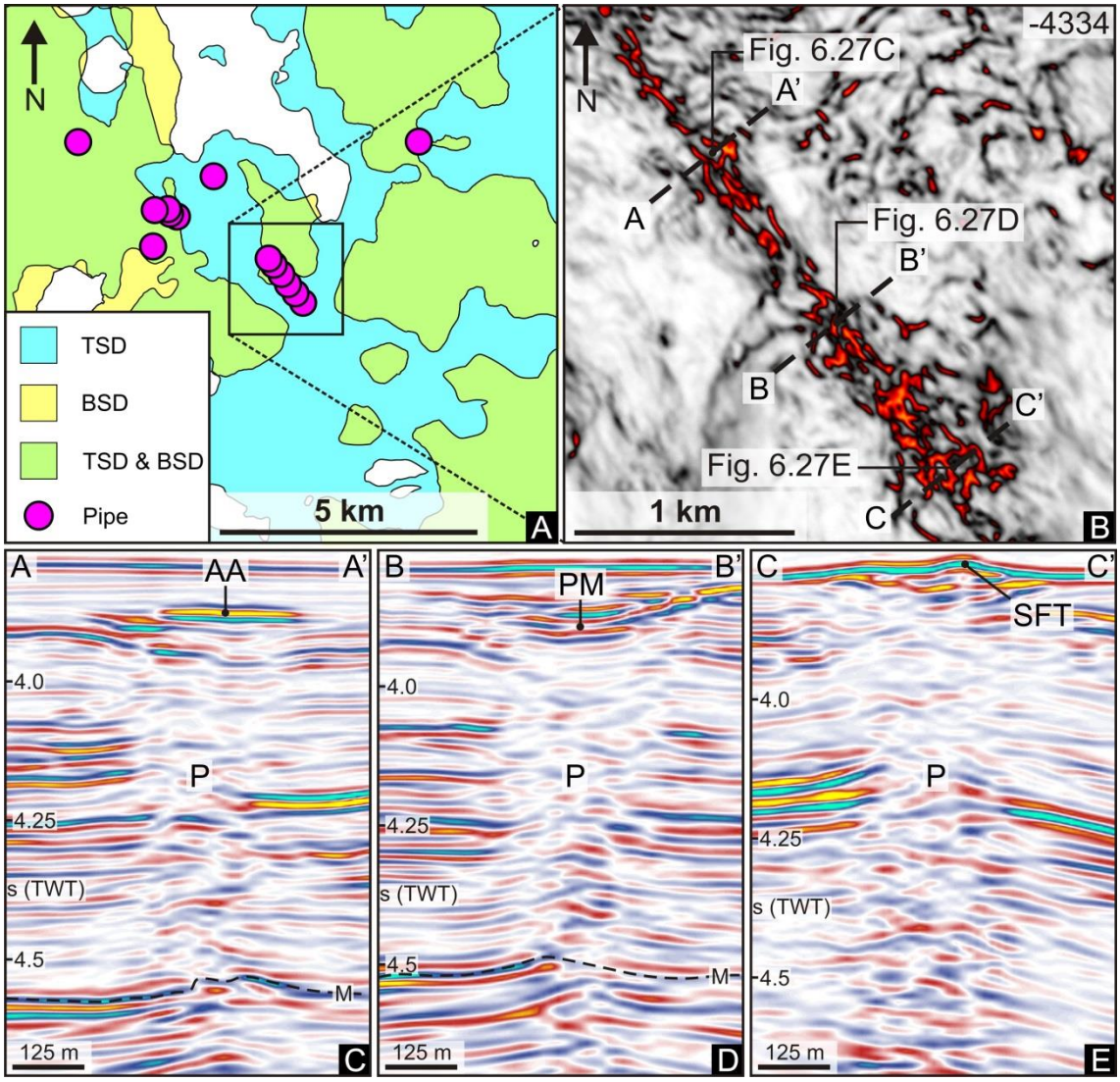

Figure 6.34 Linear trail of pipes. A: A zoomed in section of the map from Figure 6.31 showing top and base-salt depressions and fluid escape pipe data points. The box around a linear trail of pipes is the location of the variance slice in Figure 6.34B. B: A variance slice at -4334 ms through the Pliocene to Recent succession, through a linear trail of pipes. Lines of section for Figure 6.34C, Figure 6.34D and Figure 6.34E are displayed. C: Seismic profile of a pipe with an amplitude anomaly overlying the upper terminus of the pipe. D: Seismic profile of a pipe with a pockmark at its upper terminus. E: A seismic profile of a pipe which has built topography at its upper terminus at the seafloor. P – Pipe; PM – Pockmark; AA – Amplitude anomaly; SFT; Seafloor topography; TSD – Top-salt depression; BSD – Base-salt depression; M – Horizon M; TWT – Two way time.

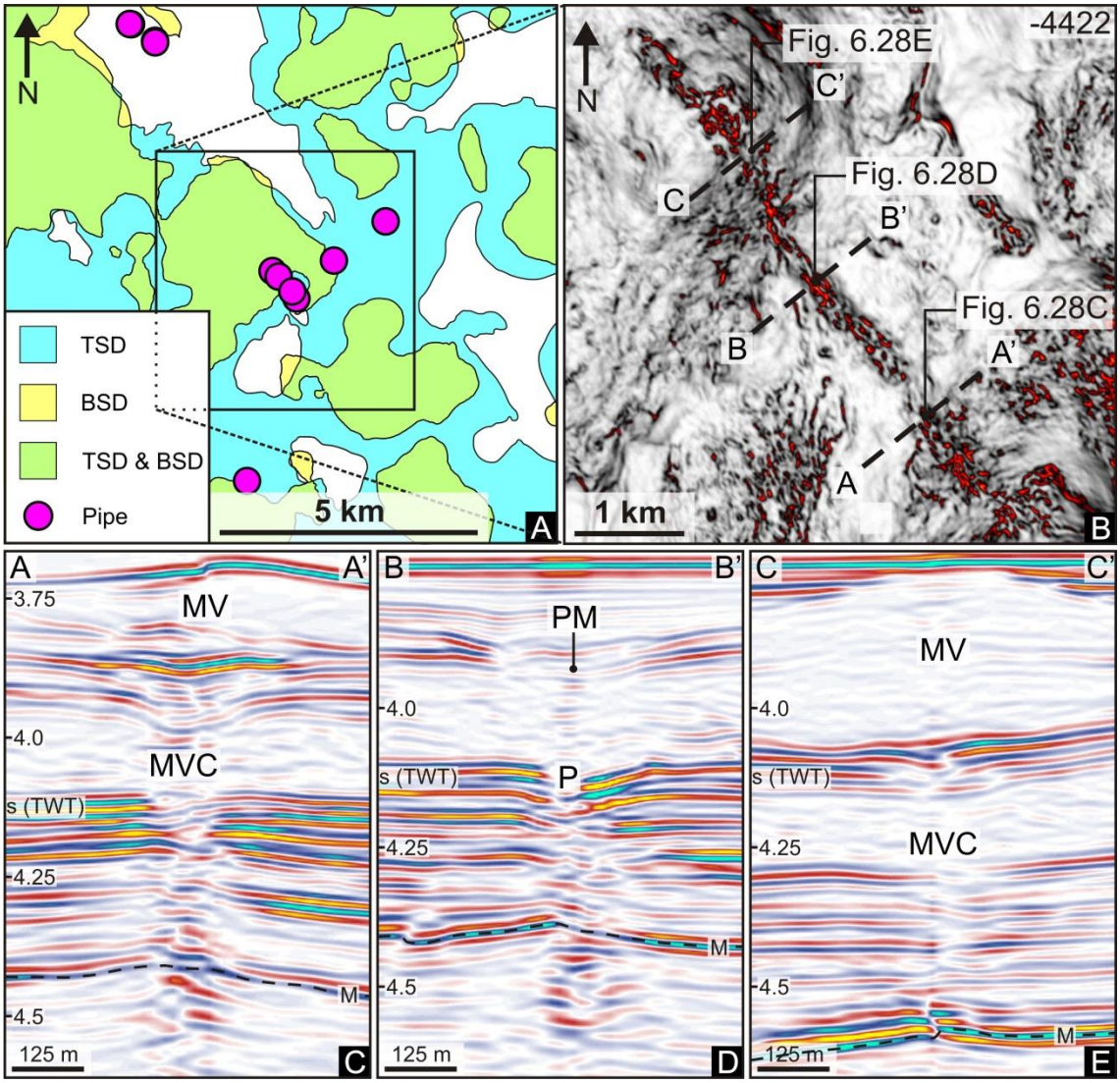

Figure 6.35 Linear trail of pipes. A: A zoomed in section of the map from Figure 6.31 showing top and base-salt depressions and fluid escape pipe data points. The box around a linear trail of pipes is the location of the variance slice in Figure 6.35B. B: A variance slice at -4334 ms through the Pliocene to Recent succession, through a linear trail of pipes. Lines of section for Figure 6.35C, Figure 6.35D and Figure 6.35E are displayed. C: Seismic profile of a mud volcano conduit with a mud volcano at the seafloor, at its upper terminus. D: Seismic profile of a pipe with a pockmark at its upper terminus. E: Seismic profile of a mud volcano conduit with a mud volcano that has been buried, at its upper terminus. P – Pipe; PM – Pockmark; MV – Mud volcano; MVC – Mud volcano conduit; SFT; Seafloor topography; TSD – Top-salt depression; BSD – Base-salt depression; M – Horizon M; TWT – Two way time.

Seismic profiles through this linear area of discontinuity clearly demonstrate that this discontinuity is associated with fluid escape pipes that transect the Pliocene to Recent interval (Figure 6.34C, Figure 6.34D and Figure 6.34E). The upper terminus of these pipes is observed at various depths ranging from -3972 ms TWT to -3886 ms TWT. Pockmarks can be observed at the upper terminus of the fluid escape pipes in Figure 6.34C and Figure 6.34D. In contrast, topography has been built at the present day seafloor above the upper terminus of the pipe in Figure 6.34E. In some examples, mud volcanoes can be clearly observed at the upper terminus of some of the conduits that are pipe-like within similar linear trails (Figure 6.35C and Figure 6.35E). This linear trail of discontinuity is, therefore, formed of not just fluid escape pipes but also mud volcano conduits that despite being part of the same linear trail, are observed at various depths (Figure 6.35C and Figure 6.35E).

6.3.5.1 Summary and interpretation

Analysis of the distribution of fluid escape pipes within this study area shows that the majority of fluid escape pipes are located within Domain B. This result, in combination with a similar observation regarding the location of mud volcanos, supports the interpretation of a specific domain within the study area which is dominated by fluid escape features. Similar to the earlier analysis of the spatial relationship between mud volcanoes and top and base-salt depressions (Chapter 5.4.7), the majority of fluid escape pipes are located overlying combined top and base-salt depressions. However, on closer inspection, it is observed that where fluid escape pipes overlie top and base-salt depressions, they are located at the periphery of the depressions (Figure 6.32 and Figure 6.33). Fluid escape pipes are never observed centred above these depressions and many of these pipes are distributed not overlying any depression. The concave base-salt geometry observed directly beneath fluid escape pipes at the margins of the depression in Figure 6.32B could be a real structure; however, it should be interpreted with caution. It is possible that it could be a pull-up velocity anomaly in response to the change in

velocity between the salt and pre-salt, and the vertical zone of noise associated with the overlying fluid escape pipe within the Pliocene to Recent succession.

Some fluid escape pipes are distributed in NW-SE linear trends. The observation of this recurring linearity and orientation in fluid escape pipe distribution could be interpreted as indicative of deeper linear NW-SE oriented structural controls. The topography observed at the seafloor at the upper terminus of the pipe in Figure 6.34E could be interpreted as a small mud cone which has formed during the early stages of mud volcano evolution. This interpretation is supported by the observation of fully formed mud volcanoes at the upper terminus of conduits which are also part of a NW-SE linear trend of fluid escape features that includes pipes (Figure 6.35). This suggests that similar deeper controls may influence the location of at least some of the fluid escape pipes and mud volcanoes. These alignments of mud volcanoes conduit and fluid escape pipes and their observed relationships to the geometry of the base-salt clearly point to a fluid source that is pre-salt.

6.4 Discussion

6.4.1 Conduit root zone

The high resolution 3D seismic data from this study area has revealed a large number of mud volcano conduits and fluid escape pipes that clearly transect the Pliocene to Recent stratigraphy. The high quality of this data allows for the seismic expression of both the mud volcano conduits and fluid escape pipes to be clearly observed and allows for detailed description and interpretation.

Ascertaining the precise depth of the root zone of many mud volcano conduits and fluid escape pipes is one of the most complicated aspects of their interpretation within this study area. It is, however, a potentially critical part of their interpretation because correctly interpreting the root zone of a conduit is

thought to give an indication as to the fluid source region involved in the conduits formation (Cartwright and Santamarina, 2015). As stated above the fluid escape pipes or mud volcano conduit is defined as a vertical zone of discontinuity, the base of which should be defined as the first continuous reflection to cross unbroken beneath the vertical zone of discontinuity (Moss and Cartwright, 2010a). In all examples, within the vertical zone of discontinuity of these conduits, the deepest reflection that can confidently be interpreted to display a genuine break in its continuity that is not artefactual, is Horizon M. Due to imaging difficulties, both within the evaporites and pre-salt, accurate interpretation of these conduits and their root zones within the evaporite succession or deeper is not possible. There is therefore no conclusive evidence for constraining the position of the root zone from the seismic data alone.

What can be inferred from directly observing these fluid escape pipes and mud volcano conduits using 3D seismic data is that in every case the conduits have clearly pierced the top of the evaporites, which is evident by the break continuity of the reflection of Horizon M, which is observed in all examples. This indicates that the fluids and mud involved in their formation have migrated at least in part through the evaporites.

Strong evidence that the root zones must be within of beneath the evaporites comes from observations of hot saline brine pools associated within the mud volcanoes within this study area (Mascle et al., 2014; Huguen et al., 2009; Dupré et al., 2014; Giresse et al., 2010). These brine pools have been interpreted to be saline rich due to dissolution of the Messinian evaporites within the ascending hot fluids. This leaves only two possibilities for the root zone of these mud volcano conduits and fluid escape pipes, which are the intra-salt or pre-salt successions.

The Messinian evaporite unit is known to include intercalations of clastic deposits (Bertoni and Cartwright, 2007a; Roveri et al., 2014) which could be isolated and overpressured and, therefore, contain pressurised pockets of trapped fluids. Whilst there is no well calibration in this study area, the presence of isolated high amplitude intra salt reflections could indicate that similar heterogeneities may

also be present within the evaporitic interval in this region of the Eastern Mediterranean. Another explanation for a source of fluid is the diagenetic transformation of gypsum into anhydrite and or carnallite into sylvite (Testa and Lugli, 2000; Jowett et al., 1993; Eruteya et al., 2015; Bertoni and Cartwright, 2015). These transitions can result in the release of significant amounts of brines and an up to 40% volume increase (Jowett et al., 1993), which can result in the development of overpressure (Davison, 2009). Whilst these are potential explanations for the fluid origin of some fluid escape pipes, these mechanisms do not factor in a fine-grained sediment source in order to form a mud volcano. A root zone within the evaporites for the mud volcano conduits is, therefore, unlikely.

As documented above, several observations were made in Chapter 4 and 5 that are indicative of a pre-salt source of mud and fluids. The spatial relationship and volumetric balance between mud volcanoes and base-salt depressions presents strong evidence for depletion of the immediate pre-salt. Numerous mud volcanoes formed directly on top of the evaporites or only a few reflections above Horizon M and the Pliocene to Recent interval beneath them shows no evidence for depletion (Figure 6.3). Lastly a velocity inversion within the immediate pre-salt observed within pre-stack depth migrated velocity data could be interpreted as indicative of undercompaction and overpressure. These observations, in combination with the observation that the conduits in this study area have clearly breached the top-salt reflection of Horizon M, indicate that the source of fluids and mud for these mud volcanoes is within the pre-salt.

The above interpretations are supported by Bentham et al. (2006), who using 2D and 3D seismic data from the Nile Delta also argued that mud volcanism within this area is related to the withdrawal and mobilisation of overpressured Tortonian shales within the immediate pre-salt. This interpretation of a pre-salt origin is further supported by published analysis, also referred to in section 5.4.1 of chapter 5, of piston core samples from mud volcanoes within this study area. These samples are reported to contain rock clasts of up to Cretaceous in age (Dupré et al., 2014; Mascle et al., 2014; Giresse et al., 2010).

Thus, the direct evidence of samples obtained from mud volcanoes at the seafloor argues powerfully that the root zone and source of fluids and mud for the mud volcano conduits is within the pre-salt stratigraphy. A similar interpretation was made by Reiche et al. (2014) with regards to the formation of a mud volcano observed at the seafloor within the Levant Basin. The root zone and source of fluids for the fluid escape pipes could also be from within the pre-salt; however there are also potential mechanisms that could lead to an intra-salt root zone. The intra-salt and pre-salt have also been previously interpreted by (Eruteya et al., 2015) as viable root zones for fluid escape pipes within the Levant basin.

6.4.2 Conduit genesis

The mud volcano conduits and fluid escape pipes within this study area both share very similar defining seismic expressions, of a steep zone of breaks in the continuity of reflections and acoustic disruption (Figure 6.6 Figure 6.7). These defining characteristics are explicable, considering the vertical migration of fluids and sediment through a lithological succession implies that the host rock has been significantly disrupted. Despite displaying varied heights and widths, they all share a similar overall three dimensional geometry which is most closely comparable to a vertically orientated cylinder (Figure 6.6 Figure 6.7). The mud volcano conduits in this study area are, therefore, pipe-like in their seismic expression and geometry. Where they differ from fluid escape pipes is in the end member at their upper terminus of a mud volcano, in contrast to a pockmark overlying upper terminus of a fluid escape pipe. These observations are similar to other documented mud volcano conduits that are pipe-like (Stewart and Davies, 2006; Reiche et al., 2014) and other fluid escape pipes (Hustoft et al., 2007; Moss and Cartwright, 2010a).

The above observations are potentially critical for understanding the genesis of both the fluid escape pipes and mud volcano conduits this study area. Bearing in mind their similar seismic expression and geometry, perhaps the mechanism for fluid escape pipe formation may give an insight into the formation of the mud

volcano conduits within this study area and other basins around the world (Fowler et al., 2000; Graue, 2000; Stewart and Davies, 2006; Reiche et al., 2014). However, a highly important difference between the fluid escape pipes and mud volcano conduits within this study area, compared to those in many other basins, is the evidence that they have bypassed a c. 2 km thick unit of low permeability evaporites. This has significant implications with regards to: (1) the sealing integrity of evaporites which are traditionally considered the perfect geological seal (Downey, 1984) and; (2) the conduit-forming mechanisms required to breach a thick unit of evaporites.

6.4.2.1 Hydraulic fracturing

The genesis of fluid escape pipes is widely considered to be through catastrophic breaching of top seals in a highly dynamic process involving hydraulic fracturing under elevated pore fluid pressures (Berndt et al., 2003; Hustoft et al., 2007; Judd and Hovland, 2007; Ligtenberg, 2005; Cartwright et al., 2007; Hustoft et al., 2010; Moss and Cartwright, 2010a; Cartwright and Santamarina, 2015; Davies et al., 2012; Løseth et al., 2011). Via this mechanism, the fluid escape pipe is thought to comprise a network of fractures that propagate to the surface within a vertical zone. It is generally believed that high overpressure within a sedimentary layer is a critical precursor to the formation of hydraulic fractures through which fluids and mobile sediments can migrate (Morley et al., 1998). Within this basin, the mechanisms with the greatest potential for generating the zone of overpressure that is required for hydraulic fracturing include build-up of gas pressure and rapid loading of evaporites (Bertoni et al., 2013; Cartwright and Santamarina, 2015; Osborne and Swarbrick, 1997). Tectonic compression can increase pore pressure where there is a horizontal direction of maximum stress (Osborne and Swarbrick, 1997). However, this study area is located within a passive margin and is not within a basin that is tectonically active. Generating overpressure via lateral compression can, therefore, be ruled out. Other mechanisms that are of secondary importance during overpressure development include aquathermal expansion and mineral

diagenesis in the form of the transformation of Smectite to Illite. These mechanisms are discussed below.

Over recent years it has been invoked that the Messinian Salinity Crisis has had a major influence on the development of pre-salt overpressure (Bertoni and Cartwright, 2015; Bertoni et al., 2013). Documented examples of mud mobilisation, cold seeps and pockmark formation and shallow laccolith intrusion have all aided in building this argument (Frey-Martnez et al., 2007; Lazar et al., 2012; Bertoni and Cartwright, 2015; Bertoni et al., 2013). In addition to being a primary driver for the formation of fluid escape pipes, overpressure is also widely invoked as a driver for the ascent of mud and pore fluids from deeper sedimentary layers during the formation of mud volcanoes (Hovland and Judd, 1988; Brown, 1990; Dimitrov, 2002).

In Chapters 4 and 5, evidence was presented in support of the interpretation of overpressure within pre-Messinian sediments. Giant mud volcanoes, described in Chapter 4, were observed directly on top of the Messinian evaporites. Based on their stratigraphic position, an interpretation was made that the timing of their extrusion coincided with the almost instantaneous loading of an estimated 1-2 km water column during the Zanclean flood, at the climax of the Messinian Salinity Crisis 5.333 Ma (Barber, 1981; Druckman et al., 1995; Garcia-Castellanos et al., 2009). This flooding event is interpreted to have delivered the critical trigger required to initiate seal failure of the “sealing” evaporites, provided the pre-salt was already in a state of overpressure.

It has been proposed that rapid basinal drawdown at the onset of the Messinian Salinity Crisis led to a dramatic increase in overpressure within shallow subsurface and fine grained pre-Messinian sediments (Bertoni et al., 2013). The rapid loading of evaporites during the Messinian Salinity Crisis could have caused high fluid retention and undercompaction and overpressure within the pre-Messinian (particularly the immediate pre-salt) (Kopf, 2002). This is due to the rapidity of deposition and loading of low permeability Messinian evaporites (ca. > 2 km thick), which produces a vertical direction of maximum compressive stress.

These giant mud volcanoes are interpreted to represent a period of massive overpressure release from the pre-salt at the end of the Messinian Salinity Crisis. It is possible that the overpressure generated within the pre-salt during the Messinian Salinity Crisis could be sufficient to exceed the fracture gradient in order to form hydraulic fractures.

In Chapter 5, 386 mud volcanoes were interpreted throughout the Pliocene to Recent succession of this study area. Mud volcanoes are extrusive features which form via an efficient mechanism for dewatering rapidly buried and overpressured clay rich sedimentary sequences (Kopf and Behrmann, 2000). The very presence of such a large number of mud volcanoes could, therefore, be considered as an indicator for overpressure.

As discussed above, the mud feeding these mud volcanoes is interpreted to be of a pre-salt origin. The formation of the giant mud volcanoes is interpreted to be associated with overpressure that was generated during the MSC and the events during its immediate aftermath. These interpretations lead to an interesting question, which is; to what extent could overpressures generated during and after the MSC still persist today?

Another possible way of generating overpressure is hydrocarbon generation within the source layer for mud directly beneath the evaporites. The formation of mud volcanoes more generally is often thought to be intimately associated with the generation of buoyant hydrocarbons. The build-up of gas pressure within a potential source region for a mud volcano can lead to it becoming highly overpressured (Hedberg, 1980; Charlou et al., 2003; Dimitrov, 2002; Kopf, 2002; Wilford, 1967; Humphrey, 1963; Stamatakis et al., 1987). Methane is almost ubiquitous in the eruption of modern mud volcanoes (Kopf, 2002).

In section 5.3.2 of Chapter 5, evidence was presented of bright spots within mud volcanoes, which were high amplitude and soft reflections with a sharp cut-off in amplitude at their margins. Gas seepage samples collected from mud volcanoes within the Nile Delta have been documented as mainly thermogenic in origin and of varying maturity (Prinzhofer and Deville, 2011; Pierre et al., 2014). Some of these

gas samples have been shown to be of very high maturity, which indicates that these seepages are sourced from great depths below the Messinian evaporites (Prinzhofer and Deville, 2011).

Within this chapter, a large number of fluid escape pipes with pockmarks at their upper terminations were described. Pockmarks are widely viewed as being formed by the escape of fluids that have migrated along a pipe, and in most, but not all instances, this fluid is interpreted to be at least in part, methane. The shallow amplitude anomalies described in this chapter and interpretation in section 6.2.4.1 as being due to the presence of free gas in porous sediments, are further indicators of the potential involvement of thermogenic methane in the formation of these fluid escape pipes and mud volcano conduits. Bearing in mind the evidence for a pre-salt fluid origin for many of the fluid escape pipes within this study area, the close spatial relationship between these DHI's and underlying fluid escape pipes suggest that they have provided pathways for deeper sourced gas. This interpretation is consistent with the evidence presented of a pre-salt source of thermogenic gas associated with mud volcanoes (Prinzhofer and Deville, 2011; Pierre et al., 2014).

The precise age of any potential pre-salt source rocks within this study area are unfortunately unknown in the absence of reliable well calibration. Mesozoic and Oligocene source rocks have been documented within the deep water region of the Nile Delta (Aal et al., 2000; Dolson et al., 2001; Vandré et al., 2007). There are also proven hydrocarbon plays documented a mere 55 km to the northeast within Shell's relinquished NEMED blocks (Economist, 2011; EGAS, 2012a; EGAS, 2012b; EGAS, 2012c). Within these blocks pre-salt terrestrial and marine deposits that developed during the Oligocene to Miocene are considered one of the main source rocks (EGAS, 2012a; EGAS, 2012b; EGAS, 2012c). Taking into account the interpretation of a pre-salt fluid and mud source and the potential for pre-salt hydrocarbon plays, it is possible that the shallow amplitude anomalies that are observed in association with the mud volcanoes and fluid escape pipes within this study area are indicative of pre-salt fluid (methane) migration and shallow gas (Judd and Hovland, 1992). This interpretation is further supported by evidence of

methane-rich and oily hydrocarbon-rich hot brine and mud samples taken from several mud volcanoes within this study area (Pierre et al., 2014; Dupré et al., 2014; Huguen et al., 2009).

A build-up of gas-pressure (methane) beneath the evaporites could contribute to overpressure generation and hydraulic fracturing. The potential to generate overpressure via this method is related to the column height, i.e. the vertical thickness of the sedimentary unit that is hosting the gas and the relative buoyancy forces applied to the sedimentary sequence (Bertoni and Cartwright, 2015). It is important to point out though that the presence of free gas within an overpressured source is not a pre-requisite for hydraulic fracturing.

Other potential overpressuring mechanisms are related to an increase in fluid volume. Aquathermal expansion is a mechanism where by a body of water that is contained within a perfectly sealed unit expands as temperature increases, which results in the generation of overpressure (Osborne and Swarbrick, 1997). The fluids within the sealed unit will expand provided they are of a temperature above 4 °C and overpressure will be generated if the thermal expansion of water at a constant pressure is greater than pore volume expansion (Osborne and Swarbrick, 1997). This mechanism is thought to be most effective within evaporite rich sedimentary sequences, where evaporites are thought to present a perfect seal. However, it is thought that fluid expansion would be relatively small and would be, therefore, insufficient to generate significant overpressure and hydraulically fracture the evaporitic seal (Osborne and Swarbrick, 1997).

As previously stated, without well calibration it is not possible to know the exact composition of the pre-salt stratigraphy. Smectite is, however, a common detrital mineral in shales, which contains an abundance of interlayered water in its crystal structure. These interlayered water molecules are arranged in a denser packing that those of ordinary water. It is thought that the dehydration of smectite during its transformation to Illite can cause an expansion in volume from the expelled water, which results in overpressuring (Osborne and Swarbrick, 1997). However, similar to aquathermal expansion, it is thought that this mechanism is

unlikely to cause significant overpressuring. This is because the volume of water that is released is relatively small and so it is thought to be insufficient to generate significant overpressure, and a build-up of pressure is actually thought to inhibit dehydration (Osborne and Swarbrick, 1997).

It is thought that a network of hydraulic fractures can form within rock salt where there is the presence of fluids either within or beneath evaporites at near-lithostatic pressure (Urai et al., 2008). In order to fracture the overlying evaporitic succession, fluid pressure within the pre-salt source unit must exceed the tensile strength and minimum horizontal stress of this sealing overburden (Jolly and Lonergan, 2002; Seldon and Flemings, 2005; Delaney et al., 1986; Cosgrove, 2001; Eruteya et al., 2015). As is suggested above, for this mechanism to be applicable, exceptionally high fluid overpressure values will be required within the pre-salt. As demonstrated above, there is the potential for generating overpressure within the pre-Messinian via both undercompaction and loading, and gas pressure build up. The evidence presented suggests that both mechanisms could have potentially contributed in generating the level of overpressure that is required to surpass the fracture gradient and hydraulically fracture the Messinian evaporite and Pliocene to Recent successions.

A key question is how can hydraulic fractures propagate across a c. 2 km thick layer of evaporites that is possibly mainly halite in composition? Despite the low permeability of salt which leads to its property as an efficient caprock, at sufficiently low effective mean stress, dilatancy and fracturing can also occur in deforming salt (Peach and Spiers, 1996; Urai et al., 2008). If deformation of the Messinian evaporites within this study area is sufficient, it is possible that significant permeability pathways could be produced, which could significantly reduce the sealing capacity of the unit and permit fluid flow through the “sealing” unit (Urai et al., 2008; Eruteya et al., 2015). It is, therefore, possible that pre-salt sourced fluids and mud may have preferentially migrated through deformations such as these within the evaporites, which could result in an intra-salt plumbing system, similar to as argued by Eruteya et al. (2015) (Figure 6.36).

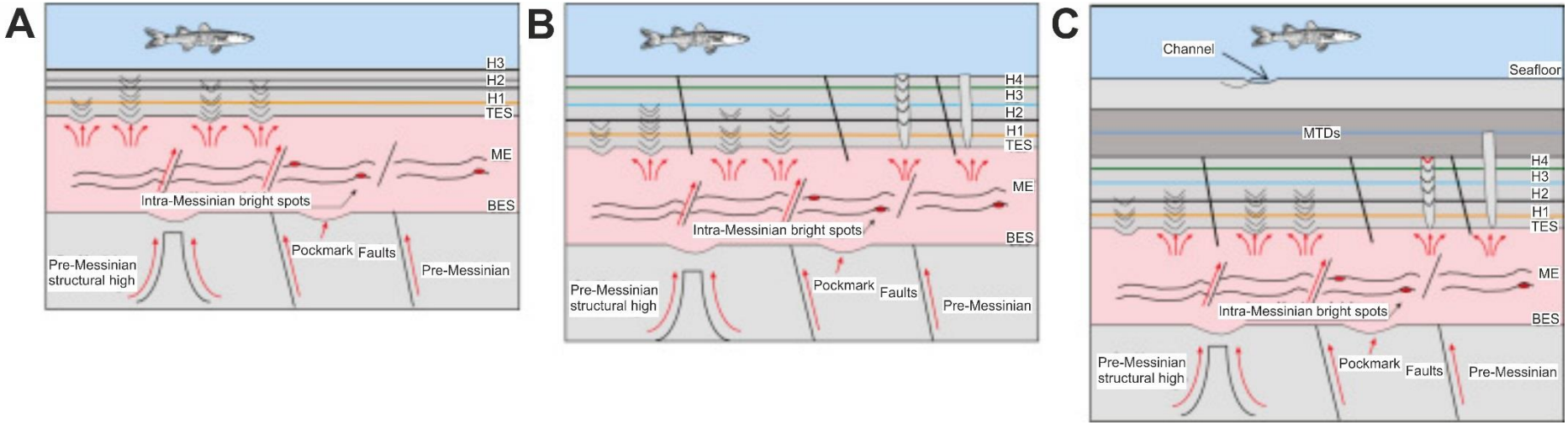

Figure 6.36 Conceptual model describing the formation process of the pipe structures documented in the central Levant Basin from Eruteya et al. (2015). The red arrows represent the direction of fluid migration, which has been interpreted by Eruteya et al. (2015) to migrate along intra-salt deformations (Modified from Eruteya et al. (2015).

In order for high pressure fluids and entrained fine grained sediment to be injected into the evaporitic and Pliocene to Recent succession along hydraulic fractures, a sustained pressure differential between the fluids within the propagating intrusion and pore fluids is required in order to achieve fracture dilation (Jolly and Lonergan, 2002; Lorenz et al., 1991). The resulting hydraulic fracture network would have to have propagated hundreds of meters above the overpressured pre-salt source unit in order to pierce the seafloor and form either a mud volcano or pockmark at its upper terminus. But could a network of hydraulic fractures have formed the columnar structures observed in these mud volcano conduits and fluid escape pipes? One proposed explanation is that erosion, driven by migrating fluid and mud and flow localization along the vertical plane of hydraulic fractures (Novikov and Slobodskoy, 1979) could eventually form a single central pipe or multiple aligned pipes with a proper exclusion distance between them (Cartwright and Santamarina, 2015; Ligtenberg, 2005).

Within the South Caspian Sea, formation of mud volcano conduits that are pipe-like have also been interpreted to be the result of hydraulic fracture propagation (Stewart and Davies, 2006). However, it is important to stress that similar to fluid escape pipes, there is thus far no direct evidence for hydraulic fracturing within any mud volcano conduit through observation using seismic data (Cartwright and Santamarina, 2015). There is, however, at least one field study which identifies and describes examples of exhumed mud volcano feeder complexes and could be used as an analogue for the mud volcano conduits observed here using 3D seismic data (Roberts et al., 2010). Peripheral fracture zones containing sinuous, conjugate and grid like fractures have been observed within several feeder complexes (Roberts et al., 2010). These fracture zones contain mud and clasts of country rock and present strong evidence for fluid and mobile sediment intrusion upwards through fracture networks (Morley et al., 1998; Clari et al., 2004; Roberts et al., 2010; Cartwright and Santamarina, 2015). The fracture density was observed to increase towards the centre of the conduit, eventually forming an highly fractured columnar zone at the centre of the conduit, where

higher mud flow is localised (Roberts et al., 2010), similar to the process hypothesised above.

6.4.2.2 Dissolution and Stoping

An alternative mechanism for the formation of fluid escape pipes that could also be relevant with regards to the formation of these mud volcano conduits is one of dissolution and stoping. Localised subsurface volume loss via dissolution of a substrate can result in later collapse of the overburden within a columnar zone, which is defined as a dissolution pipe (Cartwright and Santamarina, 2015; Sun et al., 2013). These pipes are restricted to areas where there are carbonates and/or evaporites at depth. Subsequent collapse events and fracturing of the overburden significantly increase vertical permeability and causes the pipe to propagate upwards, which promotes fluid migration within the vertical column (McDonnell et al., 2007). Within this study, dissolution of the evaporites could offer a potential mechanism in order to create the initial subsurface volume loss to initiate collapse of the overburden, and to localise highly focused fluid flow from the overpressured pre-salt succession.

Over recent years, strong evidence has been presented for subjacent dissolution of the lower Messinian evaporites by under-saturated fluids migrating along the base of the evaporites, which results in collapse of the overburden (Bertoni and Cartwright, 2005; Bertoni and Cartwright, 2006; Cartwright et al., 2007; Eruteya et al., 2015). In section 5.3.6 of Chapter 5, it was observed that where a mud volcano overlies, top and base-salt depression are correlatable with areas of localised thinning of the evaporites. The areas of anomalous thinning were clearly observed in seismic profile and in an isopach map of the evaporites. As stated above, observations from 3D seismic data combined with published analysis of the fluid and mud for these mud volcanoes are indicative of a pre-salt origin (Bentham et al., 2006; Dupré et al., 2014; Giresse et al., 2010; Mascle et al., 2014). Additionally, hot saline brine pools associated with the mud volcanoes are

interpreted as due to dissolution of the evaporites within ascending fluids (Mascle et al., 2014; Huguen et al., 2009; Dupré et al., 2014; Giresse et al., 2010). The observed volumetric loss of salt could, therefore, in part be attributed to under-saturated pre-salt fluids dissolving the base of the evaporites at the location at which a mud volcano conduit is forming.

In Chapters 4 and 5, it was discussed that the precise stratigraphy of the immediate pre-salt interval, which is Tortonian in age (Bentham et al., 2006), lacks nearby well calibration. However, by extrapolation between other well calibrated successions in the Levant Basin (Bertoni and Cartwright, 2005) and at outcrop in Sicily (Grasso et al., 1982), it is most likely that the Tortonian interval comprises a marly to muddy interval. If it is accepted that the immediate pre-salt is indeed undercompacted and has retained a large volume of pore fluid, as discussed above, it is possible that these retained fluids could potentially form dissolution associated voids at the base of the evaporites, such as those required for a dissolution and collapse mechanism (Sun et al., 2013). For this mechanism to be viable, the pre-salt fluids must be of relatively low-salinity in order dissolve the evaporites (Bertoni and Cartwright, 2005). It is also a self-limiting process because the volume of salt that can be taken into solution before the fluids become supersaturated is finite. However, a void created at the base of the evaporites by dissolution could result in subsequent and cyclic localised roof collapse events, upward propagation of fractures and further dissolution within the evaporite succession (Cartwright and Santamarina, 2015; Bertoni and Cartwright, 2015).

By analogy this collapse mechanism is similar to one suggested for the formation of presently outcropping mud volcano feeder complexes in Azerbaijan by Roberts et al. (2010), referred to as stoping. The mechanism of stoping is one that originated from igneous intrusions where by melts and volatiles invade fractures within the host rock that were formed due to pressure increases associated with thermal expansion (Pinotti et al., 2002). The invading melt widens the fractures and causes the overburden to disintegrate, break apart, and collapse resulting in a slow upwards propagating process which produces a collapse pipe (Marsh, 1982). Roberts et al. (2010) presented a compelling argument, suggesting that a similar

stoping process where the overburden collapses into a void or zone of local liquefaction may potentially be responsible for the genesis and final internal structure of mud volcano conduits.

The temperature of upwelling fluids within a mud volcano conduit range from a little as 11 °C to greater than 100 °C (Roberts et al., 2010; Martin et al., 1996; Kopf, 2002). These temperatures are an order of magnitude lower than those recorded in igneous systems (> 1000 °C) (Sweeney and Burnham, 1990), so thermal expansion and disintegration of the host rock would generally not be considered applicable in mud volcano conduits (Roberts et al., 2010). In the example presented here however, subjacent dissolution and collapse of the evaporites is possible. The stoped blocks of evaporites will fall into the migrating mud slurry and depending on the size of the block will either be carried upwards within the intruding mud or collapse. It is therefore possible that these conduits may contain numerous blocks of evaporites that have collapsed and been rotated by the upwelling intruding mud (Roberts et al., 2010), provided they have not been dissolved by ascending low-salinity fluids.

6.4.2.3 Synthesis and additional remarks on conduit genesis

It has been suggested that by drawing a comparison between fluid escape pipes and mud volcano conduits that a compelling argument can be made for their internal structure to be comprised of similar columnar zones of hydraulic fractures (Cartwright and Santamarina, 2015). Despite the exceptionally high overpressure requirements to fracture salt, a build-up of gas pressure beneath the evaporites and rapid loading of evaporites present potential mechanisms to generate pre-salt overpressure within the study area. This makes hydraulic fracturing of the evaporites one of the more acceptable hypothesised breaching mechanisms. If this is the case, hydraulic fracturing could represent a very effective transport mechanism and has the potential to rapidly deplete overpressure within parts of the pre-salt succession (Moss et al., 2012).

In most cases mud volcanoes appear as isolated bodies that do not demonstrate continued expulsion throughout the Pliocene to recent succession which suggests that these conduits do not survive to be re-used. This contrasts with some fluid escape pipes and mud volcano conduits in other basins which behave in an episodic manner (Hansen et al., 2005; Andresen and Huuse, 2011; Deville and Guerlais, 2009). Rapid sediment remobilisation and depressurising of areas that are overpressured could be one explanation for why these mud volcanoes mostly appear to be short lived episodes of extrusion and why their conduits are not exploited during later extrusive episodes. Clastic intrusions may be analogous in that the excess pressure that drives the injection and migration of fluids and entrained sand grains into a hosting sequence eventually dissipates, which in the instance of an intrusion will cause fracture propagation and the sediment injection to "freeze" (Jolly and Lonergan, 2002). In a similar manner dissipation of overpressure within the source stratigraphic unit of a mud volcano system will inevitably also result in mud intrusion and extrusion to "freeze".

Dissolution of the evaporites can lead to pipe like collapse structures with similar geometries to other pipes and is a process that does not require overpressure (Cartwright et al., 2007; Cartwright and Santamarina, 2015; Sun et al., 2013). Low-salinity fluids migrating along the base of the evaporites could initiate subjacent dissolution at the base of the evaporites. Vertically migrating fluids and sediment that exploit this depleted void may lead to further dissolution and be further aided in their migration by new fracture pathways opened within the dissolution pipe (Bertoni and Cartwright, 2005; Cartwright and Santamarina, 2015). The volumetric loss of evaporites and void formed could potentially propagate upwards through subsequent dissolution and collapse of the overburden locally within the pipe via a stoping process.

The process of stoping could also be associated with hydraulic fracture propagation as a result of blocks that are left free to collapse as a result of the fracture network. The strong possibility of stoping associated with either/or dissolution and hydraulic fracturing in combination with the strong analogue to outcrop examples (Roberts et al., 2010) makes stoping a real possibility. When

considering the mechanism for mud volcano conduit formation within this area, it is most probable that a combination of mechanisms including hydraulic fracturing, fluidisation, dissolution and stoping are culpable rather than one single mechanism (Figure 6.37).

A conceptual model for the mechanisms and stages of mud volcano conduit genesis and bypassing of the Messinian evaporites in the Eastern Mediterranean is presented in Figure 6.37:

Stage 1 (Figure 6.37A): Low-salinity fluids within the pre-Messinian stratigraphy begin to subjacently dissolve the lower evaporites. An initial fracture propagates upwards, formed due to overpressure within the immediate pre-salt that exceeds the fracture pressure.

Stage 2 (Figure 6.37B): Fluids and mud migrate into the initially formed fractures within the evaporites, driving the formation of a network of hydraulic fractures that propagate upwards and widen the fracture network. Fracturing of the evaporites combined with a volume loss through dissolution begins to result in the dissociation and collapse of blocks within the pipe structure via stoping processes.

Stage 3 (Figure 6.37C): Continued fracture propagation and dissolution drive upwards pipe propagation. The network of hydraulic fractures becomes denser and continued stoping forms an increasing accumulation of stoped blocks.

Stage 4 (Figure 6.37D): The pipe propagates to, and pierces, the seafloor. Fracture network linkage throughout the pipe results in increased focused fluids. Fracture density has further increased towards the pipe's centre forming a columnar central pipe where mud flow is at its greatest. The pipe pierces the seafloor. Mud flows through the pipe and is extruded over the seafloor, forming a constructional mud volcano.

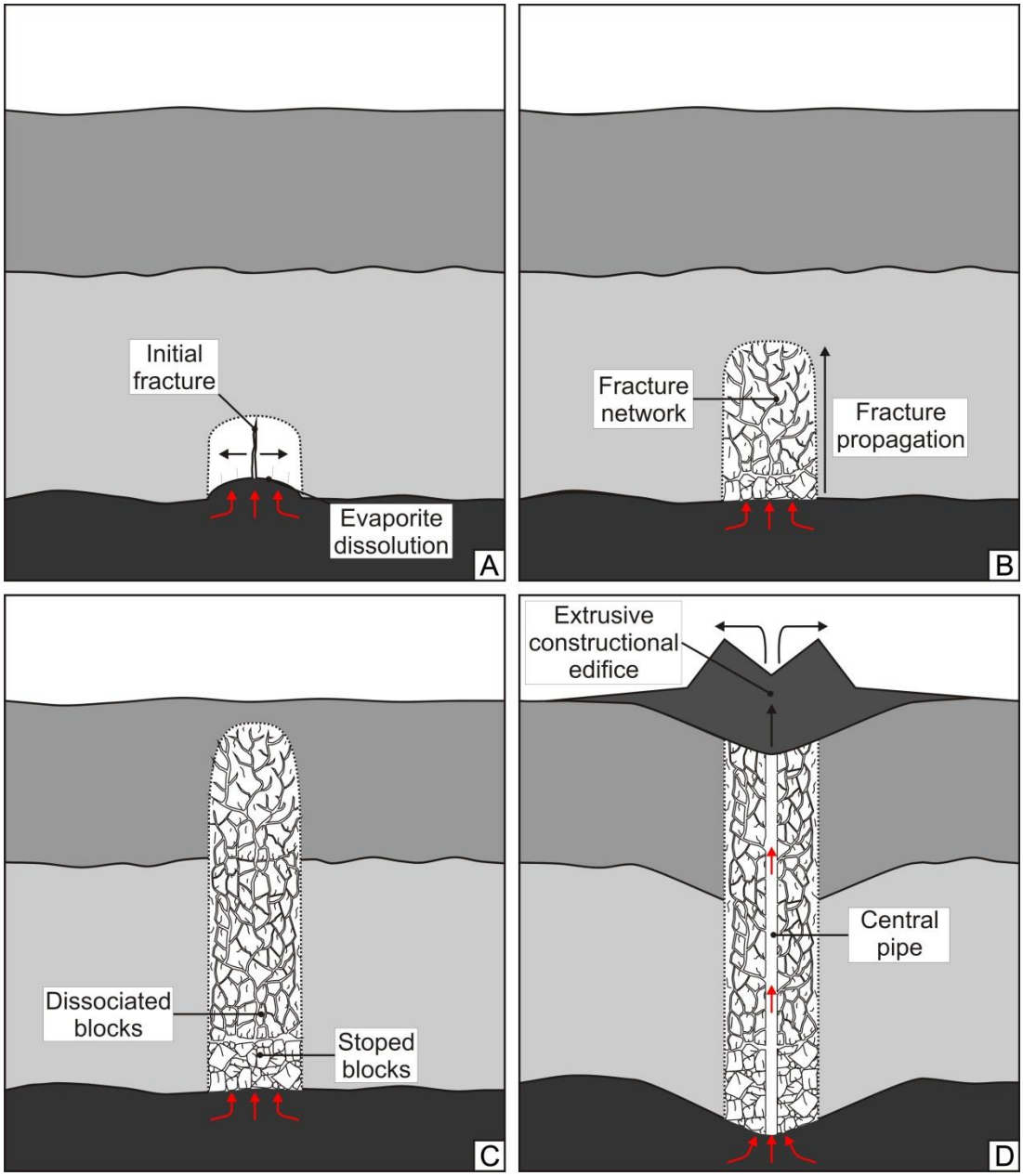

Figure 6.37 Conceptual model for the mechanisms and stages of mud volcano conduit genesis through evaporites in the Eastern Mediterranean. The various stages are described in the main body of text. The red arrows represent the direction of fluid migration.

6.4.3 Distribution of fluid escape pipes

The pockmarks observed within this study area display a large range of termination levels within the Pliocene to Recent succession. Constraining the timing of formation of these fluid escape pipes and pockmarks is, however, problematic as there is no well calibration of the chronostratigraphy. This is an issue that has been discussed in Chapter 5 with regards to the timing for the formation of the mud volcanoes. Without well calibration, constraining the exact age of these pockmarks is not possible. However, the observation of pockmarks at various levels within the Pliocene to Recent succession indicates that fluid venting has occurred at various intervals between the Pliocene to present day (Figure 6.38). Pockmarks that have been observed at the seafloor demonstrate that many fluid escape pipes are actively venting fluids in very recent times.

In Chapter 4, evidence was presented for the formation of a suite of giant mud volcanoes during a massive overpressure releasing event at the end of the Messinian Salinity Crisis (5.33 Ma). The timing of the event resulted in these giant mud volcanoes forming directly on top of the Messinian evaporites. Similar to the pockmarks, the mud volcanoes described in Chapter 5 formed at a large range of levels within the Pliocene to Recent succession. Many of these mud volcanoes formed only one of two reflections above the top-salt reflection of Horizon M as demonstrated in Figure 6.3. In this Chapter, the deepest pockmark that has been observed is 108 ms TWT above Horizon M, which is several reflections above the top of the evaporites. These observation suggest that the formation of the first fluid escape pipes and pockmarks within the Pliocene to Recent interval of this study area post-date the formation of the giant mud volcanoes and the first smaller (relative to the giant mud volcanoes) conical mud volcanoes (Figure 6.38).

An observation was made in Chapter 5 of a striking spatial correlation between top and base-salt depressions and overlying mud volcanoes. These depressions were interpreted to have developed via a combination of pre-salt depletion, subsidence, gravitational loading and dissolution. In this chapter, the location of fluid escape pipes relative to these top and base-salt depressions was

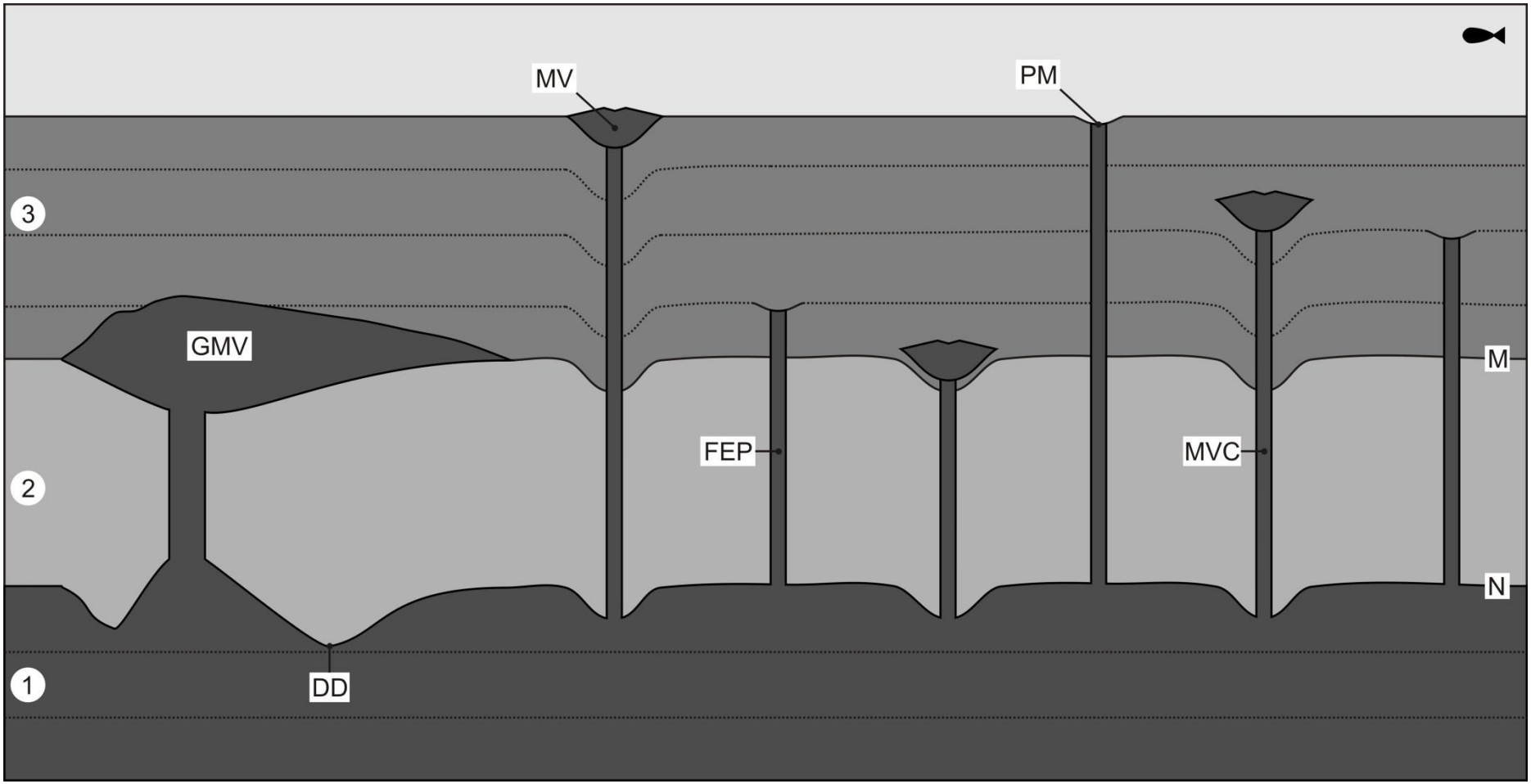

Figure 6.38 A cartoon to demonstrate the range of stratigraphic levels for the upper terminuses of mud volcano conduits and fluid escape pipes. The cartoon also shows how the top and base-salt and reflections respond to the formation of mud volcanoes and pockmarks. Areas of thinning can be observed within the pre-salt beneath mud volcano conduits. GMV – Giant mud volcano; MV – Mud volcano; PM – Pockmark; FEP – Fluid escape pipe; MVC – Mud volcano conduit; DD – Depletion depression; M – Horizon M; N – Horizon N; 1 – Pre-Messinian; 2 – Messinian evaporites; 3 – Pliocene to Recent.

shown to contrast to that of the mud volcanoes, in that they are located at the periphery of base-salt depressions (Figure 6.32 and Figure 6.33). Other fluid escape pipes have also been observed directly above a base-salt anticline (Figure 6.27) and also in NW to SE trending linear trails (Figure 6.34 and Figure 6.35).

Fluid escape pipes have historically been observed piercing lithological successions above classic structural traps, such as anticlines and footwall crests where fluids have laterally migrated up dip and accumulated, (Judd and Hovland, 2007). They are also frequently observed overlying the upper termination of faults (Gay et al., 2006; Berndt et al., 2003; Hustoft et al., 2007). Recurring linear trails (Figure 6.34 and Figure 6.35) of fluid escape pipes could be interpreted as indicative of deeper linear NW-SE oriented structural controls. Fluid flow from underlying NW-SE orientated faults or anticlinal axis could explain the clear linear arrays of pipes.

It is possible that the location of some of these fluid escape pipes is intimately associated with the undulating and highly depressed base-salt geometry, which is interpreted to be associated with sediment withdrawal of the pre-salt (See also Chapter 4 and 5) during formation of the directly overlying mud volcanoes. A potential explanation could be that the depressions formed via sediment withdrawal have produced sloping base-salt geometry in some areas which has encouraged updip lateral fluid migration and accumulation beneath an anticlinal structure at the edge of the base-salt depression (Figure 6.32 and Figure 6.39), similar to the classic structural traps described above. It is possible that the accumulation of fluids (if of low-salinity) beneath this structural trap and low permeability unit of evaporites could begin to dissolve the lower evaporites and generate a localised area of overpressure capable of initiating hydraulic fracturing if sufficient to exceed the high fracture pressure required (Figure 6.39) (Swarbrick, 1999).

These observations suggest that the formation of some of these fluid escape pipes has not contributed to the formation of the observed base-salt depressions, but rather the geometry of the base-salt depressions has influenced the location of

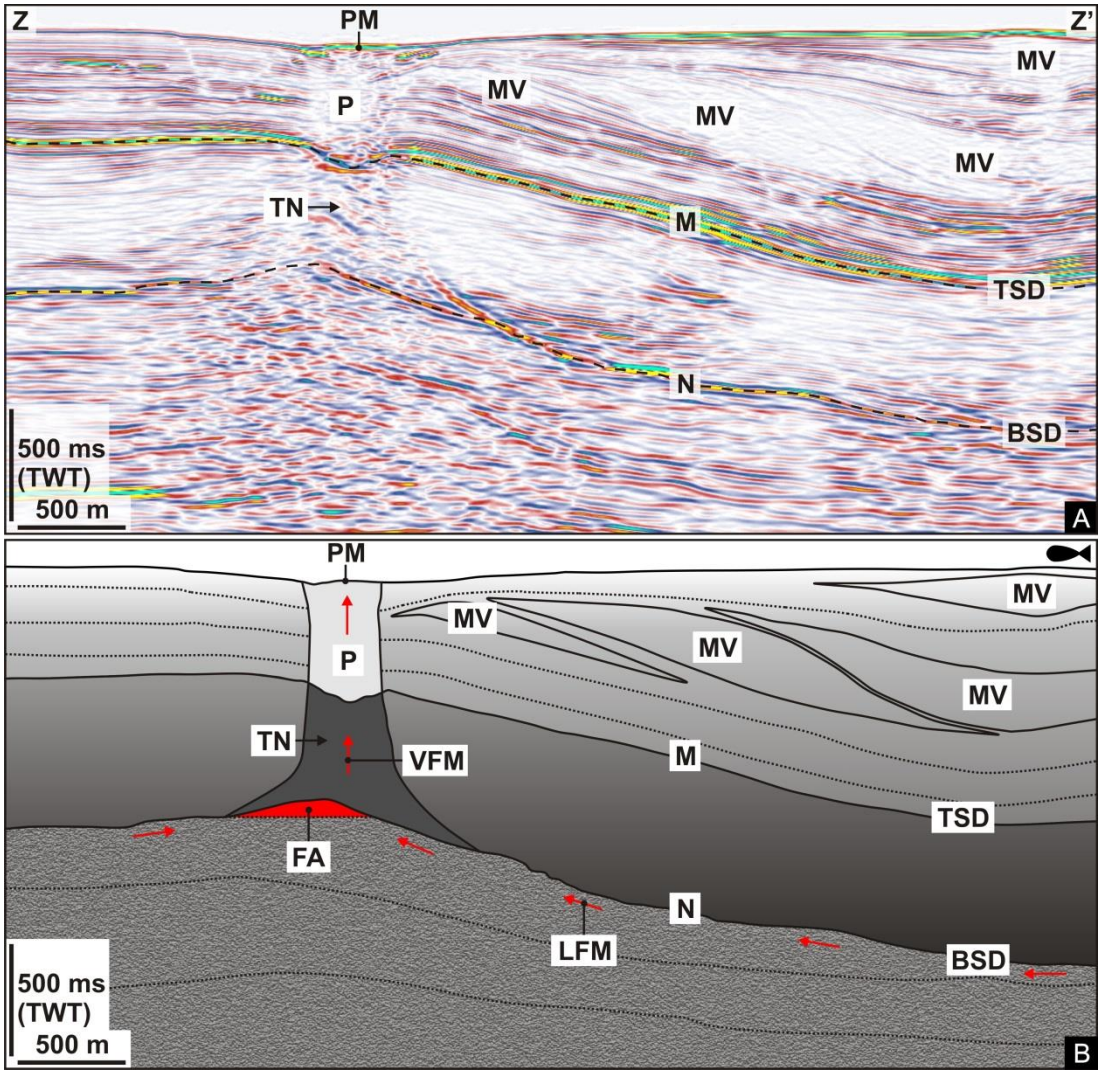

Figure 6.39 Seismic profile and cartoon showing the potential for up dip and lateral fluid migration and accumulation beneath the location where a fluid escape pipes has formed. A: Seismic profile showing top and base-salt depression formed beneath extruded mud volcanoes and a fluid escape pipe and pockmark that have formed at the margins of these depressions. B: Cartoon of the seismic profile in Figure 6.39A, demonstrating the potential for lateral fluid migration and accumulation up dip of a base-salt depression which controls the location of a fluid escape pipes formation. The red arrows represent the direction of fluid migration. P – Pipe; PM – Pockmark; MV – Mud volcano; TN – Trail of noise; TSD – Top-salt depression; BSD – Base-salt depression; LFM – Lateral fluid migration; VFM – Vertical fluid migration; FA – Fluid accumulation; M – Horizon M; N – Horizon N; TWT – Two way time.

some fluid escape pipes that root to pre-salt stratigraphy. If it is accepted that the base-salt depression have been formed by sediment withdrawal during mud volcano formation, the observed lack of base-salt depression beneath fluid escape pipes is understandable, considering the fluid escape pipes lack the solid component found within mud volcano conduits. This poses the question, in contrast to the mud volcano conduits, why do the fluid escape pipes not form extrusive mud volcanoes at their upper terminations?

One possible explanation for the lack of extrusive mud volcanoes above these fluid escape pipes could be if their root zone is different to the root zone of the mud volcano conduits. One of the pre-requisites for the formation of a mud volcano is a source of overpressured fine grained sediment that can be remobilised (Kopf, 2002). As previously discussed, the primary source of mud is interpreted to be Tortonian in age and to originate from the immediate pre-salt. If some of the fluid escape pipes do in fact root within the evaporite succession, which is a possibility discussed above, then it is conceivable that there is a source of overpressured fluids but no source of fine grained sediment. Additionally, if the root zone for some of the fluid escape pipes is even deeper than the source interval for mud, then it is possible that the fluid escape pipes bypassed the muds source interval. Sampling and geochemical analysis of the ascending fluids from one of the actively venting pockmarks at the present day seafloor could aid in constraining the fluid origin for these fluid escape pipes.

An alternative explanation is that the fluid escape pipes do in fact root to the same stratigraphic interval as the mud volcano conduits but simply did not evolve to include the solid component needed to form a mud volcano. It has previously been proposed that the initial stages of formation of mud volcano conduits may be similar to the formation of fluid escape pipes and that there may be a process whereby fluid escape pipes may evolve into mud volcano conduits as the composition of the fluids evolve to include solid components (Cartwright, 2007; Huuse et al., 2010; Cartwright and Santamarina, 2015). This interpretation could explain why the seismic characteristics and geometry of the fluid escape pipes and mud volcano conduits are so similar. It may also explain why both fluid escape pipes

and mud volcano conduits were observed within the same NW-SE orientated linear trends (Figure 6.34 and Figure 6.35). Some of the fluid escape pipes within these linear trends may have evolved into mud volcano conduits where as others within the same linear trend may not have evolved to include the solid component (Figure 6.35). The pipe with a small mud cone at its upper terminus in Figure 6.34E could be considered to be a mud volcano conduit and mud volcano in an early stage of evolution from a fluid escape pipe that has only recently begun to include a solid component within its venting fluids.

6.5 Conclusion

A large number of mud volcano conduits and fluid escape pipes from the El Dabaa study region, offshore Egypt, have been analysed based on their seismic characteristics and geometrical form. The images and interpretation presented here add further strong evidence to the growing argument of pre-salt fluid and sediment remobilisation through the Messinian evaporites, in the Eastern Mediterranean. Further key outcomes from the descriptive analysis are as follows:

- Numerous lines of evidence from seismic observations and documented studies of the composition of these mud volcanoes, brine pools and venting gas all indicate that the fluids and sediment that have migrated up these conduits is sourced within pre-Messinian stratigraphy and that the root zone of these conduits is pre-salt. The source of fluids and root zone for some fluid escape pipes could also potentially be intra-salt.
- The mud volcano conduits and fluid escape pipes within this study area share many similarities in their seismic characteristics and geometry, which could give an insight into the formation of both conduits.
- The potential mechanisms for the genesis of these fluid escape pipes and mud volcano conduits include hydraulic fracturing and dissolution and stoping.
- The high overpressure required within the pre-salt for the hydraulic fracturing of evaporites could have been achieved via rapid loading through

the rapid deposition of the evaporites and via build-up of gas pressure through fluid (methane) migration and accumulation beneath the evaporites.

- Combined, fluid escape pipes and mud volcano conduits do not survive to be re-used, potentially due to depressurising of overpressured areas within the pre-salt succession.
- Subjacent dissolution at the base of the evaporites could cause localised subsurface volume loss. Fluids could exploit the newly formed void, leading to further dissolution, fracturing and collapse of the roof of a pipe. By analogy, this mechanism is similar to a process known as stoping where the overburden collapses into the void.
- Methane-rich and oily hydrocarbon-rich hot brine and mud samples have been documented from several mud volcanoes within this study area. Bright spots observed in association with fluid escape pipes and mud volcanoes are interpreted as a response to the presence of free gas and are, hence, interpreted as direct hydrocarbon indicators.
- The stratigraphic position of the deepest pockmark within this study area demonstrates that, the formation of the first fluid escape pipe and pockmark post-dates the formation of the first mud volcanoes within the Pliocene to Recent succession.
- Fluid escape pipes have not significantly contributed to the location of base-salt depressions. Rather pipe location has been influenced by the base-salt geometry, which promotes updip lateral fluid migration and accumulation within structural traps at the margins of the depressions, which form overpressured pre-salt pockets.
- NW – SE linearity in the location of some fluid escape pipes and mud volcano conduits are indicative of fluid migration from underlying NW – SE orientated structural features such as faults and elongated anticlines.
- The initial stages of formation of mud volcano conduits may be similar to the formation of fluid escape pipes. It is possible that there is a process

whereby the solid component could be incorporated with migrating fluids within a pipe, resulting in its evolution into a mud volcano conduit.

Chapter 7

7 Discussion

7.1 Introduction

The Chapters that have proceeded have presented a detailed analysis of mud volcanoes using 3D seismic data from the El Dabaa study area, offshore Egypt within the Eastern Mediterranean. In Chapter 4, a suite of giant mud volcanoes that have been emplaced directly on top of the Messinian evaporite succession at the end of the Messinian Salinity Crisis, were described and discussed. A large number of mud volcanoes (386) that are conical and small, relative to those described in Chapter 4, were analysed in Chapter 5. The conduits that connect the source stratigraphic layer and the extruded mud volcano, and a suite of fluid escape pipes and pockmarks were the focus of Chapter 6. The analysis within these three chapters has revealed new insights into overpressure release at the end of the Messinian Salinity Crisis, the scale of mud volcanism and source of mud for mud volcanism within the Western Province of the Eastern Mediterranean, and the geometry and mechanisms for the formation of mud volcano conduits and their potential to bypass an evaporitic seal. This Chapter will focus on some of the unanswered questions regarding depletion zones, the timing and flux of mud volcanism and ultimately why such a significant scale of mud volcanism is observed here in contrast to other parts of the Eastern Mediterranean.

7.1.1 Aims

The aims of this chapter are to:

1. Summarise some of the key observations and interpretations from Chapters 4, 5 and 6 and demonstrate how they contribute to the main aims that were set out in Chapter 1.
2. Combine the results and discussion points from Chapters 4, 5 and 6 to address some of the wider questions that are yet to be discussed in full.

3. Discuss the implications of this research.
4. Outline the limitation of the research.
5. Suggest recommendations for further work.

7.1.2 Summary

The observations, interpretations and discussions in Chapters 4, 5 and 6 address many of the key aims and questions that were set out in Chapter 1. The main findings within these chapters and how they contributed to answering these questions is listed below.

7.1.2.1 The seismic expression and geometry of mud volcanoes

Chapter 4:

- Detailed description of a suite of giant mud volcanoes from Chapter 4, which display an irregular shape that contrasts with that which might be expected from a mud volcano from previously described examples (Evans et al., 2007; Fowler et al., 2000; Yusifov and Rabinowitz, 2004).
- Characteristics that contribute to defining these features as mud volcanoes include:
    1. the geometry of their upper and lower bounding surfaces, which converge to form an isolated lensoid body;
    2. their isopach distribution, which display maximum thickness centrally and a reduction in thickness with increasing proximity to the margins of the feature;
    3. the relief observed at the upper surface of the lensoid bodies, which is onlapped by the reflections of the hemipelagic deposits;
    4. the downlap of the upper surface onto Horizon M and the significant extent of Horizon M that they directly overlie;
    5. The sub-2500 m/s p-wave velocity of the bodies.

- These mud volcanoes comprise a single extrusive body which implies that their extrusion was a single phase event

Chapter 5:

- The smaller mud volcanoes within this study area that are described in Chapter 5 are characterised as single lensoid bodies which exhibit varied dimensions.
- They are identifiable as circular to elliptical features that display an overall conical geometry and exhibit similar seismic characteristics to one another in seismic profile.
- There is no scaling between the diameter and thickness of these mud volcanoes, which suggests a combination of other factors, such as the viscosity of the mud and geometry of the conduit, govern the final geometry of these mud volcanoes.
- Despite the single lensoid body of these mud volcanoes they are geometrically more similar to mud volcanoes described in other sedimentary basins than the giant mud volcanoes described in Chapter 4 (Calves et al., 2010; Evans et al., 2007; Fowler et al., 2000; Yusifov and Rabinowitz, 2004).
- Despite the geometrical differences between these mud volcanoes and the giant mud volcanoes described in Chapter 4, the two types of mud volcanoes exhibit similarities in their seismic facies.

Chapter 6

- The mud volcano conduits described in Chapter 6 exhibit a wide variety in their dimensions and geometry, which could have a significant impact on the variety in geometry of the numerous mud volcanoes.

7.1.2.2 Distribution

Chapter 4

- The giant mud volcanoes described in Chapter 4 have all been emplaced synchronously on top of the Messinian evaporite succession at the end of the Messinian Salinity Crisis.
- The location of LB1 and LB3 from the suite of giant mud volcanoes is associated with localised areas of relief at the base of the evaporite succession and pre-salt faults that display correlatable geometry and spatial correspondence to the overlying giant mud volcanoes.

Chapter 5

- There is a high frequency of mud volcanoes towards the base of the Pliocene to Recent succession, which follows the formation of the giant mud volcanoes. The frequency decreases up through the succession and then increases again nearer to the seafloor. If the correlation of a mass transport deposit within the study area, here named the El Dabaa slide, is accurate then this increase in the frequency of mud volcanism has occurred during Upper Pleistocene to Recent times.
- Statistical analysis of the spatial distribution of the conical mud volcanoes within this study area has shown that they are statistically clustered.
- Mud volcanoes that have formed more recently display a close spatial correlation to pre-existing mud volcanoes and even stack above them in some cases.
- There appears to be no spatial control between the locations of more recently formed mud volcanoes relative to the location of mud volcanoes that comprise a significant volume towards the upper end of the range of volumes.

Chapter 6

- Fluid escape pipes are distributed in a variety of configurations, from clustered and irregular patterns to linear trails and around the periphery of base-salt depressions.

The geometry of the base-salt has had a major influence on the location that fluid escape pipes and pockmarks form.

- Pockmarks and mud volcanoes are observed at various levels within the Pliocene to Recent succession and imply that fluid and mud venting has occurred at various intervals since the end of the Messinian Salinity Crisis to Recent.

7.1.2.3 Source

Chapter 4

- The giant mud volcanoes were emplaced directly on top of the Messinian evaporite succession, which indicates a source of fluids and mud that is at least pre-Pliocene.
- A clear connection can be observed in some cases between the giant mud volcanoes and the pre-salt succession, which implies that pre-salt fluids and mud have bypassed the Messinian evaporite succession.
- An anomalously low velocity (<2000 m/s) within the first 1000 m of the sub-salt section could be considered indicative of undercompaction. This would make the immediate pre-salt succession susceptible to overpressuring, which could make it a viable candidate to be a source stratigraphic succession for mud remobilisation.

Chapter 5

- There is a strong spatial correlation between conical mud volcanoes and underlying base-salt depressions.
- Anomalous thinning of the evaporite succession and the immediate pre-salt succession, beneath areas of combined base and top-salt depressions and mud volcanoes, further supports the interpretation that the immediate pre-salt succession is the primary source layer.
- Calculations of potential sediment withdrawal from the immediate pre-salt when compared to the volume of sediment calculated within overlying mud volcanoes

are found to be relatively similar. This is indicative that the mud feeding these mud volcanoes has been primarily sourced from the immediate pre-salt.

- Documented analysis of nannofossils from cores taken from mud volcanoes within this study area found clasts as old as Cretaceous in age in the mud breccia's extruded from mud volcanoes at the seafloor within this study area (Giresse et al., 2010).

Chapter 6

- All the fluid escape pipe and mud volcano conduits observed within this study area clearly pierce the top of the evaporites, which is evident by the break continuity of the reflection of Horizon M. This indicates that the fluids and mud involved in their formation have migrated at least in part through the evaporites.
- Hot saline brine pools documented in association with the mud volcanoes within this study area are saline rich and are indicative of dissolution of the Messinian evaporites within ascending hot fluids (Mascle et al., 2014; Huguen et al., 2009; Dupré et al., 2014; Giresse et al., 2010).
- The absence of a regionally extensive and significantly large source of fine grained sediment within the evaporite succession indicates that the source of mud and fluids for the mud volcanoes is within the pre-salt.

7.1.2.4 Conduits

Chapter 4

- Fluids could have been source from greater depths than the immediate pre-salt succession. Pre-salt faults that been observed at Horizon N (also described in section 3.5 of Chapter 3) and deeper directly underlying giant mud volcanoes could be exploited by migrating fluids.
- Ridges of relief at Horizon N are spatially correlatable with overlying giant mud volcanoes and underlying pre-salt faults. These observed spatial correlations are

indicative of fluid migration from deeper pre-salt layers, which locally further elevate pore fluid pressure and influence the location of formation and geometry of the overlying giant mud volcanoes.

Chapter 6

- Mud volcano conduits and fluid escape pipes can both be reliably identified as steep zones of discontinuity, disruption and attenuation to the reflections of the host succession. Their lateral margins can be accurately defined as the edge of an area of discontinuity.
- The mud volcano conduits and fluid escape pipes display variable heights and widths and exhibit a similar overall three dimensional geometry, which is most closely comparable to a vertically orientated cylinder. These mud volcano conduits are pipe-like in their seismic expression and geometry.
- Hydraulic fracturing and dissolution and stoping represent the mechanisms with the greatest potential for the genesis of the mud volcano conduits and fluid escape pipes within this study area.
- The high overpressure required for hydraulic fracturing of evaporites could have been achieved within the pre-salt via rapid loading through the rapid deposition of the evaporites and via build-up of gas pressure through fluid (methane) migration and accumulation beneath the evaporites.
- Subjacent dissolution at the base of the evaporites potentially caused localised subsurface volume loss. Fluids could exploit the newly formed void, leading to further dissolution, fracturing and collapse of the roof of a pipe via a stoping mechanism
- A striking similarity between fluid escape pipes and the conduits for these mud volcanoes has been observed, in combination with pockmarks and mud volcanoes within the same linear trends. These observations could be indicative that the initial stages of formation of a mud volcano conduit may be similar to the formation of fluid escape pipes and that some fluid escape pipes could have evolved to incorporate the solid element required for mud volcanism.

7.1.2.5 Impact on the evaporites

Chapter 4

- Some large and irregular shaped top-salt depressions are spatially correlatable to giant mud volcanoes that lie directly on top of the Messinian evaporites. These top-salt depressions are also correlatable with localised areas of anomalous thinning of the Messinian evaporites succession.
- The additional gravitational load on the salt that is applied by the overlying giant mud volcanoes has the potential to cause the withdrawal underlying mobile evaporites. This is one explanation for the anomalous thinning of the evaporites and top salt depressions that have been observed.
- The ascension of hot fluids through the evaporite succession during the extrusion of the giant mud volcanoes has the potential to result in the dissolution of the evaporites succession, therefore, contributing to the anomalous thinning and top-salt depressions that have been observed.

Chapter 5

- Similar to the giant mud volcanoes, localised gravitational loading by the extruded mud and dissolution of the evaporite succession within ascending fluids of a pre-salt origin could has caused the localised thinning of the evaporite succession and top-salt depressions that has been observed. Stacking of multiple mud volcanoes results a gradual increase in the gravitational load and the potential for multiple episodes do salt dissolution and hence, more significant salt withdrawal and removal.
- The observed of a strong spatial correlation between top-salt and base-salt depressions in combination with volumetric analysis argues that, sediment withdrawal and subsequent base-salt depressions result in subsidence of the overlying evaporites and post-salt successions.

Chapter 6

- The potential mechanisms of dissolution and stoping for the formation of these conduits involves the localised removal of evaporites from the Messinian succession and so may have attributed to the localised thinning and top-salt depression that have been observed.

7.1.2.6 Remaining questions

Many of the key questions that were set out at the start of this thesis have been discussed in prior Chapters. From this point on, this chapter will focus on some remaining questions that are yet to be discussed in full, which include:

1) Why is the scale of mud volcanism within this study area so large?
2) What governs the eruptive flux of mud over time?
3) How does depletion of the source interval impact the stacking pattern of all the mud volcanoes throughout the study area?
4) What are potential reasons why extensive mud volcanism has occurred within this study area but not all other parts of the Eastern Mediterranean?

7.2 Volumetric Considerations

A collection of five mud volcanoes with a combined volume of c. 216^3 were observed in Chapter 4. In Chapter 5, as many as 386 mud volcanoes with a combined volume of c.208 km^3 were observed. The combined volume of mud to have been extruded via mud volcanoes within this study area is c. 424 km^3.This analysis raise the question; what do the significantly large number of mud volcanoes and large volumes of mud that have been mobilised and extruded imply?

7.2.1 Fluids, mud and overpressure

The core requirements for mud volcanism are thought to include a supply of undercompacted sediment and fluids in a state of overpressure (Kopf, 2002). The mud volcanoes within this study area cover a large region, which implies a similarly extensive source of undercompacted mud from which to be sourced must be present. The rapid burial of the immediate pre-salt succession during the rapid deposition of the Messinian Salinity Crisis presents a feasible mechanism for resulting in undercompaction of the immediate pre-salt succession, which would make it a viable primary source unit of mud (See section 7.1.2.3). Despite thinning towards the southwest (See Figure 3.5. and Figure 3.7), the immediate pre-salt unit is relatively thick and laterally extensive, which in combination with the prospect that it is undercompacted presents a strong argument for its suitability as the sediment source for the similarly extensive field of mud volcanoes.

The fluids feeding these mud volcanoes are interpreted to have been sourced primarily from the pre-salt, particularly the immediate pre-salt succession, as stated in section 7.1.2.3. The process of undercompaction also presents the potential for significant retention of pore fluids within the immediate pre-salt succession (Kopf, 2002). The loading effect of the Messinian evaporite succession and the Pliocene to Recent succession also present a viable mechanism for generating overpressure within the immediate pre-salt succession (Osborne and Swarbrick, 1997; Swarbrick, 1999). However, pore fluids within the immediate pre-salt succession may not be the only source of fluids and the discussed loading mechanism may not be the only mechanism with the potential to generate significant overpressure.

It is at present not possible to ascertain the precise stratigraphic intervals from which fluids have originated from during mud volcanism within this area. It has been previously stated, however, that clasts of up to Cretaceous in age have been documented among the various clasts collected from piston cores from mud volcanoes at the seafloor (Giresse et al., 2010). In order for clasts of up to Cretaceous in age to be extruded from a mud volcano at the seafloor, they must have been entrapped within upward migrating fluids. This implies a fluids source at least as deep as within

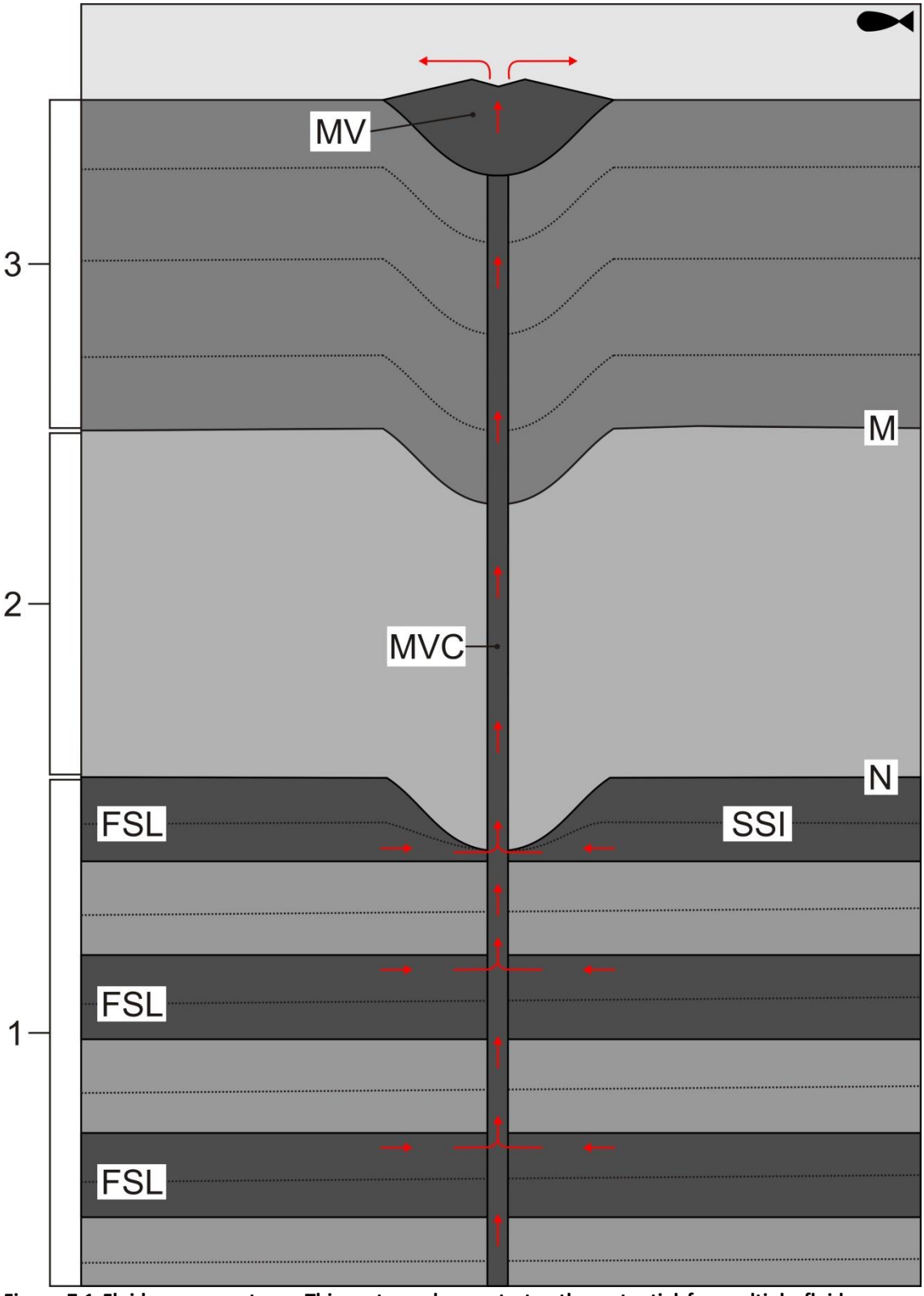

Figure 7.1 Fluid source cartoon. This cartoon demonstrates the potential for multiple fluid sources during the formation of these mud volcanoes.

Cretaceous stratigraphy and that there is more than one fluid source involved in the formation of these mud volcanoes. A similar interpretation has recently been made for the source of fluids for the modern day Lusi mud volcano (Mazzini et al., 2009; Mazzini et al., 2007; Tanikawa et al., 2010), which supports an interpretation of potentially multiple fluid sources during the formation of mud volcanoes such as those observed within this study area.

The potential that some of the fluids from these other sources could be hydrocarbons has been previously discussed (See section 3.6 of Chapter 3 and 6.4.2.1 of Chapter 6). The evidence for hydrocarbons includes direct hydrocarbon indicators in seismic data and documented evidence for nearby proven hydrocarbon plays with Oligocene to Miocene source rocks (EGAS, 2012a; EGAS, 2012b; EGAS, 2012c) and methane-rich and oily hydrocarbon-rich hot brine and mud samples taken from several mud volcanoes within this study area (Pierre et al., 2014; Dupré et al., 2014; Huguen et al., 2009). The documented analysis of natural gas formations within the western Nile Delta has found it to be a mixture of microbial methane and thermogenic gas, the thermogenic of which is interpreted to be of a pre-Miocene origin (Vandré et al., 2007).

Within the neighbouring petroleum province of the Western Desert potential source rocks for oil and gas have been interpreted as deep as coal rich Mid Jurassic sediments and also within Upper Cretaceous formations (Vandré et al., 2007). Modelling of the burial history and window for source rock maturity has found that hydrocarbon generation within the western Nile Delta is controlled by rapid burial during Miocene to Pleistocene time and is supposedly an active process at the present day (Vandré et al., 2007). The generation of hydrocarbons is another way in which overpressure can be generated (See section 6.4.2.1 of Chapter 6) and the location of formation of mud volcanoes has been documented as often found in spatial association with areas of hydrocarbon generation (Osborne and Swarbrick, 1997; Kopf, 2002). The period of hydrocarbon generation within the western Nile delta described by Vandré et al. (2007) is also correlatable with the period of time during which mud volcanoes have formed within this study area. This could be considered indicative that

the generation of hydrocarbons may have played a key role in generating the buoyancy and overpressure required for mud volcanism.

7.2.2 Depletion zone

A depletion zone is here defined as a section of a source stratigraphic layer, from which a volume of sediment has been liquefied and withdrawn during the intrusion and subsequent extrusion of liquefied sediment. Depletion zones associated with mud volcanoes have been previously interpreted in other sedimentary basins, due to the identification of a mud volcano which is underlain by sagging reflections formed due to subsidence, which overlie a stratigraphic layer that clearly displays thinning due to a volume loss at depth (Stewart and Davies, 2006; Istadi et al., 2009; Fukushima et al., 2009). Giant craters and sediment mounds within the Møre basin offshore Norway, have similarly recently been interpreted as associated with the mobilisation of sediments which has resulted in the formation of a depletion zone and subsequent crater (Lawrence and Cartwright, 2010). The vertical nature of the conduits observed in Chapter 5 and the strong spatial relation between the location of mud volcanoes and base-salt depressions that directly underlie them indicates that the mud feeding these mud volcanoes has been withdrawn from directly beneath the mud volcanoes.

Evidence for depletion of the source stratigraphic layer beneath the highly active Menes caldera was presented in section 5.4.6 of Chapter 5. A simpler example of the depletion associated with just a single mud volcano is displayed in the example in Figure 7.3. Underlying the mud volcano the reflections of the Pliocene to Recent succession, Horizon M and Horizon N all display a sagging geometry (Figure 7.3A). The first clear and continuous reflection that does not display sag geometry is here referred to as the base of the immediate pre-salt. This reflection is the base of the less coherent upper section of unit 2 that is described in 3.5.3 of Chapter 3. This reflection is relatively flat when compared to the overlying reflection of Horizon N (Figure 7.3A). The top of the immediate pre-salt succession is also Horizon N, which displays a large

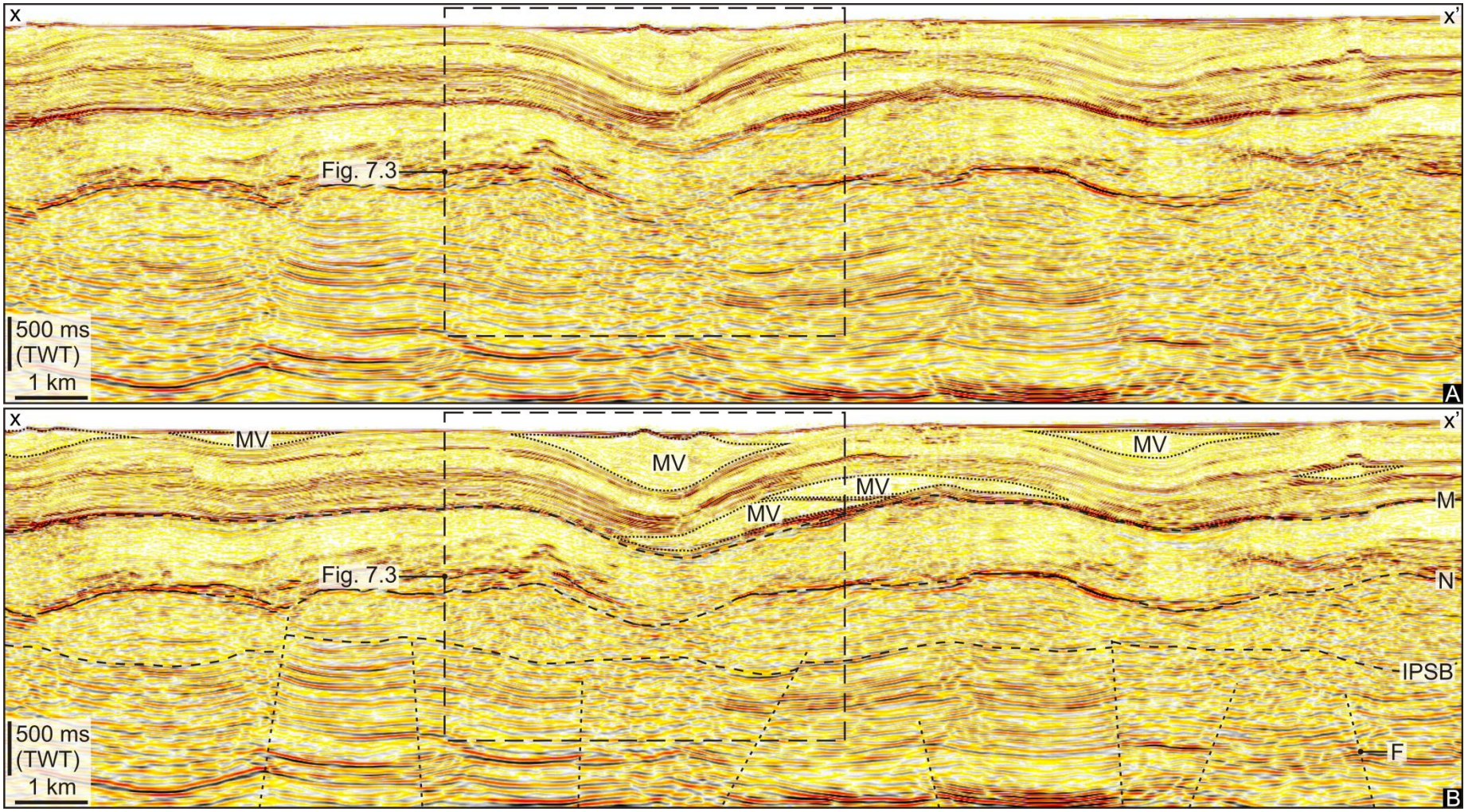

Figure 7.2 Pre-salt withdrawal. A: Seismic profile through a mud volcano. B: An interpretation of the seismic profile in Figure 7.2A, displaying a top and base-salt depression beneath a mud volcano and localised thinning of the immediate pre-salt beneath. The area of the seismic profile displayed in Figure 7.3A is highlighted. The line of section can be seen in Figure 7.3. MV – Mud volcano; F – Fault; M – Horizon M; N – Horizon N; IPSB – Immediate pre-salt base.

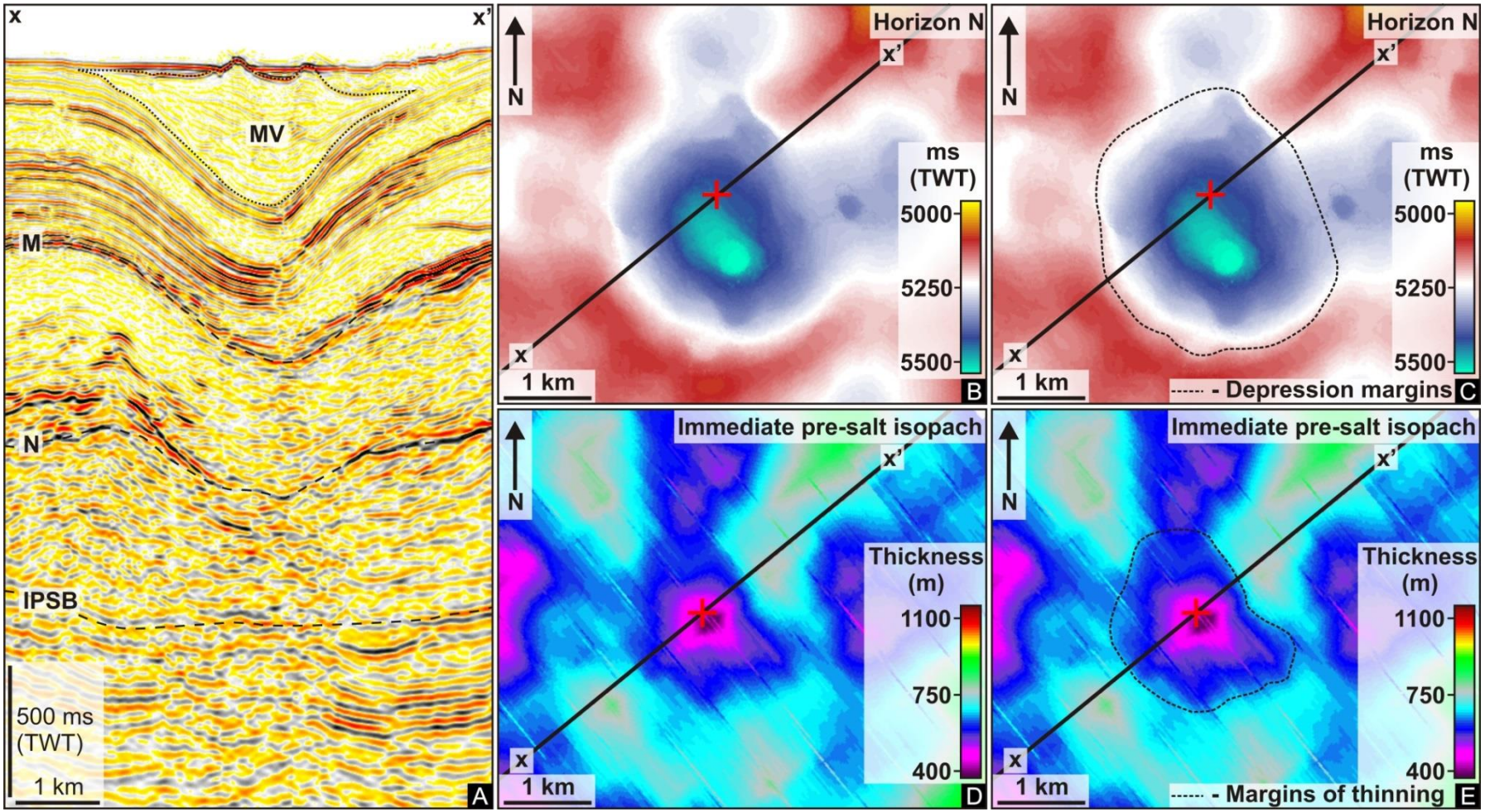

Figure 7.3 Pre-salt sediment withdrawal beneath a mud volcano. A: Interpreted seismic profile through a mud volcano. B: Base-salt depression beneath the mud volcano in Figure 7.3A. C: An interpretation of the margins of the base-salt depression in Figure 7.3B. D: Localised thinning of the immediate pre-salt beneath the mud volcano in Figure 7.3A. E: An interpretation of the margins of the localised area of thinning of the immediate pre-salt in Figure 7.3D. The red + in B to E marks the centre of the overlying mud volcano. MV – mud volcano; M – Horizon M; N – Horizon N; IPSB – Immediate pre-salt base.

and circular to sub-circular depression c. 600 m deep and up to c. 3500 m wide (Figure 7.3B and Figure 7.3C). The deepest part of this depression is off centre with respect to the mud volcano that it underlies (Figure 7.3B and Figure 7.3C). The depression observed at the upper surface of the immediate pre-salt succession results in a localised and sub-circular area of anomalous thinning, which displays a c. 360 m decrease in thickness, the thinnest part of which directly underlies the centre of the overlying mud volcano (Figure 7.3D and Figure 7.3E). Other base-salt depressions and areas of anomalous thinning of the immediate pre-salt succession can be seen in close proximity to the one described above (Figure 7.3), however, they are associated with other mud volcanoes within the Pliocene to Recent succession.

The observations made of the stratal geometries and thickness variations of stratigraphic layers beneath mud volcanoes are indicative of a zone of depletion within the immediate pre-salt interval (Figure 7.4). This interpretation is also consistent with the numerous lines of evidence presented in Chapter 4, 5 and 6 that argue that the immediate pre-salt succession is the primary source layer for the mud volcanoes within this study area.

It has previously been suggested that similar to salt structures; it should be possible to volumetrically balance a depletion zone and the extruded material within a mud volcano (Stewart and Davies, 2006). Volumetric balance calculations in section 5.3.7 of Chapter 5 found the volumes of sediment calculated to have been withdrawn from the immediate pre-salt succession and the volumes calculated within the overlying mud volcanoes are strikingly similar. A similar volumetric balance calculation for the examples in Figure 7.3 has found that the volume of sediment withdrawn from the immediate pre-salt succession and the volume of the mud volcano are 2.1 km^3 and 2.4 km^3 respectively. These two volume values are also strikingly similar and add further compelling evidence (albeit on a smaller and simpler scale) that the volume of sediment extruded during the formation of these mud volcanoes is primary depleted from within the immediate pre-salt succession. The margins of the area of anomalous thinning within the immediate pre-salt succession define the margins of the depletion zone (Figure 7.3E). A model for the withdrawal of sediment from the immediate pre-

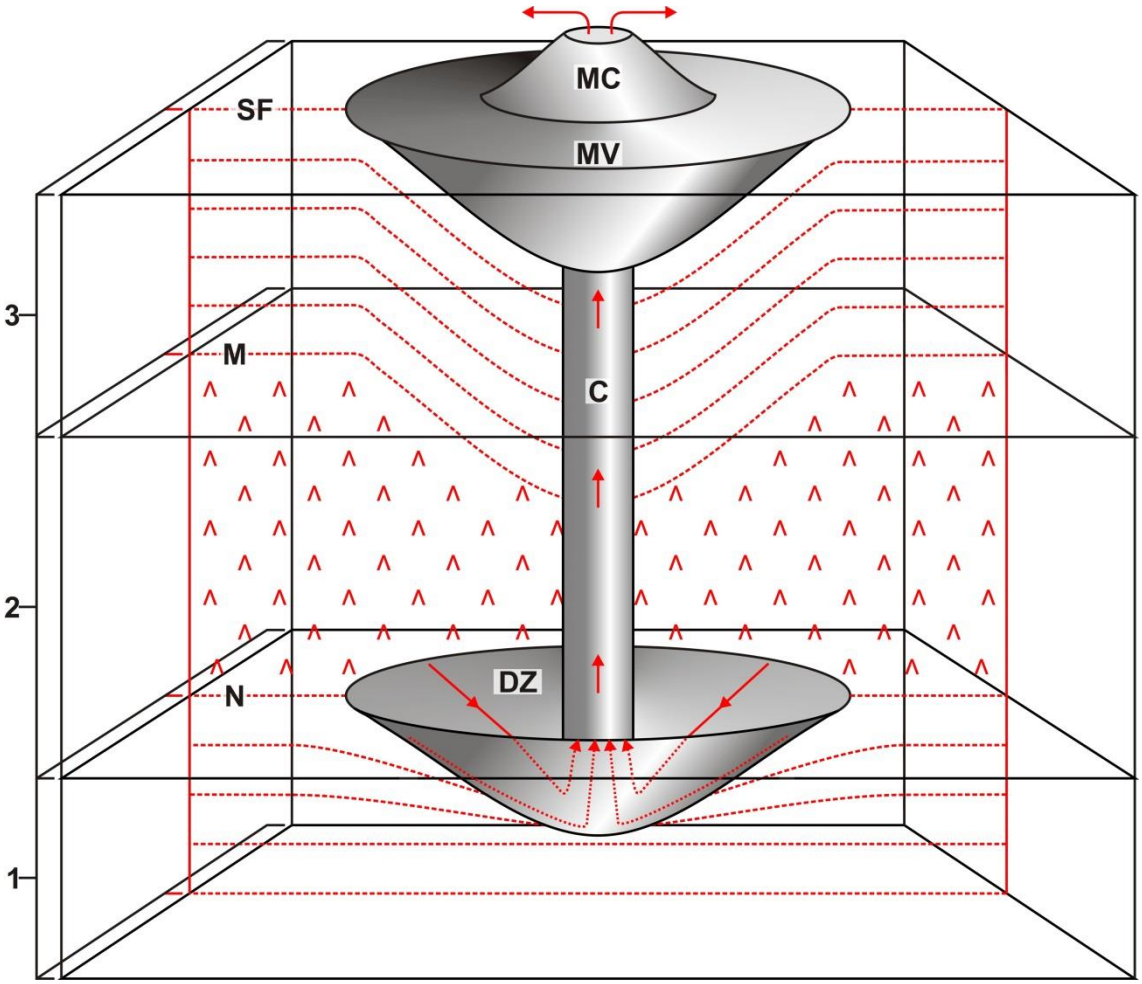

Figure 7.4 A model for the depletion zone of a mud volcano. The depletion zone, conduit and mud volcano are displayed in 3D and the red lines represent a 2D profile through the centre of the 3D structure. The red arrows represent the direction of fluid and sediment mobilisation. MC – Mud cone; MV – Mud volcano; C – Conduit; DZ – Depletion zone; SF – Seafloor; M – Horizon M; 1 – Immediate pre-salt; 2 – Messinian evaporites; 3 – Pliocene to Recent.

salt succession during the extrusion of mud and the formation of a depletion zone are displayed in the examples in Figure 7.4.

Recent analysis of nannofossils from mud volcanoes in Trinidad is thought to indicate that the sediments feeding those mud volcanoes were sourced from various levels that the mud volcano conduit transects and, therefore, not just from a single stratigraphic level (Deville et al., 2003; Deville et al., 2010). The volumetric analysis that has been undertaken in this project strongly indicates that the majority of the sediments feeding these mud volcanoes are sourced from the immediate pre-salt succession. The interpretation of depletion from the immediate pre-salt is also supported by a similar interpretation made by Bentham et al. (2006). However, slightly greater volumes have been calculated within the mud volcano than the depleted zone. This observation in combination with discovery of clasts up to Cretaceous in age within core samples from mud volcanoes within this area could imply that there are some sediments sourced from greater depths that have been mobilised within ascending fluids that originated in the Mesozoic. Some clasts from the walls of the mud volcano conduit could also be entrained in the ascending fluids.

7.2.3 The process of remobilisation

The formation of mud volcanoes via the extrusion of mud at the surface clearly implies that sediment has been removed from somewhere deeper within a lithological succession. However, solid grains do not readily ascend through a lithological succession and the mud that is extruded from a mud volcano is a combined fluid and mud slurry. This raises the question, what are the processes behind liquefying and mobilising sediment from a stratigraphic layer?

A potential mechanism that should be considered for driving the ascent of sediments up through a lithological succession is fluidization. Fluidisation is the mobilisation of granular material within migrating fluids of a sufficient velocity (Cartwright and Santamarina, 2015; Lowe, 1975). It occurs when the drag exerted on the sediments of a host succession by moving pore fluids exceeds the buoyancy weight

of the grains, which is due to the fluid velocity exceeding the settling velocity of the grains (Judd and Hovland, 2007) (See Chapter 1). The result is that the grains are lifted and carried away within the fluid flow. It is, however, difficult to imagine how the necessary flow velocity for fluidization can develop within a layered sedimentary succession where low permeability and fine grained layers impede fluid flow, and how this mechanism could result in the withdrawal of sediment from a large area of a sedimentary layer (Cartwright and Santamarina, 2015) (Figure 7.3). Perhaps once a conduit for a mud volcano is formed and a direct connection between the overpressure layer and the surface has been established, then perhaps the fluid velocity could become sufficient to internally erode the conduit and entrap some grains in the ascending flow.

An alternative mechanism for mobilising mud into a slurry is the process of liquefaction. Liquefaction is when there is a loss of friction between grain particles in a loosely packed framework and the grains become temporarily fluid supported, therefore, they are suspended in the pore fluids (Judd and Hovland, 2007). The result of liquefaction is that the sediment becomes liquefied and so can flow like a fluid. In order for liquefaction to occur, particle interaction stress must equal zero, therefore, all stress is taken temporarily by the fluid and effective stress equals zero (Judd and Hovland, 2007; Brown, 1990). It has previously been implied by Davies et al. (2008) that the requirement of increasing pore fluid pressure for liquefaction (Jolly and Lonergan, 2002) are the same conditions that are required to initiate mud volcanism.

The Lusi mud volcano represents a modern day example of a mud volcano, which despite a dispute regarding the trigger behind its formation (drilling vs earthquake) (Davies et al., 2008), is thought to be associated with liquefaction (Tanikawa et al., 2010; Mazzini et al., 2012; Davies et al., 2008). One argument that has been proposed is that a reduction in rock strength as a result of long term high fluid pressure may have resulted in mud volcanism. This is because liquefaction and hydraulic fracturing are thought to be more likely to occur in successions of low rock strength when low level and dynamic fluctuations in pore fluid pressure are exerted, such as those expected from the Yogyakarta earthquake (Tanikawa et al., 2010).

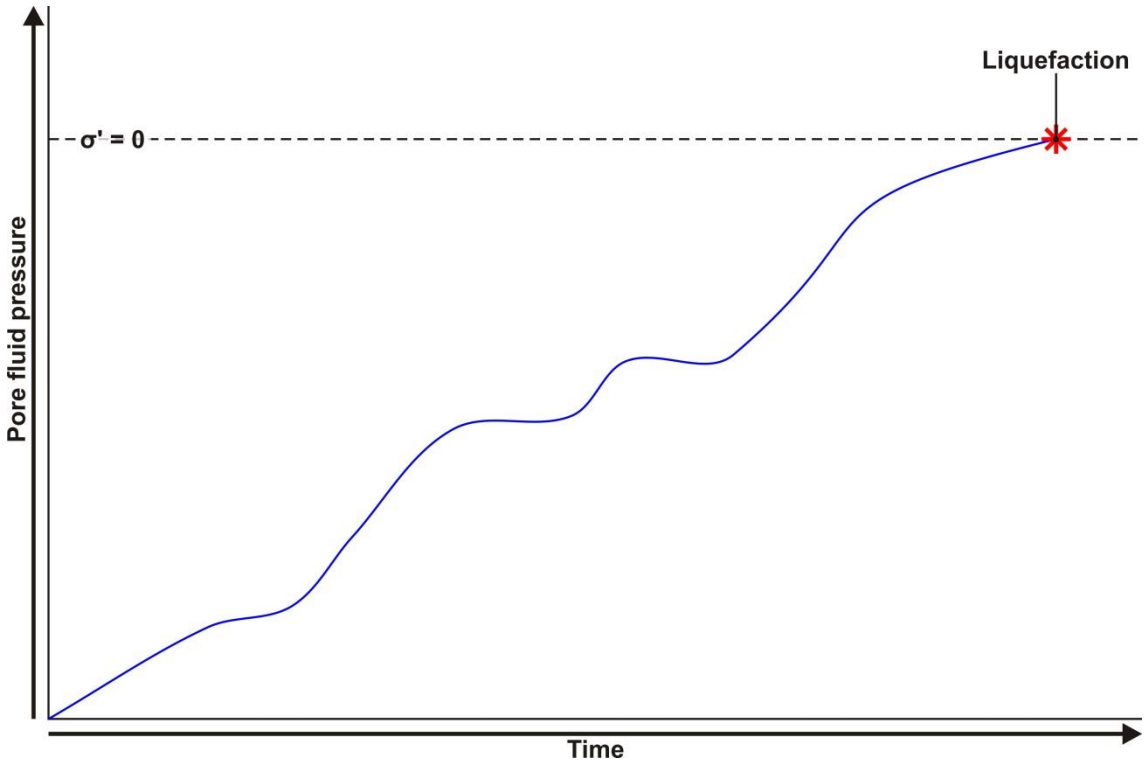

Figure 7.5 Pore fluid pressure curve leading to liquefaction. The curve displays how a gradual increase in pore fluid pressure over time can results in a state of zero effective stress (σ^1=0) and hence liquefaction.

Achieving the mobilisation and depletion of an extensive volume of sediment during mud volcanism on the scale observed within the El Dabaa study area, is more plausible if a similarly extensive zone of the source stratigraphic unit is in a consistent state of overpressure and has in part been fluidized via liquefaction, similar to as interpreted for the Lusi mud volcano (Davies et al., 2008; Tanikawa et al., 2010). If this is the case, what are the potential processes behind causing liquefaction of the source stratigraphic interval? Liquefaction and subsequently mud volcanism is a known hydrologic response to earthquakes (Davies et al., 2008; Mellors et al., 2007; Kopf, 2002; Deville and Guerlais, 2009). Liquefaction most commonly occurs in very shallow, sand rich sediments, because it is much easier for fluid pressure to reach lithostatic pressure in shallow sedimentary layers than in deep layers (Tanikawa et al., 2010). Liquefaction within deep layers, is sometimes observed but is thought to be much rarer and related more to the generation of overpressure in layers of low permeability (Kopf, 2002; Tanikawa et al., 2010).

During an earthquake, seismic waves that pass through an undercompacted and fluid rich sequence try to compact and expel fluids from the sequence. However, if the pore water cannot be drained away, pore fluid pressuring increases (Judd and Hovland, 2007). If the pore fluid pressure were to elevate to near or exceed the overburden stress then liquefaction can occur (Judd and Hovland, 2007; Tanikawa et al., 2010) (Figure 7.5). The immediate pre-salt succession within this study area has the potential to be undercompacted and fluid rich and the Messinian evaporite succession has the potential to seal the immediate pre-salt succession and prevent the expulsion of fluids, as discussed above. It is, therefore, possible that an earthquake event could result in a sudden increase in pore fluid pressure and liquefaction of the immediate pre-salt succession. This mechanism for liquefaction is made all the more plausible due to the documentation of numerous earthquake events that reportedly occurred within the Egyptian passive margin during the Quaternary at least (El-Araby and Sultan, 2000; El-Sayed et al., 2004; Garziglia et al., 2008).

A rapid increase in vertical compressive stress via a form of loading of an undercompacted succession could lead to a sudden increase in overpressure, which if sufficient could result in a reduction in effective stress and liquefaction (Osborne and

Swarbrick, 1997; Judd and Hovland, 2007). A strong argument was presented in section 4.4.2 of Chapter 4 that the loading effect from the rapid deposition of the Messinian evaporites and rapid influx of seawater during the Zanclean Flood resulted in a sudden increase in overpressure within the pre-salt succession, which led to liquefaction (Garcia-Castellanos et al., 2009; CIESM, 2008).

There are other ways in which a sudden addition of vertical load could have been applied within this study area. The large mass transport deposit within, here named the El Dabaa slide, was described in section 5.3.4.1 of Chapter 5 and covers a significant section of the study area. It has previously been suggested that slope failure and mass wasting represents a form a sediment loading that can have a significant impact on lithostatic pressure (Judd and Hovland, 2007). The formation of a large mass transport deposit such as the El Dabaa slide, therefore, present another viable mechanism for generating overpressure, due to the sudden addition of vertical load. It is possible that the overpressure generated by the El Dabaa slide may have been sufficient to cause a sufficient reduction of effective stress and trigger liquefaction for some of the mud volcanoes, or at least contribute in part to the generation of overpressure that eventually results in liquefaction.

A suite of biosiliceous ooze mounds documented within the Møre basin offshore Norway present a suitable analogy to the loading mechanism via mass wasting suggested above (Lawrence and Cartwright, 2010). One proposed model for the formation of those mounds is that a mass wasting event loaded the biosiliceous ooze and that the additional vertical load caused it to undergo liquefaction, which resulted in mobilisation of the ooze layer (Lawrence and Cartwright, 2010). The volumes of sediment within the mounds observed in the Møre basin are of a significantly large scale (ranges from 5 km^3 to 580 km^3 per mound), which implies that the resultant scale of sediment mobilised via this loading mechanism could be sufficient for the scale of mud mobilisation observed within the El Dabaa study area and could be applicable in other mud volcano hosting sedimentary basins.

Eustatic sea level variation implies the loading and unloading of the water column over time and has also been proposed to have a significant impact on pore

fluid pressure within an undercompacted succession (Judd and Hovland, 2007). Over the last 150 kyrs alone there has been significant eustatic sea level fluctuation as demonstrated in Figure 3.4 of section 3.3 of Chapter 3. The loading effect due to an increase in sea level is discussed above in relation to the Zanclean flood and smaller increases while less significant may, therefore, also result in overpressuring. A decrease in sea level can, also have a significant impact on an undercompacted sedimentary unit that is already overpressured, such as the pre-salt succession within this study area. A drop in sea level results in a reduction in hydrostatic pressure, which reduces the level of pore fluid pressure required at which zero effective stress and liquefaction is achieved (Judd and Hovland, 2007). Rapid unloading and subsequent reduction in the overburden stress can also lead to gas expansion and an increase in overpressure (Bertoni et al., 2013). It has recently been suggested that even a modest fall of ~100 m can have a significant impact on subsurface pressure conditions within a dominantly fine grained succession (Andresen and Huuse, 2011; Bertoni et al., 2013). It is possible that the drop in sea level that can be observed in Figure 3.4 in Chapter 3 could be a viable mechanism to generate overpressure within the pre-salt succession and even result in liquefaction and mud mobilisation. A similar mechanism was previously proposed regarding the formation of a suite of pockmarks that are also located within the Egyptian passive margin (Moss, 2010).

The example of a liquefaction mechanism such as an earthquake is associated with a very sudden increase in overpressure; however, an argument could also perhaps be made for a slower and more gradual process of overpressure generation. A gradual increase in pore fluid pressure within the undercompacted succession could be achieved via a gradual influx of overpressured fluids of an origin such as from diagenetic transformations and hydrocarbon generation (Jolly and Lonergan, 2002; Osborne and Swarbrick, 1997; EGAS, 2012a; EGAS, 2012b; EGAS, 2012c; Vandré et al., 2007; Bertoni and Cartwright, 2015). Perhaps over longer periods of geological time, pore fluid pressure within the undercompacted and fluid rich pre-salt succession may gradually increase, aided by the sealing evaporite succession that overlie. Fluid pressure may continue to gradually increase over time to the point where it is near or exceeds the overburden stress and liquefaction can occur (Brown, 1990) (Figure 7.5).

An important aspect to this interpretation that must be considered is that the integrity of the seal must be sufficient to withstand significant overpressure and not fracture before the point at which liquefaction can occur. If the seal were to fracture prior to liquefaction, pore fluids within the undercompacted unit would bleed-off into the fractures and result in a decrease in pore fluid pressure. The sealing capability of the thick unit of Messinian evaporites within this study area (Downey, 1984; Gluyas and Swarbrick, 2009; Warren, 1999) may, however, be sufficient to prevent fluid escape and allow pore fluid pressure to reach the point of zero effective stress and liquefaction before fracturing of the salt occurs.

An interesting question that remains with regards to the zone of liquefaction is how does the entire volume liquefy? For example, are the sediments within what eventually becomes the depletion zone liquefied all at once or is depletion achieved via a multi stage dynamic liquefaction process (Terzaghi et al., 1951)? Some key observations to consider are the internal stratification that can be observed within some of the mud volcanoes (See section 5.3.1 of Chapter 5), the circular to sub-circular geometry in planform of the depleted zone (Figure 7.3 and Figure 7.4) and the gradual sloping sides of the base-salt depressions that comprise the upper surface of the depletion zone (Figure 7.2 and Figure 7.3). Some of the more irregular base-salt depressions described in section 5.3.6 of Chapter 5 were interpreted to comprise an amalgamation of numerous depletion zones.

The geometry of the depletion zones is dictated by the zone of the pre-salt succession where liquefaction has occurred as a result of sufficient pore fluid pressure. It is, however, unlikely that the zone of liquefaction would be consistently circular to sub-circular unless, perhaps pore fluid pressure was locally rapidly increased via a mechanism such as a sudden gravitational point load (Osborne and Swarbrick, 1997). It could, therefore, be proposed that the circular to sub-circular geometry in planform of the depletion zone for each mud volcano argues against the sudden liquefaction of the entire depletion zone.

An alternative solution to the style of liquefaction of these depletion zones is via a dynamic liquefaction mechanism (Terzaghi et al., 1951) (Figure 7.6). This process

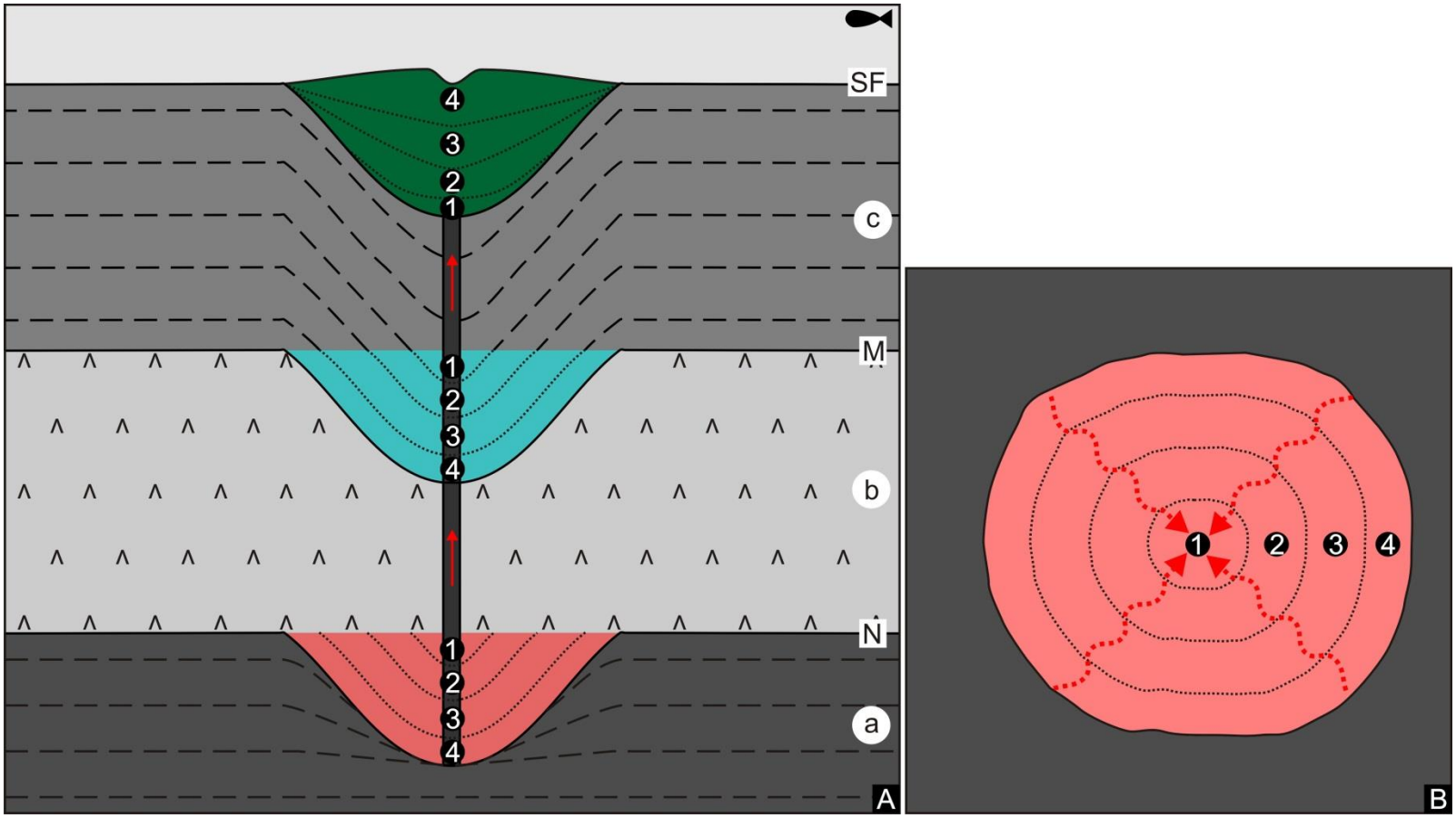

Figure 7.6 A cartoon of a dynamic liquefaction process. A: A cartoon demonstrating the various stages of dynamic liquefaction. In this example, there are four episodes of liquefaction and mobilisation numbered 1-4. The liquefaction and mobilisation of a volume of mud (i.e. episode 1) results in the extrusion of that volume at the seafloor and subsidence and collapse of the overburden, which triggers the liquefaction of the next episode (i.e. episode 2) and so on. B: Planform cartoon of the liquefaction and depletion zone demonstrating how it builds out during dynamic liquefaction. Red arrows represent mud and fluid mobilisation. The light red represents the liquefaction and depletion zone, the green represents the mud volcano and the blue represents the clear areas of downsagging within the Pliocene to Recent succession. SF – Seafloor; M – Horizon M; N – Horizon N; a – pre-salt; b – Messinian evaporites; c – Pliocene to Recent.

involves a progressive increase in pore fluid pressure that leads to liquefaction and mobilisation of a small volume, the removal of which triggers the subsequent liquefaction of a further volume (Figure 7.6). This process is cyclic and causes the liquefaction and depletion zone to grow out from its central starting point (Figure 7.6). The gradual nature of this process could explain why the sides of the top-salt depressions are gradually sloping as opposed to a more abrupt geometry, such as the craters associated with mud mobilisation within the Møre basin offshore Norway (Lawrence and Cartwright, 2010). This mechanism may also explain the circular to sub-circular geometry in planform of the depletion zone, as the liquefied slurry is mobilised towards the conduit (Figure 7.6). The process of dynamic liquefaction is a multi-stage process and so could also have contributed toward the internal stratification described within the mud volcanoes.

By analogy, the mechanisms for quick clay landslides present an appropriate comparison for this process of dynamic liquefaction (Ter-Stepanian, 2000). Similar to as observed with the depletion zones of these mud volcanoes, quick clay landslides result in the formation of a zone from which clay has been liquefied and mobilised, which has a bowl shaped geometry (Ter-Stepanian, 2000). Quick clay landslides initiate as a small rotation landslide event, which leads to larger subsequent landslide events after a short period of time. Similar to the process of dynamic liquefaction proposed here, each subsequent episode of sliding is as a result of liquefaction of a volume of mud that is triggered by the prior slide (Ter-Stepanian, 2000; Terzaghi et al., 1951).

The reflections that comprise the Pliocene to Recent succession and notably Horizon M display downsagging geometry beneath the extruded mud volcano and above the depletion zone (Figure 7.2 and Figure 7.4). The geometry of these reflections suggests that the various stages of liquefaction and withdrawal of mud from the depletion zone also coincide with subsiding and collapse of the overburden above Horizon N (Figure 7.6). The subsidence and collapse of this overburden also presents an elegant mechanism to increase pore fluid pressure within the depletion zone in order to trigger the next stage of liquefaction.

.

7.3 Timing and flux

7.3.1 Depletion and exclusion zone

The location of all the giant mud volcanoes described in Chapter 4 and the smaller and conical mud volcanoes described in Chapter 5 are displayed in Figure 7.7. It is clear that the small and conical mud volcanoes are clustered and often stacked (Figure 7.7 and Figure 7.8), as was demonstrated in Chapter 5 where spatial analysis showed that these mud volcanoes are statistically of a clustered distribution and also in many areas a stacking relationship. By comparison, the formation of fluid escape pipes driven by fluid-pressure has previously been interpreted to potentially explain clustering patterns and exclusion distances between pipes determined by lateral drainage efficiency within the overpressured zone (Moss and Cartwright, 2010b). Voronoi polygon analysis was also undertaken in Chapter 5, to assess whether there is a spatial ordering to the location that mud volcanoes form relative to those that have already been emplaced and are of a significantly large volume. The observation of mud volcanoes of a large scale clearly implies that a similarly large volume of mud and fluid has been depleted from the source stratigraphic interval. The results of this analysis showed that there is no spatial ordering in the distribution of the conical mud volcanoes based on their volumes.

The Voronoi polygon analysis described above does not take into account the giant mud volcanoes that are described in Chapter 4 and exhibit significantly larger volumes. This raises the question, is there spatial ordering between the giant mud volcanoes and the smaller and conical mud volcanoes? The giant mud volcanoes were emplaced directly on top of the Messinian evaporite succession and formed prior to any of the smaller and conical mud volcanoes within the study area. Small and conical mud volcanoes can be observed overlying the giant mud volcanoes of LB2, LB4 and LB5, despite their extruded volumes, other than LB5, being significantly larger than the conical mud volcanoes. LB4 is larger of the three, covering an area of c. 105 km^2 with an extruded volume of c. 36 km^3. Despite the significant scale of LB4, it is overlain by as

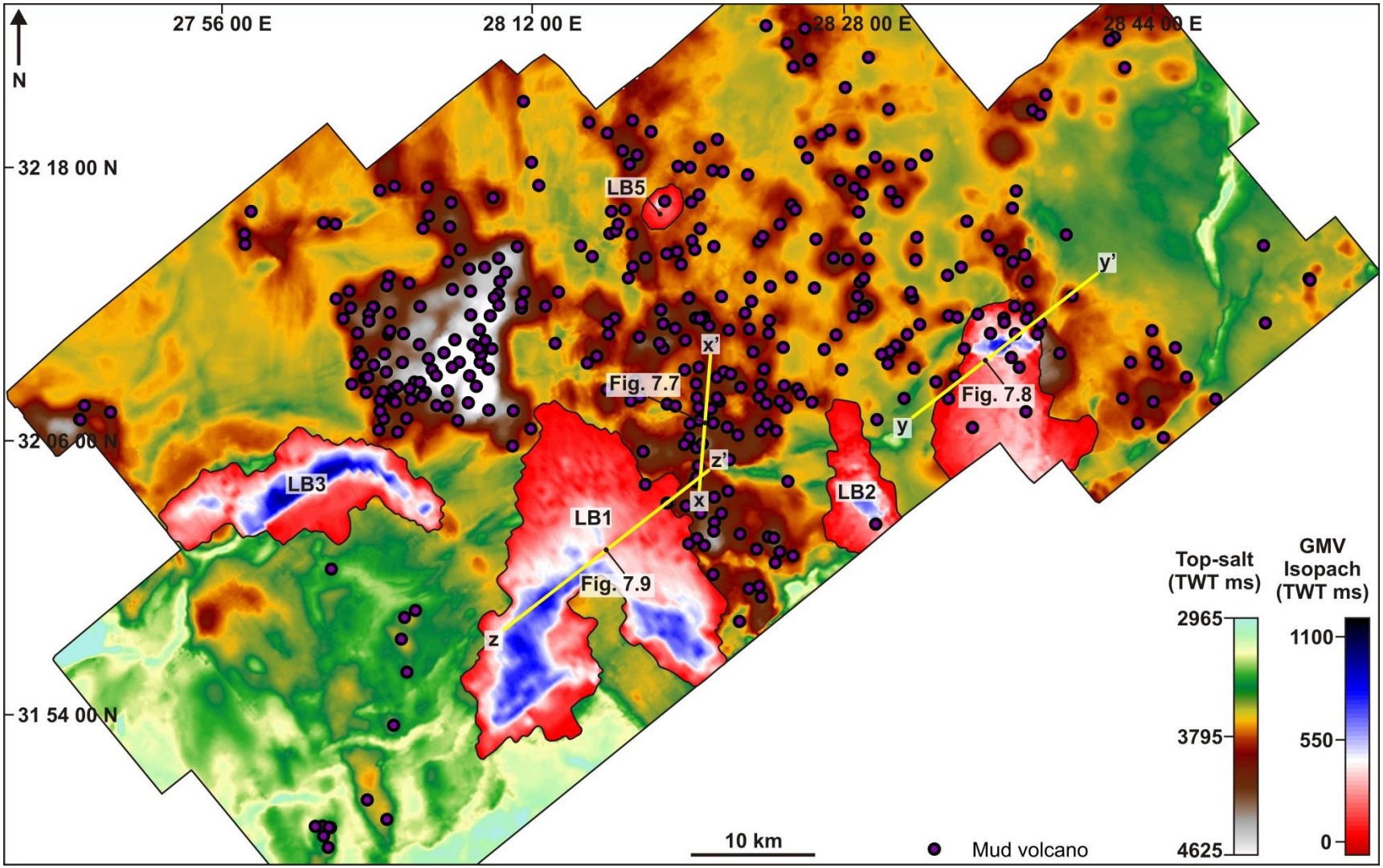

Figure 7.7 The location of all giant mud volcanoes and all small and conical mud volcanoes. The lines of section for Figure 7.8, Figure 7.9 and Figure 7.10 are displayed.

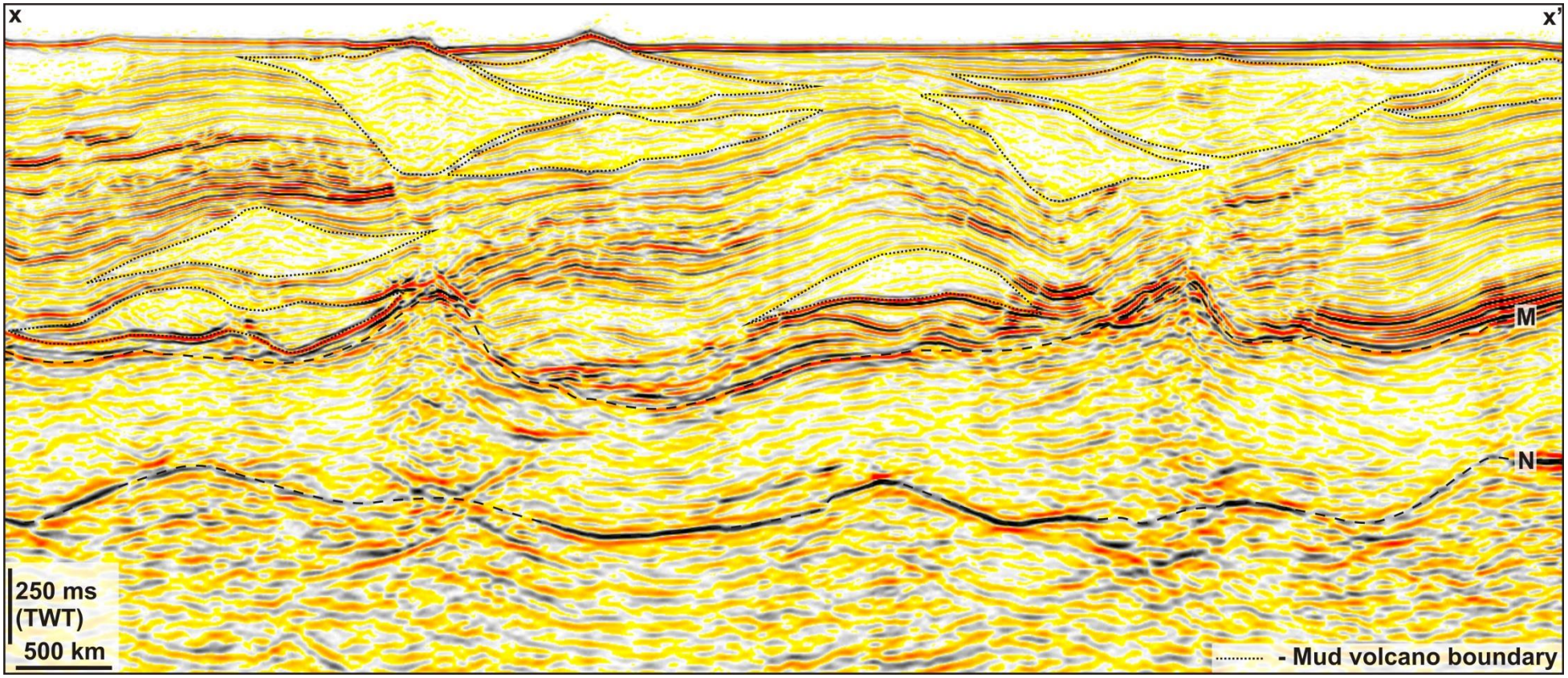

Figure 7.8 Stacked mud volcanoes. A seismic profile that displays numerous mud volcanoes at various levels throughout the Pliocene to Recent succession, some of which are stacked. The line of section for this seismic profile is displayed in Figure 7.7. M – Horizon M; Horizon N.

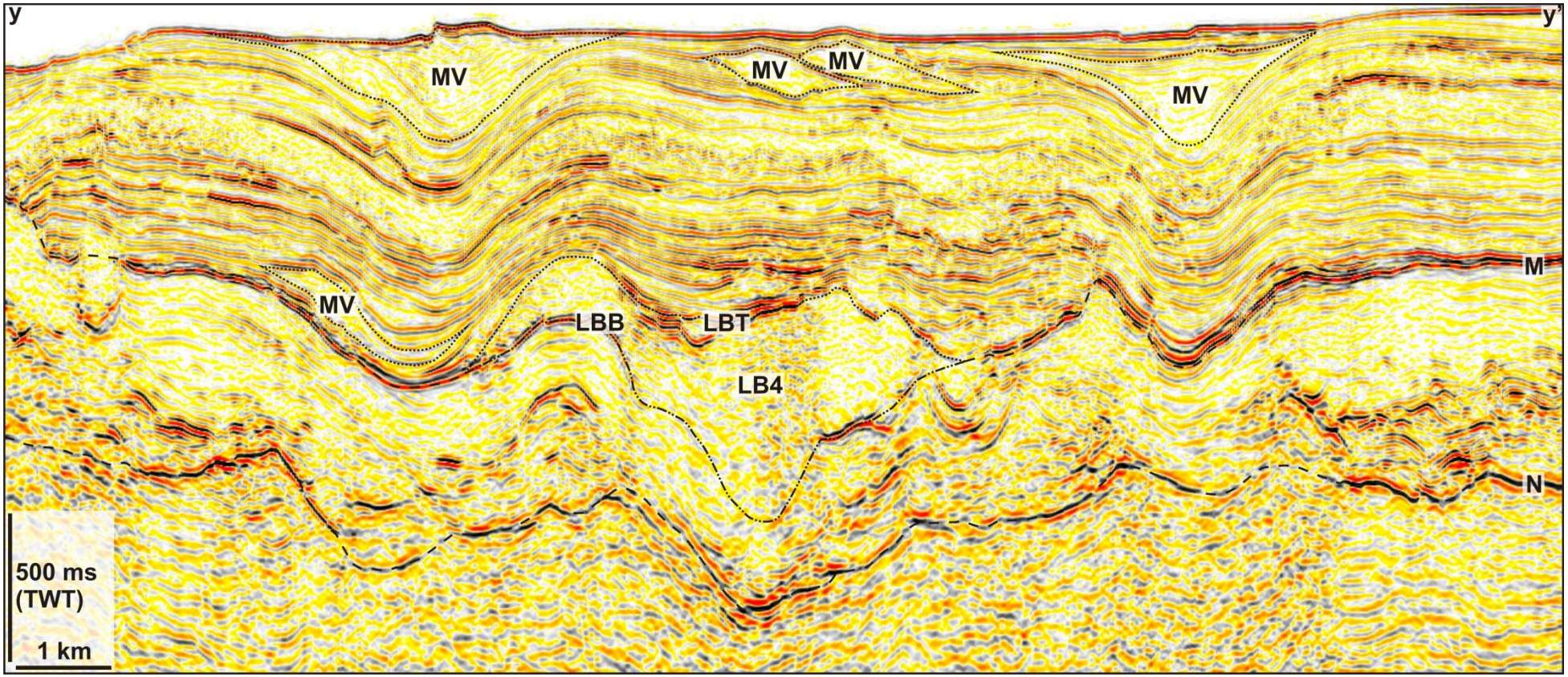

Figure 7.9 Mud volcanoes overlying LB4. A seismic profile displaying numerous mud volcanoes and the giant mud volcano of LB4. The smaller and conical mud volcanoes can be observed at the margins LB4 and directly overlying. The location of this seismic profile is displayed in Figure 7.7. MV – Mud volcano; LB4 – Lensoid body 4; LBT – Lensoid body top; LBB – Lensoid body base; M – Horizon M; N – Horizon N.

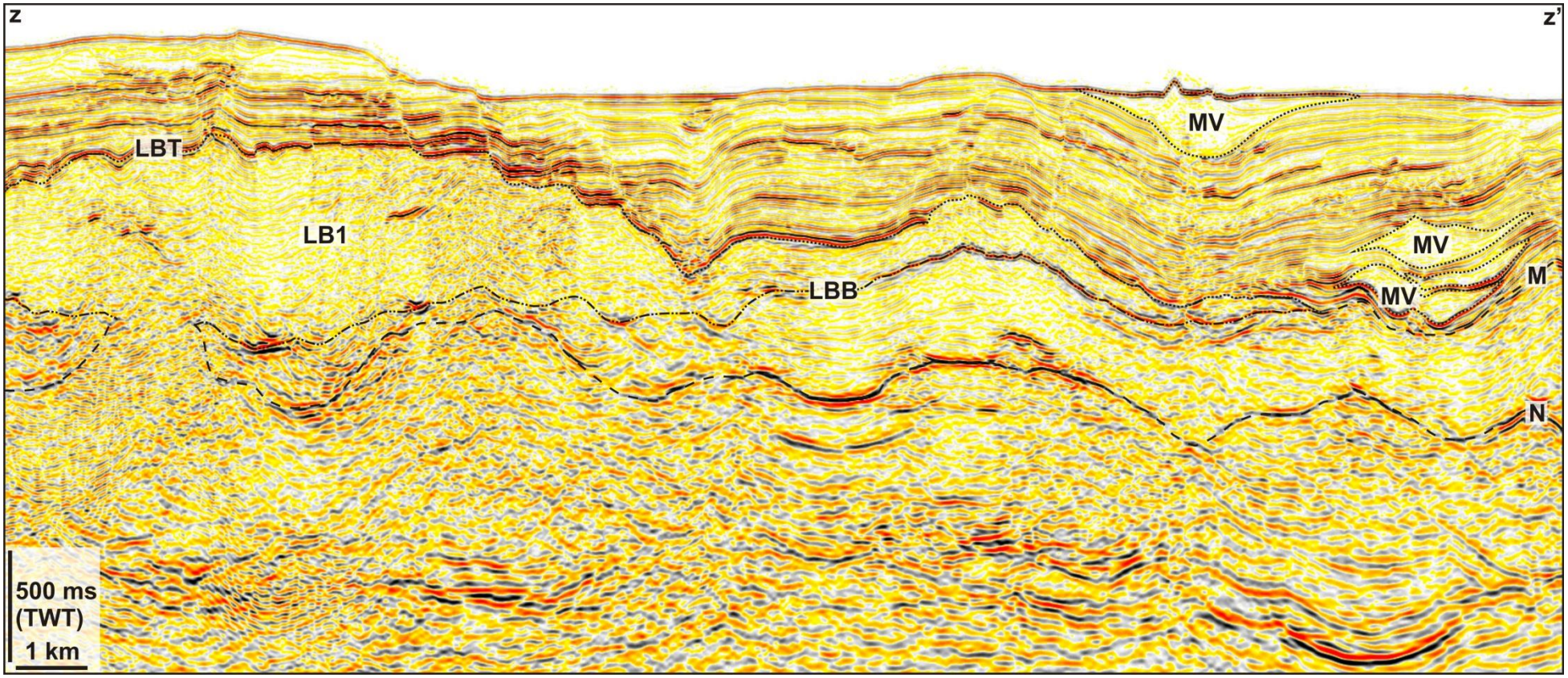

Figure 7.10 Mud volcanoes at the margins of LB1. A seismic profile displaying numerous mud volcanoes and the giant mud volcano of LB1. The smaller and conical mud volcanoes can be observed at the margin of LB1, however, cannot be seen overlying LB1. The location of this seismic profile is displayed in Figure 7.7. MV – Mud volcano; LB1 Lensoid body 1; LBT – Lensoid body top; LBB – Lensoid body base; M – Horizon M; N – Horizon N.

many as 15 of the smaller and conical mud volcanoes (Figure 7.7 and Figure 7.9). A number of these mud volcanoes are located at the margins of LB4 and also directly above its central region (Figure 7.7 and Figure 7.9).

The giant mud volcanoes of LB1 and LB3 display a contrasting spatial relationship with the smaller and conical mud volcanoes to that which has been observed for LB2, LB4 and LB5. LB1 and LB3 are the largest two of the giant mud volcanoes having extruded volumes of mud of c. 116km^3 and c. 52 km^3 respectively. LB3 covers an area of c. 122 km^2, and yet not a single smaller and conical mud volcano can be observed overlying the giant mud volcano (Figure 7.7). LB1 covers a region of up to c. 315 km^2, which is a significantly large section of the overall 4300 km^2 of the study area, and yet none of the smaller and conical mud volcanoes directly overlie (Figure 7.7 and Figure 7.10). The smaller mud volcanoes can only be observed at the distal margins of LB1 at significant distance from its central region where it exhibits its maximum thickness and a connection between the pre-salt and the giant mud volcano (Described in section 4.3.2.1 of Chapter 4).

During mud volcanism, the extrusion of fluid and mud during a period of overpressure venting implies that there is a zone of depletion of fluid and mud at depth and also a decrease in pore fluid pressure within the source stratigraphic interval beneath the mud volcano (Deville et al., 2010; Deville and Guerlais, 2009; Stewart and Davies, 2006). This would suggest that over time, fluid and mud and overpressure will eventually deplete sufficiently beneath where a mud volcano has formed that it will cease to erupt. The implications of this are that due to insufficient fluid and mud and overpressure within this depleted zone, an area within which no other mud volcanoes can originate is formed, which is here referred to as an exclusion zone. This could potentially result in the spatial ordering of mud volcanoes, whereby newer forming mud volcanoes will be emplaced outside of an exclusion zone (Figure 7.11). This could present a possible explanation for the observed spatial relationship between the conical mud volcanoes and LB1 and LB3 (Figure 7.7 and Figure 7.11). This hypothesis is similar to one which was proposed by Moss et al. (2012) who demonstrated the potential of an exclusion zone surrounding pockmarks, which results in a tendency for pockmarks to form just beyond an exclusion zone limit.

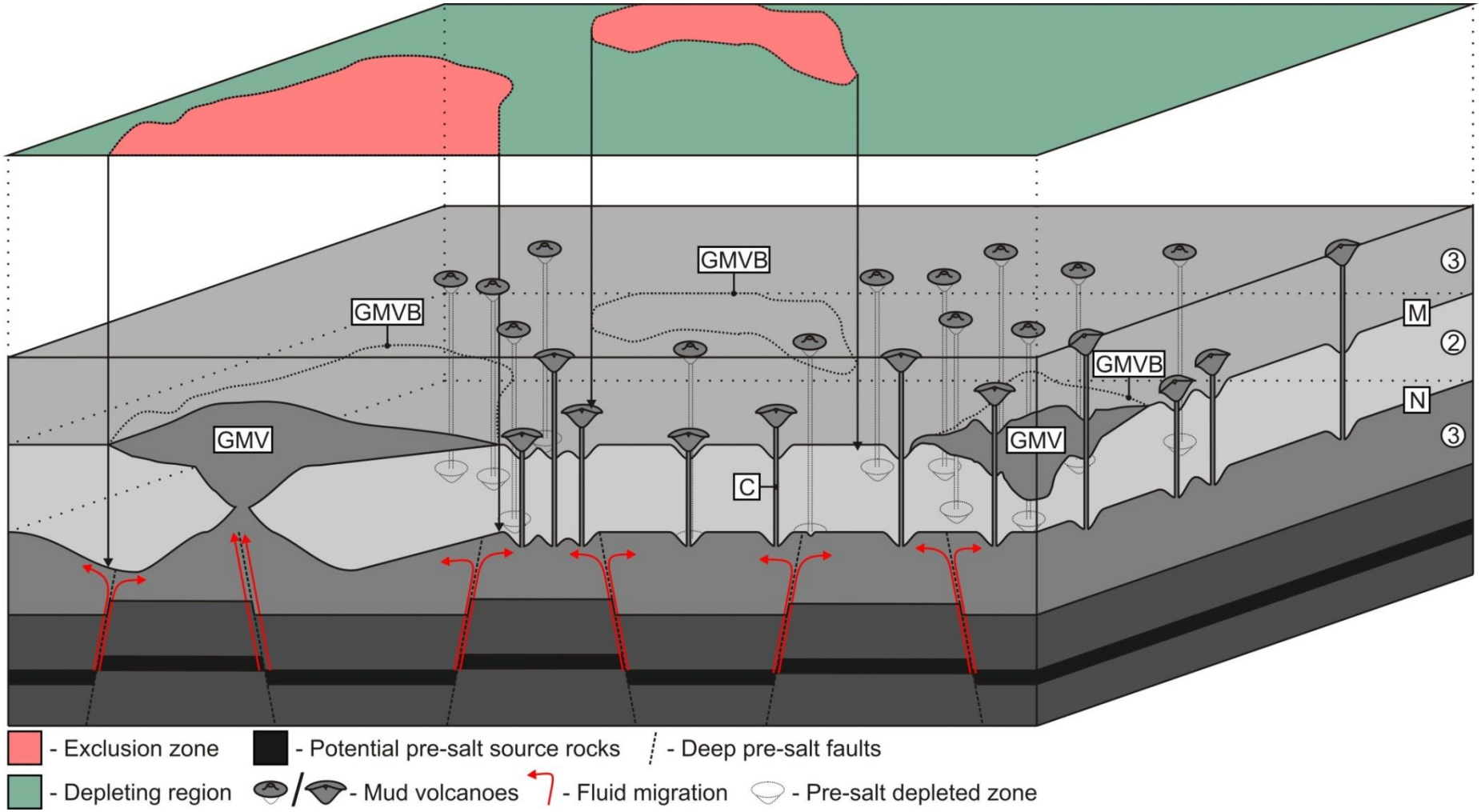

Figure 7.11 Exclusion zone and depleting region cartoon. The red areas represent exclusion zones which are spatially correlatable with giant mud volcanoes of a sufficient scale. The green areas represent regions within which depletion pre-salt and mud volcanism is still active. GMV – Giant mud volcano; GMVB – Giant mud volcano boundary; C – conduit; M – Horizon M; N – Horizon N; 3 – Pre-salt succession; 2 – Messinian evaporite succession; 1 – Pliocene to Recent succession.

The sources of fluid and sediment for the giant mud volcanoes have previously been argued to be from similar parts of the pre-salt succession (See section 4.4.1 of Chapter 4 and 5.4.1 and 5.4.3 of Chapter 5). The observed spatial relationship between LB2, LB4 and LB5 and smaller and conical mud volcanoes could imply that the scale of depletion of mud and fluid and overpressure during their formation has not been sufficient enough to form an exclusion zone and so they remain within a region of continued depletion (Figure 7.11). However, LB1 and LB3 comprise exceptional volumes of extruded mud, which combined with the absence of directly overlying smaller and conical mud volcanoes, argues for an associated exclusion zone (Figure 7.11). The above observations imply that the extrusion of LB1 and LB3 at the end of the Messinian Salinity Crisis was of such significant scale that fluids and mud and overpressure depletion was sufficient enough to form an exclusion zone, above which no further mud extrusion has occur (Figure 7.11). The observation of the formation of smaller and conical mud volcanoes only at the margins LB1 could indicate that the areal extent of the exclusion zone may be similar to that of the giant mud volcano (Figure 7.11).

7.3.2 Source of overpressure

The total extruded volume of mud within the small and conical mud volcanoes within this study area described in Chapter 5 have been calculated to have a combined volume of c. 208 km^3. By comparison, the total extruded volume of the giant mud volcanoes described in chapter 4 is c. 216 km^3. A schematic histogram that represents the observed changes in volume of mud extruded over time is presented in (Figure 7.12). This histogram is based on observations of the frequency of mud volcanoes through the Pliocene to Recent succession and their individual volumes. A large peak can be seen between 5.3 Ma and 5.1 Ma that represents the large volume of mud that was extruded during the formation of the giant mud volcanoes. A gradual decrease in extruded volume can then be observed to follow, during the Pliocene (Figure 7.12). An increase in volume can eventually be seen, which represents the observed increase in mud volcanoes towards the top of the Pliocene to Recent succession (Figure 7.12). An

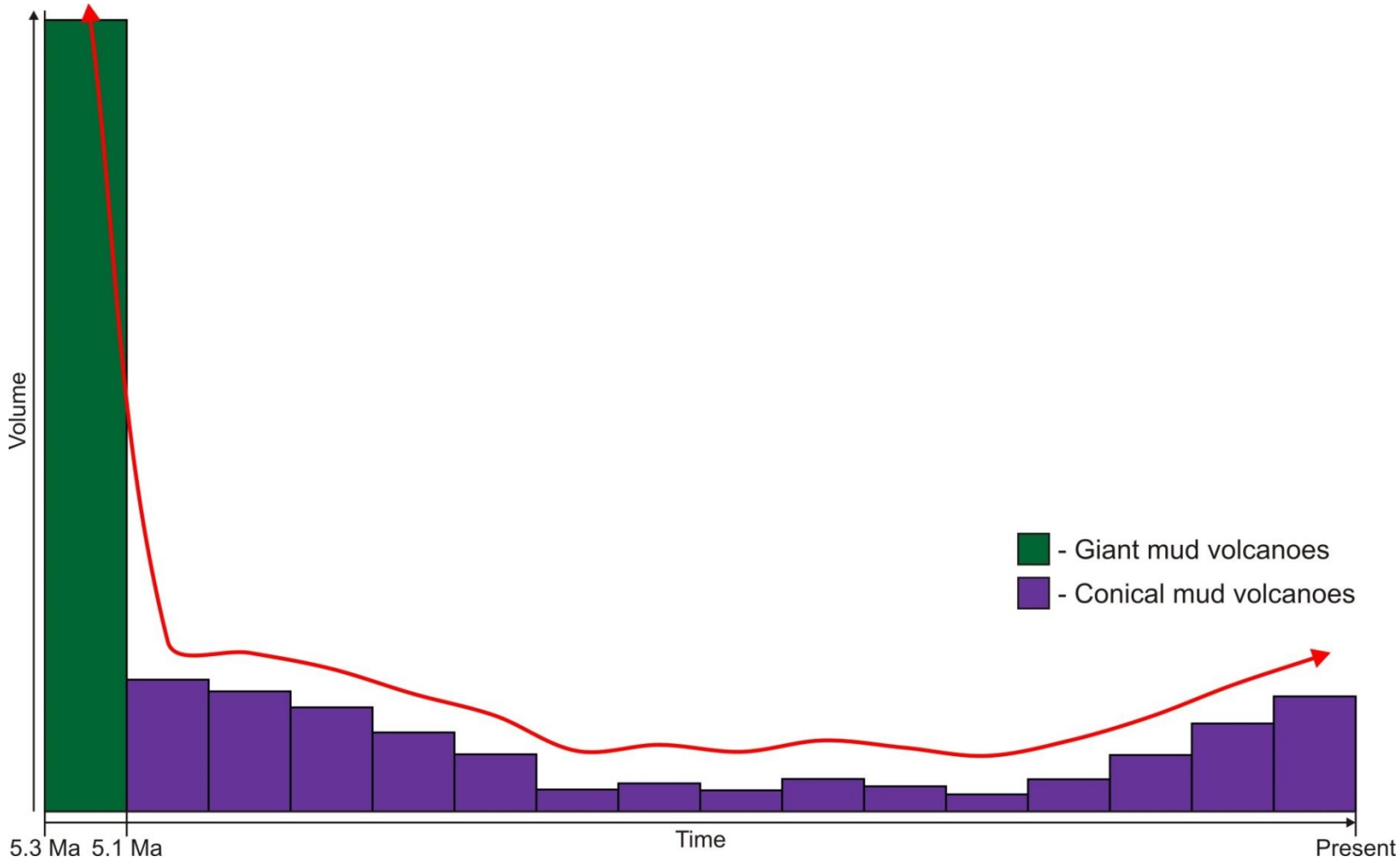

Figure 7.12 Volume of extruded mud over time. This schematic histogram displays the variation in the volume of mud extruded via mud volcanism since the climax of the Messinian Salinity Crisis. This histogram is an approximation based on the observed frequency of mud volcanoes through the Pliocene to Recent succession and their recorded volume of mud.

important question to consider is what mechanisms controls the frequency of mud volcano formation and also the volume of mud extruded during their formation?

Overpressure within a sedimentary layer is believed to be the primary driving mechanism behind the formation of a mud volcanoes (Kopf, 2002; Osborne and Swarbrick, 1997; Milkov, 2000; Deville and Guerlais, 2009; Dimitrov, 2002). The description of several giant mud volcanoes in Chapter 4 is interpreted to be indicative of a massive overpressure release event at the end of the Messinian Salinity Crisis, as a result of the overpressuring effect of the rapid loading of evaporites and Zanclean flood. The premise of overpressure generation associated with the Messinian Salinity Crisis is one that has recently also been suggested by Bertoni and Cartwright (2015). The smaller and conical mud volcanoes described in Chapter 5 formed after the giant mud volcanoes and are distributed at various stratigraphic levels throughout the Pliocene to Recent succession. These smaller and conical mud volcanoes represent numerous smaller events of overpressure release. If the mechanism for generating overpressure for the extrusion of the giant mud volcanoes was the rapid loading of the Messinian evaporites, what is the mechanism for generating overpressure that subsequently has led to the extrusion of the smaller and conical mud volcanoes? Two possible and contrasting mechanisms are considered below for generating the required overpressure.

7.3.2.1 Persistent overpressure and depletion

It could be argued that the original overpressure that was generated within the pre-salt succession across this study area due to the rapid loading of evaporites has in fact persisted since the end of the Messinian Salinity Crisis. If a significantly high level of overpressure has been retained since that event, only low level fluctuations in pore fluid pressure may be required to trigger liquefaction and mud mobilisation (Tanikawa et al., 2010) (Figure 7.13). The fluctuations in pore fluid pressure that are required could be caused by earthquakes, eustatic variation, rapid loading and a build-up of fluid pressure via the generation and addition of secondary fluids such as

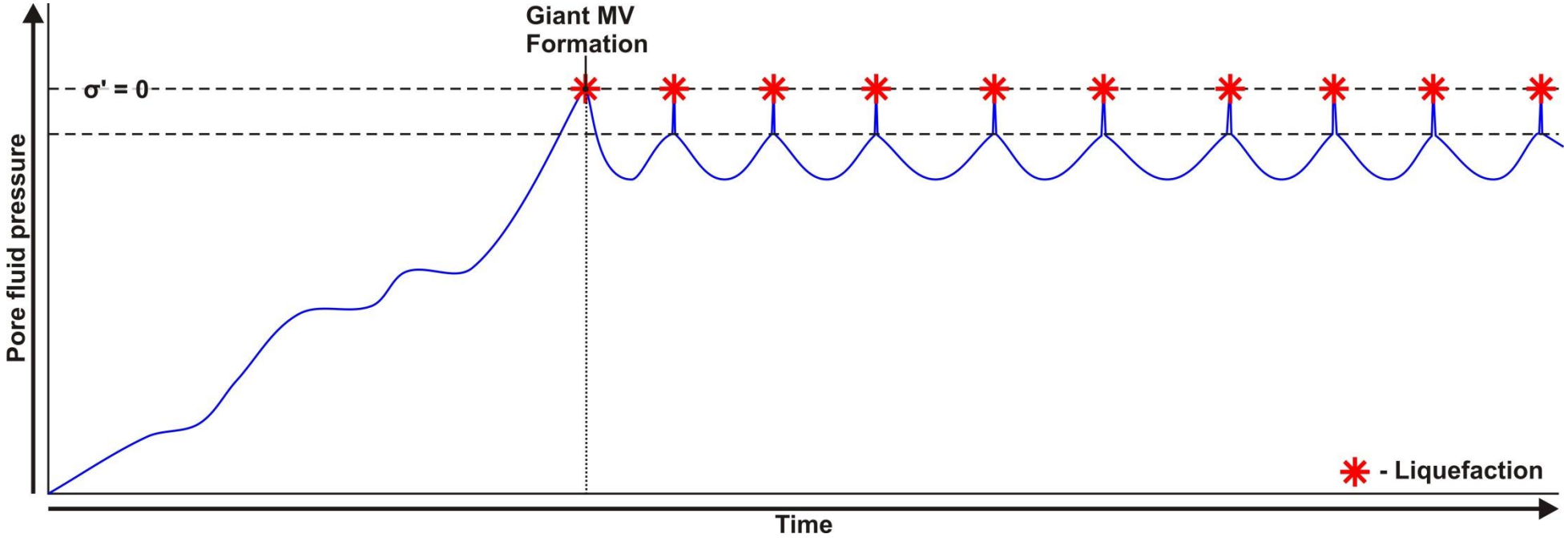

Figure 7.13 Persistent overpressure and liquefaction. This is a schematic representation of how variations in pore fluid pressure and liquefaction within the pre-salt succession during the Messinian and Pliocene to Recent. The initial increase in pore fluid pressure represents the overpressuring effect of the Messinian Salinity Crisis which subsequently leads to liquefaction and formation of the giant mud volcanoes. The hypothesis of persistent overpressure since the Messinian Salinity Crisis results in liquefaction being active numerous times due to low level fluctuations in pore fluids pressure.

hydrocarbons (Judd and Hovland, 2007; Osborne and Swarbrick, 1997), the potential for all of which has been discussed above in section 7.2.3. By analogy, a similar mechanism was recently proposed for triggering the eruption of the Lusi mud volcano (Tanikawa et al., 2010). It has been suggested that the primary source succession of mud feeding the Lusi mud volcano (thought to be the Kalibeng Formation) was in a long-term state of high fluid pressure and low level of dynamic pore pressure fluctuations, potentially from the Yogyakarta earthquake, could have triggered liquefaction and hydraulic fracturing (Tanikawa et al., 2010).

Although this mechanism of persistent overpressure requires secondary influences to trigger a slight increase in pore fluid pressure, the implication is that the primary mechanism for increasing pore fluid pressure is still from the initial overpressuring effect of the Messinian Salinity Crisis (Figure 7.13). Heterogeneities in the supply of fluid and mud and the level of overpressure within the pre-salt succession across the study area could potentially govern the timing of when the pore fluid pressure reaches the point at which liquefaction can occur (Figure 7.13). Over time, the overpressure that was generated during the Messinian Salinity Crisis within a particular area could be depleted via episodes of mud volcanism. These episodes of overpressure venting could eventually result in a zone of sufficient depletion of mud and fluid and overpressure, above which no more mud volcanoes can form, as discussed in section 7.3.1.

7.3.2.2 Recharge

An alternative to the hypothesis of persistent overpressure suggested above is that the formation of the smaller and conical mud volcanoes is in fact not primarily associated with a generation of overpressure during the Messinian Salinity Crisis, but rather an overpressure recharging mechanism such as via the generation of hydrocarbons. The presence of known nearby hydrocarbon plays, the observation of direct hydrocarbon indicators associated with these mud volcanoes and the documentation of methane-rich and oily hydrocarbon-rich hot brine and mud samples

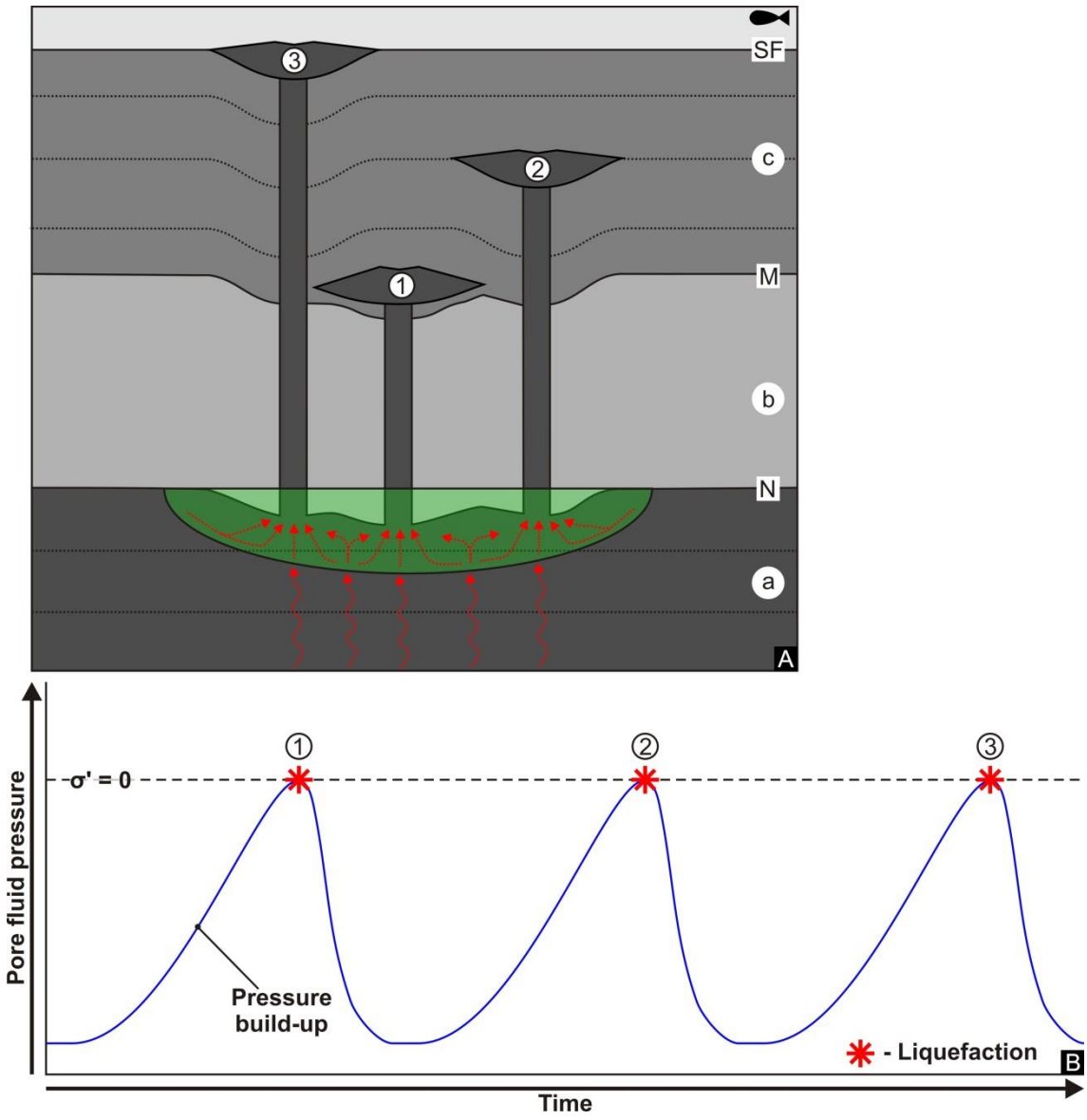

Figure 7.14 Recharge and cyclical build-up of pore fluid pressure. A: A schematic cartoon showing the generation and migration of fluids to a depletion zone that becomes overpressured due to a build-up in pore fluid pressure (green), which results in liquefaction and the formation of the mud volcanoes. B: A schematic representation of the increase in pore fluid pressure associated with the generation and migration of fluids depicted in Figure 7.14A. It demonstrates a potential cyclic recharge mechanism where by a build-up in pore fluid pressure could result in liquefaction and mud mobilisation and a drop in pore fluid pressure. This process could potentially be followed by another build-up in pore fluid pressure due to fluid migration. The numbers 1-3 represent extrusive events which are displayed as mud volcanoes in Figure 7.14A, the numbering of which is correlatable. SF – Seafloor; M – Horizon M; N – Horizon N; a – Pre-salt succession; b – Messinian evaporite succession; c – Pliocene to Recent succession.

associated with the mud volcanoes within this study area present a strong argument for the generation of hydrocarbons having influenced the formation of these mud volcanoes (Pierre et al., 2014; Dupré et al., 2014; Huguen et al., 2009; EGAS, 2012a; EGAS, 2012b; EGAS, 2012c).

Hydrocarbon generation and accumulation beneath the Messinian evaporite succession could potentially result in a gradual elevation in pore fluid pressure within the immediate pre-salt succession over time (Hedberg, 1980; Charlou et al., 2003; Dimitrov, 2002; Kopf, 2002; Wilford, 1967; Humphrey, 1963; Stamatakis et al., 1987). A progressive increase in overpressure may continue over time until the pore fluid pressure reaches a critical point at which the pore fluids temporarily sustain the entire stress exerted on the sediment, resulting in liquefaction (Maltman and Bolton, 2003) (Figure 7.14). Subsequently the overpressure will bleed off via the extrusion of fluids and mud during mud volcanism (Figure 7.14). This process of generating overpressure via hydrocarbon generation could result in cyclicity to the formation of mud volcanoes, whereby the fluids and subsequently overpressure may recharge again, until the pore fluid pressure once again reached the critical point for liquefaction (Deville and Guerlais, 2009) (Figure 7.14).

7.3.2.3 Persistent overpressure vs overpressure recharging

When evaluating which of the potential mechanisms for overpressure generation suggested above is the most viable, a key observation to make is the absence of any mud volcanoes above the two largest giant mud volcanoes. If the mud volcanoes within this study area are indeed formed in association with a recharge mechanism, it could be expected that mud volcanoes would have formed overlying LB1 and LB3. These giant mud volcanoes represent clear evidence of previous overpressure release and proven mud volcanism in those regions of the study area (Figure 7.7). The observation of no other mud volcanoes overlying LB1 and LB3 argues in favour of a mechanism for depletion of the overpressure generated during the Messinian Salinity Crisis and implies that it has not be recharged and has ultimately

lead to the formation of an exclusion zone (Moss and Cartwright, 2010b) (Figure 7.7). Hence this explains why the two largest mud volcanoes within this study area are not overlain by subsequent extrusive episodes associated with the venting of overpressure at depth.

Another observation that should be considered is that the conduits for these mud volcanoes are not re-used. A pre-existing conduit that is connected to the source stratigraphic unit could potentially represent a weakness in the overlying seal as it is a location where seal bypass has previously occurred. If fluids and overpressure were recharged within an area of the source unit that was previously overpressured and depleted, then it could be considered reasonable to assume that a pre-existing conduit would represent a preferential pathway for fluid and mud remobilisation, similar to as observed in other mud volcano conduits and fluid escape pipes (Hansen et al., 2005; Andresen and Huuse, 2011; Deville and Guerlais, 2009; Deville et al., 2010). In contrast, the depletion of overpressure within an area of the source unit for mud that was primed during the Messinian Salinity Crisis and is not recharged could explain why these conduits are not re-used. The evidence presented here, suggests that while a recharge mechanism is possible it is complex, and a mechanism where by the initial overpressure generated during the Messinian Salinity Crisis persists and is gradually depleted over time is more plausible.

7.4 Why not the entire Mediterranean?

The exact reasons behind the precise location that mud volcanoes form is something that is at present still not fully understood. The broader regions in which they form are known to primarily include areas of high tectonic stresses, such as major sheer or compression zones near plate boundaries (Brown, 1990; Van Rensbergen et al., 1999; Kopf et al., 2001; Kopf, 2002; Deville and Guerlais, 2009; Deville et al., 2006; Milkov, 2000; Dimitrov, 2002) and in areas of high sedimentation rates such as the Niger Delta (Graue, 2000; Milkov, 2000; Kopf, 2002) or within the Nile Deep Sea Fan (Loncke et al., 2004). The reason mud volcanoes are often found in these types of

settings is in part associated with the generation of overpressure associated with high compressive stress (Charlou et al., 2003; Osborne and Swarbrick, 1997).

Fluid escape activity within the Mediterranean during the Messinian Salinity Crisis is thought to be largely governed by events that occurred Mediterranean-wide (Bertoni and Cartwright, 2015). The deposition of a thick unit of evaporites during the Messinian Salinity Crisis played a significant role in the development of undercompaction and overpressure within pre-salt layers (Bertoni and Cartwright, 2015). It is this mechanism for generating overpressure that is here thought to be the primary source of overpressure that drives mud volcanism within this area. A case can also be made for the build-up of additional overpressure due to the generation of hydrocarbons. However, it must be taken into consideration that the entire Mediterranean was subjected to rapid burial beneath the Messinian evaporites and there are numerous other areas within the Eastern Mediterranean where hydrocarbon generation is proven and yet there are no mud volcanoes (Aal et al., 2000; Prinzhofer and Deville, 2011).

Considering the potential priming mechanisms for mud volcanism exist throughout the Eastern Mediterranean as stated above, an important question is raised which is, of the entire Eastern Mediterranean, why has such a large volume of mud been mobilised here, resulting in such a large number of mud volcanoes? One of the least understood aspects of these mud volcanoes is what the exact sediment composition is within the source stratigraphic succession. It was previously suggested in Chapter 3 that the immediate pre-salt succession, which as stated above is interpreted as the primary source of mud, most likely comprises a marly to muddy interval based on extrapolation from other well calibrated pre-Messinian successions in the Levant Basin (Bertoni and Cartwright, 2005) and at outcrop in Sicily (Grasso et al., 1982). Perhaps an improved understanding of the minerals present in the sediments that have been mobilised could give in an insight into why these mud volcanoes have formed within the El Dabaa study area.

Typically minerals with low densities such as kaolinite, smectite and vermiculite, all of which have densities lower than quartz or feldspar, are ideal for mud

mobilisation (Kopf, 2002). These clay minerals are common in marine environments and have the capability to incorporate large volumes of water into their mineral structure (Kopf, 2002). Samples from the brines and extruded sediment from the Cheops mud volcano within the Menes Caldera are characterised by predominantly clay-size particles and detrital silicates (quartz, feldspars, micas and clay minerals) and dark grey silty clay, which contains oily hydrocarbons, as well as mm size rounded clasts or rock fragments (Pierre et al., 2014).

Other samples from mud volcanoes within this region have found the extruded mud to range from light brown to light grey and comprise of a silty, marly and sandy slurry with poorly lithified clasts < 1 cm large and are H_2S rich (Giresse et al., 2010; Huguen et al., 2009). The main component of the cement associated with these muds is siderite, which is indicative that the source of some clasts is from shallow or deltaic deposits (Giresse et al., 2010). As well as in the present day, an environment such as this is known to have existed prior to the Messinian Salinity Crisis and evaporite deposition as a result of sedimentary output from the proto-Nile Delta, which is thought to have onset as early as the Eocene (See section 3.3 of Chapter 3) (Said, 1962; Salem, 1976; Barber, 1981). During Tortonian times, a substantial delta complex was established; however, a significant proportion of these deltaic sediments were eroded during the early stages of the Messinian Salinity Crisis (Barber, 1981; Ryan and Cita, 1978; Hsü, 1978; Rizzini et al., 1978). This is evident by the observation of some base-salt depressions, including a submarine canyon, which are associated with erosion during the drawdown of the Mediterranean Sea (See section 5.4.6 of Chapter 5). The primary source of mud has been established as pre-salt and so it is implied that the mud that feeds these mud volcanoes originates from the sediment output of the proto-Nile Delta prior to the Messinian Salinity Crisis.

An example of extensive analysis of the remobilised sediment from other mud volcanoes that can be compared to those of the El Dabaa study area are found within Trinidad and the Barbados prism (Deville et al., 2010). Analysis of these muds has found them to largely comprise clays (smectite, illite, kaolinite and vermiculite), chlorite and muscovite, an abundance of quartz and feldspar grains and carbonates (calcite, dolomite and siderite) (Deville et al., 2003; Deville et al., 2010). Other

examples that are geographically closer to the El Dabaa study area include the Milano and Napoli mud volcanoes, which are located within the Mediterranean ridge region and have been described to comprise nannofossil oozes and clays (Robertson, 1996). Core samples from these mud volcanoes exhibit a matrix-supported, clast-rich muddy sediment, the matrix of which contains silty clay and sometime sandy silt, clay, quartz, rock fragments and nannofossils that range from Eocene to mid Miocene in age (Robertson, 1996). A suite of mounds within the Møre Basin offshore Norway, the scale of which base on volume are comparable to the giant mud volcanoes described here, are also documented to comprise remobilised ooze, similar to the Milano and Napoli mud volcanoes (Lawrence and Cartwright, 2010).

By comparison with the samples from the mud volcanoes within the El Dabaa study area, it is clear that the extruded slurry from these mud volcanoes originates from a source stratigraphy that is primarily comprised of clays. The analysis of the mud samples from the El Dabaa study area lack specifics on the type of clays that have been erupted (Giresse et al., 2010; Huguen et al., 2009). However, if the erupted mud contains clays which comprise of minerals such as smectite and kaolinite, similar to those observed in the other submarine mud volcanoes, there is a strong possibility that their relatively low density could add buoyancy (Kopf, 2002). Large volumes of water could also be incorporated into their mineral structure, which due to the rapid loading of evaporites during the Messinian Salinity Crisis could result in a particularly fluid rich, undercompacted and buoyant sedimentary layer (Kopf, 2002).

Variation in the thickness of the evaporite and post-salt successions has also been suggested to influence the location at which mud volcanoes form in Chapter 5. In the up dip regions of the western province and El Dabaa study area, the Messinian evaporites decrease in thickness due to the successions overall depositional wedge shape geometry and due to down dip gravitational sliding of the evaporites, which has subsequently led to gravitational collapse of the post-salt overburden (See sections 3.3 and 3.5.3 in Chapter 3). The gradual but significant decrease in the thickness of the evaporites and post-salt successions further up the continental margin, which clearly be seen within Domain A of the El Dabaa study area, will result in a lesser loading effect on the pre-salt succession. This could result in a gradual decrease in

overpressure within the pre-salt succession further towards the continental slope, which subsequently leads to insufficient overpressure to drive mud volcanism.

Fan deposits associated with the sedimentary output from the proto-Nile Delta extends and gradually thins towards the north (Ross and Uchupi, 1977; Ryan and Cita, 1978). The quantity of sediment sourced from the proto-Nile Delta will decrease towards the north, towards the Mediterranean ridge. Another limiting factor to consider regarding the distribution of mud volcanoes is that it is possible that the decrease in deltaic sediment input towards the North could also result in a gradual decrease in suitable source sediments such as clays that are required for mud volcanism. This may explain why the density of mud volcanoes decreases slightly within Domain C of the study area. The extent of the mud volcano field described here will almost certainly extend beyond the margin of this study area, provided the required clays, fluids and overpressure are present within the pre-salt succession. Mud mobilisation and extrusion is sure to continue within this area until the depletion of mud and fluids and overpressure within the source stratigraphic succession is sufficient that liquefaction and bypassing of the evaporite succession are no longer possible.

7.5 Research limitations

The research presented in the Chapters that have preceded would have benefited from well calibration. At least one or ideally multiple deep boreholes that penetrate as deep at the pre-salt succession within the study area or nearby would have significantly helped this research. With the aid of well calibration it would have been possible to confirm the geology of various stratigraphic units. Knowing the exact geology of the immediate pre-salt would have helped greatly in assessing its viability as the source stratigraphic interval for mud volcanism. Knowing the age of numerous reflections within the Pliocene to Recent succession would also have aided significantly in the analysis of the temporal distribution of mud volcanoes. Analysis of mud volcanoes and exhumed mud volcano conduits via fieldwork may have provided a different perspective to this research. Fieldwork could have allowed smaller scale observations that are below the resolution of 3D seismic data and may have given a

further insight into the mechanisms behind the formation of mud volcanoes and their conduits.

7.6 Further work

7.6.1 Additional datasets

Additional datasets located near the current study area or in more distal parts of the Eastern Mediterranean could be analysed to see if there is any evidence for fluid escape features associated with the release of overpressure that are correlatable with the end of the Messinian Salinity Crisis. This would further substantiate the interpretation of a massive overpressure release event at the end of the Messinian Salinity Crisis. Other high resolution 3D seismic data that contains mud volcanoes, from any region of the world, could allow further analysis and comparison of the geometry and potentially different types of conduits that can be observed in seismic data feeding mud volcanoes.

7.6.2 Gas release and climate change

An interesting open question remains regarding the impact that the gases released during the formation of mud volcanoes has on climate change. As a source of hydrocarbon gases they may provide sufficient supply of gases to the hydrosphere and atmosphere to possibly affect climate change (Kopf, 2002; Milkov, 2000). However, the extent to which the gases have an impact on the global greenhouse gas budget is something that remains poorly quantified. It has been previously suggested that mud volcanoes may contribute ~9% of fossil CH_4 missing in the modern atmospheric CH_4 budget and ~12% in the preindustrial budget (Milkov et al., 2003). This also raises the question, considering the massive scale of the giant mud volcanoes, what impact if

any; did the massive overpressure release event at the end of the Messinian Salinity Crisis have on the global greenhouse gas budget and climate change?

Chapter 8

8 Conclusions

This chapter presents the main conclusions of this thesis, which draw discussion and conclusion points from all the previous chapters. For a summary of the main results chapter, see section 7.1.2 of Chapter 7. Please refer to section 4.5 of Chapter 4, section 5.5 of Chapter 5 and section 6.5 of Chapter 6 for individual conclusion sections for each main results chapter.

8.1 The generation and release of overpressure associated with the Messinian Salinity Crisis

Chapter 4:

- A suite of previously unknown giant lensoid bodies that have been emplaced onto the upper surface of the c. > 1 km thick Messinian evaporite succession have been described. The convergence of the bounding reflections of these lensoid bodies, their isopach distribution, relief at their upper surface and the stratal geometries of the bodies and underlying and overlying deposits leads to the conclusion that these lensoid bodies are in fact giant mud volcanoes. The formation of mud volcanoes is often associated with the generation of overpressure within a succession. The rapid deposition and loading of the Messinian evaporite succession presents a viable mechanism for undercompaction and the generation of overpressure within pre-salt stratigraphy. Their stratigraphic position directly on top of the Messinian evaporite succession implies that they formed at the end of the Messinian Salinity Crisis. The timing of their emplacement is correlatable with a short period of rapid loading of seawater during the Zanclean flood, which presents an effective mechanism for a sudden increase in overpressure, which triggered liquefaction and large scale mud mobilisation. The analysis presented here demonstrates the potential for significant overpressure generation associated with the Messinian Salinity Crisis. It also presents strong evidence for a major phase of overpressure

release at the end of the Messinian Salinity Crisis within the Eastern Mediterranean, and the potential for significant volumes of fluid and mud to bypass the Messinian evaporite succession.

Chapter 5 and Chapter 7:

- As many as 386 small (relative to the giant mud volcanoes described in Chapter 4) and conical mud volcanoes have been observed throughout the Pliocene to Recent succession, the formation of which post-dates the formation of the giant mud volcanoes. In order for these mud volcanoes to form, there must be a mechanism for generating overpressure, similar to the example of the giant mud volcanoes. The interpretation of an exclusion zone around the giant mud volcanoes of LB1 and LB3 presents strong evidence for the depletion of mud and fluids and overpressure that was generated during the Messinian Salinity Crisis. The lack of stacking of mud volcanoes above these giant mud volcanoes argues against a recharge mechanism, as they clearly represent proven areas of previous overpressuring and mud mobilisation. Despite the clustered distribution of mud volcanoes, their conduits are not re-used during the formation of later forming mud volcanoes, which opposes what might be expected from a recharge mechanism as they represent pre-existing points of weakness. The analysis present here suggests that the overpressure generated during the Messinian Salinity Crisis may have persisted within many parts of the pre-salt succession across this study area. Only low level fluctuations in pore fluid pressure may be required to reach the point at which effective stress is equal to zero and liquefaction and mud mobilisation can be achieved. This implies that the initial overpressuring effect of the Messinian Salinity Crisis continues to have a major impact on fluid and sediment mobilisation.

8.2 Extend the general descriptive base of mud volcano conduits using 3D seismic data and their potential to bypass salt

Chapter 6:

- A large number of mud volcano conduits have been described within this study area, all of which display significant variety in their dimensions. However, all of these mud volcano conduits share very similar seismic characteristics that allow them to be easily identified and their overall geometry is observable as a vertical to sub-vertical columnar structure that has a circular to elliptical form. Their seismic characteristics and geometry are in fact strikingly similar to that of fluid escape pipes, a large number of which have also been described within this study. The descriptions presented confirm previous interpretations that fluid escape pipes and mud volcanoes are in fact very similar seal bypass systems. Observations regarding the upper terminations and spatial association of mud volcano conduits and fluid escape pipes indicate that the initial stages of the formation of mud volcano conduits may be similar to that of fluid escape pipes and that some fluid escape pipes could potentially evolve into mud volcano conduits. Analysis of the stratal origin of these conduits, combined with numerous lines of evidence including volumetric balance calculations between the mud volcanoes and pre-salt depletion zones, and the analysis of core samples from published literature are indicative of a pre-salt fluid and mud source for these conduits. Considering the observed similarities between the fluid escape pipes and mud volcano conduits, it is possible that the mechanisms that drive the formation of one of these seal bypass systems may be analogous to the other. Therefore, the mechanisms with the greatest potential to bypass the Messinian evaporite succession include hydraulic fracturing associated with the generation of overpressure and dissolution and stoping.

8.3 Extend the understanding of the depletion zone for mud volcanoes

Chapter 5 and 7:

- A strong argument has been built throughout this thesis for the source of mud and fluids for these mud volcanoes being of pre-salt in origin. This interpretation is based on numerous lines of evidence including: the stratigraphic position of mud volcanoes; the observable connection between some giant mud volcanoes and the pre-salt succession; a p-wave velocity inversion within the immediate pre-salt succession; the spatial relationship between mud volcanoes and underlying pre-salt depressions and areas of anomalous thinning of the immediate pre-salt succession that are localised; volumetric balance calculations between the mud volcanoes and the immediate pre-salt succession and; evidence from published literature. The zone of depletion associated with these mud volcanoes is defined by the margins of the area of anomalous thinning of the immediate pre-salt. The geometry in planform of these depletion zones is circular to sub-circular and appears irregular in shape where more than a single depletion zone overlaps, due to the clustered distribution of mud volcanoes. Mud mobilisation is initiated via a process where by an increase in pore fluid pressure leads to a state of zero effective stress, which triggers liquefaction. The formation of the depletion zone may have occurred via a dynamic liquefaction process, which is comprised of multiple phases of liquefaction and progressive outward growth of the circular to sub-circular depletion zone. The depletion of fluids and mud and overpressure will eventually be sufficient to form an exclusion zone, within which no further mud volcanism can occur, similar to as observed in the largest mud volcanoes of LB1 and LB3. Subsidence and collapse of the successions that overlie the depletion zone, coincides with the mobilisation and withdrawal of sediment from the depletion zone and the extrusion of mud at the seafloor, which could potentially trigger the next phase of liquefaction.

8.4 Investigate the controls on the location of mud volcano formation within the Nile Deep Sea Fan

Chapter 7:

- There are numerous factors have been identified that could ultimately govern the region within the modern Nile Deep Sea Fan that mud volcanoes form. Mechanisms such as vertical compressive stress via loading, and the generation of hydrocarbons could potentially result in the required fluid and overpressure for mud volcanism. However, these mechanisms are known to be present across the Eastern Mediterranean and Nile Deep Sea Fan within areas where no mud volcanoes have formed. The types of minerals present within the immediate pre-salt succession within this particular region of the Nile Deep Sea Fan may, therefore, have a significant influence on the formation of mud volcanoes. The analysis of samples from mud volcanoes within this study area contain siderite, which is indicative of sediments sourced from a succession comprised of deltaic output, such as from the proto-Nile Delta. Clay minerals such as kaolinite, smectite and vermiculite, if present similar to as observed in other mud volcano provinces, could potentially incorporate large volumes of water into their mineral structure. In combination with the rapid loading of evaporites this could result in a source stratigraphic succession that is particularly fluid rich, undercompacted and buoyant. Variation in the thickness of the evaporite and Pliocene to Recent succession could result in regional fluctuations in overpressure within the pre-salt succession. Limitations in the extent of proto-Nile deltaic deposits and erosion during the drawdown of the Mediterranean may also influence the region within which these minerals are present and mud volcanoes can form.

References

References

AAL, A. A., EL BARKOOKY, A., GERRITS, M., MEYER, H., SCHWANDER, M. & ZAKI, H. 2000. Tectonic evolution of the Eastern Mediterranean Basin and its significance for hydrocarbon prospectivity in the ultradeepwater of the Nile Delta. *The Leading Edge,* 19**,** 1086-1102.

ABIKH, G. 1863. New Islands on the Caspian Sea and the cognition of Mud Volcanoes of the Caspian Region. *Mem. Acad. Sci. Peterbourg, Ser. VIII,* 6.

ANDRESEN, K. J. & HUUSE, M. 2011. 'Bulls-eye' pockmarks and polygonal faulting in the Lower Congo Basin: Relative timing and implications for fluid expulsion during shallow burial. *Marine Geology,* 279**,** 111-127.

ANTONIOLI, F., BARD, E., POTTER, E.-K., SILENZI, S. & IMPROTA, S. 2004. 215-ka History of sea-level oscillations from marine and continental layers in Argentarola Cave speleothems (Italy). *Global and planetary change,* 43**,** 57-78.

ARNTSEN, B., WENSAAS, L., LØSETH, H. & HERMANRUD, C. 2007. Seismic modeling of gas chimneys. *Geophysics,* 72**,** SM251-SM259.

AYDIN, A. 2000. Fractures, faults, and hydrocarbon entrapment, migration and flow. *Marine and Petroleum Geology,* 17**,** 797-814.

BACON, M., SIMM, R. & REDSHAW, T. 2007. *3-D seismic interpretation*, Cambridge University Press.

BARBER, P. M. 1981. Messinian subaerial erosion of the proto-Nile Delta. *Marine Geology,* 44**,** 253-272.

BARKER, C. 1987. Development of abnormal and subnormal pressures in reservoirs containing bacterially generated gas. *AAPG Bulletin,* 71**,** 1404-1413.

BARRY, K. M. & SHUGART, T. R. Seismic hydrocarbon indicators and models. Offshore Technology Conference, 1974. Offshore Technology Conference.

BENTHAM, P., PASLEY, M. & BIRT, C. The style and timing of mud volcanism in the offshore Nile Delta, Egypt. Paris 2005 AAPG International Conference and Exhibition, 2006.

BERNDT, C. 2005. Focused fluid flow in passive continental margins. *Philosophical Transactions of the Royal Society A: Mathematical, Physical and Engineering Sciences,* 363**,** 2855-2871.

BERNDT, C., BÜNZ, S. & MIENERT, J. 2003. Polygonal fault systems on the mid-Norwegian margin: a long-term source for fluid flow. *Geological Society, London, Special Publications,* 216**,** 283-290.

BERRYHILL, H. L., SUTER, J. R. & HARDIN, N. S. 1987. *Late Quaternary facies and structure, northern Gulf of Mexico: interpretations from seismic data*, American Association of Petroleum Geologists.

BERTONI, C. & CARTWRIGHT, J. 2005. 3D seismic analysis of circular evaporite dissolution structures, Eastern Mediterranean. *Journal of the Geological Society,* 162**,** 909-926.

BERTONI, C. & CARTWRIGHT, J. 2007a. Clastic depositional systems at the base of the late Miocene evaporites of the Levant region, Eastern Mediterranean. *Geological Society, London, Special Publications,* 285**,** 37-52.

BERTONI, C. & CARTWRIGHT, J. 2015. Messinian evaporites and fluid flow. *Marine and Petroleum Geology*.

BERTONI, C., CARTWRIGHT, J. & HERMANRUD, C. 2013. Evidence for large-scale methane venting due to rapid drawdown of sea level during the Messinian Salinity Crisis. *Geology,* 41**,** 371-374.

BERTONI, C. & CARTWRIGHT, J. A. 2006. Controls on the basinwide architecture of late Miocene (Messinian) evaporites on the Levant margin (Eastern Mediterranean). *Sedimentary Geology,* 188**,** 93-114.

BERTONI, C. & CARTWRIGHT, J. A. 2007b. Major erosion at the end of the Messinian Salinity Crisis: evidence from the Levant Basin, Eastern Mediterranean. *Basin Research,* 19**,** 1-18.

BOWMAN, S. A. 2011. Regional seismic interpretation of the hydrocarbon prospectivity of offshore Syria. *Geoarabia,* 16**,** 95-124.

BRANNEY, M. J. 1995. Downsag and extension at calderas: new perspectives on collapse geometries from ice-melt, mining, and volcanic subsidence. *Bulletin of Volcanology,* 57**,** 303-318.

BROWN, A. R., BROWN, A. R., BROWN, A. R. & BROWN, A. R. 2004. *Interpretation of three-dimensional seismic data*, American Association of Petroleum Geologists Tulsa.

BROWN, K. M. 1990. The nature and hydrogeologic significance of mud diapirs and diatremes for accretionary systems. *Journal of Geophysical Research,* 95**,** 8969-8982.

BRYAN, S. E., PEATE, I. U., PEATE, D. W., SELF, S., JERRAM, D. A., MAWBY, M. R., MARSH, J. & MILLER, J. A. 2010. The largest volcanic eruptions on Earth. *Earth-Science Reviews,* 102**,** 207-229.

BUCHBINDER, B. & ZILBERMAN, E. 1997. Sequence stratigraphy of Miocene-Pliocene carbonate-siliciclastic shelf deposits in the eastern Mediterranean margin (Israel): Effects of eustasy and tectonics. *Sedimentary Geology,* 112**,** 7-32.

CALVES, G., SCHWAB, A., HUUSE, M., VAN RENSBERGEN, P., CLIFT, P., TABREZ, A. & INAM, A. 2010. Cenozoic mud volcano activity along the Indus Fan: offshore Pakistan. *Basin Research,* 22**,** 398-413.

CAMERLENGHI, A. & CITA, M. 1987. Setting and tectonic evolution of some Eastern Mediterranean deep-sea basins. *Marine geology,* 75**,** 31-55.

CARTWRIGHT, J. 2007. The impact of 3D seismic data on the understanding of compaction, fluid flow and diagenesis in sedimentary basins. *Journal of the Geological Society,* 164**,** 881-893.

CARTWRIGHT, J. & HUUSE, M. 2005. 3D seismic technology: the geological 'Hubble'. *Basin Research,* 17**,** 1-20.

CARTWRIGHT, J., HUUSE, M. & APLIN, A. 2007. Seal bypass systems. *AAPG Bulletin,* 91**,** 1141-1166.

CARTWRIGHT, J. & SANTAMARINA, C. 2015. Seismic characteristics of fluid escape pipes in sedimentary basins: implications for pipe genesis. *Marine and Petroleum Geology*.

CARTWRIGHT, J. A. & JACKSON, M. P. A. 2008. Initiation of gravitational collapse of an evaporite basin margin: The Messinian saline giant, Levant Basin, eastern Mediterranean. *Geological Society of America Bulletin,* 120**,** 399-413.

CATHLES, L., SU, Z. & CHEN, D. 2010. The physics of gas chimney and pockmark formation, with implications for assessment of seafloor hazards and gas sequestration. *Marine and Petroleum Geology,* 27**,** 82-91.

CHARLOU, J., DONVAL, J., ZITTER, T., ROY, N., JEAN-BAPTISTE, P., FOUCHER, J. & WOODSIDE, J. 2003. Evidence of methane venting and geochemistry of brines on mud volcanoes of the eastern Mediterranean Sea. *Deep Sea Research Part I: Oceanographic Research Papers,* 50**,** 941-958.

CHIODINI, G., D'ALESSANDRO, W. & PARELLO, F. 1996. Geochemistry of gases and waters discharged by the mud volcanoes at Paternò, Mt. Etna (Italy). *Bulletin of volcanology,* 58**,** 51-58.

CIESM 2008. The Messinian Salinity Crisis from mega-deposits to microbiology - A consensus report. *N° 33 in CIESM Workshop Monographs [F. Briand, Ed.], 168 pages, Monaco.*

CLARI, P., CAVAGNA, S., MARTIRE, L. & HUNZIKER, J. 2004. A Miocene mud volcano and its plumbing system: a chaotic complex revisited (Monferrato, NW Italy). *Journal of Sedimentary Research,* 74**,** 662-676.

CLARK, P. J. & EVANS, F. C. 1954. Distance to nearest neighbor as a measure of spatial relationships in populations. *Ecology***,** 445-453.

CLAUZON, G., SUC, J. P., GAUTIER, F., BERGER, A. & LOUTRE, M. F. 1996. Alternate interpretation of the Messinian salinity crisis: Controversy resolved? *Geology,* 24**,** 363.

COCHRAN, W. G. 1952. The $\chi 2$ test of goodness of fit. *The Annals of Mathematical Statistics***,** 315-345.

COSGROVE, J. W. 2001. Hydraulic fracturing during the formation and deformation of a basin: A factor in the dewatering of low-permeability sediments. *AAPG bulletin,* 85**,** 737-748.

DADASHEV, F. 1963. Hydrocarbon gases of mud volcanoes of Azerbaijan. *Azerneshr, Baku,* 5.

DAINES, S. R. 1982. Aquathermal Pressuring and Geopressure Evaluation: GEOLOGIC NOTES. *AAPG Bulletin,* 66**,** 931-939.

DAVIES, R. J. 2003. Kilometer-scale fluidization structures formed during early burial of a deep-water slope channel on the Niger Delta. *Geology,* 31**,** 949-952.

DAVIES, R. J., BRUMM, M., MANGA, M., RUBIANDINI, R., SWARBRICK, R. & TINGAY, M. 2008. The East Java mud volcano (2006 to present): An earthquake or drilling trigger? *Earth and Planetary Science Letters,* 272**,** 627-638.

DAVIES, R. J. & CLARKE, A. L. 2010. Methane recycling between hydrate and critically pressured stratigraphic traps, offshore Mauritania. *Geology,* 38**,** 963-966.

DAVIES, R. J., MATHIAS, S. A., MOSS, J., HUSTOFT, S. & NEWPORT, L. 2012. Hydraulic fractures: How far can they go? *Marine and petroleum geology,* 37**,** 1-6.

DAVIES, R. J., MATHIAS, S. A., SWARBRICK, R. E. & TINGAY, M. J. 2011. Probabilistic longevity estimate for the LUSI mud volcano, East Java. *Journal of the Geological Society,* 168**,** 517-523.

DAVIES, R. J. & STEWART, S. A. 2005. Emplacement of giant mud volcanoes in the South Caspian Basin: 3D seismic reflection imaging of their root zones. *Journal of the Geological Society,* 162**,** 1-4.

DAVIES, R. J., SWARBRICK, R. E., EVANS, R. J. & HUUSE, M. 2007. Birth of a mud volcano: East Java, 29 May 2006. *GSA TODAY,* 17**,** 4.

DAVIS, J. C. & SAMPSON, R. J. 2002. *Statistics and data analysis in geology*, Wiley New York.

DAVISON, I. 2009. Faulting and fluid flow through salt. *Journal of the Geological Society,* 166**,** 205-216.

DE LANGE, G., MIDDELBURG, J., VAN DER WEIJDEN, C., CATALANO, G., LUTHER III, G., HYDES, D., WOITTIEZ, J. & KLINKHAMMER, G. 1990. Composition of anoxic hypersaline brines in the Tyro and Bannock Basins, eastern Mediterranean. *Marine chemistry,* 31**,** 63-88.

DELANEY, P. T., POLLARD, D. D., ZIONY, J. I. & MCKEE, E. H. 1986. Field relations between dikes and joints: emplacement processes and paleostress analysis. *Journal of Geophysical Research: Solid Earth (1978–2012),* 91**,** 4920-4938.

DEMING, D. 1994. Factors necessary to define a pressure seal. *AAPG bulletin,* 78**,** 1005-1009.

DEVILLE, E., BATTANI, A., GRIBOULARD, R., GUERLAIS, S., HERBIN, J., HOUZAY, J., MULLER, C. & PRINZHOFER, A. 2003. The origin and processes of mud volcanism: New insights from Trinidad. *Geological Society, London, Special Publications,* 216**,** 475-490.

DEVILLE, E., GUERLAIS, S.-H., CALLEC, Y., GRIBOULARD, R., HUYGHE, P., LALLEMANT, S., MASCLE, A., NOBLE, M., SCHMITZ, J. & GROUP, C. O. T. C. W. 2006. Liquefied vs stratified sediment mobilization processes: insight from the South of the Barbados accretionary prism. *Tectonophysics,* 428**,** 33-47.

DEVILLE, E. & GUERLAIS, S. H. 2009. Cyclic activity of mud volcanoes: Evidences from Trinidad (SE Caribbean). *Marine and Petroleum Geology,* 26**,** 1681-1691.

DEVILLE, É., GUERLAIS, S. H., LALLEMANT, S. & SCHNEIDER, F. 2010. Fluid dynamics and subsurface sediment mobilization processes: an overview from Southeast Caribbean. *Basin research,* 22**,** 361-379.

DIA, A., CASTREC-ROUELLE, M., BOULEGUE, J. & COMEAU, P. 1999. Trinidad mud volcanoes: where do the expelled fluids come from? *Geochimica et Cosmochimica Acta,* 63**,** 1023-1038.

DIMITROV, L. I. 2002. Mud volcanoes--the most important pathway for degassing deeply buried sediments. *Earth-Science Reviews,* 59**,** 49-76.

DOLSON, J., BOUCHER, P., SIOK, J. & HEPPARD, P. Key challenges to realizing full potential in an emerging giant gas province: Nile Delta/Mediterranean offshore, deep water, Egypt. Geological Society, London, Petroleum Geology Conference series, 2005. Geological Society of London, 607-624.

DOLSON, J., SHANN, M., MATBOULY, S., HAMMOUDA, H. & RASHED, R. 2001. Egypt in the twenty-first century: petroleum potential in offshore trends. *GEOARABIA-MANAMA-,* 6**,** 211-230.

DOWNEY, M. W. 1984. Evaluating seals for hydrocarbon accumulations. *AAPG Bulletin,* 68**,** 1752-1763.

DRUCKMAN, Y., BUCHBINDER, B., MARTINOTTI, G. M., TOV, R. & AHARON, P. 1995. The buried Afiq Canyon (eastern Mediterranean, Israel): a case study of a Tertiary submarine canyon exposed in Late Messinian times. *Marine Geology,* 123**,** 167-185.

DUCASSOU, E., CAPOTONDI, L., MURAT, A., BERNASCONI, S. M., MULDER, T., GONTHIER, E., MIGEON, S., DUPRAT, J., GIRAUDEAU, J. & MASCLE, J. 2007. Multiproxy Late Quaternary stratigraphy of the Nile deep-sea turbidite system—Towards a chronology of deep-sea terrigeneous systems. *Sedimentary Geology,* 200**,** 1-13.

DUGGEN, S., HOERNLE, K., VAN DEN BOGAARD, P., RÜPKE, L. & MORGAN, J. P. 2003. Deep roots of the Messinian salinity crisis. *Nature,* 422**,** 602-606.

DUPRÉ, S., MASCLE, J., FOUCHER, J.-P., HARMEGNIES, F., WOODSIDE, J. & PIERRE, C. 2014. Warm brine lakes in craters of active mud volcanoes, Menes caldera off NW Egypt: evidence for deep-rooted thermogenic processes. *Geo-Marine Letters,* 34**,** 153-168.

DUPRE, S., WOODSIDE, J., FOUCHER, J.-P., DE LANGE, G., MASCLE, J., BOETIUS, A., MASTALERZ, V., STADNITSKAIA, A., ONDREAS, H., HUGUEN, C., HARMEGNIES, F. O., GONTHARET, S., LONCKE, L., DEVILLE, E., NIEMANN, H., OMOREGIE, E., ROY, K. O.-L., FIALA-MEDIONI, A., DAHLMANN, A., CAPRAIS, J.-C., PRINZHOFER, A., SIBUET, M., PIERRE, C., DAMSTE, J. S. S. & PARTY, N. S. 2007. Seafloor geological studies above active gas chimneys off Egypt (Central nile deep sea fan). *Deep-Sea Research Part I-Oceanographic Research Papers,* 54**,** 1146-1172.

DUPRÉ, S., WOODSIDE, J., KLAUCKE, I., MASCLE, J. & FOUCHER, J.-P. 2010. Widespread active seepage activity on the Nile Deep Sea Fan (offshore Egypt) revealed by high-definition geophysical imagery. *Marine Geology,* 275**,** 1-19.

DUPRE, S., WOODSIDE, J., KLAUCKE, I., MASCLE, J. & FOUCHER, J. P and the NAUTINIL & MIMES Scientific Parties (2005)-Multi-scale seafloor mapping of active seep-related structures, offshore Egypte. CIESM Workshop, Bologna, Working document, 2005.

ECONOMIST, P. 2011. *Shell gives up on deep water Nemed* [Online]. Petroleum Economist. Available: http://www.petroleum-

economist.com/Article/2949653/Shell-gives-up-on-deep-water-Nemed.html [Accessed 26th July 2014].

EGAS. 2012a. *Technical report Block 11 N. Leil offshore* [Online]. Available: http://www.egas.com.eg/BidRound2012/block0011.pdf [Accessed 22nd May 2013].

EGAS. 2012b. *Technical report Block 12 N. Leil offshore* [Online]. Available: http://www.egas.com.eg/BidRound2012/block0011.pdf [Accessed 22nd May 2013].

EGAS. 2012c. *Technical report Block 13 N. Leil offshore* [Online]. Available: http://www.egas.com.eg/BidRound2012/block0011.pdf [Accessed 22nd May 2013].

EL-ARABY, H. & SULTAN, M. 2000. Integrated seismic risk map of Egypt. *Seismological Research Letters,* 71**,** 53-66.

EL-SAYED, A., KORRAT, I. & HUSSEIN, H. 2004. Seismicity and seismic hazard in Alexandria (Egypt) and its surroundings. *Seismic Ground Motion in Large Urban Areas.* Springer.

ERUTEYA, O. E., WALDMANN, N., SCHALEV, D., MAKOVSKY, Y. & BEN-AVRAHAM, Z. 2015. Intra-to Post-Messinian deep-water gas piping in the Levant Basin, SE Mediterranean. *Marine and Petroleum Geology*.

ESRI. 2013a. *Average Nearest Neighbor (Spatial Statistics)* [Online]. Available: http://resources.arcgis.com/EN/HELP/MAIN/10.1/index.html#/Average_Nearest_Neighbor/005p00000008000000/ [Accessed: 08 Octorber 2014].

ESRI. 2013b. *Create Thiessen Polygons (Analysis)* [Online]. Available: http://resources.arcgis.com/EN/HELP/MAIN/10.1/index.html#//00080000001m000000 [Accessed: 08 Octorber 2014].

ESRI. 2013c. *Kernel Density (Spatial Analyst)* [Online]. Available: http://resources.arcgis.com/en/help/main/10.1/index.html#/Kernel_Density/009z0000000s000000/ [Accessed: 08 Octorber 2014].

ESRI. 2013d. *Multi-Distance Spatial Cluster Analysis (Ripley's K Function) (Spatial Statistics)* [Online]. Available: http://resources.arcgis.com/en/help/main/10.1/index.html#//005p0000000m000000 [Accessed: 08 Octorber 2014].

ETIOPE, G., BACIU, C., CARACAUSI, A., ITALIANO, F. & COSMA, C. 2004a. Gas flux to the atmosphere from mud volcanoes in eastern Romania. *Terra Nova,* 16**,** 179-184.

ETIOPE, G., CARACAUSI, A., FAVARA, R., ITALIANO, F. & BACIU, C. 2002. Methane emission from the mud volcanoes of Sicily (Italy). *Geophysical Research Letters,* 29**,** 56-1-56-4.

ETIOPE, G., FEYZULLAYEV, A., BACIU, C. & MILKOV, A. 2004b. Methane emission from mud volcanoes in eastern Azerbaijan. *Geology,* 32**,** 465-468.

ETIOPE, G. & KLUSMAN, R. W. 2002. Geologic emissions of methane to the atmosphere. *Chemosphere,* 49**,** 777-789.

EVANS, R. 2007. *The structure, evolution and geopysical expression of mud volcano systems from the South Caspian Basin.* PhD, Cardiff University.

EVANS, R. J., DAVIES, R. J. & STEWART, S. A. 2007. Internal structure and eruptive history of a kilometre-scale mud volcano system, South Caspian Sea. *Basin Research,* 19**,** 153-163.

EVANS, R. J., STEWART, S. A. & DAVIES, R. J. 2008. The structure and formation of mud volcano summit calderas. *Journal of the Geological Society,* 165**,** 769-780.

FAUGÈRES, J.-C., STOW, D. A., IMBERT, P. & VIANA, A. 1999. Seismic features diagnostic of contourite drifts. *Marine Geology,* 162**,** 1-38.

FISHER, K. & WARPINSKI, N. Hydraulic fracture-height growth: real data. Paper SPE 145949 presented at the Annual Technical Conference and Exhibition, Denver, Colorado. DOI, 2011.

FOSCHI, M., CARTWRIGHT, J. A. & PEEL, F. J. 2014. Vertical anomaly clusters: Evidence for vertical gas migration across multilayered sealing sequences. *AAPG Bulletin,* 98**,** 1859-1884.

FOWLER, S., MILDENHALL, J., ZALOVA, S., RILEY, G., ELSLEY, G., DESPLANQUES, A. & GULIYEV, F. 2000. Mud volcanoes and structural development on Shah Deniz. *Journal of Petroleum Science and Engineering,* 28**,** 189-206.

FREY-MARTÍNEZ, J., CARTWRIGHT, J. & JAMES, D. 2006. Frontally confined versus frontally emergent submarine landslides: a 3D seismic characterisation. *Marine and Petroleum Geology,* 23**,** 585-604.

FREY-MARTNEZ, J., CARTWRIGHT, J., HALL, B. & HUUSE, M. 2007. Clastic intrusion at the base of deep-water sands: A trap-forming mechanism in the eastern Mediterranean.

FUKUSHIMA, Y., MORI, J., HASHIMOTO, M. & KANO, Y. 2009. Subsidence associated with the LUSI mud eruption, East Java, investigated by SAR interferometry. *Marine and Petroleum Geology,* 26**,** 1740-1750.

GARCIA-CASTELLANOS, D., ESTRADA, F., JIMÉNEZ-MUNT, I., GORINI, C., FERNÁNDEZ, M., VERGÉS, J. & DE VICENTE, R. 2009. Catastrophic flood of the Mediterranean after the Messinian salinity crisis. *Nature,* 462**,** 778-781.

GARZIGLIA, S., MIGEON, S., DUCASSOU, E., LONCKE, L. & MASCLE, J. 2008. Mass-transport deposits on the Rosetta province (NW Nile deep-sea turbidite system, Egyptian margin): characteristics, distribution, and potential causal processes. *Marine Geology,* 250**,** 180-198.

GAULLIER, V., MART, Y., BELLAICHE, G., MASCLE, J., VENDEVILLE, B. C., ZITTER, T. & PARTY, S. L. P. I. I. S. 2000. Salt tectonics in and around the Nile deep-sea fan: insights from the PRISMED II cruise. *Geological Society, London, Special Publications,* 174**,** 111-129.

GAY, A., LOPEZ, M., BERNDT, C. & SERANNE, M. 2007. Geological controls on focused fluid flow associated with seafloor seeps in the Lower Congo Basin. *Marine Geology,* 244**,** 68-92.

GAY, A., LOPEZ, M., COCHONAT, P., SÉRANNE, M., LEVACHÉ, D. & SERMONDADAZ, G. 2006. Isolated seafloor pockmarks linked to BSRs, fluid chimneys, polygonal faults and stacked Oligocene–Miocene turbiditic palaeochannels in the Lower Congo Basin. *Marine Geology,* 226**,** 25-40.

GIRESSE, P., LONCKE, L., HUGUEN, C., MULLER, C. & MASCLE, J. 2010. Nature and origin of sedimentary clasts associated with mud volcanoes in the Nile deep-sea fan. Relationships with fluid venting. *Sedimentary Geology,* 228**,** 229-245.

GLUYAS, J. & SWARBRICK, R. 2009. *Petroleum geoscience*, John Wiley & Sons.

GONTHARET, S., PIERRE, C., BLANC-VALLERON, M.-M., ROUCHY, J.-M., FOUQUET, Y., BAYON, G., FOUCHER, J.-P., WOODSIDE, J. & MASCLE, J. 2007a. Nature and origin of diagenetic carbonate crusts and concretions from mud volcanoes and pockmarks of the Nile deep-sea fan (eastern Mediterranean Sea). *Deep Sea Research Part II: Topical Studies in Oceanography,* 54**,** 1292-1311.

GONTHARET, S., PIERRE, C., BLANC-VALLERON, M.-M., ROUCHY, J., FOUQUET, Y., BAYON, G., FOUCHER, J., WOODSIDE, J. & MASCLE, J. 2007b. Nature and origin of diagenetic carbonate crusts and concretions from mud volcanoes and pockmarks of the Nile deep-sea fan (eastern Mediterranean Sea). *Deep Sea Research Part II: Topical Studies in Oceanography,* 54**,** 1292-1311.

GOUBKIN, I. & FEDOROV, S. 1938. Mud volcanoes of the Soviet Union and their Connection with the genesis of petroleum fields in

Crimean-Caucasus geologic province. *USSR Academy of Science, Moscow) in Russian*.

GRANLI, J. R., ARNTSEN, B., SOLLID, A. & HILDE, E. 1999. Imaging through gas-filled sediments using marine shear-wave data. *Geophysics,* 64**,** 668-677.

GRASSO, M., LENTINI, F. & PEDLEY, H. 1982. Late tortonian—lower messinian (miocene) palaeogeography of SE Sicily: information from two new formations of the sorting group. *Sedimentary Geology,* 32**,** 279-300.

GRAUE, K. 2000. Mud volcanoes in deepwater Nigeria. *Marine and Petroleum Geology,* 17**,** 959-974.

GULIYEV, I., FEIZULLAYEV, A., JEVANSHIR, R. D. & AKADEMIĬASY, A. J. E. 1996. *All about mud volcanoes*, Geology Institute, Azerbaijan Academy of Sciences.

HAESE, R. R., MEILE, C., VAN CAPPELLEN, P. & DE LANGE, G. J. 2003. Carbon geochemistry of cold seeps: methane fluxes and transformation in sediments from Kazan mud volcano, eastern Mediterranean Sea. *Earth and Planetary Science Letters,* 212**,** 361-375.

HANSEN, J., CARTWRIGHT, J., HUUSE, M. & CLAUSEN, O. R. 2005. 3D seismic expression of fluid migration and mud remobilization on the Gjallar Ridge, offshore mid-Norway. *Basin Research,* 17**,** 123-139.

HART, B. S. 1999. Definition of subsurface stratigraphy, structure and rock properties from 3-D seismic data. *Earth-Science Reviews,* 47**,** 189-218.

HEDBERG, H. D. 1980. Methane generation and petroleum migration. *AAPG Special Volumes,* 10**,** 179-206.

HEGGLAND, R. 1997. Detection of gas migration from a deep source by the use of exploration 3D seismic data. *Marine Geology,* 137**,** 41-47.

HEGGLAND, R. 1998. Gas seepage as an indicator of deeper prospective reservoirs. A study based on exploration 3D seismic data. *Marine and Petroleum Geology,* 15**,** 1-9.

HIGGINS, G. E. & SAUNDERS, J. B. 1974. Mud volcanoes—their nature and origin. *Verh. Naturforsch. Ges. Basel,* 84**,** 101-152.

HIRSCH, F., FLEXER, A., ROSENFELD, A. & YELLINDROR, A. 1995. Palinspastic and crustal setting of the Eastern Mediterranean. *Journal of Petroleum Geology,* 18**,** 149-170.

HOOPER, E. 1991. Fluid migration along growth faults in compacting sediments. *Journal of Petroleum Geology,* 14**,** 161-180.

HOVLAND, M. & JUDD, A. 1988. *Seabed pockmarks and seepages: impact on geology, biology, and the marine environment*, Springer.

HSÜ, K., RYAN, W. & CITA, M. 1973. Late Miocene desiccation of the Mediterranean. *Nature,* 242**,** 240-244.

HSÜ, K. J. 1978. Initial reports of the Deep Sea Drilling Project: Washington. *DC, US Government Printing Office,* 42**,** 1249.

HSÜ, K. J., MONTADERT, L., BERNOULLI, D., CITA, M. B., GARRISON, R. E., KIDD, R. B., MELIERES, F., MÜLLER, C. & WRIGHT, R. 1977. History of the Mediterranean salinity crisis. *Structural history of the Mediterranean basins***,** 421.

HUBBERT, M. K. & WILLIS, D. G. 1972. Mechanics of hydraulic fracturing. *Mem.-Am. Assoc. Pet. Geol.;(United States),* 18.

HUDEC, M. R. & JACKSON, M. 2007. Terra infirma: Understanding salt tectonics. *Earth-Science Reviews,* 82**,** 1-28.

HUGUEN, C., FOUCHER, J. P., MASCLE, J., ONDREAS, H., THOUEMENT, M., GONTHARET, S., STADNITSKAIA, A., PIERRE, C., BAYON, G. & LONCKE, L. 2009. Menes caldera, a highly active site of brine seepage in the Eastern Mediterranean sea:" In situ" observations from the NAUTINIL expedition (2003). *Marine Geology,* 261**,** 138-152.

HUGUEN, C., MASCLE, J., CHAUMILLON, E., KOPF, A., WOODSIDE, J. & ZITTER, T. 2004. Structural setting and tectonic control of mud volcanoes from the Central Mediterranean Ridge (Eastern Mediterranean). *Marine Geology,* 209**,** 245-263.

HUGUEN, C., MASCLE, J., CHAUMILLON, E., WOODSIDE, J. M., BENKHELIL, J., KOPF, A. & VOLKONSKAïA, A. 2001. Deformational styles of the eastern Mediterranean Ridge and surroundings from combined swath mapping and seismic reflection profiling. *Tectonophysics,* 343**,** 21-47.

HUMPHREY, W. E. 1963. Sedimentary volcanism in eastern Mexico and northern Colombia. *Geological Society of America Bulletin,* 74**,** 125-128.

HUNT, M. 1979. *Petroleum geochemistry and geology*, WH Freeman and Company.

HUSTOFT, S., BÜNZ, S. & MIENERT, J. 2010. Three-dimensional seismic analysis of the morphology and spatial distribution of chimneys beneath the Nyegga pockmark field, offshore mid-Norway. *Basin Research,* 22**,** 465-480.

HUSTOFT, S., DUGAN, B. & MIENERT, J. 2009. Effects of rapid sedimentation on developing the Nyegga pockmark field: Constraints from hydrological modeling and 3-D seismic data, offshore mid-Norway. *Geochemistry, Geophysics, Geosystems,* 10.

HUSTOFT, S., MIENERT, J., BÜNZ, S. & NOUZÉ, H. 2007. High-resolution 3D-seismic data indicate focussed fluid migration pathways above polygonal fault systems of the mid-Norwegian margin. *Marine Geology,* 245**,** 89-106.

HUUSE, M., JACKSON, C. A. L., VAN RENSBERGEN, P., DAVIES, R. J., FLEMINGS, P. B. & DIXON, R. J. 2010. Subsurface sediment remobilization and fluid flow in sedimentary basins: an overview. *Basin Research,* 22**,** 342-360.

HUUSE, M., SHOULDERS, S. J., NETOFF, D. I. & CARTWRIGHT, J. 2005. Giant sandstone pipes record basin-scale liquefaction of buried dune sands in the Middle Jurassic of SE Utah. *Terra Nova,* 17**,** 80-85.

ISTADI, B. P., PRAMONO, G. H., SUMINTADIREJA, P. & ALAM, S. 2009. Modeling study of growth and potential geohazard for LUSI mud volcano: East Java, Indonesia. *Marine and Petroleum Geology,* 26**,** 1724-1739.

JACKSON, M. 1995. Retrospective salt tectonics. *AAPG Special Volume***,** 1-28.

JOLLY, R. J. & LONERGAN, L. 2002. Mechanisms and controls on the formation of sand intrusions. *Journal of the Geological Society,* 159**,** 605-617.

JOWETT, E. C., CATHLES III, L. M. & DAVIS, B. W. 1993. Predicting depths of gypsum dehydration in evaporitic sedimentary basins. *AAPG Bulletin,* 77**,** 402-413.

JUDD, A. & HOVLAND, M. 1992. The evidence of shallow gas in marine sediments. *Continental Shelf Research,* 12**,** 1081-1095.

JUDD, A. G. & HOVLAND, M. 2007. *Seabed fluid flow: the impact of geology, biology and the marine environment*, Cambridge University Press.

KARAKIN, A., KARAKIN, S. & KAMBAROVA, G. 2001. Movement of a mud mixture through a mud volcano channel. *IZVESTIIA PHYSICS OF THE SOLID EARTH C/C OF FIZIKA ZEMLI-ROSSIISKAIA AKADEMIIA NAUK,* 37**,** 812-824.

KEAREY, P., BROOKS, M. & HILL, I. 2009. *An introduction to geophysical exploration*, John Wiley & Sons.

KHOLODOV, V. 2002. Mud volcanoes: distribution regularities and genesis (communication 2. geological–geochemical peculiarities and formation model). *Lithology and Mineral Resources,* 37**,** 293-310.

KING, L. H. & MACLEAN, B. 1970. Pockmarks on the Scotian shelf. *Geological Society of America Bulletin,* 81**,** 3141-3148.

KNIPE, R. J. 1997. Juxtaposition and seal diagrams to help analyze fault seals in hydrocarbon reservoirs. *AAPG Bulletin,* 81**,** 187-195.

KOPF, A. & BEHRMANN, J. H. 2000. Extrusion dynamics of mud volcanoes on the Mediterranean Ridge accretionary complex. *Geological Society, London, Special Publications,* 174**,** 169-204.

KOPF, A., BEN CLENNELL, M. & CAMERLENGHI, A. Variations in sediment physical properties and permeability of mud-volcano deposits from Napoli dome and adjacent mud volcanoes. Proceedings of the Ocean Drilling Program. Scientific results, 1998. Ocean Drilling Program, 625-643.

KOPF, A., KLAESCHEN, D. & MASCLE, J. 2001. Extreme efficiency of mud volcanism in dewatering accretionary prisms. *Earth and Planetary Science Letters,* 189**,** 295-313.

KOPF, A. J. 2002. Significance of mud volcanism. *Reviews of Geophysics,* 40**,** 1-52.

KRIJGSMAN, W., HILGEN, F. J., RAFFI, I., SIERRO, F. J. & WILSONK, D. S. 1999. Chronology, causes and progression of the Messinian salinity crisis. *Nature,* 400**,** 652-655.

LAWRENCE, G. W. & CARTWRIGHT, J. A. 2010. The stratigraphic and geographic distribution of giant craters and remobilised sediment mounds on the mid Norway margin, and their relation to long term fluid flow. *Marine and Petroleum Geology,* 27**,** 733-747.

LAZAR, M., SCHATTNER, U. & RESHEF, M. 2012. The great escape: An intra-Messinian gas system in the eastern Mediterranean. *Geophysical Research Letters,* 39.

LIGTENBERG, J. 2005. Detection of fluid migration pathways in seismic data: implications for fault seal analysis. *Basin Research,* 17**,** 141-153.

LOFI, J., DÉVERCHÈRE, J., GAULLIER, V., GILLET, H., GORINI, C., GUENNOC, P., LONCKE, L., MAILLARD, A., SAGE, F. & THINON, I. 2011. Seismic atlas of the Messinian Salinity Crisis markers in the Mediterranean and Black Seas. *Mémoire de la Société Géologique ns,* 179**,** 1-72.

LONCKE, L., GAULLIER, V., BELLAICHE, G. & MASCLE, J. 2002. Recent depositional patterns of the Nile deep-sea fan from echo-character mapping. *AAPG Bulletin,* 86**,** 1165-1186.

LONCKE, L., GAULLIER, V., DROZ, L., DUCASSOU, E., MIGEON, S. & MASCLE, J. 2009. Multi-scale slope instabilities along the Nile deep-sea fan, Egyptian margin: A general overview. *Marine and Petroleum Geology,* 26**,** 633-646.

LONCKE, L., GAULLIER, V., MASCLE, J., VENDEVILLE, B. & CAMERA, L. 2006. The Nile deep-sea fan: an example of interacting sedimentation, salt tectonics, and inherited subsalt paleotopographic features. *Marine and Petroleum Geology,* 23**,** 297-315.

LONCKE, L., MASCLE, J. & PARTIES, F. S. 2004. Mud volcanoes, gas chimneys, pockmarks and mounds in the Nile deep-sea fan (Eastern Mediterranean): geophysical evidences. *Marine and Petroleum Geology,* 21**,** 669-689.

LORENZ, J. C., TEUFEL, L. W. & WARPINSKI, N. R. 1991. Regional Fractures I: A Mechanism for the Formation of Regional Fractures at Depth in Flat-Lying Reservoirs (1). *AAPG Bulletin,* 75**,** 1714-1737.

LØSETH, H., GADING, M. & WENSAAS, L. 2009. Hydrocarbon leakage interpreted on seismic data. *Marine and Petroleum Geology,* 26**,** 1304-1319.

LØSETH, H., WENSAAS, L., ARNTSEN, B., HANKEN, N.-M., BASIRE, C. & GRAUE, K. 2011. 1000 m long gas blow-out pipes. *Marine and Petroleum Geology,* 28**,** 1047-1060.

LØSETH, H., WENSAAS, L., ARNTSEN, B., HANKEN, N., BASIRE, C. & GRAUE, K. 1000 m long gas blow-out pipes. 63rd EAGE Conference & Exhibition, 2001.

LOWE, D. R. 1975. Water escape structures in coarse-grained sediments. *Sedimentology,* 22**,** 157-204.

LUNDEGARD, P. D. 1992. Sandstone porosity loss - A big picture view of the importance of compaction. *Journal of Sedimentary Petrology,* 62**,** 250-260.

MACDONALD, I., LEIFER, I., SASSEN, R., STINE, P., MITCHELL, R. & GUINASSO, N. 2002. Transfer of hydrocarbons from natural seeps to the water column and atmosphere. *Geofluids,* 2**,** 95-107.

MACDONALD, I. R., BUTHMAN, D. B., SAGER, W. W., PECCINI, M. B. & GUINASSO, N. L. 2000. Pulsed oil discharge from a mud volcano. *Geology,* 28**,** 907-910.

MAGARA, K. 1978. *Compaction and fluid migration*, Elsevier.

MALTMAN, A. J. & BOLTON, A. 2003. How sediments become mobilized. *Geological Society, London, Special Publications,* 216**,** 9-20.

MALTMAN, A. J., HUBBARD, B. & HAMBREY, M. J. 2000. Deformation of glacial materials: introduction and overview. *Geological Society, London, Special Publications,* 176**,** 1-9.

MANDL, G. & HARKNESS, R. M. 1987. Hydrocarbon migration by hydraulic fracturing. *Geological Society, London, Special Publications,* 29**,** 39-53.

MARSH, B. D. 1982. On the mechanics of igneous diapirism, stoping, and zone melting. *American Journal of Science,* 282**,** 808-855.

MARTIN, J. B., KASTNER, M., HENRY, P., LE PICHON, X. & LALLEMENT, S. 1996. Chemical and isotopic evidence for sources of fluids in a mud volcano field seaward of the Barbados accretionary wedge. *Journal of Geophysical Research: Solid Earth (1978–2012),* 101**,** 20325-20345.

MASCLE, J., BENKHELIL, J., BELLAICHE, G., ZITTER, T., WOODSIDE, J., LONCKE, L. & PARTY, P. I. I. S. 2000. Marine geologic evidence for a Levantine-Sinai plate, a new piece of the Mediterranean puzzle. *Geology,* 28**,** 779-782.

MASCLE, J., MARY, F., PRAEG, D., BROSOLO, L., CAMERA, L., CERAMICOLA, S. & DUPRÉ, S. 2014. Distribution and geological control of mud volcanoes and other fluid/free gas seepage features in the Mediterranean Sea and nearby Gulf of Cadiz. *Geo-Marine Letters,* 34**,** 89-110.

MASCLE, J., SARDOU, O., LONCKE, L., MIGEON, S., CAMÉRA, L. & GAULLIER, V. 2006. Morphostructure of the Egyptian continental margin: insights from swath bathymetry surveys. *Marine Geophysical Researches,* 27**,** 49-59.

MAZZINI, A., ETIOPE, G. & SVENSEN, H. 2012. A new hydrothermal scenario for the 2006 Lusi eruption, Indonesia. Insights from gas geochemistry. *Earth and Planetary Science Letters,* 317**,** 305-318.

MAZZINI, A., NERMOEN, A., KROTKIEWSKI, M., PODLADCHIKOV, Y., PLANKE, S. & SVENSEN, H. 2009. Strike-slip faulting as a trigger mechanism for overpressure release through piercement structures. Implications for the Lusi mud volcano, Indonesia. *Marine and Petroleum Geology,* 26**,** 1751-1765.

MAZZINI, A., SVENSEN, H., AKHMANOV, G., ALOISI, G., PLANKE, S., MALTHE-SØRENSSEN, A. & ISTADI, B. 2007. Triggering and dynamic evolution of the LUSI mud volcano, Indonesia. *Earth and Planetary Science Letters,* 261**,** 375-388.

MCCLUSKY, S., BALASSANIAN, S., BARKA, A., DEMIR, C., ERGINTAV, S., GEORGIEV, I., GURKAN, O., HAMBURGER, M., HURST, K. & KAHLE, H. 2000. Global Positioning System constraints on plate kinematics and dynamics in the eastern Mediterranean and Caucasus. *Journal of Geophysical Research: Solid Earth (1978–2012),* 105**,** 5695-5719.

MCDONNELL, A., LOUCKS, R. G. & DOOLEY, T. 2007. Quantifying the origin and geometry of circular sag structures in northern Fort Worth Basin, Texas: Paleocave collapse, pull-apart fault systems, or hydrothermal alteration? *AAPG bulletin,* 91**,** 1295-1318.

MCKENZIE, D. P. 1970. PLATE TECTONICS OF MEDITERRANEAN REGION. *Nature,* 226**,** 239-&.

MCKENZIE, J. A. 1999. From desert to deluge in the Mediterranean. *Nature,* 400**,** 613-613.

MEISSNER, F. F. 1978. Petroleum geology of the Bakken Formation, Williston Basin, North Dakota and Montana: Proceedings from 1978 Williston Basin Symposium, September 24-27. *Montana Geological Society, Billings***,** 207-227.

MELLORS, R., KILB, D., ALIYEV, A., GASANOV, A. & YETIRMISHLI, G. 2007. Correlations between earthquakes and large mud volcano eruptions. *Journal of Geophysical Research: Solid Earth (1978–2012),* 112.

MILKOV, A. V. 2000. Worldwide distribution of submarine mud volcanoes and associated gas hydrates. *Marine Geology,* 167**,** 29-42.

MILKOV, A. V., SASSEN, R., APANASOVICH, T. V. & DADASHEV, F. G. 2003. Global gas flux from mud volcanoes: a significant source of fossil methane in the atmosphere and the ocean. *Geophysical Research Letters,* 30**,** 1037.

MILLAHN, K., KOITKA, H., JURCZYK, D. & JANKOWSKY, W. 1979. Direct detection of hydrocarbons using seismic procedures. *Final Report Prakla-Seismos GmbH, Hanover (Germany, FR).* 1.

MILLER, K. G., KOMINZ, M. A., BROWNING, J. V., WRIGHT, J. D., MOUNTAIN, G. S., KATZ, M. E., SUGARMAN, P. J., CRAMER, B. S., CHRISTIE-BLICK, N. & PEKAR, S. F. 2005. The Phanerozoic record of global sea-level change. *science,* 310**,** 1293-1298.

MITCHELL, A. 2005. The ESRI guide to GIS analysis, Volume 2: Spatial Measurements and Statistics. Redlands. CA: Esri Press.

MORELLI, C. 1978. EASTERN MEDITERRANEAN - GEOPHYSICAL RESULTS AND IMPLICATIONS. *Tectonophysics,* 46**,** 333-346.

MORLEY, C. 2003. Outcrop examples of mudstone intrusions from the Jerudong anticline, Brunei Darussalam and inferences for hydrocarbon reservoirs. *Geological Society, London, Special Publications,* 216**,** 381-394.

MORLEY, C., CREVELLO, P. & AHMAD, Z. H. 1998. Shale tectonics and deformation associated with active diapirism: the Jerudong Anticline, Brunei Darussalam. *Journal of the Geological Society,* 155**,** 475-490.

MOSS, J. & CARTWRIGHT, J. 2010a. 3D seismic expression of km-scale fluid escape pipes from offshore Namibia. *Basin Research,* 22**,** 481-501.

MOSS, J. & CARTWRIGHT, J. 2010b. The spatial and temporal distribution of pipe formation, offshore Namibia. *Marine and Petroleum Geology,* 27**,** 1216-1234.

MOSS, J., CARTWRIGHT, J., CARTWRIGHT, A. & MOORE, R. 2012. The spatial pattern and drainage cell characteristics of a pockmark field, Nile Deep Sea Fan. *Marine and Petroleum Geology,* 35**,** 321-336.

MOSS, J. L. 2010. The spatial and temporal distribution of pipe and pockmark formation. *PhD Thesis, Cardiff University*.

MUERDTER, D. & RATCLIFF, D. 2001. Understanding subsalt illumination through ray-trace modeling, Part 1: Simple 2-D salt models. *The Leading Edge,* 20**,** 578-594.

MURTON, B. J. & BIGGS, J. 2003. Numerical modelling of mud volcanoes and their flows using constraints from the Gulf of Cadiz. *Marine Geology,* 195**,** 223-236.

NEWTON, C., SHIPP, R., MOSHER, D. & WACH, G. Importance of mass transport complexes in the Quaternary development of the Nile Fan, Egypt. Offshore Technology Conference, 2004. Offshore Technology Conference.

NOVIKOV, L. & SLOBODSKOY, R. 1979. Mechanism of formation of diatremes. *International Geology Review,* 21**,** 1131-1139.

O'BRIEN, M. J. & GRAY, S. H. 1996. Can we image beneath salt? *The Leading Edge,* 15**,** 17-22.

OKABE, A., BOOTS, B., SUGIHARA, K. & CHIU, S. N. 2009. *Spatial tessellations: concepts and applications of Voronoi diagrams*, John Wiley & Sons.

OSBORNE, M. J. & SWARBRICK, R. E. 1997. Mechanisms for generating overpressure in sedimentary basins; a reevaluation. *AAPG Bulletin,* 81**,** 1023-1041.

PEACH, C. J. & SPIERS, C. J. 1996. Influence of crystal plastic deformation on dilatancy and permeability development in synthetic salt rock. *Tectonophysics,* 256**,** 101-128.

PICKERING, K. T., AGAR, S. M. & OGAWA, Y. 1988. Genesis and deformation of mud injections containing chaotic basalt-limestone-chert associations: Examples from the southwest Japan forearc. *Geology,* 16**,** 881-885.

PIERRE, C., BAYON, G., BLANC-VALLERON, M.-M., MASCLE, J. & DUPRÉ, S. 2014. Authigenic carbonates related to active seepage of methane-rich hot brines at the Cheops mud volcano, Menes

caldera (Nile deep-sea fan, eastern Mediterranean Sea). *Geo-Marine Letters,* 34**,** 253-267.

PINOTTI, L., CONIGLIO, J., ESPARZA, A., D'ERAMO, F. & LLAMBıAS, E. 2002. Nearly circular plutons emplaced by stoping at shallow crustal levels, Cerro Aspero batholith, Sierras Pampeanas de Córdoba, Argentina. *Journal of South American Earth Sciences,* 15**,** 251-265.

PRINZHOFER, A. & DEVILLE, E. 2011. Origins of hydrocarbon gas seeping out from offshore mud volcanoes in the Nile delta. *Tectonophysics*.

QUIRK, D. G., SCHØDT, N., LASSEN, B., INGS, S. J., HSU, D., HIRSCH, K. K. & VON NICOLAI, C. 2012. Salt tectonics on passive margins: examples from Santos, Campos and Kwanza basins. *Geological Society, London, Special Publications,* 363**,** 207-244.

REICHE, S., HÜBSCHER, C. & BEITZ, M. 2014. Fault-controlled evaporite deformation in the Levant Basin, Eastern Mediterranean. *Marine Geology,* 354**,** 53-68.

REILLY, M. J. & FLEMINGS, P. B. 2010. Deep pore pressures and seafloor venting in the Auger Basin, Gulf of Mexico. *Basin Research,* 22**,** 380-397.

RIDER, M. H. 1986. The geological interpretation of well logs. Second edition. 91-132.

RIZZINI, A., VEZZANI, F., COCOCCETTA, V. & MILAD, G. 1978. Stratigraphy and sedimentation of a Neogene—Quaternary section in the Nile Delta area (ARE). *Marine Geology,* 27**,** 327-348.

ROBERTS, K. 2010. *Mud volcano systems: Structure, evolution and processes.* Doctor of Philosophy, Durham University.

ROBERTS, K., DAVIES, R. & STEWART, S. 2010. Structure of exhumed mud volcano feeder complexes, Azerbaijan. *Basin Research,* 22**,** 439-451.

ROBERTS, S. J. & NUNN, J. A. 1995. Episodic fluid expulsion from geopressured sediments. *Marine and Petroleum Geology,* 12**,** 195-204.

ROBERTSON, A. 1996. Mud volcanism on the Mediterranean Ridge: Initial results of Ocean Drilling Program Leg 160. *Geology,* 24**,** 239-242.

ROBERTSON, A. H. 1998. Tectonic significance of the Eratosthenes Seamount: a continental fragment in the process of collision with a subduction zone in the eastern Mediterranean (Ocean Drilling Program Leg 160). *Tectonophysics,* 298**,** 63-82.

ROBERTSON, A. H. & KOPF, A. 1998. Tectonic setting and processes of mud volcanism on the Mediterranean Ridge accretionary complex: evidence from Leg 160. *Proceedings of the Ocean Drilling Program, Scientific Results, Vol. 160; Chapter 50*.

ROBINSON, J. E. & EAKINS, B. W. 2006. Calculated volumes of individual shield volcanoes at the young end of the Hawaiian Ridge. *Journal of volcanology and geothermal research,* 151**,** 309-317.

ROSS, D. A. & UCHUPI, E. 1977. Structure and sedimentary history of southeastern Mediterranean Sea-Nile Cone area. *American Association of Petroleum Geologists Bulletin,* 61**,** 872-902.

ROVERI, M., FLECKER, R., KRIJGSMAN, W., LOFI, J., LUGLI, S., MANZI, V., SIERRO, F. J., BERTINI, A., CAMERLENGHI, A. & DE LANGE, G. 2014. The Messinian Salinity Crisis: past and future of a great challenge for marine sciences. *Marine Geology,* 352**,** 25-58.

RUDOLPH, M., SHIRZAEI, M., MANGA, M. & FUKUSHIMA, Y. 2013. Evolution and future of the Lusi mud eruption inferred from ground deformation. *Geophysical Research Letters,* 40**,** 1089-1092.

RUDOLPH, M. L., KARLSTROM, L. & MANGA, M. 2011. A prediction of the longevity of the Lusi mud eruption, Indonesia. *Earth and Planetary Science Letters,* 308**,** 124-130.

RYAN, W. B. & CITA, M. B. 1978. The nature and distribution of Messinian erosional surfaces—Indicators of a several-kilometer-deep Mediterranean in the Miocene. *Marine Geology,* 27**,** 193-230.

RYAN, W. B. F. 1978. Messinian badlands on the southeastern margin of the Mediterranean Sea. *Marine Geology,* 27**,** 349-363.

SAGE, L. & LETOUZEY, J. 1990. Convergence of the African and Eurasian plate in the eastern Mediterranean. *Petroleum and tectonics in mobile belts***,** 49-68.

SAID, R. 1962. The geology of Egypt. *New york*.

SALEM, R. 1976. Evolution of Eocene-Miocene sedimentation patterns in parts of northern Egypt. *AAPG Bulletin,* 60**,** 34-64.

SAMUEL, A., KNELLER, B., RASLAN, S., SHARP, A. & PARSONS, C. 2003. Prolific deep-marine slope channels of the Nile Delta, Egypt. *AAPG bulletin,* 87**,** 541-560.

SCHOENHERR, J., URAI, J. L., KUKLA, P. A., LITTKE, R., SCHLEDER, Z., LARROQUE, J.-M., NEWALL, M. J., AL-ABRY, N., AL-SIYABI, H. A. & RAWAHI, Z. 2007. Limits to the sealing capacity of rock salt: A case study of the infra-Cambrian Ara Salt from the South Oman salt basin. *AAPG bulletin,* 91**,** 1541-1557.

SCHOLZ, C. H., SYKES, L. R. & AGGARWAL, Y. P. 1973. Earthquake prediction: A physical basis. *Science,* 181**,** 803-810.

SCHROOT, B. M. & SCHÜTTENHELM, R. T. E. 2003. Shallow gas and gas seepage: expressions on seismic and otheracoustic data from the Netherlands North Sea. *Journal of Geochemical Exploration,* 78**,** 305-309.

SCLATER, J. G. & CHRISTIE, P. A. F. 1980. CONTINENTAL STRETCHING - AN EXPLANATION OF THE POST-MID-CRETACEOUS SUBSIDENCE OF THE CENTRAL NORTH-SEA BASIN. *Journal of Geophysical Research,* 85**,** 3711-3739.

SECOR, D. T. 1969. Mechanics of natural extension fracturing at depth in the earth's crust. *Research in tectonics: Geological Survey of Canada Special Paper***,** 68-52.

SELDON, B. & FLEMINGS, P. B. 2005. Reservoir pressure and seafloor venting: Predicting trap integrity in a Gulf of Mexico deepwater turbidite minibasin. *AAPG bulletin,* 89**,** 193-209.

SHACKLETON, N. 1987. Oxygen isotopes, ice volume and sea level. *Quaternary Science Reviews,* 6**,** 183-190.

SIBSON, R., MOORE, J. M. M. & RANKIN, A. 1975. Seismic pumping—a hydrothermal fluid transport mechanism. *Journal of the Geological Society,* 131**,** 653-659.

SIBSON, R. H. 1990. Conditions for fault-valve behaviour. *Geological Society, London, Special Publications,* 54**,** 15-28.

SILVERMAN, B. W. 1986. *Density estimation for statistics and data analysis*, CRC press.

STAMATAKIS, M. G., BALTATZIS, E. G. & SKOUNAKIS, S. B. 1987. Sulfate minerals from a mud volcano in the Katakolo area, western Peloponnesus, Greece. *American Mineralogist,* 72**,** 839-841.

STEWART, S. 1999. Seismic interpretation of circular geological structures. *Petroleum Geoscience,* 5**,** 273-285.

STEWART, S. A. & DAVIES, R. J. 2006. Structure and emplacement of mud volcano systems in the South Caspian Basin. *AAPG bulletin,* 90**,** 771-786.

STROZYK, F., VAN GENT, H., URAI, J. & KUKLA, P. 2012. 3D seismic study of complex intra-salt deformation: An example from the Upper Permian Zechstein 3 stringer, western Dutch offshore. *Geological Society, London, Special Publications,* 363**,** 489-501.

SULTAN, N. Excess Pore Pressure and Slope Failures Resulting From Gas-Hydrates Dissociation and Dissolution. Offshore Technology Conference, 2007. Offshore Technology Conference.

SUN, Q., CARTWRIGHT, J., WU, S. & CHEN, D. 2013. 3D seismic interpretation of dissolution pipes in the South China Sea:

Genesis by subsurface, fluid induced collapse. *Marine Geology,* 337**,** 171-181.

SUN, Q., WU, S., CARTWRIGHT, J. & DONG, D. 2012. Shallow gas and focused fluid flow systems in the Pearl River Mouth Basin, northern South China Sea. *Marine Geology,* 315**,** 1-14.

SVENSEN, H., PLANKE, S., MALTHE-SØRENSSEN, A., JAMTVEIT, B., MYKLEBUST, R., EIDEM, T. R. & REY, S. S. 2004. Release of methane from a volcanic basin as a mechanism for initial Eocene global warming. *Nature,* 429**,** 542-545.

SWARBRICK, R. E. 1999. Overpressure in Petroeum Systems. *Joint Association for Petroelum Exploration Courses (UK)*

Geological society: Imperial College London.

SWEENEY, J. J. & BURNHAM, A. K. 1990. Evaluation of a Simple Model of Vitrinite Reflectance Based on Chemical Kinetics (1). *AAPG Bulletin,* 74**,** 1559-1570.

TANIKAWA, W., SAKAGUCHI, M., WIBOWO, H. T., SHIMAMOTO, T. & TADAI, O. 2010. Fluid transport properties and estimation of overpressure at the Lusi mud volcano, East Java Basin. *Engineering Geology,* 116**,** 73-85.

TER-STEPANIAN, G. 2000. Quick clay landslides: their enigmatic features and mechanism. *Bulletin of Engineering Geology and the Environment,* 59**,** 47-57.

TERZAGHI, K., TERZAGHI, K., ENGINEER, C., CZECHOSLOWAKIA, A., TERZAGHI, K., CIVIL, I., TCHÉCOSLOVAQUIE, A. & UNIS, E. 1951. *Mechanism of landslides*, Harvard University, Department of Engineering.

TESTA, G. & LUGLI, S. 2000. Gypsum–anhydrite transformations in Messinian evaporites of central Tuscany (Italy). *Sedimentary Geology,* 130**,** 249-268.

TIGERT, V. & AL-SHAIEB, Z. 1990. Pressure seals: their diagenetic banding patterns. *Earth-Science Reviews,* 29**,** 227-240.

URAI, J., SCHLÉDER, Z., SPIERS, C. & KUKLA, P. 2008. Flow and transport properties of salt rocks. *Dynamics of Complex Intracontinental Basins: The Central European Basin System***,** 277-290.

VAN RENSBERGEN, P., DEPREITER, D., PANNEMANS, B. & HENRIET, J. P. 2005. Seafloor expression of sediment extrusion and intrusion at the El Arraiche mud volcano field, Gulf of Cadiz. *Journal of Geophysical Research: Earth Surface (2003–2012),* 110.

VAN RENSBERGEN, P., HILLIS, R. R., MALTMAN, A. J. & MORLEY, C. K. 2003. Subsurface sediment mobilization: introduction. *Geological Society, London, Special Publications,* 216**,** 1-8.

VAN RENSBERGEN, P., MORLEY, C., ANG, D., HOAN, T. & LAM, N. 1999. Structural evolution of shale diapirs from reactive rise to mud volcanism: 3D seismic data from the Baram delta, offshore Brunei Darussalam. *Journal of the Geological Society,* 156**,** 633-650.

VAN RENSBERGEN, P. & MORLEY, C. K. 2003. Re-evaluation of mobile shale occurrences on seismic sections of the Champion and Baram deltas, offshore Brunei. *Geological Society, London, Special Publications,* 216**,** 395-409.

VAN RENSBERGEN, P., RABAUTE, A., COLPAERT, A., GHISLAIN, T. S., MATHIJS, M. & BRUGGEMAN, A. 2007. Fluid migration and fluid seepage in the Connemara Field, Porcupine Basin interpreted from industrial 3D seismic and well data combined with high-resolution site survey data. *International Journal of Earth Sciences,* 96**,** 185-197.

VAN RENSBERGEN, P. M., C.K. 2003. Re-evaluation of mobile shale occurences on seismic sections of the Champion and Baram deltas, offshore Brunei. *In:* Van Rensbergen, P., Hillis, R.R., Maltman, C.K. (eds) *Subsurface sediment mobilization. Geological Society, London, Special Publications,* 216**,** 395-411.

VANDRÉ, C., CRAMER, B., GERLING, P. & WINSEMANN, J. 2007. Natural gas formation in the western Nile delta (Eastern Mediterranean): thermogenic versus microbial. *Organic Geochemistry,* 38**,** 523-539.

WARREN, J. 1999. *Evaporites: their evolution and economics*, Blackwell Science Oxford.

WATTS, N. 1987. Theoretical aspects of cap-rock and fault seals for single-and two-phase hydrocarbon columns. *Marine and Petroleum Geology,* 4**,** 274-307.

WEIJERMARS, R., JACKSON, M. P. A. & VENDEVILLE, B. 1993. Rheological and tectonic modeling of salt provinces. *Tectonophysics,* 217**,** 143-174.

WILFORD, G. 1967. The mud volcanoes of Sabah. *J. Sabah Soc,* 3**,** 12-21.

WU, X. & LIU, T. 2009. Spectral decomposition of seismic data with reassigned smoothed pseudo Wigner–Ville distribution. *Journal of Applied Geophysics,* 68**,** 386-393.

YUSIFOV, M. & RABINOWITZ, P. D. 2004. Classification of mud volcanoes in the South Caspian Basin, offshore Azerbaijan. *Marine and Petroleum Geology,* 21**,** 965-975.

Appendices

Appendices on DVD

Supplementary data for Chapter 5.

- Table of data recorded from Phase 1 mud volcanoes.
- Table of data recorded from Phase 2 mud volcanoes.
- A map showing the location of Phase 1 mud volcanoes.
- A map showing the location of Phase 2 mud volcanoes.
- A map showing the location of Phase 1 and Phase 2 mud volcanoes.
- Table of data showing the frequency of mud volcano volumes.
- Table of data used in the Chi-square test.
- Table of data used in the analysis of the Poisson distribution model.
- Table of data used in the analysis of the Negative Binomial model.

Supplementary data for Chapter 6

- Table of data recorded from fluids escape pipes.